Efficient Upcycling of Low-Functionality Polymers Using Trifluoromethyl Aryl Diazirine Chemistry

by

Liting Bi
B.Sc (Honours), University of Manitoba, 2019
B.Sc, Lanzhou University, 2019

A Dissertation Submitted in Partial Fulfillment
of the Requirements for the Degree of

DOCTOR OF PHILOSOPHY

in the Department of Chemistry

Supervisory Committee

Efficient Upcycling of Low-Functionality Polymers Using Trifluoromethyl Aryl Diazirine Chemistry

by

Liting Bi
B.Sc (Honours), University of Manitoba, 2019
B.Sc, Lanzhou University, 2019

Supervisory Committee

Dr. Jeremy E. Wulff, Department of Chemistry
Supervisor

Dr. Ian Manners, Department of Chemistry
Departmental Member

Dr. Stephanie Willerth, Department of Mechanical Engineering
Outside Member

Abstract

Crosslinking technologies are widely employed in our daily life: from silicone bakeware to epoxy adhesives and rubber tires. Traditionally, however, each type of commodity polymer substrate requires the use of a specific crosslinking method. Many desirable polymers—especially low-functionality polyolefins—cannot be crosslinked using these existing methods. To address this limitation, our group developed a family of *bis*-aryl-diazirine reagents that function through C−H, O–H or N–H insertions, and that can thereby act as universal crosslinkers for aliphatic polymers.

Despite their increasing popularity as crosslinkers in a variety of fields (e.g. photopatterning, bioadhesives), little attention has been given to the synthesis of highly efficient reagents with reduced or eliminated side-products. In Chapter 2, structure–function relationships of *mono*-aryl-diazirines were studied, highlighting the fundamental role played by electronic properties in the thermal and photo-activation of the molecules, as well as their insertion efficiency.

Building upon this study, Chapter 3 introduces a new generation of ether-linked trifluoromethyl *bis*-diazirine crosslinker, which is more than 10 times as effective as previous generations. The new reagent can also be activated using lower temperatures and longer wavelengths than earlier *bis*-diazirines—permitting the use of visible light for photopatterning. The efficacy of the electron-rich tether has been demonstrated at both the molecular and polymer level, showcasing the ability of the new linker to covalently adhere to low-surface energy materials and strengthen ultra-high molecular weight polyethylene fabrics.

The covalent inter-chain crosslinks in thermoset materials make them difficult to reprocess and recycle. To address this issue, Chapter 4 introduces chemically cleavable groups (e.g. carbonates, oxalates, silyl ethers) into the *bis*-diazirine crosslinker, allowing for further reprocessing of commodity polymers after the initial crosslinking step. This new class of crosslinkers exhibits rapid reactions during both the crosslinking and decrosslinking steps across a wide range of substrates, including small-molecule models and low-functionality polymers (e.g. LDPE, aPP/LDPE, PEG, PDMS). By employing specific chemical uncoupling methods, these materials can be efficiently converted from

thermoset to thermoplastic, presenting a new strategy for circularization of the polymer economy.

Chapter 5 describes the synthesis of *mono*-aryl-diazirine reagents along with their successful use for the non-destructive surface modification of polydimethylsiloxane (PDMS) substrates by both thermal and ultraviolet activation. Bovine serum albumin (BSA) and immunoglobulin G (IgG) are immobilized as a model protein and antibody, respectively, and sensitive quantification of their amounts along with their stability on the surface is achieved by radiolabeling with iodine-125. Through both thermal and ultraviolet activation, two types of trifluoromethyl aryl diazirine reagents with electrophilic motifs were able to enhance the amount and stability of BSA and IgG immobilization on the surface. These techniques show great promise for multi-material modifications, patterning of biomolecules on surfaces and various other important biological and medical device applications.

Author's Note: In the context of this thesis, the term "low-functionality polymers" refers to materials like polyethylene and polypropylene that lack conventional organic functional groups such as alcohols, alkenes, aromatic rings, or halogens. Materials lacking these groups are intrinsically more challenging to crosslink, because one cannot make use of traditional organic reactions (e.g. alkylation, acylation, hydrosilylation, thiol-ene reactions, etc.) to form new covalent bonds.

Table of Contents

List of Tables

List of Figures

List of Schemes

Abbreviations

°C	Degrees Celsius
3D	three-dimensional
AFM	Atomic force microscopy
aPP	Amorphous polypropylene
aq	Aqueous
Ar	Aromatic
ATR	Attenuated total reflectance
Bn	Benzyl
BSA	Bovine serum albumin
CDI	Carbonyldiimidazole
DCM	Dichloromethane
DLPNO	Domain based local pair natural orbital
DMAP	4-Dimethylaminopyridine
DMDHEU	Dimethylol-dihydroxyethyleneurea
DMF	Dimethylformamide
DMSO	Dimethyl sulfoxide
DMTA	Dynamic mechanical thermal analysis
DSC	Differential scanning calorimetry
E'	Storage modulus
EDG	Electron-donating group
Et_2O	Diethyl ether
EtOAc	Ethyl acetate
EWG	Electron-withdrawing group
FD	Field desorption
FITC	Fluorescein isothiocyanate
FT-IR	Fourier-transform infrared spectroscopy
g/mol	Grams per mole
SEC	Size exclusion chromatography
HCl	Hydrochloric acid

HDPE	High-density polyethylene
HMDSO	Hexamethyldisiloxane
HRMS	High resolution mass spectrometry
i-Pr	Isopropyl
IgG	Immunoglobulin G
iPP	Isotactic polypropylene
IR	Infrared
ISC	Intersystem crossing
K_2CO_3	Potassium carbonate
LDPE	Low-density polyethylene
LRMS	Low resolution mass spectrometry
MA	Maleic anhydride
M_c	Average molecular weight between two adjacent crosslinks
MeOH	Methanol
$MgSO_4$	Magnesium sulfate
M_n	Number average of molecular weight
MPa	Megapascals
M_w	Weight average of molecular weight
Na_2SO_4	Sodium sulfate
NH_4Cl	Ammonium Chloride
NHS	N-hydroxysuccinimide
nm	Nanometer
NMR	Nuclear magnetic resonance
OLED	Organic light-emitting diodes
PAL	Photoaffinity labeling
PAMAM	Polyamidoamine
PCL	Polycaprolactone
PDA	Polydopamine
PDI	Polydispersity PDI=M_w/M_n
PDMS	Polydimethylsiloxane
PEG	Polyethylene glycol

PEI	Polyethylenimine
PMMA	Polymethylmethacrylate
ppm	parts per million
PW	Paraffin wax
SDS	Sodium dodecyl sulfate
SEM	Scanning electron microscopy
TBAF	Tetrabutylammonium fluoride
TEM	Transmission electron microscopy
T_g	Glass transition temperature
THF	Tetrahydrofuran
T_{init}	Initiation temperature
T_m	Melting temperature
T_{onset}	Onset temperature for diazirine activation
TPD	Trifluoromethyl phenyl diazirine
T_{peak}	The temperature at which the diazirine activation exotherm reaches maximal heat flow
TS	Transition state
UHMWPE	Ultra-high-molecular weight polyethylene
UV	Ultraviolet
UV/Vis	Ultraviolet–visible
VC	Vehicle control
W	Watt
WAXS	Wide-angle X-ray scattering
wt%	Weight percent
XLPE	crosslinked polyethylene
XPS	X-ray photoelectron spectroscopy
XRD	X-ray diffraction
$\Delta G^{\ddagger}$	Activation free energy
ΔH	Enthalpy

Acknowledgments

I would first like to thank my committee for reading and contributing to this dissertation. A special thanks to Professor Ian Manners and Professor Stephanie M. Willerth for their support and advice during the past four and a half years.

A huge thank you goes to my supervisor, Professor Jeremy E. Wulff. Thank you for allowing me to grow into the scientist that I am. I am sincerely grateful for your supervision and guidance. You have not only taught me how to become a better communicator, but also emphasized the importance of it. I would also like to thank Rebecca Hof (Becky) for her work behind the scenes and her delicious cookies during Christmas times throughout my PhD.

I have engaged with numerous people throughout my PhD, and to acknowledge them all appropriately would require an appendix. Instead, I would like to highlight those with whom I worked closely and who had the biggest impact on my PhD.

Firstly, I would like to thank Dr. Stefania F. Musolino, Dr. Rashid Nazir, Dr. Mathieu L. Lepage and Dr. Chakravarthi Simhadri for their contributions to the various projects I have been a part of. I particularly wish to thank Stefania for her mentoring, answering my questions, providing endless support and engaging in stimulating discussions—thank you. I also want to thank Mathieu for his support and guidance at the start of my PhD. I wish to extend my gratitude to our collaborators: Professor Heather L. Buckley group (Grace M.O. Tieman and Dr. Fatima Shatila), Professor Kyla N. Sask group (Jie Li), Professor Kevin Golovin group (Dr. Xiaoxiao Zhao), Professor Abbas S. Milani group (Dr. Mahdi Takaffoli, Olivia H. Margoto, Mahshid Mahbod and Bryn Crawford) and Professor Gino A. DiLabio group (Zhipeng Pei).

During my PhD, I have had an incredible time at UVic and have been very fortunate to be surrounded by so many amazing and inspiring people during my studies. There are too many people to individually list here; however, I would like to give a special thanks to present and past Wulff group members who have made my last few years truly enjoyable: Dr. Tong Li, Dr. Chang Liu, Jon Sader, Dr. Derek Blevins, Austin Burman, Ben Godwin and Spencer Petras. On a similar note, I would like to acknowledge

all the staff from the Department of chemistry, with special thanks to Chris Barr, Erin Hodgson, Sandra Carlson, Hiromi Kurata and Dave Berry for all the work behind scenes.

I would like to give a special thanks to my undergraduate programs at both Lanzhou University and the University of Manitoba. I was taught by passionate and extraordinarily smart mentors. With too many people to name, I would like to highlight some of those that had the greatest impact. Thank you to Professor Rebecca Davis, Professor Scott Kroeker, Dr. Horace Luong, Professor Hélène Perreault, Professor Jennifer van Wijngaarden, Professor. Mario Bieringer and Professor Philip Hultin. But most importantly, I would like to thank Professor Frank Schweizer and his group, where I learned the fundamentals of synthetic and medicinal chemistry.

Last but not least, I would like to thank my parents and close friends for their caring support throughout not only my PhD but at every stage that led me to where I am now.

Publication List

(1) Li, J.; **Bi, L.**; Wulff, J. E.; Sask, K. Surface Modification of Polydimethylsiloxane (PDMS) with Diazirine Molecules for Protein Immobilization. *manuscript submitted*, **2023**.

(2) **Bi, L.**; Godwin, B.; Baran, M.; Nazir, R., Wulff, J. E. A Cleavable Crosslinking Strategy for Commodity Polymer Functionalization and Generation of Reprocessable Thermosets. *Angew. Chem. Int. Ed.* **2023**, e202304708.

(3) Musolino, S. F.; Mahbod, M.; Nazir, R.; **Bi, L.**; Graham, H. A.; Milani, A. S.; Wulff, J. E. Electronically Optimized Diazirine-Based Polymer Crosslinkers. *Polym. Chem.* **2022**, 13, 3833–3839.

(4) Zhao, X.; **Bi, L.**; Khatir, B.; Serles, P.; Filleter, T.; Wulff, J. E.; Golovin, K. Crosslinking Inert Liquidlike Polydimethylsiloxane Brushes Using Bis-Diazirine Chemical Insertion for Enhanced Mechanical Durability. *Chem. Eng. J.* **2022**, 442, 136017.

(5) Nazir, R.; **Bi, L.**; F. Musolino, S.; H. Margoto, O.; Çelebi, K.; Mobuchon, C.; Takaffoli, M.; S. Milani, A.; Falck, G.; E. Wulff, J. Polyamine–Diazirine Conjugates for Use as Primers in UHMWPE–Epoxy Composite Materials. *ACS Appl. Polym. Mater*. **2022**, 4 (3), 1728–1742.

(6) L. Lepage, M.; Takaffoli, M.; Simhadri, C.; Mandau, R.; Parvinzadeh Gashti, M.; Nazir, R.; Mohseni, M.; Li, W.; Liu, C.; **Bi, L.**; Falck, G.; Berrang, P.; Golovin, K.; S. Milani, A.; A. DiLabio, G.; E. Wulff, J. Influence of Topical Cross-Linking on Mechanical and Ballistic Performance of a Woven Ultra-High-Molecular-Weight Polyethylene Fabric Used in Soft Body Armor. *ACS Appl. Polym. Mater.* **2021**, 3 (11), 6008–6018.

(7) Musolino, S. F.; Pei, Z.; **Bi, L.**; DiLabio, G. A.; Wulff, J. E. Structure–Function Relationships in Aryl Diazirines Reveal Optimal Design Features to Maximize C–H Insertion. *Chem. Sci.* **2021**, 36 (12), 12138–12148.

(8) Simhadri, C.; **Bi, L.**; Lepage, M. L.; Takaffoli, M.; Pei, Z.; Musolino, S. F.; Milani, A. S.; DiLabio, G. A.; Wulff, J. E. Flexible Polyfluorinated Bis-Diazirines as Molecular Adhesives. *Chem. Sci.* **2021**, 11 (12), 4147–4153.

(9) Lepage, M. L.; Simhadri, C.; Liu, C.; Takaffoli, M.; **Bi, L.**; Crawford, B.; Milani, A. S.; Wulff, J. E. A Broadly Applicable Cross-Linker for Aliphatic Polymers Containing C–H Bonds. *Science.* **2019**, 366 (6467), 875–878.

Chapter 1: Introduction

1.1. Commodity Polymer Crosslinking: Mechanisms and Utility

Polymeric materials can be divided into thermoplastics and thermosets, based on the presence or absence of covalent linkages between the polymer chains. Thermoplastics contain unlinked polymer chains which under high temperatures might lose their rigidity and slide past one another, whereas thermosets contain covalent crosslinks that lock the polymeric matrix into a single molecular unit. Crosslinked polymeric materials are widely employed in our daily life: from rubber tires and epoxy adhesives to silicone bakeware and polyethylene insulation. Crosslinked polymers are a ubiquitous class of materials comprising ca. 15–20% of polymers produced, with a worldwide annual production of about 65 million tons during 2010–2015.[1,2] Crosslinking of natural and synthetic polymer materials offers various enhanced mechanical properties such as impact strength, improved chemical resistance to degradation by solvents or microbial contaminants, dimensional stability and high-temperature performance.[3,4] Thermoplastics can be melted, deformed, and processed in the molten state, whereas thermosets are virtually unrecyclable due to their permanent network structure.

Regarding conventional polymer crosslinking reactions, the vulcanization of rubber, which turns liquid rubber into a hard and durable material, is arguably the most widely applied crosslinking method in industry (the process is used for tires, conveyor belts, tubes, wires and cables, shoe soles, hoses, and window and door seals).[5] Natural and synthetic rubber consumptions were 14.8 million metric tons in 1990 and grew to 26.9 million tonnes in 2020 worldwide.[6] In 1839–1844, Charles Goodyear (American) and Thomas Hancock (English) independently discovered the vulcanization process.[7] The essence of vulcanization lies in creating crosslinks between precursor polymer strands, consequently leading to a three-dimensional (3D) rubber matrix network by incorporation of vulcanizing agents into unsaturated hydrocarbon backbones (Figure 1.1).[8] Various reagents are involved in vulcanization such as polymeric sulphur, which introduces short chains of sulphur atoms linking the polymer strands in rubber materials, accelerators (e.g. sulphenamides), and activators (e.g. zinc oxide).[7] Thanks to the sulphur vulcanization process, crosslinked rubber materials present good physical, mechanical, and dynamic

properties, as well as outstanding abrasive resistance and relatively low cost.[9] The vulcanization process, curing time, temperature, and type of filler can affect the chemical and physical properties of thermoset rubbers.[10] However, this covalently crosslinked network comes at a price—vulcanized rubber as an elastic, insoluble, and infusible thermoset material cannot be directly reprocessed and recycled.[11]

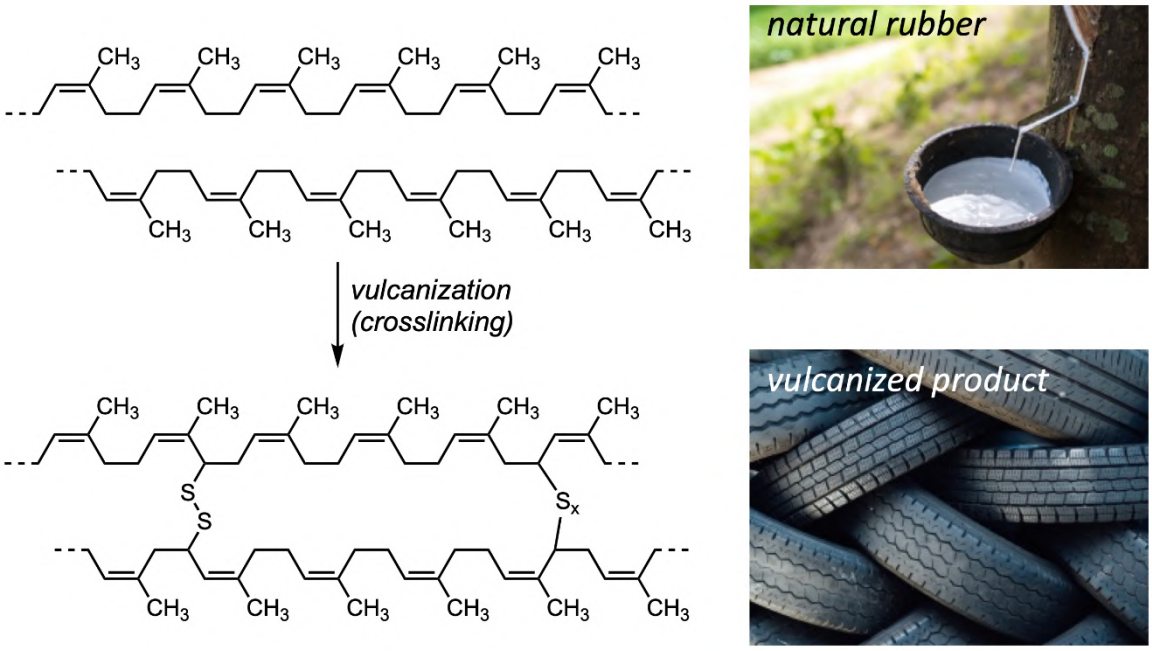

Figure 1.1 Crosslinking of polymer strands leads to the formation of network polymers through vulcanization.

Similarly, cellulose (a high-functionality linear polysaccharide) is the most abundant natural terrestrial biopolymer and is a source of many sustainable fuels, chemicals, and apparel materials.[12,13] However, when an external distortion force is applied (such as laundering), untreated cotton fabrics wrinkle easily due to the weak hydrogen bonds in their crystalline and amorphous structures.[14] Crosslinking of cellulose has been applied as a beneficial process for creating cotton fabrics with wrinkle-resistance properties for over 90 years.[15] DMDHEU (dimethylol-dihydroxyethyleneurea, used as an electrophilic reagent) and its derivatives are the most important and widely used reactants for crosslinking cellulose-based materials.[16] At elevated temperatures, the principal reaction of DMDHEU with the cellulose is etherification of hydroxyl groups in presence of an acid catalyst, causing crosslinking of adjacent cellulose molecules

(Figure 1.2). Therefore, the newly formed network prevents movement of fibre chains under stress and hinders wrinkle formation and shrinkage.[17]

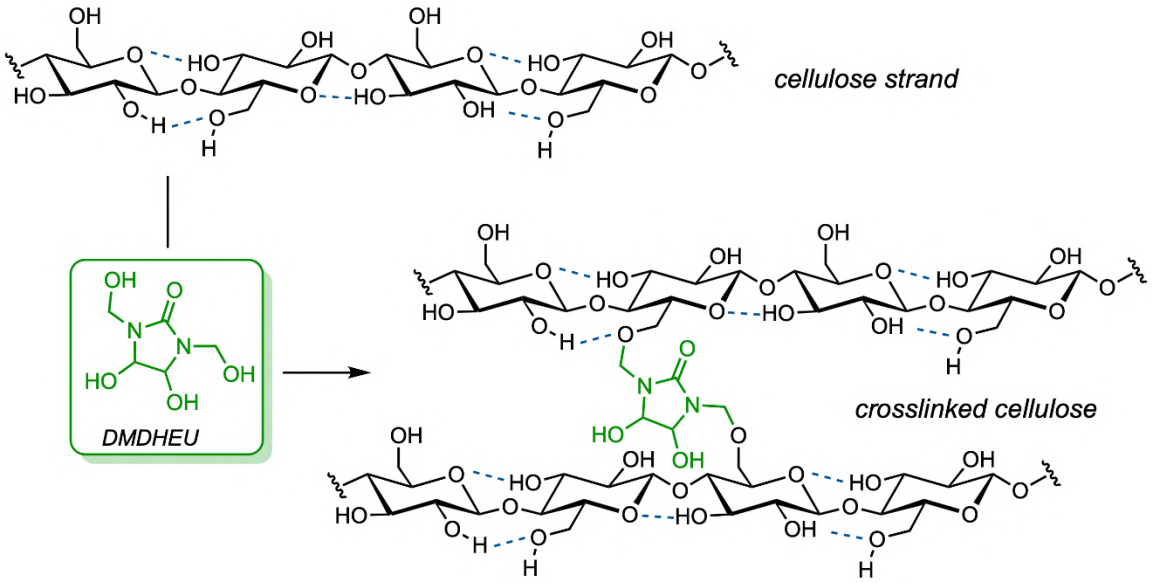

Figure 1.2 Conventional crosslinking reaction between molecular chains of cellulose using DMDHEU. Adapted from literature.[18]

Synthetic polymers like polyurethanes make up 31% of the commercial crosslinked polymer market.[19] Thermosetting polyurethanes are a family of crosslinked polymeric materials widely used as high-performance elastomers, sealants, adhesives, foams, coatings, or insulators due to their excellent adhesive properties, good stability to weather, and versatility of formulation.[20] Similar to the polar crosslinking mechanisms harnessed for cellulose, crosslinked polyurethanes are usually formed by reacting polyols (polyether, polyester, or polycarbonate) with excess diisocyanate (aromatic or aliphatic) or polymeric isocyanates, and lead to a densely interconnected network (Figure 1.3a).[21] When increased rigidity and thermal stability of polyurethane foams are desired, further crosslinking may be accomplished via cyclotrimerization of alkyl and aryl isocyanates (isocyanurate formation, Figure 1.3b).[22]

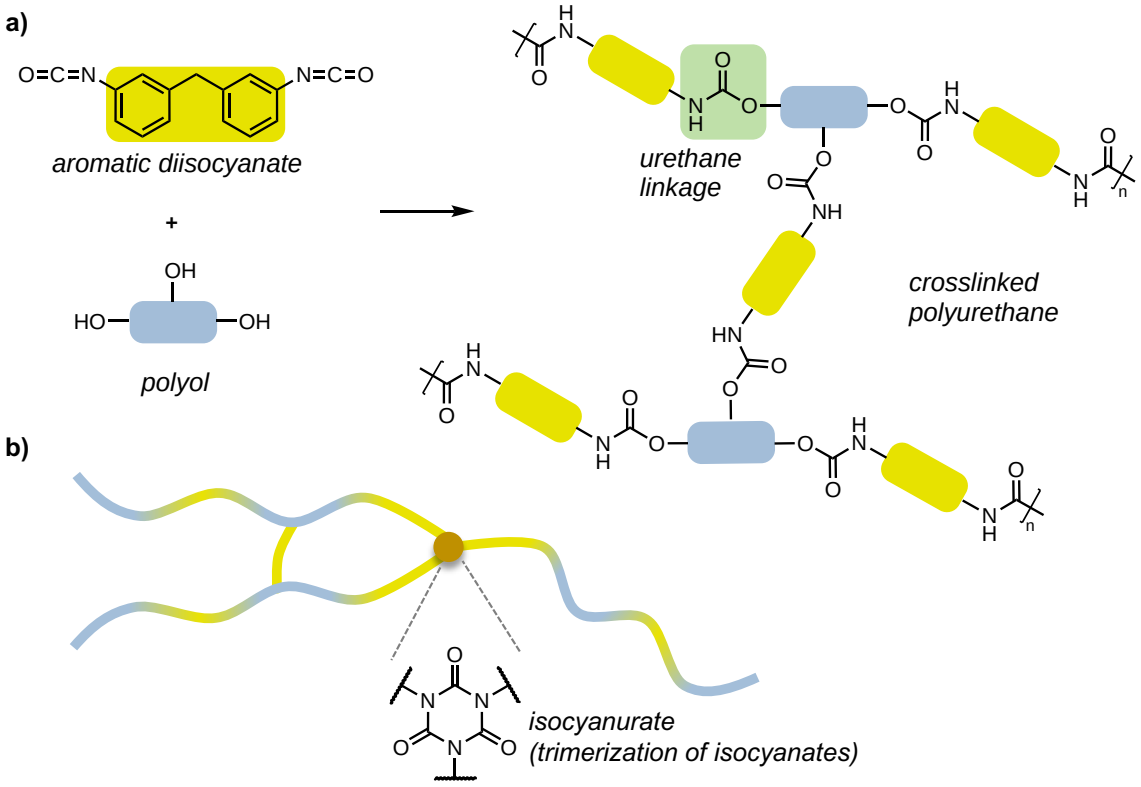

Figure 1.3 a) General synthesis of thermoset polyurethane. b) Isocyanate self-cyclization formed isocyanurate-based crosslinked polyurethane.

Likewise, the commercial epoxy curing process is also a well-studied example of polar crosslinking method, where the combination of an epoxy resin (i.e., reactive polymer) with a hardener (i.e., curing agent), containing typically multiple amine groups, generates a crosslinked network. The epoxide groups present on the resin (linear telechelic chains) react with the nucleophilic amines (or other nucleophilic groups contained in the hardener reagents) to form multiple crosslinks throughout the polymeric network (Figure 1.4). This results in the liquid epoxy resin (a thermoplastic) transforming into a hard, nonmeltable solid (a thermoset). After crosslinking, epoxy resins possess high chemical and heat resistance (useful for thermoset polymer matrix composites), good mechanical performance, and outstanding adhesion to many different substrates (useful for construction of aircraft and automobile components).[23]

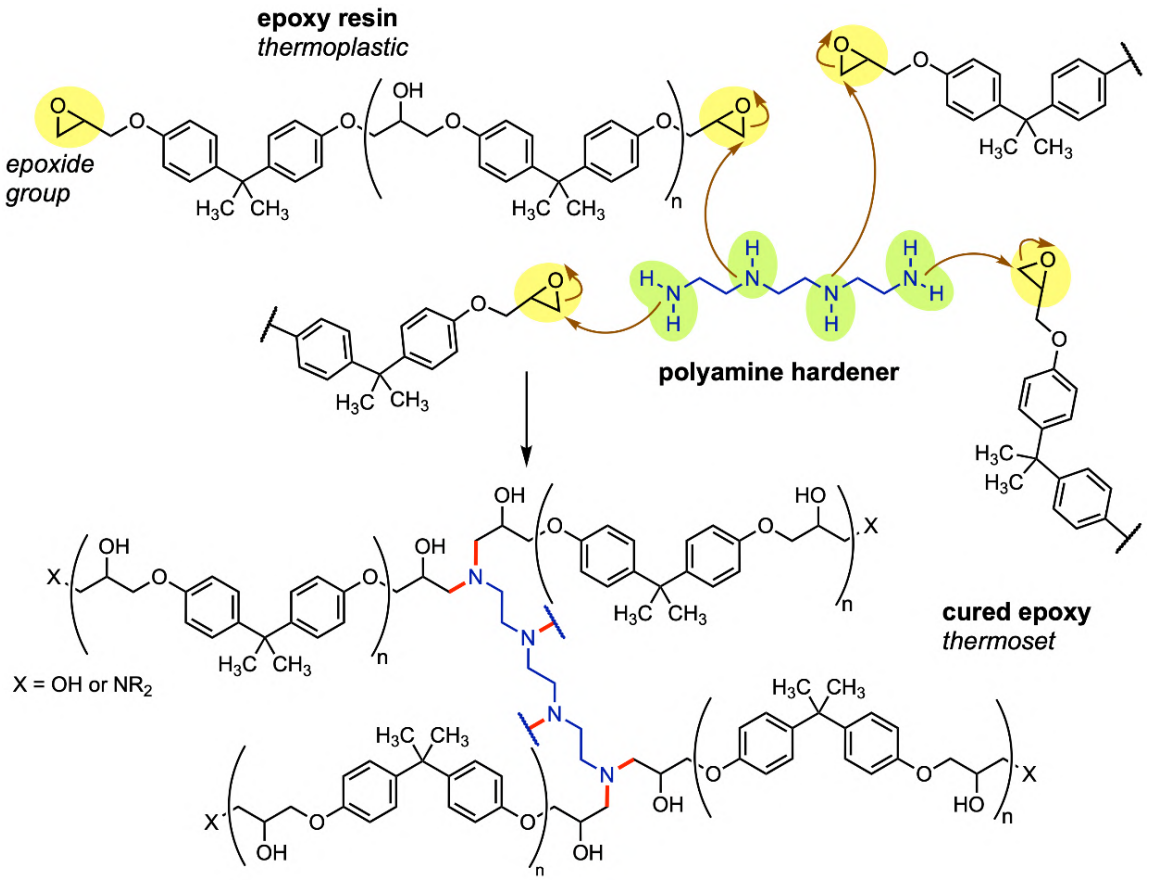

Figure 1.4 Two-component epoxy system curing process. Epoxide and amine groups are highlighted in yellow and green, respectively. The covalent bonds between hardener and resin are highlighted in red. Adapted from literature.[24]

Silicone elastomers are widely used in kitchenware, fabrication of wearable biomedical and soft robotic parts, stretchable electronics, and microfluidic devices, owing to their unique combination of chemical and thermal stability, gas permeability, biocompatibility, hydrophobicity and flexibility, among others.[25–27] Thermoset silicone elastomers are prepared by platinum-catalyzed hydrosilylation, organotin-catalyzed condensation, or peroxide-catalyzed radical curing.[28] Addition cure silicone elastomers are generally synthesized by a hydrosilylation process that involves a multi-hydrosilane (Si–H) functional linear polydimethylsiloxane (PDMS) reacting with a vinyl-functional PDMS-based crosslinker in the presence of a platinum catalyst (Figure 1.5a).[29] On the other hand, condensation cure silicone elastomers, generally used in protective coatings and sealants, are synthetized using organotin-catalyzed crosslinking reactions, which commonly occur between hydroxy-terminated PDMS and an alkoxysilane-based

crosslinker at room temperature to provide a silicone elastomer network (Figure 1.5b).[30] Peroxide curing involves organic peroxides such as dicumyl peroxide. At elevated temperatures (150–200 °C), the radical initiators decompose to form highly reactive radicals that covalently connect the linear PDMS chains and lead to three-dimensional networks.[31]

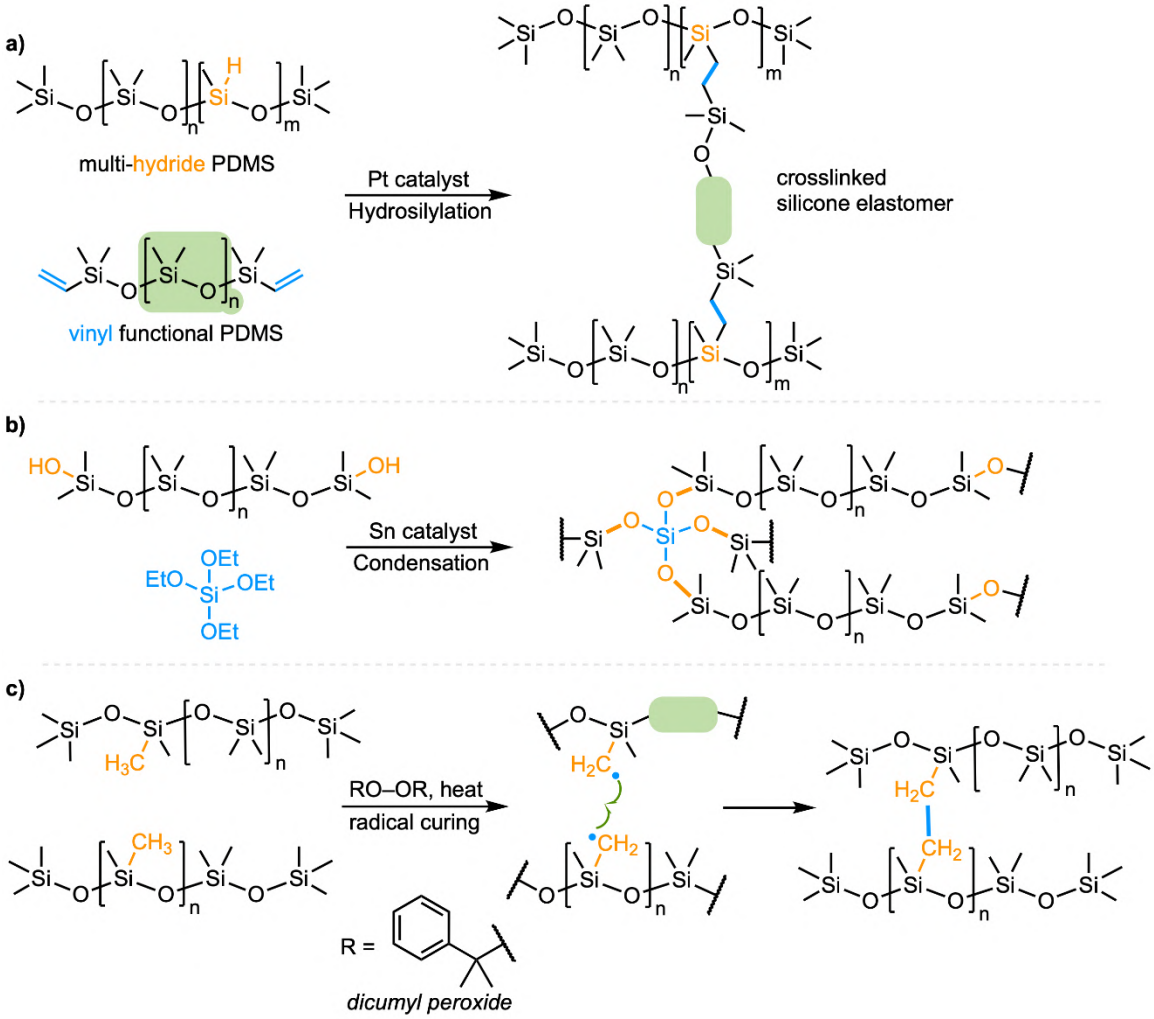

Figure 1.5 Thermoset silicone elastomer crosslinking via a) platinum-catalyzed hydrosilylation; b) organotin-catalyzed condensation; and c) organic peroxide-induced free-radical crosslinking.

In recent years, crosslinked polyethylene (XLPE) has become widely used in industry for applications ranging from electrical wire and cable insulation to heat-shrinkable products (tubing, packaging film, and bags).[32] Covalent crosslinking of polyethylene increases its strength and extends the upper temperature limit at which this

plastic can be used. However, crosslinking low-functionality macromolecules (e.g. polyethylene, polypropylene) in a well-controlled manner has been a major challenge in the field of polymer chemistry for more than 50 years.[33] Crosslinking of polyethylene to produce XLPE requires the breakage of a carbon-hydrogen (C–H) bond, which is typically accomplished using high-energy irradiation (γ rays or electron beams) or peroxide-induced radicals. This method limits control over the degree and type of crosslinks, which reduces the possibility to easily tune the mechanical properties of the final material.[32] Moreover, competing fragmentation and branching through β-scission processes can compromise the integrity of the material, due to the fact that C–H bonds (ca. 389 to 400 kJ/mol) are cleaved in the vicinity of relatively weaker C–C bonds (ca. 350 kJ/mol) (Figure 1.6a). These undesirable reactions become even more favored when polypropylene is used as the polymer substrate, since more stable secondary radicals are produced following C–C bond cleavage (Figure 1.6b).[34,35] As a result, polypropylene, along with many other aliphatic polymers, is unsuitable for crosslinking using the radical methods employed in manufacturing XLPE.

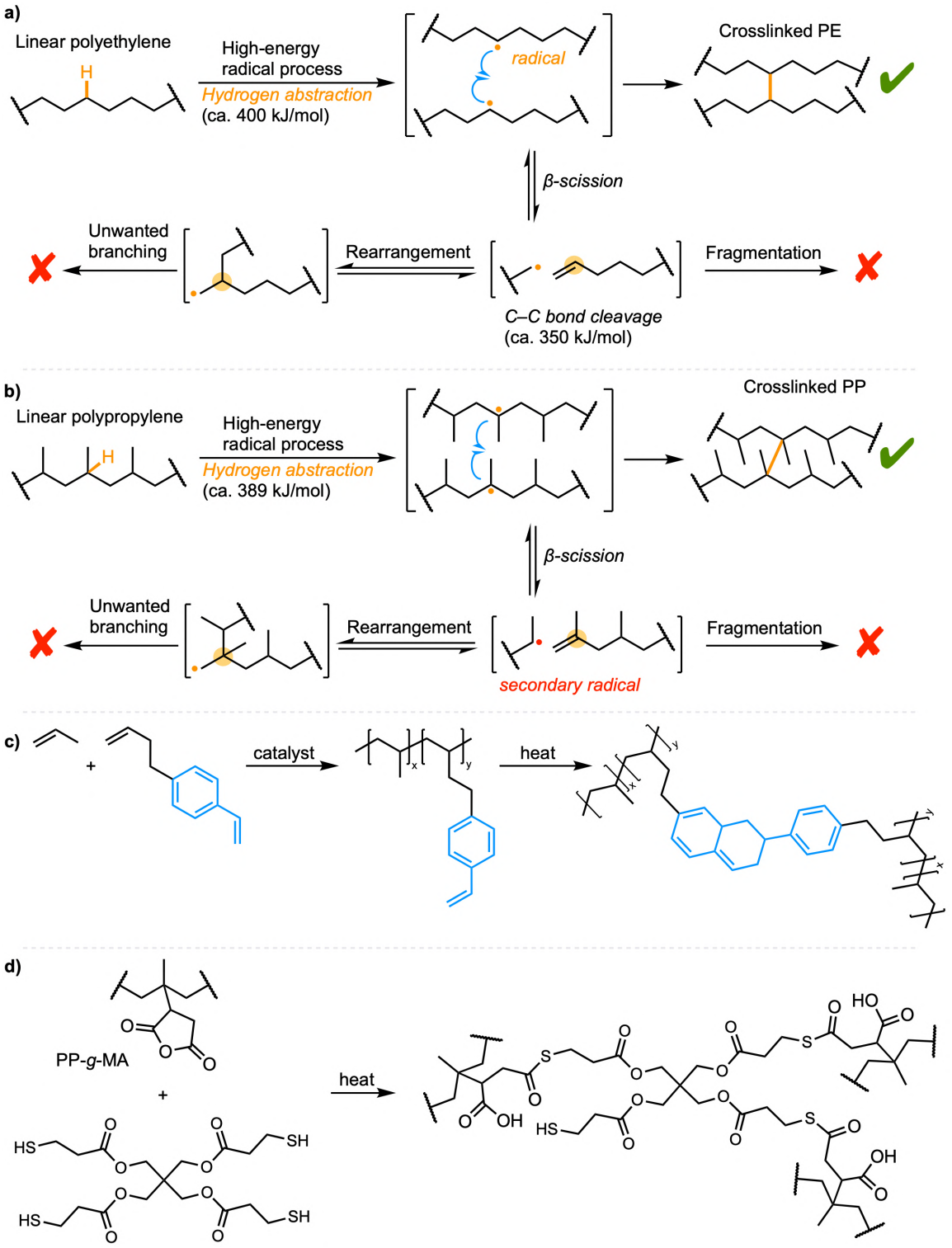

Figure 1.6 Challenges for high-energy crosslinking processes: a) polyethylene and b) polypropylene. Recent literatures on polypropylene crosslinking methods: c) copolymerization of propylene and *p*-(3-butenylstyrene), and the subsequent inter-chain

thermal crosslinking reaction and d) the reaction of PP-grafted-MA and four-functional thiol crosslinker. The stoichiometric ratio of 1.25 thiol bonds per one anhydride left with one free thiol group to facilitate bond exchange. Adapted from literature.[4,36,37]

Several studies have explored alternative crosslinking methods specifically tailored for polypropylene and other aliphatic polymers. One approach involves the utilization of copolymers, in which one of the monomer constituents incorporates a linkable fragment, such as styrene units. Lin et al. (Figure 1.6c) developed a linear poly(propylene-*co*-*p*-(3-butenylstyrene)) copolymer containing pendent styrene groups that can undergo interchain cycloaddition reactions, leading to the formation of a crosslinked network.[4] Furthermore, researchers have investigated the functionalization of polypropylene chains using maleic anhydride (MA) units. Saed et al. employed a four-functional thiol reagent as a crosslinker to react with the polypropylene-grafted-MA, resulting in crosslinked polyolefins with exchangeable thioester bonds (Figure 1.6d).[37] However, both grafting and chain scission occur simultaneously, competing with each other, and their outcomes are influenced by factors such as process temperature, the quantities of peroxide, and crosslinking agents.[38] Additionally, the copolymerization method is not suitable for existing polyolefin materials. Consequently, the development of a broadly applicable method for preparing crosslinked polypropylenes remains a technological challenge.

1.2. Uses of Diazirine Chemistry for Biological Applications

1.2.1 Reactive intermediates for photoaffinity labeling

Protein, along with nucleic acids, and carbohydrates comprise one of the three fundamental classes of biopolymers within organisms. The elucidation of interactions between small molecules and biomolecules provides a crucial link between biomolecular structure information and novel therapeutic strategies.[39] However, it remains challenging to interpret these fundamental biochemical interactions due to the complexity of native cellular environments.[40] In light of this challenge, photoaffinity labeling (PAL) has emerged as a powerful technology for investigating new small molecule–protein interactions within the complex proteome (Figure 1.7).[41] In this process, small molecules, tagged with a photoreactive group, bind within a protein pocket and then, upon ultraviolet (UV) irradiation, can reveal reactive intermediates (radicals, nitrenes, or carbenes) that can covalently label the target biomolecules.[40] After covalent modification the reacted protein is then usually purified by chromatography and characterized using mass spectrometry.[42] The concept of PAL was first introduced by Westheimer in 1962 using aliphatic diazo groups to generate reactive carbene intermediates,[43] and since then three major types of photoreactive groups have emerged: benzophenone, aryl azide, and diazirine (Figure 1.8).[44]

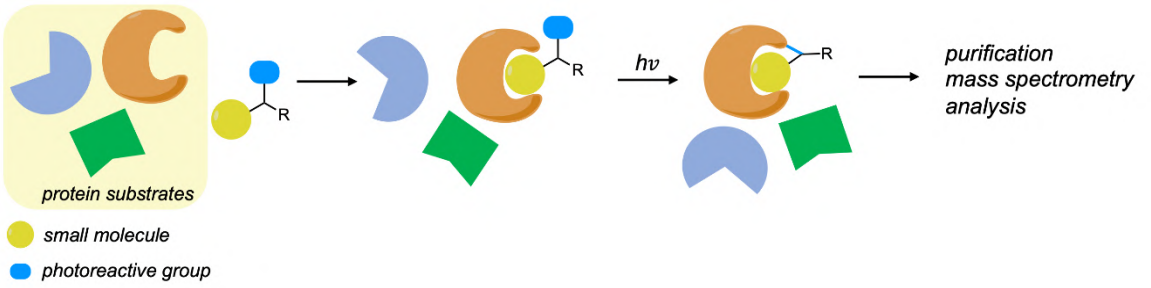

Figure 1.7 General schematic of a diazirine-based photoaffinity labeling experiment.

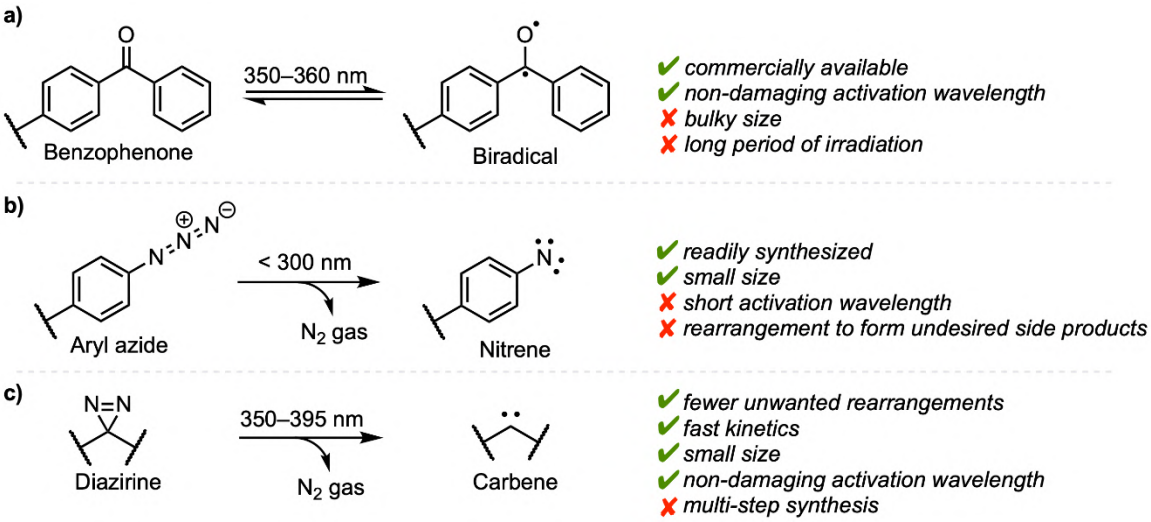

Figure 1.8 Comparison of commonly used photoreactive groups.

Benzophenones generate reactive biradicals upon UV irradiation, which can abstract hydrogen atoms from accessible C–H bonds, leading to pairs of carbon-centred radicals that can subsequently recombine, creating stable covalent C–C bonds (Figure 1.9a).[45] Despite their large steric size and requirement for long irradiation times (seconds to minutes), benzophenones have been employed extensively in PAL because of their commercial availability, less damaging activation wavelength (normally 350–360 nm) to the protein substrate, and relative stability under ambient light.[46] By comparison, aryl azides have smaller steric demands, but the shorter wavelengths (< 300 nm) at which they are excited can damage biomolecules.[47] Upon photoirradiation, the azide is activated to form a singlet nitrene accompanied by the release of nitrogen. However, the generated singlet nitrene not only undergoes a C–H insertion reaction for the labeling but also intramolecular ring expansion and subsequent rearrangement to a ketenimine, which only reacts with nucleophiles to generate azepine, thus decreasing the photolabeling efficiency (Figure 1.9b).[48] Moreover, the singlet nitrenes can generate triplet nitrene intermediates

via intersystem crossing (ISC), which can be quenched by O_2 or dimerized to form side products as minor pathways.[49]

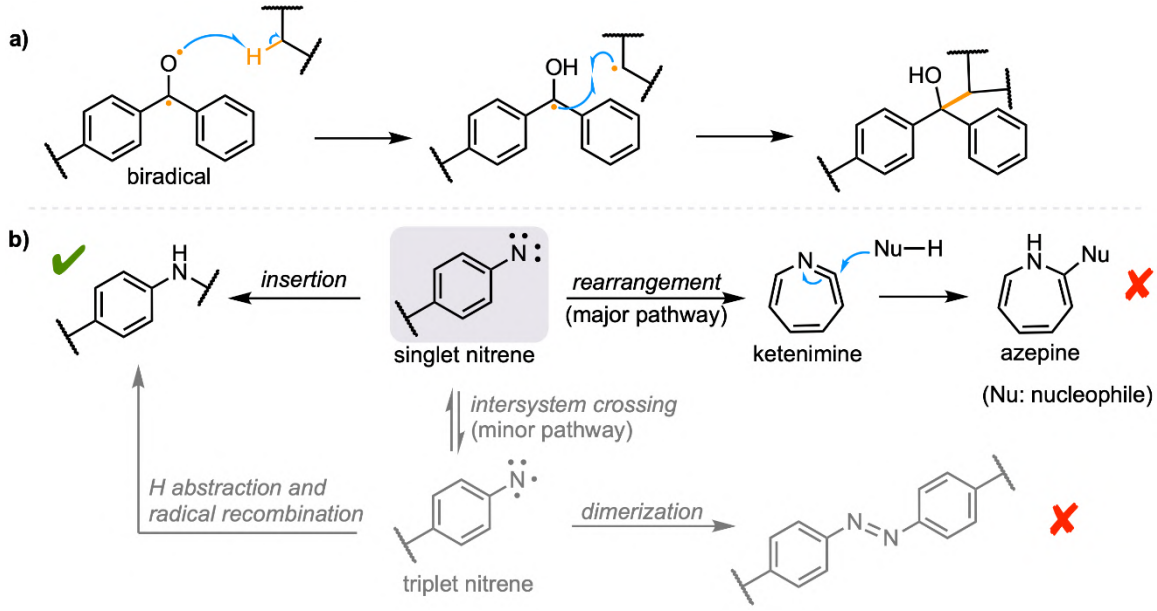

Figure 1.9 The photochemical reaction pathways of a) benzophenone and b) aryl azide.

Diazirines are three-membered rings containing two nitrogen atoms bound by a double bond. Upon excitation with heat or near-UV light (350–395 nm), diazirines release N_2 and generate highly reactive carbenes, either directly or via initial isomerization to the linear diazo species.[50] Carbenes can undergo a range of reactions depending on their electronic spin state, either spin-paired singlet or unpaired triplet.[51] Crucially, singlet carbenes display polar reactivity, rapidly forming covalent bonds with any nearby available substrates through C–H, N–H, and O–H insertions.[52] Intersystem crossing can generate triplet carbenes, which can be quenched by O_2 or covalent crosslinking by a two-step mechanism: hydrogen abstraction and radical recombination (Figure 1.10).[40] Among the different photoreactive groups, diazirines are generally preferred due to their few unwanted rearrangements, short solution half-lives (< 1 ns), small steric demands, and longer excitation wavelengths.[52] In addition to their superior photo-physical properties, diazirines (below their thermal activation temperatures) are stable to acids and bases, and are unreactive towards common nucleophiles and electrophiles.[51]

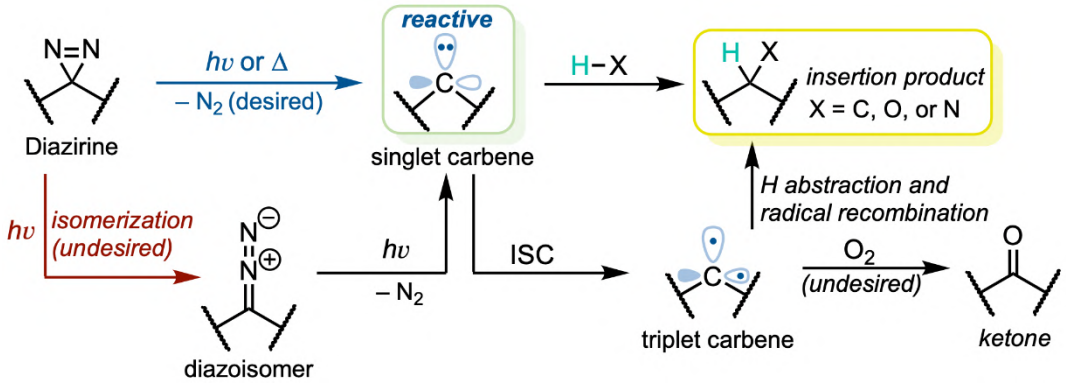

Figure 1.10 Generation of reactive intermediates from diazirines activation.

1.2.2 Development of diazirines

Diazirine motifs can be categorized in two types: aliphatic and aromatic, both of which have been used extensively in chemical biology over the last 40 years as photoreactive groups to create covalent links between small molecules and their protein binding partners. The first chemically synthesized diazirines were dialkyl versions made in the 1960s by Paulsen and Schmitz.[53,54] However, aliphatic diazirines have limited applications due to intramolecular rearrangements (1,2-hydride migration, Figure 1.11a).[55] In 1973, Smith and Knowles showed that 3*H*-3-phenyl diazirines (Figure 1.11b) can be applied as potential photoreactive groups for PAL, but photoactivation of this aryl diazirine produced primarily undesired diazo species, from which relatively slow extrusion of N_2 can lead to nonspecific labeling as a result of dispersion from the active site.[56,57] In an attempt to address these limitations, in the early 1980s, Brunner and co-workers introduced the 3-trifluoromethyl-3-phenyl diazirine (Figure 1.11c) as a superior alternative. The strong inductive electron-withdrawing effect of the trifluoromethyl group reduced the proportion and non-specific labeling reactivity of the formed diazo species.[57,58] Although trifluoromethyl aryl diazirines have been extensively applied in biology, their utility in materials science has been much less well explored.

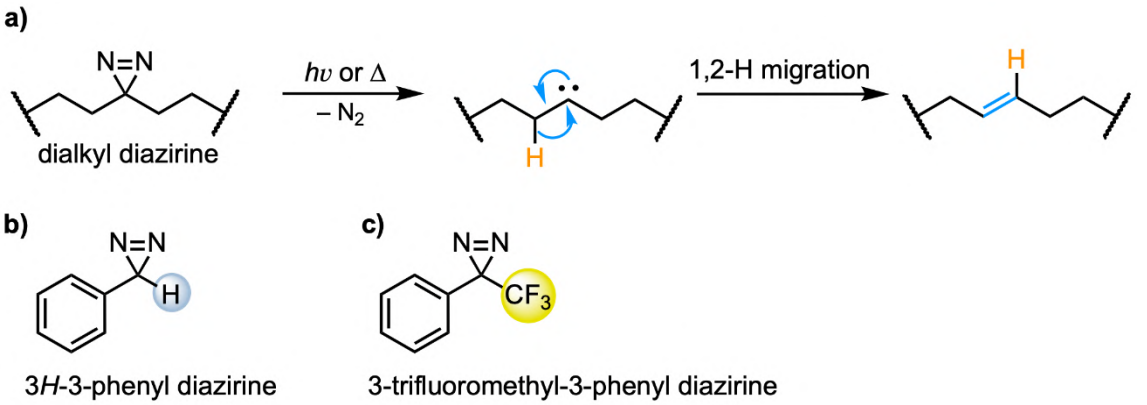

Figure 1.11 a) Intramolecular rearrangement of aliphatic diazirine. b) and c) General structures of aryl diazirines.

1.3. Emerging Applications of Trifluoromethyl Aryl Diazirines in Materials Science

1.3.1 Developments in diazirine-based polymer crosslinkers

The highly reactive and non-specific nature of carbenes has enabled a multitude of macromolecules to be functionalized without the need for specialized substrates or additives. The use of diazirines as stable carbene precursors has increased significantly over the past years for biological and material applications. Among different types of diazirine structures, trifluoromethyl aryl diazirines have found promising applications as polymer crosslinkers for a variety of polymer substrates, such as polyethylene glycol (PEG)[59,60] and low-functionality polyolefins.[36] In 2008, Hayes et al. designed and synthesized a *bis*-diazirine crosslinker **1.1** (Figure 1.12a) that enables the preparation of crosslinked PEG gels via photoactivation of mixtures of **1.1** and PEG.[59]

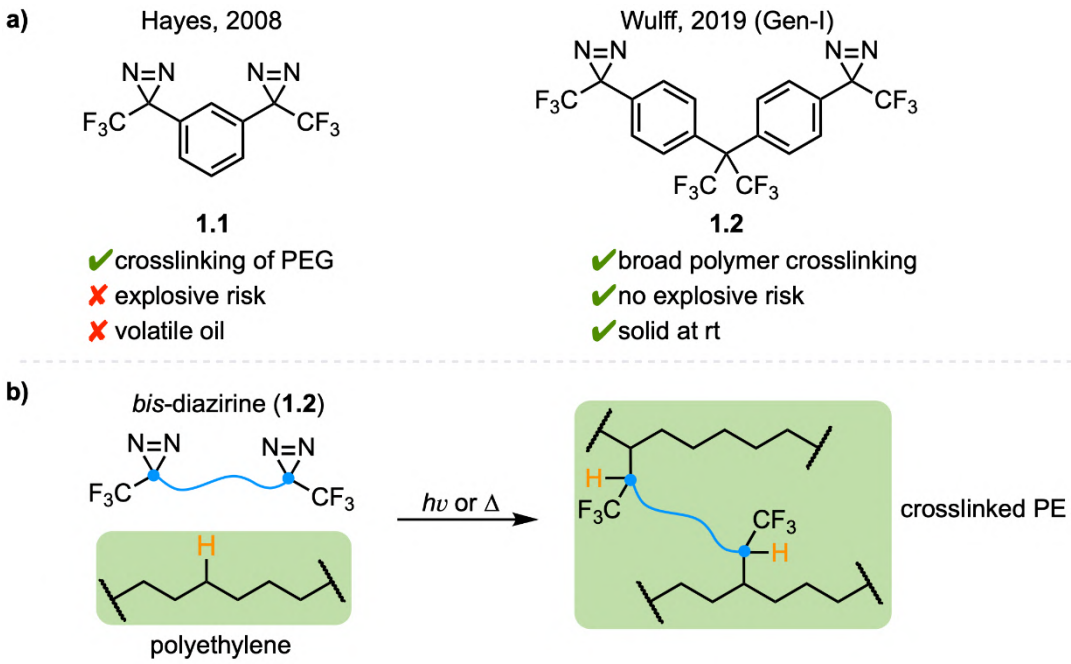

Figure 1.12 a) Structures of *bis*-diazirine crosslinkers **1.1** and **1.2**. b) Crosslinking of low-functionality polyethylene via double C–H insertions of *bis*-diazirines.

In 2019, our group used the thermal and photochemical activation of trifluoromethyl aryl *bis*-diazirines to perform C−H insertion on unfunctionalized saturated hydrocarbon polymers like polyethylene and polypropylene (Figure 1.12b). We rationally designed and synthesized improved *bis*-diazirine crosslinker **1.2**, which finely balances explosion risk and reactivity (Figure 1.12a). A variety of polymer substrates (paraffin, polycarprolactone, polyisoprene, silicone, PE, PP) were successfully crosslinked, resulting in increased polymer molecular weights and glass transition temperatures, and decreased solubility.[36] Subsequently, in collaboration with Golovin group, we explored the use of *bis*-diazirine molecule **1.2** to crosslink nanoscale polydimethylsiloxane (PDMS) brushes on surfaces through a chemically non-destructive C–H insertion.[27] This strategy provides a new pathway for the design of durable inert nanoscale coatings that maintain their attractive surface properties after mechanical wear.

Crosslinker **1.2** is also an effective fabric strengthen. In particular, 1 wt% crosslinker of **1.2** doubled the tear strength of woven ultra-high-molecular weight polyethylene (UHMWPE) fabric, and significantly increased the resistance to perforation (antiballistic performance) of composite soft body armour constructed using treated UHMWPE.[18] Building upon these results, we later designed a diazirine–grafted

polyamine (polyethylenimine, PEI) conjugate (Figure 1.13) that can be used as a topically applied primer for UHMWPE fabric.[24] Activation of the diazirine groups can lead to strong covalent bonds between the fabrics and the polyamine coating, which in turn can participate directly in nucleophilic reactions with epoxy resin to achieve significant adhesive forces and improve the mechanical properties of manufactured UHMWPE-epoxy composite materials.

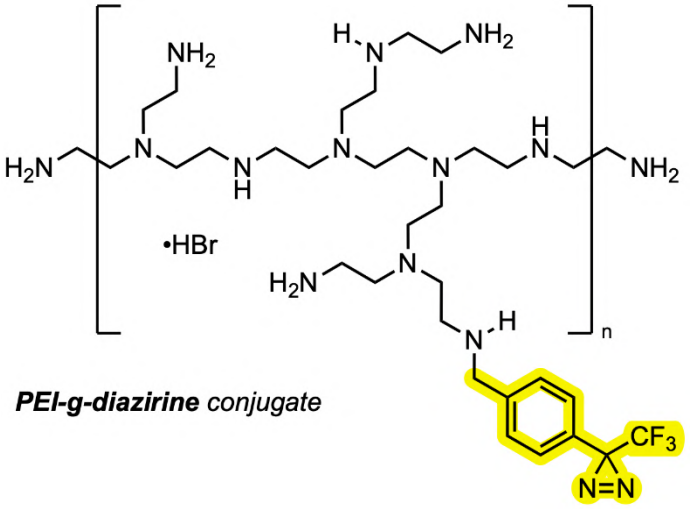

Figure 1.13 Structure of conjugate PEI-*grafted*-diazirine.

1.3.2 Molecular adhesives

As an added benefit, our group's first-generation trifluoromethyl aryl *bis*-diazirine crosslinker **1.2** can be employed as a broadly useful covalent adhesive, especially to low surface energy material such as high-density PE (HDPE) where commercial adhesives (e.g. SuperGlue) show poor bonding. Motivated by a desire to develop flexible crosslinkers that show some degree of malleability in the adhesive layer as traditional polymer-based adhesives, we designed and synthesized two flexible, highly fluorinated *bis*-diazirines **1.3** and **1.4** (Figure 1.14).[61] Both molecules were shown to be effective in lap-shear adhesion experiments with a wide variety of hard plastics (HDPE, PP, UHMWPE, poly(methyl methacrylate), polycarbonate). Crosslinker **1.4** generally outperformed **1.3** in adhesion measurements, presumably because the increased length of its perfluorinated alkyl tether (providing greater molecular flexibility) is correlated with improved mechanical compliance in the adhesive layer.

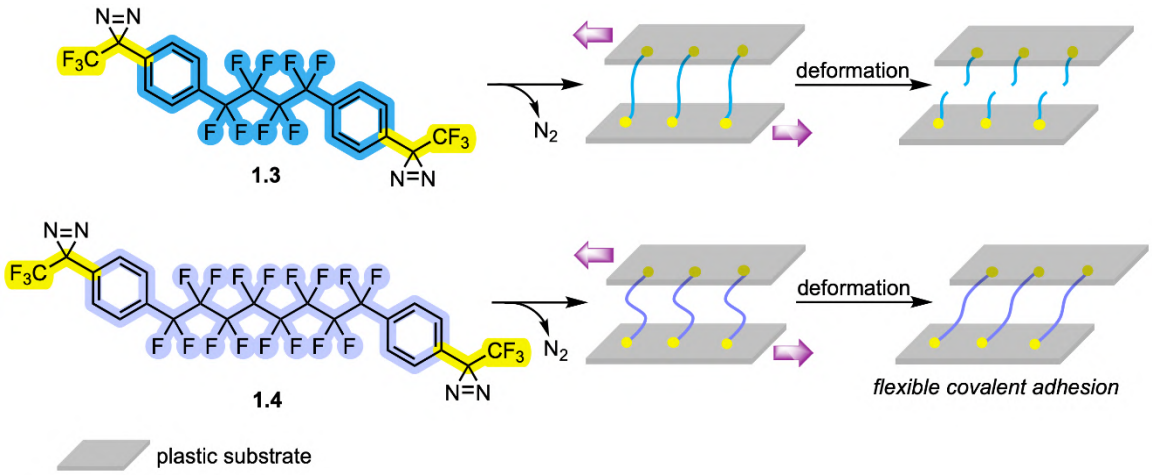

Figure 1.14 Structures of second generation of *bis*-diazirine crosslinkers.

Meanwhile, Steele and co-workers developed tissue adhesives by incorporating trifluoromethyl aryl diazirines into polyamidoamine (PAMAM) dendrimer[62,63] or food-grade polycaprolactone (PCL) substrates (Figure 1.15).[64,65] Upon photoactivation, the grafted diazirine end-groups can crosslink hydrated tissue surfaces rapidly. After crosslinking, the leachable components of hydrolyzed PCL tissue adhesives are evaluated for *in vitro* biocompatibility assessment and reveal little to no risk of genotoxicity or skin sensitization effects.[66]

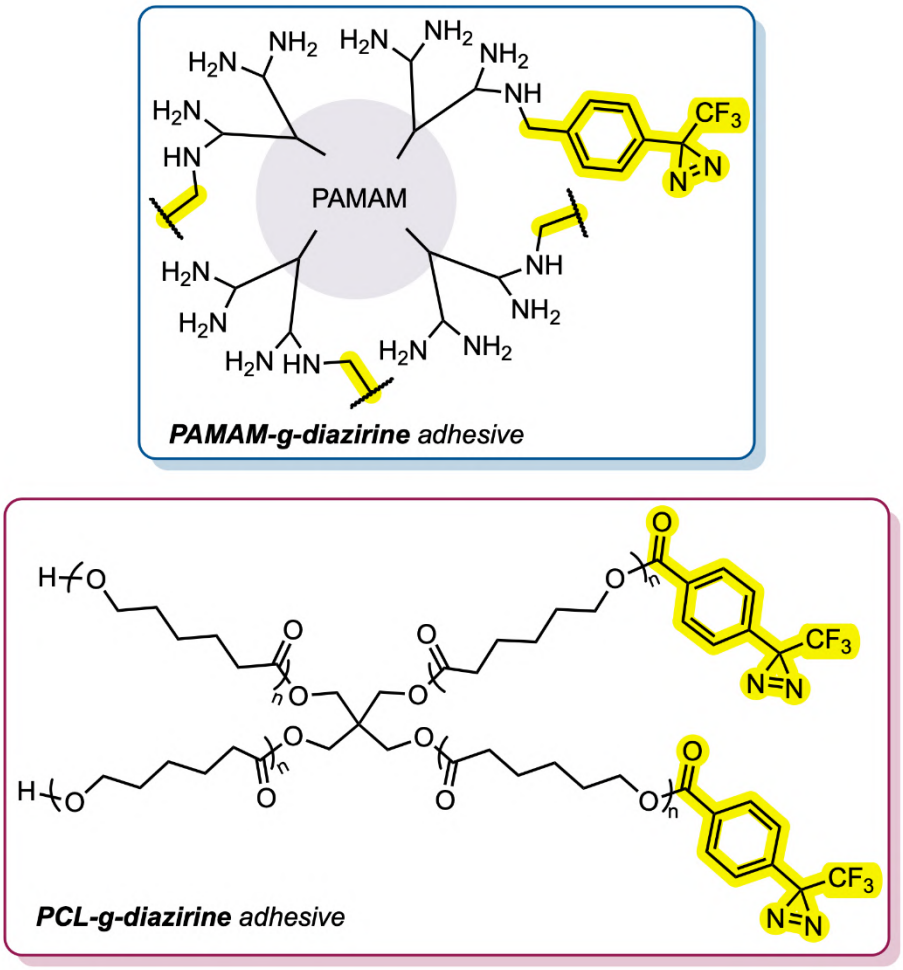

Figure 1.15 General structures of Steele group adhesives, which are synthesized by grafting PAMAM-NH_2 and PCL-OH endgroups with benzyl bromide or benzoic acid trifluoromethyl aryl diazirine.

1.3.3 Recent applications in photopatterning

In early 2020, Burgoon and co-workers synthesized a *bis*-(trifluoromethyl aryl diazirine) derivative **1.5** (depicted in Figure 1.16), which was utilized for photopatterning unreactive, aliphatic cycloolefin polymer films.[67] Later in the same year, the Anzenbacher group developed two *bis*-diazirine crosslinkers **1.6** and **1.7** (Figure 1.16) that enable the crosslinking of organic electronic materials in organic light-emitting diodes (OLEDs).[68] The process of creating solution deposited OLEDs poses numerous challenges, primarily due to interlayer mixing and surface erosion during the layer-by-layer deposition process.[69] These diazirine-based crosslinkers can react with blue-

emitting polydioctylfluorene to transform soluble organic materials into highly crosslinked insoluble networks. The resulting crosslinked polymer layers exhibit no interlayer mixing when overlaid with red-emitting poly(alkylthiophene), and instead, display a clear and distinct boundary. This demonstrates that diazirine-based crosslinking effectively prevents interfacial mixing between two material layers, thereby improving structural stability, device lifetime, and overall performance. Furthermore, diazirine groups allow easy-to-achieve photo-crosslinking without the presence of any catalyst or initiator while liberating molecular nitrogen as the only side product for fabrication of solution-processed OLEDs.[70]

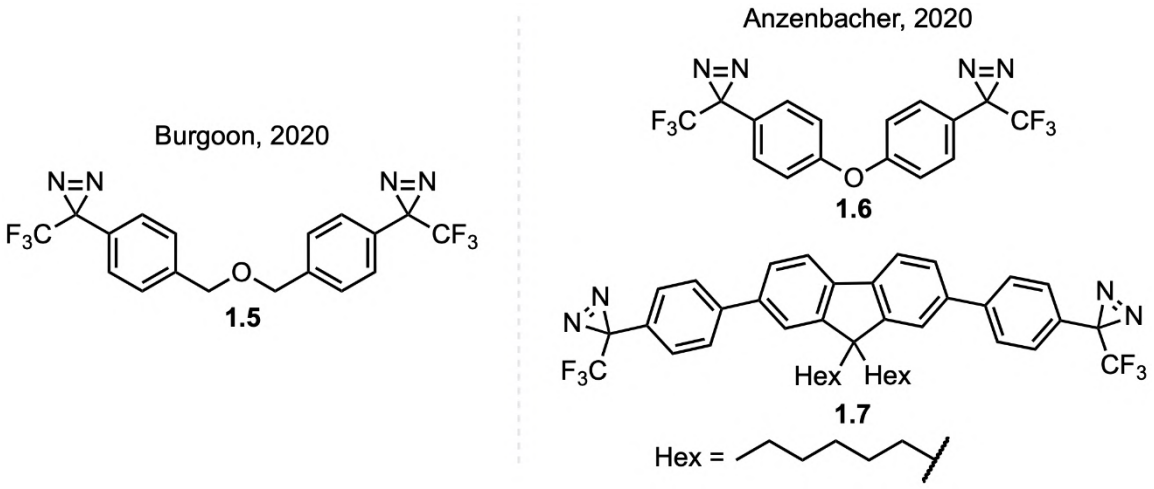

Figure 1.16 *bis*-Diazirine derivatives **1.5**–**1.7** from Burgoon and Anzenbacher groups.

In 2021, the Bao group introduced *bis*-diazirine crosslinker **1.8** (Figure 1.17) where they selected a branched alkyl chain as the linker to reduce crosslinker crystallization and to improve miscibility with semiconducting polymers for efficient photo-crosslinking and greater film deformability.[71] The carbene-based photo-crosslinking enabled the layer-by-layer deposition of stretchable polymer semiconductors during photolithography. Additionally, Zhang et al. presented a diazirine-based four-armed crosslinker **1.9** with a tetrahedral geometry, allowing for low loadings to achieve efficient photopatterning of polymeric semiconductors.[72]

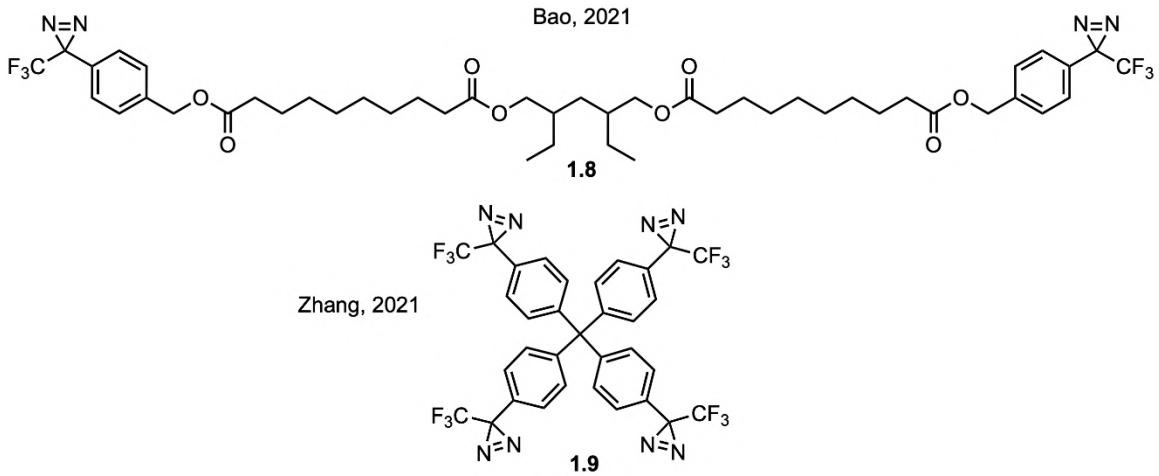

Figure 1.17 Structures of diazirine-based crosslinkers **1.8** and **1.9** from Bao and Zhang groups.

The introduction of this thesis has provided an overview of common commodity polymers crosslinking methods and challenges in crosslinking low-functionality plastics. This chapter has also covered the notable applications of trifluoromethyl aryl diazirine systems in materials science—in particular their use in polymer crosslinking. While diazirines are well recognized as powerful tools for use in photoaffinity labeling experiments, the broad scope of application found within this class of highly reactive systems is clearly a useful property to be investigated in materials science. This research work represents a comprehensive study on design, synthesis, and optimization strategies of new diazirine containing molecules, and their applications towards upcycling and functionalization of low-functionality commodity polymers. The aim of this thesis is to expand the versatile and unexplored uses of diazirine containing molecules into materials science, with the ambition of broadening the scope of applications of such old tools, known for years in chemical biology, and opening endless doors towards new unexplored directions.

1.4. Thesis Summary

The work presented in this thesis is a compilation of interrelated research projects focusing on the investigation and applications of trifluoromethyl aryl diazirine chemistry. This thesis comprises four results chapters in addition to a final summary and outlook

chapter, highlighting the impact of this work and possible future research directions. The chapters are organised as follows:

Chapter 2 explores structure–function relationships in aryl diazirines by using a combination of experimental and computational methods. We show that aryl diazirine activation temperature can be tuned through changing the substituent groups on the phenyl ring. Additionally, electron-rich diazirines have greatly enhanced C–H insertion performance.

Chapter 3 focuses on applying the findings from Chapter 2 to design a new generation of *bis*-diazirine crosslinker, where we obtained >10-fold improvement in efficacy, relative to earlier first- and second-generation crosslinkers (**1.2**–**1.4**).

Chapter 4 describes a new strategy for recycling and upcycling of low-functionality plastics, by installing a cleavable site into our electronically optimized *bis*-diazirine scaffold. For the first time in this Chapter, we were able to process crosslinked bulk materials (and non-crosslinked controls) into macro-scale objects suitable for dynamic mechanical thermal analysis (DMTA) and tensile tests. As expected, crosslinked materials displayed clear rubbery plateaus indicative of thermoset behaviour. Hydrolysis of the cleavable linker group restored thermoplastic performance to the materials, while also facilitating further installation of functional groups.

Chapter 5 describes the use of electronically optimized *mono*-diazirines covalently linked to electrophilic groups, for protein immobilization on PDMS substrates.

Chapter 2: Structure–Function Relationships in Aryl Diazirines Reveal Optimal Design Features to Maximize C–H Insertion

This chapter has been adapted with permission from a previously published paper.

Stefania F. Musolino[†], Zhipeng Pei[†], Liting Bi, Gino A. DiLabio, and Jeremy E. Wulff, *Chem. Sci.*, **2021**, *12*, 12138–12148.

[†] Equal contribution

Contributions:

Synthetic work was performed by Dr. Stefania F. Musolino with assistance from Liting Bi. Dr. Stefania F. Musolino also undertook the cyclohexane insertion experiments. DSC experiments were performed by Liting Bi. Computational work was performed by Zhipeng Pei working under the supervision of Prof. Gino DiLabio (The University of British Columbia, Okanagan Campus).

2.1. Abstract

Diazirine reagents allow for the ready generation of carbenes upon photochemical, thermal, or electrical stimulation. Because carbenes formed in this way can undergo rapid insertion into any nearby C–H, O–H or N–H bond, molecules that encode diazirine functions have emerged as privileged tools in applications ranging from biological target identification and proteomics through to polymer crosslinking and adhesion. Here we use a combination of experimental and computational methods to complete the first comprehensive survey of diazirine structure–function relationships, with a particular focus on thermal activation methods. We reveal a striking ability to vary the activation energy and activation temperature of aryl diazirines through the rational manipulation of electronic properties. Of even greater importance, we show that electron-rich aryl diazirines have vastly superior efficacy toward C–H insertion, under both thermal and photochemical activation conditions. We expect these results to lead to significant improvements in the design of diazirine-based chemical probes and polymer crosslinkers.

2.2. Introduction

The insertion of high-energy carbene or nitrene species into unactivated C–H, O–H and N–H bonds constitutes a powerful strategy for forming new bonds in complex biological, chemical, or mechanical mixtures.[73,74] The ability to rapidly and controllably generate carbenes from stable and readily accessed precursor molecules allows one to label (or 'tag') binding partners,[51] isolate reaction products,[75] or crosslink polymer materials.[36,67,68]

In recent years, diazirine motifs have enjoyed enormous popularity as carbene precursors, for applications ranging from biological target identification through to adhesion of commodity plastics (Figure 2.1). Part of this popularity can be attributed to their small size and ready synthetic access.[58,76–79] Of course, for any reactive reporter group the most important criteria are that the reporter be stable under any required synthesis, handling, and experimental conditions, yet be easy to activate (ideally with good control over spatial localization) when needed. Diazirines excel when measured against these criteria as well; most diazirines are stable to commonly used synthetic reaction conditions (including strong Brønsted[36] and Lewis[80,81] acids), and many

diazirine-containing molecules are thermally stable. When desired, diazirines can be readily activated using light (*ca.* 350–365 nm),[58] heat (typically 110–130 °C),[36,61] resonance energy transfer[82] or electrical potential,[62,83,84] resulting in the expulsion of nitrogen gas and the formation of the corresponding carbene. The long wavelength of light required for photochemical activation (outside the window where biological and polymer materials absorb) and the low temperature required for thermal activation (below the melting temperature of many commodity polymers) are critical factors that have contributed to the broad uptake of diazirines by research groups around the world.

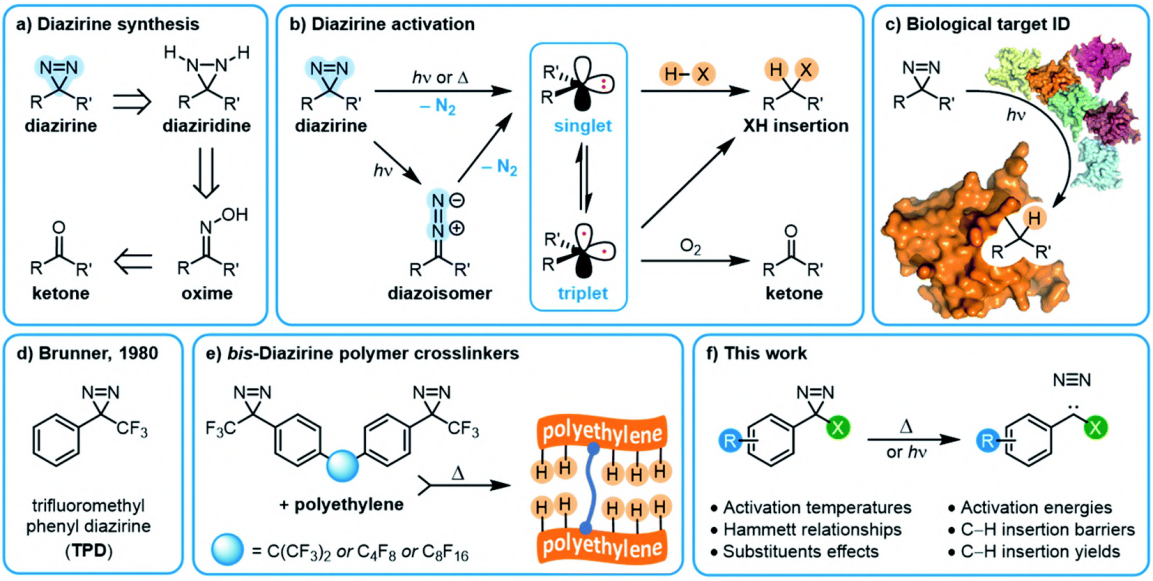

Figure 2.1 Overview of diazirine synthesis, activation, and applications. a) Synthetic strategies for producing aryl diazirines. b) Diazirine activation and carbene formation. c) The use of diazirines for biological target identification. d) Trifluoromethyl phenyl diazirine (TPD). e) *bis*-Diazirine polymer crosslinkers based upon the TPD monomeric structure. f) This work: structure–function relationships within trifluoromethyl aryl diazirines. Adapted with permission from literature.[50]

The substituents on either side of the CN_2 core are known to influence the properties of both the parent diazirine molecule and the product carbene. For example, dialkyl diazirines generally give rise to ground-state singlet carbenes, due to hyperconjugative donation of filled C–H orbitals into the unoccupied p orbital of the singlet carbene group.[85,86] Carbenes generated from phenyl diazirines (or from the isomeric linear diazo compound) can exist in either singlet or triplet forms; the triplet is

generally found to be the ground state for these species,[87] but in many cases the singlet carbene is believed to be produced initially,[88,89] after which intersystem crossing (ISC) facilitates relaxation to the observed triplet (Figure 2.1b).[87] The energy gap between the singlet and triplet states is crucially important, since the two types of carbenes undergo different types of reactions with X–H bonds. Triplet reactivity is dominated by stepwise hydrogen abstraction/radical recombination pathways that can lead to undesirable side reactions, while singlet X–H insertion is believed to proceed by a concerted—but two-phase—pathway wherein the empty carbene p orbital first receives electron donation from the X–H σ bonding orbital, and then the lone pair on the carbene back-donates into the X–H σ* orbital.[86] Further complicating matters, triplet carbenes are known to undergo rapid reactions with adventitious O_2 (ultimately leading to the production of ketone byproducts) while singlet carbenes appear to be immune to this undesirable reaction pathway.[90]

As is the case with nitrene species, diazirines and carbenes can undergo unwanted rearrangement reactions; Brunner showed in 1980 that the installation of an α-trifluoromethyl group reduced the likelihood of such rearrangements, leading to improved overall stability and more controllable reactivity.[58]

Since Brunner's seminal report, the trifluoromethyl phenyl diazirine group (TPD; Figure 2.1d) has become the most widely employed carbene precursor in the chemical literature. Trifluoromethyl aryl diazirines are now used in a host of biological target identification experiments (Figure 2.1c)[51,91–95] where they are found to outperform alternative labeling groups like nitrenes or benzophenones,[96,97] and the TPD motif has been genetically encoded into protein structures using expanded genome techniques.[98] TPD has also been used to map the localized protein environment on T cells using an innovative μ-mapping technique facilitated by Dexter energy transfer,[82] and trifluoromethyl aryl diazirines have been designed into bio-adhesives to expedite wound closure.[62,83,84] In polymer science, trifluoromethyl aryl diazirines have been conjugated to fluorophores and photosensitizers in order to imbue nylon[99] and spunbond polypropylene[100] materials with new functionality. Silicon and silicon nitride surfaces can be similarly functionalized.[101] TPD groups have also been used on surfaces to capture small molecule reaction products[75] and drug molecules,[102] and have been incorporated

into polymer crosslinkers that can be used to strengthen woven polyethylene fabric[36] or provide adhesion between polypropylene or polyethylene surfaces (Figure 2.1e).[61] These latter applications using commodity aliphatic polymers provide a particularly stringent test of a diazirine's ability to support C–H insertion, since (to a first approximation, at least) such polymers only contain C–C and C–H bonds, and therefore lack anything that would be traditionally viewed as a reactive functional group.

Given the extensive utility of TPD groups, it is surprising that linear free energy relationships in trifluoromethyl aryl diazirines have received very little attention. (By contrast, Hammett relationships in α-chloro diazirines have been extensively studied, but these species are known to participate in a variety of reactions that are not available to the much more important α-trifluoromethyl congeners.[103–111]) As a result, incorporation of a trifluoromethyl aryl diazirine group into a molecule of interest (whether for biological or materials science applications) has typically been done in an ad hoc manner, without any consideration of how the electronics of the aryl diazirine group will influence the generation and reactivity of the resulting carbene. While a variety of electron-rich, electron-poor, and electron-neutral trifluoromethyl aryl diazirines have been described in the literature, only in very rare cases has the influence of electron-donating or electron-withdrawing groups on reaction outcome (especially under thermal activation conditions) been discussed, and the conclusions from these reports are somewhat contradictory.

In 2011, Song and Sheridan reported a study of *meta*-methoxy *vs. para*-methoxyphenyl trifluoromethyl diazirine, and showed that the *para*-methoxy substituent was capable of supporting a singlet carbene ground state (at 7 K in a frozen nitrogen matrix) due to resonance stabilization.[90] Two years later, Raimer and Lindel studied this same *para*-methoxy trifluoromethyl diazirine molecule, and found that activation in the presence of phenols (including tyrosine derivatives) led to production of the desired singlet carbene, which could then undergo formal O–H and C–H insertions with the substrate.[112] Interestingly, however, these reactions were shown in all cases to be the result of initial protonation of the singlet carbene to generate a benzylic cation, which could then either be quenched by reaction with the phenol (or phenoxide anion) or else undergo Friedel–Crafts reaction with the electron-rich aromatic ring.[112] Various lines of evidence were used to rule out the existence of any direct C–H insertion reactions. While

the Sheridan and Lindel papers provide important precedent in favour of the hypothesis that electron-rich trifluoromethyl aryl diazirines might provide an improved reactivity profile relative to electron-poor or electron-neutral analogues, neither report demonstrated direct C–H insertion reactions with aliphatic substrates. As a result, it remains an open question whether electron-rich aryl diazirines would be preferred or not, in the applications described above.

To further complicate matters, a recent report by Kumar, Tipton and Manetsch provided compelling evidence that electron-poor diazirines are superior, due to improved stability under ambient light, and that this lack of electron density does not impair the molecules' ability to undergo C–H insertion.[113] Meanwhile, Kanaoka and co-workers have advocated for the use of diazirines bearing both an electron-donating alkoxy group and an electron-withdrawing nitro substituent, due to improved optical properties.[114–116] While the Kanaoka group showed the performance of their molecules in reacting with cyclohexane (an important benchmarking experiment for diazirine reactivity) they did not compare the efficacy of their structures to that of the parent TPD molecule.

These sparse reports leave the experimentalist who might want to employ a diazirine for a particular application in a quandary. Should an electron-rich or electron-poor trifluoromethyl aryl diazirine be used if one wants to maximize the potential for C–H insertion under standard laboratory conditions? If an electron-rich system is preferred in order to stabilize a singlet carbene intermediate, how electron rich does it need to be? Given that the optimized electronic properties will likely increase the synthetic challenge in preparing the molecule, is the improved performance sufficient to justify the increased synthetic effort and/or increased cost of reagents?

The situation becomes even more complex when activation temperature is taken into account. The few structure–function studies on trifluoromethyl aryl diazirines alluded to above all focused on photochemical activation, since this is the dominant excitation method used for biological studies. For materials science work, however, thermal activation is generally preferred;[36,61] while commodity polymers like polyethylene and polypropylene do not absorb light in the window used for photochemical diazirine activation, they do very efficiently *scatter* light and are therefore visibly opaque or white solids—making the use of photochemical activation techniques a

substantial challenge for real-world samples. An understanding of how activation temperature changes with diazirine electronics is therefore critically important to the design of new polymer crosslinkers and adhesives.[117] Moreover, the thermal activation temperature dictates the explosivity (or lack thereof) for the diazirine molecule being used:[36,118] an understanding of how activation temperature can be tuned is therefore necessary for designing safe and effective diazirine-based reagents for all manner of applications.

This chapter (Figure 2.1f) employs a combination of experimental and computational methods to conduct an extensive structure–function study of the properties and reactivity of aryl diazirines, with a particular emphasis on those bearing an α-trifluoromethyl substituent. The experimental work focuses on measuring activation temperatures by differential scanning calorimetry (DSC) and explicitly comparing the ability of electron-rich, electron-neutral, and electron-poor molecules to engage in C–H insertion reactions under both thermal and photochemical activation conditions. The results of this study have the potential to inform the design of molecular probes, small-molecule capture agents, and polymer crosslinkers with improved efficacy.

2.3. Results and Discussion

2.3.1 Tunability of optical absorbance characteristics

We synthesized (or, in a few cases, purchased) several representative trifluoromethyl aryl diazirines, incorporating electron-rich, electron-neutral, and electron-withdrawing groups on the aromatic ring (see Table 2.1 for substituents).

Table 2.1 Effect of aryl substituent electronics on activation temperature and on activation free energy

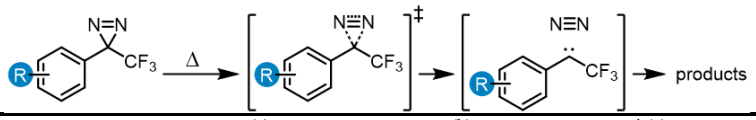

Entry	R	T_{onset} [a] (°C)	T_{peak} [b] (°C)	$\Delta G^{\ddagger}$ [c] (kJ mol^{-1})
1	4-OCH_3	88.0 ±0.5	113.0 ±0.7	141.6
2	4-OPh	90.2 ±0.2	116.6 ±0.1	140.3
3	4-*t*-Bu	100.0 ±0.1	125.5 ±1.5	147.0
4	H	103.3 ±0.5	127.4 ±0.7	149.8
5	4-Br	105.6 ±0.5	132.4 ±0.6	147.8
6	4-CH_2OH	106.8 ±0.2	132.2 ±0.3	149.1
7	4-CH_2Br	102.0 ±0.2	133.0 ±0.2	148.1
8	3-OCH_3	108.7 ±0.4	135.5 ±0.1	152.5
9	3-OH	110.5 ±0.2	135.8 ±0.1	152.1
10	3,5-OCH_3	112.5 ±0.1	137.9 ±0.1	149.3
11	4-CF_3	115.7 ±0.4	138.9 ±0.6	150.7
12	4-CHO	113.2 ±0.5	139.1 ±0.3	153.2
13	4-NO_2	117.6 ±1.0	143.9 ±0.8	154.3

(a) Experimentally determined by extrapolation of the tangent of the upward slope observed in the DSC experiment, to the fitted baseline of the plot. Data are presented as the average of three independent measurements ± standard deviation. (b) Experimentally determined from the peak maxima in the DSC experiment. Data are presented as the average of three independent measurements ± standard deviation. (c) Calculated free energy (298.15 K, 1 atm) of activation (M06-2X-D3/6-31+G(d,p)//M06-2X-D3/6-31G(d,p)) associated with conversion of the diazirine into the corresponding carbene in vacuum.

Characterization of archetypal electron-rich (4-OMe-C_6H_4, 4-OPh-C_6H_4), electron-neutral (C_6H_5, 4-*t*-Bu-C_6H_4), and electron-poor (3-OMe-C_6H_4, 3,5-$(OMe)_2$-C_6H_3, 4-NO_2-C_6H_4) trifluoromethyl aryl diazirines by UV/Vis spectroscopy revealed interesting trends. As shown in Figure 2.2, electron-rich and highly electron-poor diazirines both showed strong absorbances in the diazirine activation window of *ca.* 320–410 nm. However, electron-neutral and moderately electron-poor trifluoromethyl aryl diazirines had attenuated absorbances in this range. It would seem, therefore, that strongly electron-rich or electron-poor diazirines might be preferred for photochemical activation, simply

on the basis of their improved extinction coefficients. This is an important observation, given that the vast majority of biological target identification studies in which diazirines have been used have featured electron-neutral substrates.

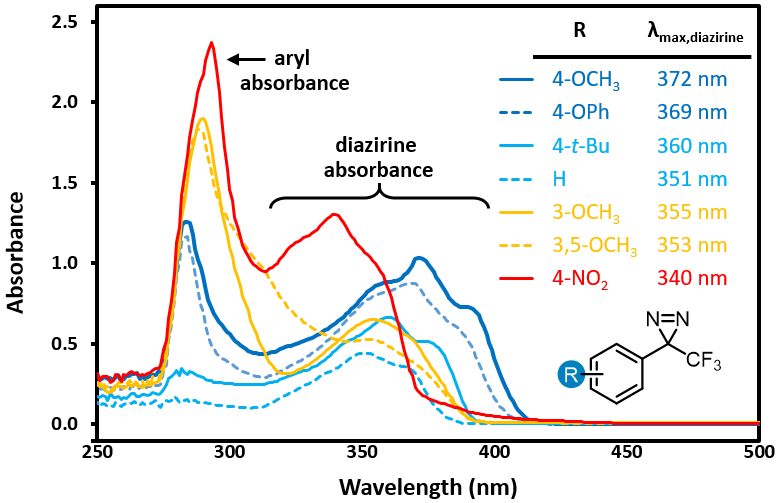

Figure 2.2 Variation in UV/Vis absorption spectra for representative trifluoromethyl aryl diazirines. All data were acquired using 5 mM samples in *n*-hexane. Refer to Figure S2.1 for comparative spectra obtained in methanol. Adapted with permission from literature.[50]

Of equal importance, we observed a >30 nm shift to higher wavelengths when moving from electron-poor to electron-rich trifluoromethyl aryl diazirines. The ability to shift the diazirine activation bands to longer wavelength is useful both in terms of evading background absorbance and allowing the use of cheaper and more readily purchased light sources.

2.3.2 Tunability of activation temperature and activation free energy

Each of the trifluoromethyl aryl diazirine molecules was analyzed by DSC (refer to the section 2.5 for representative traces) to measure the onset temperature for diazirine activation (T_{onset})[119] and the peak temperature (T_{peak}; the temperature at which the diazirine activation exotherm reaches maximal heat flow). At the same time, we computationally determined the activation free energy ($\Delta G^{\ddagger}$) for the diazirine activation reaction.

The data (Table 2.1) revealed a difference of *ca.* 30 °C in thermal activation temperatures, as we moved from electron-rich trifluoromethyl aryl diazirines (e.g. R = 4-OCH_3; T_{onset} = 88 °C; T_{peak} = 113 °C) to electron-poor analogues (e.g. R = 4-NO_2; T_{onset} =

118 °C; T_{peak} = 144 °C). This substantial difference in activation temperature corresponded to an equally significant difference in calculated activation free energy ($\Delta\Delta G^{\ddagger}$ > 12 kJ mol^{-1}). Indeed, a strong positive correlation between all of the experimentally determined T_{onset} and T_{peak} values and the corresponding calculated activation free energies was observed (Figure 2.3). This agreement between theory and experiment, confirming that T_{onset} is a reflection of the reaction barrier, is a necessary prerequisite for using computational methods to interrogate features of the reaction that cannot be easily observed experimentally.

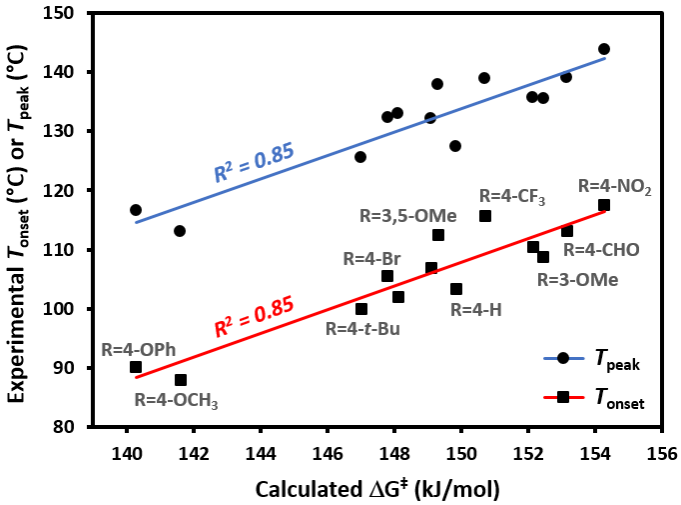

Figure 2.3 Comparison of experimentally determined T_{onset} and T_{peak} (°C) with calculated activation free energies (kJ mol^{-1}) for the conversion of representative trifluoromethyl aryl diazirines into the corresponding carbene. Adapted with permission from literature.[50]

The 30 °C span in activation temperatures is important from the perspective of experimental planning. For some applications where increased thermal stability is required (e.g. application of diazirine crosslinkers to polymer melts, or certain biological experiments where size limitations on a molecule may preclude the addition of molecular weight necessary to mitigate the explosivity risk that would otherwise accompany a low activation temperature) electron-poor diazirines with high activation temperatures will be preferred. For many applications, however (especially for polymer adhesion applications where one does not wish to melt the underlying polymer substrate), lower activation temperatures are highly desirable. In this context, the observation that electron-rich

trifluoromethyl aryl diazirines can be activated at <90 °C is particularly relevant to the development of improved reagents for materials science.

2.3.3 Quantification of linear free-energy relationships

The observed variation in activation temperatures can also shed light onto the mechanism of diazirine activation. To explore this, we plotted the data from Table 2.1 against various empirically derived Hammett σ values available from prior studies of reactions that are known to occur by polar or radical mechanisms. These included: (1) Hammett's original σ parameters derived from the study of *para*-substituted benzoic acid ionization;[120] (2) Brown's σ_p^+ parameters derived from observation of solvolysis of substituted *t*-cumyl chlorides;[121] (3) Arnold's $\sigma_\alpha^\bullet$ parameters derived from the study of EPR hyperfine coupling of benzyl radicals;[122] (4) Creary's $\sigma_C^\bullet$ parameters derived from the rearrangement of methylenecyclopropane ring systems;[123,124] and (5) Jiang and Ji's $\sigma_{jj}^\bullet$ parameters derived from the cyclodimerization of trifluorostyrenes.[125,126] In comparisons of this type, a strong positive correlation to σ^+ is generally taken as evidence in favour of some degree of carbocation character in the transition state, while correlation with any of the various $\sigma^\bullet$ parameters is taken as evidence of radical character.[127]

Experimental T_{onset} and T_{peak} data were found to give robust linear fits ($R^2 \geq 0.95$) to empirically derived σ_p^+ values (Figure 2.4). Calculated $\Delta G^\ddagger$ values likewise showed a strong correlation to σ_p^+ ($R^2 = 0.91$). By contrast, very poor fits ($R^2 < 0.1$) were observed to empirically derived $\sigma^\bullet$ values from Creary or Jiang (see Figure S2.2 in the section 2.5 for plots of T_{onset} and T_{peak} *vs.* all σ parameters). Together, these results argue in favour of an emerging vacant orbital at the benzylic centre during the transition state, and against the presence of any significant spin density at this position. These data provide compelling additional experimental support for the hypothesis that trifluoromethyl aryl diazirines initially form singlet carbenes upon activation, and that triplet carbenes are formed via a subsequent relaxation step.

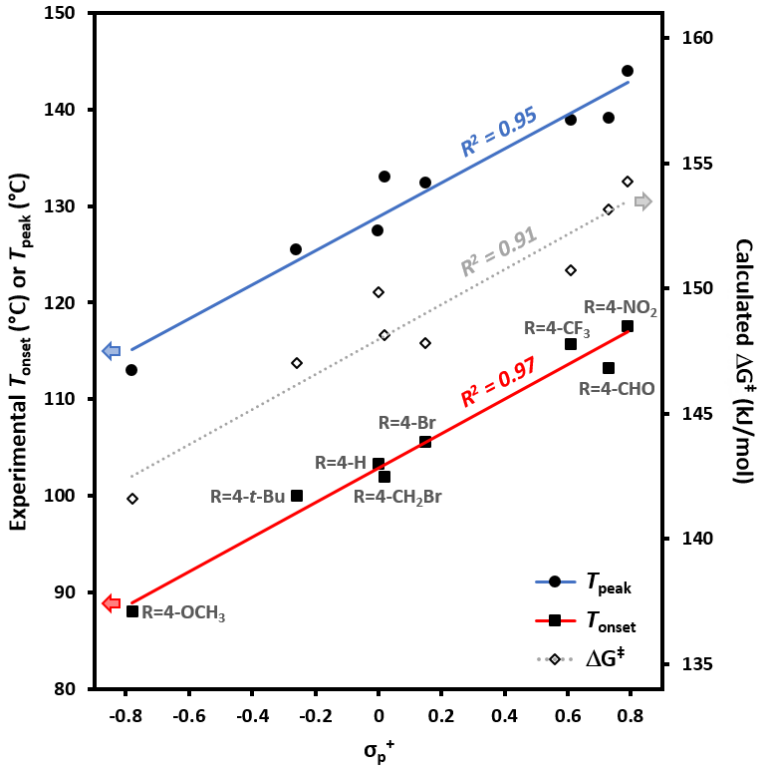

Figure 2.4 Variation in trifluoromethyl aryl diazirine activation temperatures and energies with the Hammett parameter σ_p^+. T_{onset}, T_{peak}, and $\Delta G^{\ddagger}$ are defined as in Table 2.1. The strong correlations and positive slopes are indicative of carbocation character in the transition state resulting from diazirine activation. Adapted with permission from literature.[50]

As discussed above, trifluoromethyl aryl diazirines have dominated diazirine research ever since Brunner's publication in 1980. Perhaps because of this dominance, there are few direct comparisons of α-trifluoromethyl diazirines to diazirines containing different α-substituents. In an effort to partially address this deficiency, we surveyed five other α-substituents and compared their T_{onset} and T_{peak} values (Table 2.2).

Table 2.2 Effect of α-substituent electronics on activation temperature and activation free energy[(a)]

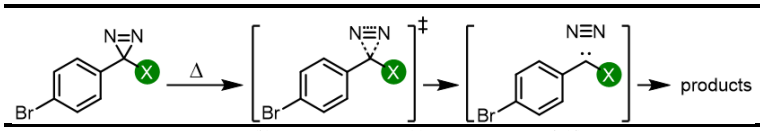

Entry	X	T_{onset} [(b)] (°C)	T_{peak} [(c)] (°C)	$\Delta G^{‡}$ [(d)] (kJ mol^{-1})
1	Cl	76.5 ± 0.1	99.6 ± 0.2	152.7
2	H	84.6 ± 1.8	104.5 ± 0.5	147.2
3	CH_3	93.5 ± 0.4	120.2 ± 0.1	153.8
4	CF_3	105.6 ± 0.5	132.4 ± 0.6	147.8
5	F	108.4 ± 0.3	133.4 ± 0.4	156.8
6	OCH_3	n.d.[(e)]	n.d.[(e)]	116.2

(a) In order to increase the molecular weight of the substrate (and thereby reduce volatility) experiments were carried out on *p*-brominated aryl diazirines. (b) Experimentally determined by extrapolation of the tangent of the upward slope observed in the DSC experiment, to the fitted baseline of the plot. Data are presented as the average of three independent measurements ± standard deviation. (c) Experimentally determined from the peak maxima in the DSC experiment. Data are presented as the average of three independent measurements ± standard deviation. (d) Calculated free energy (298.15 K, 1 atm) of activation (M06-2X-D3/6-31+G(d,p)//M06-2X-D3/6-31G(d,p)) associated with conversion of the diazirine into the corresponding carbene in vacuum. (e) The α-methoxy diazirine was too unstable to be analyzed by DSC, which is consistent with the low $\Delta G^{‡}$ that was found computationally, and with results from a different group.[128]

Lower activation temperatures were observed for α-H, α-chloro and α-methyl diazirines relative to α-CF3, while a representative α-fluoro diazirine had slightly higher T_{onset} and T_{peak} temperatures. The only α-methoxy compound studied was too unstable to properly study experimentally, but appeared to have a very low decomposition temperature.[128] Preliminary multi-reference calculations indicate that there are varying degrees of multi-reference character in the transition states of the alpha-substituted species. The poor treatment of multi-reference systems by M06-2X leads to a weaker correlation between the calculated barrier heights and T_{onset} for the data in Table 2.2 than was seen for the equivalent data in Table 2.1.

2.3.4 Expanded *in silico* Hammett studies

The robust linear free energy relationship observed in Figure 2.4 stimulated several additional questions:

1. Would aryl diazirines with alpha substituents other than CF_3 reveal similar tunability in activation temperature through the addition of electron donating or electron withdrawing groups on the aromatic ring? We were particularly interested here to study molecules with π donor groups at the alpha position (e.g. OMe or F). By donating into the unfilled p orbital of the singlet carbene, such groups could in principle alter the electronic preferences of the carbene intermediate, as well as the transition state energies.

2. Is it possible through judicious tuning of the electronics of an aryl diazirine to stabilize the singlet carbene sufficiently well that it becomes the lower energy state for the molecule? As discussed above, data from Sheridan and Lindel strongly implicate the involvement of singlet carbenes following activation of trifluoromethyl 4-methoxyphenyl diazirine, but it was not clear how this molecule fits into a larger trend.[129]

3. If a singlet state were favoured, would this improve the ability of the molecule to undergo C–H insertion with aliphatic substrates? Or would the stabilization that is necessary to lower the energy of the singlet state below that of the triplet necessarily then raise the activation barrier for C–H insertion, such that this becomes a less efficient process?

4. Given the very low activation barrier for α-methoxy diazirines, would these species be better or worse reagents from the perspective of C–H insertion? Alkoxy diazirines are valuable intermediates in glycoside synthesis,[130,131] but less is known about how their properties compare to the more commonly exploited trifluoromethyl diazirines.[128,132,133]

Some of these questions are challenging to study experimentally. For example, the difficulty of working with α-methoxy diazirines (as noted above) makes it a challenge to derive analytically precise data describing their activation. Similarly, exploring the farther reaches of the Hammett plot by studying the inclusion of stronger electron donating groups like NMe_2 ($\sigma_p^+ = -1.7$) or NH_2 ($\sigma_p^+ = -1.3$) was ruled out as potentially hazardous to laboratory personnel, since these molecules would have significantly lower activation temperatures. Even studying the difference in performance for a *p*-OH group

(σ_p^+ = –0.92) relative to the *p*-OMe substituent (σ_p^+ = –0.78) was ruled out experimentally, due to concerns that hydrogen bonding for the phenol in the solid state might complicate our analysis. Moreover, Hatanaka and co-workers have previously reported that this phenol is unstable and difficult to isolate.[80]

Of course, none of the above concerns apply to *in silico* experiments. We therefore sought to explore the above questions computationally, using an expanded Hammett series (R = 4-NMe_2, 4-NH_2, 4-OH, 4-OMe, 4-*t*-Bu, 4-CH_3, 4-H, 4-Cl, 4-CF_3, 4-CN and 4-NO_2) and four different alpha substituents (X = CF_3, Cl, F, and OCH_3).

All 44 diazirine activation reactions were modelled using M06-2X-D3/6-31G(d,p) methods, and the calculated activation free energies ($\Delta G^{\ddagger}$) are shown in Figure 2.5 (see Table S2.3 for complete tabulated data). The series of α-trifluoromethyl diazirines gave the largest positive slope of any of the four families of substrates. Because we know from Figure 2.3 and 2.4 that diazirine activation energy tightly corresponds to T_{onset} and T_{peak} temperatures, this means that activation temperature would be much less tunable for α-fluoro, α-chloro and α-methoxy diazirines. In fact, the slope is essentially zero across the Hammett series when X = F (see Table S2.3 for tabulated slopes), and becomes negative when X = OCH_3.

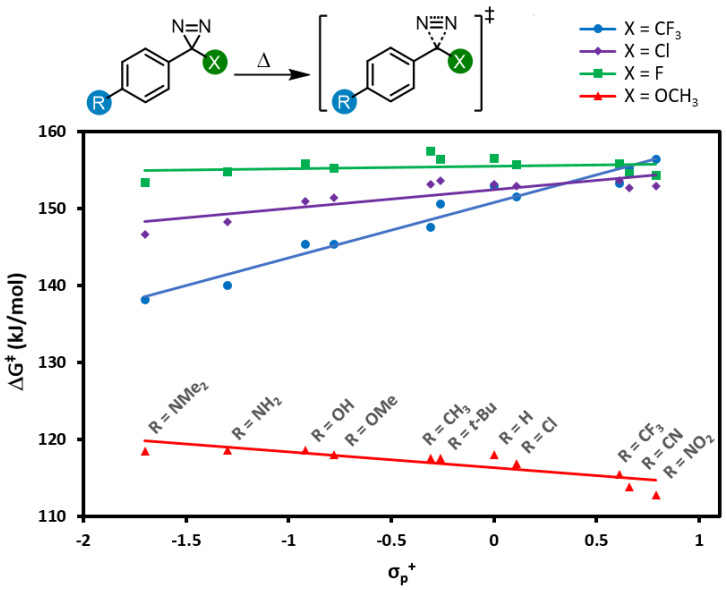

Figure 2.5 Variation in diazirine activation free energy (M06-2X-D3/6-31G(d,p)) with the Hammett parameter σ_p^+ for four different series of aryl diazirines. Adapted with permission from literature.[50]

A series of computed isodesmic reactions (Figure S2.3) suggested that the trends observed in Figure 2.5 are principally due to (de)stabilization of the transition states, rather than alteration of the ground-state diazirine energies. These data indicate that when X = CF_3, electron-donating groups located across the aromatic ring from the diazirine centre can help to stabilize the empty p orbital that is evolving within the transition state. Once again this is consistent with a transition structure that is singlet-like, rather than triplet-like, and provides additional data in support of the hypothesis that singlet carbenes are initially formed following diazirine activation. This effect is blunted by incorporation of groups with increasing π-donating ability (X = Cl < F < OCH_3) since these groups can themselves donate electron density to help stabilize the evolving empty p orbital. By the time we reach the strongest π-donor (X = OCH_3), the evolving empty p orbital is fully stabilized, and we therefore observe no change in transition-state stabilization with differing substituents on the aromatic ring.

2.3.5 Assessment of singlet–triplet gaps

We next calculated the singlet–triplet energy gaps for our four Hammett series using domain based local pair natural orbital (DLPNO) coupled cluster methods (Figure 2.6; see Table S2.6 for comparative data using different levels of theory).[134]

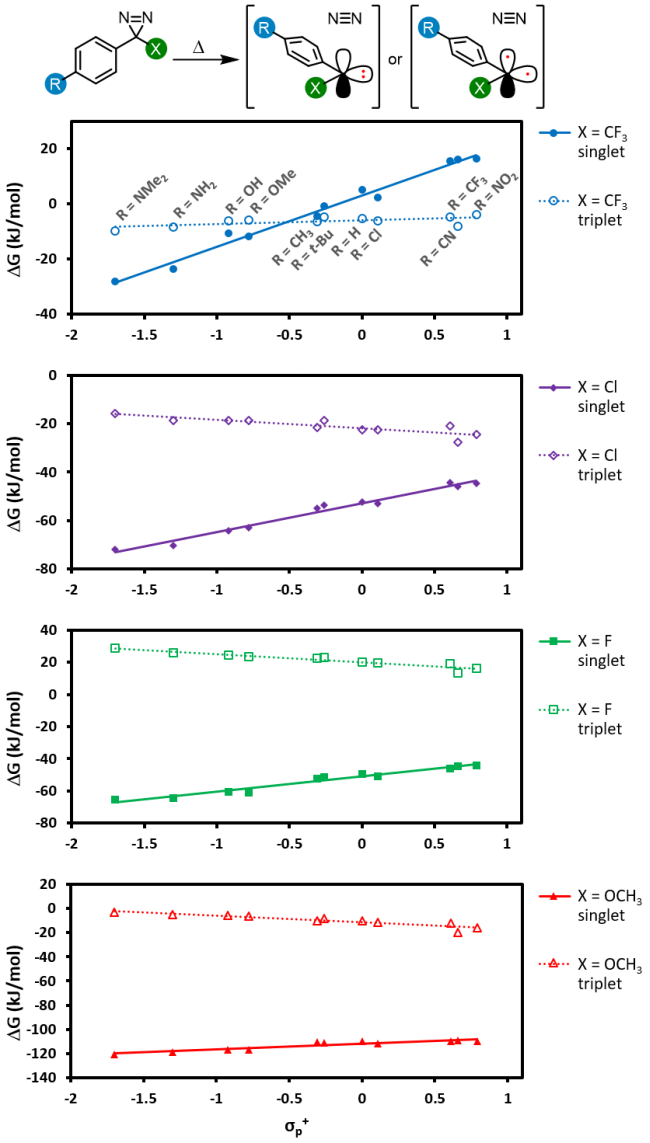

Figure 2.6 Free energy of reaction (DLPNO-CCSD(T)/cc-pV(D-T)Z CBS//M06-2X-D3/6-31G(d,p)) leading from diazirine starting materials to the corresponding singlet or triplet carbene. Refer to Figure S2.4 for an equivalent plot where the same y-axis is used for each panel. Adapted with permission from literature.[50]

For each of the π-donors included in our study (X = Cl, F, or OCH_3), the singlet was always the lowest energy state for the carbene, regardless of the identity of the *para* substituent (R) on the aromatic ring. As we saw with transition state energies, the ability of the α-substituent to stabilize the singlet carbene through the donation of electron density into the empty p orbital evidently outweighs other effects due to resonance donation by the distal R group.

For the α-trifluoromethyl series, we saw more interesting behaviour, wherein the singlet energy was dramatically affected by the ability of the R group to donate electron density, while the triplet energy remained essentially constant across the Hammett series. The result is a switch in the energy ordering of the two possible carbenes—when the aryl group was substituted with electron-neutral or electron-poor groups at the *para*-position, the triplet carbene was the lower energy species, but when a strong electron-donating group was added to the *para*-position of the aromatic ring, the singlet carbene became lower in energy. When R = OCH_3, the singlet was calculated to be 6.9 kJ mol^{-1} lower in free energy (DLPNO-CCSD(T)/cc-pV(T-Q)Z//M06-2X-D3/6-31G(d,p)).

The data in Figure 2.6 indicate two different options for producing aryl carbenes in which the singlet state is predominant: one may either employ an electron-donating α substituent such as an alkoxy group (in which case the electronics of the aromatic ring are largely immaterial) or else one can maintain the α-CF_3 group that is widely used in literature crosslinking studies but add a sufficiently electron-donating *para* substituent to the aromatic ring.

2.3.6 Calculation of C–H insertion barriers

Applications of diazirine groups in chemical biology or materials science demand that the carbene generated *in situ* be able to undergo efficient C–H insertion (or occasionally O–H insertion). However, the percent conversion for this process is typically quite poor (often <10%) because of the occurrence of side reactions. One particularly troublesome side-reaction for carbenes—often accounting for >50% of the mass balance in model studies of C–H insertion reactions—is quenching by adventitious oxygen to produce undesired ketone side products. It is thought that this mainly occurs through reaction of $^3O_2$ with the triplet carbene. As such, the use of stabilized singlet

carbenes (wherein little if any triplet is ever formed) may provide improved C–H insertion yields. On the other hand, if the singlet carbenes are too stabilized, then a higher energy barrier will be required for C–H insertion.

Mindful of the potential benefits of improved C–H insertion reactions elicited by an ability to favour a singlet carbene intermediate, we computed the energy barriers for aliphatic C–H insertion (using the central CH_2 motif of propane as a model of a typical aliphatic group), for all 88 singlet and triplet carbenes derived from aryl diazirines where X = CF_3, Cl, F, or OCH_3, and R = 4-NMe_2, 4-NH_2, 4-OH, 4-OMe, 4-*t*-Bu, 4-CH_3, 4-H, 4-Cl, 4-CF_3, 4-CN or 4-NO_2. Complete numerical data are tabulated in Table S2.3, and are summarized graphically in Figure 2.7.

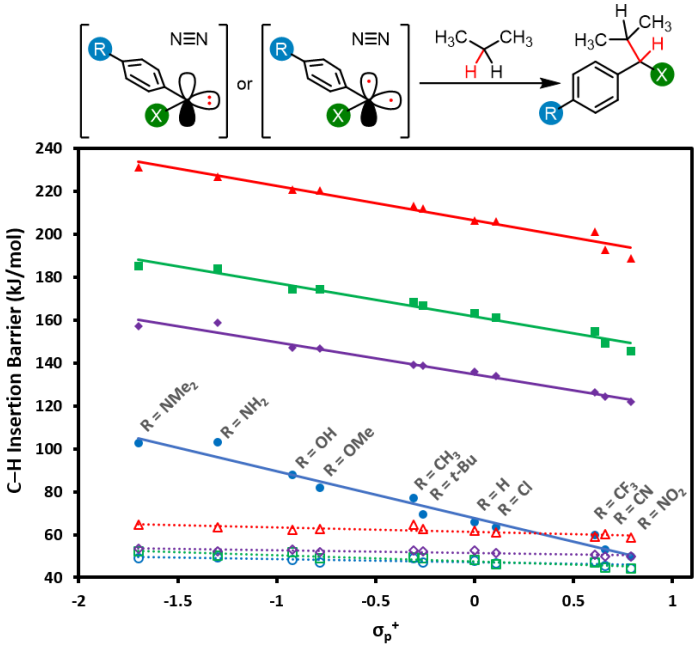

Figure 2.7 Calculated free energy barriers (M06-2X-D3/6-31G(d,p)) for insertion of singlet or triplet carbenes into the central C–H bond of propane. Data points and linear fits are reported as in Figure 2.6: blue circles: X = CF_3; purple diamonds: X = Cl; green square: X = F; red triangles: X = OCH_3; solid lines: data and fits for singlet species; dashed lines: data and fits for triplets. Refer to Figure S2.5 for plots showing singlet and triplet insertions on separate axes. Adapted with permission from literature.[50]

The data reveal that for all four series of carbenes, the triplet C–H insertion barriers are always lower in energy than the corresponding singlet barriers, although the numbers are relatively close for electron-poor trifluoromethyl aryl diazirines ($\Delta[\Delta G]$ =

5.5 kJ mol^{-1} when R = NO_2). The lowest singlet C–H insertion barriers are found for the trifluoromethyl aryl diazirine series. Critically, these barriers are all lower than the $\Delta G^{\ddagger}$ for the initial production of carbenes from the diazirine parent compounds (*ca*. 140–155 kJ mol^{-1}; see Table 2.1 and Figure 2.5).

Therefore, although the singlet C–H insertion barriers shown in Figure 2.7 are higher than the barriers for the corresponding triplets, they must still be energetically achievable if the system had enough energy for diazirine activation. In other words, if a singlet α-CF_3 carbene is produced, it should be able to undergo insertion with nearby C–H bonds; the rate-determining step for the process will be loss of N_2 from the diazirine, and the subsequent insertion will be kinetically invisible.

This is not the case for the other carbene series. For α-OCH_3 carbenes in particular, the singlet C–H insertion barriers are very high in free energy, which removes any possible benefit associated with the facile diazirine activation for these molecules.

2.3.7 Optimal C–H insertion efficiency from an electron-rich diazirine

Taken together, the above data suggest that trifluoromethyl aryl diazirines bearing an electron-donating substituent at the *para*-position of the aromatic ring may be optimal: they will require a lower temperature for thermal activation, they should favour a singlet ground state for the carbene intermediate, and that singlet carbene should have sufficient energy to undergo C–H insertion. But what would be the most appropriate electron-donating group to use, when seeking to balance a desirable reactivity profile with good handling characteristics? Extrapolation of the red line in Figure 2.4 and estimation of initiation temperature from T_{onset} (refer to Figure S2.40 for further details) suggests that *p*-amino trifluoromethyl phenyl diazirines would be unstable above *ca*. 40 °C. In addition to obvious concerns around shock sensitivity or explosive propagation[36,118] simply making and handling such a molecule on large scale could be problematic.

We therefore identified a *p*-alkoxy group as the optimal substituent to attach to the trifluoromethyl aryl diazirine scaffold. Our calculations suggest that it is sufficiently electron donating to favour the singlet ground state in the carbene (i.e. it falls just to the left of the intersection point in the top panel of Figure 2.6), and yet our experimental measurements indicate that it is not so electron-donating as to result in an impractically

low activation temperature. As an added benefit, *p*-alkoxy trifluoromethyl aryl diazines will have a longer wavelength λ_{max} and increased extinction coefficient associated with the diazirine activation band in the UV/Vis spectrum (Figure 2.2).

Notwithstanding occasional earlier reports on the use of *p*-alkoxy trifluoromethyl aryl diazirines by Sheridan,[90] Lindel,[112] Kanaoka[114–116] and Hashimoto,[135] direct comparisons of efficacy between electron-rich, electron-neutral, and electron-poor aryl diazirines in their ability to insert into challenging (i.e. high energy) C–H bonds are lacking in the literature. Moreover, the few literature examples where electron-rich trifluoromethyl aryl diazirines are used are limited to photochemical activation methods. These examples are therefore relevant to chemical biology applications (where diazirines are almost always excited photochemically or else through energy transfer) but are less relevant to materials science applications, where thermal activation tends to predominate.

We therefore conducted a series of thermally and photochemically promoted C–H insertions with representative electron-rich, electron-neutral, and electron-poor trifluoromethyl aryl diazirines, employing cyclohexane as a substrate (C–H bond dissociation energy = 416 kJ mol^{-1}).[136] Consistent with our prediction from Figure 2.6 that electron-donating groups at the *para*-position of the aromatic ring would stabilize a singlet carbene and allow for more selective C–H insertion reactions, we found that the installation of 4-OPh or 4-OCH_3 substituents dramatically improved the isolated yield of the desired product (Table 2.3). This was particularly true for thermal activation conditions, in which the best-performing diazirine substrate was >10-fold more efficacious toward C–H insertion than the worst substrate. Regardless of the activation method, the 4-OCH_3 group was found to be superior to the 4-OPh group, consistent with the improved electron-donating ability of the former substituent.

Table 2.3 Effect of aryl substituent electronics on cyclohexane C–H insertion

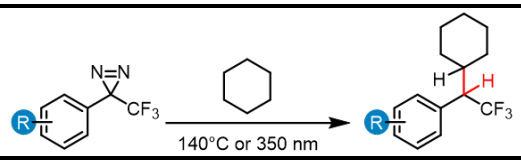

Entry	R	Thermal C–H insertion yield[(a)] (%)	Photochemical C–H insertion yield[(b)] (%)
1	4-CF_3	6	25
2	4-H	15	35
3	3-OCH_3	18	19
4	4-OPh	75	77
5	4-OCH_3	91	94

(a) Thermal C–H insertion reactions were performed using 15 mM of the desired diazirine in dry, degassed cyclohexane. Reaction mixtures were heated in a sealed tube at 140 °C for 2 h. (b) Photochemical C–H insertion reactions were performed using 15 mM of the desired diazirine in dry, degassed cyclohexane. Reaction mixtures were irradiated at 350 nm for 4 h using a Rayonet reactor.

Careful examination of the crude NMR spectra for each of the reactions in Table 2.3 (see Figure S2.30 and S2.31) indicated the presence of significant quantities of ketone side products for the less-successful reactions, consistent with the hypothesis that for electron-poor or electron-neutral trifluoromethyl aryl carbenes, the triplet is the ground-state species. As further evidence for the mechanism of ketone formation, we examined the addition of triplet trifluoromethyl aryl carbenes to O_2 computationally, and found this process to be essentially barrierless. Other side products appear to result from self-insertion pathways where one carbene molecule undergoes undesirable C–H insertion reactions with the aromatic moiety of the starting material.

Whereas the data in Table 2.3 were collected using dry, degassed solvent, we also sought to study the reaction of the optimized substrate in less rigorous reaction conditions that might better mimic "real world" circumstances where diazirines need to be used. Thermal and photochemical reactions of *p*-methoxy trifluoromethyl phenyl diazirine were therefore repeated using 9 : 1 cyclohexane : water, and each reaction was run under air instead of inert atmosphere (Scheme 2.1). Remarkably, the desired C–H insertion adduct was once again the only isolable product, and could be obtained in ≥90% yield. Indeed, the crude NMR spectra for these "wet" reactions were identical to those obtained when the reaction was run using dry, deoxygenated cyclohexane (Figure S2.32).

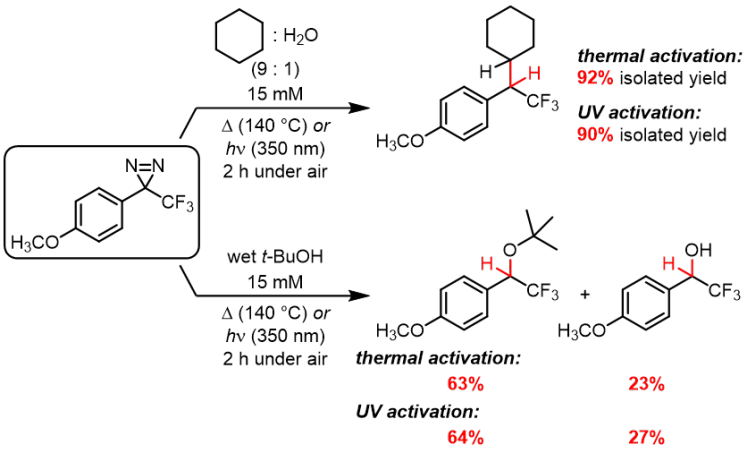

Scheme 2.1 C–H and O–H insertions in the presence of air and moisture. Adapted with permission from literature.[50]

While C–H insertions are often desired, O–H insertions can be equally useful for both protein labeling[112,137] and polymer crosslinking.[36,61] Raimer and Lindel had previously shown that *p*-methoxy trifluoromethyl phenyl diazirine could react with phenols,[112] but because the proposed mechanism involved initial protonation by the acidic phenol, it was unclear what the efficiency of O–H insertion would be with alcohols. We therefore reacted our electronically optimized diazirine with *tert*-butanol under both photochemical and thermal activation conditions, once again intentionally carrying out the reaction under air and using non-anhydrous solvent (Scheme 2.1). Satisfyingly, the total yield of O–H insertion products was approximately 90% in both cases.

2.4. Conclusions

Aryl diazirine reagents already find broad application in biological target identification, small molecule capture, and protein- and polymer-crosslinking, as well as in experimental adhesives for both commodity polymers and living tissue.[71,138] However, in the vast majority of cases, the structure of the diazirine unit within these reagents has been chosen based on synthetic expedience rather than a consideration of what electronic properties might be optimal. In other words, all aryl diazirines have been assumed to be more or less equivalent in their ability to function as reactive “warheads”. In contrast to this view, the data presented in the current work provide compelling evidence that the properties of aryl diazirines can be readily adjusted by tuning the electronics of the aryl substituent. In particular, the observation that simply adding an alkoxy group to an aryl

diazirine can improve the C–H insertion efficiency by >10-fold relative to an electronically unoptimized diazirine should stimulate the development of ever more effective reagents for the diverse array of applications discussed above.

2.5. Experimental and Supplementary Information

2.5.1 Supplemental figures

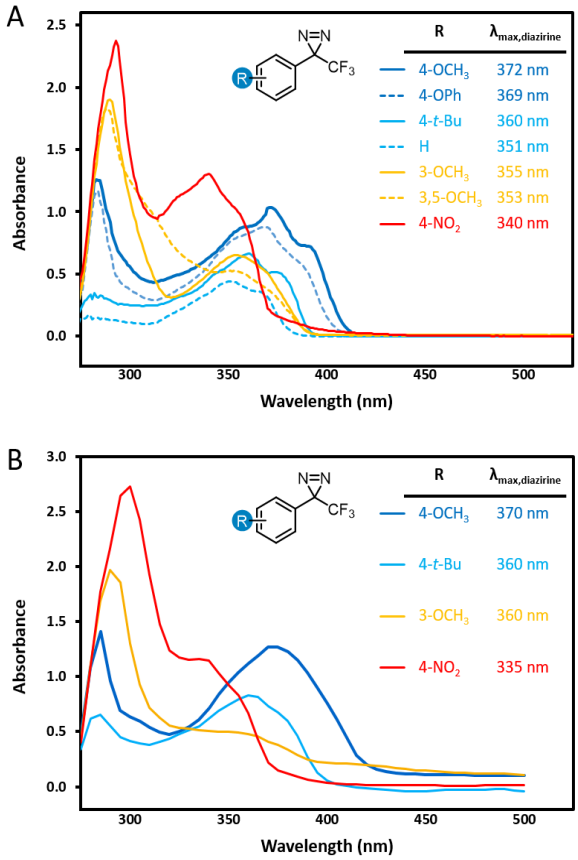

Figure S2.1 Comparison of UV/Vis spectra for representative diazirines in nonpolar and polar solvents. (A) Spectra recorded in *n*-hexane, using 1 nm steps. (B) Spectra recorded in methanol, using 5 nm steps. Adapted with permission from literature.[50]

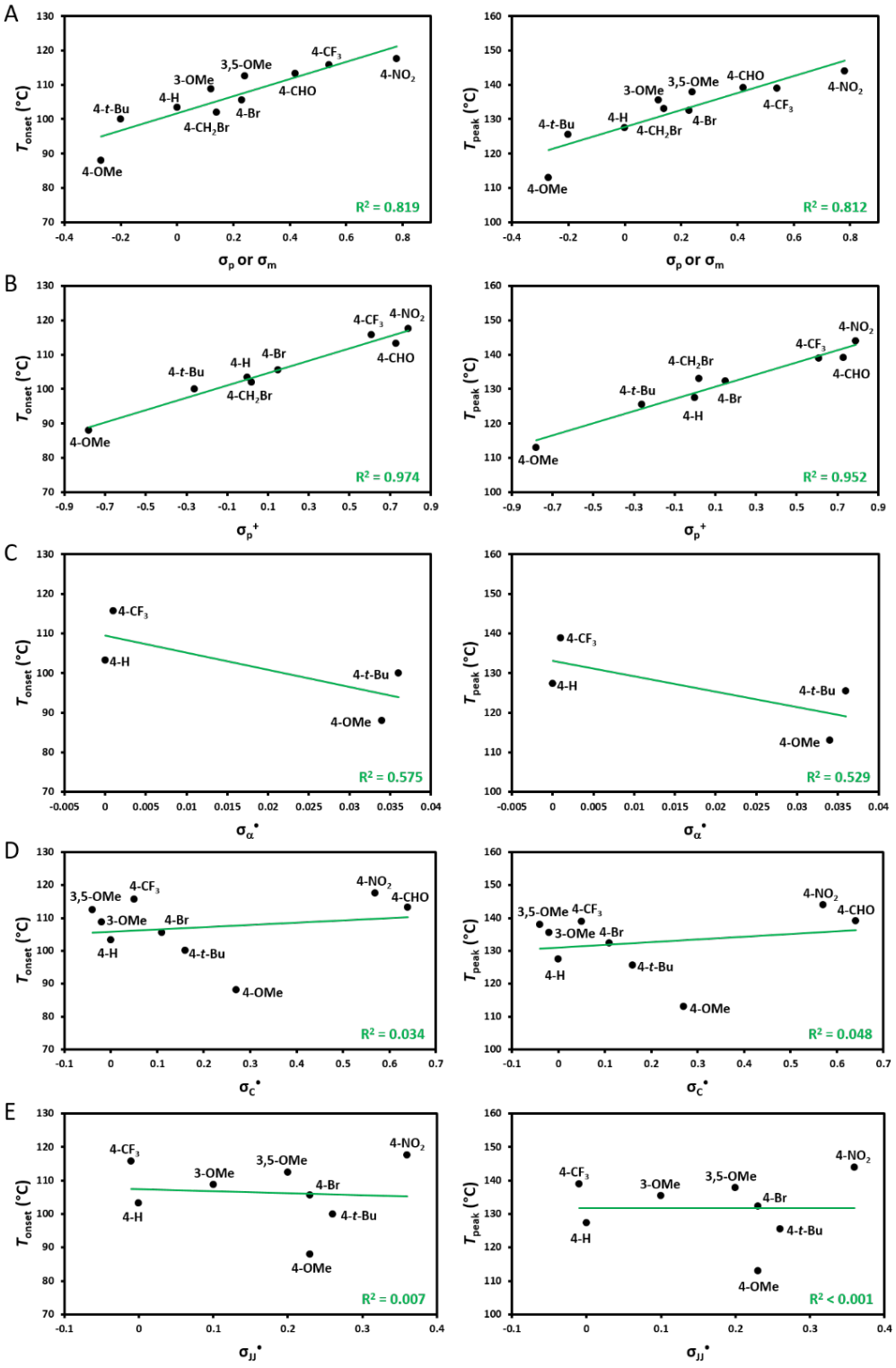

Figure S2.2 Fits of experimental T_{onset} and T_{peak} data to empirically derived Hammett parameters. (A) Fits generated using Hammett's original σ parameters derived from the study of *para*-substituted benzoic acid ionization. (B) Fits generated using Brown's σ_p^+

parameters derived from observation of solvolysis of substituted *t*-cumyl chlorides. (C) Fits generated using Arnold's $\sigma_{\alpha}^{\bullet}$ parameters derived from the study of EPR hyperfine coupling of benzyl radicals. (D) Fits generated using Creary's $\sigma_{C}^{\bullet}$ parameters derived from the rearrangement of methylenecyclopropane ring systems. (E) Fits generated using Jiang and Ji's $\sigma_{jj}^{\bullet}$ parameters derived from the cyclodimerization of trifluorostyrenes. Excellent fits are observed using Brown's σ_{p}^{+} parameters, while very poor fits are observed using any of the $\sigma^{\bullet}$ parameters. These data support some degree of carbocation character in the transition state, and are not consistent with radical character at the benzylic center during the rate-determining step. Adapted with permission from literature.[50]

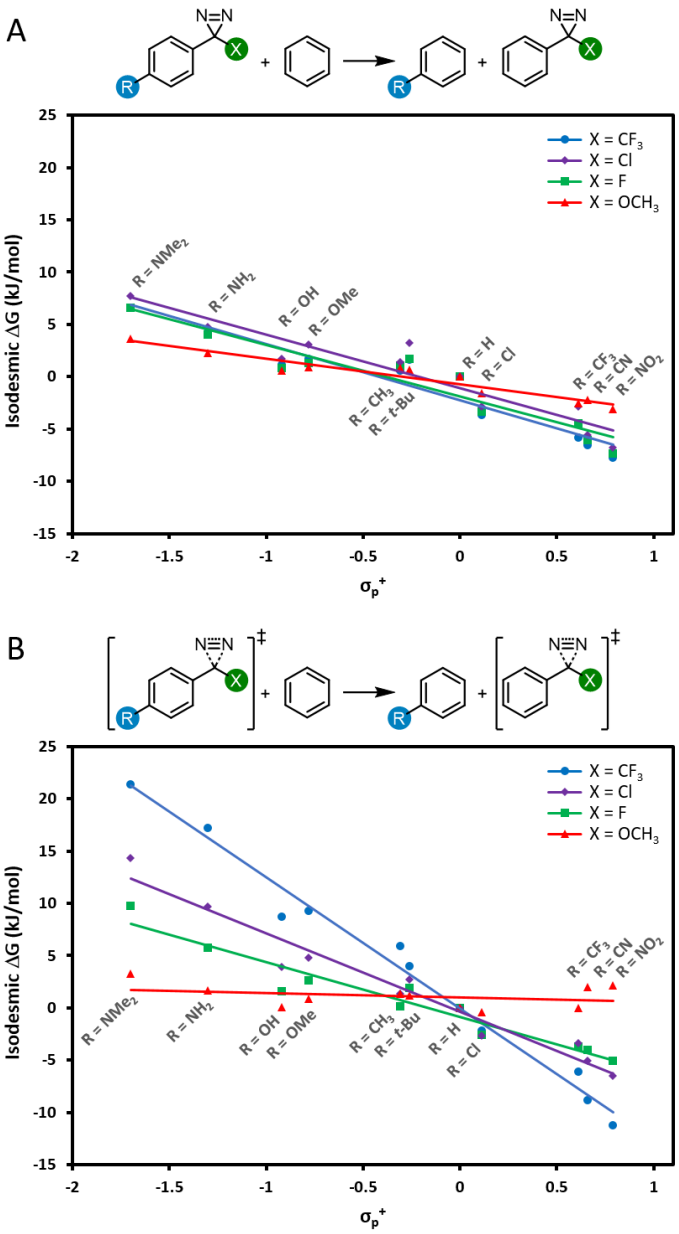

Figure S2.3 Isodesmic equations used to explore the effect of aryl substituents on energetics of the diazirine ground state (panel A) and transition state (panel B). All calculations were performed using M06-2X-D3/6-31G(d,p). The data in panel A indicate that varying the electronic properties of the aryl substituent has only minor (and very consistent) effects on the energy of the ground-state diazirine; the consistent negative slope across all four series of isodesmic reactions indicates that the CN_2X function constitutes a weak electron withdrawing group. The data in panel B indicate that when $X=CF_3$, electron-donating groups located across the aromatic ring from the diazirine

centre can help to stabilize the empty p orbital that is evolving within the transition state. However, this effect is blunted by incorporation of groups with increasing π-donating ability (X=Cl < F < OCH_3) since these groups can themselves donate electron density to help stabilize the evolving empty p orbital. Adapted with permission from literature.[50]

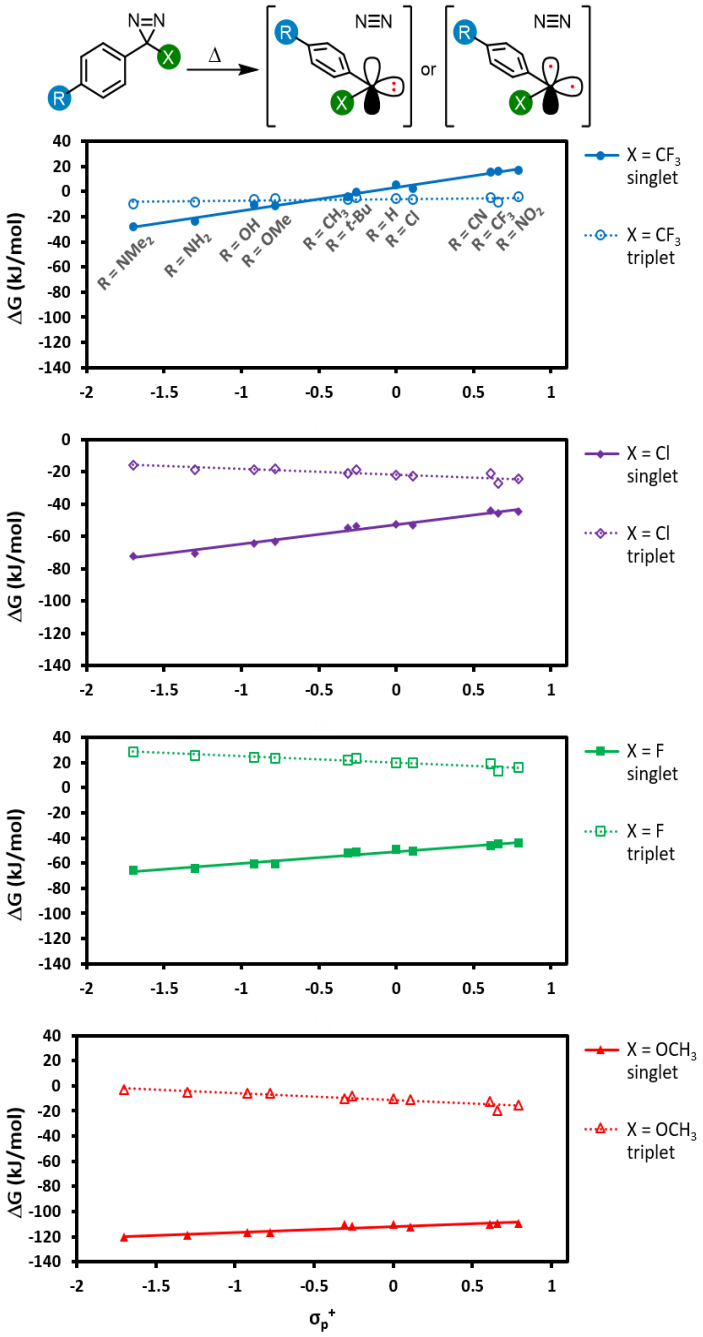

Figure S2.4 Alternative presentation of the data in Figure 2.6, in which the same y-axis is used for each panel. Adapted with permission from literature.[50]

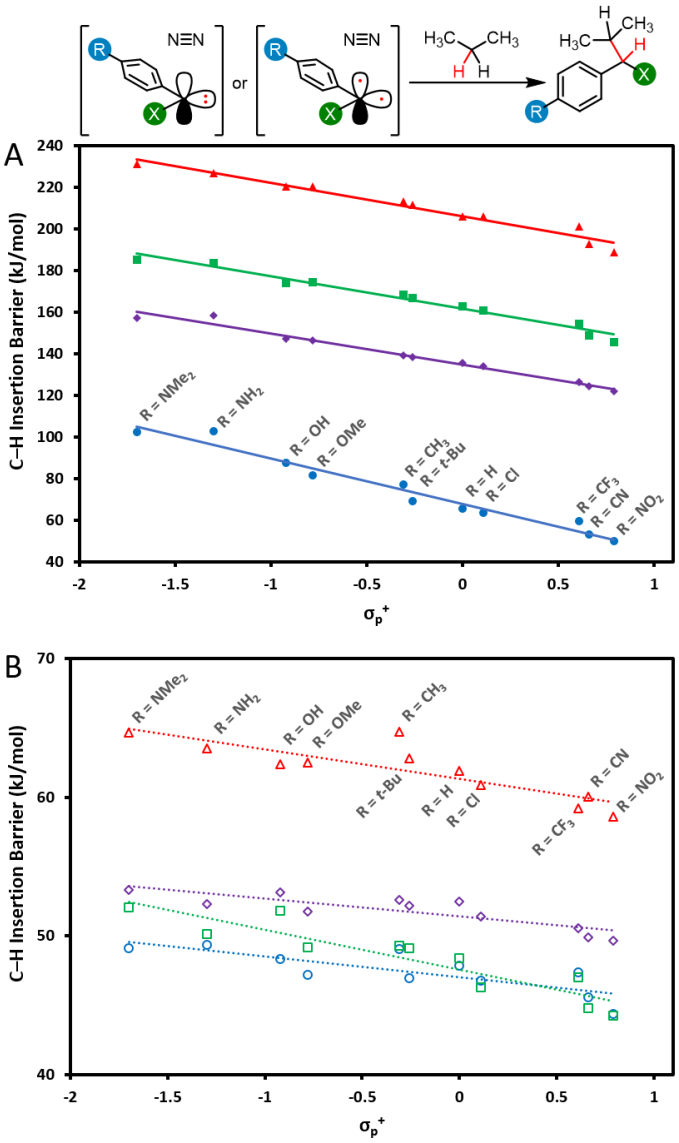

Figure S2.5 Alternative presentation of the data in Figure 2.7, in which the data for the singlet insertions and triplet insertions are plotted separately to improve visibility. Data and fits for singlet species (solid lines) are shown in panel A. Data and fits for triplet species (dashed lines) are shown in panel B. Adapted with permission from literature.[50]

2.5.2 Materials and methods

2.5.2.1 General considerations

All commercial materials were used as received. THF was freshly dried over Na/benzophenone. Dichloromethane (DCM) was freshly dried by passage over alumina in a commercial solvent purification system. Anhydrous cyclohexane was used in crosslinking experiments. Spectranalyzed™ pentane was used for purification of diazirines. Unless otherwise stated, all reactions were performed in flame-dried glassware equipped with rubber septa under a positive pressure of argon. NMR spectra were acquired on either a Bruker AVANCE 300 (300.27 MHz for ^{1}H, 282.54 MHz for ^{19}F, 75.5 MHz for ^{13}C) or a Bruker AVANCE Neo 500 (500.27 MHz for ^{1}H, 470.72 MHz for ^{19}F, 125 MHz for ^{13}C) spectrometer. Chemical shifts were reported in parts per million (ppm) and were calibrated to the central peak of residual NMR solvent (central peak of chloroform-d: ^{1}H NMR δ = 7.26 ppm, ^{13}C NMR δ = 77.16 ppm; dichloromethane-d_2: ^{1}H NMR δ = 5.32 ppm, ^{13}C NMR δ = 53.84 ppm). ^{13}C spectra and ^{19}F spectra were ^{1}H decoupled. Data is reported as follows: chemical shift (multiplicity [s = singlet, d = doublet, t = triplet, q = quartet, qd = quartet of doublet, p = pentet, dt = doublet of triplet, tt = triplet of triplet, td = triplet of doublet, br-s = broad singlet, m = multiplet], coupling constant in Hz, integration). Chemical shifts in ^{19}F spectra are reported in ppm and reported as obtained. IR spectra were recorded using a Perkin-Elmer ATR spectrometer. IR wave numbers (ν) are reported in cm^{-1}. Rayonet UV chamber equipped with eight 350 nm UV lamps and an operating fan was used for photochemical C–H insertion experiments. High resolution electrospray ionization mass spectrometry (HRMS) data were acquired using a Thermo Scientific Orbitrap Exactive Plus spectrometer using electrospray ionization experiments. GC-MS experiments were conducted using a Finnigan Trace GC Ultra and DSQ mass spectrometer system coupled with an AI 3000 autosampler (Thermo, MA). Samples were dissolved in Optima™ Acetonitrile (Fisher Chemical, NH) and then 2 µL was injected into the GC with a carrier flow of He gas set at 1 mL/min. The column used was a RTX-5MS capillary column with dimensions of 15 m x 0.25 mm x 0.5 µm (Restek, PA). The inlet temperature was set to 220 °C with a split flow of 10 mL/min. The oven temperature was held at 50 °C for 1 min and then raised to

250 °C using a ramp rate of 20 °C/min. The oven then was held for three minutes at 250 °C resulting in a total run time of 9 min. The DSQ mass spectrometer was scanned continuously in positive mode in the range of m/z = 50 to 650 Da. The source temperature was set to 150 °C and electron impact energy 70 eV. Differential scanning calorimetry analysis was performed using a DSC 25 TA instrument.

All diazirine-forming reactions were performed in the dark. Removal of solvent was done at 25 °C, avoiding the use of excessive vacuum.

Diazirines are numbered in order of appearance in the manuscript **D2.1**−**D2.17**.

2.5.2.2 Synthesis of aryl diazirines

Diazirine **D2.4** was purchased from Amadis Chemical and diazirines **D2.6** and **D2.7** were purchased from TCI America.

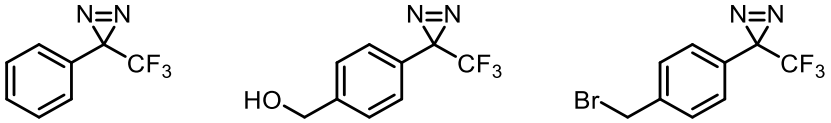

D2.4 **D2.6** **D2.7**

Synthesis of 2,2,2-trifluoro-1-(4-methoxyphenyl)ethan-1-one (**S2.1**).

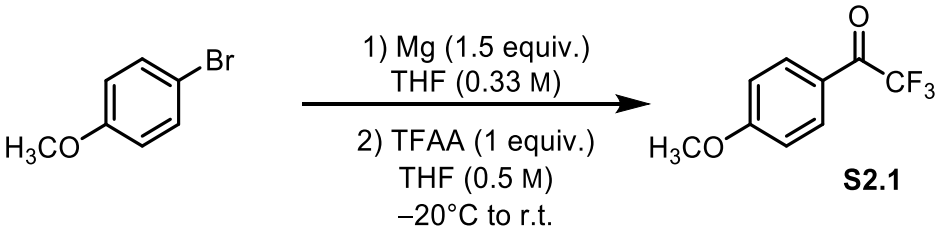

S2.1

To a suspension of magnesium turnings (182 mg, 7.5 mmol, 1.5 equiv.) in anhydrous THF (7.5 mL) stirred under argon was added drop wise a solution of 4-bromoanisole (0.6 mL, 5 mmol, 1 equiv.) in anhydrous THF (7.5 mL). The reaction was left for 2 h stirring and the product, (4-methoxyphenyl)magnesium bromide (14 mL of 0.33 M solution in THF fresh-made, 4.62 mmol) was added drop wise to a solution of trifluoroacetic anhydride (TFAA, 0.64 mL, 4.2 mmol, 1 equiv.) in anhydrous THF at –20 °C. The reaction was stirred at –20 °C for 2 h, then it was quenched with NH_4Cl and it was extracted with diethyl ether (× 3) and the combined organic layers were washed with brine and dried over magnesium sulfate. The crude compound **S2.1** was purified by silica gel column chromatography using petroleum ether: EtOAc (9:1, R_f = 0.35) as eluent to

afford the desired ketone **S2.1** (713 mg, 3.49 mmol, 83%) as a yellow solid with spectroscopic data in accordance with the literature.[112] ^{1}H NMR (300 MHz, $CDCl_3$) δ 8.06 (dd, *J* = 9.1, 1.0 Hz, 2H), 7.01 (d, *J* = 9.1 Hz, 2H), 3.92 (s, 3H). ^{19}F NMR (283 MHz, $CDCl_3$) δ –71.01.

Synthesis of 2,2,2-trifluoro-1-(4-methoxyphenyl)ethan-1-one oxime (**S2.2**) (mixture of *E*-, *Z*-isomers).

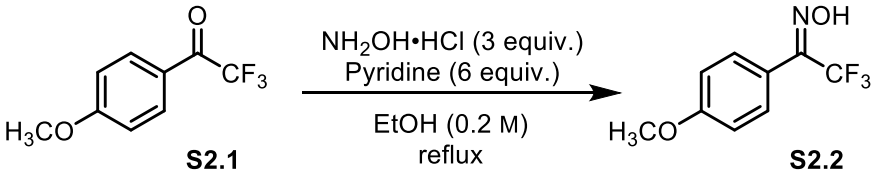

To a stirred solution of compound **S2.1** (713 mg, 3.49 mmol, 1 equiv.) in ethanol (0.2 M), hydroxylamine hydrochloride (728 mg, 10.5 mmol, 3 equiv.) and pyridine (1.7 mL, 20.9 mmol, 6 equiv.) were added and the reaction mixture was heated to reflux for 21 h. The mixture was then cooled to room temperature and the mixture was treated with 2 M HCl and extracted with diethyl ether (3 times). The combined organic layers were washed with distilled water until the pH of the washing layer became neutral, and then dried with sodium sulfate, filtered, and concentrated. The residue was dried under high vacuum for a prolonged time to afford the desired crude oxime **S2.2** (as a mixture of geometric isomers) as a white solid, with spectroscopic data in accordance with the literature.[112] The compound was submitted to the next step without further purification. ^{1}H NMR (300 MHz, $CDCl_3$) δ 8.36 (br-s, 1H, OH), 8.12 – 8.01 (m, 0.3H, OH, minor isomer), 7.53 (d, *J* = 8.7 Hz, 2H), 7.44 (dd, *J* = 9.0, 1.0 Hz, 0.75H, minor isomer), 6.98 (d, *J* = 9.0 Hz, 2H), 6.95 – 6.90 (m, 0.75H, minor isomer), 3.85 (s, 3H), 3.84 (s, 1.3H, minor isomer). ^{19}F NMR (283 MHz, $CDCl_3$) δ –62.36 (minor isomer), –66.31.

Synthesis of 2,2,2-trifluoro-1-(4-methoxyphenyl)ethan-1-one *O*-tosyl oxime (**S2.3**) (mixture of *E*-, Z-isomers).

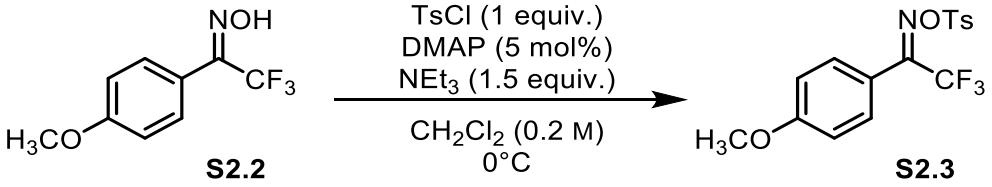

Compound **S2.2** (764 mg, 3.49 mmol, 1 equiv.) was dissolved in CH_2Cl_2 (0.2 M), and triethylamine (0.7 mL, 5.2 mmol, 1.5 equiv.), DMAP (21 mg, 0.17 mmol, 5 mol%) and tosyl chloride (665 mg, 3.49 mmol, 1 equiv.) were successively added at 0 °C. The ice bath was removed after 5 min, and the reaction mixture was stirred at room temperature for 1 h. The mixture was then treated with sat. aq. NH_4Cl and extracted with CH_2Cl_2. The combined organic extracts were dried with sodium sulfate, filtered, and concentrated to afford the desired crude tosyl oxime **S2.3** as a white solid, with spectroscopic data in accordance with the literature.[112] The compound was submitted to the next step without further purification. ^{1}H NMR (300 MHz, $CDCl_3$) δ 7.89 (d, J = 8.3 Hz, 2H), 7.45 (d, J = 8.9 Hz, 2H), 7.38 (d, J = 8.2 Hz, 2H), 6.96 (d, J = 9.0 Hz, 2H), 3.86 (s, 3H), 2.48 (s, 3H). ^{19}F NMR (283 MHz, $CDCl_3$) δ –61.42 (minor isomer), –66.03.

Synthesis of 3-(4-methoxyphenyl)-3-(trifluoromethyl)diaziridine (**S2.4**).

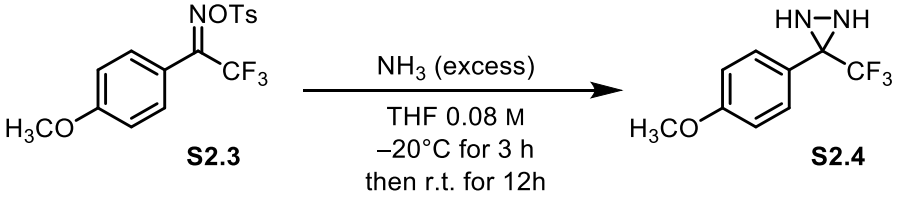

Tosyl oxime **S2.3** (856 mg, 2.29 mmol, 1 equiv.) was transferred to a flame-dried 3-neck flask under argon in anhydrous THF (0.08 M) and cooled to –20 °C. Anhydrous gaseous ammonia was bubbled into the stirred solution for 3 h. Then, the reaction was left stirring for 12 h, during which time it was allowed to warm from –20 °C to room temperature. The mixture was quenched with sat. aq. NH_4Cl and extracted with diethyl ether (3 times). The combined organic layers were washed with brine and then dried with sodium sulfate, filtered, and concentrated to afford the desired crude diaziridine **S2.4** as a colourless solid, which was submitted to the next step without further purification. The analytical data were in accordance with literature.[112] ^{1}H NMR (300 MHz, $CDCl_3$) δ 7.53

(d, J = 8.7 Hz, 2H), 6.93 (d, J = 8.7 Hz, 2H), 3.83 (s, 3H), 2.75 (d, J = 8.6 Hz, 1H, NH), 2.16 (d, J = 8.6 Hz, 1H, NH). ^{19}F NMR (283 MHz, $CDCl_3$) δ –75.81.

Synthesis of 3-(4-methoxyphenyl)-3-(trifluoromethyl)-3*H*-diazirine (**D2.1**).

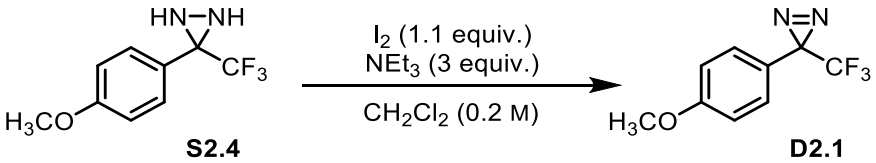

S2.4 **D2.1**

To a solution of the crude diaziridine **S2.4** (298 mg, 1.37 mmol, 1 equiv.) in CH_2Cl_2 (0.2 M) at 0 °C were added successively triethylamine (0.57 mL, 4.11 mmol, 3 equiv.) and iodine (382 mg, 1.5 mmol, 1.1 equiv.). The colored mixture was stirred at 0 °C for 1 h. The mixture was diluted with CH_2Cl_2 and washed with sat. aq. sodium thiosulfate. The aqueous layer was re-extracted with CH_2Cl_2 (3 times). Then the combined organic extracts were washed with brine and dried with sodium sulfate, filtered, and concentrated. The residue was purified by silica gel column chromatography using pentane: diethyl ether (9:1, R_f = 0.33) as eluent to afford the desired diazirine **D2.1** (291 mg, 1.34 mmol, 98%) as a yellow oil, with spectroscopic data in accordance with the literature.[112] ^{1}H NMR (500 MHz, $CDCl_3$) δ 7.15 (dd, J = 9.1, 0.7 Hz, 2H), 6.91 (d, J = 9.0 Hz, 2H), 3.81 (s, 3H).^{13}C NMR (126 MHz, $CDCl_3$) δ 160.78, 128.30, 122.41 (q, J = 274.6 Hz), 121.09, 114.51, 55.51. ^{19}F NMR (283 MHz, $CDCl_3$) δ –65.63. UV (*n*-hexane): $\lambda_{max,\ diazirine}$ = 372 nm. IR (diamond-ATR) ν: 2937, 2844, 1606, 1514, 1297, 1261, 1176, 1133, 1032, 969, 835.

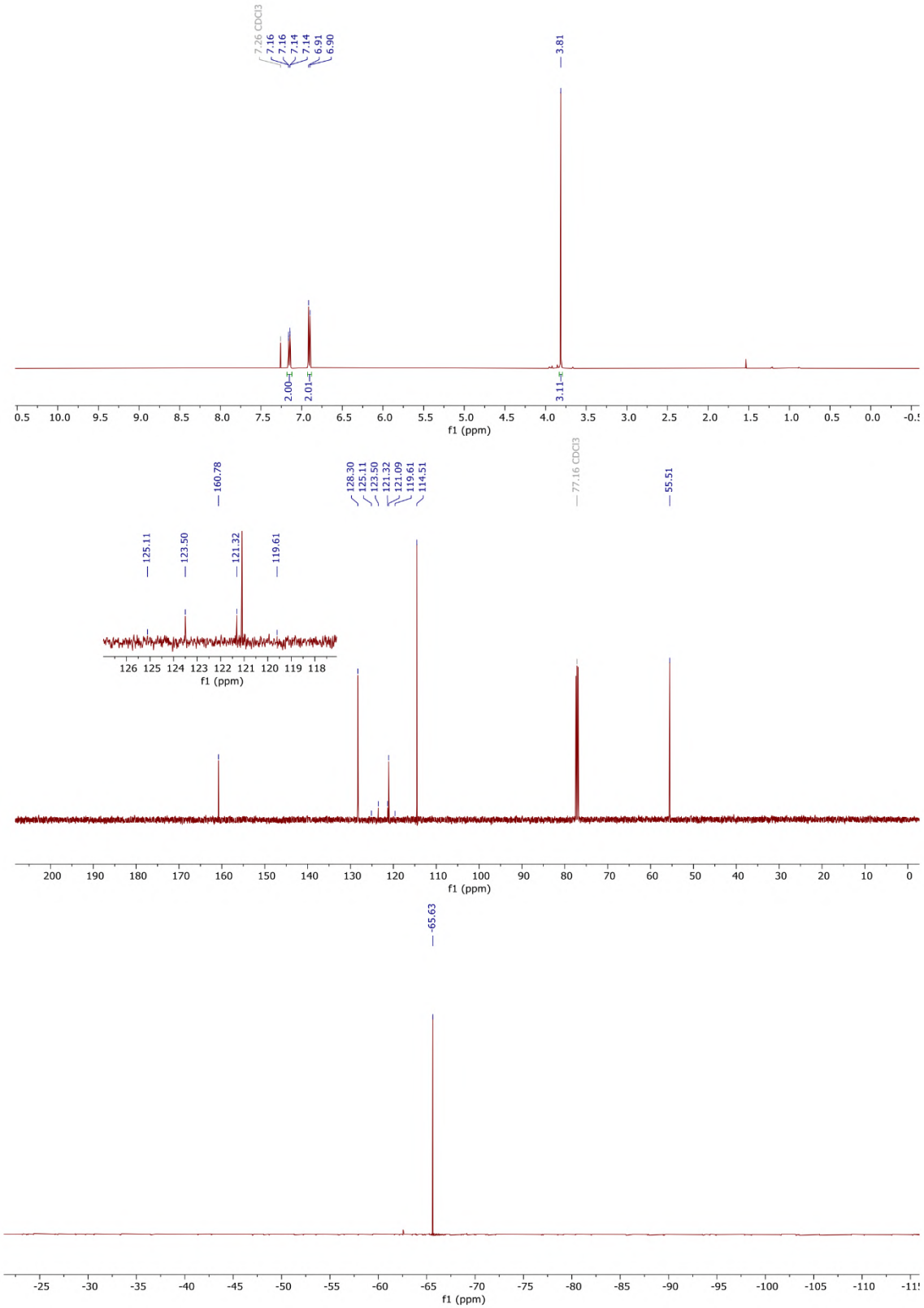

Figure S2.6 ^{1}H, ^{13}C, and ^{19}F NMR spectra of **D2.1** in $CDCl_3$.

Synthesis of 2,2,2-trifluoro-1-(4-phenoxyphenyl)ethan-1-one (**S2.5**).

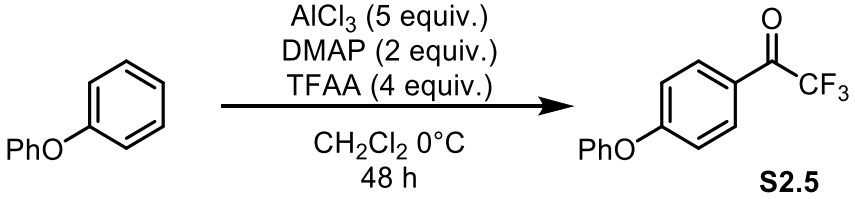

To a solution of diphenyl ether (1 g, 5.87 mmol, 1 equiv.) and 4-dimethylaminopyridine (DMAP, 1.4 g, 11.7 mmol, 2 equiv.) in dry dichloromethane (10 mL), trifluoroacetic anhydride (TFAA, 3.2 mL, 23.4 mmol, 4 equiv.) was injected dropwise at 0 °C under argon atmosphere. Then, anhydrous aluminum chloride (3.9 g, 29.35 mmol, 5 equiv.) was added to the mixture. The reaction was warmed to room temperature and stirred for 48 h. The reaction mixture was poured into ice water and extracted with dichloromethane. The organic layer was washed with brine and dried over sodium sulfate. After evaporation of the solvent the reaction afforded the desired pure product **S2.5** as a colorless oil (1.25 g, 4.69 mmol, 80%) in agreement with literature data.[139] ^{1}H NMR (300 MHz, $CDCl_3$) δ 8.05 (d, J = 8.2 Hz, 2H), 7.44 (t, J = 7.9 Hz, 2H), 7.29 – 7.21 (m, 1H), 7.10 (d, J = 7.6 Hz, 2H), 7.04 (d, J = 9.0 Hz, 2H). ^{19}F NMR (283 MHz, $CDCl_3$) δ –71.15.

Synthesis of 2,2,2-trifluoro-1-(4-phenoxyphenyl)ethan-1-one oxime (**S2.6**) (mixture of *E*-, *Z*-isomers).

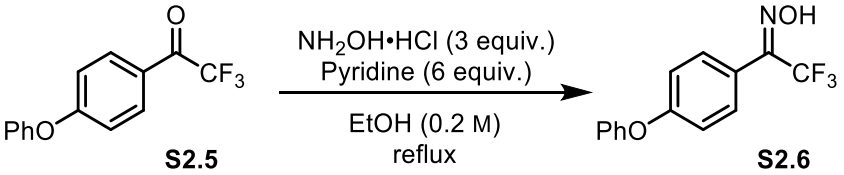

To a stirred solution of compound **S2.5** (443 mg, 1.66 mmol, 1 equiv,) in ethanol (0.2 M), hydroxylamine hydrochloride (1.15 g, 16.5 mmol, 3 equiv.) and pyridine (2.6 mL, 33 mmol, 6 equiv.) were added and the reaction mixture was heated to reflux for 21 h. The mixture was then cooled to room temperature and the mixture was treated with 2 M HCl and extracted with diethyl ether (3 times). The combined organic layers were washed with distilled water until the pH of the washing layer became neutral, and then dried with sodium sulfate, filtered, and concentrated. The residue was dried under high vacuum for a prolonged time to afford the desired crude oxime **S2.6** (as a mixture of

geometric isomers) as a yellow oil (464 mg). The compound was submitted to the next step without further purification. ^{1}H NMR (300 MHz, $CDCl_3$) δ 8.30 (d, *J* = 8.9 Hz, 2H), 8.25 (d, *J* = 9.0 Hz, 1.6H, minor isomer), 7.68 (d, *J* = 8.6 Hz, 3.6H, major and minor isomers). ^{19}F NMR (283 MHz, $CDCl_3$) δ –62.28, –66.06.

Synthesis of 2,2,2-trifluoro-1-(4-phenoxyphenyl)ethan-1-one *O*-tosyl oxime (**S2.7**) (mixture of *E*-, *Z*-isomers).

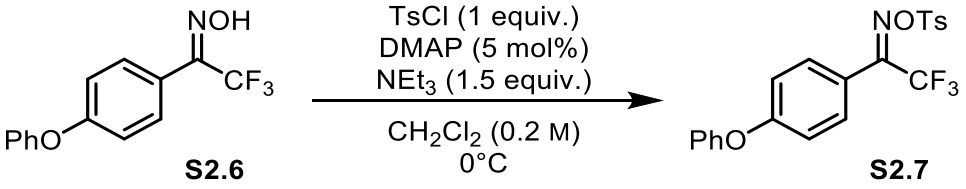

Compound **S2.6** (464 mg, 1.65 mmol, 1 equiv.) was dissolved in CH_2Cl_2 (0.2 M), and triethylamine (0.35 mL, 2.47 mmol, 1.5 equiv.), DMAP (10 mg, 0.082 mmol, 5 mol%) and tosyl chloride (315 mg, 1.65 mmol, 1 equiv.) were successively added at 0 °C. The ice bath was removed after 5 min, and the reaction mixture was stirred at room temperature for 1 h. The mixture was then treated with sat. aq. NH_4Cl and extracted with CH_2Cl_2. The combined organic extracts were dried with sodium sulfate, filtered, and concentrated to afford the desired crude tosyl oxime **S2.7** as a yellow solid, which was submitted to the next step without further purification. ^{1}H NMR (300 MHz, $CDCl_3$) δ 7.89 (d, *J* = 8.3 Hz, 2.90H, major and minor isomers), 7.48 – 7.33 (m, 9H, major and minor isomers), 7.24 – 7.16 (m, 1.55H, minor isomer), 7.14 – 6.92 (m, 6H, major and minor isomers), 2.48 (s, 3H), 2.46 (s, 1.39H, minor isomer). ^{19}F NMR (283 MHz, $CDCl_3$) δ –61.45 (minor isomer), –66.26.

Synthesis of 3-(4-phenoxyphenyl)-3-(trifluoromethyl)diaziridine (**S2.8**).

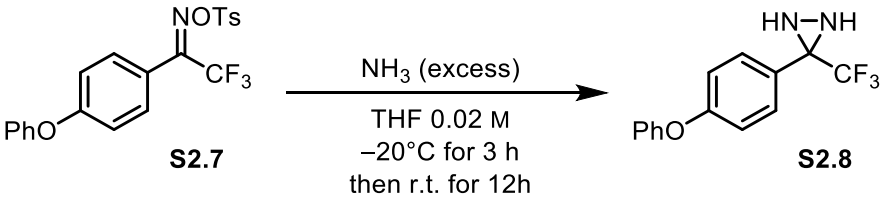

Tosyl oxime **S2.7** (714 mg, 1.60 mmol, 1 equiv.) was transferred to a flame-dried 3-neck flask under argon in anhydrous THF (0.02 M) and cooled to –20°C. Anhydrous gaseous ammonia was bubbled into the stirred solution for 3 h. Then, the reaction was left stirring for 12 h, during which time it was allowed to warm from –20°C to room

temperature. The mixture was quenched with sat. aq. NH_4Cl and extracted with diethyl ether (3 times). The combined organic layers were washed with brine and then dried with sodium sulfate, filtered and concentrated to afford the desired crude diaziridine **S2.8**, which was submitted to the next step without further purification.^{19}F NMR (283 MHz, $CDCl_3$) δ –75.69.

Synthesis of 3-(4-phenoxyphenyl)-3-(trifluoromethyl)-3*H*-diazirine (**D2.2**).

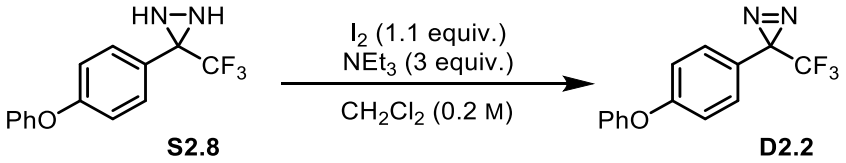

S2.8 **D2.2**

To a solution of the crude diaziridine **S2.8** in CH_2Cl_2 (0.2 M) at 0 °C were added successively triethylamine (3 equiv.) and iodine (1.1 equiv.). The colored mixture was stirred at 0 °C for 1 h. The mixture was diluted with CH_2Cl_2 and washed with sat. aq. sodium thiosulfate. The aqueous layer was re-extracted with CH_2Cl_2 (3 times). Then the combined organic extracts were washed with brine and dried with sodium sulfate, filtered, and concentrated. The residue was purified by silica gel column chromatography using pentane as eluent (R_f = 0.44) to afford the desired diazirine **D2.2** (216 mg, 0.77 mmol, 48% over two steps) as a pale-yellow oil. ^{1}H NMR (500 MHz, $CDCl_3$) δ 7.40 – 7.33 (m, 2H), 7.19 – 7.12 (m, 3H), 7.04 – 7.01 (m, 2H), 7.01 – 6.97 (m, 2H). ^{13}C NMR (126 MHz, $CDCl_3$) δ 159.09, 156.11, 130.14, 128.45, 124.40, 123.34, 119.83, 118.56, 29.86. ^{19}F NMR (471 MHz, $CDCl_3$) δ –65.52. UV (*n*-hexane): $\lambda_{max,\ diazirine}$ = 369 nm. IR (diamond-ATR) ν: 3044, 2927, 2856, 1614, 1589, 1512, 1489, 1344, 1232, 1186, 1148, 937, 691. GC–MS *m/z* (% relative intensity) [ion]: 291 (70) $[M - N_2 + CH_3CN]^+$, 250 (40) $[M - N_2]^+$, 157 (100) $[C_8H_4F_3]^+$, 137 (10) $[C_8H_3F_2]^+$, 76 (45) $[C_6H_4]^+$. [M = $C_{14}H_9F_3N_2O$ (278.06)].

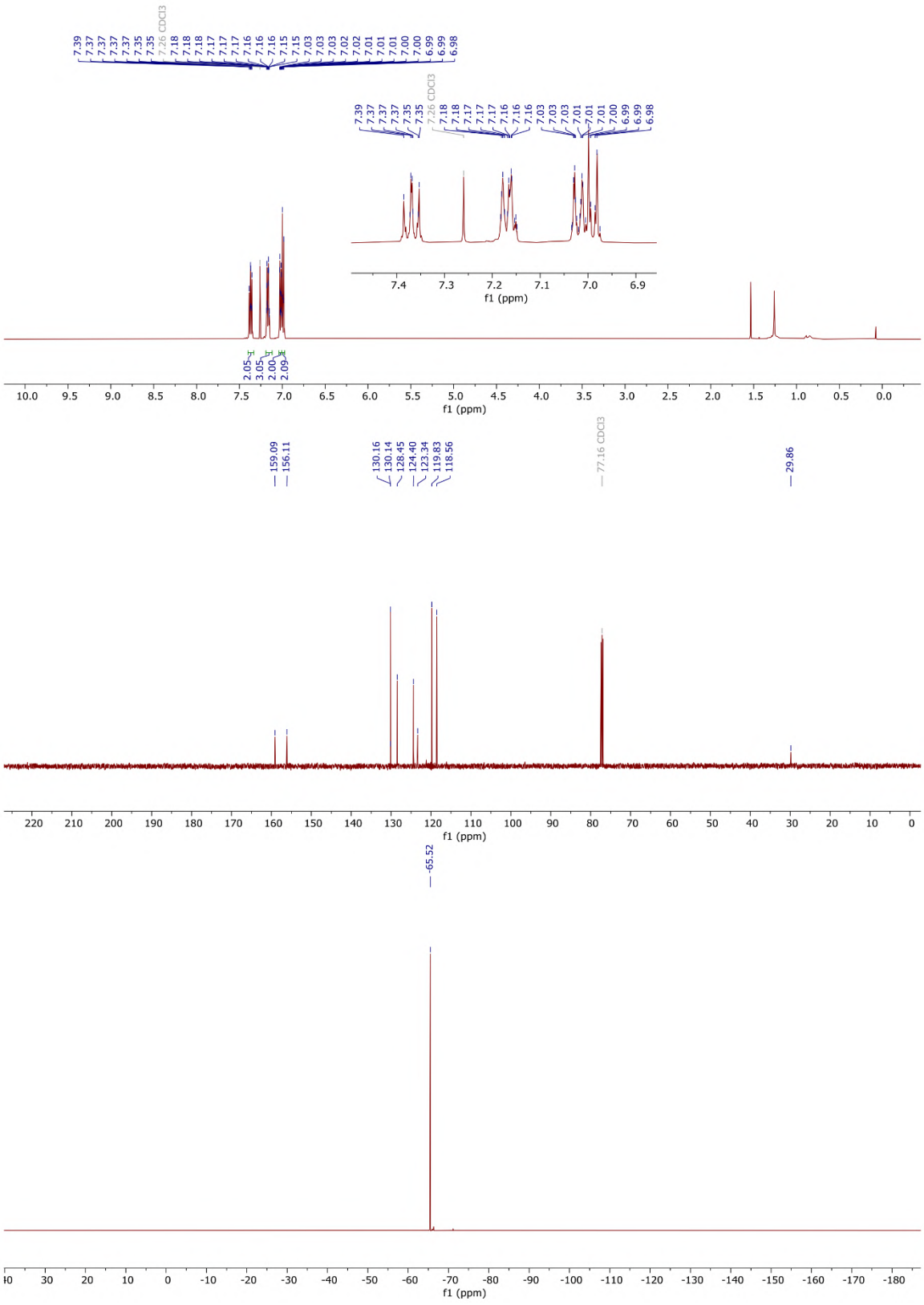

Figure S2.7 ^{1}H, ^{13}C, and ^{19}F NMR spectra of **D2.2** in $CDCl_3$.

Synthesis of 1-(4-(tert-butyl)phenyl)-2,2,2-trifluoroethan-1-one (**S2.9**).

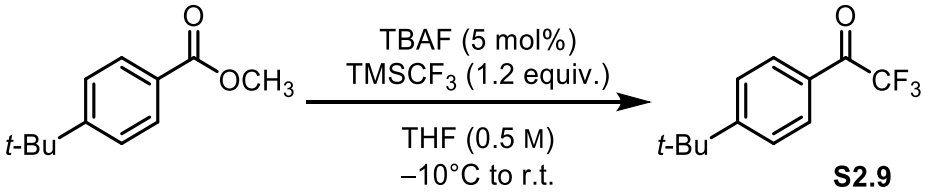

In a flame-dried flask, to a stirring solution of commercially available methyl 4-(tert-butyl)benzoate (1.0 mL, 5.2 mmol, 1 equiv.) in distilled THF (8.2 mL) under argon atmosphere at –10 °C, $TMSCF_3$ (0.92 mL, 6.24 mmol, 1.2 equiv.) and then TBAF (0.26 mL, 1 M in THF, 5 mol%) were slowly added dropwise. The resulting solution was allowed to warm to room temperature with continued stirring for an hour and the colour changed from transparent to orange. The reaction was left stirring for 16 h and then quenched with NH_4Cl, extracted with diethyl ether (2 times) and the combined organic extracts were washed with brine and dried with sodium sulfate. The filtered and concentrated orange oil was purified by silica gel column chromatography using pentane: chloroform (6:4, R_f = 0.62) as eluent to afford the desired ketone **S2.9** (446 mg, 1.94 mmol, 37%) as a yellow oil, in accordance with literature data.[140] ^{1}H NMR (300 MHz, $CDCl_3$) δ 8.02 (d, *J* = 8.8 Hz, 2H), 7.56 (d, *J* = 8.8 Hz, 2H), 1.36 (s, 9H). ^{19}F NMR (283 MHz, $CDCl_3$) δ –71.34.

Synthesis of 1-(4-(tert-butyl)phenyl)-2,2,2-trifluoroethan-1-one oxime (**S2.10**) (mixture of *E*-, *Z*-isomers).

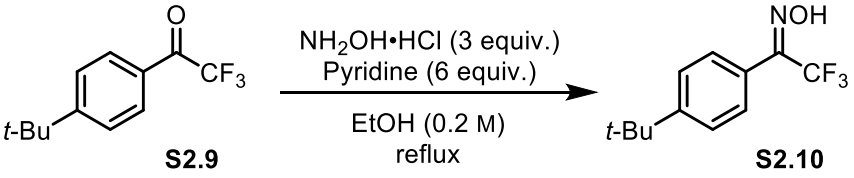

To a stirred solution of compound **S2.9** (400 mg, 1.74 mmol, 1 equiv,) in ethanol (0.2 M), hydroxylamine hydrochloride (363 mg, 5.22 mmol, 3 equiv.) and pyridine (0.9 mL, 10.42 mmol, 6 equiv.) were added and the reaction mixture was heated to reflux for 21 h. The mixture was then cooled to room temperature and the mixture was treated with 2 M HCl and extracted with diethyl ether (3 times). The combined organic layers were washed with distilled water until the pH of the washing layer became neutral, and then dried with sodium sulfate, filtered, and concentrated. The residue was dried under high

vacuum for a prolonged time to afford the desired crude oxime **S2.10** (as a mixture of geometric isomers) as a white solid (410 mg, 96%). The compound was submitted to the next step without further purification. ^{1}H NMR (300 MHz, $CDCl_3$) δ7.47 (d, J = 2.3 Hz, 2H), 7.43 (s, 2H), 1.33 (s, 9H). ^{19}F NMR (283 MHz, $CDCl_3$) δ –62.36 (minor isomer), –66.44.

Synthesis of 1-(4-(tert-butyl)phenyl)-2,2,2-trifluoroethan-1-one *O*-tosyl oxime (**S2.11**) (mixture of *E*-, *Z*-isomers).

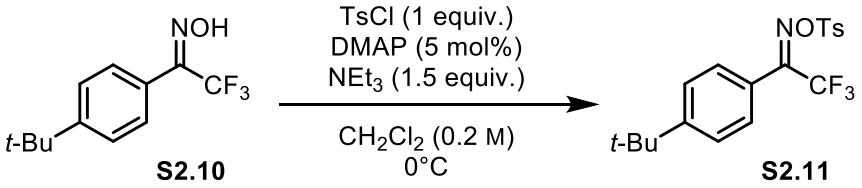

Compound **S2.10** (410 mg, 1.67 mmol, 1 equiv.) was dissolved in CH_2Cl_2 (0.8 mL), and triethylamine (0.35 mL, 2.5 mmol, 1.5 equiv.), DMAP (10 mg, 0.083 mmol, 5 mol%) and tosyl chloride (319 mg, 1.67 mmol, 1 equiv.) were successively added at 0 °C. The ice bath was removed after 5 min, and the reaction mixture was stirred at room temperature for 1 h. The mixture was then treated with sat. aq. NH_4Cl and extracted with CH_2Cl_2. The combined organic extracts were dried with magnesium sulfate, filtered, and concentrated to afford the desired crude tosyl oxime **S2.11** (587 mg, 91%) as a yellow oil, which was submitted to the next step without further purification. ^{1}H NMR (300 MHz, $CDCl_3$) δ 7.95 – 7.84 (m, 2H), 7.80 (d, J = 8.3 Hz, 2H), 7.48 (d, J = 8.8 Hz, 2H), 7.42 – 7.29 (m, 2H), 2.45 (s, 3H), 1.34 (s, 9H). ^{19}F NMR (283 MHz, $CDCl_3$) δ –61.49 (minor isomer), –66.46.

Synthesis of 3-(4-(tert-butyl)phenyl)-3-(trifluoromethyl)diaziridine (**S2.12**).

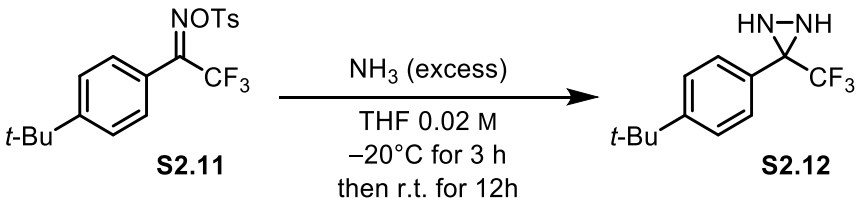

Tosyl oxime **S2.11** (533 mg, 1.3 mmol, 1 equiv.) was transferred to a flame-dried 3-neck flask under argon in anhydrous THF (65 mL) and cooled to –20°C. Anhydrous gaseous ammonia was bubbled into the stirred solution for 3 h. Then, the reaction was left stirring for 12 h, during which time it was allowed to warm from –20°C to room

temperature. The mixture was quenched with sat. aq. NH_4Cl and extracted with CH_2Cl_2 (3 times). The combined organic layers were washed with brine and then dried with sodium sulfate, filtered and concentrated to afford the desired crude diaziridine **S2.12**, which was submitted to the next step without further purification. ^{1}H NMR (300 MHz, $CDCl_3$) δ 7.54 (d, *J* = 8.3 Hz, 2H), 7.43 (d, *J* = 8.7 Hz, 2H), 2.76 (d, *J* = 9.1 Hz, 1H), 2.19 (d, *J* = 9.1 Hz, 1H), 1.32 (s, 9H). ^{19}F NMR (283 MHz, $CDCl_3$) δ –75.59.

Synthesis of 3-(4-(tert-butyl)phenyl)-3-(trifluoromethyl)-3*H*-diazirine (**D2.3**).

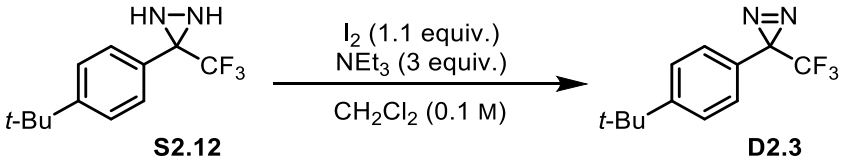

To a solution of the crude diaziridine **S2.12** (318 mg, 1.3 mmol, 1 equiv.) in CH_2Cl_2 (10 mL) at 0 °C were added successively triethylamine (0.54 mL, 3.9 mmol, 3 equiv.) and iodine (363 mg, 1.43 mmol, 1.1 equiv.). The colored mixture was stirred at 0°C for 1 h. The mixture was diluted with CH_2Cl_2 and washed with sat. aq. sodium thiosulfate. The aqueous layer was re-extracted with CH_2Cl_2 (3 times). Then the combined organic extracts were washed with brine and dried with sodium sulfate, filtered, and concentrated. The residue was purified by silica gel column chromatography using pentane as eluent to afford the desired diazirine **D2.3** (282 mg, 1.16 mmol, 80%) as a pale-yellow oil. ^{1}H NMR (500 MHz, $CDCl_3$) δ 7.41 (d, *J* = 8.6 Hz, 2H), 7.13 (d, *J* = 8.1 Hz, 2H), 1.31 (s, 9H). ^{13}C NMR (126 MHz, $CDCl_3$) δ 153.08, 126.36, 126.32, 125.96, 122.38 (q, *J* = 274.7, 274.3 Hz), 34.88, 31.27, 29.87. ^{19}F NMR (283 MHz, $CDCl_3$) δ –65.30. UV (*n*-hexane): $\lambda_{max,\ diazirine}$ = 360 nm. IR (diamond-ATR) ν: 2960, 2925, 2855, 1616, 1514, 1464, 1344, 1238, 1188, 1158, 941, 703. HRMS (ESI-) m/z [M – N_2 + HO^-] calculated for $[C_{12}H_{14}F_3O]^-$: 231.1002, found: 231.1006.

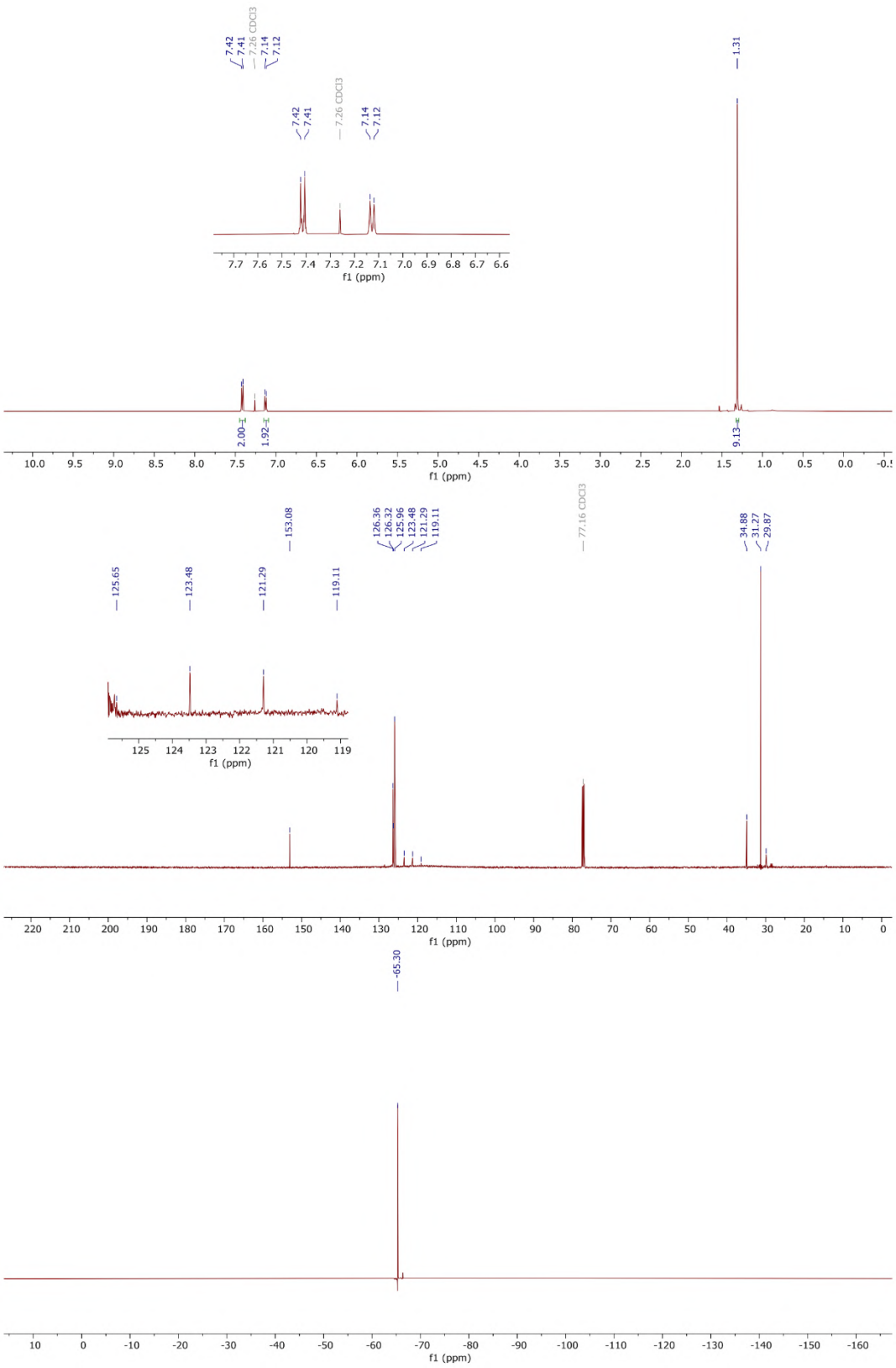

Figure S2.8 ^{1}H, ^{13}C, and ^{19}F NMR spectra of **D2.3** in $CDCl_3$.

Synthesis of 1-(4-bromophenyl)-2,2,2-trifluoroethan-1-one (**S2.13**).

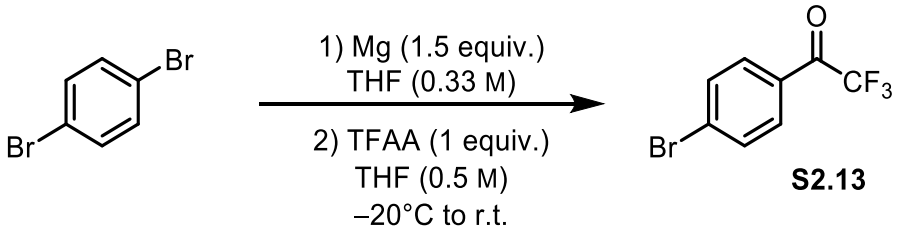

To a suspension of magnesium turnings (250 mg, 10.4 mmol, 1.5 equiv.) in anhydrous THF (11 mL) stirred under argon was added drop wise a solution of 1,4-dibromobenzene (1.63 g, 6.9 mmol, 1 equiv.) in anhydrous THF (9 mL). The reaction was left for 2 h stirring and the product, (4-bromophenyl)magnesium bromide (16 mL of 0.33 M solution in THF fresh-made, 5.4 mmol) was added drop wise to a solution of trifluoroacetic anhydride (TFAA, 0.83 mL, 5 mmol, 1 equiv.) in anhydrous THF at –20 °C. The reaction was stirred at –20 °C for 2 h, then it was quenched with NH_4Cl and it was extracted with diethyl ether (× 3) and the combined organic layers were washed with brine and dried over magnesium sulfate. The crude compound **S2.13** was purified by silica gel column chromatography using petroleum ether: EtOAc (9:1, R_f = 0.40) as eluent to afford the desired ketone **S2.13** (898 mg, 3.55 mmol, 71%) as a pale-yellow oil with spectroscopic data in accordance with the literature.[141] ^{1}H NMR (300 MHz, $CDCl_3$) δ 7.93 (d, *J* = 8.7 Hz, 2H), 7.71 (d, *J* = 8.7 Hz, 2H). ^{19}F NMR (283 MHz, $CDCl_3$) δ –71.54.

Synthesis of 1-(4-bromophenyl)-2,2,2-trifluoroethan-1-one oxime (**S2.14**) (mixture of *E*-, *Z*-isomers).

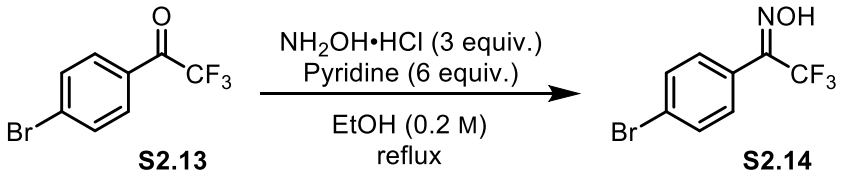

To a stirred solution of compound **S2.13** (815 mg, 3.22 mmol, 1 equiv.) in ethanol (0.2 M), hydroxylamine hydrochloride (672 mg, 9.66 mmol, 3 equiv.) and pyridine (1.5 mL, 19.3 mmol, 6 equiv.) were added and the reaction mixture was heated to reflux for 21 h. The mixture was then cooled to room temperature and the mixture was treated with 2 M HCl and extracted with diethyl ether (3 times). The combined organic layers were washed with distilled water until the pH of the washing layer became neutral, and then dried with sodium sulfate, filtered, and concentrated. The residue was dried under high

vacuum for a prolonged time to afford the desired crude oxime **S2.14** (as a mixture of geometric isomers) as a yellow oil, with spectroscopic data in accordance with the literature.[142] The compound was submitted to the next step without further purification. ^{1}H NMR (300 MHz, $CDCl_3$) δ 8.61 (s, OH), 8.34 (s, OH, minor isomer), 7.60–7.53 (m, 2H), 7.40–7.37 (m, 2H). ^{19}F NMR (283 MHz, $CDCl_3$) δ ─62.32, ─66.60 (minor isomer).

Synthesis of 1-(4-bromophenyl)-2,2,2-trifluoroethan-1-one *O*-tosyl oxime (**S2.15**) (mixture of *E*-, *Z*-isomers).

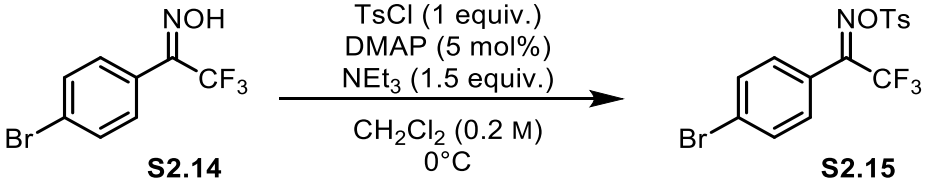

Compound **S2.14** (787 mg, 2.94 mmol, 1 equiv.) was dissolved in CH_2Cl_2 (0.2 M), and triethylamine (0.20 mL, 4.41 mmol, 1.5 equiv.), DMAP (18 mg, 0.14 mmol, 5 mol%) and tosyl chloride (560 mg, 2.94 mmol, 1 equiv.) were successively added at 0 °C. The ice bath was removed after 5 min, and the reaction mixture was stirred at room temperature for 1 h. The mixture was then treated with sat. aq. NH_4Cl and extracted with CH_2Cl_2. The combined organic extracts were dried with sodium sulfate, filtered, and concentrated to afford the desired crude tosyl oxime **S2.15** as a white solid, with spectroscopic data in accordance with the literature.[142] The compound was submitted to the next step without further purification. ^{1}H NMR (300 MHz, $CDCl_3$) δ 7.87 (d, J = 8.3 Hz, 2H), 7.58 (d, J = 8.6 Hz, 2H), 7.37 – 7.42 (m, 2H), 7.27 (d, J = 8.6 Hz, 2H), 2.46 (s, 3H). ^{19}F NMR (283 MHz, $CDCl_3$) δ –61.53 (minor isomer), –66.70.

Synthesis of 3-(4-bromophenyl)-3-(trifluoromethyl)diaziridine (**S2.16**).

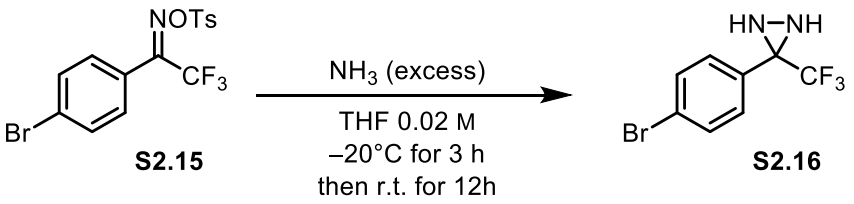

Tosyl oxime **S2.15** (1.22 g, 2.89 mmol, 1 equiv.) was transferred to a flame-dried 3-neck flask under argon in anhydrous THF (0.02 M) and cooled to –20°C. Anhydrous gaseous ammonia was bubbled into the stirred solution for 3 h. Then, the reaction was left stirring for 12 h, during which time it was allowed to warm from –20°C to room temperature. The mixture was quenched with sat. aq. NH_4Cl and extracted with diethyl ether (3 times). The combined organic layers were washed with brine and then dried with sodium sulfate, filtered and concentrated to afford the desired crude diaziridine **S2.16** as a colourless solid, which was submitted to the next step without further purification. The analytical data were in accordance with literature.[142] ^{1}H NMR (300 MHz, $CDCl_3$) δ 7.56 (d, J = 8.6 Hz, 2H), 7.49 (d, J = 8.6 Hz, 2H), 2.21 (d, J = 8.4 Hz, 1H), 2.81 (d, J = 8.4 Hz, 1H). ^{19}F NMR (283 MHz, $CDCl_3$) δ –75.48.

Synthesis of 3-(4-bromophenyl)-3-(trifluoromethyl)-3*H*-diazirine (**D2.5**).

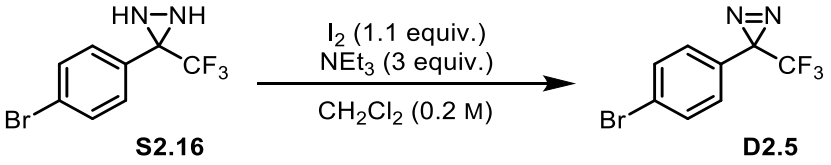

To a solution of the crude diaziridine **S2.16** (774 mg, 2.89 mmol, 1 equiv.) in CH_2Cl_2 (0.2 M) at 0 °C were added successively triethylamine (1.21 mL, 8.69 mmol, 3 equiv.) and iodine (809 mg, 3.18 mmol, 1.1 equiv.). The colored mixture was stirred at 0 °C for 1 h. The mixture was diluted with CH_2Cl_2 and washed with sat. aq. sodium thiosulfate. The aqueous layer was re-extracted with CH_2Cl_2 (3 times). Then the combined organic extracts were washed with brine and dried with sodium sulfate, filtered, and concentrated. The residue was purified by silica gel column chromatography using pentane as eluent (R_f = 0.75) to afford the desired diazirine **D2.5** (742 mg, 2.80 mmol, 96%) as a pale-yellow oil, with spectroscopic data in accordance with the literature.[142] ^{1}H NMR (500 MHz, $CDCl_3$) δ7.54 (d, J = 8.7 Hz, 2H), 7.07 (d, J = 8.1 Hz, 2H).^{13}C NMR

(126 MHz, $CDCl_3$) δ 132.13, 124.28, 121.92 (q, J = 274.8 Hz), 28.22 (q, J = 43.2, 41.9 Hz). ^{19}F NMR (283 MHz, $CDCl_3$) δ –65.33. IR (diamond-ATR) ν: 2928, 1614, 1497, 1339, 1232, 1185, 1151, 936, 814, 747, 532.

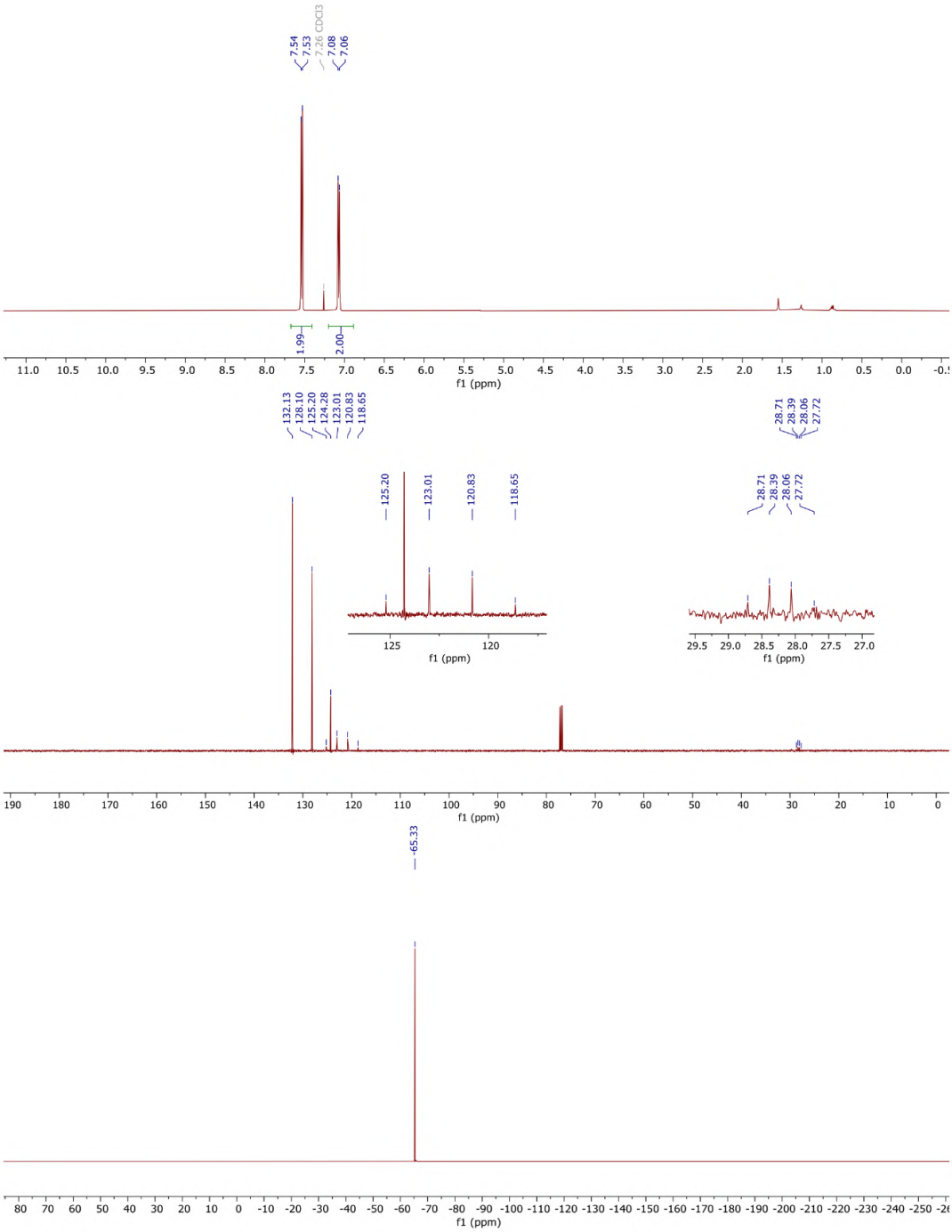

Figure S2.9 ^{1}H, ^{13}C, and ^{19}F NMR spectra of **D2.5** in $CDCl_3$.

Synthesis of 2,2,2-trifluoro-1-(3-methoxyphenyl)ethan-1-one (**S2.17**).

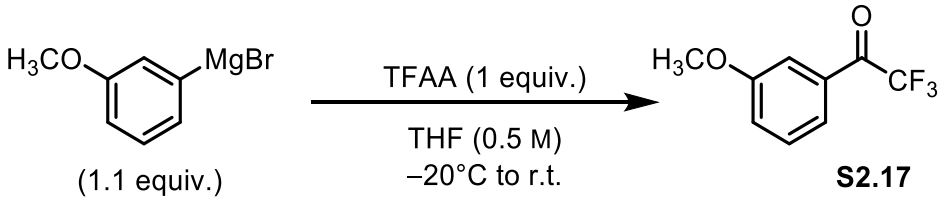

In a round bottom flask equipped with a magnetic stir bar and a condenser, to a stirring mixture of trifluoroacetic anhydride (0.66 mL, 4.76 mmol, 1 equiv.) in distilled THF (0.5 M) at –20°C, 3-methoxyphenyl magnesium Grignard (5.2 mL, 1 M in THF, 1.1 equiv.) was added. The mixture was stirred for 4 h and then quenched with NH_4Cl and extracted with EtOAc (3 times). Then the combined organic extracts were washed with brine and dried with magnesium sulfate, filtered, and concentrated. The crude compound **S2.17** was purified by silica gel column chromatography using petroleum ether: EtOAc (8:2, R_f= 0.6) as eluent to afford the desired ketone **S2.17** (766 mg, 3.75 mmol, 79%) as a yellow oil. ^{1}H NMR (300 MHz, $CDCl_3$) δ 7.66 (d, *J* = 7.7 Hz, 1H), 7.57 (s, 1H), 7.46 (t, *J* = 8.0 Hz, 1H), 7.03 – 6.88 (m, 1H), 3.88 (s, 3H). ^{19}F NMR (283 MHz, $CDCl_3$) δ –71.22.

Synthesis of 2,2,2-trifluoro-1-(3-methoxyphenyl)ethan-1-one oxime (**S2.18**) (mixture of *E*-, *Z*-isomers).

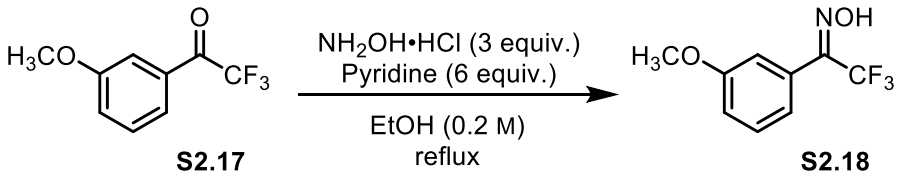

To a stirred solution of compound **S2.17** (673 mg, 3.3 mmol, 1 equiv,) in ethanol (0.2 M), hydroxylamine hydrochloride (688 mg, 9.9 mmol, 3 equiv.) and pyridine (1.6 mL, 19.8 mmol, 6 equiv.) were added and the reaction mixture was heated to reflux for 1 h. The mixture was then cooled to room temperature and the mixture was treated with 2 M HCl and extracted with diethyl ether (3 times). The combined organic layers were washed with distilled water until the pH of the washing layer became neutral, and then dried with sodium sulfate, filtered, and concentrated. The residue was dried under high vacuum for a prolonged time to afford the desired crude oxime **S2.18** (as a mixture of geometric isomers) as a white solid (720 mg). The compound was submitted to the next step without further purification. The analytical data were in accordance with literature.[99]

^{1}H NMR (300 MHz, $CDCl_3$) δ 9.64 (br-s, 1H), 9.33 (s, 0.3H, minor isomer), 7.47 – 7.28 (m, 1H and 0.3H minor isomer), 7.14 – 6.80 (m, 3H and 0.9H minor isomer), 3.83 (s, 3H), 3.78 (s, 1H, minor isomer).^{19}F NMR (283 MHz, $CDCl_3$) δ –62.37, –66.67.

Synthesis of 2,2,2-trifluoro-1-(3-methoxyphenyl)ethan-1-one *O*-tosyl oxime (**S2.19**) (mixture of *E*-, *Z*-isomers).

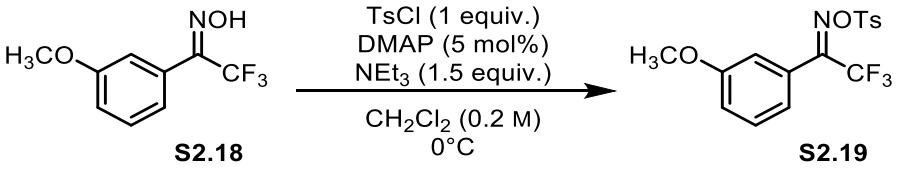

S2.18 **S2.19**

Compound **S2.18** (720 mg, 3.3 mmol, 1 equiv.) was dissolved in CH_2Cl_2 (0.2 M), and triethylamine (0.69 mL, 4.95 mmol, 1.5 equiv.), DMAP (20 mg, 0.165 mmol, 5 mol%) and tosyl chloride (629 mg, 3.3 mmol, 1 equiv.) were successively added at 0 °C. The ice bath was removed after 5 min, and the reaction mixture was stirred at room temperature for 1 h. The mixture was then treated with sat. aq. NH_4Cl and extracted with CH_2Cl_2. The combined organic extracts were dried with sodium sulfate, filtered, and concentrated to afford the desired crude tosyl oxime **S2.19** (1.05 g) as a yellow oil, which was submitted to the next step without further purification. The analytical data were in accordance with literature.[99] ^{1}H NMR (300 MHz, $CDCl_3$) δ 7.92 – 7.85 (m, 2H), 7.41 – 7.36 (m, 2H), 7.34 – 7.29 (m, 1H), 7.08 – 7.02 (m, 1H), 6.97 – 6.91 (m, 1H), 6.90 – 6.84 (m, 1H), 3.82 (s, 3H), 2.48 (s, 3H). ^{19}F NMR (283 MHz, $CDCl_3$) δ –61.51 (minor isomer), –66.93.

Synthesis of 3-(3-methoxyphenyl)-3-(trifluoromethyl)diaziridine (**S2.20**).

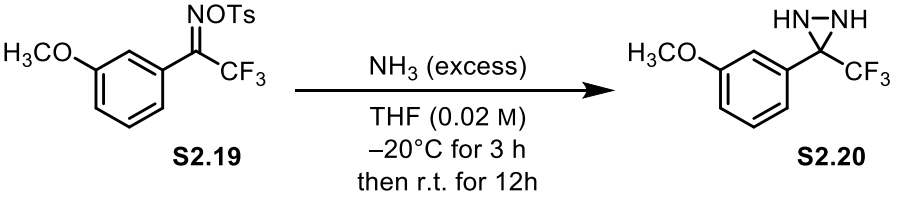

S2.19 **S2.20**

Tosyl oxime **S2.19** (1 g, 2.68 mmol, 1 equiv.) was transferred to a flame-dried 3-neck flask under argon in anhydrous THF (30 mL) and cooled to –20°C. Anhydrous gaseous ammonia was bubbled into the stirred solution for 3 h. Then, the reaction was left stirring for 12 h, during which time it was allowed to warm from –20°C to room temperature. The mixture was quenched with sat. aq. NH_4Cl and extracted with CH_2Cl_2

(3 times). The combined organic layers were washed with brine and then dried with sodium sulfate, filtered and concentrated to afford the desired crude diaziridine **S2.20**, which was submitted to the next step without further purification. The analytical data were in accordance with literature.[99] ^{1}H NMR (300 MHz, $CDCl_3$) δ 7.34 (t, *J* = 8.0 Hz, 1H), 7.20 (d, *J* = 7.7 Hz, 1H), 7.15 (s, 1H), 7.02 – 6.93 (m, 1H), 3.83 (s, 3H).^{19}F NMR (283 MHz, $CDCl_3$) δ –75.49.

Synthesis of 3-(3-methoxyphenyl)-3-(trifluoromethyl)-3*H*-diazirine (**D2.8**).

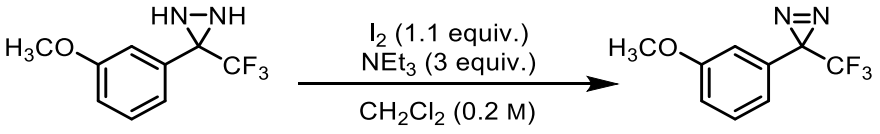

S2.20 **D2.8**

To a solution of the crude diaziridine **S2.20** (585 mg, 2.68 mmol, 1 equiv.) in CH_2Cl_2 (0.2 M) at 0 °C were added successively triethylamine (1.1 mL, 8.04 mmol, 3 equiv.) and iodine (748 mg, 2.94 mmol, 1.1 equiv.). The colored mixture was stirred at 0 °C for 1 h. The mixture was diluted with CH_2Cl_2 and washed with sat. aq. sodium thiosulfate. The aqueous layer was re-extracted with CH_2Cl_2 (3 times). Then the combined organic extracts were washed with brine and dried with sodium sulfate, filtered, and concentrated. The residue was purified by silica gel column chromatography using pentane: EtOAc (9:1) as eluent to afford the desired diazirine **D2.8** (241 mg, 1.1 mmol, 42%) as a pale-yellow oil, in accordance with literature data.[99] ^{1}H NMR (500 MHz, $CDCl_3$) δ 7.31 (t, *J* = 8.0 Hz, 1H), 6.95 (ddd, *J* = 8.3, 2.6, 0.9 Hz, 1H), 6.78 (ddq, *J* = 7.8, 1.7, 0.9 Hz, 1H), 6.69 (t, *J* = 2.3 Hz, 1H), 3.81 (s, 3H). ^{13}C NMR (126 MHz, $CDCl_3$) δ 159.94, 130.70, 130.17, 122.25 (d, *J* = 274.7 Hz), 118.89, 115.35, 112.39, 55.48, 29.86. ^{19}F NMR (283 MHz, $CDCl_3$) δ –65.16. UV (*n*-hexane): $\lambda_{max,\ diazirine}$ = 355 nm. IR (diamond-ATR) ν: 2959, 2929, 2874, 2860, 1606, 1462, 1265, 1247, 1115, 1100, 1019, 729.

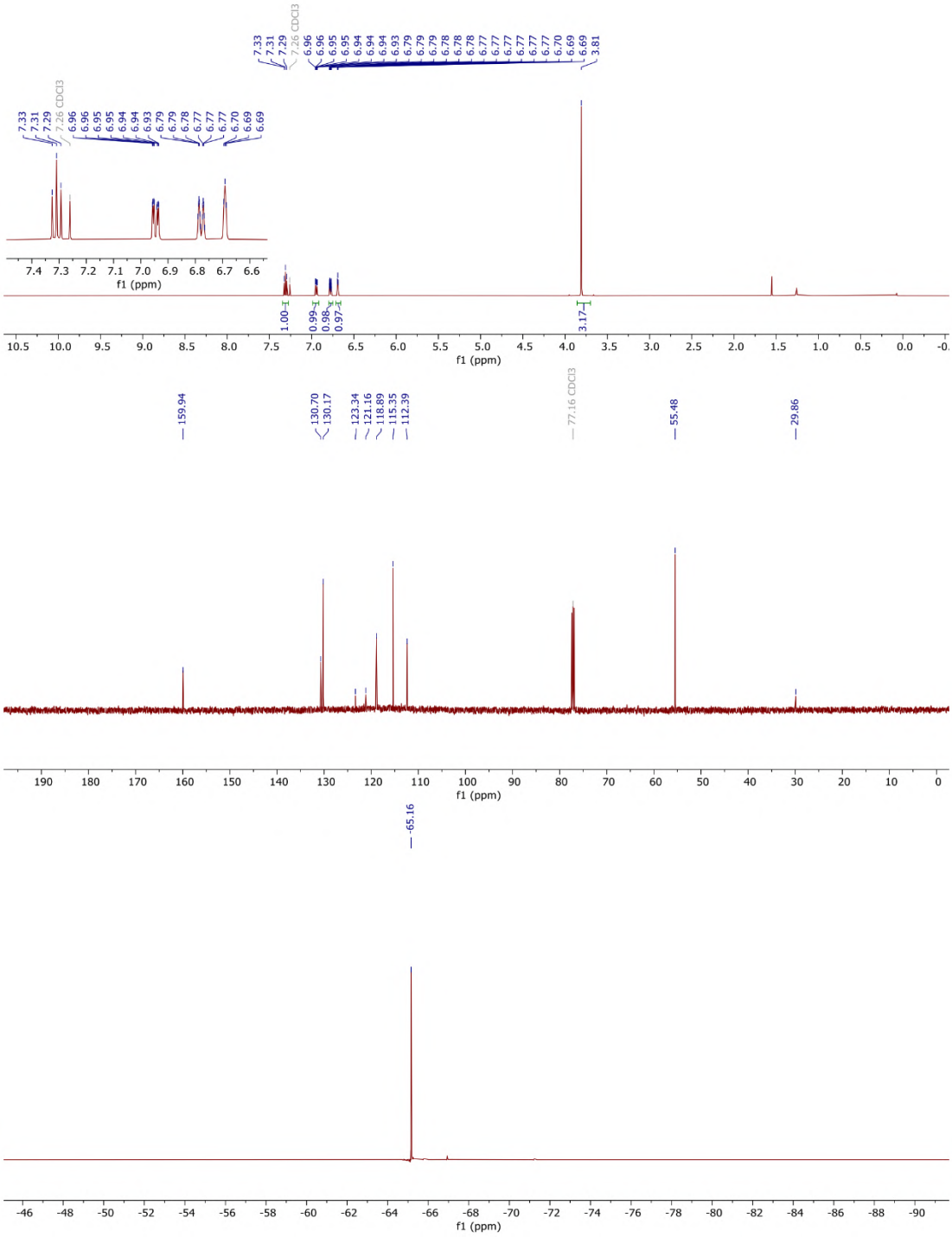

Figure S2.10 ^{1}H, ^{13}C, and ^{19}F NMR spectra of **D2.8** in $CDCl_3$.

Synthesis of 3-(3-hydroxyphenyl)-3-(trifluoromethyl)-3*H*-diazirine (**D2.9**).

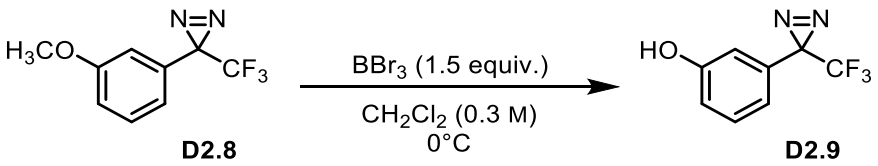

D2.8 **D2.9**

The reaction was carried out in dim light: to a solution of compound **D2.8** (400 mg, 1.85 mmol, 1 equiv.) in CH_2Cl_2 (0.3 M) at 0 °C were added successively a solution of 1 M boron tribromide in CH_2Cl_2 (2.8 mL, 2.78 mmol, 1.5 equiv.). The colored mixture was stirred at 0 °C and slowly warm up to room temperature for 4 h. Water (5 mL) was added to the reaction mixture followed by CH_2Cl_2. The aqueous layer was re-extracted with CH_2Cl_2 (2 times). Then the combined organic extracts were dried with sodium sulfate, filtered, and concentrated. The residue was characterized directly without further purification, affording the desired diazirine **D2.9** (365 mg, 1.81 mmol, 98%) as a brown-yellow oil. The analytical data were in accordance with literature.[99] ^{1}H NMR (500 MHz, CD_2Cl_2) δ 7.28 (t, J = 8.0 Hz, 1H), 6.90 (dd, J = 8.2, 2.4 Hz, 1H), 6.74 (d, J = 7.8 Hz, 1H), 6.68 (s, 1H), 5.42 (s, 1H). ^{13}C NMR (126 MHz, CD_2Cl_2) δ 156.69, 131.20, 130.86, 122.67 (q, J = 274.8 Hz), 119.22, 117.46, 114.02, 30.28. ^{19}F NMR (283 MHz, CD_2Cl_2) δ –65.60. IR (diamond-ATR) ν: 3343.8, 2954, 2924, 2854, 1588, 1456, 1158.

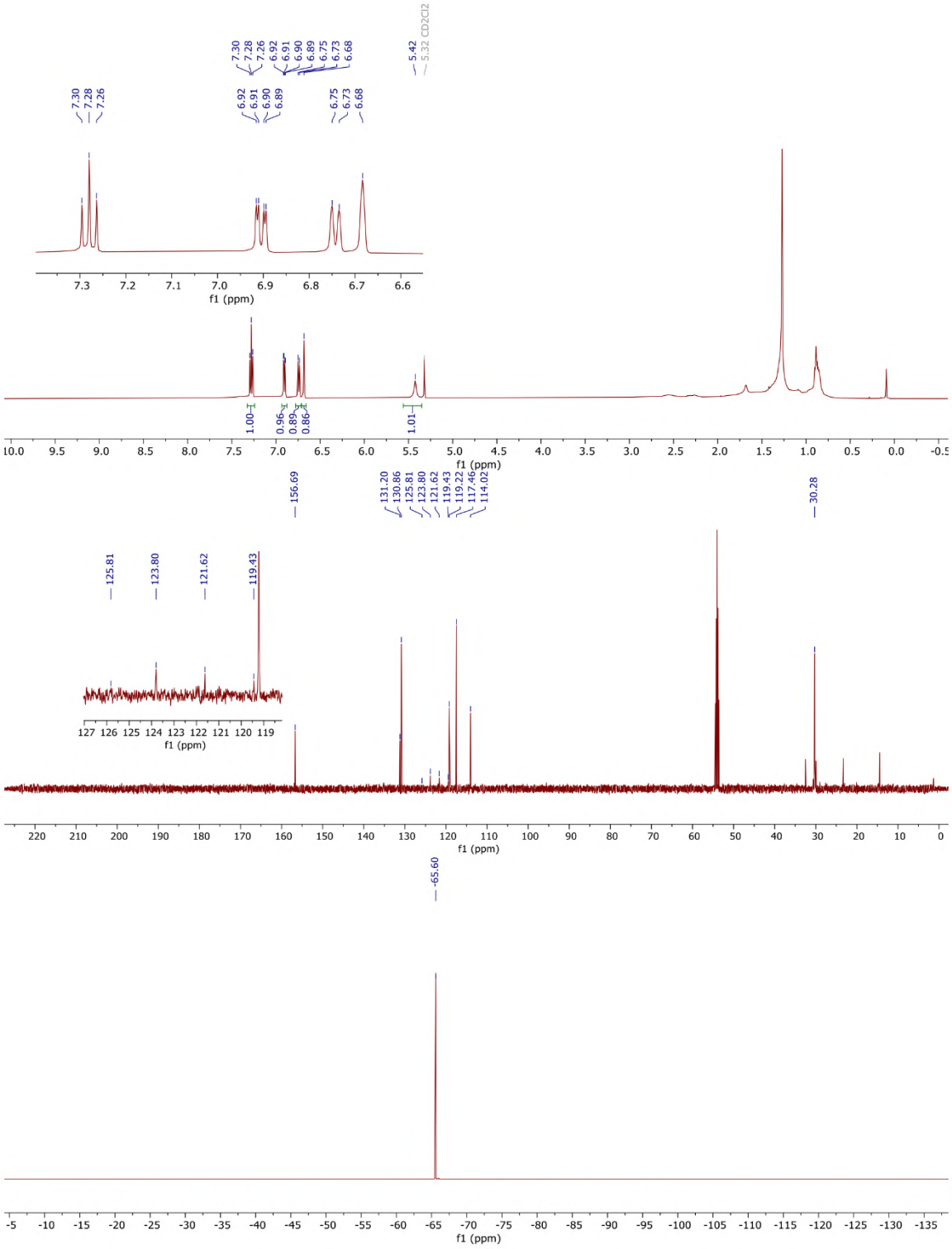

Figure S2.11 ^{1}H, ^{13}C, and ^{19}F NMR spectra of **D2.9** in CD_2Cl_2.

Synthesis of methyl 3,5-dimethoxybenzoate (**S2.21**).

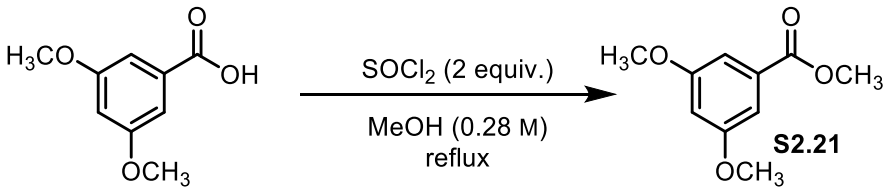

To a stirring solution of commercially available 3,5-dimethoxybenzoic acid (1.06 g, 5.8 mmol, 1 equiv.) in MeOH (40 mL), thionyl chloride (0.84 mL, 11.6 mmol, 2 equiv.) was slowly added dropwise. The suspension was heated to reflux for 16 h. The mixture was then cooled to room temperature and it was treated with $NaHCO_3$ until pH is around 7–8. The organic layer was extracted with diethyl ether (3 times) and washed with sat. $NaHCO_3$ and brine, and then dried over anhydrous sodium sulfate. Solvent was removed to afford the desired ester **S2.21** as a white solid (1.07 g, 5.49 mmol, 95%), in accordance with literature data.[143] ^{1}H NMR (300 MHz, $CDCl_3$) δ 7.19 (d, J = 2.4 Hz, 2H), 6.65 (t, J = 2.4 Hz, 1H), 3.91 (s, 3H), 3.83 (s, 6H).

Synthesis of 1-(3,5-dimethoxyphenyl)-2,2,2-trifluoroethan-1-one (**S2.22**).

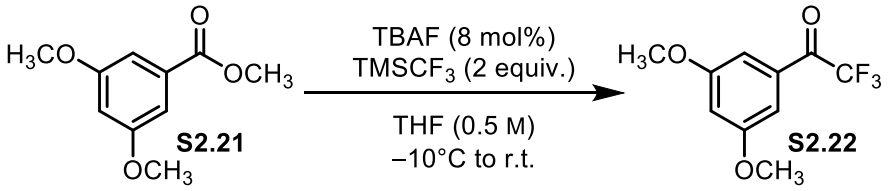

In a flame-dried flask, to a stirring solution of **S2.21** (1 g, 5.48 mmol, 1 equiv.) in distilled THF (1 M) under argon atmosphere at –10 °C, $TMSCF_3$ (1.2 mL, 8.2 mmol, 2 equiv.) and then TBAF (0.43 mL, 1 M in THF, 8 mol%) were slowly added dropwise. The resulting solution was allowed to warm to room temperature with continued stirring for an hour. The reaction was left stirring for 1 h and then quenched with NH_4Cl, extracted with diethyl ether (2 times) and the combined organic extracts were washed with brine and dried with sodium sulfate to afford the desired ketone **S2.22**, which was submitted to the next step without further purification. The analytical data were in accordance with literature.[144] ^{1}H NMR (300 MHz, $CDCl_3$) δ 6.71 (d, J = 2.2 Hz, 2H), 6.45 (t, J = 2.1 Hz, 1H), 3.83 ppm (s, 6H). ^{19}F NMR (283 MHz, $CDCl_3$) δ –71.19.

Synthesis of 1-(3,5-dimethoxyphenyl)-2,2,2-trifluoroethan-1-one oxime (**S2.23**) (mixture of *E*-, *Z*-isomers).

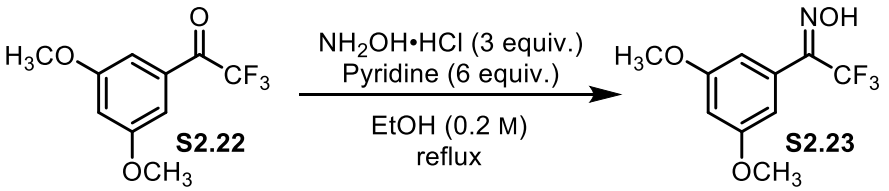

To a stirred solution of compound **S2.22** in ethanol (0.2 M), hydroxylamine hydrochloride (1.14 g, 16.5 mmol, 3 equiv.) and pyridine (2.6 mL, 33 mmol, 6 equiv.) were added and the reaction mixture was heated to reflux for 21 h. The mixture was then cooled to room temperature and the mixture was treated with 2 M HCl and extracted with diethyl ether (3 times). The combined organic layers were washed with distilled water until the pH of the washing layer became neutral, and then dried with sodium sulfate, filtered, and concentrated. The residue was dried under high vacuum for a prolonged time to afford the desired crude oxime **S2.23** (as a mixture of geometric isomers) as a yellow oil. The compound was submitted to the next step without further purification. The analytical data were in accordance with literature.[144] ^{1}H NMR (300 MHz, $CDCl_3$) δ 7.18 (d, *J* = 2.4 Hz, 2H), 6.64 (t, *J* = 2.4 Hz, 1H), 3.82 (s, 6H). ^{19}F NMR (283 MHz, $CDCl_3$) δ –62.35, –66.61.

Synthesis of 1-(3,5-dimethoxyphenyl)-2,2,2-trifluoroethan-1-one *O*-tosyl oxime (**S2.24**) (mixture of *E*-, *Z*-isomers).

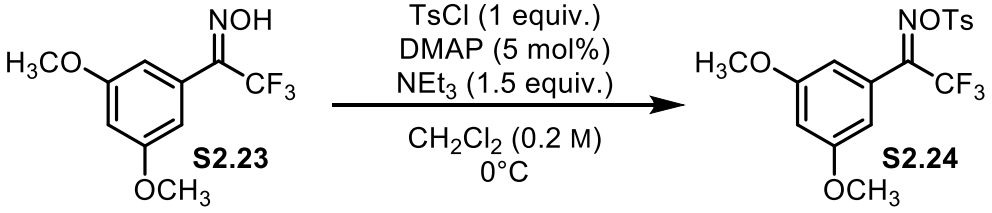

Compound **S2.23** (1.3 g, 5.49 mmol, 1 equiv.) was dissolved in CH_2Cl_2 (0.2 M), and triethylamine (1.15 mL, 8.2 mmol, 1.5 equiv.), DMAP (34 mg, 0.27 mmol, 5 mol%) and tosyl chloride (1.05 g, 5.49 mmol, 1 equiv.) were successively added at 0 °C. The ice bath was removed after 5 min, and the reaction mixture was stirred at room temperature for 1 h. The mixture was then treated with sat. aq. NH_4Cl and extracted with CH_2Cl_2. The combined organic extracts were dried with sodium sulfate, filtered, and concentrated to afford the desired crude tosyl oxime **S2.24** (714 mg) as a colourless solid, which was

submitted to the next step without further purification. The analytical data were in accordance with literature.[144] ^{1}H NMR (300 MHz, $CDCl_3$) δ 7.89 (d, *J* = 8.1 Hz, 2H), 7.38 (d, *J* = 8.2 Hz, 2H), 6.56 (t, *J* = 2.0 Hz, 1H), 6.44 (d, *J* = 2.1 Hz, 2H), 3.81 (s, 6H), 2.46 ppm (s, 3H). ^{19}F NMR (283 MHz, $CDCl_3$) δ –61.55, –67.11 (minor isomer).

Synthesis of 3-(3,5-dimethoxyphenyl)-3-(trifluoromethyl)diaziridine (**S2.25**).

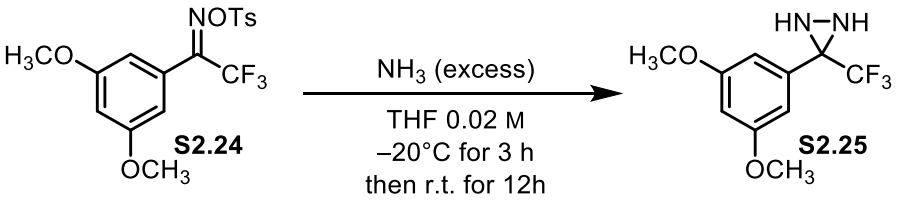

Tosyl oxime **S2.24** (1 equiv.) was transferred to a flame-dried 3-neck flask under argon in anhydrous THF (0.02 M) and cooled to –20 °C. Anhydrous gaseous ammonia was bubbled into the stirred solution for 3 h. Then, the reaction was left stirring for 12 h, during which time it was allowed to warm from –20 °C to room temperature. The mixture was quenched with sat. aq. NH_4Cl and extracted with diethyl ether (3 times). The combined organic layers were washed with brine and then dried with sodium sulfate, filtered and concentrated to afford the desired crude diaziridine **S2.25**, which was submitted to the next step without further purification. The analytical data were in accordance with literature.[144] ^{1}H NMR (300 MHz, $CDCl_3$) δ 6.77 (d, *J* = 2.0 Hz, 2H), 6.51 (d, *J* = 2.0 Hz, 1H), 3.81 (s, 6H), 2.74 (d, *J* = 9.0 Hz, 1H), 2.21 ppm (d, *J* = 9.0 Hz, 1H). ^{19}F NMR (283 MHz, $CDCl_3$) δ –75.41.

Synthesis of 3-(3,5-dimethoxyphenyl)-3-(trifluoromethyl)-3*H*-diazirine (**D2.10**).

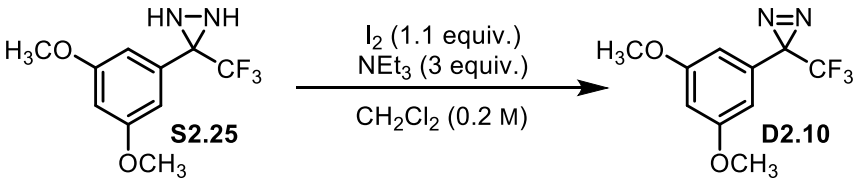

To a solution of the crude diaziridine **S2.25** (1.3 g, 5.48 mmol, 1 equiv.) in CH_2Cl_2 (0.2 M) at 0 °C were added successively triethylamine (2.2 mL, 16.4 mmol, 3 equiv.) and iodine (1.5 g, 6.04 mmol, 1.1 equiv.). The colored mixture was stirred at 0 °C for 1 h. The mixture was diluted with CH_2Cl_2 and washed with sat. aq. sodium thiosulfate. The aqueous layer was re-extracted with CH_2Cl_2 (3 times). Then the combined organic extracts were washed with brine and dried with sodium sulfate, filtered, and concentrated. The residue was purified by silica gel column chromatography using pentane: diethyl ether (8:2, R_f = 0.76), as eluent mixture to afford the desired diazirine **D2.10** (1.16 g, 4.72 mmol, 86%) as a pale-yellow oil, in accordance with literature data.[144] ^{1}H NMR (500 MHz, $CDCl_3$) δ 6.48 (t, *J* = 2.2 Hz, 1H), 6.32 – 6.27 (m, 2H), 3.78 (s, 6H). ^{13}C NMR (126 MHz, $CDCl_3$) δ 161.25, 131.32, 104.90, 122.20 (q, *J* = 274.3 Hz), 101.72, 55.59, 28.67 (d, *J* = 40.1 Hz). ^{19}F NMR (283 MHz, $CDCl_3$) δ –65.07. UV (*n*-hexane): $\lambda_{max,\ diazirine}$ = 353 nm. IR (diamond-ATR) ν: 2963, 2942, 2846, 1595, 1460, 1429, 1288, 1207, 1151, 999, 704.

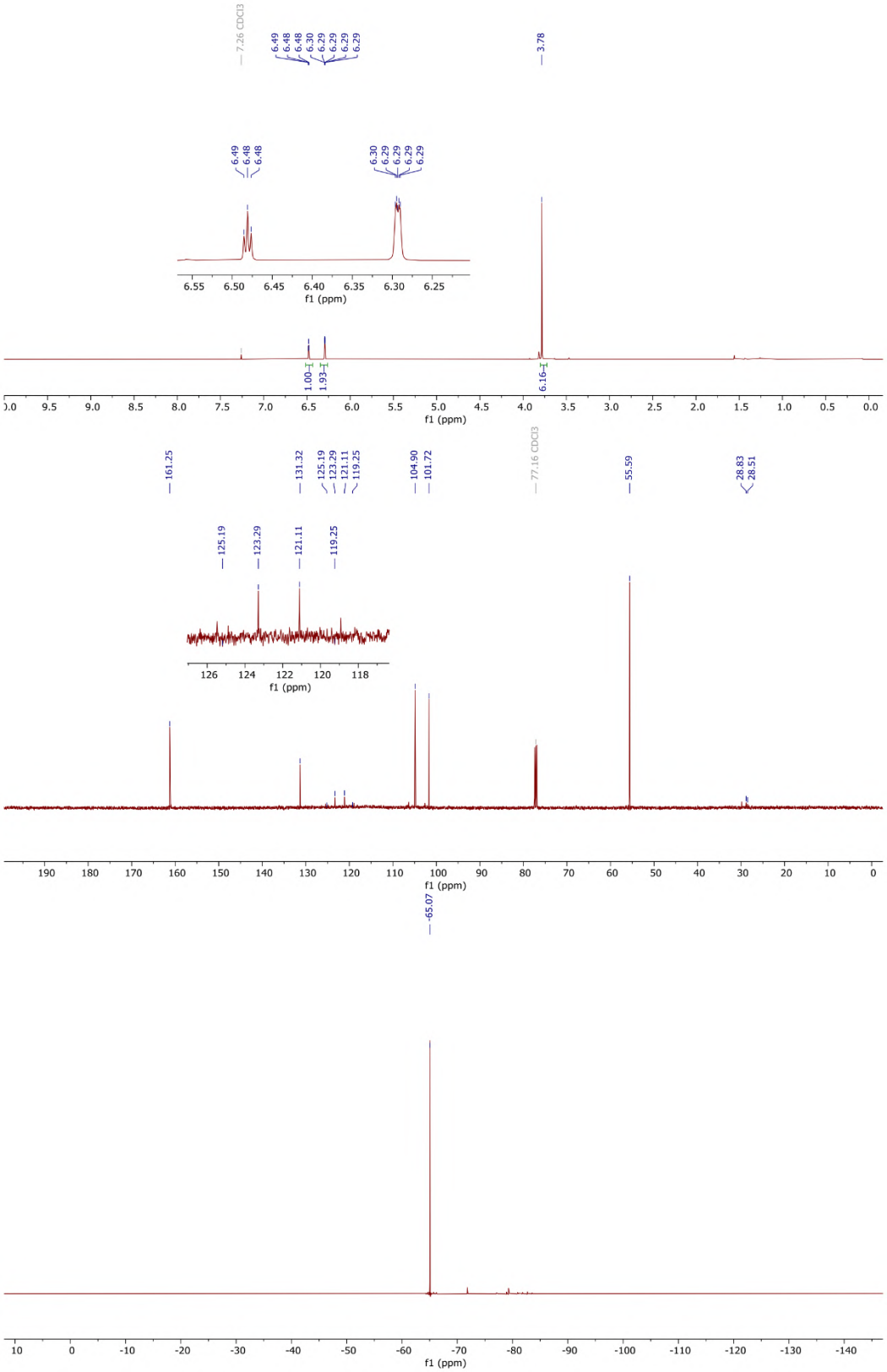

Figure S2.12 ^{1}H, ^{13}C, and ^{19}F NMR spectra of **D2.10** in $CDCl_3$.

Synthesis of methyl 4-(trifluoromethyl)benzoate (**S2.26**).

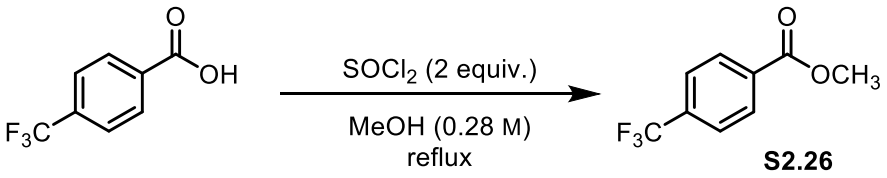

To a stirring solution of commercially available 4-(trifluoromethyl)benzoic acid (1 g, 5.26 mmol, 1 equiv.) in MeOH (20 mL), thionyl chloride (0.76 mL, 10.5 mmol, 2 equiv.) was slowly added dropwise. The suspension was heated to reflux for 2 h. The mixture was then cooled to room temperature and it was treated with $NaHCO_3$ until pH is around 7–8. The organic layer was extracted with diethyl ether (3 times) and washed with sat. $NaHCO_3$ and brine, and then dried over anhydrous magnesium sulfate. Solvent was removed to afford the desired ester **S2.26** as pale-yellow oil (1.2 g, 5 mmol, 95%), in accordance with literature data.[145] ^{1}H NMR (300 MHz, $CDCl_3$) δ 8.16 (d, J = 8.1 Hz, 2H), 7.71 (d, J = 8.2 Hz, 2H), 3.96 (s, 3H). ^{19}F NMR (471 MHz, $CDCl_3$) δ –63.13.

Synthesis of 2,2,2-trifluoro-1-(4-(trifluoromethyl)phenyl)ethan-1-one (**S2.27**).

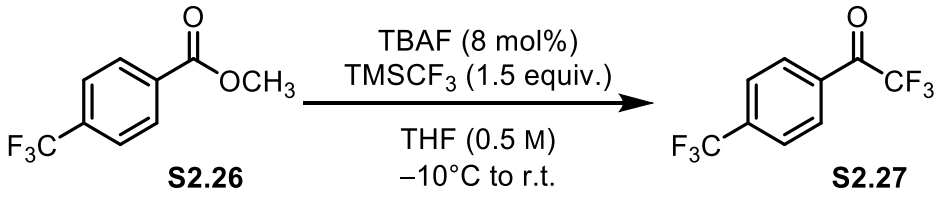

In a flame-dried flask, to a stirring solution of compound **S2.26** (1.1 g, 5.5 mmol, 1 equiv.) in distilled THF (11 mL) under argon atmosphere at –10 °C, $TMSCF_3$ (1.2 mL, 8.22 mmol, 1.5 equiv.) and then TBAF (0.5 mL, 1 M in THF, 8 mol%) were slowly added dropwise. The resulting solution was allowed to warm to room temperature with continued stirring for 2 h. The reaction was quenched with NH_4Cl, extracted with diethyl ether (2 times) and the combined organic extracts were washed with brine and dried with sodium sulfate. The filtered and concentrated oil was purified by silica gel column chromatography using pentane: ethyl acetate (9:1, R_f = 0.42) as eluent to afford the desired ketone **S2.27** (892 mg, 3.68 mmol, 67%) as a colourless oil, in accordance with literature data.[146] ^{1}H NMR (300 MHz, $CDCl_3$) δ 8.14 (d, J = 8.4 Hz, 2H), 7.77 (d, J = 8.4 Hz, 2H). ^{19}F NMR (283 MHz, $CDCl_3$) δ –63.63 (p-CF_3), –71.83.

Synthesis of 2,2,2-trifluoro-1-(4-(trifluoromethyl)phenyl)ethan-1-one oxime (**S2.28**) (mixture of *E*-, *Z*-isomers).

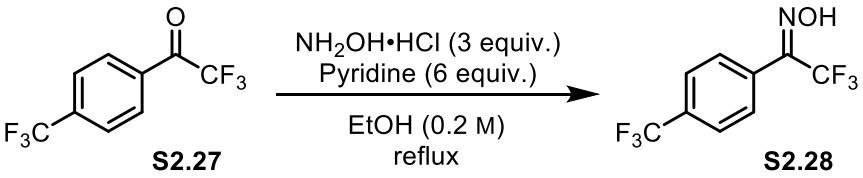

To a stirred solution of compound **S2.27** (892 mg, 3.68 mmol, 1 equiv.) in ethanol (0.2 M), hydroxylamine hydrochloride (767 mg, 11.4 mmol, 3 equiv.) and pyridine (1.8 mL, 22 mmol, 6 equiv.) were added and the reaction mixture was heated to reflux for 21 h. The mixture was then cooled to room temperature and the mixture was treated with 2 M HCl and extracted with diethyl ether (3 times). The combined organic layers were washed with distilled water until the pH of the washing layer became neutral, and then dried with sodium sulfate, filtered, and concentrated. The residue was dried under high vacuum for a prolonged time to afford the desired crude oxime **S2.28** (as a mixture of geometric isomers) as a colorless oil. The compound was submitted to the next step without further purification. ^{1}H NMR (300 MHz, $CDCl_3$) δ 8.62 (d, *J* = 1.8 Hz, 1H, OH), 8.60 (d, *J* = 1.6 Hz, 1H, OH, minor isomer), 7.74 (d, *J* = 7.9 Hz, 2H), 7.39 – 7.32 (m, 2H). ^{19}F NMR (283 MHz, $CDCl_3$) δ –62.36 (minor isomer), –62.96 (minor isomer, *p*-CF_3), –63.13 (*p*-CF_3), –66.24.

Synthesis of 2,2,2-trifluoro-1-(4-(trifluoromethyl)phenyl)ethan-1-one *O*-tosyl oxime (**S2.29**) (mixture of *E,Z*-isomers).

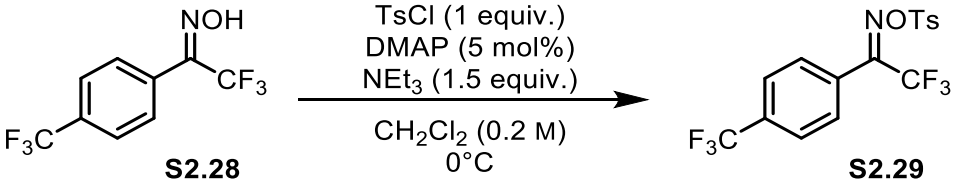

Compound **S2.28** (789 mg, 3.07 mmol, 1 equiv.) was dissolved in CH_2Cl_2 (0.2 M), and triethylamine (0.65 mL, 4.6 mmol, 1.5 equiv.), DMAP (19 mg, 0.15 mmol, 5 mol%) and tosyl chloride (585 mg, 3.07 mmol, 1 equiv.) were successively added at 0 °C. The ice bath was removed after 5 min, and the reaction mixture was stirred at room temperature for 1 h. The mixture was then treated with sat. aq. NH_4Cl and extracted with CH_2Cl_2. The combined organic extracts were dried with sodium sulfate, filtered, and

concentrated to afford the desired crude tosyl oxime **S2.29** as a yellow oil. The compound was submitted to the next step without further purification. ^{1}H NMR (300 MHz, $CDCl_3$) δ 7.90 (d, *J* = 8.5 Hz, 2H, minor isomer), 7.89 (d, *J* = 8.4 Hz, 2H), 7.76 (d, *J* = 8.2 Hz, 2H), 7.70 (d, *J* = 8.3 Hz, 2H, minor isomer), 7.58 (d, *J* = 8.7 Hz, 2H, minor isomer), 7.51 (d, *J* = 8.4 Hz, 1H), 7.44 – 7.33 (m, 4H, both isomers), 2.49 (s, 3H), 2.47 (s, 3H, minor isomer). ^{19}F NMR (283 MHz, $CDCl_3$) δ –61.53 (minor isomer), –63.26 (minor isomer, *p*-CF_3), –63.36 (*p*-CF_3), –66.93.

Synthesis of 3-(trifluoromethyl)-3-(4-(trifluoromethyl)phenyl)diaziridine (**S2.30**).

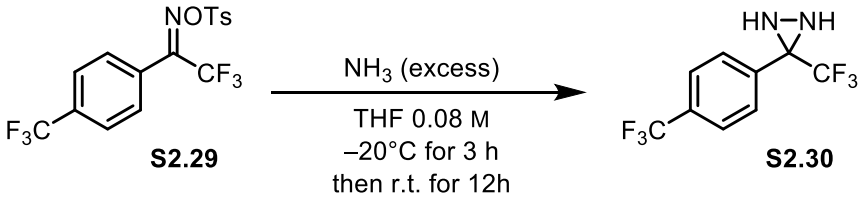

Tosyl oxime **S2.29** (1.2 g, 3 mmol, 1 equiv.) was transferred to a flame-dried 3-neck flask under argon in anhydrous THF (0.08 M) and cooled to –20 °C. Anhydrous gaseous ammonia was bubbled into the stirred solution for 3 h. Then, the reaction was left stirring for 12 h, during which time it was allowed to warm from –20 °C to room temperature. The mixture was quenched with sat. aq. NH_4Cl and extracted with diethyl ether (3 times). The combined organic layers were washed with brine and then dried with sodium sulfate, filtered, and concentrated to afford the desired crude diaziridine **S2.30** as a colourless oil, which was submitted to the next step without further purification. ^{1}H NMR (300 MHz, $CDCl_3$) δ 7.78 (d, *J* = 8.5 Hz, 2H), 7.70 (d, *J* = 8.4 Hz, 2H), 2.88 (d, *J* = 8.8 Hz, 1H, NH), 2.26 (d, *J* = 8.8 Hz, 1H, NH). ^{19}F NMR (283 MHz, $CDCl_3$) δ –63.03 (*p*-CF_3), –75.23.

Synthesis of 3-(trifluoromethyl)-3-(4-(trifluoromethyl)phenyl)-3*H*-diazirine (**D2.11**).

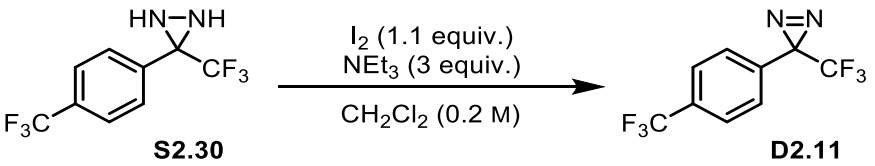

S2.30 **D2.11**

To a solution of the crude diaziridine **S2.30** (644 mg, 2.5 mmol, 1 equiv.) in CH_2Cl_2 (0.2 M) at 0 °C were added successively triethylamine (1.1 mL, 7.5 mmol, 3 equiv.) and iodine (702 mg, 2.8 mmol, 1.1 equiv.). The colored mixture was stirred at 0 °C for 1 h. The mixture was diluted with CH_2Cl_2 and washed with sat. aq. sodium thiosulfate. The aqueous layer was re-extracted with CH_2Cl_2 (3 times). Then the combined organic extracts were washed with brine and dried with sodium sulfate, filtered, and concentrated (the title compound is very volatile and decomposes very easily). The residue was purified by silica gel column chromatography using pentane (R_f = 0.86) as eluent to afford the desired diazirine **D2.11** (400 mg, 1.57 mmol, 63%) as a colourless oil. ^{1}H NMR (300 MHz, $CDCl_3$) δ 7.67 (d, *J* = 8.2 Hz, 1H), 7.32 (dd, *J* = 8.3, 0.7 Hz, 1H).^{13}C NMR (126 MHz, $CDCl_3$) δ 133.13, 132.00 (d, *J* = 33.0 Hz), 127.05(d, *J* = 1.5 Hz), 126.00 (q, *J* = 3.7 Hz), 124.74, 123.07, 122.58, 120.89, 34.29, 29.86. ^{19}F NMR (471 MHz, $CDCl_3$) δ –63.09 (*p*-CF_3), –65.09. IR (diamond-ATR) ν: 2959, 2928, 2860, 1265, 1247, 1115, 1101, 1019, 729. GC–MS *m/z* (% relative intensity) [ion]: 254 (2) $[M]^+$, 226 (100) $[M - N_2]^+$, 207 (40) $[C_9H_4F_5]^+$, 187 (20) $[C_9H_3F_4]^+$, 176 (60) $[C_8H_4F_4]^+$, 157 (60) $[C_8H_4F_3]^+$, 138 (18) $[C_8H_4F_2]^+$, 137 (32) $[C_8H_3F_2]^+$, 126 (18) $[C_7H_4F_2]^+$, 107 (26) $[C_7H_4F_1]^+$, 87 (20) $[C_7H_3]^+$, 81 (10) $[C_2F_3]^+$, 69 (12) $[CF_3]^+$. [M = $C_9H_4F_6N_2$ (254.03)].

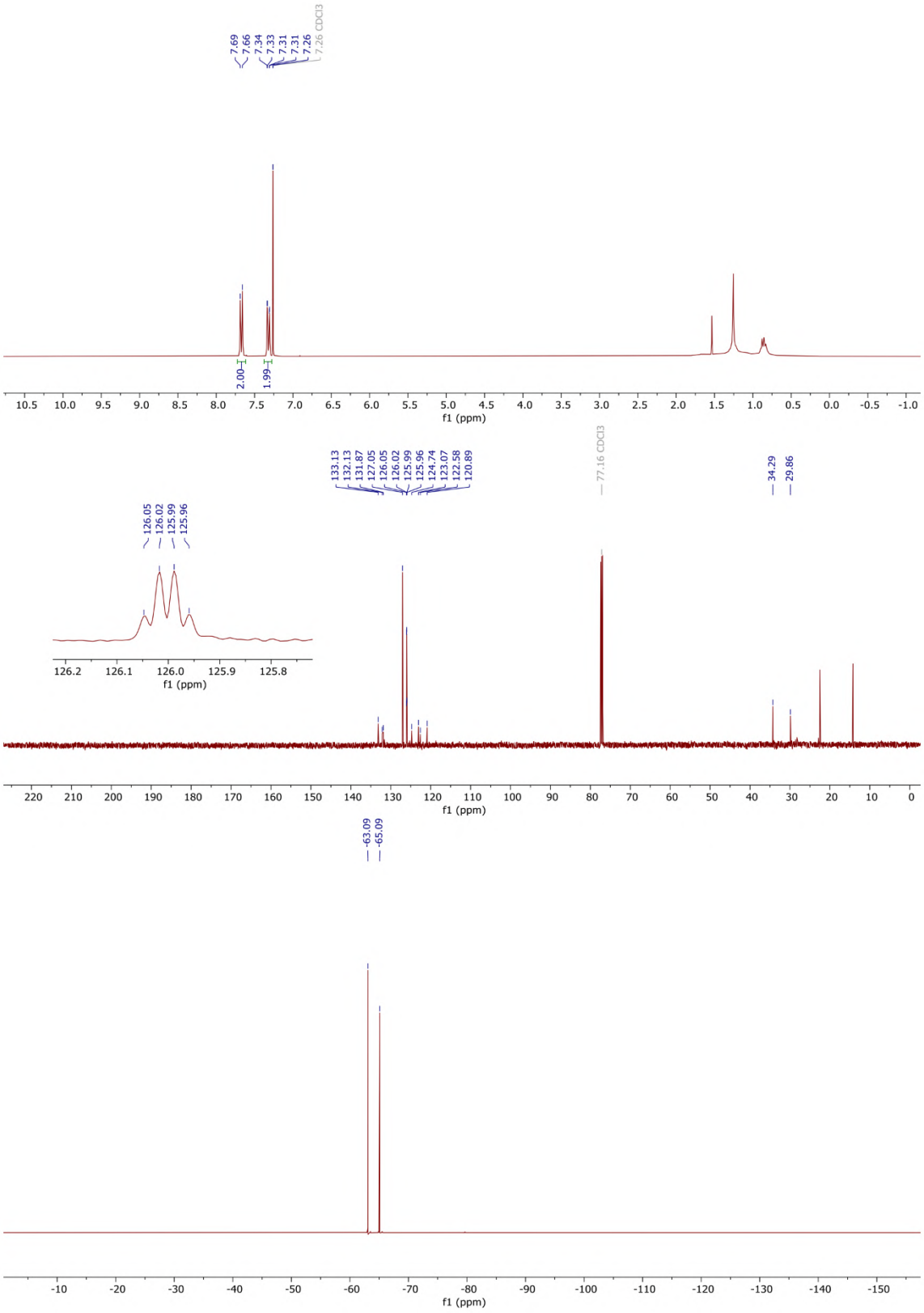

Figure S2.13 ^{1}H, ^{13}C, and ^{19}F NMR spectra of **D2.11** in $CDCl_3$.

Synthesis of 4-[3-(Trifluoromethyl)-3*H*-diazirin-3-yl]benzaldehyde (**D2.12**).

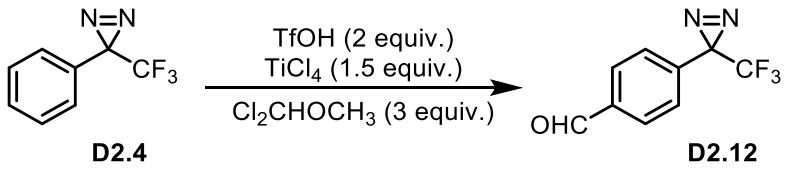

D2.4 **D2.12**

Following the procedure reported by Hatanaka,[81] in a flame dried two-neck flask under argon a yellow bright solid was prepared mixing TfOH (1.8 mL, 20 mmol, 2 equiv.) and $TiCl_4$ (1.6 mL, 15 mmol, 1.5 equiv.). The fuming solid was added portion wise to a second flame dried flask containing a mixture of 3-phenyl-3-(trifluoromethyl)-3*H*-diazirine **D2.4** (1.86 g, 10 mmol, 1 equiv.) and dichloromethyl methyl ether (2.7 mL, 30 mmol, 3 equiv.) (*Warning: acute toxicity, carcinogens*). The colour changed from pale yellow to dark brown and the reaction mixture started bubbling. The reaction was allowed to proceed for 1 h and quenched with a cold water at –20 °C. The resulting mixture was neutralized with Na_2CO_3, left stirring for 1 hour, and extracted with pentane. The organic phase was washed with brine and dried over magnesium sulfate. After removal of solvent, the residue was purified by chromatography using pentane: diethyl ether (gradient 10:0 to 8:2, R_f = 0.62 (8:2)) to afford compound **D2.12** as a pale-yellow oil (899 mg, 4.2 mmol, 42%). The analytical data were in accordance with literature.[147] ^{1}H NMR (500 MHz, $CDCl_3$) δ 10.04 (s, 1H), 7.92 (d, *J* = 8.6 Hz, 2H), 7.35 (d, *J* = 8.1 Hz, 2H). ^{13}C NMR (126 MHz, $CDCl_3$) δ 191.19, 136.95, 135.41, 130.00, 127.14, 121.95 (d, *J* = 274.9 Hz), 22.49. ^{19}F NMR (283 MHz, $CDCl_3$) δ –64.82. IR (diamond-ATR) ν: 2833, 2744, 1707, 1609, 1342, 1187, 1153, 939, 737.

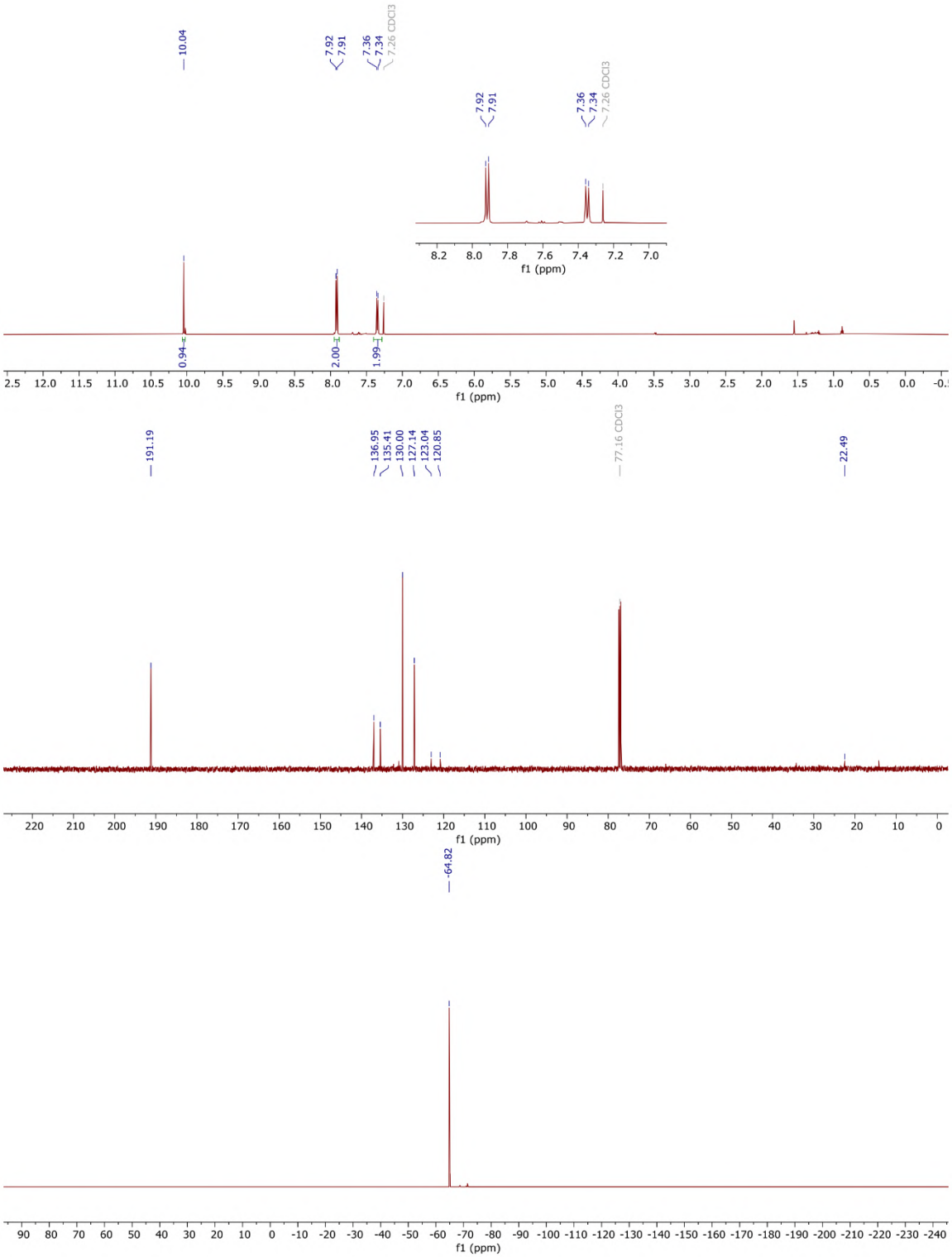

Figure S2.14 ^{1}H, ^{13}C, and ^{19}F NMR spectra of **D2.12** in $CDCl_3$.

Synthesis of 2,2,2-trifluoro-1-(4-nitrophenyl)ethan-1-one (**S2.31**).

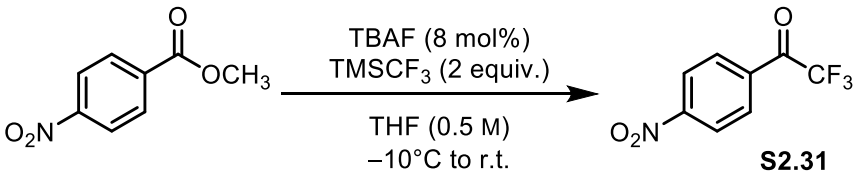

In a flame-dried flask, to a stirring solution of commercially available methyl 4-nitrobenzoate (1 g, 5.52 mmol, 1 equiv.) in distilled THF (11 mL) under argon atmosphere at –10 °C, $TMSCF_3$ (1.6 mL, 11 mmol, 2 equiv.) and then TBAF (0.44 mL, 1 M in THF, 8 mol%) were slowly added dropwise. The resulting solution was allowed to warm to room temperature with continued stirring for an hour and the colour changed from transparent to orange. The reaction was left stirring for 16 h and then quenched with NH_4Cl., extracted with diethyl ether (2 times) and the combined organic extracts were washed with brine and dried with sodium sulfate to afford the desired ketone **S2.31**, which was submitted to the next step without further purification. The analytical data are in accordance with the literature.[148] ^1H NMR (300 MHz, $CDCl_3$) 8.39 (d, J = 8.9 Hz, 1H), 8.23 (d, J = 9.0 Hz, 2H). ^{19}F NMR (283 MHz, $CDCl_3$) δ –71.92.

Synthesis of 2,2,2-trifluoro-1-(4-nitrophenyl)ethan-1-one oxime (**S2.32**) (mixture of *E*-, *Z*-isomers).

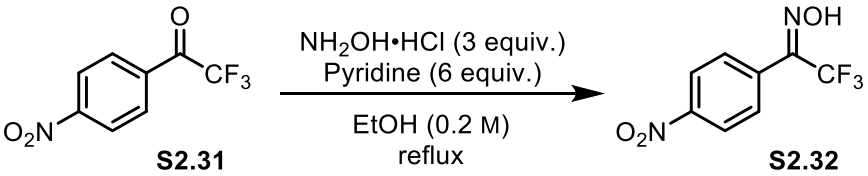

To a stirred solution of compound **S2.31** (1.2 g, 5.5 mmol, 1 equiv,) in ethanol (0.2 M), hydroxylamine hydrochloride (1.15 g, 16.5 mmol, 3 equiv.) and pyridine (2.6 mL, 33 mmol, 6 equiv.) were added and the reaction mixture was heated to reflux for 21 h. The mixture was then cooled to room temperature and the mixture was treated with 2 M HCl and extracted with diethyl ether (3 times). The combined organic layers were washed with distilled water until the pH of the washing layer became neutral, and then dried with sodium sulfate, filtered, and concentrated. The residue was dried under high vacuum for a prolonged time to afford the desired crude oxime **S2.32** (as a mixture of geometric isomers) as a yellow oil (1.3 g). The compound was submitted to the next step without further purification. ^1H NMR (300 MHz, $CDCl_3$) δ 8.30 (d, J = 8.9 Hz, 2H), 8.25

(d, J = 9.0 Hz, 1.6H, minor isomer), 7.68 (d, J = 8.6 Hz, 3.6H, major and minor isomers). ^{19}F NMR (283 MHz, $CDCl_3$) δ –62.28, –66.06.

Synthesis of 2,2,2-trifluoro-1-(4-nitrophenyl)ethan-1-one *O*-tosyl oxime (**S2.33**) (mixture of *E*-, *Z*-isomers).

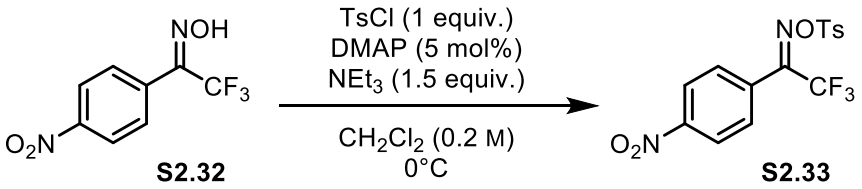

Compound **S2.32** (1.2 g, 5.5 mmol, 1 equiv.) was dissolved in CH_2Cl_2 (28 mL), and triethylamine (1.15 mL, 8.25 mmol, 1.5 equiv.), DMAP (34 mg, 0.275 mmol, 5 mol%) and tosyl chloride (1.05 g, 5.5 mmol, 1 equiv.) were successively added at 0 °C. The ice bath was removed after 5 min, and the reaction mixture was stirred at room temperature for 1 h. The mixture was then treated with sat. aq. NH_4Cl and extracted with CH_2Cl_2. The combined organic extracts were dried with magnesium sulfate, filtered, and concentrated to afford the desired crude tosyl oxime **S2.33** (1.5 g), which was submitted to the next step without further purification. ^{1}H NMR (300 MHz, $CDCl_3$) δ 8.36 (d, J = 8.9 Hz, 2H), 8.30 (d, J = 8.9 Hz, 1.7H, minor isomer), 7.91 (d, J = 8.3 Hz, 1.6H, minor isomer), 7.89 (d, J = 8.3 Hz, 2H), 7.66 (d, J = 8.6 Hz, 1.8H, minor isomer), 7.59 (d, J = 8.8 Hz, 2H), 7.42 (d, J = 8.2 Hz, 2H), 7.40 (d, J = 8.3 Hz, 1.8H, minor isomer), 2.50 (s, 3H), 2.48 (s, 2.6H, minor isomer). ^{19}F NMR (283 MHz, $CDCl_3$) δ –61.43 (minor isomer), –66.82.

Synthesis of 3-(4-nitrophenyl)-3-(trifluoromethyl)diaziridine (**S2.34**).

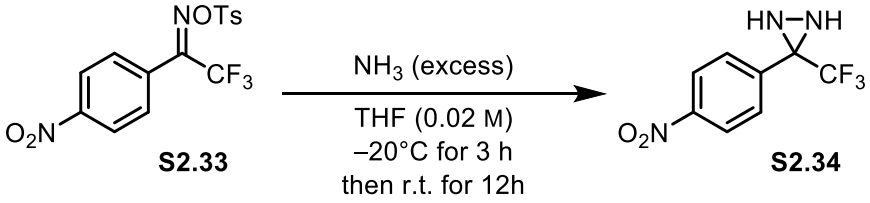

Tosyl oxime **S2.33** (1.5 g, 4.4 mmol, 1 equiv.) was transferred to a flame-dried 3-neck flask under argon in anhydrous THF (200 mL) and cooled to –20 °C. Anhydrous gaseous ammonia was bubbled into the stirred solution for 3 h. Then, the reaction was left stirring for 12 h, during which time it was allowed to warm from –20 °C to room temperature. The mixture was quenched with sat. aq. NH_4Cl and extracted with CH_2Cl_2

(3 times). The combined organic layers were washed with brine and then dried with sodium sulfate, filtered and concentrated to afford the desired crude diaziridine **S2.34** (930 mg), which was submitted to the next step without further purification. ^{1}H NMR (300 MHz, $CDCl_3$) δ 8.29 (d, *J* = 8.9 Hz, 2H), 7.84 (d, *J* = 8.6 Hz, 2H), 2.95 (d, *J* = 8.6 Hz, 1H), 2.33 (d, *J* = 9.0 Hz, 1H).^{19}F NMR (283 MHz, $CDCl_3$) δ –74.92.

Synthesis of 3-(4-nitrophenyl)-3-(trifluoromethyl)-3*H*-diazirine (**D2.13**).

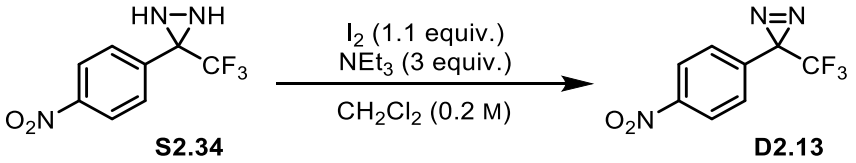

To a solution of the crude diaziridine **S2.34** (930 mg, 4 mmol, 1 equiv.) in CH_2Cl_2 (20 mL) at 0 °C were added successively triethylamine (1.7 mL, 12 mmol, 3 equiv.) and iodine (1.12 g, 4.4 mmol, 1.1 equiv.). The colored mixture was stirred at 0 °C for 1 h. The mixture was diluted with CH_2Cl_2 and washed with sat. aq. sodium thiosulfate. The aqueous layer was re-extracted with CH_2Cl_2 (3 times). Then the combined organic extracts were washed with brine and dried with sodium sulfate, filtered, and concentrated. The residue was purified by silica gel column chromatography using pentane: EtOAc (0 to 20%) as eluent to afford the desired diazirine **D2.13** (632 mg, 2.7 mmol, 68%) as a pale-yellow oil, in accordance with literature data.[149] ^{1}H NMR (300 MHz, $CDCl_3$) δ 8.27 (d, *J* = 8.8 Hz, 2H), 7.37 (d, *J* = 8.6 Hz, 2H). ^{13}C NMR (126 MHz, $CDCl_3$) δ 148.57, 135.95, 127.58, 124.12, 120.59 (q, *J* = 274.8 Hz), 28.45 (q, *J* = 41.0 Hz). ^{19}F NMR (283 MHz, $CDCl_3$) δ –64.81. UV (*n*-hexane): $\lambda_{max,\ diazirine}$ = 340 nm. IR (diamond-ATR) ν: 3089, 1604, 1525, 1352, 1338, 1225, 1185, 1151, 1046. HRMS (ESI-) m/z [M – N_2 + HO^-] calculated for $[C_8H_5F_3NO_3]^-$: 220.0227, found: 220.0228.

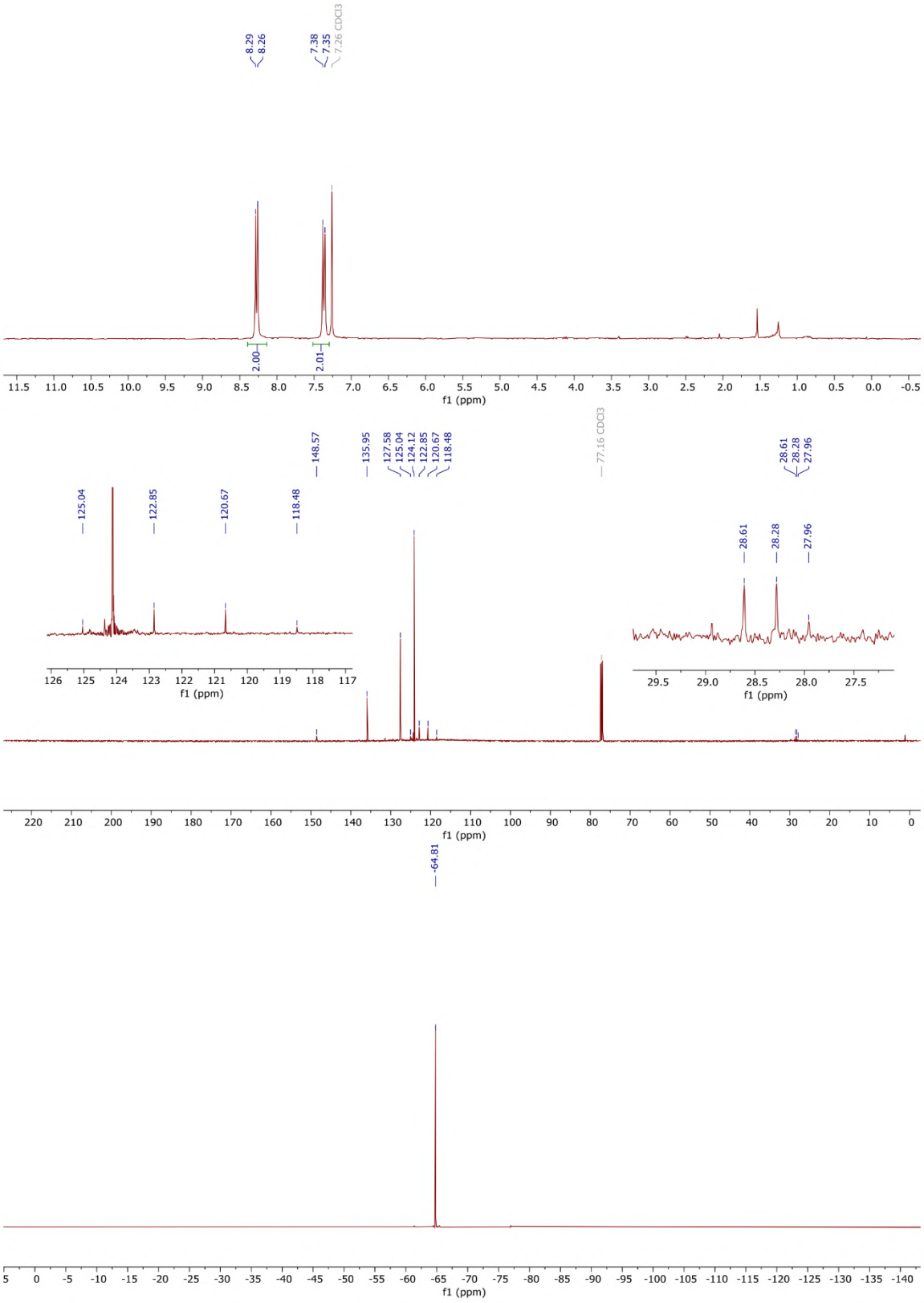

Figure S2.15 ^{1}H, ^{13}C, and ^{19}F NMR spectra of **D2.13** in $CDCl_3$.

Synthesis of 3-(4-bromophenyl)-3-chloro-3*H*-diazirine (**D2.14**).

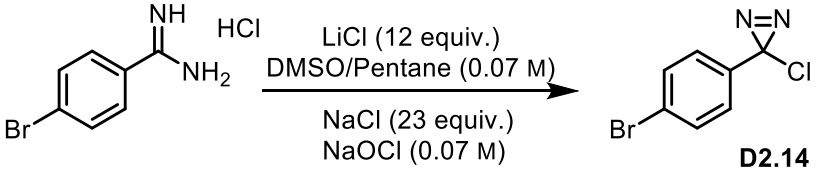

In a three-neck flask fitted with a dropping funnel and thermometer, to a mixture of lithium chloride (1 g, 25.4 mmol, 12 equiv.) and DMSO (15 mL), commercially available 4-bromobenzamidine hydrochloride (500 mg, 2.21 mmol, 1 equiv.) and pentane (15 mL) were added and the reaction was cooled to 0 °C. Aqueous NaOCl solution (30 mL, 8.25% hypochlorite) saturated with sodium chloride (2.8 g, 48.7 mmol, 23 equiv.) was added slowly, maintaining the temperature between 35 and 40 °C with an ice bath. After 5 min, 15 mL of DMSO, 15 mL of pentane, and 40 mL of aqueous NaOCl were added, and the mixture was allowed to stir for 1 h at room temperature. The reaction solution was poured into a separatory funnel containing ice water, and the pentane layer was separated, washed with brine (4 times), and dried over $CaCl_2$. The crude was purified by silica gel column chromatography using pentane (R_f = 0.72), as eluent mixture to afford the desired diazirine **D2.14** (351 mg, 1.51 mmol, 71%) as a colourless oil, in accordance with literature data.[150] ^{1}H NMR (300 MHz, $CDCl_3$) δ 7.53 (d, *J* = 8.9 Hz, 2H), 6.98 (d, *J* = 8.9 Hz, 2H). ^{13}C NMR (126 MHz, $CDCl_3$) δ 134.92, 131.87, 127.72, 124.00, 29.86. IR (diamond-ATR) ν: 2925, 2853, 1594, 1578, 1491, 1398, 1080, 1020, 905, 814, 536. GC–MS *m/z* (% relative intensity) [ion]: 243/245/247 (42) $[M - N_2 + CH_3CN]^+$, 208/210 (52) $[C_7H_4Br + CH_3CN]^+$, 202/204/206 (68) $[C_7H_4BrCl]^+$, 167/169 (20) $[C_7H_4Br]^+$, 164/166 (48) $[C_7H_4Cl + CH_3CN]^+$, 155/157 (18) $[C_6H_4Br]^+$, 123/125 (100) $[C_7H_4Cl]^+$, 88 (50) $[C_7H_4]^+$, 76 (44) $[C_6H_4]^+$. [M = $C_7H_4BrClN_2$ (229.92)].

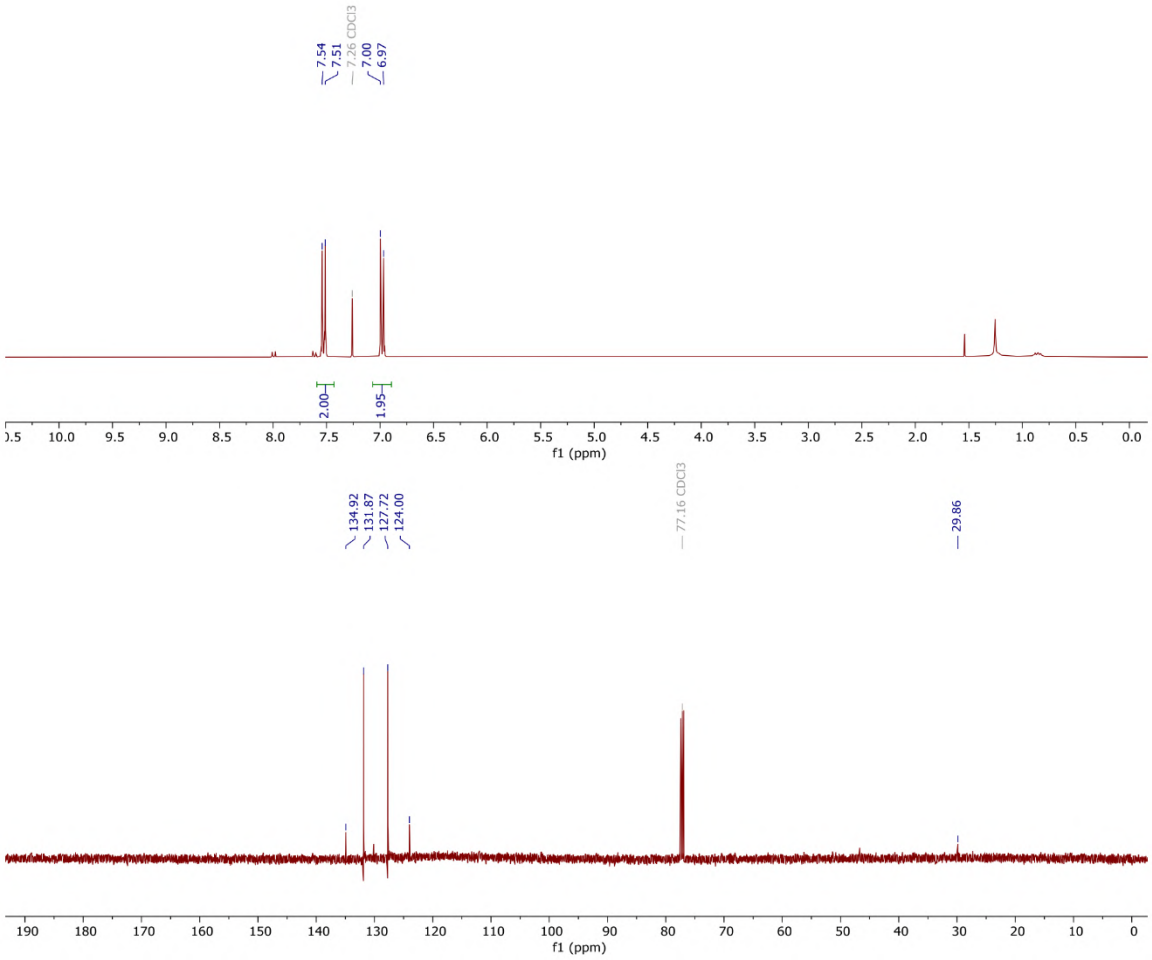

Figure S2.16 ^{1}H and ^{13}C NMR spectra of **D2.14** in $CDCl_3$.

Synthesis of 3-(4-bromophenyl)-3*H*-diazirine (**D2.15**).

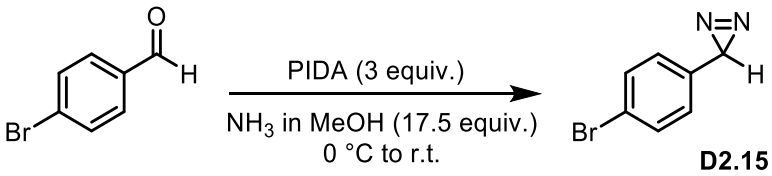

(Diacetoxyiodo)benzene (PIDA, 7.5 mmol, 3 equiv.) was added in one portion to a stirred solution of 4-bromobenzaldehyde (2.5 mmol, 1 equiv.) in NH_3 in MeOH 7 M (6.3 mL, 17.5 equiv.) at 0 °C under argon. After 30 minutes at 0 °C, the batch was allowed to reach room temperature and was left stirred for 2 h. After completion (monitored by TLC and ^{1}H NMR), the batch was concentrated under reduced pressure and the crude was purified by flash chromatography on silica gel. Pentane was employed to afford diazirine **D2.15** (122 mg, 0.618 mmol, 25% yield) as a pale-yellow oil. ^{1}H NMR (500 MHz, $CDCl_3$) δ 7.44 (d, J = 8.5 Hz, 2H), 6.78 (d, J = 8.5 Hz, 2H), 2.03 (s, 1H). ^{13}C

NMR (126 MHz, $CDCl_3$) δ 135.55, 131.63, 126.86, 122.23, 23.17. IR (diamond-ATR) ν: 3054, 1622, 1608, 1490, 1013, 831, 818, 782, 535. GC–MS *m/z* (% relative intensity) [ion]: 209/211 (25) $[M - N_2 + CH_3CN]^+$, 208/210 (25) $[C_7H_4Br + CH_3CN]^+$, 168/170 (10) $[C_7H_5Br]^+$, 130 (64) $[C_7H_5 + CH_3CN]^+$, 89 (100) $[C_7H_5]^+$. [M = $C_7H_5BrN_2$ (195.96)].

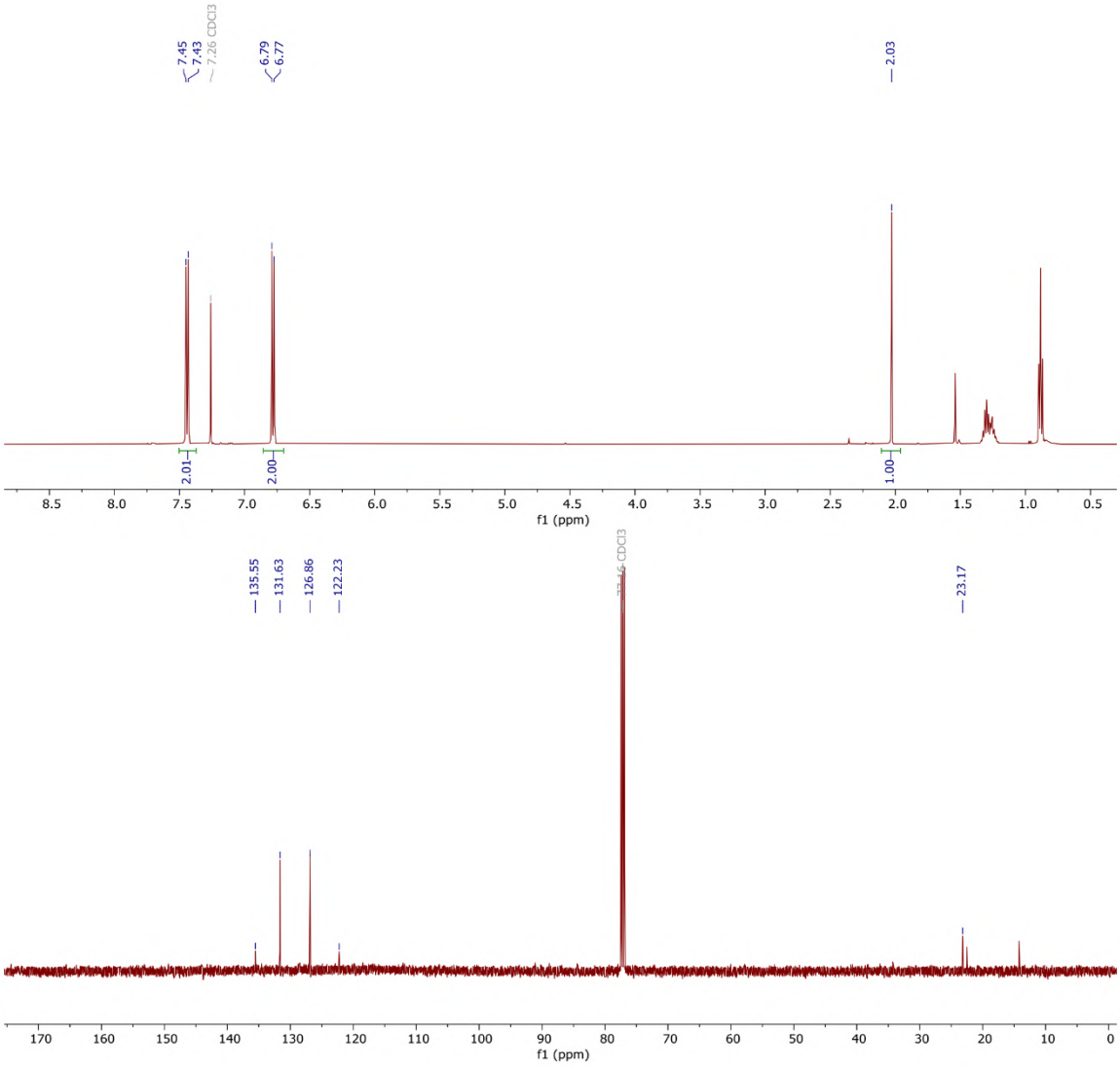

Figure S2.17 ^1H and ^{13}C NMR spectra of **D2.15** in $CDCl_3$.

Synthesis of 3-(4-bromophenyl)-3-methyl-3*H*-diazirine (**D2.16**).

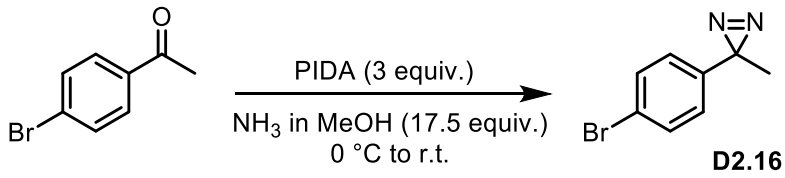

(Diacetoxyiodo)benzene (PIDA, 10.5 mmol, 3 equiv.) was added in one portion to a stirred solution of 4-bromoacetophenone (3.5 mmol, 1 equiv.) in NH_3 in MeOH 7M (8.8 mL, 17.5 equiv.) at 0 °C under argon. After 30 minutes at 0 °C, the batch was allowed to reach room temperature and was left stirred for 2 h. After completion (monitored by TLC and ^{1}H NMR), the batch was concentrated under reduced pressure and the crude was purified by flash chromatography on silica gel. Pentane was employed to afford diazirine **D2.16** (150 mg, 0.711 mmol, 20% yield) as a pale-yellow oil. ^{1}H NMR (500 MHz, Chloroform-*d*) δ 7.51 – 7.42 (m, 2H), 6.85 – 6.75 (m, 2H), 1.50 (s, 3H). ^{13}C NMR (126 MHz, $CDCl_3$) δ 138.96, 131.48, 127.24, 121.82, 26.10, 17.68. IR (diamond-ATR) ν: 2964, 2930, 1607, 1591, 1494, 1404, 1082, 1008, 829, 728, 540. HRMS (ESI+) m/z [M+H] calculated for $[C_8H_8BrN_2]^+$: 210.9865, found: 210.9864.

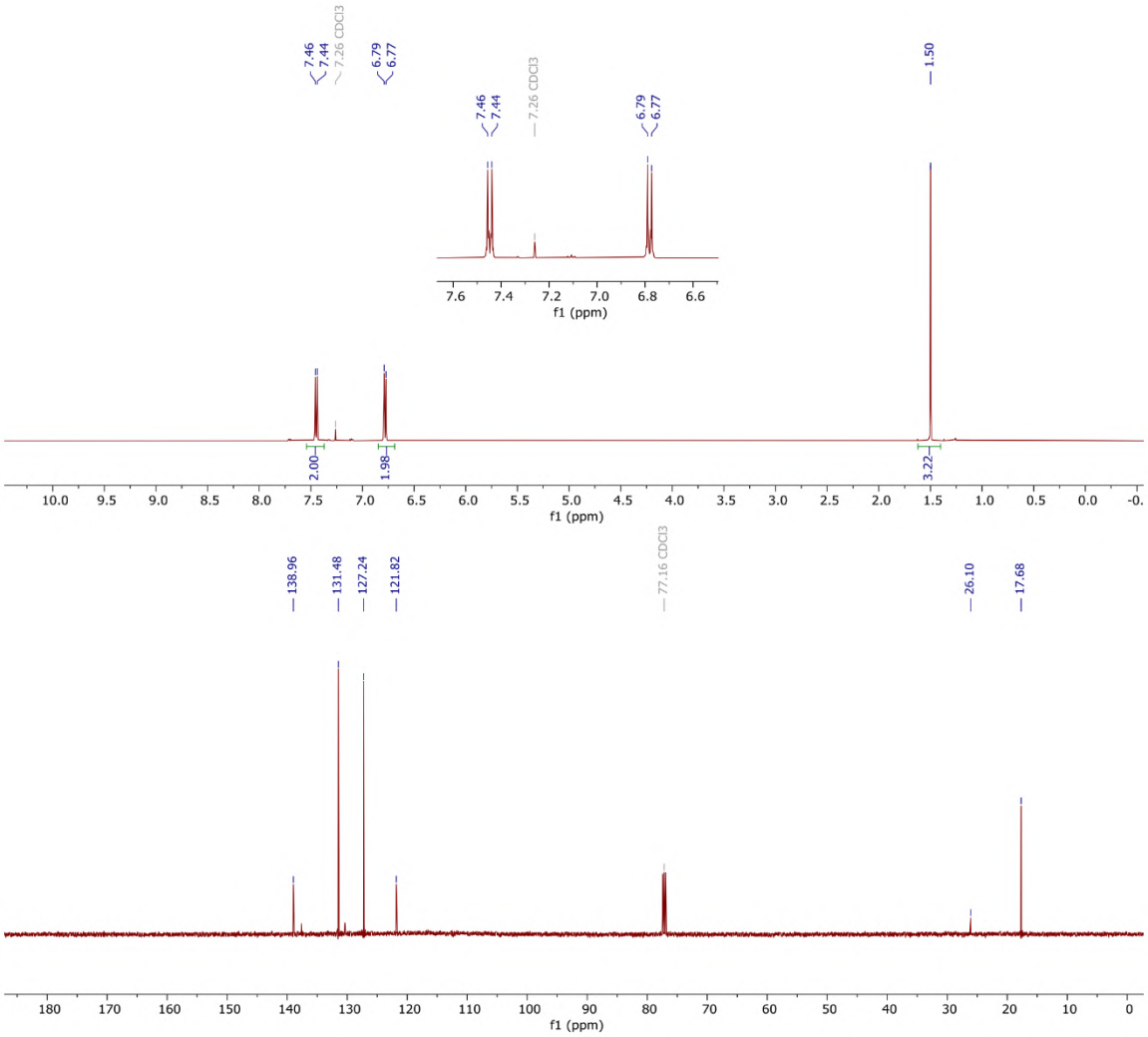

Figure S2.18 ^{1}H and ^{13}C NMR spectra of **D2.16** in $CDCl_3$.

Synthesis of 3-(4-bromophenyl)-3-fluoro-3*H*-diazirine (**D2.17**).

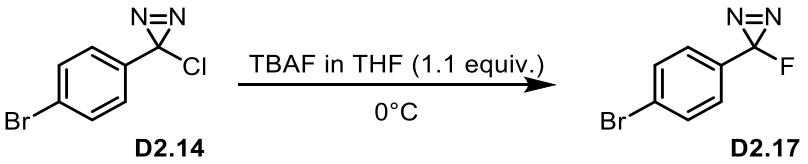

D2.14 **D2.17**

To a stirred solution of TBAF (4.4 mL, 1 M in THF, 1.1 equiv.) under argon at 0 °C, 3-(4-bromophenyl)-3-chloro-3*H*-diazirine **D2.14** (107 mg, 0.4 mmol, 1 equiv.) was added dropwise. The reaction mixture was stirred for 2 h and then quenched with NH_4Cl. The resulting mixture was extracted with pentane (3 times). The combined organic layers were dried over magnesium sulfate. The desired diazirine **D2.17** was afforded as a clean colourless oil (86 mg, 0.39 mmol, 99%), in accordance with literature data.[151] ^{1}H NMR (500 MHz, $CDCl_3$) δ 7.56 (d, J = 7.9 Hz, 2H), 6.90 (d, J = 8.6 Hz, 2H). ^{13}C NMR (126 MHz, $CDCl_3$) δ 129.39 (q, J = 258.0 Hz). ^{13}C NMR (126 MHz, $CDCl_3$) δ 132.66, 132.11, 129.39 (q, J = 258.0 Hz), 126.37 (q, J = 4.1 Hz), 124.53, 29.85. ^{19}F NMR (283 MHz, $CDCl_3$) δ −154.09. IR (diamond-ATR) ν: 2957, 2925, 2854, 1601, 1491, 1400, 1021, 817, 552, 537. GC–MS *m/z* (% relative intensity) [ion]: 227/229 (80) $[M - N_2 + CH_3CN]^+$, 212/214 (10) $[M - N_2 + CN]^+$, 186/188 (10) $[M - N_2]^+$, 148 (100) $[C_7H_4F + CH_3CN]^+$, 107 (95) $[C_7H_4F]^+$, 76 (50) $[C_6H_4]^+$. [M = $C_7H_4BrFN_2$ (213.95)].

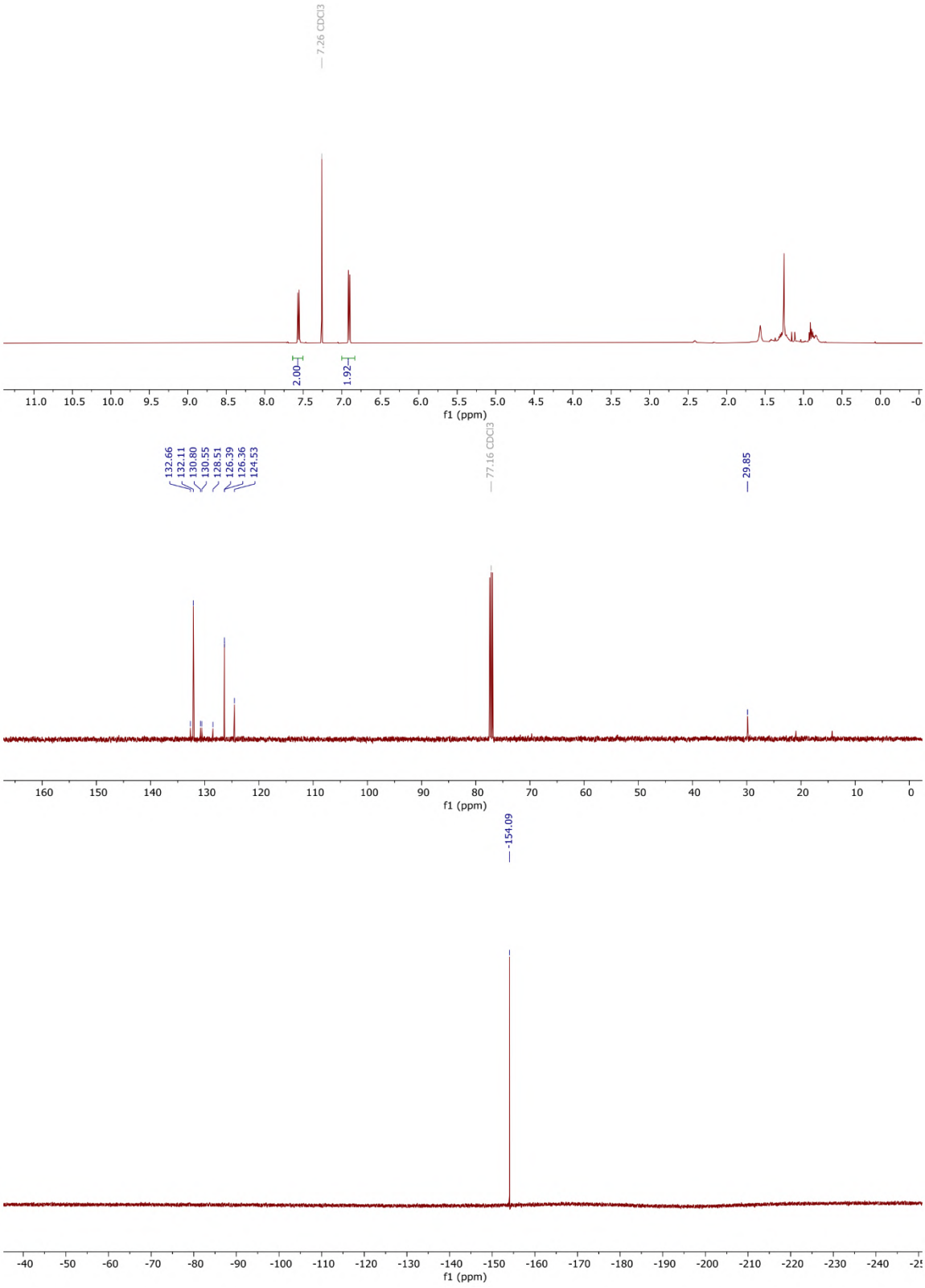

Figure S2.19 ^{1}H, ^{13}C, and ^{19}F NMR spectra of **D2.17** in $CDCl_3$.

2.5.3 General protocols for insertion reactions

(A) **Thermal C–H insertion reaction**: a 15 mM solution of the desired diazirine in anhydrous, degassed cyclohexane was prepared in a heavy wall pressure vessel with PTFE bushing as pressure seal. Glassware was previously flame dried and kept under argon pressure. After sealing the vessel, the reaction was immerged in an oil bath at 140 °C and stirred at that temperature for 2 h. After cooling the mixture to room temperature, the reaction was transferred into a round bottom flask and concentrated in vacuo to provide crude product.

(B) **Photochemical C–H insertion reaction**: a 15 mM solution of the desired diazirine in anhydrous, degassed cyclohexane was prepared in a long neck round bottom flask. Glassware was previously flame dried and kept under argon pressure. The flask was sealed with a septum and placed under a balloon of argon to maintain an inert atmosphere. The flask was suspended into a Rayonet UV chamber that was equipped with eight 350 nm UV lamps and an operating fan. The reaction contents were irradiated for 4 h. The reaction was then concentrated in vacuo to provide crude product.

(C) **Thermal insertion reaction in a "wet environment"**: a 15 mM solution of the desired diazirine in a specific, moisture-containing solvent was prepared in a heavy wall pressure vessel with PTFE bushing as pressure seal. The reaction was prepared under air. After sealing the vessel, the reaction was immerged in an oil bath at 140 °C and stirred at that temperature for 2 h. After cooling the mixture to room temperature, the reaction was transferred into a round bottom flask and concentrated in vacuo to provide crude product.

(D) **Photochemical insertion reaction in a "wet environment"**: a 15 mM solution of the desired diazirine in a specific, moisture-containing solvent was prepared in a long neck round bottom flask. The reaction was prepared under air. The flask was sealed with a septum and suspended into a Rayonet UV chamber that was equipped with eight 350 nm UV lamps and an operating fan. The reaction contents were irradiated for 2 h. The reaction was then concentrated in vacuo to provide crude product.

Crude ^{19}F NMR ($CDCl_3$) spectra were collected and compared to show the effect of aryl substituent electronics on the type of insertion products. The crude materials were purified by chromatography using petroleum ether as eluent, unless otherwise specified.

Several 2–4 mL fractions were collected in 12 x 75 mm test tubes. Fractions that contained the desired product were combined and concentrated.

2.5.3.1 Insertion reactions in cyclohexane

Preparation of 1-(1-cyclohexyl-2,2,2-trifluoroethyl)-4-(trifluoromethyl)benzene (**S2.35**).

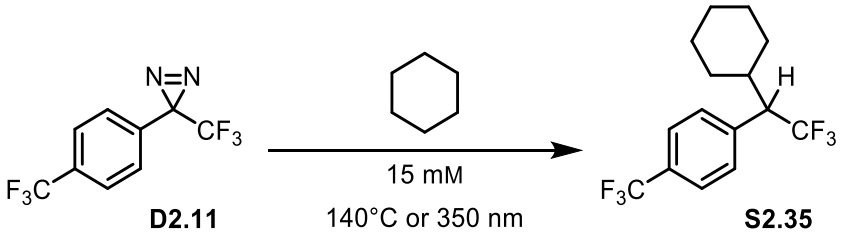

Following the above general protocols (**A** and **B**) for insertion experiments, the reaction was performed using: **A) Thermal insertion:** diazirine **D2.11** (55.5 mg, 0.218 mmol) dissolved in cyclohexane (14 mL). The desired product **S2.35** (4 mg, 0.013 mmol, 6%) was isolated following chromatography. **B) Photochemical insertion**: diazirine **D2.11** (29 mg, 0.114 mmol) dissolved in cyclohexane (7.6 mL). The desired product **S2.35** (9.2 mg, 0.029 mmol, 25%) was isolated following chromatography. ^{1}H NMR (500 MHz, $CDCl_3$) δ 7.60 (d, *J* = 8.1 Hz, 2H), 7.36 (d, *J* = 8.0 Hz, 2H), 3.12 (qd, *J* = 9.6, 8.5 Hz, 1H), 2.05 – 1.93 (m, 2H), 1.82 – 1.74 (m, 1H), 1.68 – 1.58 (m, 2H), 1.49 – 1.41 (m, 1H), 1.36 – 1.30 (m, 1H), 1.15 – 1.03 (m, 3H), 0.82 – 0.75 (m, 1H). ^{13}C NMR (126 MHz, $CDCl_3$) δ 129.71, 125.59 (q, *J* = 3.8 Hz), 56.21 (q, *J* = 26.0 Hz), 38.65, 31.54, 30.82, 29.85, 26.21, 26.12, 26.02. ^{19}F NMR (471 MHz, $CDCl_3$) δ –62.65 (*p*-CF_3), –63.23. IR (diamond-ATR) ν: 2954, 2920, 2851, 1464, 1267, 1168, 1131, 1116, 730. GC–MS *m/z* (% relative intensity) [ion]: 310 (10) $[M]^+$, 291 (8) $[C_{15}H_{16}F_5]^+$, 177 (14) $[C_8H_5F_4]^+$, 159 (8) $[C_8H_6F_3]^+$, 83 (100) $[C_6H_{11}]^+$, 67 (15) $[C_5H_7]^+$, 55 (96) $[C_4H_7]^+$. [M = $C_{15}H_{16}F_6$ (310.12)].

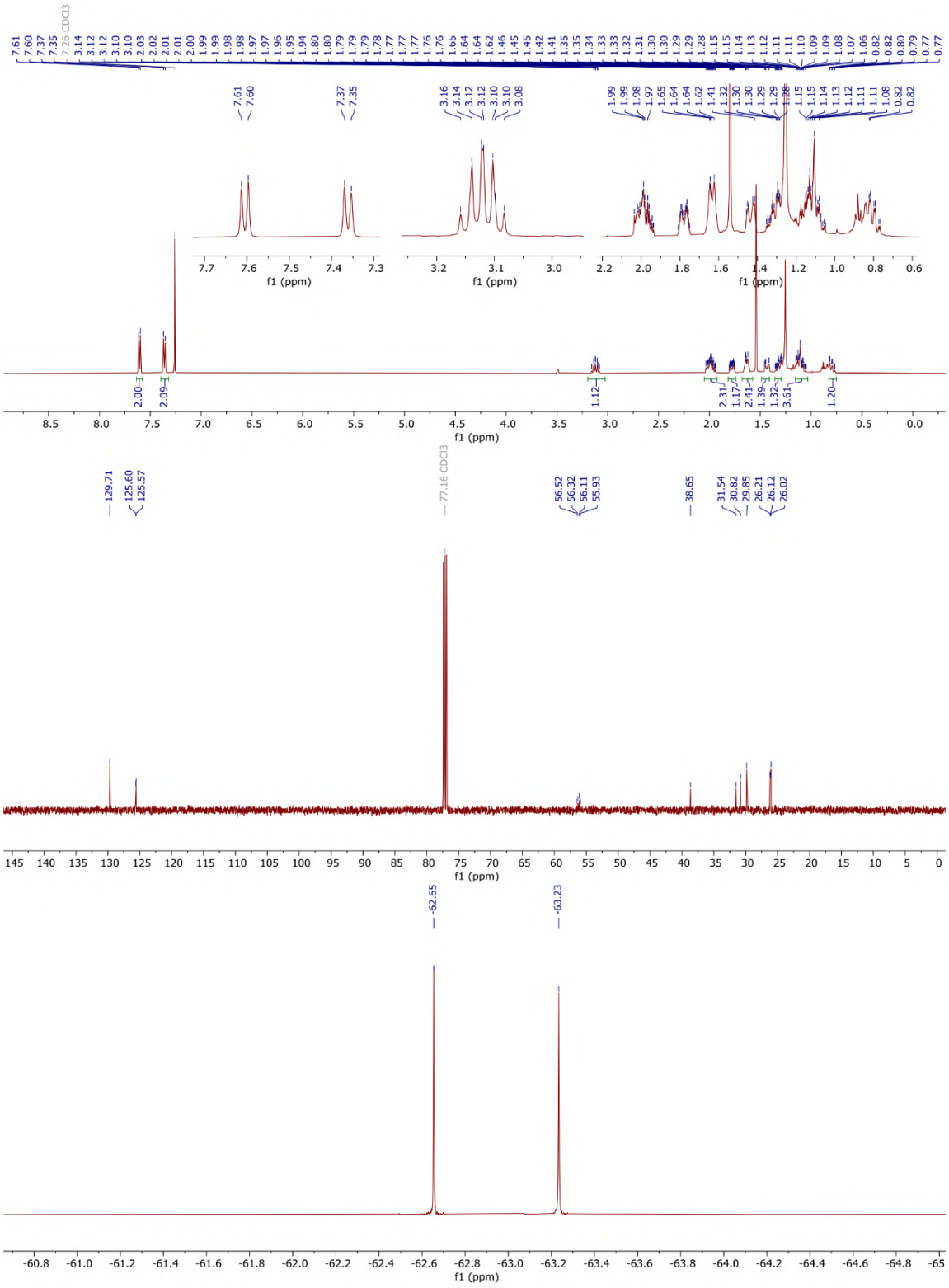

Figure S2.20 ^{1}H, ^{13}C, and ^{19}F NMR spectra of cyclohexane adduct **S2.35** in $CDCl_3$.

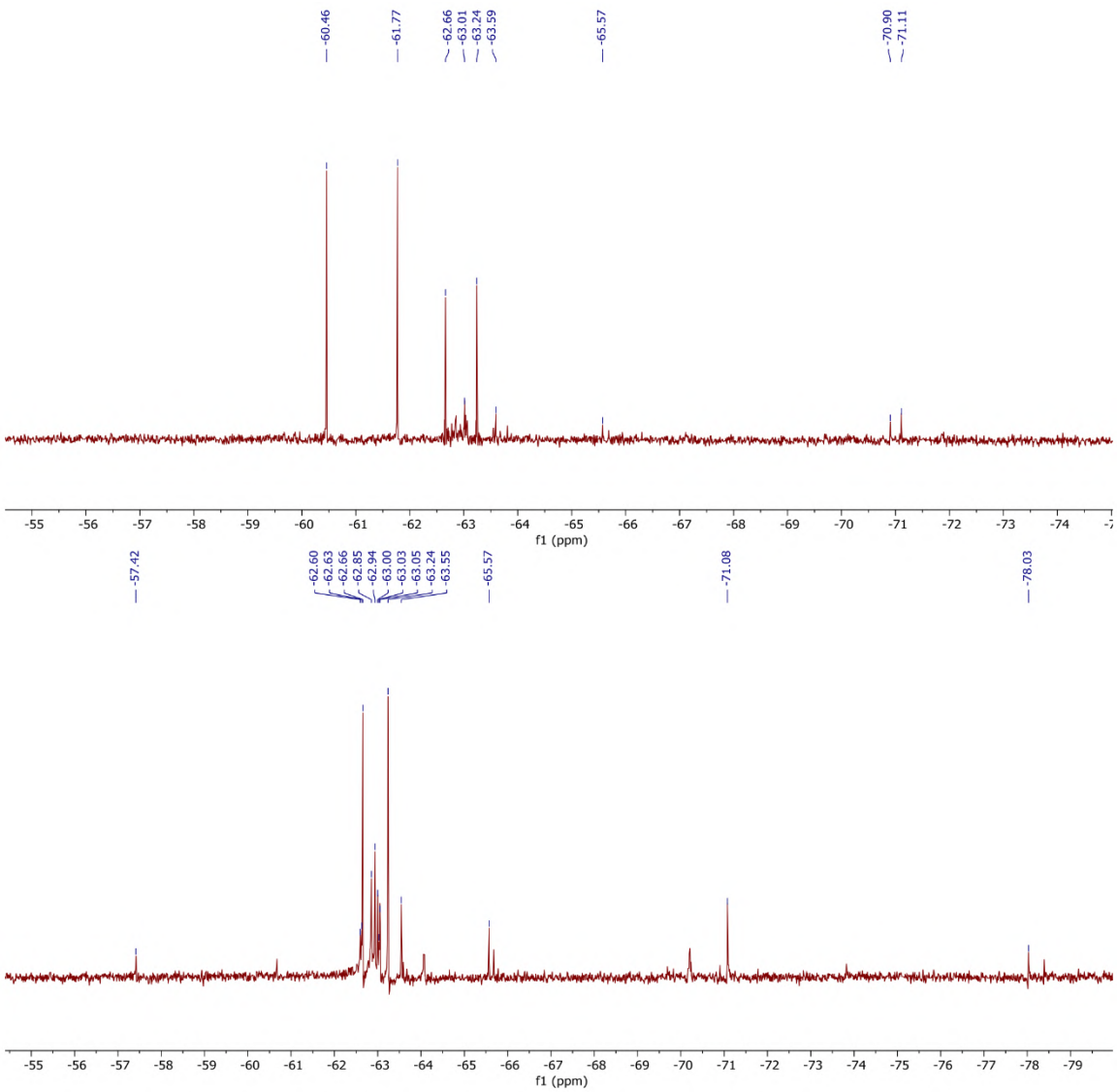

Figure S2.21 Crude ^{19}F NMR spectra: under thermal (top) and photochemical (bottom) insertion conditions.

Preparation of (1-cyclohexyl-2,2,2-trifluoroethyl)benzene (**S2.36**).

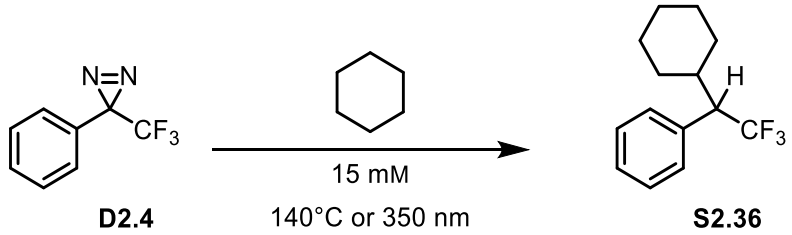

D2.4 **S2.36**

Following the above general protocols (**A** and **B**) for insertion experiments, the reaction was performed using: **A) Thermal insertion:** diazirine **D2.4** (66 mg, 0.35 mmol) dissolved in cyclohexane (24 mL). The desired product **S2.36** (12.7 mg, 0.053 mmol, 15%) was isolated following chromatography. **B) Photochemical insertion**: diazirine **D2.4** (66 mg, 0.35 mmol) dissolved in cyclohexane (24 mL). The desired product **S2.36** (30.1 mg, 0.124 mmol, 35%) was isolated following chromatography. The analytical data were in accordance with literature.[152] ^{1}H NMR (300 MHz, $CDCl_3$) δ 7.39 – 7.28 (m, 3H), 7.26 – 7.20 (m, 2H), 3.03 (qd, *J* = 10.2, 8.0 Hz, 1H), 2.06 – 1.98 (m, 1H), 1.98 – 1.89 (m, 1H), 1.84 – 1.71 (m, 1H), 1.70 – 1.57 (m, 2H), 1.52 – 1.41 (m, 1H), 1.39 – 1.27 (m, 1H), 1.21 – 1.03 (m, 3H), 0.85 – 0.72 (m, 1H). ^{13}C NMR (126 MHz, $CDCl_3$) δ 129.34, 128.58, 127.84, 38.69, 30.90, 29.86, 26.31, 26.23, 26.15. ^{19}F NMR (283 MHz, $CDCl_3$) δ –63.31. IR (diamond-ATR) ν: 2931, 2857, 1169, 1104, 700.

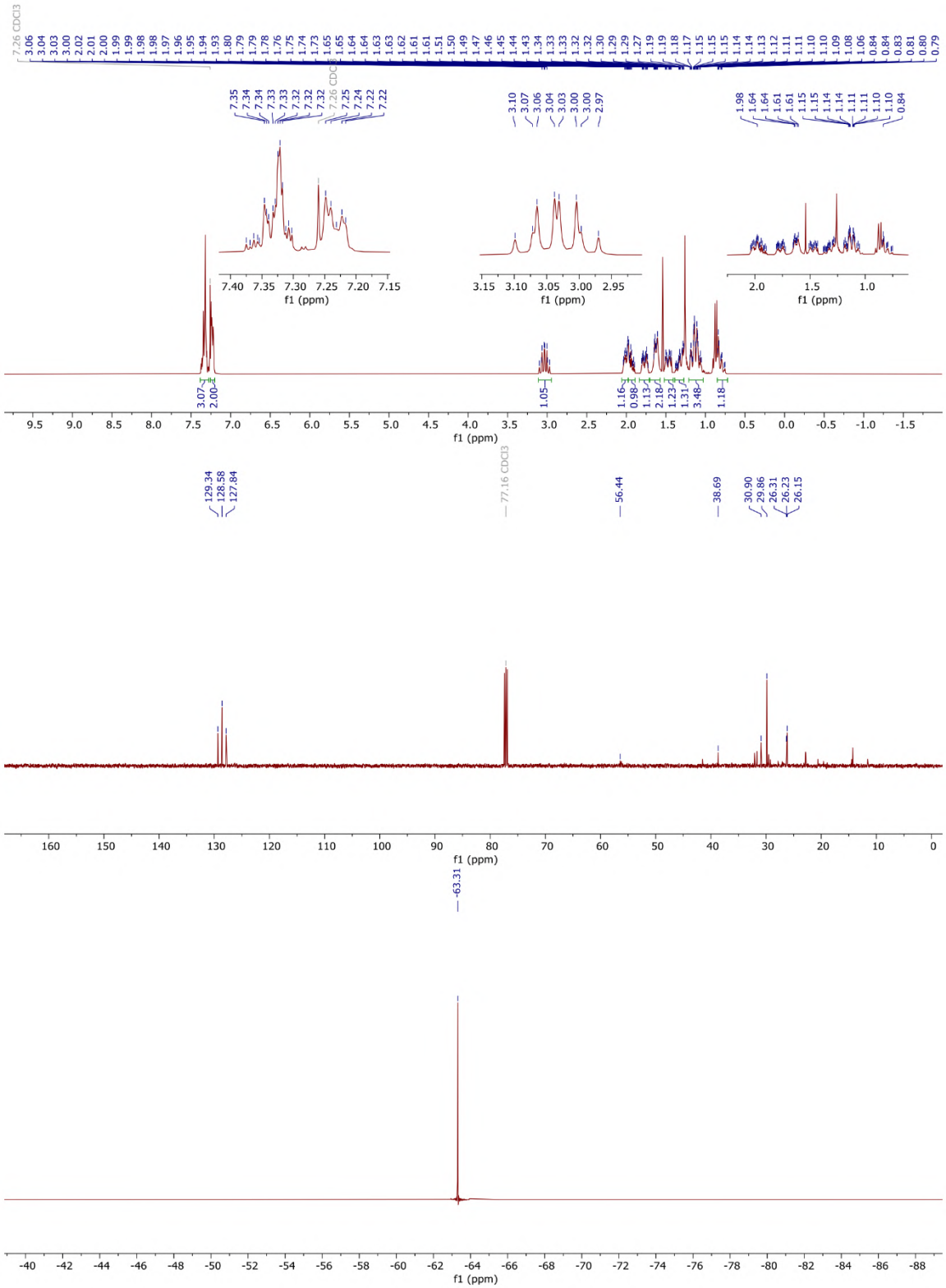

Figure S2.22 ^{1}H, ^{13}C, and ^{19}F NMR spectra of cyclohexane adduct **S2.36** in $CDCl_3$.

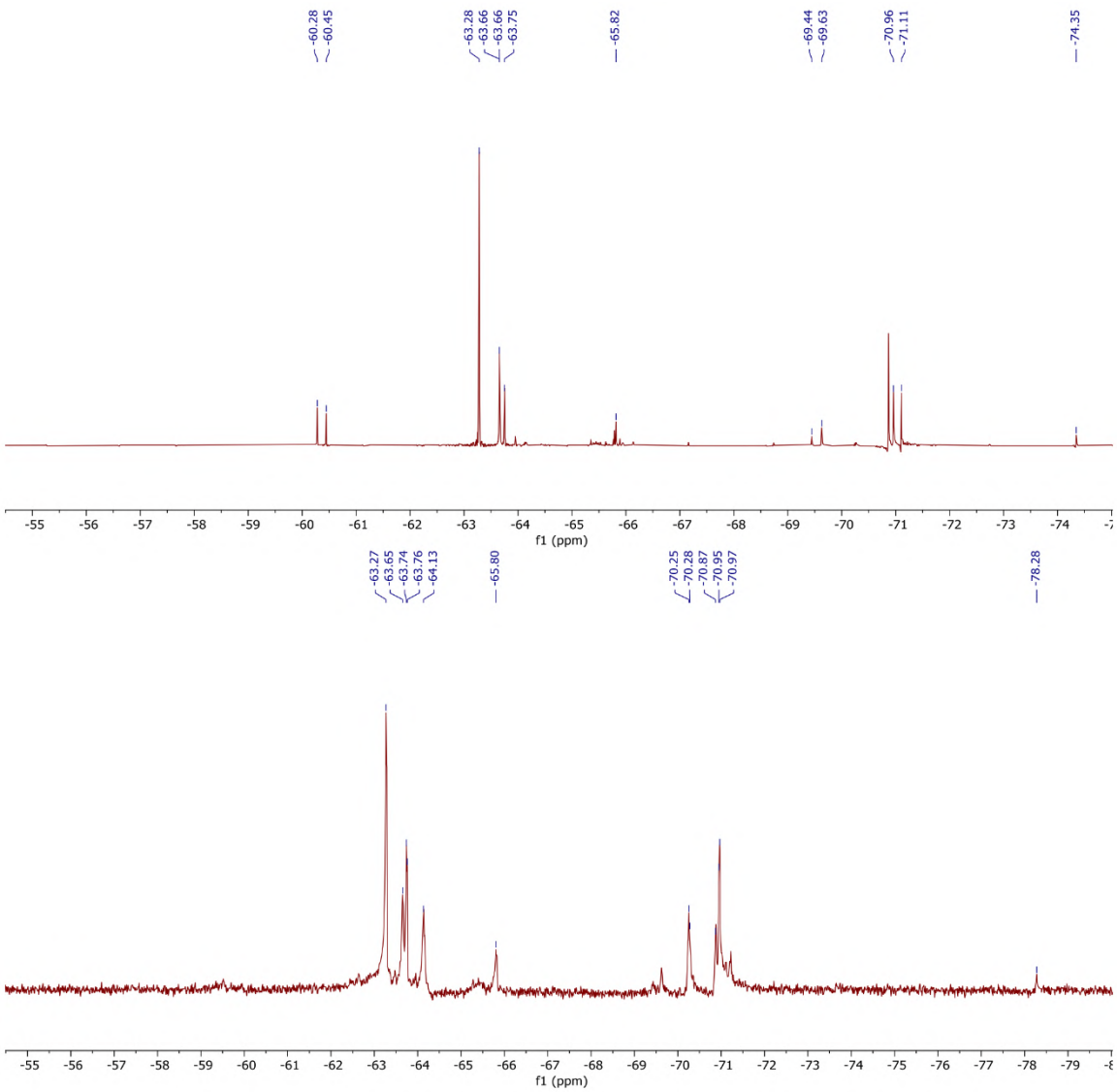

Figure S2.23 Crude ^{19}F NMR spectra: under thermal (top) and photochemical (bottom) insertion conditions.

Preparation of 1-(1-cyclohexyl-2,2,2-trifluoroethyl)-3-methoxybenzene (**S2.37**).

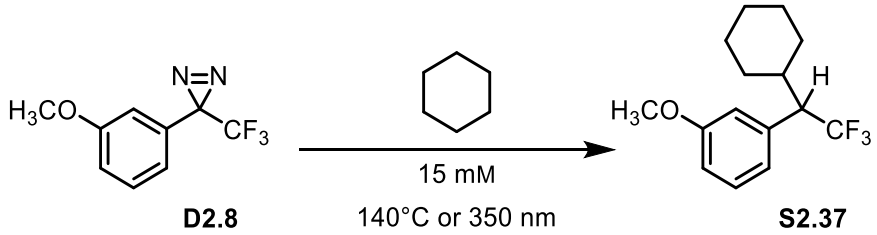

D2.8 **S2.37**

Following the above general protocols (**A** and **B**) for insertion experiments, the reaction was performed using: **A) Thermal insertion:** diazirine **D2.8** (64.3 mg, 0.3 mmol) dissolved in cyclohexane (20 mL). The desired product **S2.37** (14.7 mg, 0.054 mmol, 18%) was isolated following chromatography. **B) Photochemical insertion**: diazirine **D2.8** (45.1 mg, 0.208 mmol) dissolved in cyclohexane (14 mL). The desired product **S2.37** (11 mg, 0.04 mmol, 19%) was isolated following chromatography. ^{1}H NMR (500 MHz, $CDCl_3$) δ 7.25 (t, *J* = 7.9 Hz, 1H), 6.85 (ddd, *J* = 8.3, 2.6, 1.0 Hz, 1H), 6.82 (d, *J* = 7.7 Hz, 1H), 6.78 (t, *J* = 2.1 Hz, 1H), 3.81 (s, 3H), 3.00 (qd, *J* = 10.1, 8.3 Hz, 1H), 2.03 – 1.96 (m, 1H), 1.96 – 1.88 (m, 1H), 1.81 – 1.72 (m, 1H), 1.68 – 1.58 (m, 2H), 1.48 (dt, *J* = 14.0, 3.4 Hz, 1H), 1.32 – 1.24 (m, 1H), 1.20 – 1.07 (m, 3H), 0.83 (qd, *J* = 12.1, 3.3 Hz, 1H). ^{13}C NMR (126 MHz, $CDCl_3$) δ 159.68, 129.52, 121.79, 115.43, 112.76, 56.31 (q, *J* = 25.3 Hz), 55.34, 38.69, 31.61, 30.93, 26.30, 26.24, 26.15. ^{19}F NMR (283 MHz, $CDCl_3$) δ –63.28. IR (diamond-ATR) ν: 2928, 2855, 1603, 1586, 1251, 1156, 1132, 712.

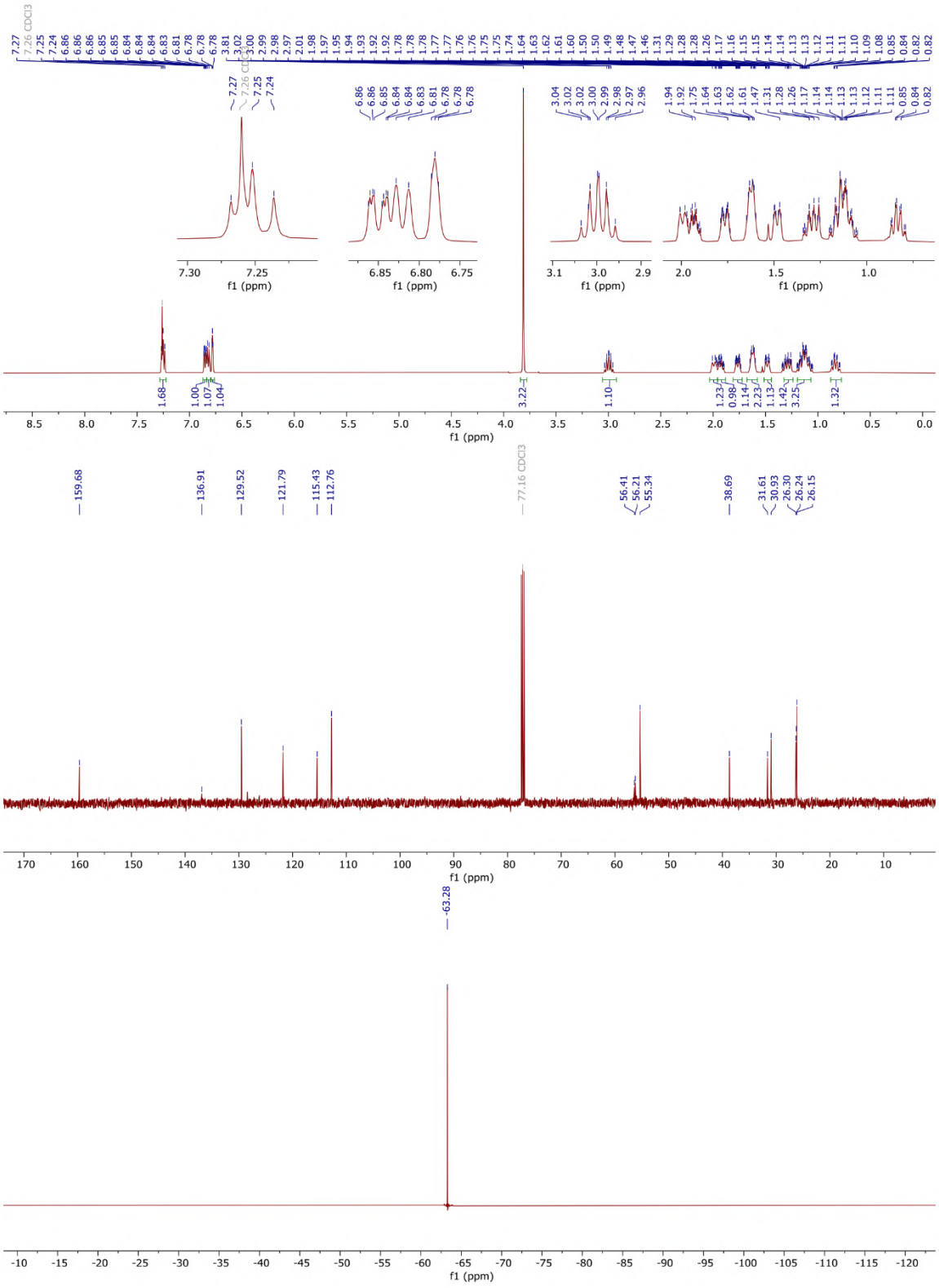

Figure S2.24 ^{1}H, ^{13}C, and ^{19}F NMR spectra of cyclohexane adduct **S2.37** in $CDCl_3$.

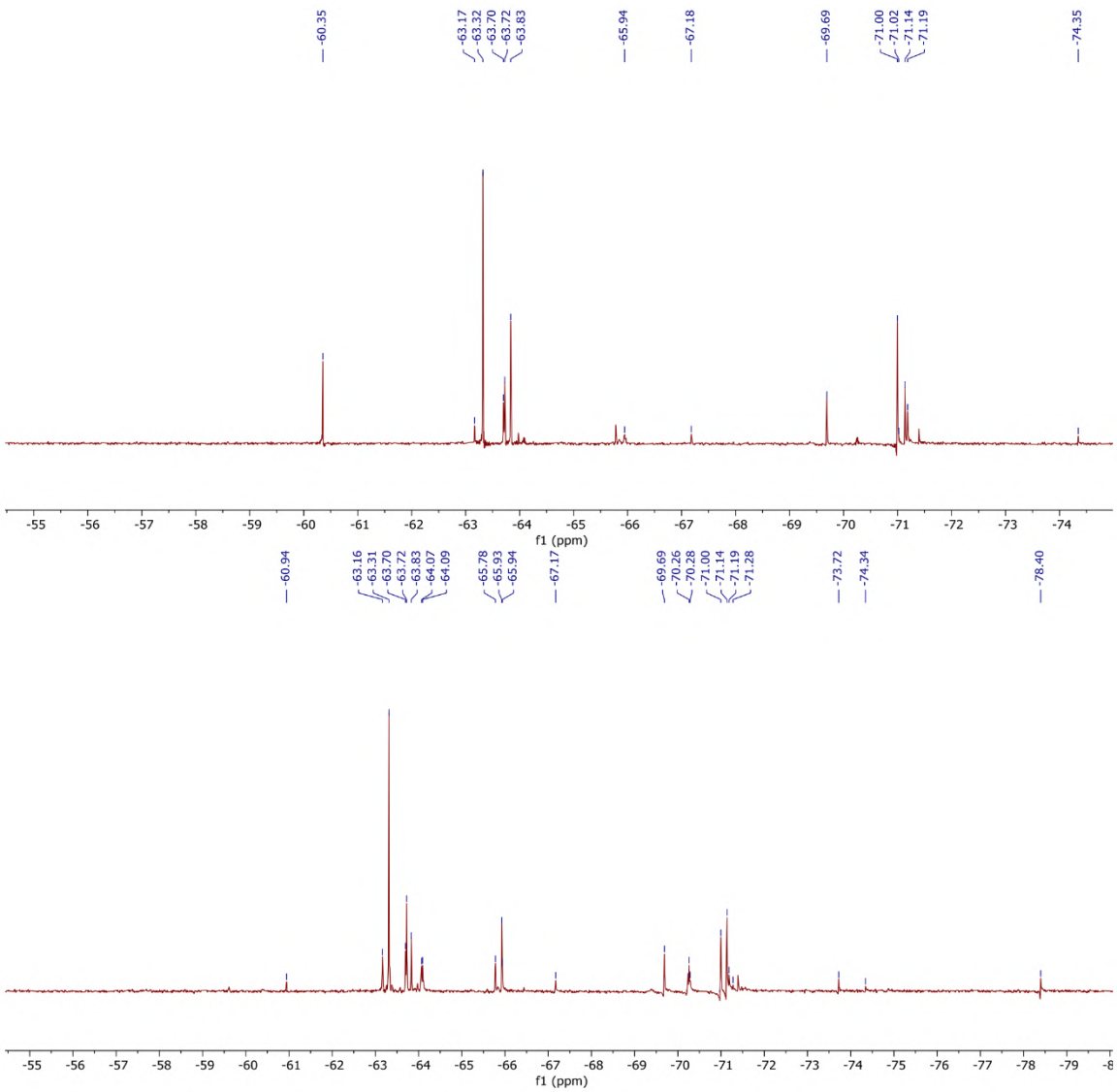

Figure S2.25 Crude ^{19}F NMR spectra: under thermal (top) and photochemical (bottom) insertion conditions.

Preparation of 1-(1-cyclohexyl-2,2,2-trifluoroethyl)-4-phenoxybenzene (**S2.38**).

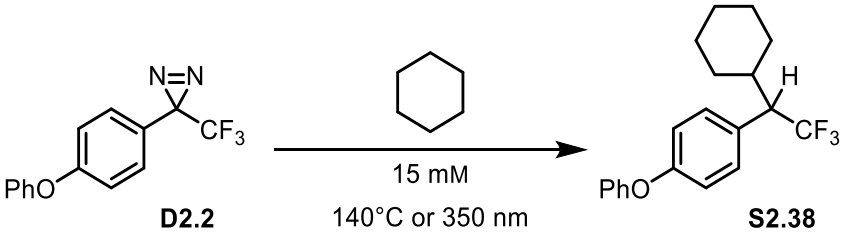

Following the above general protocols (**A** and **B**) for insertion experiments, the reaction was performed using: **A) Thermal insertion:** diazirine **D2.2** (51 mg, 0.183 mmol) dissolved in cyclohexane (12 mL). The desired product **S2.38** (45.9 mg, 0.137 mmol, 75%) was isolated following chromatography. **B) Photochemical insertion**: diazirine **D2.2** (22.9 mg, 0.082 mmol) dissolved in cyclohexane (5.5 mL). The desired product **S2.38** (21.2 mg, 0.063 mmol, 77%) was isolated following chromatography. ^{1}H NMR (500 MHz, $CDCl_3$) δ 7.40 – 7.31 (m, 2H), 7.18 (d, *J* = 8.5 Hz, 2H), 7.12 (t, *J* = 7.4 Hz, 1H), 7.03 (d, *J* = 7.6 Hz, 2H), 6.96 (d, *J* = 8.7 Hz, 2H), 3.02 (qd, *J* = 9.9, 8.5 Hz, 1H), 1.98 (d, *J* = 13.9 Hz, 1H), 1.95 – 1.88 (m, 1H), 1.83 – 1.72 (m, 1H), 1.70 – 1.59 (m, 2H), 1.50 (s, 1H), 1.37 – 1.28 (m, 1H), 1.20 – 1.04 (m, 3H), 0.83 – 0.76 (m, 1H). ^{13}C NMR (126 MHz, $CDCl_3$) δ 157.11, 156.94, 130.62, 129.94, 123.68, 119.39, 118.53, 38.70, 31.63, 30.86, 26.31, 26.24, 26.15. ^{19}F NMR (283 MHz, $CDCl_3$) δ –63.60. IR (diamond-ATR) ν: 2925, 2854, 1508, 1489, 1238, 1154, 1099. GC–MS *m/z* (% relative intensity) [ion]: 334 (90) $[M]^+$, 315 (2) $[C_{20}H_{21}F_2O]^+$, 252 (76) $[C_{14}H_{11}F_3O]^+$, 251 (72) $[C_{14}H_{10}F_3O]^+$, 183 (32) $[C_{13}H_{11}O]^+$, 159 (16) $[C_8H_6F_3]^+$, 83 (100) $[C_6H_{11}]^+$, 77 (46) $[C_6H_5]^+$, 55 (96) $[C_4H_7]^+$. [M = $C_{20}H_{21}F_3O$ (334.15)].

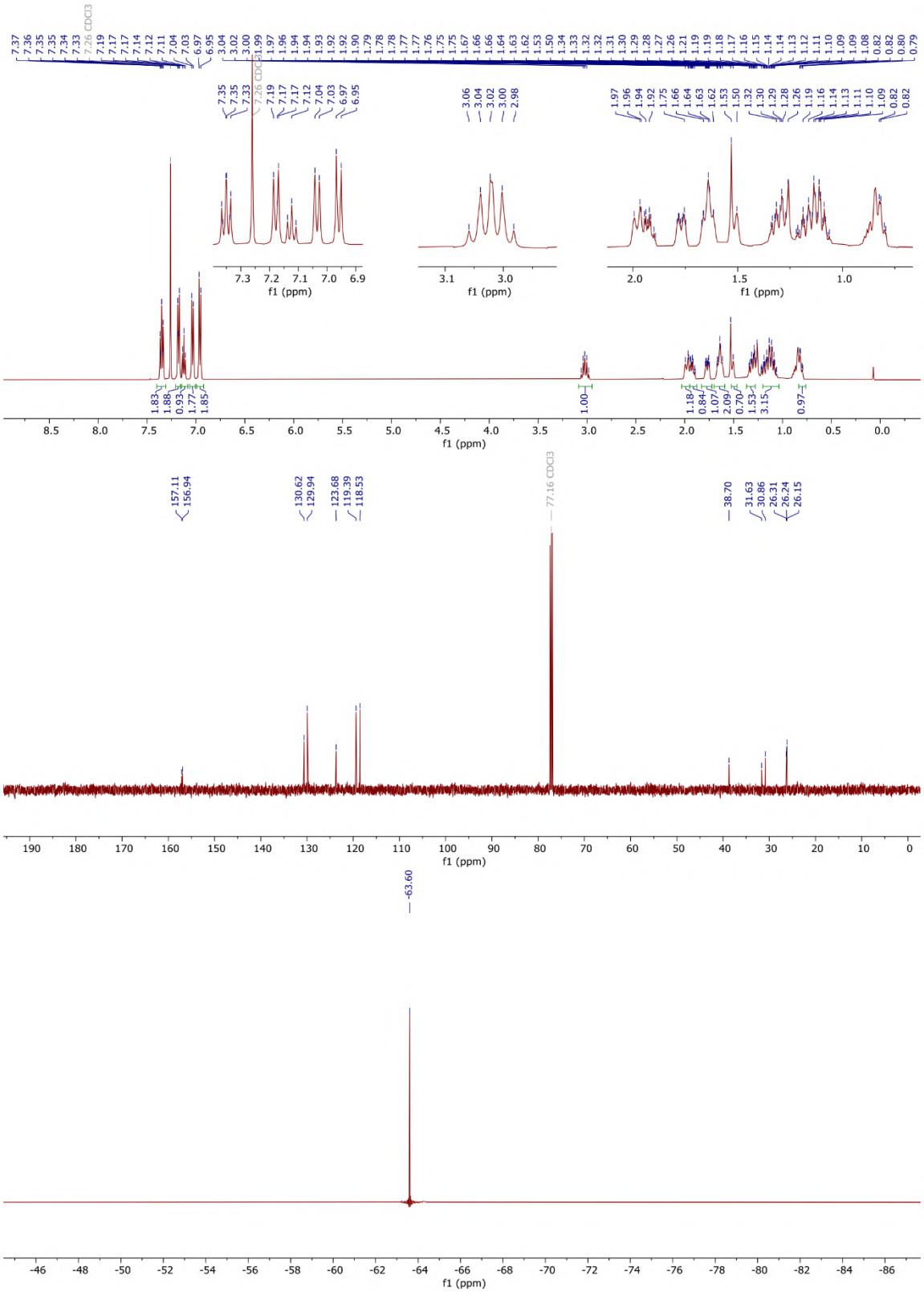

Figure S2.26 ^{1}H, ^{13}C, and ^{19}F NMR spectra of cyclohexane adduct **S2.38** in $CDCl_3$.

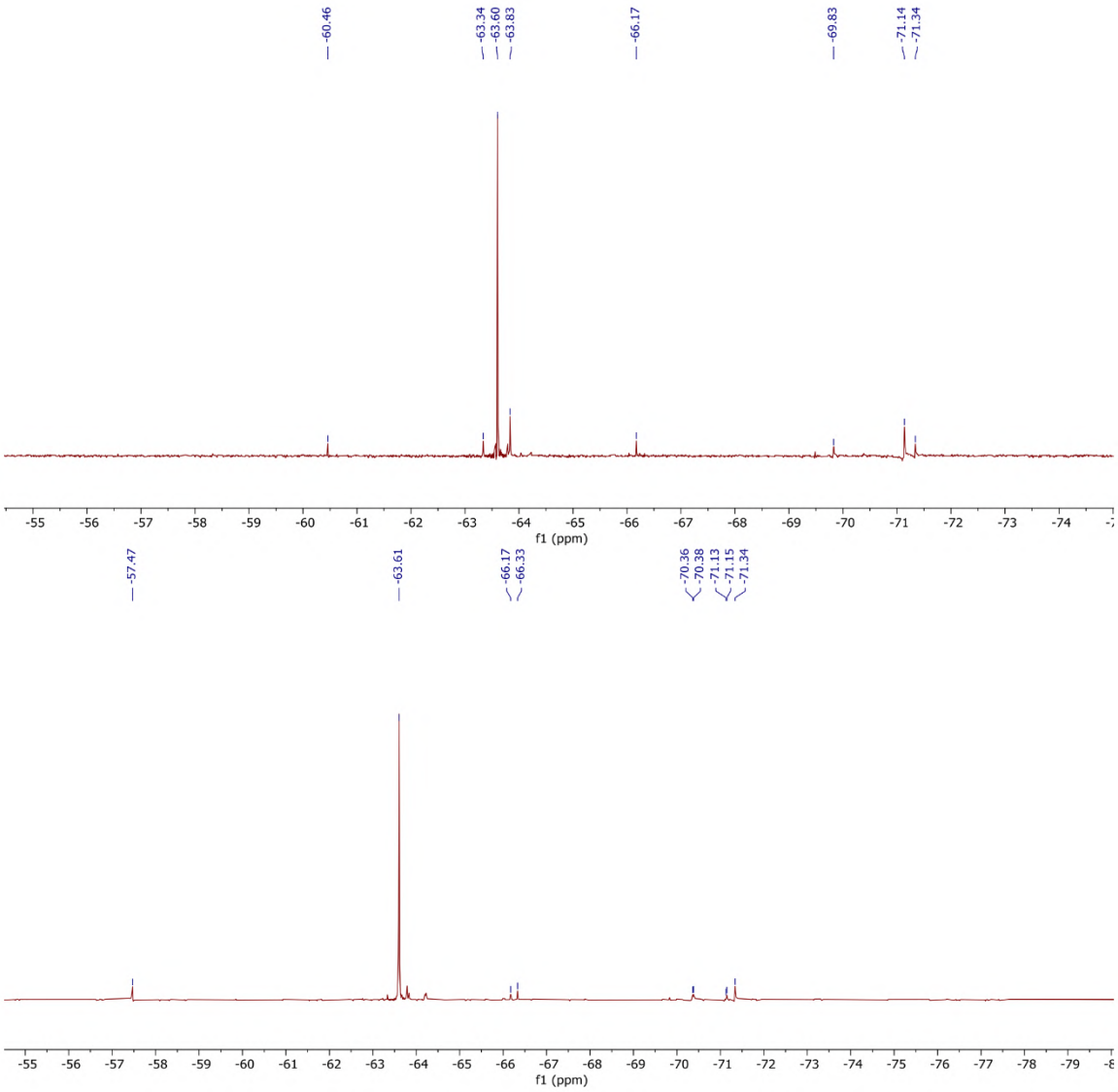

Figure S2.27 Crude ^{19}F NMR spectra: under thermal (top) and photochemical (bottom) insertion conditions.

Preparation of 1-(1-cyclohexyl-2,2,2-trifluoroethyl)-4-methoxybenzene (**S2.39**).

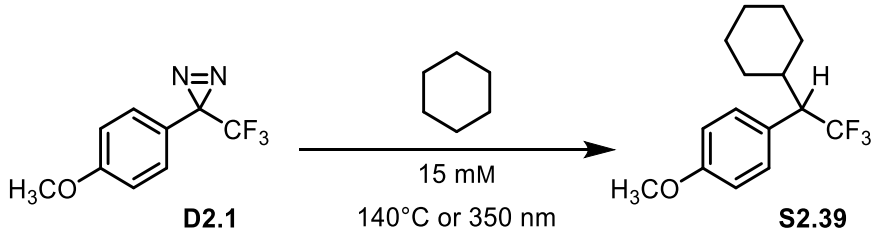

Following the above general protocols (**A** and **B**) for insertion experiments, the reaction was performed using: **A) Thermal insertion:** diazirine **D2.1** (108 mg, 0.5 mmol) dissolved in cyclohexane (35 mL). The desired product **S2.39** (124 mg, 0.455 mmol, 91%) was isolated following chromatography. **B) Photochemical insertion**: diazirine **D2.1** (56.1 mg, 0.259 mmol) dissolved in cyclohexane (17 mL). The desired product **S2.39** (66.4 mg, 0.244 mmol, 94%) was isolated following chromatography. Spectroscopic data are in accordance with the literature.[112] ^{1}H NMR (500 MHz, $CDCl_3$) δ 7.15 (d, *J* = 8.6 Hz, 2H), 6.87 (d, *J* = 8.7 Hz, 2H), 3.81 (s, 3H), 3.01 (qd, *J* = 10.0, 8.4 Hz, 1H), 1.96 (d, *J* = 14.0 Hz, 1H), 1.90 (ddt, *J* = 11.4, 6.8, 3.3 Hz, 1H), 1.81 – 1.72 (m, 1H), 1.67 – 1.57 (m, 2H), 1.50 (d, *J* = 13.6 Hz, 1H), 1.36 – 1.23 (m, 1H), 1.22 – 1.02 (m, 3H), 0.87 – 0.75 (m, 1H). ^{13}C NMR (126 MHz, $CDCl_3$) δ 159.20, 130.38, 113.96, 55.35, 38.68, 31.66, 30.82, 26.33, 26.26, 26.17. ^{19}F NMR (283 MHz, $CDCl_3$) δ –63.74. IR (diamond-ATR) ν: 2927, 2855, 1515, 1247, 1153, 1134, 1099, 831, 820.

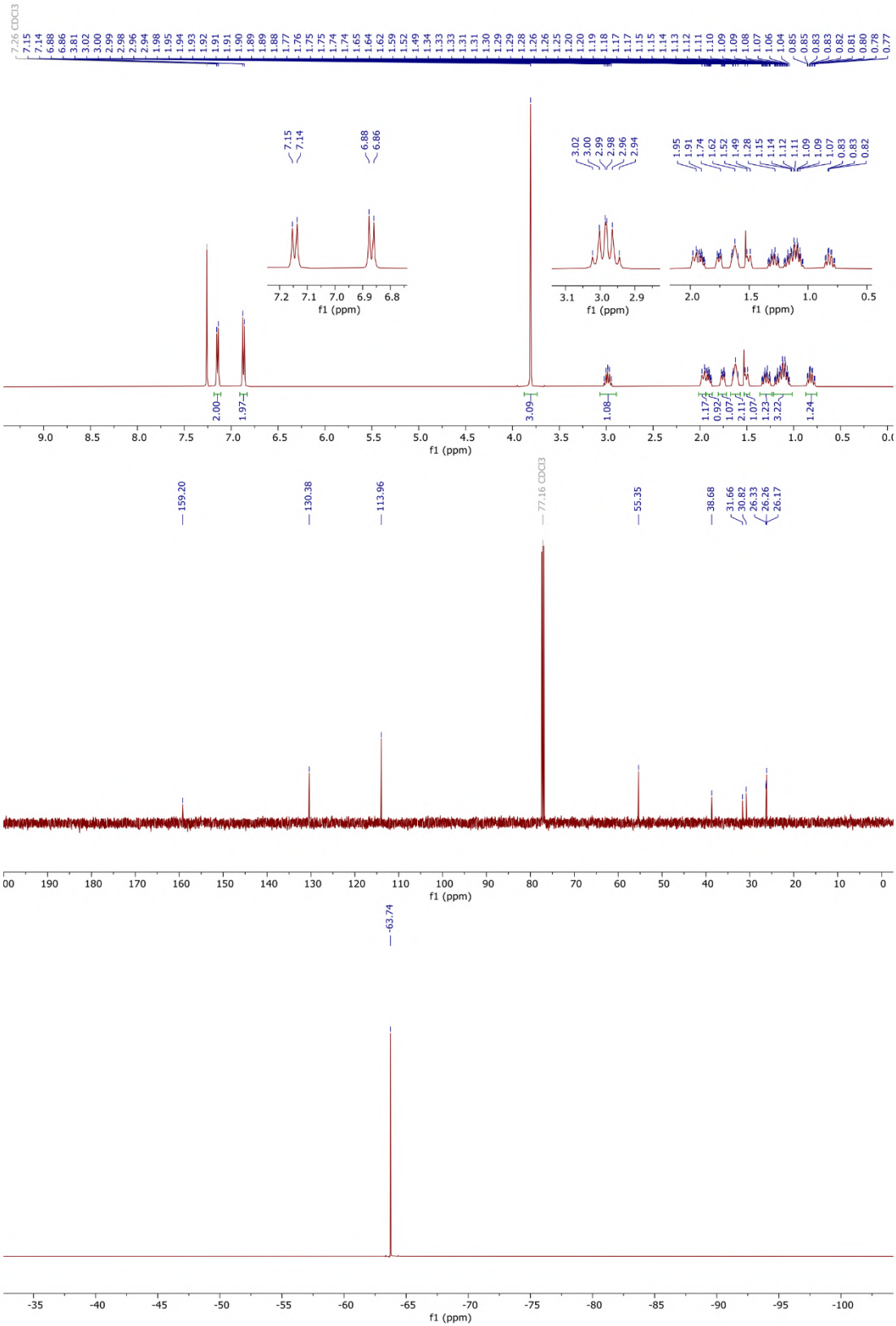

Figure S2.28 ^{1}H, ^{13}C, and ^{19}F NMR spectra of cyclohexane adduct **S2.39** in $CDCl_3$.

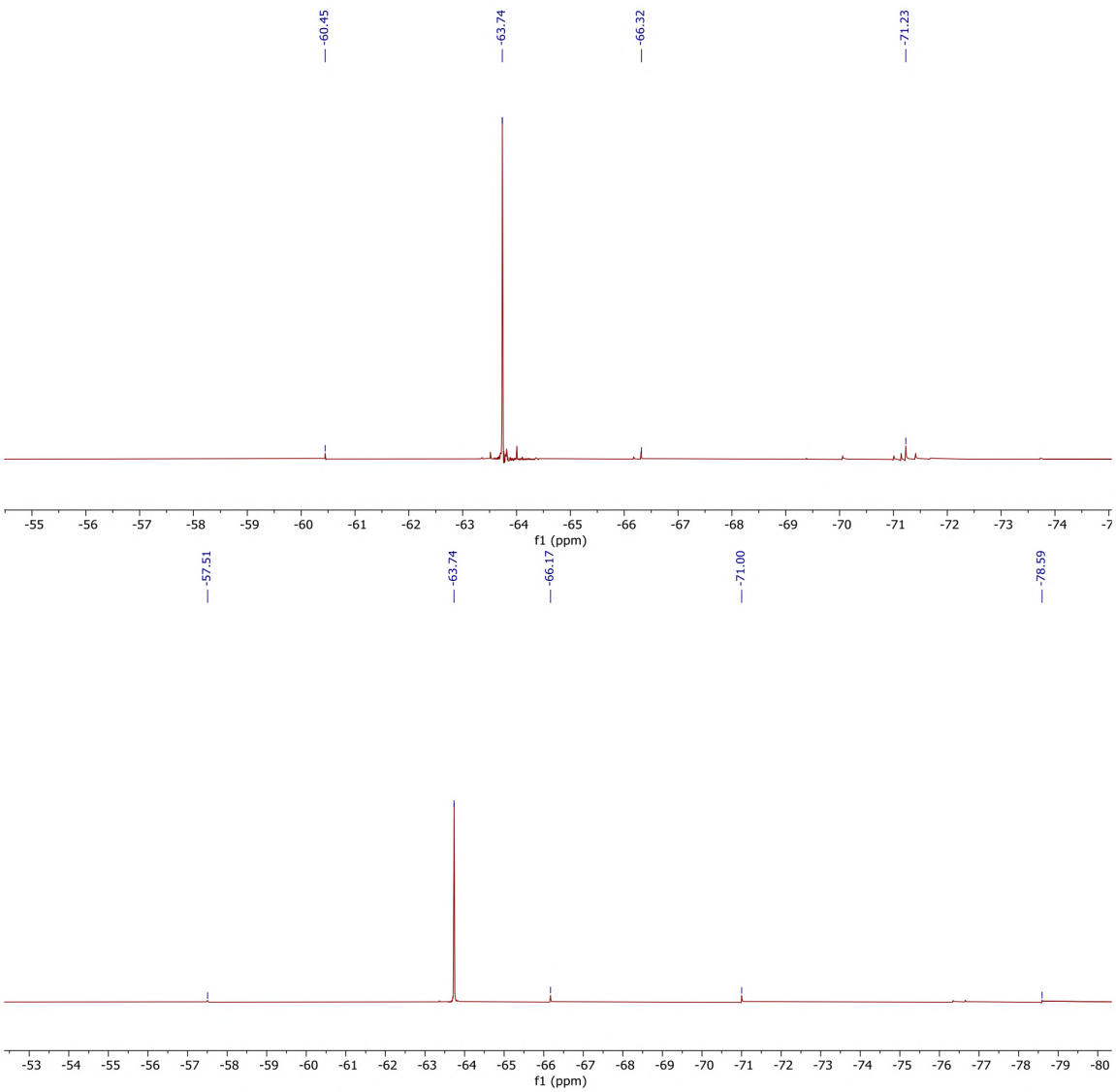

Figure S2.29 Crude ^{19}F NMR spectra: under thermal (top) and photochemical (bottom) insertion conditions.

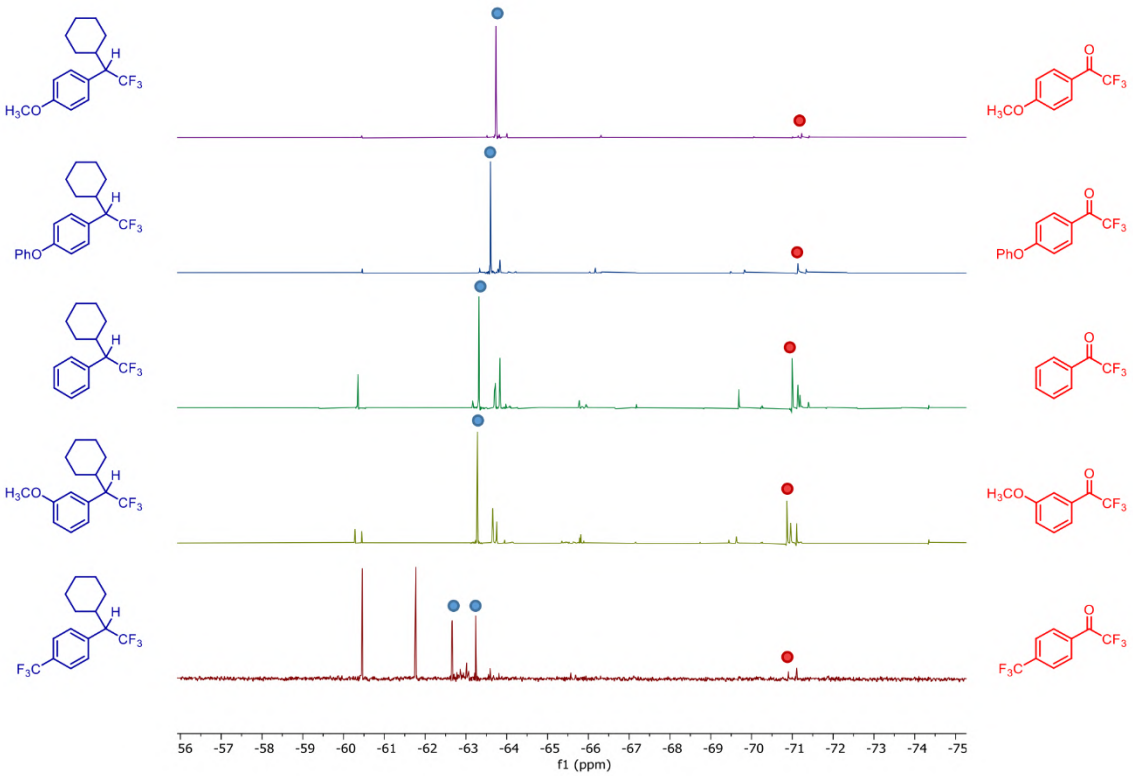

Figure S2.30 Comparison of crude ^{19}F NMR spectra under thermal C–H insertion experiments.

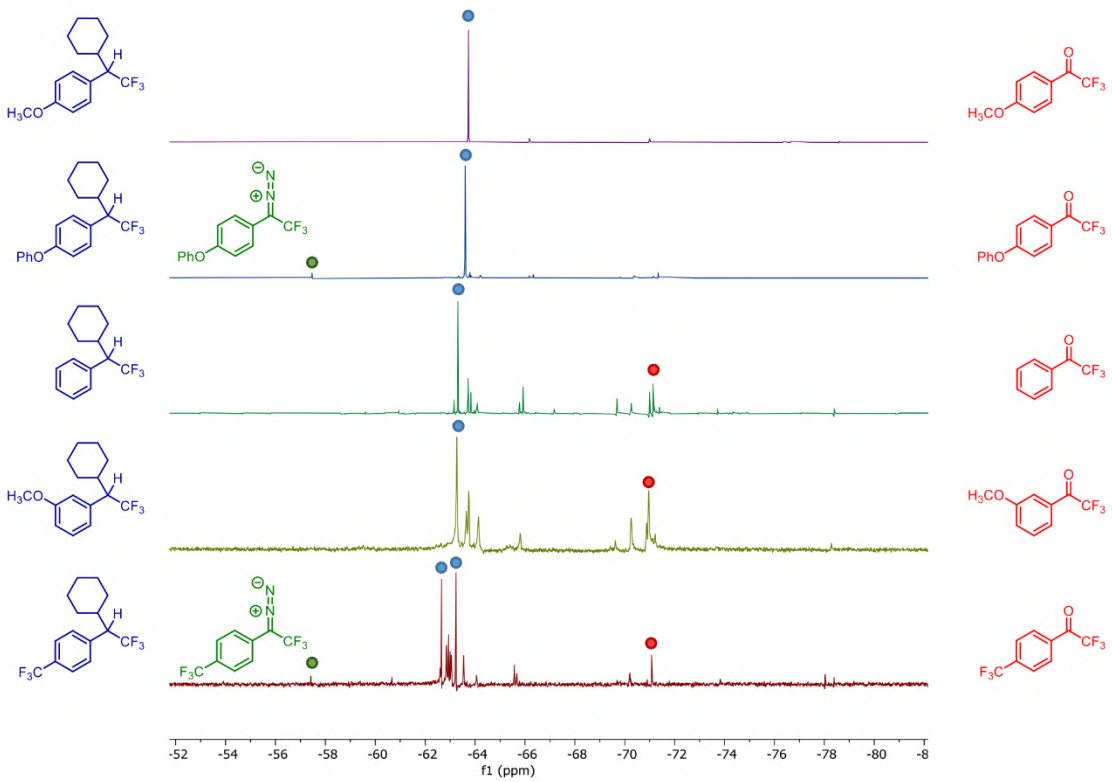

Figure S2.31 Comparison of crude ^{19}F NMR spectra under photochemical C–H insertion experiments.

2.5.3.2 Insertion reactions in a wet environment

Insertion to cyclohexane:water (9:1)

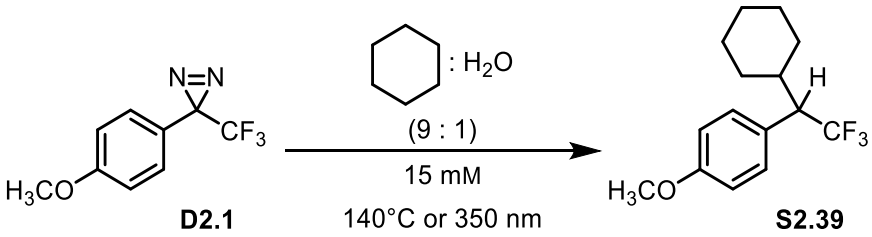

Following the above general protocols (**C** and **D**) for insertion experiments, the reaction was performed using: **C) Thermal insertion:** diazirine **D2.1** (8.5 mg, 0.039 mmol) dissolved in cyclohexane:water (9:1, 2.6 mL). The desired product **S2.39** (9.8 mg, 0.0359 mmol, 92%) was isolated following chromatography. **D) Photochemical insertion**: diazirine **D2.1** (10 mg, 0.046 mmol) dissolved in cyclohexane:water (9:1, 3 mL). The desired product **S2.39** (11.2 mg, 0.041 mmol, 90%) was isolated following chromatography. Spectroscopic data are consistent with the ones reported above for compound **S2.39**.

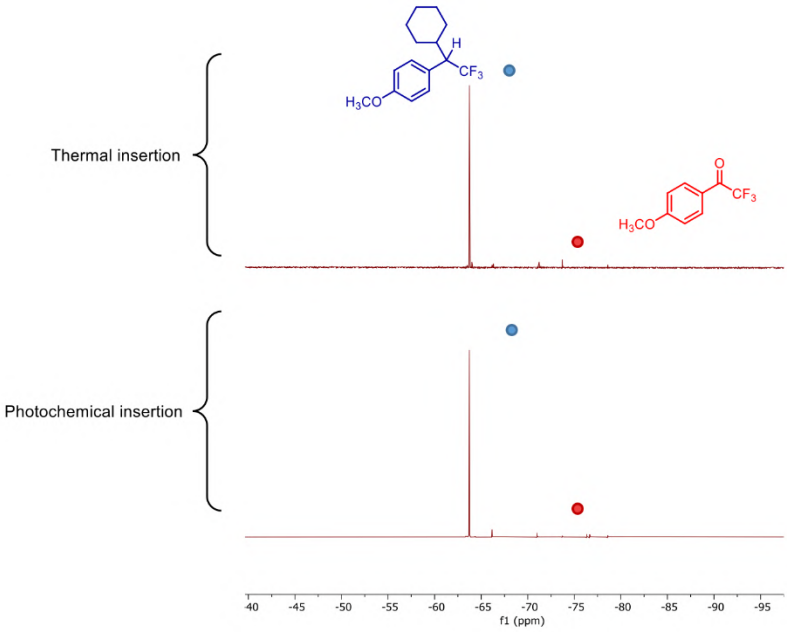

Figure S2.32 Crude ^{1}H NMR spectra of insertion reaction in cyclohexane:water 9:1 (top: thermal; bottom: photochemical).

Insertion to *tert*-Butanol

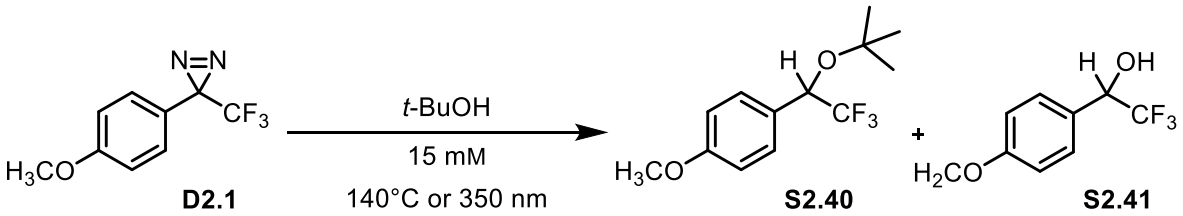

Following the above general protocols (**C** and **D**) for insertion experiments, the reaction was performed using: **C) Thermal insertion:** diazirine **D2.1** (10.7 mg, 0.049 mmol) dissolved in *tert*-butanol (3.2 mL). Compound **S2.40** (8.1 mg, 0.031 mmol, 63%) and compound **S2.41** (2.3 mg, 0.017 mmol, 23%) were isolated following chromatography using petroleum ether: diethyl ether (9:1, R_f= 0.72 (**S2.40**) and R_f= 0.25 (**S2.41**)). **D) Photochemical insertion**: diazirine **D2.1** (16.2 mg, 0.075 mmol) dissolved in *tert*-butanol (5 mL). Compound **S2.40** (12.5 mg, 0.048 mmol, 64%) and compound **S2.41** (4.2 mg, 0.020 mmol, 27%) were isolated following chromatography.

1-(1-(*tert*-Butoxy)-2,2,2-trifluoroethyl)-4-methoxybenzene (S2.40): ^{1}H NMR (500 MHz, $CDCl_3$) δ 7.38 (d, *J* = 8.7 Hz, 2H), 6.89 (d, *J* = 8.8 Hz, 2H), 4.73 (q, *J* = 7.0 Hz, 1H), 3.81 (s, 3H), 1.18 (s, 9H). ^{13}C NMR (126 MHz, $CDCl_3$) δ 160.07, 129.15, 113.81, 72.29 (q, *J* = 31.1 Hz), 55.38, 29.85, 28.29. ^{19}F NMR (283 MHz, $CDCl_3$) δ – 77.22. IR (diamond-ATR) ν: 2960, 2928, 2858, 1613, 1514, 1269, 1249, 1129. GC–MS *m/z* (% relative intensity) [ion]: 262 (10) $[M]^+$, 193 (24) $[C_{12}H_{17}O_2]^+$, 189 (30) $[C_9H_8F_3O]^+$, 137 (100) $[C_8H_9O_2]^+$, 107 (5) $[C_7H_7O]^+$, 77 (10) $[C_6H_5]^+$, 57 (30) $[C_4H_9]^+$. [M = $C_{13}H_{17}F_3O_2$ (262.12)].

(4-(2,2,2-Trifluoro-1-hydroxyethyl)phenoxy)methylium (S2.41): ^{1}H NMR (500 MHz, $CDCl_3$) δ 7.48 – 7.33 (m, 2H), 6.94 (d, *J* = 8.8 Hz, 2H), 4.98 (q, *J* = 6.7 Hz, 1H), 3.83 (s, 3H), 2.08 (d, *J* = 5.0 Hz, 1H, OH). ^{19}F NMR (283 MHz, $CDCl_3$) δ – 78.59. Spectroscopic data in accordance with the literature.[112]

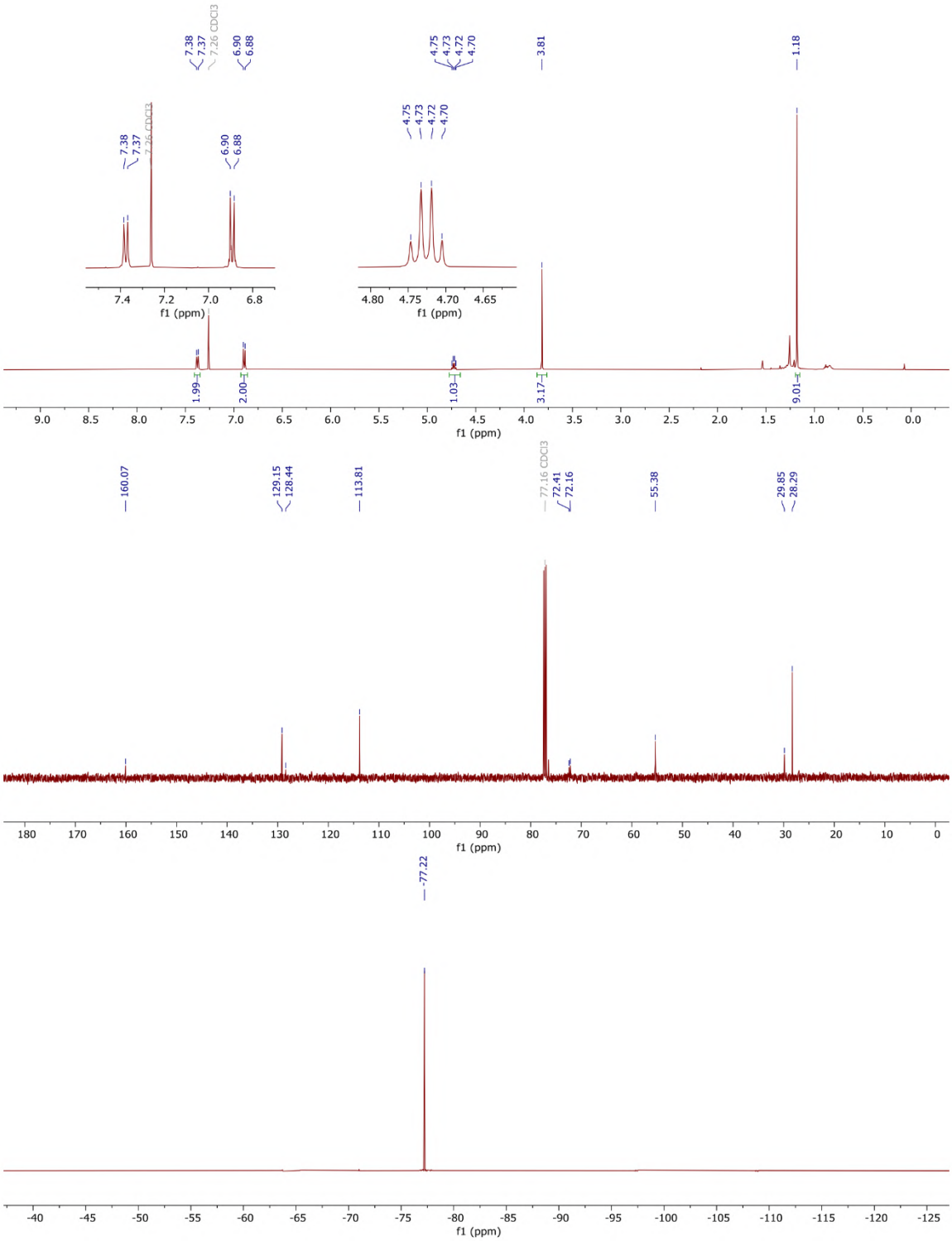

Figure S2.33 ^{1}H, ^{13}C, and ^{19}F NMR spectra of **S2.40** in $CDCl_3$.

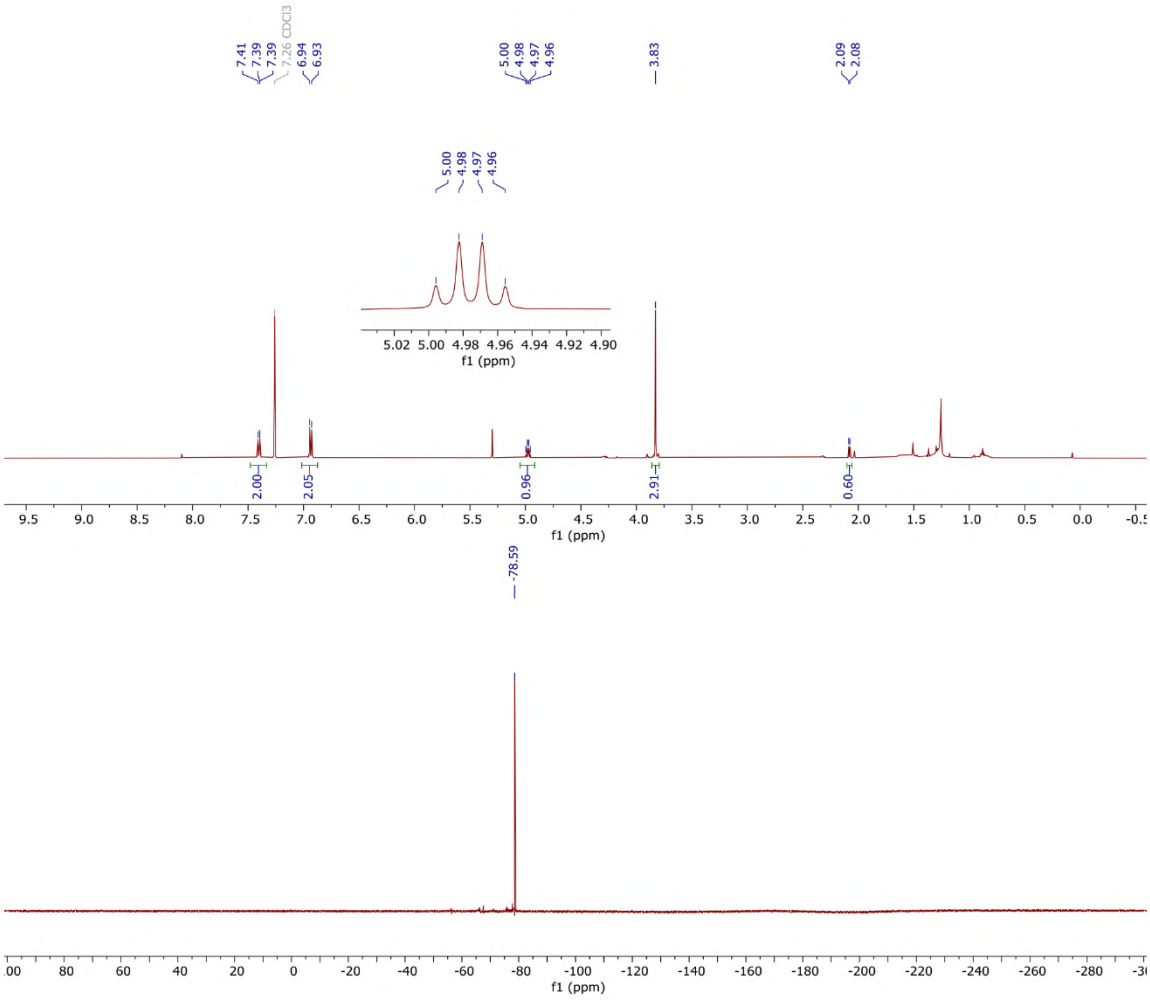

Figure S2.34 ^{1}H and ^{19}F NMR spectra of **S2.41** in $CDCl_3$.

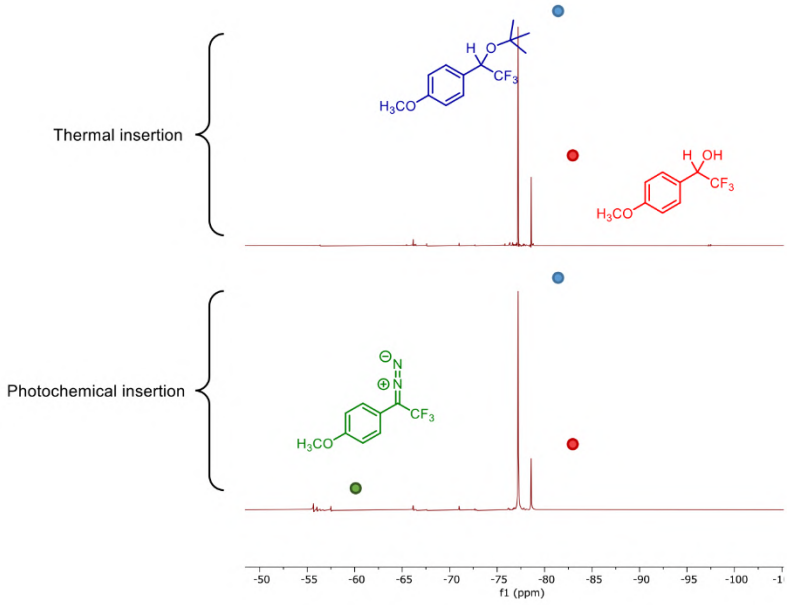

Figure S2.35 Crude ^{1}H NMR spectra of insertion reaction in *tert*-butanol (top: thermal; bottom: photochemical).

2.5.4 Monitoring of diazo-isomer formation during thermal activation of diazirines

Diazirines are known to undergo partial rearrangement to linear diazo species upon excitation, although this isomerization is known to be less significant for α-trifluoromethyl diazirines than for other diazirine species,[58] and is also known to be less significant under conditions of thermal activation compared with photochemical activation.[36] The weak correlation between experimentally determined activation temperature and calculated activation energy observed in Table 2.2 led us to question whether the α-H, -CH_3 and -Cl substrates may have followed a different reaction pathway (possibly involving the diazo-isomer) in the DSC experiment, compared to the α-CF_3 substrate. Therefore, we carried out thermal activation experiments on four representative α-substituted diazirines while monitoring the progress of the reaction by UV/Vis spectroscopy, in order to determine if the formation of the diazo-isomer during thermal activation could be detected.

Traces of diazo-isomer formation (indicated by a signal in the characteristic diazo absorption region of 450–550 nm) were observed only with the α-CH_3 sample. We

observed a gradual consumption of the α-CF_3 diazirine over the course of 20 mins, whereas the other three α-substituted diazirines were consumed in less than 6 mins.

Decomposition of **D2.14**, **D2.15**, **D2.16**, and **D2.5** under thermal activation.

A SpectraMax M5 multi-channel platereader was used for all spectral measurements. The diazirine solution in cyclohexane was prepared as described above for the cyclohexane C–H insertion experiment. For each substrate, thermal activation was performed in ten high-pressure glass tubes, under an atmosphere of argon, at 140 °C. Each tube was withdrawn from the heating bath at the appropriate time, and the UV/Vis spectrum was recorded.

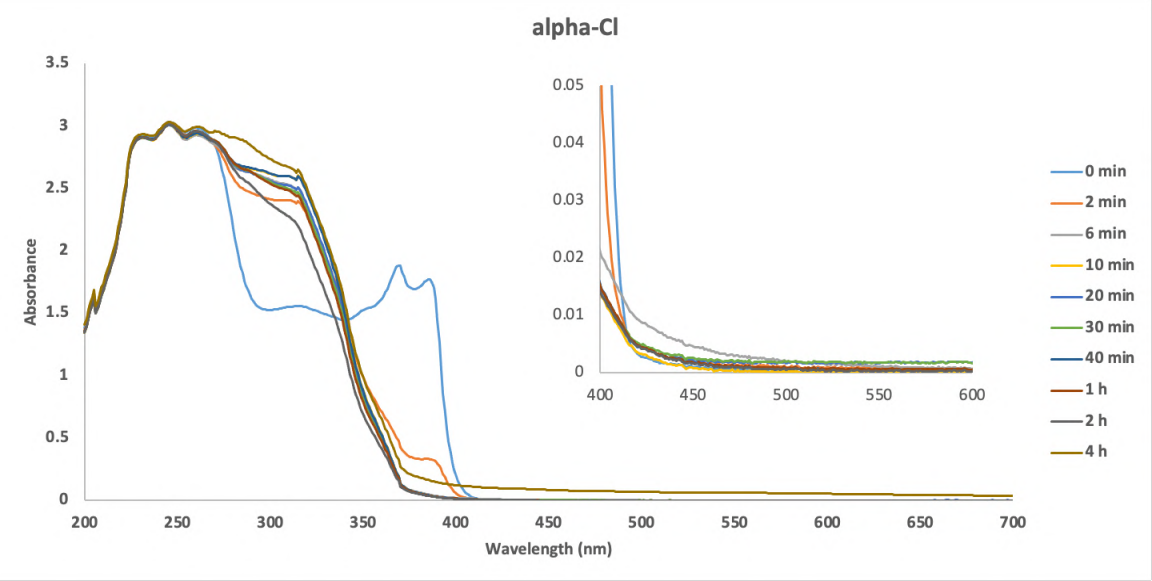

Figure S2.36 UV absorbance spectra of **D2.14** showing consumption of starting material over time. The diazirine was consumed over the first 6 mins, and examination of the spectrum between 400–600 nm (inset) indicated the absence of the diazo-isomer.

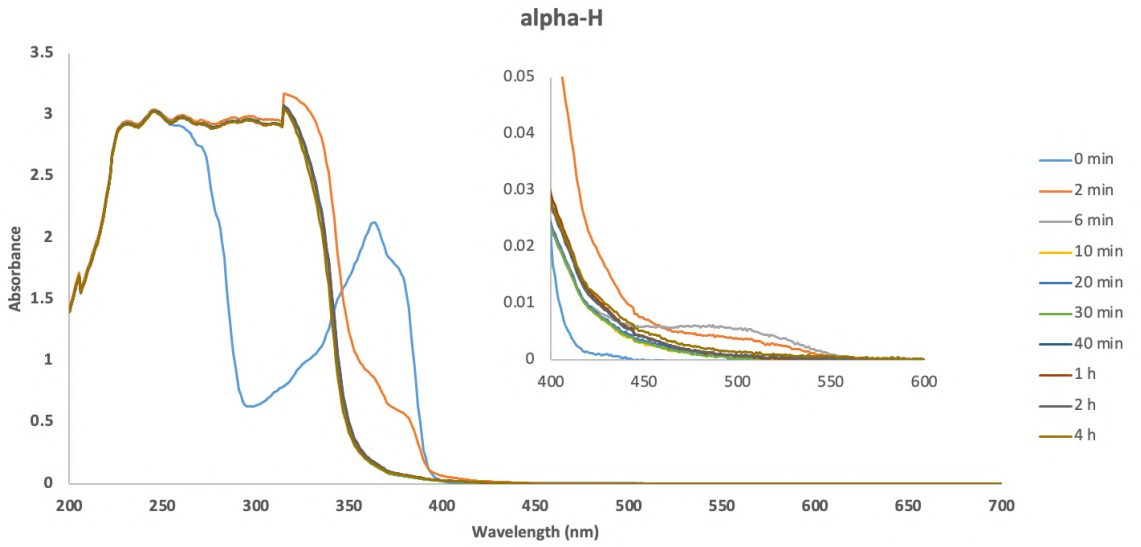

Figure S2.37 UV absorbance spectra of **D2.15** showing consumption of starting material over time. The diazirine was consumed over the first 6 mins, and examination of the spectrum between 400–600 nm (inset) indicated only trace amounts of the diazo-isomer.

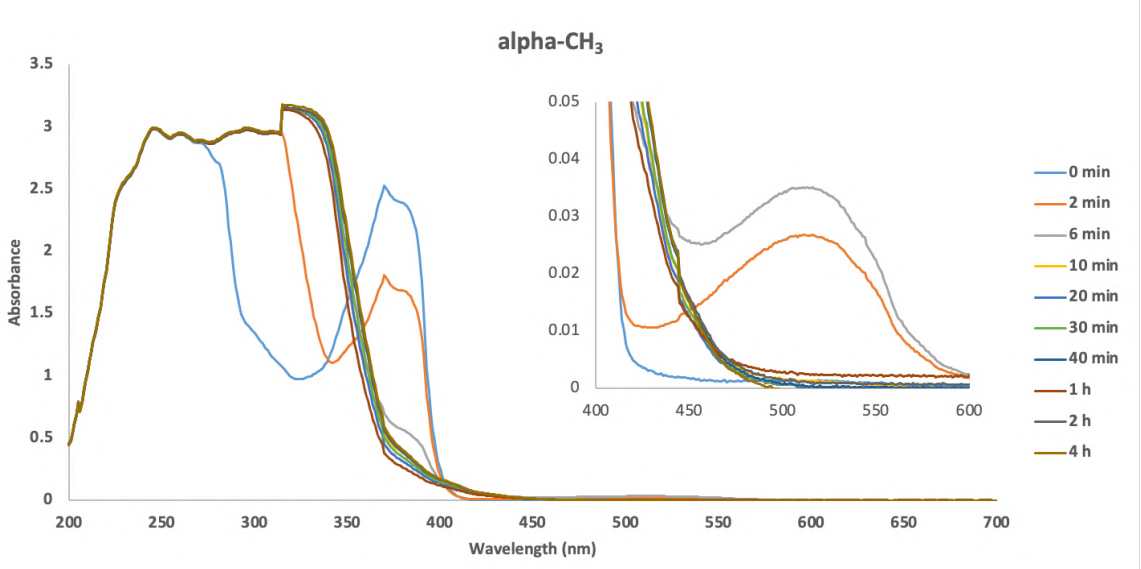

Figure S2.38 UV absorbance spectra of **D2.16** showing consumption of starting material over time. The diazirine was consumed over the first 6 mins, and examination of the spectrum between 400–600 nm (inset) indicated the diazo-isomer as a transient isomerization product.

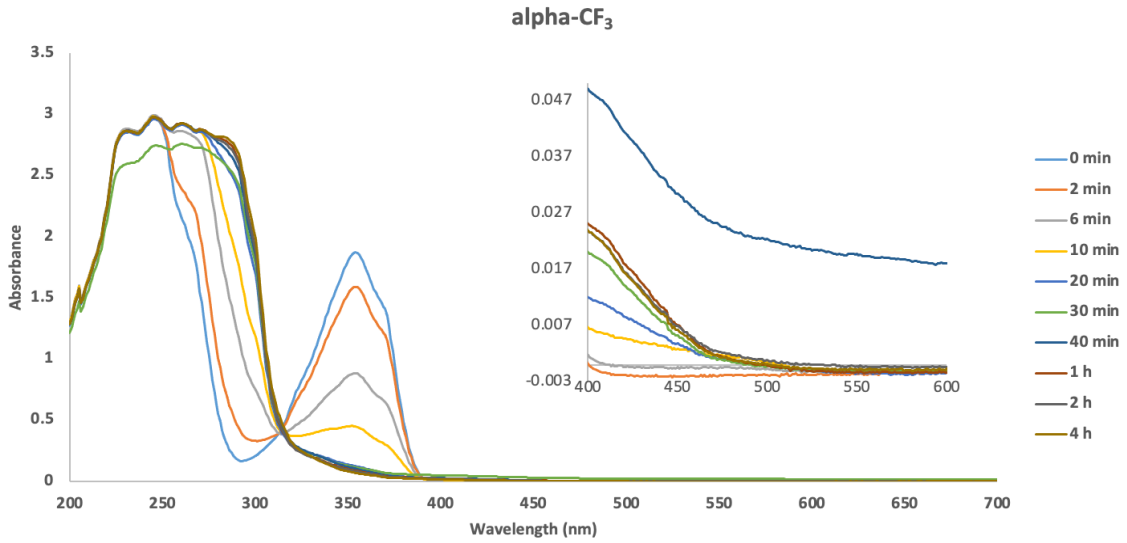

Figure S2.39 UV absorbance spectra of **D2.5** showing consumption of starting material over time. The diazirine was consumed over the first 20 mins, and examination of the spectrum between 400–600 nm (inset) indicated the absence of the diazo-isomer.

2.5.5 Differential scanning calorimetry (DSC)

General Protocol for DSC analysis

A sample of the substance to be analyzed (typically 2 to 7 mg) was placed in a Tzero aluminum hermetic pan and sealed by a matching lid. The pan was pierced with a small pinhole to allow evolution of nitrogen gas. The pan was placed in the oven of a DSC25 device (TA instruments) and heated from 40 °C to 200 °C at a rate of 5 °C/min, with an identical empty pan as a reference. The oven was constantly flushed by a 50 mL/min flow of nitrogen. The device recorded the difference in heat flow between the reference and the studied sample, allowing the assignment of T_{onset} and T_{peak}. No significant differences were observed in the T_{onset} and T_{peak} values when the DSC experiment was repeated using stainless steel high-pressure capsules sealed with gold-plated copper sealing disks. The T_{onset} value is determined from the intersection of the computed baseline in the DSC trace, with the tangent of the upward slope corresponding to the diazirine activation exotherm. T_{onset} is typically ca. 20–30 °C higher than the true initiation temperature (T_{init}), but is more reliably determined experimentally.

DSC analysis for each aryl diazirine substrate was conducted in triplicate. A representative plot for each diazirine is reported in **Appendix B**.

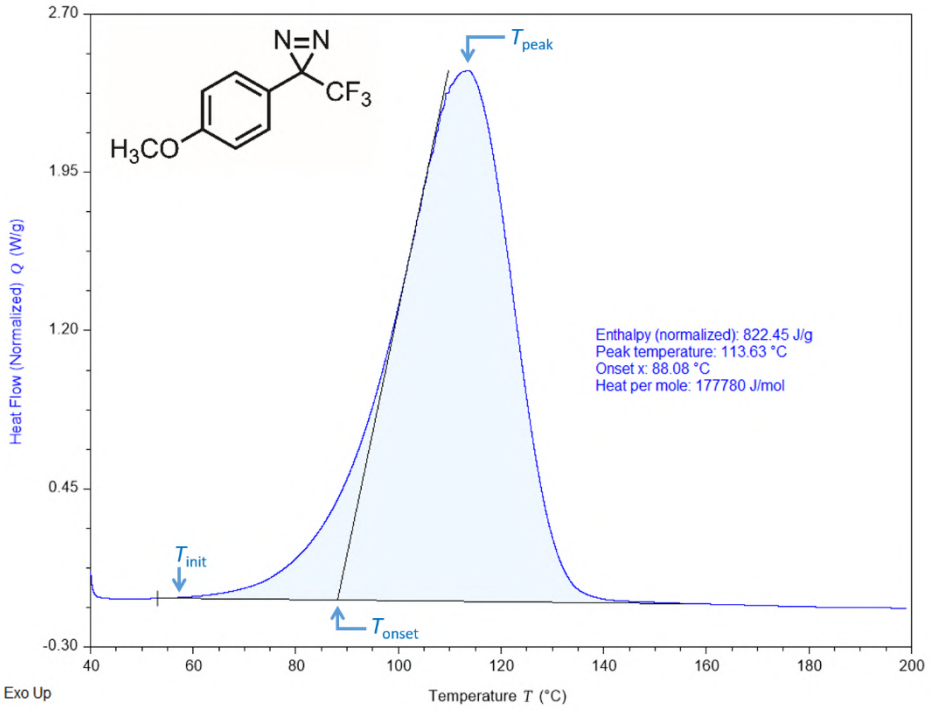

Figure S2.40 Representative DSC data for **D2.1**, illustrating the positions of T_{init}, T_{onset} and T_{peak}.

2.5.6 Computational details

2.5.6.1 General considerations

Geometry optimization and frequency calculations were performed using M06-2X[1]-D3[2]/6-31G(d,p) at 298 K and 1 atm. A minima point was confirmed when all of the vibrations associated with a molecule's normal modes were positive, and a transition state (TS) structure was characterized by the presence of only one imaginary frequency that connects reactants to products. Additional single-point energies were calculated using the 6-31+G(d,p) basis set for data in Table 2.1 and Table 2.2. All DFT results were obtained with the Gaussian 16 package.[3]

For Figure 2.6, DLPNO-CCSD(T)[4]/CBS with TightPNO option single-point energies were included, using the extrapolation scheme of cc-pVDZ and cc-pVTZ recommended in the ORCA manual.[5] All these calculations were carried out using the ORCA 4.2.1 package.[6]

The computational techniques used here were chosen on the basis of parallel work from DiLabio group,[7] wherein it is shown that M06-2X-D3 had some of the lowest absolute errors and lowest mean errors in computed barrier heights and energies for 449 reactions amongst the 12 common functionals tested. It is also shown that complete basis set DLPNO-CCSD(T) produced barrier heights and reaction energies for a cross-section of the 449 reactions that were within 0.5 kcal/mol of canonical, complete basis set CCSD(T).

Table S2.1 Summary of the calculated free energy barriers (298 K, 1 atm) of carbene formations at M06-2X-D3/6-31+G(d,p)//M06-2X-D3/6-31G(d,p) for X=CF_3 diazirines. The units of single-point energies and free energy corrections are in E_h, and the barriers are in kJ/mol. These data are used in Table 2.1.

X=CF_3			diazirine		carbene formation TS		carbene formation barrier (kJ/mol)
T_{onset}	#	R	single-point	thermal	single-point	thermal	
88.0	1	4-OCH_3	-831.0795518	0.114832	-831.0213133	0.110526	141.6
90.2	2	4-OPh	-1022.754237	0.161346	-1022.695422	0.155958	140.3
100.0	3	4-*t*-Bu	-873.7851535	0.192149	-873.724229	0.187219	147.0
103.3	4	4-H	-716.5958686	0.085054	-716.5340457	0.080302	149.8
105.6	5	4-Br	-3287.800083	0.072023	-3287.738626	0.066862	147.8
106.8	6	4-CH_2OH	-831.0852765	0.112979	-831.0244056	0.108895	149.1
102.0	7	4-CH_2Br	-3327.092416	0.097804	-3327.030973	0.092775	148.1
108.7	8	3-OCH_3	-831.0792245	0.114743	-831.0165079	0.110092	152.5
110.5	9	3-OH	-791.7974855	0.087953	-791.7346427	0.083055	152.1
112.5	10	3,5-OCH_3	-945.5620573	0.144616	-945.5006585	0.140083	149.3
115.7	11	4-CF_3	-1053.549729	0.08415	-1053.486691	0.078515	150.7
113.2	12	4-CHO	-829.8813742	0.091449	-829.8185819	0.086989	153.2
117.6	13	4-NO_2	-921.0272248	0.084011	-920.9637568	0.079302	154.3

Table S2.2 Summary of the calculated free energy barriers (298 K, 1 atm) of carbene formations at M06-2X-D3/6-31+G(d,p)//M06-2X-D3/6-31G(d,p) for R=Br diazirines. The units of single-point energies and free energy corrections are in E_h, and the barriers are in kJ/ mol. These data are used in Table 2.2.

R=Br			diazirine		carbene formation TS		carbene formation barrier (kJ/mol)
T_{onset}	#	X	single-point	thermal	single-point	thermal	
76.5	1	Cl	-3410.41549	0.059615	-3410.353335	0.055608	152.7
84.6	2	H	-2950.84887	0.07169	-2950.787209	0.066082	147.2
93.5	3	CH_3	-2990.15124	0.098135	-2990.087606	0.093075	153.8
105.6	4	CF_3	-3287.80008	0.072023	-3287.738626	0.066862	147.8
108.4	5	F	-3050.06402	0.062596	-3050.000009	0.058312	156.8
N/A	6	OCH_3	-3065.33306	0.100734	-3065.285585	0.097526	116.2

Table S2.3 Summary of the calculated free energy (298 K, 1 atm) S-T gaps[a] and barriers of carbene formation, singlet carbene insertion, and triplet carbene abstraction using M06-2X-D3/6-31G(d,p) for X=CF_3, Cl, F, and OMe. The central C–H bond in propane is targeted for insertion or abstraction reaction modeling. The units are in kJ/mol. These data are used in Figure 2.5 and Figure 2.7.

X=CF_3					
σ_p^+	R	S-T gap	formation barrier	insertion barrier	abstraction barrier
-1.7	NMe_2	10.4	138.2	102.6	49.1
-1.3	NH_2	7.3	140.0	103.0	49.3
-0.92	OH	19.7	145.4	87.6	48.3
-0.78	OMe	18.8	145.4	81.6	47.2
-0.31	CH_3	27.1	147.6	77.1	49.0
-0.26	*t*-Bu	29.9	150.6	69.2	47.0
0	H	34.1	153.0	65.6	47.9
0.11	Cl	33.9	151.5	63.5	46.7
0.61	CF_3	43.1	153.2	59.6	47.4
0.66	CN	45.6	155.3	53.0	45.6
0.79	NO_2	46.7	156.5	49.8	44.4
		slope =	*+ 7.2*		

X=Cl					
σ_p^+	R	S-T gap	formation barrier	insertion barrier	abstraction barrier
-1.7	NMe_2	-38.9	146.6	157.1	53.3
-1.3	NH_2	-39.1	148.2	158.6	52.3
-0.92	OH	-28.4	150.9	147.1	53.1
-0.78	OMe	-28.1	151.5	146.6	51.7
-0.31	CH_3	-18.8	153.2	139.2	52.6
-0.26	*t*-Bu	-18.7	153.7	138.6	52.2
0	H	-15.5	153.2	135.8	52.5
0.11	Cl	-14.6	152.9	133.9	51.4
0.61	CF_3	-6.3	153.7	126.4	50.5
0.66	CN	-2.3	152.7	124.4	49.9
0.79	NO_2	0.8	152.9	121.8	49.7
		slope =	*+ 2.4*		

X=F					
σ_p^+	R	S-T gap	formation barrier	insertion barrier	abstraction barrier
-1.7	NMe_2	-75.1	153.4	185.2	52.0
-1.3	NH_2	-73.7	154.8	183.8	50.1
-0.92	OH	-66.6	155.8	174.2	51.8
-0.78	OMe	-66.2	155.2	174.5	49.2
-0.31	CH_3	-59.0	157.5	168.5	49.3
-0.26	*t*-Bu	-57.8	156.4	166.7	49.1
0	H	-54.7	156.6	163.0	48.4
0.11	Cl	-54.4	155.8	161.0	46.3
0.61	CF_3	-48.1	155.8	154.6	47.0
0.66	CN	-42.4	154.6	149.0	44.8
0.79	NO_2	-39.6	154.3	145.5	44.2
		slope =	*+ 0.3*		

X=OMe					
σ_p^+	R	S-T gap	formation barrier	insertion barrier	abstraction barrier
-1.7	NMe_2	-97.8	118.4	231.4	64.7
-1.3	NH_2	-95.4	118.6	226.7	63.5
-0.92	OH	-92.3	118.6	220.6	62.4
-0.78	OMe	-91.3	118.0	220.4	62.5
-0.31	CH_3	-83.8	117.5	213.2	64.7
-0.26	*t*-Bu	-85.4	117.6	211.8	62.8
0	H	-84.2	118.0	206.3	61.9
0.11	Cl	-84.0	116.8	205.9	60.9
0.61	CF_3	-79.4	115.5	201.2	59.2
0.66	CN	-72.6	113.8	192.8	60.0
0.79	NO_2	-70.7	112.8	188.8	58.6
		slope =	*– 2.0*		

[a] A positive S-T gap indicates that the ground state is in a triplet state.

Table S2.4 Summary of the calculated (298 K, 1 atm) isodesmic free energies (of the parent reaction or TS reaction) using M06-2X-D3/6-31G(d,p) for X=CF_3, Cl, F, and OMe. The units are in kJ/mol. These data are used in Figure S2.3.

X=CF_3			
σ_p^+	R	isodesmic free energy (parent)	isodesmic free energy (TS)
-1.7	NMe_2	6.6	21.4
-1.3	NH_2	4.3	17.2
-0.92	OH	1.1	8.7
-0.78	OMe	1.7	9.3
-0.31	CH_3	0.6	6.0
-0.26	*t*-Bu	1.6	4.0
0	H	0.0	0.0
0.11	Cl	-3.6	-2.2
0.61	CF_3	-5.8	-6.1
0.66	CN	-6.5	-8.8
0.79	NO_2	-7.7	-11.2
	slope =	*– 5.4*	– 12.5

X=Cl			
σ_p^+	R	isodesmic free energy (parent)	isodesmic free energy (TS)
-1.7	NMe_2	7.8	14.3
-1.3	NH_2	4.7	9.7
-0.92	OH	1.7	3.9
-0.78	OMe	3.0	4.8
-0.31	CH_3	1.4	1.4
-0.26	*t*-Bu	3.2	2.7
0	H	0.0	0.0
0.11	Cl	-2.9	-2.7
0.61	CF_3	-2.9	-3.3
0.66	CN	-5.6	-5.1
0.79	NO_2	-6.8	-6.5
	slope =	*– 5.1*	– 7.5

X group=F			
σ_p^+	R	isodesmic free energy (parent)	isodesmic free energy (TS)
-1.7	NMe_2	6.6	9.8
-1.3	NH_2	4.0	5.8
-0.92	OH	0.9	1.6
-0.78	OMe	1.3	2.6
-0.31	CH_3	1.1	0.2
-0.26	*t*-Bu	1.7	1.9
0	H	0.0	0.0
0.11	Cl	-3.4	-2.6
0.61	CF_3	-4.4	-3.7
0.66	CN	-6.0	-4.0
0.79	NO_2	-7.3	-5.1
	slope =	*– 4.9*	– 5.3

X=OMe			
σ_p^+	R	isodesmic free energy (parent)	isodesmic free energy (TS)
-1.7	NMe_2	3.7	3.3
-1.3	NH_2	2.3	1.7
-0.92	OH	0.6	0.1
-0.78	OMe	0.9	0.9
-0.31	CH_3	0.8	1.3
-0.26	*t*-Bu	0.7	1.2
0	H	0.0	0.0
0.11	Cl	-1.6	-0.4
0.61	CF_3	-2.6	0.0
0.66	CN	-2.2	2.0
0.79	NO_2	-3.1	2.1
	slope =	*– 2.5*	– 0.4

Table S2.5 Summary of the calculated free energy of carbene formations Δ*G* (298 K, 1 atm) at DLPNO-CCSD(T)/CBS//M06-2X-D3/6-31G(d,p) using cc-pV(D-T)Z for X=CF_3, Cl, F, and OMe. The high-level corrected free energy of N_2 is –109.435558328013 E_h. The units of final Gibbs free energies are in E_h, and Δ*G* are in kJ/mol. These data are used in Figure 2.6.

X=CF_3						
σ_p^+	R	diazirine	singlet carbene	triplet carbene	Δ*G* (singlet)	Δ*G* (triplet)
-1.7	NMe_2	-849.7679547	-740.3430655	-740.3361249	-28.0	-9.8
-1.3	NH_2	-771.3194645	-661.8928763	-661.88708	-23.6	-8.3
-0.92	OH	-791.1941893	-681.7627094	-681.7609716	-10.7	-6.1
-0.78	OMe	-830.4123156	-720.9812062	-720.9789479	-11.7	-5.8
-0.31	CH_3	-755.267888	-645.8340032	-645.8347959	-4.4	-6.5
-0.26	*t*-Bu	-872.9716236	-763.5363741	-763.53786	-0.8	-4.7
0	H	-716.0275523	-606.5900275	-606.5940309	5.2	-5.3
0.11	Cl	-1175.212266	-1065.775821	-1065.779023	2.3	-6.1
0.61	CF_3	-1052.856771	-943.4153379	-943.4230487	15.4	-4.8
0.66	CN	-808.163276	-698.7216225	-698.7308207	16.0	-8.1
0.79	NO_2	-920.3539023	-810.9120569	-810.9198491	16.5	-4.0

X=Cl						
σ_p^+	R	diazirine	singlet carbene	triplet carbene	Δ*G* (singlet)	Δ*G* (triplet)
-1.7	NMe_2	-972.1260473	-862.7179391	-862.6964872	-72.1	-15.7
-1.3	NH_2	-893.677363	-784.2686337	-784.2488785	-70.4	-18.6
-0.92	OH	-913.5521539	-804.1411027	-804.1237454	-64.3	-18.8
-0.78	OMe	-952.7705419	-843.3590024	-843.3420274	-63.1	-18.5
-0.31	CH_3	-877.6259946	-768.2113494	-768.1985676	-54.9	-21.3
-0.26	*t*-Bu	-995.3299626	-885.9148193	-885.9015305	-53.6	-18.7
0	H	-838.3853105	-728.9697445	-728.9583101	-52.5	-22.5
0.11	Cl	-1297.570446	-1188.155095	-1188.14348	-53.1	-22.6
0.61	CF_3	-1175.215881	-1065.797208	-1065.788261	-44.3	-20.8
0.66	CN	-930.5217074	-821.1036191	-821.0966442	-45.9	-27.6
0.79	NO_2	-1042.71229	-933.2937615	-933.2860351	-44.7	-24.4

X=F						
σ_p^+	R	diazirine	singlet carbene	triplet carbene	Δ*G* (singlet)	Δ*G* (triplet)
-1.7	NMe_2	-612.1358394	-502.7252733	-502.6894244	-65.6	28.5
-1.3	NH_2	-533.6874531	-424.2763436	-424.2420508	-64.2	25.8
-0.92	OH	-553.5618957	-444.1493504	-444.1170748	-60.4	24.3
-0.78	OMe	-592.7799314	-483.3675455	-483.3354003	-60.8	23.6
-0.31	CH_3	-517.6359311	-408.2202432	-408.1919048	-52.2	22.2
-0.26	*t*-Bu	-635.3394467	-525.9235265	-525.8950691	-51.6	23.2
0	H	-478.3953286	-368.9785601	-368.9521205	-49.3	20.1
0.11	Cl	-937.5801908	-828.1639494	-828.1371375	-50.7	19.7
0.61	CF_3	-815.2250991	-705.8070995	-705.7822079	-46.1	19.3
0.66	CN	-570.5312352	-461.1127491	-461.090625	-44.8	13.3
0.79	NO_2	-682.7217083	-573.3029851	-573.2799927	-44.2	16.2

X=OMe						
σ_p^+	R	diazirine	singlet carbene	triplet carbene	Δ*G* (singlet)	Δ*G* (triplet)
-1.7	NMe_2	-627.3266876	-517.937063	-517.8923537	-120.6	-3.2
-1.3	NH_2	-548.878565	-439.4882194	-439.44495	-118.7	-5.1
-0.92	OH	-568.753901	-459.3627794	-459.3204945	-116.7	-5.6
-0.78	OMe	-607.9718126	-498.5807972	-498.5386439	-116.9	-6.3
-0.31	CH_3	-532.8278622	-423.4343948	-423.3961121	-110.5	-10.0
-0.26	*t*-Bu	-650.5310368	-541.1379472	-541.0985569	-111.5	-8.1
0	H	-493.5873668	-384.1937892	-384.1556017	-110.2	-10.0
0.11	Cl	-952.7727654	-843.3798918	-843.3415037	-112.1	-11.3
0.61	CF_3	-830.4179481	-721.024299	-720.9870833	-110.0	-12.3
0.66	CN	-585.7248119	-476.3309406	-476.2967454	-109.4	-19.7
0.79	NO_2	-697.9154032	-588.5216064	-588.4858059	-109.6	-15.7

Table S2.6 Summary of the calculated free energy S–T gaps[a] (298 K, 1 atm) of X=CF_3, Cl, F, and OMe carbenes using DLPNO-CCSD(T)/CBS//M06-2X-D3/6-31G(d,p). (D-T)CBS stands for cc-pV(D-T)Z, and (T-Q) stands for cc-pV(T-Q)Z. The units are in kJ/mol. Highlighted cells indicate the calculated singlet–triplet gap (at the two levels of theory noted above) for *para*-methoxyphenyl trifluoromethyl diazirine. Good agreement is found between the two methods, and in each case we find the singlet to be the lower-energy carbene when R=4-OMe and X=CF_3.

σ_p^+	R	X=CF_3		X=Cl	X=F	X=OMe
		(D-T)CBS	(T-Q)CBS	(D-T)CBS	(D-T)CBS	(D-T)CBS
-1.7	NMe_2	-18.2	-19.5	-56.3	-94.1	-117.4
-1.3	NH_2	-15.2	-16.8	-51.9	-90.0	-113.6
-0.92	OH	-4.6	-5.2	-45.6	-84.7	-111.0
-0.78	OMe	-5.9	-6.9	-44.6	-84.4	-110.7
-0.31	CH_3	2.1	1.1	-33.6	-74.4	-100.5
-0.26	*t*-Bu	3.9	2.8	-34.9	-74.7	-103.4
0	H	10.5	9.7	-30.0	-69.4	-100.3
0.11	Cl	8.4	7.8	-30.5	-70.4	-100.8
0.61	CF_3	20.2	19.7	-23.5	-65.4	-97.7
0.66	CN	24.1	22.9	-18.3	-58.1	-89.8
0.79	NO_2	20.5	19.6	-20.3	-60.4	-94.0

[a] A positive S-T gap indicates that the ground state is in a triplet state.

2.5.6.2 Supplementary references

[1] Y. Zhao and D. G. Truhlar, *Theor. Chem. Acc.*, **2008**, *120*, 215–241.

[2] S. Grimme, J. Antony, S. Ehrlich and H. Krieg, *J. Chem. Phys.*, **2010**, *132*, 154104.

[3] Gaussian 16, Revision C.01, M. J. Frisch, G. W. Trucks, H. B. Schlegel, G. E. Scuseria, M. A. Robb, J. R. Cheeseman, G. Scalmani, V. Barone, G. A. Petersson, H. Nakatsuji, X. Li, M. Caricato, A. V. Marenich, J. Bloino, B. G. Janesko, R. Gomperts, B. Mennucci, H. P. Hratchian, J. V. Ortiz, A. F. Izmaylov, J. L. Sonnenberg, D. Williams-Young, F. Ding, F. Lipparini, F. Egidi, J. Goings, B. Peng, A. Petrone, T. Henderson, D. Ranasinghe, V. G. Zakrzewski, J. Gao, N. Rega, G. Zheng, W. Liang, M. Hada, M. Ehara, K. Toyota, R. Fukuda, J. Hasegawa, M. Ishida, T. Nakajima, Y. Honda, O. Kitao, H. Nakai, T. Vreven, K. Throssell, J. A. Montgomery, Jr., J. E. Peralta, F. Ogliaro, M. J. Bearpark, J. J. Heyd, E. N. Brothers, K. N. Kudin, V. N. Staroverov, T. A. Keith, R. Kobayashi, J. Normand, K. Raghavachari, A. P. Rendell, J. C. Burant, S. S. Iyengar, J. Tomasi, M. Cossi, J. M. Millam, M. Klene, C. Adamo, R. Cammi, J. W. Ochterski, R. L. Martin, K. Morokuma, O. Farkas, J. B. Foresman and D. J. Fox, Gaussian, Inc., Wallingford CT, 2016.

[4] (a) C. Riplinger and F. Neese, *J. Chem. Phys.*, **2013**, *138*, 034106; (b) C. Riplinger, B. Sandhoefer, A. Hansen and F. Neese, *J. Chem. Phys.*, **2013**, *139*, 134101; (c)

M. Saitow, U. Becker, C. Riplinger, E. F. Valeev and F. Neese, *J. Chem. Phys.*, **2017**, *146*, 164105.

[5] W. Schneider, S. Lehnhausenm and F. Neese, ORCA Manual Version 4.2.1; 2020; p 72.

[6] (a) F. Neese, *WIREs Comput. Mol. Sci.*, **2018**, *8*, e1327; (b) F. Neese, *WIREs Comput. Mol. Sci.*, **2012**, *2*, 73–78.

[7] V. K. Prasad, Z. Pei, S. Edelmann, A. Otero-de-la-Roza and G. A. DiLabio, *J. Chem. Theory Comput*. **2022**, *18*, 151–166.

Chapter 3: Electronically Optimized Diazirine-Based Polymer Crosslinkers

This chapter has been adapted with permission from a previously published paper.

Stefania F. Musolino, Mahshid Mahbod, Rashid Nazir, Liting Bi, Hamish A. Graham, Abbas S. Milani and Jeremy E. Wulff, *Polym. Chem.*, **2022**, *13*, 3833–3839.

Contributions:

Dr. Stefania F. Musolino contributed to the design and synthesis of the molecules, as well as to the crosslinking experiments and the preparation of crosslinked fabrics and lap-shear samples. Mahshid Mahbod performed the mechanical measurements. Rashid Nazir carried out the gravimetric experiments. Liting Bi performed the DSC measurements and contributed to data discussions. Hamish A. Graham prepared the crosslinked apparel fabrics.

3.1. Abstract

Topical application of diazirine-based crosslinkers can upgrade mechanical properties of low-functionality commodity plastics by engaging in rapid C–H insertions along the polymer chain. Here we describe an effective strategy to improve the performance of diazirine reagents through electronic optimization of the trifluoromethyl aryl diazirine warhead. A prototypically optimized *bis*-diazirine is shown to be >10-fold more effective than earlier best-in-class crosslinkers. The superior performance—attributed to better stabilization of intermediate singlet carbenes—confers increased tear resistance and enhanced tensile strength to ultra-high molecular weight polyethylene fabric, at lower loadings than was previously achievable for any crosslinking reagent. Electronically optimized diazirines can also be activated at lower temperatures and longer wavelengths than traditionally employed analogues, for the first time enabling fast, high-yield crosslinking of unfunctionalized aliphatic substrates using visible light. These advances pave the way for far-ranging improvements to the design of new diazirine-containing crosslinkers, biological probes, adhesives, and related reagents.

3.2. Introduction

Incorporation of crosslinker molecules into a polymer network increases mechanical strength and thermal stability, reduces material creep at high temperatures, provides resistance to electrical discharge, offers increased stability to solvents and stress cracking, and introduces new surface functionalities.[4,153,154] Traditionally, however, each polymer substrate required the use of a particular crosslinking technology (e.g. vulcanization for rubber,[9] hydrosilylation for silicone,[155] etc.). Moreover, many types of desirable polymer materials lack the functional groups required for coupling, and so cannot be crosslinked using traditional technologies.

First popularized for use in biological target identification,[58,156–158] trifluoromethyl aryl diazirines offer an attractive, and near-universal, solution to the challenge of polymer crosslinking.[159] When activated with heat or light, the diazirine group loses an equivalent of nitrogen gas to liberate a reactive carbene that can undergo rapid insertion into nearby C–H, O–H, or N–H bonds.[58,85,160,161] Shortly after our report in 2019 of a rationally designed *bis*-diazirine reagent (**3.1**) for crosslinking polyethylene, polypropylene, and

other aliphatic polymers[36,59,67,162] the use of *bis*- and *tetrakis*-diazirines in materials science experienced an explosion of interest (**Figure 3.1**). For example, Burgoon and co-workers reported the use of *bis*-(benzyl) ether **3.2** for photopatterning of cycloolefin polymers,[67] while the Anzenbacher group developed *bis*-(aryl) ether **3.3** for crosslinking the components of organic light-emitting diodes,[68,70] and the Zhang lab used *tetrakis*-diazirine **3.4** for photopatterning polymeric semiconductors.[72] Meanwhile the Bao group reported compound **3.5** (linked with an aliphatic tether) for use in patterning wearable elastic circuits,[71] while our lab developed **3.6** (linked with flexible perfluoroalkyl chains) for adhesion of commodity plastics.[61] Polymeric analogues (e.g. **3.7**), created by adding electrophilic diazirine reagents to nucleophilic polymer supports, have also been extensively explored for biological wound healing applications[62,64,83,163,164] and as primers for fibre-reinforced polymer composites[24] and enzyme–polymer assemblies.[165] Diazirine reagents can also add functionality to commodity polymers;[99,166,167] for example porphyrin conjugate **3.8** can be used to generate antiviral coatings on woven polypropylene filter material.[100]

The aryl diazirines discussed above range from moderately electron rich (**3.3**) to moderately electron poor (**3.1** and **3.6**), with the majority being electron neutral. This raises an important but unaddressed question: *what kind of aryl diazirine is preferred in order to maximize the efficacy of polymer crosslinking?* The optimal electron density of the aryl diazirine unit has generally not been taken into account in the design of diazirine-based crosslinkers. Instead, *bis*- and *tetrakis*-diazirines have largely been designed around synthetic expedience and the availability of electron-neutral, diazirine-containing starting materials.

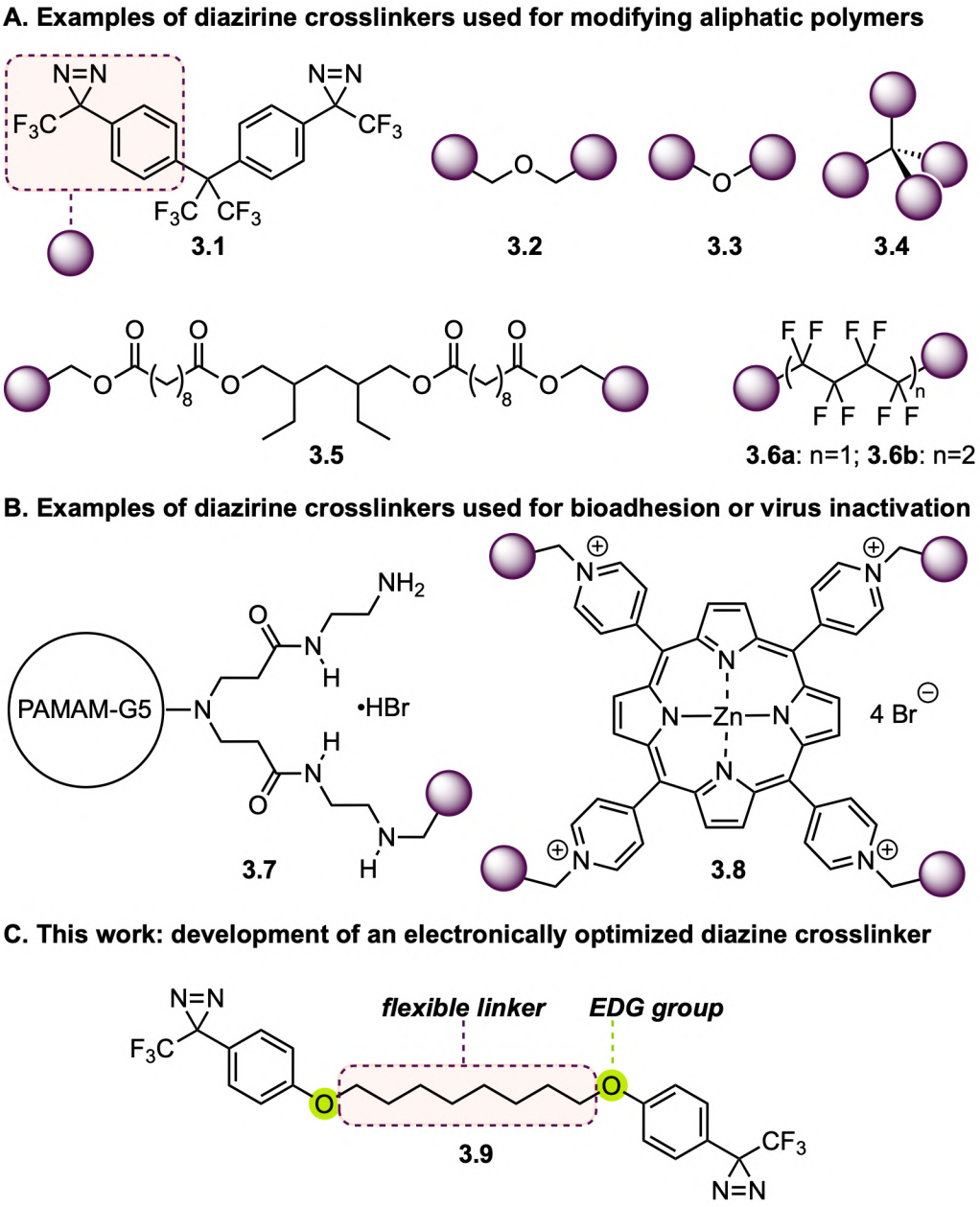

Figure 3.1 Examples of diazirine-based crosslinkers reported in the literature, and design of an electronically optimized *bis*-diazirine. Adapted with permission from literature.[168]

As part of a comprehensive structure–function survey of aryl diazirines, we recently examined the effect of aryl group electronics on spectral properties, activation energy, activation temperature, singlet-triplet carbene gap, C–H insertion barriers, and efficiency of insertion into an aliphatic substrate in Chapter 2.[50] We found that electron-poor and electron-neutral trifluoromethyl aryl diazirines were relatively inefficient at reacting with unactivated C–H bonds, regardless of whether thermal or photochemical

excitation was used to generate the reactive carbene intermediate. By contrast, the addition of a *para*-alkoxy group to the aryl diazirine motif conferred a number of important advantages: the UV/Vis absorbance spectrum was shifted to longer wavelengths, the activation temperature was lowered, and—most significantly—the efficiency of C–H insertion to a model aliphatic substrate was improved by up to an order of magnitude.[50] Here we apply these lessons toward the design of an electronically optimized *bis*-diazirine crosslinker, and show that significantly enhanced mechanical performance can be achieved through small changes to the structure of the crosslinking reagent. Taken together, these findings represent the first concrete answer to the molecular design question posed above.

3.3. Results and Discussion

3.3.1 Crosslinker design, synthesis, and characterization

We targeted crosslinker **3.9** (Figure 3.1C) as a representative electron-rich *bis*-diazirine, in which an 8-carbon aliphatic tether is incorporated between two ether-linked aryl diazirine motifs. The tether serves two distinct purposes. First, as with the flexible tethers found in **3.5** and **3.6**, it allows the diazirine units to effectively bridge polymer strands that are >20 Å apart, providing a competitive advantage for crosslinker **3.9** over shorter, more rigid molecules like **3.1**–**3.4**. At the same time, the simple aliphatic tether in **3.9** lacks the labile ester linkages found in **3.5** (which could present a liability for some materials applications) and is easier to install than the perfluorinated alkyl tether in **3.6**. Second, the molecular weight of the tether was chosen specifically to reduce the risk of explosion that is present for densely packed compounds like **3.3**–**3.4**, in which the energetic diazirine groups are insufficiently balanced by mass elsewhere in the molecule.

Trifluoromethyl aryl diazirines are typically synthesized from the corresponding trifluoromethyl ketone, via a 4-step protocol: (1) condensation with hydroxylamine to afford the corresponding oxime; (2) activation of the oxime with tosyl chloride; (3) addition of ammonia to produce the diaziridine intermediate; and (4) oxidation to the desired diazirine. In initial attempts to synthesize **3.9** using this route, we found that the electron-rich aryl group favours formation of the *E*-isomer at the tosyloxime stage, and makes this intermediate resistant to nucleophilic attack by ammonia. While the minor Z-

isomer could be converted to the desired product, the overall yield of **3.9** using this sequence was low. After considerable experimentation, we found that using nosyl chloride in place of tosyl chloride (allowing reaction through the more electrophilic nosyloxime intermediate) provided efficient conversion to the desired diaziridine, affording **3.9** in good overall yield on multi-gram scale (refer to the section 3.5 for full experimental details). Similar protocols were then used to produce *bis*-(aryl) ether **3.3**[68,70] as a rigid and less electron-rich control compound. The properties and crosslinking performance of **3.1**, **3.3**, and **3.9** were then directly compared.

As anticipated from our earlier survey of differentially functionalized *mono*-diazirines, crosslinker **3.9** absorbs light at significantly longer wavelengths than **3.1** (Figure 3.2A), while biaryl ether **3.3** was intermediate between the two. Perhaps most importantly, the absorbance spectrum for **3.9** includes a discrete band at *ca.* 390 nm—inside the visible region of the electromagnetic spectrum. This represents an important advantage for industrial applications where UV light may be disallowed due to safety concerns.

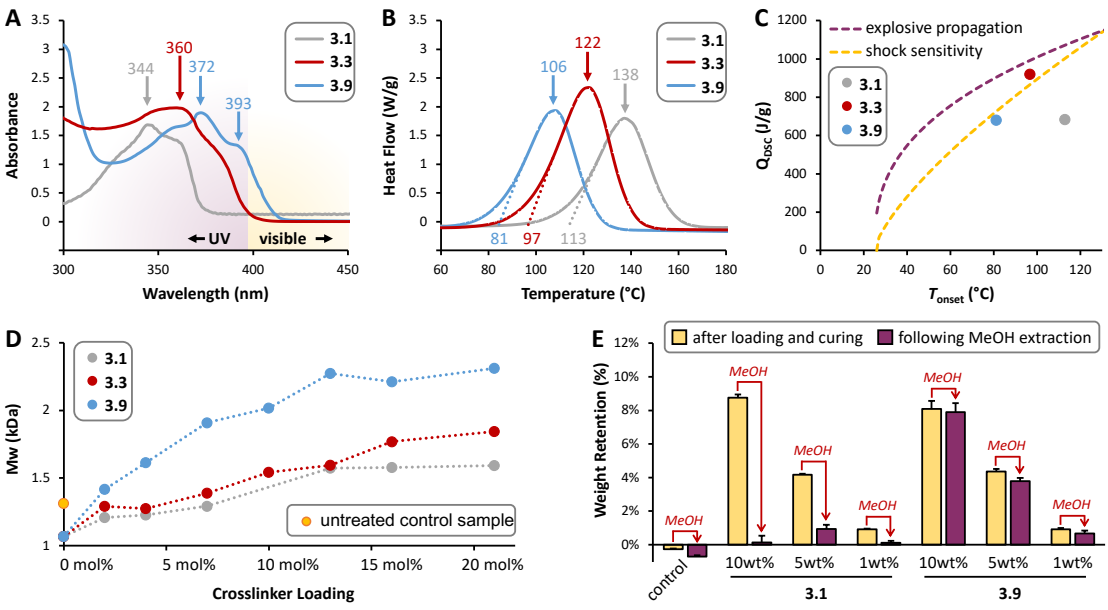

Figure 3.2 Comparison of physicochemical properties and crosslinking efficiency for crosslinkers **3.1**, **3.3**, and **3.9**. (A) UV/Vis spectra recorded at 5 mM in hexane, showing longer-wavelength absorbance for **3.9**. (B) Collected DSC data, showing lower-temperature activation for **3.9**; dotted lines indicate tangents used to determine onset temperatures. (C) Prediction of explosivity for the three representative crosslinkers;

points on or above the curves indicate potentially hazardous reagents. (D) SEC data showing increasing PEG molecular weight as a result of crosslinking. (E) Gravimetric analysis following methanolic extraction of crosslinked UHMWPE fabric, revealing significantly improved crosslinking by **3.9** relative to **3.1**. Error bars indicate standard error across a minimum of three replicate samples. Adapted with permission from literature.[168]

With a T_{onset} of 81 °C, **3.9** can also be activated at much lower temperatures than **3.1** (T_{onset}=113 °C) or **3.3** (T_{onset}= 97 °C) as shown by the differential scanning calorimetry (DSC) traces in Figure 3.2B—a feature advantageous for adhesion or topical crosslinking applications using polyethylene, which softens above *ca.* 90 °C. With lower activation temperatures, however, comes an intrinsically greater risk of explosion, if the total molecular mass is too low. To interrogate the risk of shock sensitivity or explosive propagation associated with the three prototypical *bis*-diazirines, we applied Yoshida's correlations[118] to the thermal data obtained from the DSC measurements. As shown in Figure 3.2C, **3.9** falls below both the shock-sensitivity and explosive-propagation curves, indicating that the C8 tether contains sufficient mass to offset the energetic diazirine groups. By contrast, **3.3** (containing only a single-atom tether) lies above the shock-sensitivity curve despite having a higher activation temperature. These data underscore the need to balance energetics against molecular weight, in order to produce safe and effective diazirine reagents. A complete list of thermal properties for **3.1**, **3.3**, and **3.9** is provided in Table S3.3.

3.3.2 Benchmarking of crosslinker performance

To probe the crosslinking efficacy of **3.9** *vs.* **3.1** and **3.3**, we first employed cyclohexane as a molecular model for polyethylene. As shown in Table 3.1, the yield of the *bis*-cyclohexane adduct generated from **3.1** was only 7%,[36] similar to the yields reported for cyclohexane crosslinking using **3.6a** and **3.6b**.[61] By contrast, *bis*-(aryl) ether **3.3** afforded 54% yield of crosslinked cyclohexane, while the most electron-rich *bis*-diazirine, **3.9**, gave a 91% yield of the desired adduct. Based upon prior studies from Sheridan and Raimer,[90,112] as well as our recent Hammett experiments with *mono*-diazirines in Chapter 2,[50] we attribute the >10-fold increase in crosslinking efficiency for

3.9 *vs.* **3.1** to the different degrees of stabilization of the singlet carbene that is generated following diazirine activation. Significantly, despite the use of a flexible, non-fluorinated tether, we observed no cyclization products forming from compound **3.9**.

Table 3.1 Effect of aryl substituent electronics on crosslinking efficiency for a representative aliphatic substrate

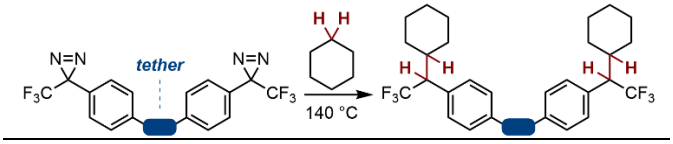

Reagent	Tether	C–H insertion yield
3.1	–$C(CF_3)_2$–	7% *(ref. 35)*
3.6a	–$(CF_2)_4$–	6% *(ref. 58)*
3.6b	–$(CF_2)_8$–	7% *(ref. 58)*
3.3	–O–	54%
3.9	–$O(CH_2)_8O$–	91%

To confirm the relative performance of the three proto-typical crosslinkers in the context of a polymeric system, we added varying amounts (0–21 mol%) of **3.1**, **3.3**, and **3.9** to monodisperse polyethylene glycol (PEG; 1,000 g/mol) and analyzed the products by SEC. Once again the electronically optimized crosslinker **3.9** significantly outperformed first-generation *bis*-diazirine **3.1**, with *bis*-(aryl) ether **3.3** occupying second place. As shown in Figure 3.2D, **3.9** more than doubled the average molecular weight of the polymer, while **3.1** and **3.3** triggered more modest increases. As expected, crosslinking also leads to increased polydispersity (Figure S3.15); by this metric as well the relative performance ranking was **3.9** > **3.3** > **3.1**.

Diazirine reagents are known to be useful in bonding low-surface-energy plastics.[33,61] To evaluate the performance of **3.1**, **3.3**, and **3.9** in adhesion, we painted each crosslinker between two pieces of HDPE, heated (110 °C) to initiate diazirine activation, and then challenged the resulting crosslinked polyethylene sandwich in a lap-shear experiment. At low loadings (1 mg crosslinker in each 3.2 cm^2 overlap region), we found that **3.9** and **3.3** afforded superior adhesion to **3.1** (Figure 3.3A), as would be predicted from the molecular data in Table 3.1. At higher loadings, however (5 mg per sample; Figure S3.16), **3.1** performed better, likely due to its ability to undergo oligomerization.[61] To confirm that the observed adhesion (at low loadings) was due to interfacial crosslinking rather than simple surface functionalization, control experiments

were conducted with *mono*-diazirine **3.10**. As expected, lap-shear samples prepared with **3.10** showed no detectable adhesion.

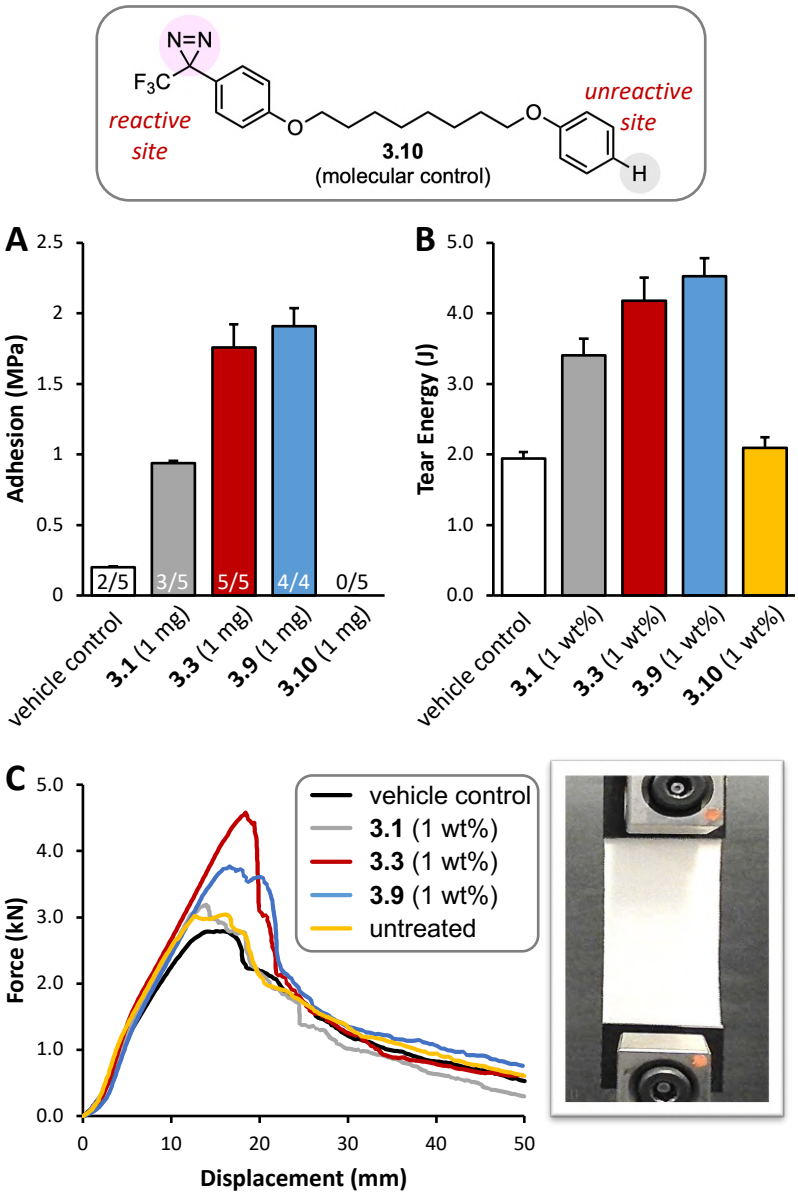

Figure 3.3 Mechanical characterization of crosslinked HDPE lap-shear samples and crosslinked UHMWPE fabric. (A) Adhesion strength of HDPE–crosslinker–HDPE lap-shear composites; numerical values indicate the samples that were sufficiently well adhered to be measured. (B) Tear strength of crosslinked 75 g/m^2 UHMWPE fabric (100 mm × 100 mm). (C) Tensile strength of crosslinked 75 g/m^2 UHMWPE fabric (75 mm × 250 mm). Error bars in panels A and B indicate standard error. Curves in panel C indicate

averaged data over 3 independent tests at 10 mm/min. Adapted with permission from literature.[168]

3.3.3 Mechanical testing of crosslinked polymer materials

One of the major applications for crosslinkers like **3.1** is the strengthening of woven ultra-high molecular weight polyethylene (UHMWPE) fabric.[18] To explore the advantages of **3.9** in this context, we thermally crosslinked 75 g/m^2 UHMWPE fabric with varying loadings of **3.1** vs. **3.9** (*ca.* 10 wt%, 5 wt% and 1 wt%), and then exhaustively extracted the crosslinked product with methanol. In keeping with the modest cyclohexane crosslinking yield shown in Table 3.1, we found that an average of 61% of the mass added from **3.1** was lost upon methanolic extraction (Figure 3.2E and Table S3.6), presumably due to ketone byproducts, oligomers, and other impurities. By contrast, >95% of the mass added from **3.9** was retained following extraction—indicating a much greater efficiency of bonding to the polyethylene matrix. Tear testing of crosslinked UHMWPE samples further reinforced the trends observed above. While **3.1** is capable of significantly improving tear strength in woven UHMWPE fabric (Figure 3.3B), **3.3** and **3.9** both offer even greater performance. As expected, samples treated with the *mono*-diazirine control, **3.10**, performed equivalently to vehicle control samples treated with crosslinker-free solvent and subjected to the same thermal conditions as the other test samples.

Increasing the tensile strength of woven UHMWPE is more challenging than improving the tear strength, because UHMWPE fabric is already extremely strong in the warp and weft directions—a key factor underpinning its use in ballistic protection garments. Our lab previously showed that loadings of 2 wt% **3.1** afforded only a modest increase to warp/weft tensile strength.[18] To probe whether more electron-rich diazirines would perform better, we lowered the loading to 1 wt% and compared the effects of **3.1**, **3.3**, and **3.9** (Figure 3.3C).

Unsurprisingly, at this low crosslinker loading, compound **3.1** had no effect, and force–displacement curves of fabric treated with 1 wt% of **3.1** were indistinguishable from curves of untreated UHMWPE or vehicle-control fabric. Crucially, however, much better performance was observed for both **3.3** and **3.9**. Peak force for fabric treated with

3.3 was improved by 64% relative to vehicle-control fabric, and by 35% for fabric treated with **3.9**. The better performance of **3.3** in this experiment probably relates to its physical properties. Compound **3.3** is an oil and so can be evenly dispersed throughout the fabric, while **3.9** is a crystalline solid (mp. 49 °C). These data suggest that further improvements to **3.9** may be possible through modification of the tether to disfavour crystal packing. In any event, the ability to effect such significant enhancements to the tensile strength of a material like UHMWPE that is already extremely strong—by simple topical application at 1 wt%—represents an impressive validation of the power of chemical crosslinking. In separate experiments (refer to section 3.5) we studied the performance of **3.1** and **3.9** in apparel fabrics. We found that both crosslinkers were capable of increasing stretch modulus within the fabric, but that **3.9** was the more effective of the two reagents.

3.3.4 Crosslinking under milder reaction conditions

The mechanical testing data reported above were obtained following thermal crosslinking under conditions that were known to be applicable to first-generation *bis*-diazirine **3.1**, so that the mechanical upgrades offered by **3.1** and **3.9** could be directly compared. However, the data in Figure 3.2B indicated that significantly lower temperatures could be used to activate **3.9**, while data in Figure 3.2A suggested the tantalizing possibility of visible-light photocuring. To confirm the viability of these desirable activation conditions using crosslinker **3.9**, we turned once again to reaction with cyclohexane, since this system (which serves as a useful model for low-functionality polymers) allowed crosslinking progress to be followed over time by simply monitoring the reaction by NMR spectroscopy.

Reaction of **3.9** with cyclohexane was found to proceed efficiently at 80 °C, with 75% of the desired *bis*-cyclohexane adduct being formed after 3 hours (Figure 3.4). Increasing the temperature to 90 °C led to 82% conversion after only 2 hours. These observations are consistent with the DSC data in Figure 3.2B, and indicate that not only crosslinker *activation* but also the subsequent C–H insertion event can be induced at modest temperatures. By contrast, efficient reaction of **3.1** with cyclohexane was previously shown to require prolonged heating at 140 °C.[36]

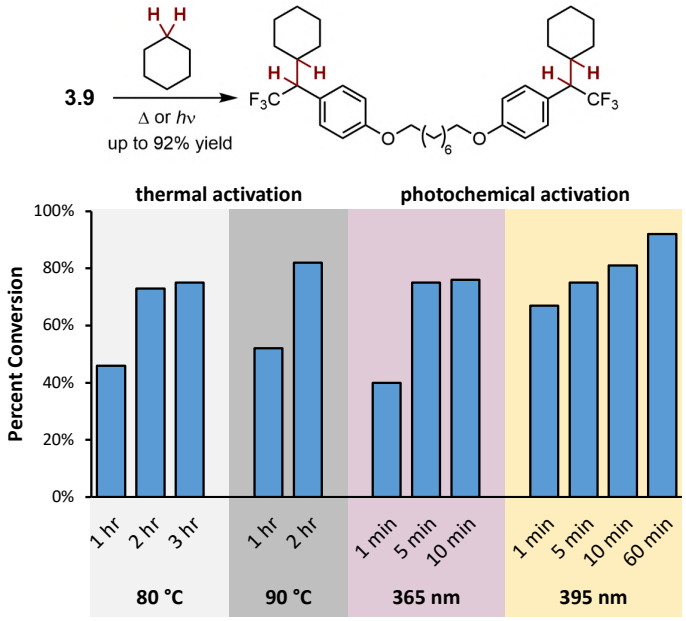

Figure 3.4 Low-temperature thermal crosslinking of cyclohexane using **3.9**, and photochemical crosslinking under UV and visible light. The 365 nm light-source operated at 38 W/m^2. The 395 nm light-source operated at 53 W/m^2. Adapted with permission from literature.[168]

Similarly, photoreaction of **3.9** in cyclohexane could be carried out using inexpensive LED strip lights centred at 395 nm. Notably, the half-life for this reaction was <1 minute at room temperature (Figure 3.4), and 92% isolated yield of the desired *bis*-adduct was obtained after allowing the reaction to proceed to completion. By contrast, no reaction was observed for compound **3.1** under equivalent reaction conditions (Table S3.2).

To further demonstrate the utility of visible light curing, we impregnated UHMWPE fabric with varying amounts of crosslinker **3.9**, and irradiated the material for 5 minutes at 395 nm (53 W/m^2). Subsequent mechanical testing (Figure S3.19) indicated that as little as 0.2 wt% of **3.9** was capable of significantly improving the tear-strength of the UHMWPE fabric following photocuring. Using this low loading, no discoloration of the fabric was observed (Figure S3.21).

3.4. Conclusions

We rationally designed *bis*-diazirine **3.9** as a prototype to explore the use of electronically optimized trifluoromethyl aryl diazirines in the crosslinking of commodity polymers. Notwithstanding the use of a simple 8-carbon tether to link the two diazirine warheads together, we found that **3.9** was >10-fold better at crosslinking a molecular model of polyethylene than was crosslinker **3.1**, and led to significant improvements in the crosslinking of a representative linear polymer (PEG) and in the bonding of an exemplary low-surface-energy plastic (HDPE). These improvements were attributed to the stabilization of the intermediate singlet carbene, in such a way as to favour C–H insertion over unwanted radical reactivity.

Topical application of crosslinkers represents an attractive and operationally simple "top-down" method to improve the mechanical properties of commodity polymers without the need to synthesize bespoke polymer or co-polymer precursors containing functional groups that are amenable to traditional crosslinking chemistry. Crosslinker **3.9** was capable of increasing the tear resistance and tensile strength of a high-performance UHMWPE material, to a degree that was significantly greater than that observed for the first-generation crosslinker **3.1**. It will be recognized that a range of simple modifications to *bis*-diazirine **3.9** could be used to generate useful next-generation reagents. For example, the 8-carbon tether could be increased in mass to further defend against the risk of shock sensitivity, or could have branching installed to minimize crystallinity—thereby making the reagent easier to apply onto surfaces. Likewise, the introduction of tethers that undergo chemical or enzymatic cleavage would immediately afford new families of degradable crosslinkers. At the same time, replacement of the aliphatic tether with functional groups such as the photosensitizer used in porphyrin conjugate **3.8** would provide reagents that are capable of effectively imbuing commodity polymers with useful new functionality. Similarly, installation of electron-rich trifluoromethyl aryl diazirines into polyamines would afford valuable polymer reagents with a wide range of enhanced properties relative to existing polydiazirines like **3.7**. Finally, the fact that **3.9** permitted the fast crosslinking of a representative low-functionality aliphatic substrate in excellent yield and with a half-life of <1 minute using inexpensive visible-light LEDs suggests

numerous additional applications in the rapid, efficient patterning of photoresist materials and other substrates.

3.5. Experimental and Supplementary Information

3.5.1 Materials and methods

3.5.1.1 General considerations

All commercial materials were used as received. THF was freshly dried over Na/benzophenone. Anhydrous cyclohexane was used in crosslinking experiments. Spectranalyzed™ pentane was used for purification of diazirines.

NMR spectra were acquired on either a Bruker AVANCE 300 (300.27 MHz for ^{1}H, 282.54 MHz for ^{19}F, 75.5 MHz for ^{13}C) or a Bruker AVANCE Neo 500 (500.27 MHz for ^{1}H, 470.72 MHz for ^{19}F, 125.7 MHz for ^{13}C) spectrometer. Chemical shifts were reported in parts per million (ppm) and were calibrated to the central peak of residual NMR solvent (central peak of chloroform-d: ^{1}H NMR δ = 7.26 ppm, ^{13}C NMR δ = 77.16 ppm; dichloromethane-d_2: ^{1}H NMR δ = 5.32 ppm, ^{13}C NMR δ = 53.84 ppm; acetone-d_6: ^{1}H NMR δ = 2.04 ppm, ^{13}C NMR δ = 29.8 ppm; methanol-d_4: ^{1}H NMR δ = 3.31 ppm). ^{13}C spectra and ^{19}F spectra were ^{1}H decoupled. Data is reported as follows: chemical shift (multiplicity [s = singlet, d = doublet, t = triplet, q = quartet, qd = quartet of doublet, p = pentet, dt = doublet of triplet, tt = triplet of triplet, td = triplet of doublet, br-s = broad singlet, m = multiplet], coupling constant in Hz, integration). Chemical shifts in ^{19}F spectra are reported in ppm and reported as obtained. Melting points were measured using a Gallenkamp melting point apparatus and are uncorrected.

High resolution mass spectrometry (HRMS) data were acquired using field desorption (FD) ionization on a JEOL AccuTOF GCx mass spectrometer. IR spectra were recorded using a Perkin-Elmer ATR spectrometer. IR wave numbers (ν) are reported in cm^{-1}. UV spotlight 365 nm (ThorLabs, 3685 lux, 38 W/m^2) and LED Strip Lights 395 nm (Waveform Lighting, 5129 lux, 53 W/m^2) were used for photochemical C–H insertion experiments. Illuminance readings were made using a wireless light sensor from PASCO (PS-3213). Differential Scanning Calorimetry analysis was performed using a DSC 25 TA instrument.

All diazirine-forming reactions were performed in the dark. Removal of solvent was done at 25 °C, avoiding the use of excessive vacuum.

3.5.1.2 Synthesis of aryl ether crosslinker 3.9 with a flexible aliphatic linker

Synthetic scheme for compound **3.9**

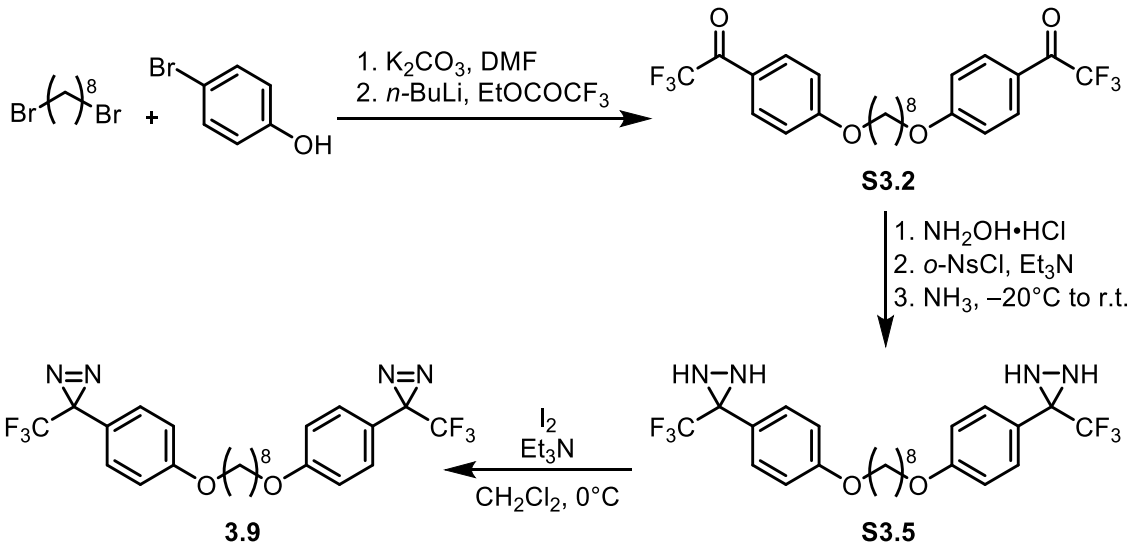

Synthesis of 1,8-bis(4-bromophenoxy)octane (**S3.1**)

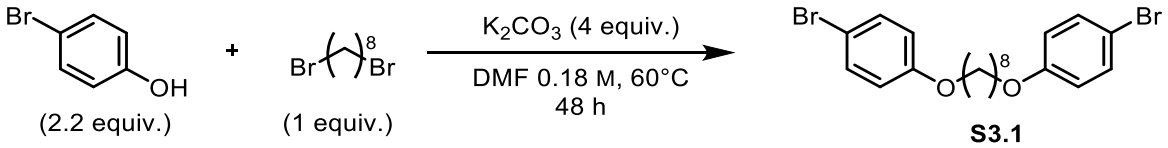

In a 1 L round bottom flask equipped with a magnetic stir bar and a condenser, to a stirring mixture of 4-bromophenol (14.8 g, 85.8 mmol, 2.2 equiv.) and potassium carbonate (21.5 g, 155.9 mmol, 4 equiv.) in DMF (200 mL), 1,8-dibromooctane (10.6 g, 38.9 mmol, 1 equiv.) was added. The mixture was heated to 60 °C for two days. The reaction mixture was cooled to room temperature, diluted with Et2O followed by water, the aqueous layer was extracted with Et2O (3 times) and EtOAc (1 time). The organic layers were combined, washed subsequently with brine, dried over Na2SO4, and concentrated in vacuo. The crude compound S3.1 was obtained as colourless crystals (17.6 g, 38.6 mmol, 99%). Melting point = 39–40 °C. 1H NMR (500 MHz, CDCl3) δ 7.36 (d, J = 8.9 Hz, 4H), 6.77 (d, J = 8.9 Hz, 4H), 3.91 (t, J = 6.5 Hz, 4H), 1.77 (p, J = 6.6 Hz, 4H), 1.46 (qt, J = 6.8, 2.9 Hz, 4H), 1.42 – 1.34 (m, 4H). 13C NMR (126 MHz,

CDCl3) δ 158.36, 132.33, 116.43, 112.72, 68.32, 29.40, 29.28, 26.07. HRMS (FD+) m/z [M•]+ calculated for C20H24Br2O2: 454.0138, found: 454.0142.

Synthesis of 1,1'-((octane-1,8-diylbis(oxy))bis(4,1-phenylene))bis(2,2,2-trifluoroethan-1-one) (**S3.2**)

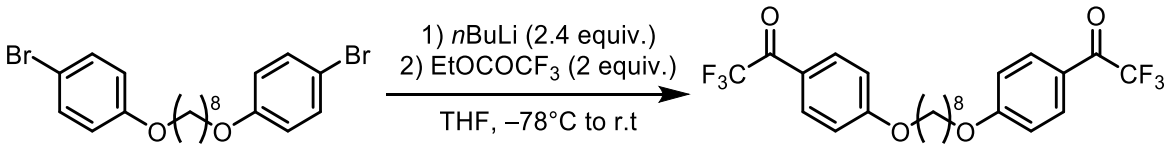

S3.1 **S3.2**

To a stirring solution of compound **S3.1** (1.2 g, 2.6 mmol, 1 equiv.) in dry THF (15 mL) under argon atmosphere at ─78 °C, *n*-butyllithium (2.5 ml, 6.3 mmol, 2.4 equiv.) was slowly added and stirring was maintained at ─78 °C for 1 h. Then ethyl trifluoroacetate (0.6 mL, 5.3 mmol, 2 equiv.) was added dropwise, and the mixture was stirred for a further 1 h at –78 °C and then allowed to warm to room temperature with continued stirring. After 6 h the reaction was quenched with sat. aq. NH_4Cl, and the aqueous layer was extracted with diethyl ether (3 times) and dried over $MgSO_4$. The dried organic layer was filtered and concentrated under reduced pressure. Flash-column chromatography over silica gel using petroleum ether:Et_2O (8:2) as eluent yielded pure compound **S3.2** as a white solid (1.2 g, 2.4 mmol, 92%). Melting point = 64–65 °C. ^{1}H NMR (500 MHz, $CDCl_3$) δ 8.04 (d, *J* = 7.9 Hz, 4H), 6.98 (d, *J* = 9.0 Hz, 4H), 4.07 (t, *J* = 6.5 Hz, 4H), 1.88 – 1.79 (m, 4H), 1.56 – 1.46 (m, 4H), 1.44 – 1.40 (m, 4H).^{13}C NMR (126 MHz, $CDCl_3$) δ 165.15, 132.91, 122.77, 114.98, 68.67, 29.36, 29.11, 26.03. ^{19}F NMR (283 MHz, $CDCl_3$) δ –70.97. HRMS (FD+) m/z $[M^{\bullet}]^+$ calculated for $C_{24}H_{24}F_6O_4$: 490.1573, found: 490.1557.

Synthesis of 1,1'-((octane-1,8-diylbis(oxy))bis(4,1-phenylene))bis(2,2,2-trifluoroethan-1-one) dioxime (**S3.3**)

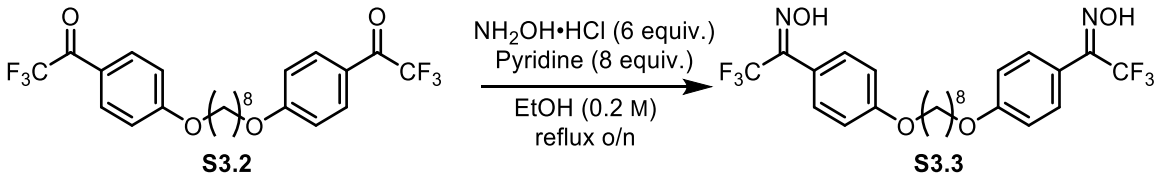

To a stirred solution of compound **S3.2** (4.4 g, 8.97 mmol, 1 equiv.) in ethanol (0.2 M), hydroxylamine hydrochloride (3.7 g, 53.83 mmol, 6 equiv.) and pyridine (5.8 mL, 71.77 mmol, 8 equiv.) were added and the reaction mixture was heated to reflux for 16 h. The mixture was then cooled to room temperature and the mixture was treated with 2M HCl and extracted with Et_2O (3 times). The combined organic layers were washed with distilled water until the pH of the washing layer became neutral, and then dried with sodium sulfate, filtered and concentrated. The residue was dried under high vacuum for a prolonged time to afford the desired crude *bis*-oxime **S3.3** (as a mixture of geometric isomers) as a white solid (4.6 g, 8.84 mmol, 99%). The compound was submitted to the next step without further purification. ^{19}F NMR (283 MHz, $CDCl_3$) δ –62.32, –66.26 (major isomer).

On one occasion, for the purpose of NMR characterization, the residue was purified by flash-column chromatography over silica gel using pentane:EtOAc (7:3) to afford the pure *bis*-oxime (major isomer). Melting point = 127–131 °C. ^1H NMR (500 MHz, Acetone) δ 7.53 (d, J = 8.8 Hz, 4H), 7.05 (d, J = 8.9 Hz, 4H), 4.08 (t, J = 6.4 Hz, 4H), 1.86 – 1.76 (m, 4H), 1.56 – 1.48 (m, 4H), 1.44 (p, J = 3.3 Hz, 4H). ^{19}F NMR (471 MHz, Acetone) δ –66.40. HRMS (FD+) m/z $[M^{\bullet}]^+$ calculated for $C_{24}H_{26}F_6N_2O_4$: 520.1791, found: 520.1773.

Synthesis of 1,1'-((octane-1,8-diylbis(oxy))bis(4,1-phenylene))bis(2,2,2-trifluoroethan-1-one) O,O-di((2-nitrophenyl)sulfonyl) dioxime (**S3.4**)

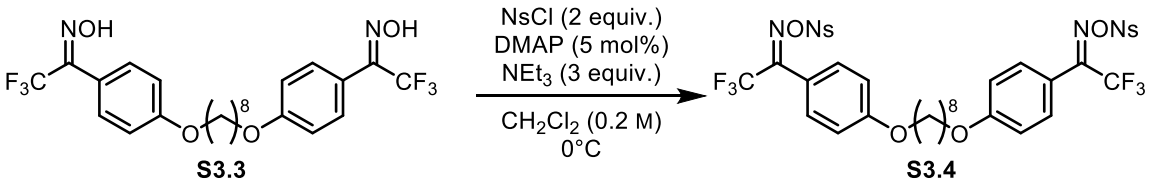

Compound **S3.3** (5.2 g, 10.0 mmol, 1 equiv.) was dissolved in CH_2Cl_2 (50 mL), and triethylamine (4.2 mL, 30.18 mmol, 3 equiv.), DMAP (61 mg, 0.50 mmol, 5 mol%) and 2-nitrobenzenesulfonyl chloride (4.5 g, 20.0 mmol, 2 equiv.) were successively added at 0 °C. The ice bath was removed after 5 min, and the reaction mixture was stirred at room temperature for 1 h. The mixture was then treated with sat. aq. NH_4Cl and extracted with CH_2Cl_2. The combined organic extracts were dried with magnesium sulfate, filtered, and concentrated to afford the desired crude *bis*-nosyloxime **S3.4**, which was submitted to the next step without further purification.

On one occasion, for the purpose of NMR characterization, the residue was purified by flash-column chromatography over silica gel using pentane:EtOAc (7:3) to afford the pure *bis*-nosyloxime as an off-white solid (7.48 g, 8.39 mmol, 84%). Melting point = 114–117 °C. ^{1}H NMR (500 MHz, $CDCl_3$) δ 8.27 (d, J = 7.8 Hz, 2H), 7.94 – 7.74 (m, 6H), 7.60 (d, J = 8.6 Hz, 4H), 7.00 (d, J = 8.9 Hz, 4H), 4.03 (t, J = 6.4 Hz, 4H), 1.88 – 1.76 (m, 4H), 1.49 (q, J = 6.4, 5.5 Hz, 4H), 1.42 (p, J = 3.4 Hz, 4H). ^{19}F NMR (471 MHz, $CDCl_3$) δ –65.59. HRMS (FD+) m/z $[M^{\bullet}]^+$ calculated for $C_{36}H_{32}F_6N_4O_{12}S_2$: 890.1357, found: 890.1341.

Synthesis of 1,8-bis(4-(3-(trifluoromethyl)diaziridin-3-yl)phenoxy)octane (**S3.5**)

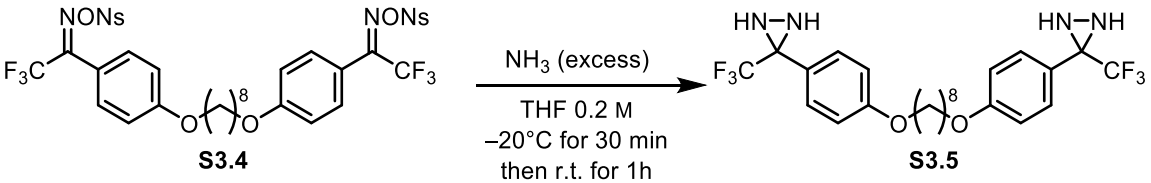

Bis-nosyloxime **S3.4** (7.48 g, 8.39 mmol, 1 equiv.) in anhydrous THF (42 mL) was transferred to a flame-dried 3-neck flask under argon and cooled to –20 °C. Anhydrous gaseous ammonia was bubbled into the stirred solution for 30 min. Then, the reaction was left stirring for 1 h, during which time it was allowed to warm from –20 °C to room temperature. The mixture was quenched with sat. aq. NH_4Cl and extracted with

Et_2O (3 times). The combined organic layers were washed with brine and then dried with magnesium sulfate, filtered and concentrated to afford the desired crude *bis*-diaziridine **S3.5**, which was submitted to the next step without further purification.

On one occasion, for the purpose of NMR characterization, the residue was purified by flash-column chromatography over silica gel using pentane:EtOAc (7:3) to afford the pure *bis*-diaziridine as a white solid (4.2 g, 8.1 mmol, 96%). Melting point = 81–83 °C. ^{1}H NMR (500 MHz, $CDCl_3$) δ 7.52 (d, *J* = 8.7 Hz, 4H), 6.91 (d, *J* = 8.8 Hz, 4H), 3.97 (t, *J* = 6.5 Hz, 4H), 2.74 (d, *J* = 8.8 Hz, 2H, N-H), 2.15 (d, *J* = 8.9 Hz, 2H, N-H), 1.84 – 1.74 (m, 4H), 1.52 – 1.43 (m, 4H), 1.39 (p, *J* = 3.5 Hz, 4H). ^{13}C NMR (126 MHz, $CDCl_3$) δ 160.55, 129.60, 123.65, 114.76, 68.21, 29.40, 29.26, 26.09. ^{19}F NMR (471 MHz, $CDCl_3$) δ –75.78. IR (diamond-ATR) ν: 3675, 3260, 2930, 2858, 1742, 1613, 1519, 1247, 1153, 1053, 939, 832, 755. HRMS (FD+) m/z $[M^{\bullet}]^+$ calculated for $C_{24}H_{28}F_6N_4O_2$: 518.2111, found: 518.2091.

Synthesis of 1,8-bis(4-(3-(trifluoromethyl)-3H-diazirin-3-yl)phenoxy)octane (**3.9**)

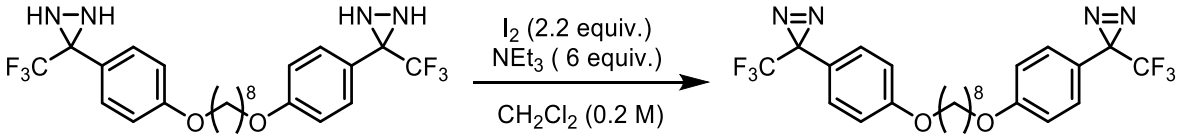

S3.5 **3.9**

To a solution of *bis*-diaziridine **S3.5** (4.2 g, 8.1 mmol, 1 equiv.) in CH_2Cl_2 (41 mL) at 0 °C were added successively triethylamine (6.8 mL, 48.6 mmol, 6 equiv.) and iodine (4.52 g, 17.8 mmol, 2.2 equiv.). The coloured mixture was stirred at 0 °C for 1 h. The mixture was diluted with CH_2Cl_2 and washed with sat. aq. sodium thiosulfate. The aqueous layer was re-extracted with CH_2Cl_2 (3 times). Then the combined organic extracts were washed with brine and dried with magnesium sulfate, filtered, and concentrated. The residue was purified by silica gel column chromatography using pentane: Et_2O (8:2) as eluent to afford the desired *bis*-diazirine **3.9** (3.04 g, 5.91 mmol, 73%) as a pale-yellow solid. Melting point = 48–49 °C. ^{1}H NMR (500 MHz, $CDCl_3$) δ 7.13 (d, *J* = 8.4 Hz, 4H), 6.88 (d, *J* = 8.9 Hz, 4H), 3.95 (t, *J* = 6.5 Hz, 4H), 1.78 (p, *J* = 6.6 Hz, 4H), 1.46 (dp, *J* = 12.4, 6.5 Hz, 4H), 1.43 – 1.35 (m, 4H). ^{13}C NMR (126 MHz, $CDCl_3$) δ 160.32, 129.55, 128.25, 123.50, 121.32, 120.85, 114.99, 68.22, 29.38, 29.23, 26.07. ^{19}F NMR (283 MHz, $CDCl_3$) δ –65.63. IR (diamond-ATR) ν: 2939, 2860, 1707, 1603, 1519, 1259, 1235, 1181, 1155, 939, 825, 626, 525. UV (*n*-hexane): $\lambda_{max,\ diazirine}$ =

372 nm. HRMS (FD+) m/z $[M^{\bullet}]^{+}$ calculated for $C_{24}H_{24}F_6N_4O_2$: 514.1798, found: 514.1779.

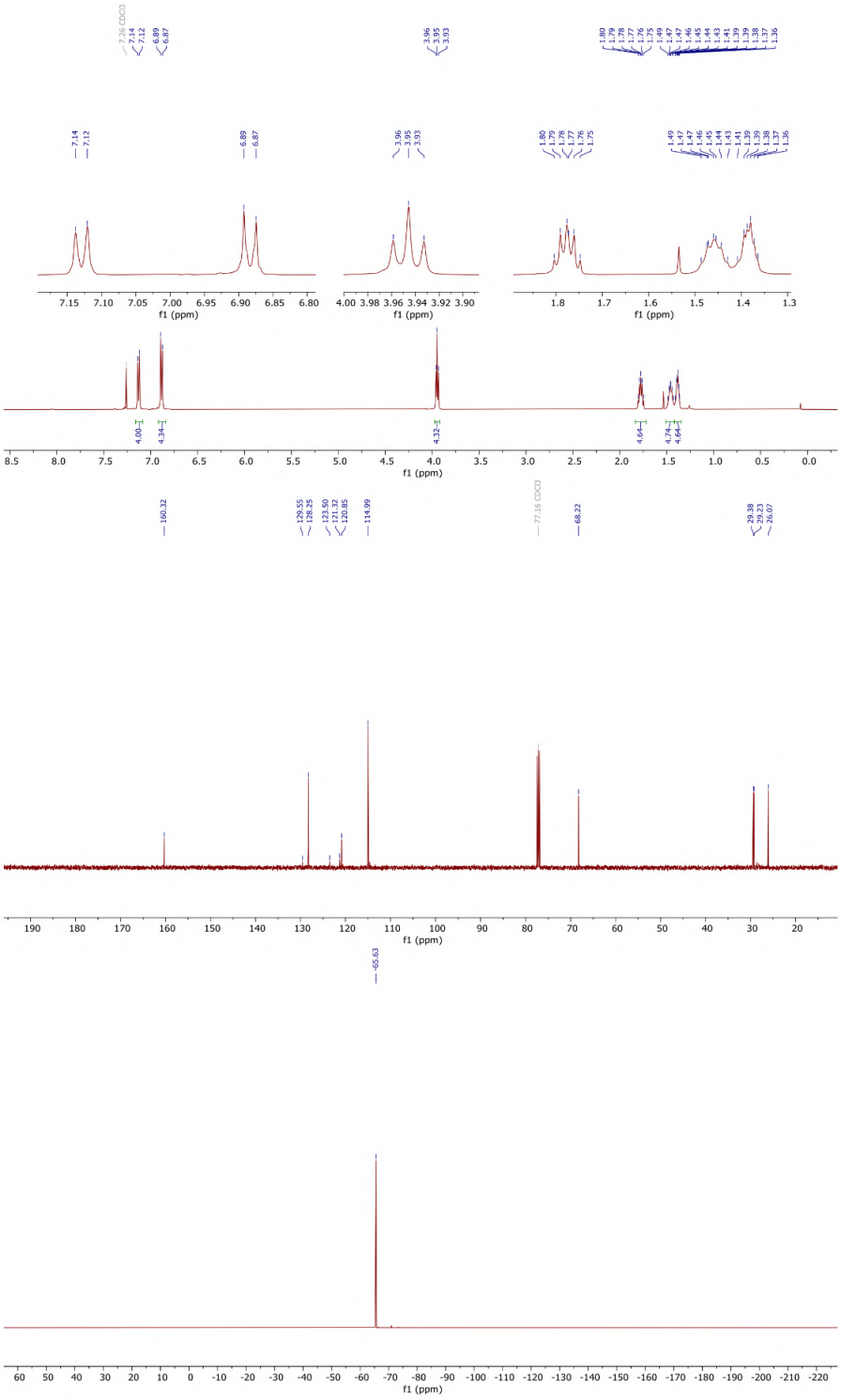

Figure S3.1 ^{1}H, ^{13}C, and ^{19}F NMR spectra of **3.9** in $CDCl_3$.

3.5.1.3 Synthesis of rigid *bis*-aryl ether crosslinker 3.3

Synthetic scheme for compound **3.3**

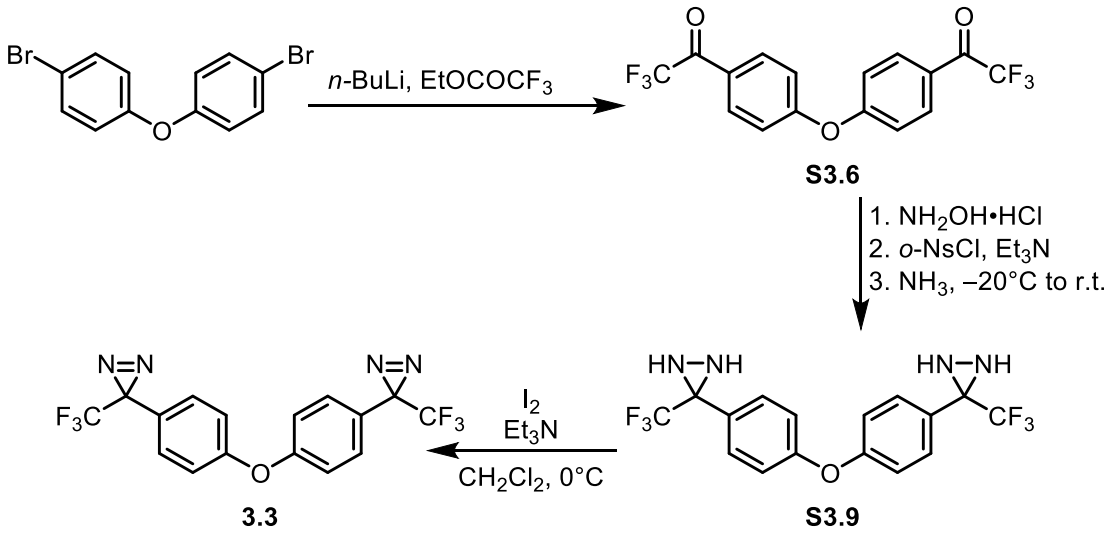

Synthesis of 1,1'-(oxybis(4,1-phenylene))bis(2,2,2-trifluoroethan-1-one) (**S3.6**)

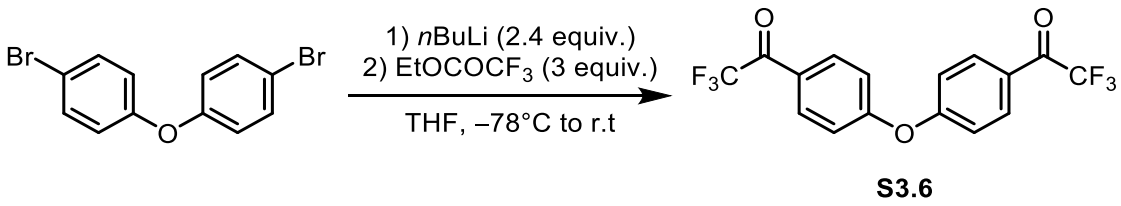

To a stirring solution of 4,4'-oxybis(bromobenzene) (5.12 g, 15.61 mmol, 1 equiv.) in dry THF (90 ml) under argon atmosphere at –78 °C, *n*-butyllithium (15 mL, 37.48 mmol, 2.4 equiv., 2.5 M) was slowly added and stirring was maintained at –78 °C for 1 h. Then ethyl trifluoroacetate (5.6 mL, 46.8 mmol, 3 equiv.) was added dropwise, and the mixture was stirred for a further 1 h at –78 °C and then allowed to warm to room temperature with continued stirring. After 6 h the reaction was quenched with sat. aq. NH_4Cl, and the aqueous layer was extracted with Et_2O (3 times) and dried over $MgSO_4$. The dried organic layer was filtered and concentrated under reduced pressure. Flash-column chromatography over silica gel using petroleum ether:Et_2O (8:2) as eluent yielded pure compound **S3.6** as a colourless oil (5.46 g, 15.07 mmol, 97%) with spectroscopic data in accordance with the literature.[68] ^{1}H NMR (300 MHz, $CDCl_3$) δ 8.14 (d, *J* = 8.0 Hz, 4H), 7.20 (d, *J* = 8.9 Hz, 4H). ^{19}F NMR (283 MHz, $CDCl_3$) δ ─71.32.

Synthesis of 1,1'-(oxybis(4,1-phenylene))bis(2,2,2-trifluoroethan-1-one) dioxime (**S3.7**)

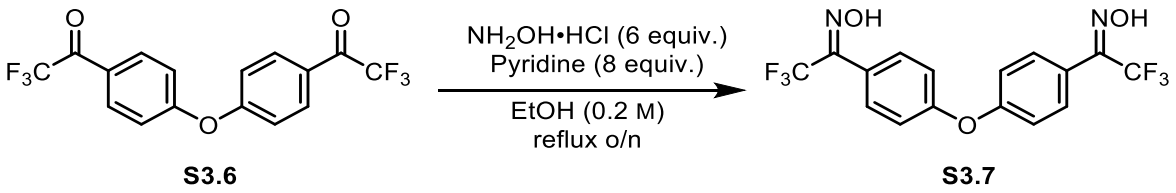

S3.6 **S3.7**

To a stirred solution of compound **S3.6** (5.36 g, 14.8 mmol, 1 equiv.) in ethanol (0.2 M), hydroxylamine hydrochloride (6.17 g, 88.85 mmol, 6 equiv.) and pyridine (9.5 mL, 118.4 mmol, 8 equiv.) were added and the reaction mixture was heated to reflux for 16 h. The mixture was then cooled to room temperature and the mixture was treated with 2M HCl and extracted with Et_2O (3 times). The combined organic layers were washed with distilled water until the pH of the washing layer became neutral, and then dried with sodium sulfate, filtered, and concentrated. The residue was dried under high vacuum for a prolonged time to afford the desired crude *bis*-oxime **S3.7** (as a mixture of geometric isomers) (5.8 g, 14.78 mmol, 99%) with spectroscopic data in accordance with the literature.[68] The compound was submitted to the next step without further purification. ^{1}H NMR (300 MHz, CD_3OD) δ 7.53 (d, J = 8.6 Hz, 4H), 7.13 (d, J = 8.8 Hz, 4H).^{19}F NMR (283 MHz, $CDCl_3$) δ –62.26, –66.42.

Synthesis of 1,1'-(oxybis(4,1-phenylene))bis(2,2,2-trifluoroethan-1-one) O,O-di((2-nitrophenyl)sulfonyl) dioxime (**S3.8**)

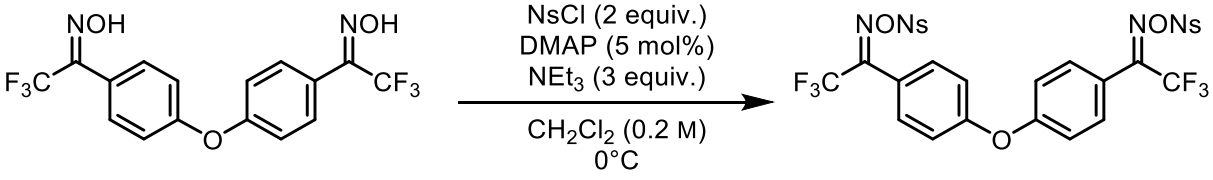

S3.7 **S3.8**

Compound **S3.7** (5.8 g, 14.8 mmol, 1 equiv.) was dissolved in CH_2Cl_2 (74 mL), and triethylamine (6.2 mL, 44.4 mmol, 3 equiv.), DMAP (90 mg, 0.74 mmol, 5 mol%) and 2-nitrobenzenesulfonyl chloride (6.89 g, 31.8 mmol, 2.1 equiv.) were successively added at 0 °C. The ice bath was removed after 5 min and the reaction mixture was stirred at room temperature for 1 h. The mixture was then treated with sat. aq. NH_4Cl and extracted with CH_2Cl_2. The combined organic extracts were dried with magnesium sulfate, filtered, and concentrated to afford the desired crude *bis*-nosyloxime **S3.8** which was submitted to the next step without further purification.

On one occasion, for the purpose of NMR characterization, the residue was purified by flash-column chromatography over silica gel using pentane:EtOAc (7:3) to afford the pure *bis*-nosyloxime (10.91 g, 14.29 mmol, 96%) as a pale-yellow solid. Melting point = 116–117 °C. ^{1}H NMR (500 MHz, $CDCl_3$) δ 8.29 (d, *J* = 7.8 Hz, 2H), 7.96 – 7.79 (m, 6H), 7.65 (d, *J* = 8.7 Hz, 4H), 7.21 (d, *J* = 8.9 Hz, 4H). ^{13}C NMR (126 MHz, $CDCl_3$) δ 159.11, 136.10, 133.80, 132.38, 131.32, 127.51, 125.13, 119.59. ^{19}F NMR (471 MHz, $CDCl_3$) δ –66.09. HRMS (FD+) m/z $[M^{\bullet}]^{+}$ calculated for $C_{28}H_{16}F_6N_4O_{11}S_2$: 762.0156, found: 762.0176.

Synthesis of 3,3'-(oxybis(4,1-phenylene))bis(3-(trifluoromethyl)diaziridine) (**S3.9**)

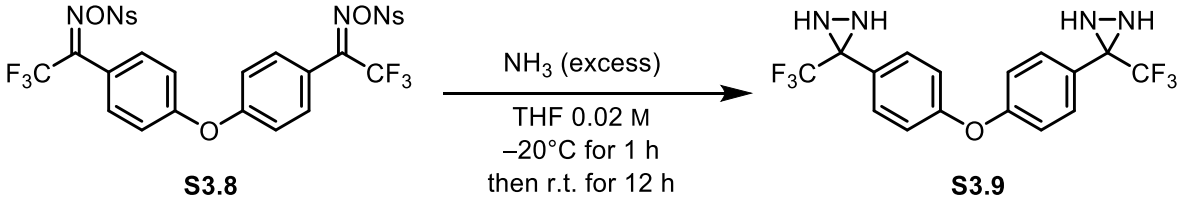

S3.8 **S3.9**

Bis-nosyloxime **S3.8** (10.91 g, 14.29 mmol, 1 equiv.) in anhydrous THF (70 mL) was transferred to a flame-dried 3-neck flask under argon and cooled to ─20 °C. Anhydrous gaseous ammonia was bubbled into the stirred solution for 1 h. Then, the reaction was left stirring for 12 h, during which time it was allowed to warm from ─20 °C to room temperature. The mixture was quenched with sat. aq. NH_4Cl and extracted with Et_2O (3 times). The combined organic layers were washed with brine and then dried with magnesium sulfate, filtered, and concentrated to afford the desired crude *bis*-diaziridine **S3.9** (5.4 g, 13.83 mmol, 96%) with spectroscopic data in accordance with the literature.[68] The compound was submitted to the next step without further purification. ^{1}H NMR (500 MHz, $CDCl_3$) δ 7.61 (d, *J* = 8.7 Hz, 4H), 7.06 (d, *J* = 8.7 Hz, 4H), 2.80 (d, *J* = 9.1 Hz, 2H), 2.21 (d, *J* = 8.9 Hz, 2H).^{19}F NMR (283 MHz, $CDCl_3$) δ –75.81. IR (diamond-ATR) ν: 3675, 3262, 2972, 2901, 1603, 1507, 1247, 1153, 884.

Synthesis of 3,3'-(oxybis(4,1-phenylene))bis(3-(trifluoromethyl)-3H-diazirine) (**3.3**)

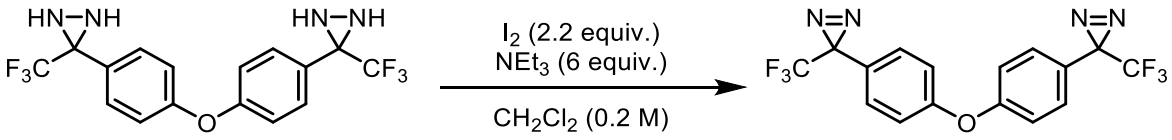

S3.9 **3.3**

To a solution of *bis*-diaziridine **S3.9** (5.77 g, 14.8 mmol, 1 equiv.) in CH_2Cl_2 (74 mL) at 0 °C were added successively triethylamine (12.4 mL, 88.8 mmol, 6 equiv.) and iodine (7.5 g, 29.6 mmol, 2 equiv.). The coloured mixture was stirred at 0 °C for 1 h. The mixture was diluted with CH_2Cl_2 and washed with sat. aq. sodium thiosulfate. The aqueous layer was re-extracted with CH_2Cl_2 (3 times). Then the combined organic extracts were washed with brine and dried with magnesium sulfate, filtered, and concentrated. The residue was purified by silica gel column chromatography using pentane as eluent to afford the desired *bis*-diazirine **3.3** (4.66 g, 12.06 mmol, 81%) as a colourless liquid. ^{1}H NMR (300 MHz, $CDCl_3$) δ 7.20 (d, J = 8.8 Hz, 4H), 7.01 (d, J = 8.9 Hz, 4H). ^{13}C NMR (126 MHz, $CDCl_3$) δ 157.79, 128.67, 124.52, 119.45, 29.86. ^{19}F NMR (283 MHz, $CDCl_3$) δ –65.45. IR (diamond-ATR) ν: 2971, 1603, 1508, 1251, 1154, 938, 827, 539. UV (*n*-hexane): $\lambda_{max,\ diazirine}$ = 360 nm. HRMS (FD+) m/z $[M^{\bullet}]^{+}$ calculated for $C_{28}H_{32}F_6O$: 386.0597, found: 386.0599.

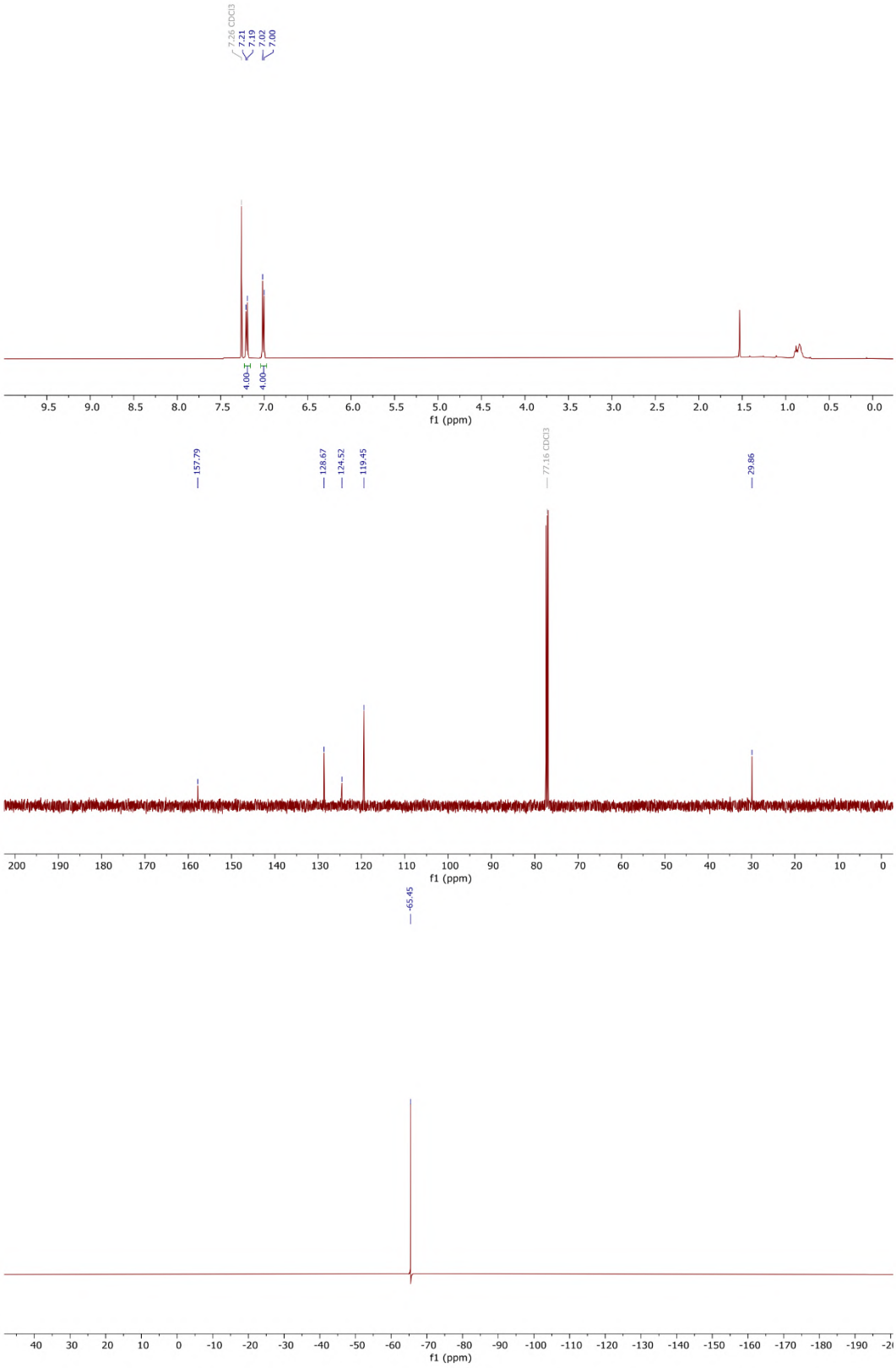

Figure S3.2 ^{1}H, ^{13}C, and ^{19}F NMR spectra of **3.3** in $CDCl_3$.

3.5.1.4 Synthesis of molecular control 3.10

Synthesis of 2,2,2-trifluoro-1-(4-((8-phenoxyoctyl)oxy)phenyl)ethan-1-one (**S3.10**)

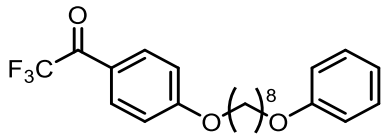

S3.10

During the purification of 1,1'-((octane-1,8-diyl*bis*(oxy))*bis*(4,1-phenylene))*bis*(2,2,2-trifluoroethan-1-one) **S3.2** described above, the corresponding mono-ketone **S3.10**, precursor of molecular control **3.10**, was isolated in small amounts (260 mg, 0.6591 mmol). ^{1}H NMR (300 MHz, CD_2Cl_2) δ 8.04 (d, *J* = 8.0 Hz, 2H), 7.26 (tt, *J* = 7.5, 2.3 Hz, 2H), 7.01 (d, *J* = 9.0 Hz, 2H), 6.97 – 6.82 (m, 3H), 4.08 (t, *J* = 6.5 Hz, 2H), 3.95 (t, *J* = 6.5 Hz, 2H), 1.90 – 1.69 (m, 4H), 1.51 – 1.35 (m, 8H). ^{13}C NMR (126 MHz, CD_2Cl_2) δ 182.61, 165.66, 159.63, 133.05, 129.77, 122.84, 120.77, 115.31, 114.80, 69.14, 68.23, 29.68, 29.63, 29.35, 26.37, 26.23. ^{19}F NMR (283 MHz, $CDCl_3$) δ –70.95. HRMS (FD+) m/z $[M^{\bullet}]^+$ calculated for $C_{22}H_{25}F_3O_3$: 394.1750, found: 394.1771.

Synthesis of 2,2,2-trifluoro-1-(4-((8-phenoxyoctyl)oxy)phenyl)ethan-1-one oxime (**S3.11**)

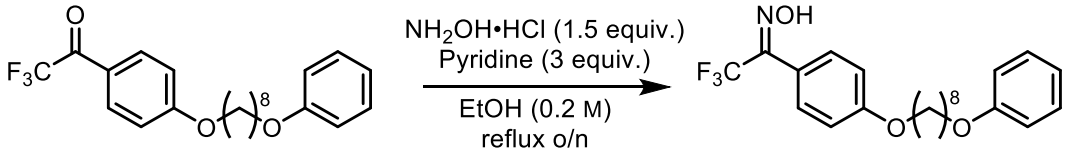

S3.10 **S3.11**

To a stirred solution of compound **S3.10** (260 mg, 0.6591 mmol, 1 equiv.) in ethanol (0.2 M), hydroxylamine hydrochloride (65.6 mg, 0.943 mmol, 1.5 equiv.) and pyridine (0.16 mL, 1.97 mmol, 3 equiv.) were added and the reaction mixture was heated to reflux for 16 h. The mixture was then cooled to room temperature and the mixture was treated with 2M HCl and extracted with Et_2O (3 times). The combined organic layers were washed with distilled water until the pH of the washing layer became neutral, and then dried with sodium sulfate, filtered, and concentrated. The residue was dried under high vacuum for a prolonged time to afford the desired crude oxime **S3.11** (as a mixture of geometric isomers) as a white solid (261.3 mg). ^{1}H NMR (500 MHz, Acetone) δ 11.63 (s, 1H), 7.52 (d, *J* = 8.8 Hz, 2H), 7.26 (dd, *J* = 8.8, 7.2 Hz, 2H), 7.05 (d, *J* = 8.9 Hz, 2H), 6.93 – 6.85 (m, 3H), 4.07 (t, *J* = 6.5 Hz, 2H), 3.99 (t, *J* = 6.5 Hz, 2H), 1.85 – 1.73 (m,

4H), 1.51 (q, *J* = 6.8, 6.3 Hz, 4H), 1.43 (dt, *J* = 14.5, 7.4 Hz, 4H). ^{19}F NMR (471 MHz, Acetone) δ –63.02, –66.41.

Synthesis of 2,2,2-trifluoro-1-(4-((8-phenoxyoctyl)oxy)phenyl)ethan-1-one O-((2-nitrophenyl)sulfonyl) oxime (**S3.12**)

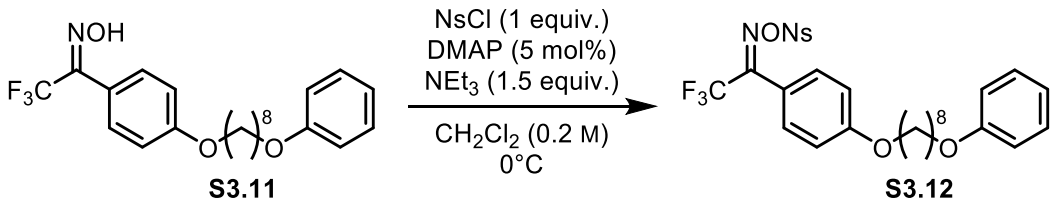

Compound **S3.11** (261 mg, 0.638 mmol, 1 equiv.) was dissolved in CH_2Cl_2 (4 mL), and triethylamine (0.133 mL, 0.957 mmol, 1.5 equiv.), DMAP (4 mg, 0.032 mmol, 5 mol%) and nosyl chloride (141.4 mg, 0.638 mmol, 1 equiv.) were successively added at 0 °C. The ice bath was removed after 5 min, and the reaction mixture was stirred at room temperature for 30 min. The mixture was then treated with sat. aq. NH_4Cl and extracted with CH_2Cl_2. The combined organic extracts were dried with magnesium sulfate, filtered, and concentrated to afford the desired crude nosyloxime **S3.12** (380 mg), which was submitted to the next step without further purification. ^{1}H NMR (500 MHz, $CDCl_3$) δ 8.28 (d, *J* = 7.8 Hz, 1H), 7.93 – 7.78 (m, 3H), 7.60 (d, *J* = 8.7 Hz, 2H), 7.31 – 7.25 (m, 2H), 7.00 (d, *J* = 8.9 Hz, 2H), 6.92 – 6.86 (m, 3H), 4.00 – 3.91 (m, 4H), 1.87 – 1.73 (m, 8H), 1.65 – 1.57 (m, 2H), 1.52 – 1.45 (m, 8H).^{19}F NMR (471 MHz, $CDCl_3$) δ –61.16, 65.60 (major isomer).

Synthesis of 3-(4-((8-phenoxyoctyl)oxy)phenyl)-3-(trifluoromethyl)diaziridine (**S3.13**)

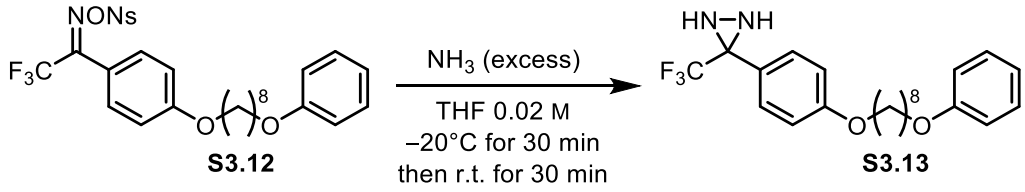

Nosyloxime **S3.12** (380 mg, 0.63 mmol, 1 equiv.) in anhydrous THF (20 mL) was transferred to a flame-dried 3-neck flask under argon and cooled to –20 °C. Anhydrous gaseous ammonia was bubbled into the stirred solution for 30 min. Then, the reaction was left stirring for 30 min, during which time it was allowed to warm from –20 °C to room temperature. The mixture was quenched with sat. aq. NH_4Cl and extracted with Et_2O (3 times). The combined organic layers were washed with brine and then dried with

magnesium sulfate, filtered, and concentrated to afford the desired crude diaziridine **S3.13** (256 mg) as yellow solid, which was submitted to the next step without further purification. ^{1}H NMR (500 MHz, $CDCl_3$) δ 7.52 (d, *J* = 8.5 Hz, 2H), 7.31 – 7.25 (m, 2H), 6.98 – 6.84 (m, 5H), 3.96 (q, *J* = 6.3 Hz, 4H), 2.74 (d, *J* = 8.8 Hz, 1H), 2.16 (d, *J* = 8.9 Hz, 1H), 1.79 (p, *J* = 6.7 Hz, 4H), 1.54 – 1.44 (m, 4H), 1.43 – 1.36 (m, 4H). ^{13}C NMR (126 MHz, $CDCl_3$) δ 160.56, 159.24, 129.58, 129.55, 123.61, 122.51 (d, *J* = 41.7 Hz), 120.62, 114.76, 114.63, 68.21, 67.94, 29.85, 29.46, 29.44, 29.41, 29.26, 26.15, 26.08. ^{19}F NMR (471 MHz, $CDCl_3$) δ –75.87. IR (diamond-ATR) ν: 3258, 2928, 2856, 1727, 1613, 1518, 1471, 1245, 1152, 1033, 754, 692.

Synthesis of 3-(4-((8-phenoxyoctyl)oxy)phenyl)-3-(trifluoromethyl)-3*H*-diazirine (**3.10**)

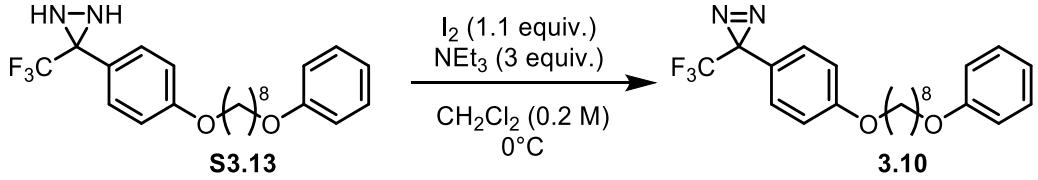

To a solution of the crude diaziridine **S3.13** (256 mg) in CH_2Cl_2 (4 mL) at 0 °C were added successively triethylamine (0.27 mL, 1.91 mmol, 3 equiv.) and iodine (178 mg, 0.702 mmol, 1.1 equiv.). The coloured mixture was stirred at 0 °C for 1 h. The mixture was diluted with CH_2Cl_2 and washed with sat. aq. sodium thiosulfate. The aqueous layer was re-extracted with CH_2Cl_2 (3 times). Then the combined organic extracts were washed with brine and dried with magnesium sulfate, filtered, and concentrated. The residue was purified by silica gel column chromatography using pentane: Et_2O (8:2, R_f =0.71) as eluent to afford the desired diazirine **3.10** (250 mg, 0.62 mmol, 98%) as a yellow solid. Melting point = 41–42 °C. ^{1}H NMR (500 MHz, CD_2Cl_2) δ 7.26 (dd, *J* = 8.7, 7.2 Hz, 2H), 7.15 (d, *J* = 8.7 Hz, 2H), 6.98 – 6.89 (m, 1H), 6.95 (d, *J* = 9.0 Hz, 2H), 3.95 (q, *J* = 6.5 Hz, 4H), 1.81 – 1.73 (m, 4H), 1.52 – 1.43 (m, 4H), 1.40 (dt, *J* = 6.7, 4.6 Hz, 4H). ^{13}C NMR (126 MHz, CD_2Cl_2) δ 160.81, 159.63, 129.77, 128.50, 123.86, 120.78, 120.76, 120.74, 115.28, 114.80, 68.63, 68.25, 29.70, 29.68, 29.48, 26.38, 26.29. ^{19}F NMR (471 MHz, $CDCl_3$) δ –65.67. IR (diamond-ATR) ν: 2929, 2857, 1723, 1601, 1518, 1497, 1244, 1180, 1154, 1054, 939, 754, 692. HRMS (FD+) m/z $[M^{\bullet}]^{+}$ calculated for $C_{22}H_{25}F_3N_2O_2$: 406.1863, found: 406.1877.

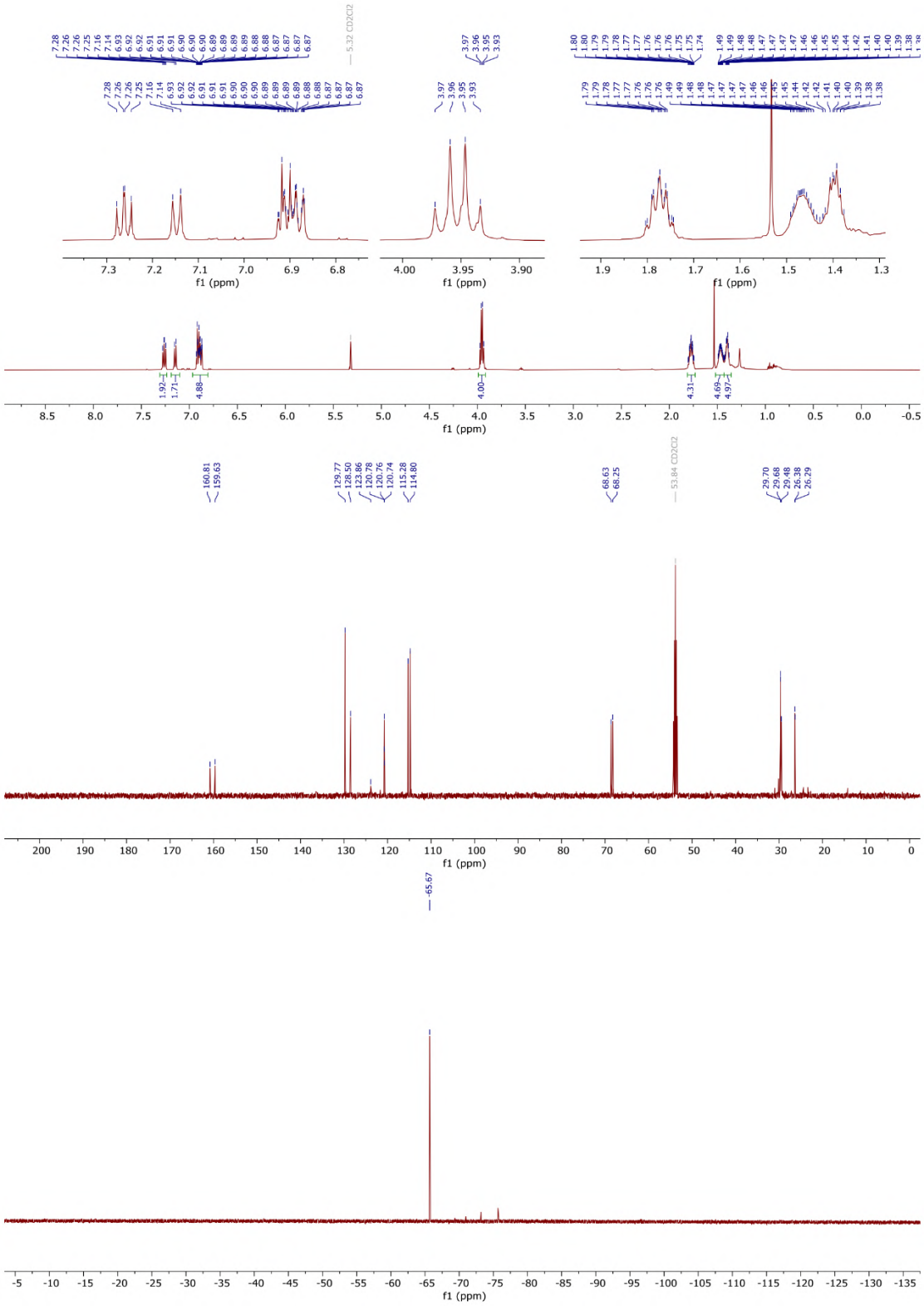

Figure S3.3 ^{1}H and ^{13}C NMR spectra of **3.10** in CD_2Cl_2, and ^{19}F NMR spectrum of **3.10** in $CDCl_3$.

3.5.1.5 Evaluation of crosslinker efficacy by crosslinking of cyclohexane

Cyclohexane crosslinking with *bis*-diazirine **3.9**

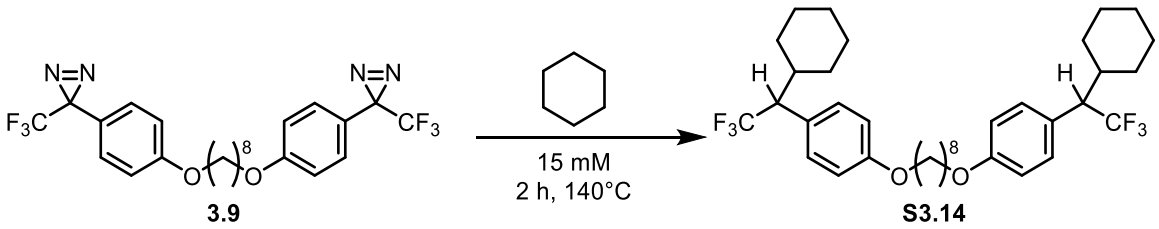

In a flame-dried sealed tube, *bis*-diazirine **3.9** (11.3 mg, 0.022 mmol, 1 equiv.) in cyclohexane (15 mM), flushed gently with argon and capped, was heated at 140 °C for 2 h. After cooling the mixture to room temperature, the reaction mixture was transferred into a round bottom flask and concentrated in vacuo to provide crude product (14 mg). Flash-column chromatography over silica gel using 100% petroleum ether afforded 1,8-*bis*(4-(1-cyclohexyl-2,2,2-trifluoroethyl)phenoxy)octane **S3.14** (12 mg, 0.02 mmol) in 91% yield. ^{1}H NMR (300 MHz, $CDCl_3$) δ 7.13 (d, *J* = 8.6 Hz, 4H), 6.85 (d, *J* = 8.7 Hz, 4H), 3.94 (t, *J* = 6.5 Hz, 4H), 2.97 (qd, *J* = 10.3, 7.9 Hz, 2H), 2.04 – 1.86 (m, 4H), 1.84 – 1.65 (m, 8H), 1.68 – 1.57 (m, 4H), 1.45 – 1.35 (m, 8H), 1.34 – 1.28 (m, 2H), 1.20 – 1.02 (m, 6H), 0.84 – 0.72 (m, 2H). ^{13}C NMR (126 MHz, $CDCl_3$) δ 158.78, 132.34, 130.34, 128.94 (q, *J* = 118.0 Hz), 114.45, 68.01, 55.31 (q, *J* = 25.8 Hz), 38.68, 31.67, 30.81, 29.85, 29.46, 29.43, 26.34, 26.26, 26.17. ^{19}F NMR (283 MHz, $CDCl_3$) δ –63.73. HRMS (FD+) m/z $[M^{\bullet}]^{+}$ calculated for $C_{36}H_{48}F_6O_2$: 626.3553, found: 626.3565.

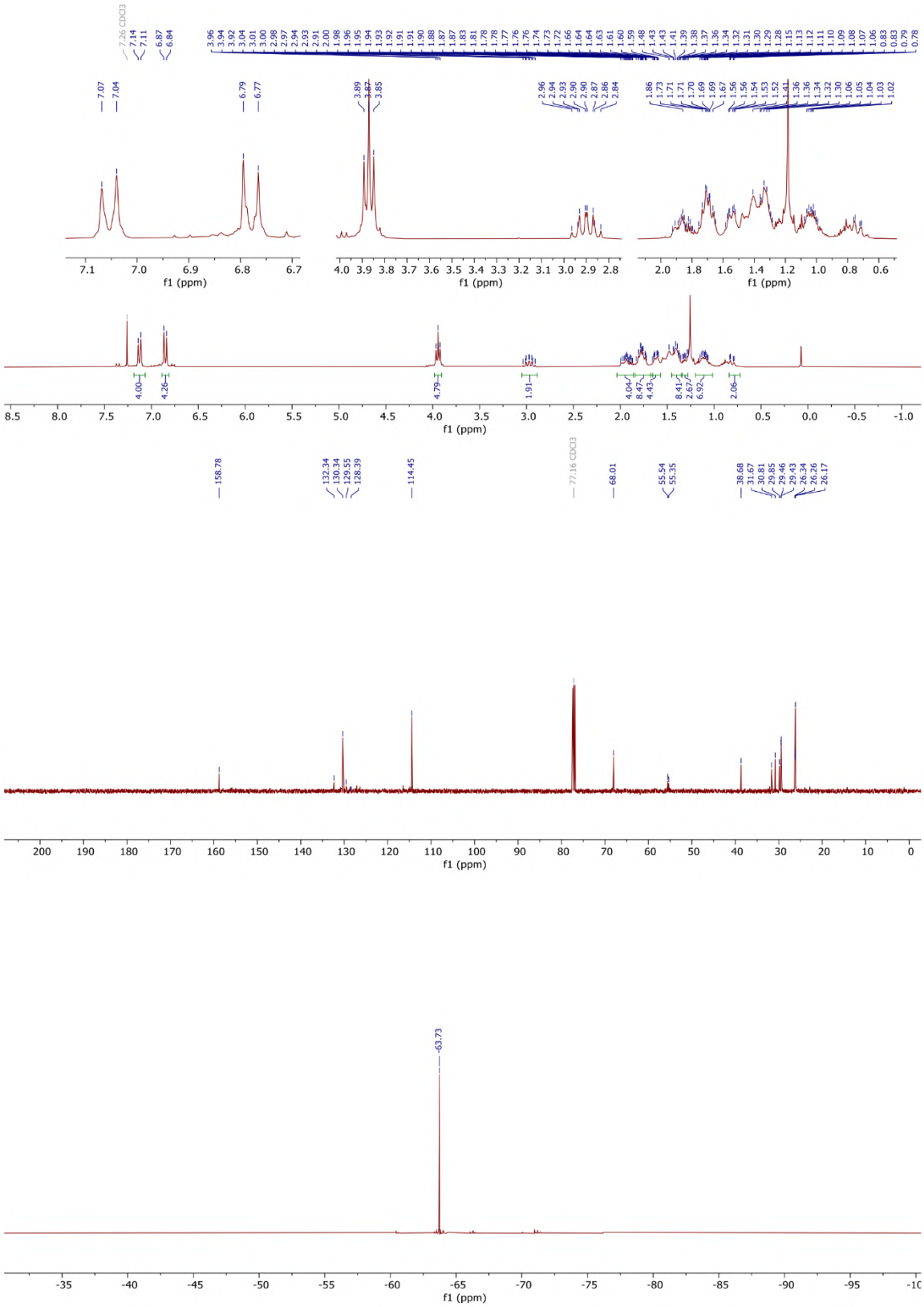

Figure S3.4 ^{1}H, ^{13}C, and ^{19}F NMR spectra of **S3.14** in $CDCl_3$.

Cyclohexane crosslinking with *bis*-diazirine **3.3**

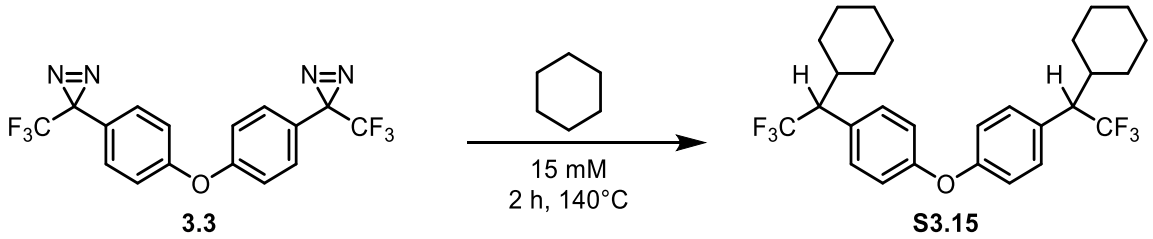

In a flame-dried sealed tube, *bis*-diazirine **3.3** (24.9 mg, 0.064 mmol, 1 equiv.) in cyclohexane (15 mM), flushed gently with argon and capped, was heated at 140 °C for 2 h. After cooling the mixture to room temperature, the reaction mixture was transferred into a round bottom flask and concentrated in vacuo to provide crude product (34.6 mg). Flash-column chromatography overs silica gel 100% petroleum ether afforded 4,4'-oxy-*bis*((1-cyclohexyl-2,2,2-trifluoroethyl)benzene) **S3.15** (17.6 mg, 0.034 mmol) in 54% yield. ^{1}H NMR (300 MHz, $CDCl_3$) δ 7.20 (d, *J* = 8.7 Hz, 4H), 6.98 (d, *J* = 8.7 Hz, 4H), 3.03 (qd, *J* = 10.4, 9.9 Hz, 2H), 2.03 – 1.84 (m, 5H), 1.84 – 1.71 (m, 2H), 1.68 – 1.59 (m, 5H), 1.22 – 1.01 (m, 8H), 0.85 – 0.72 (m, 2H).^{13}C NMR (126 MHz, $CDCl_3$) δ 156.68, 130.69, 118.92, 55.61 (q, *J* = 25.2 Hz), 38.69, 31.63, 30.85, 29.85, 26.30, 26.24, 26.15. ^{19}F NMR (283 MHz, $CDCl_3$) δ –63.60. HRMS (FD+) m/z $[M^{\bullet}]^{+}$ calculated for $C_{28}H_{32}F_6O$: 498.2352, found: 498.2340.

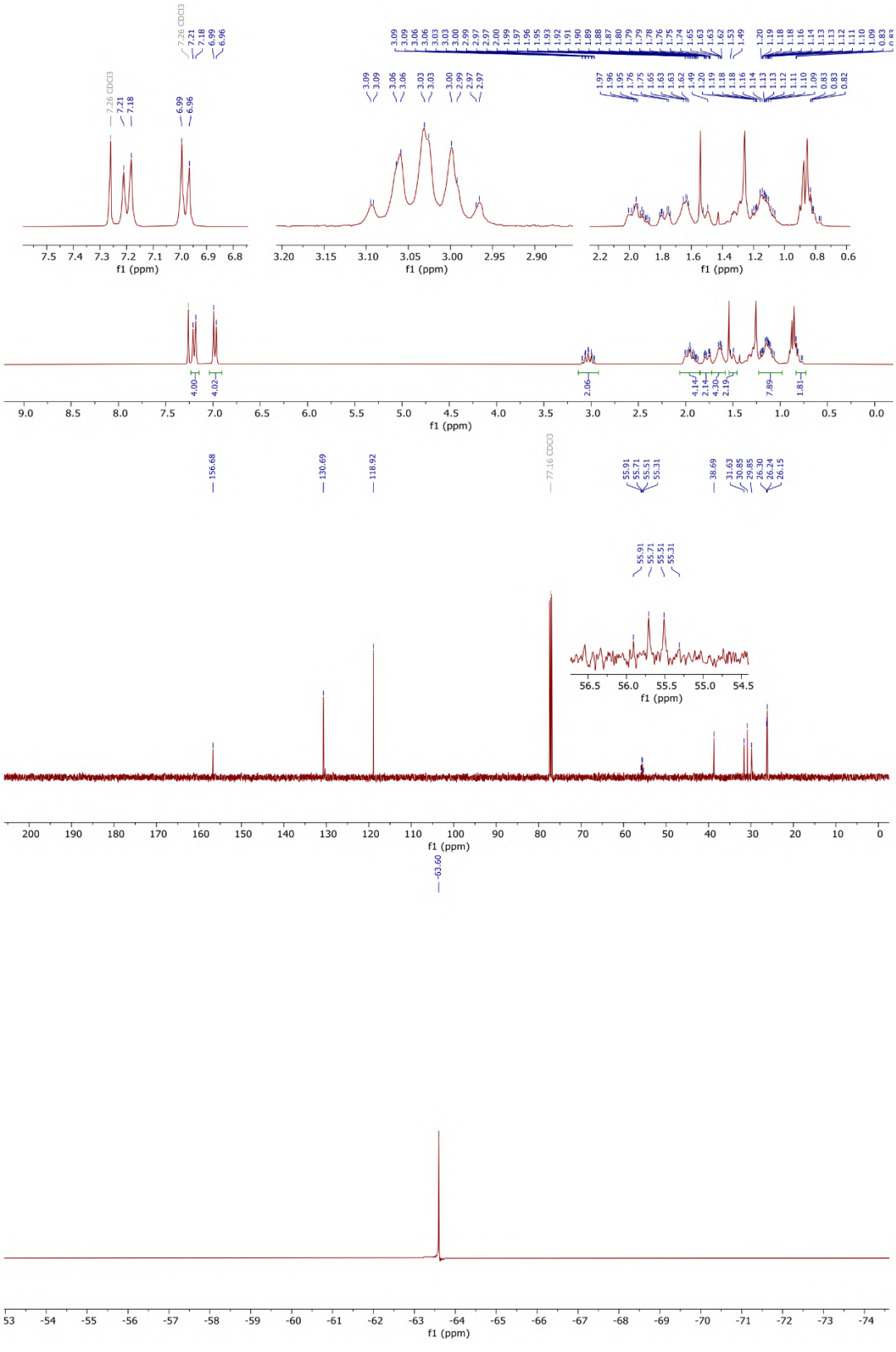

Figure S3.5 ^{1}H, ^{13}C, and ^{19}F NMR spectra of **S3.15** in $CDCl_3$.

3.5.1.6 Crosslinking of cyclohexane under mild conditions

General protocols for insertion reactions

A) Thermal insertion reaction: a 15 mM solution of the desired crosslinker in cyclohexane was prepared in a vial. The reaction was immersed in an oil bath at the desired temperature and stirred at that temperature for the desired time. After cooling the mixture to room temperature, the reaction was concentrated in vacuo to provide the crude product.

B) Photochemical insertion reaction (365 nm): a 15 mM solution of the desired crosslinker in cyclohexane was prepared in a vial. The reaction was irradiated with a 365 nm UV spotlight (ThorLabs, 3685 lux, 38 W/m^2) for the desired time. The reaction was concentrated in vacuo to provide the crude product.

C) Photochemical insertion reaction (395 nm): a 15 mM solution of the desired crosslinker in cyclohexane was prepared in a vial. The reaction was irradiated with 395 nm LED Strip Lights (Waveform Lighting, 5129 lux, 53 W/m^2) for the desired time. The reaction was concentrated in vacuo to provide the crude product.

All reactions were conducted under an air atmosphere. Crude ^{19}F NMR ($CDCl_3$) spectra were collected and compared.

Cyclohexane crosslinking of *bis*-diazirine **3.9** at low temperatures

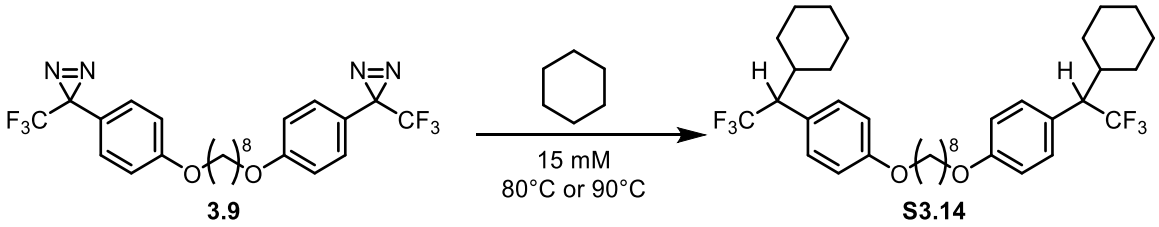

3.9 **S3.14**

Following the above general protocol (**A**), three reactions (***a***, ***b***, ***c***) were performed at 80 °C, and two reactions were performed at 90 °C using compound **3.9** (12.4 mg, 0.024 mmol) dissolved in cyclohexane (1.6 mL). The reactions were heated for 1 h (***a*** and ***d***); 2 h (***b*** and ***e***); 3 h (***c***). Silica plug filtration using petroleum ether as eluent afforded *bis*-adduct product **S3.14;** yields are reported in the following table. Spectroscopic data are consistent with those reported above for compound **S3.14**.

Table S3.1 Thermal insertion reactions at low temperatures

	temperature (°C)	time (h)	*bis*-adduct (%)
a	80	1	46
b	80	2	73
c	80	3	75
d	90	1	52
e	90	2	82

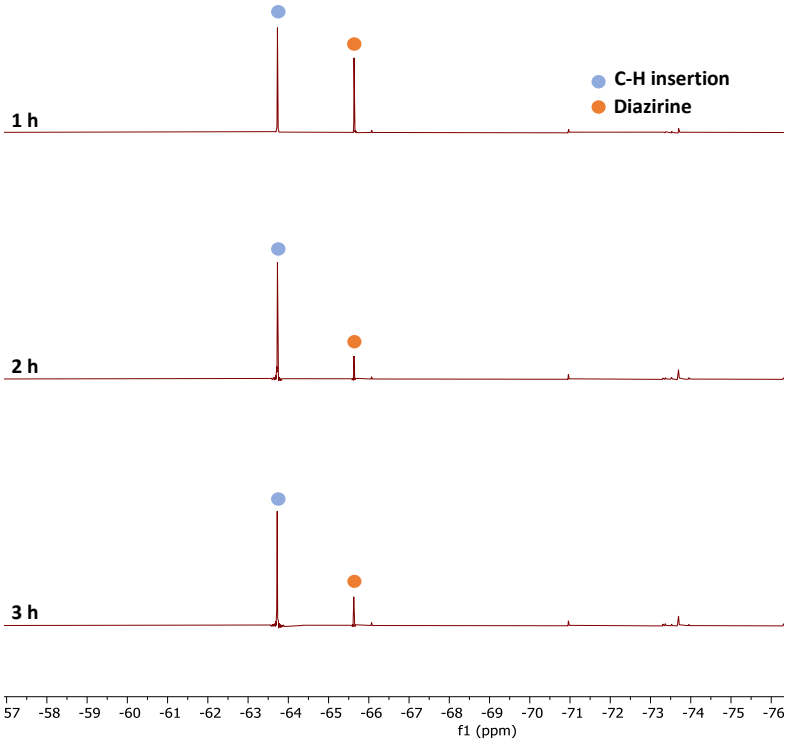

Figure S3.6 Crude ^{19}F NMR spectra of compound **3.9** under thermal C–H insertion condition at 80 °C.

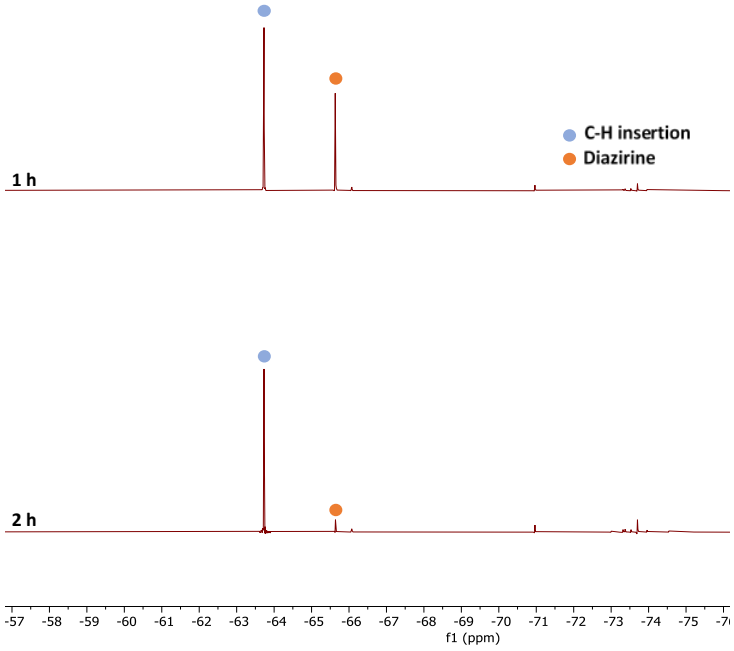

Figure S3.7 Crude ^{19}F NMR spectra of compound **3.9** under thermal C─H insertion condition at 90 °C.

Cyclohexane crosslinking of *bis*-diazirines **3.9** and **3.1** at 365 and 395 nm.

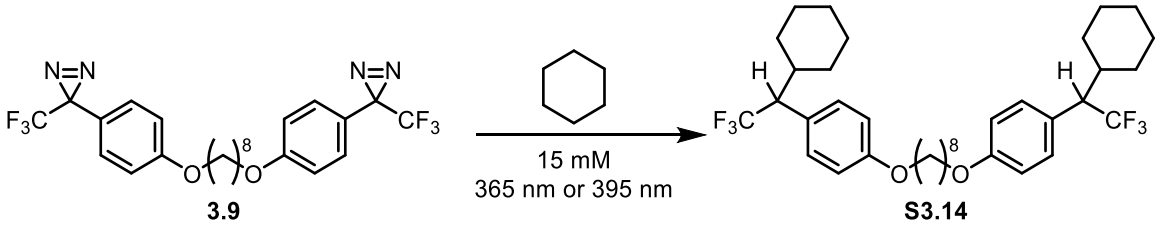

3.9 **S3.14**

Following the above general protocol (**B**), three reactions (***a***, ***b***, ***c***) were performed under 365 nm light using compound **3.9** (12.6 mg, 0.024 mmol) dissolved in cyclohexane (1.6 mL). The reactions were irradiated for 1 min (***a***); 5 min (***b***); 10 min (***c***).

Following the above general protocol (**C**), three reactions (***d***, ***e***, ***f***) were performed under 395 nm light using compound **3.9** (12.4 mg, 0.024 mmol) dissolved in cyclohexane (1.6 mL). The reactions were irradiated for 1 min (***d***); 5 min (***e***); 10 min (***f***); 60 min (***g***).

Following the above general protocol (**C**), two reactions (***h***, ***i***) were performed under 395 nm light using compound **3.1** (12.5 mg, 0.024 mmol) dissolved in cyclohexane (1.6 mL). The reactions were irradiated for 1 min (***h***); 10 min (***i***). *Bis*-adduct product was not observed.

Conversions of *bis*-adduct product **S3.14** are reported in the following table. Product **S3.14** in reaction (***g***) was isolated after filtration through a silica plug, using petroleum ether as eluent. Spectroscopic data are consistent with the ones reported above for compound **S3.14**.

Table S3.2 Photochemical insertion reactions

	compound	λ (nm)	time (min)	*bis*-adduct (%)
a	**3.9**	365	1	40
b	**3.9**	365	5	75
c	**3.9**	365	10	76
d	**3.9**	395	1	67
e	**3.9**	395	5	75
f	**3.9**	395	10	81
g	**3.9**	395	60	93 (92)*
h	**3.1**	395	1	-
i	**3.1**	395	10	-

* Numbers in parentheses indicate isolated yield.

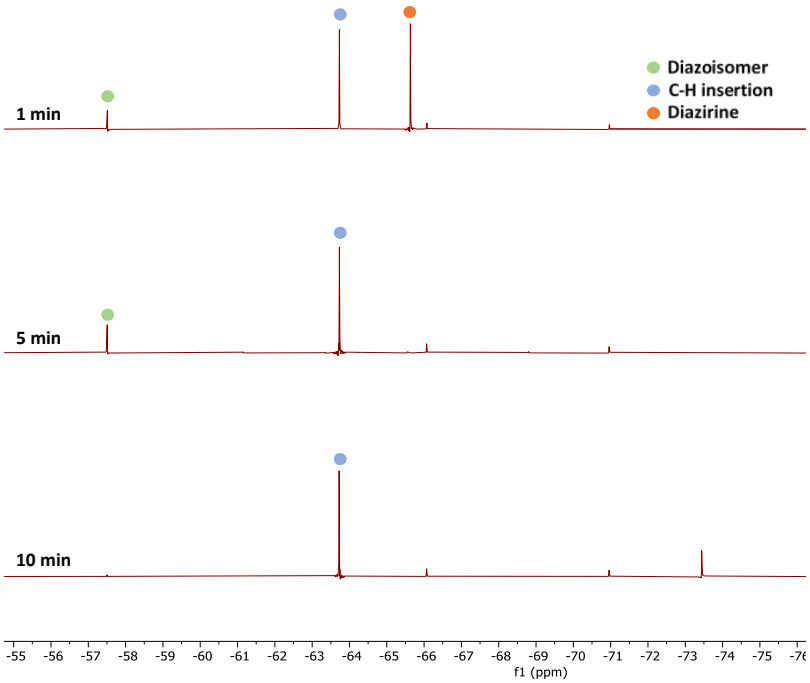

Figure S3.8 Crude ^{19}F NMR spectra of compound **3.9** under photochemical C–H insertion condition, 365 nm.

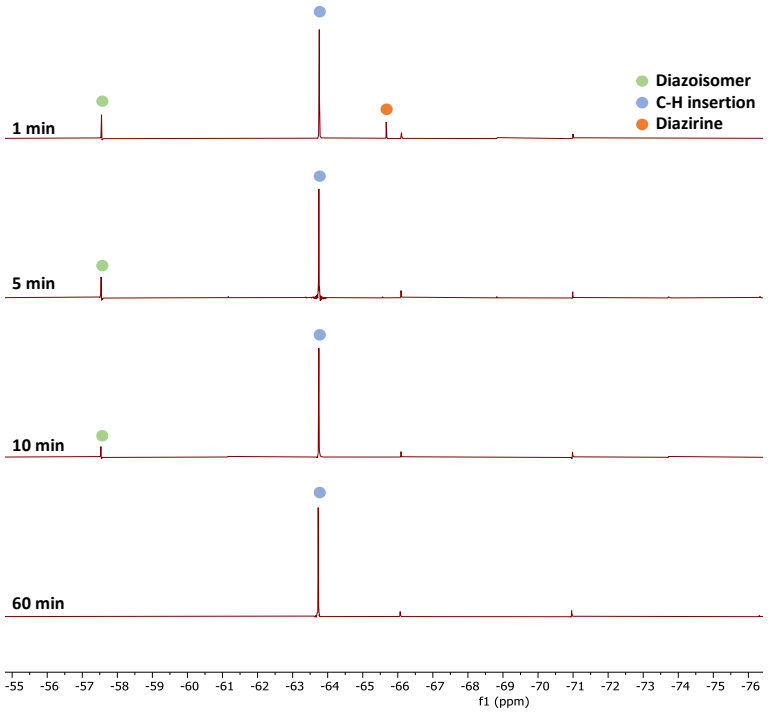

Figure S3.9 Crude ^{19}F NMR spectra of compound **3.9** under photochemical C─H insertion condition, 395 nm.

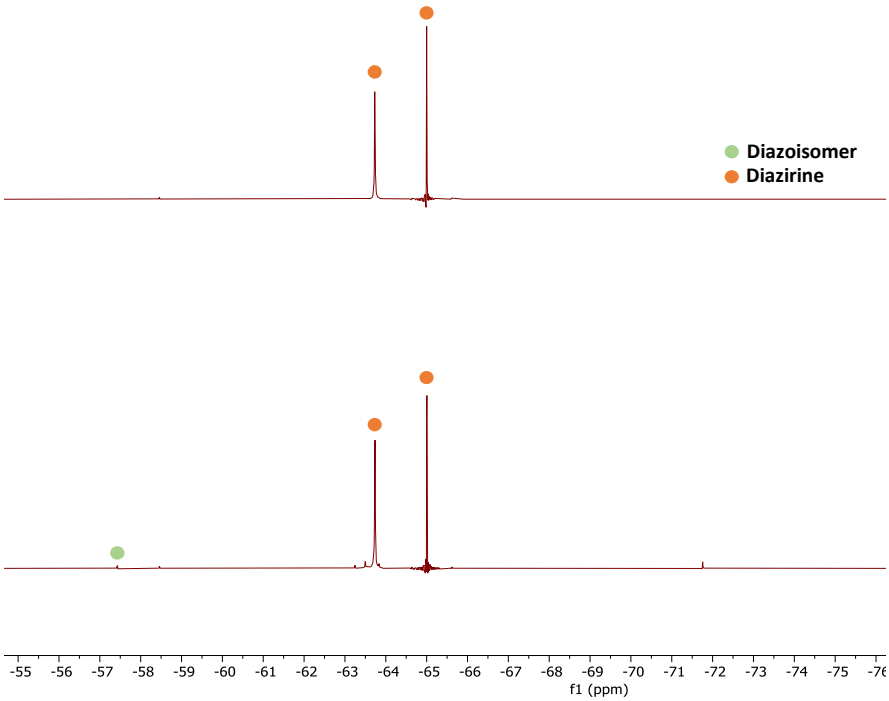

Figure S3.10 Crude ^{19}F NMR spectra of compound **3.1** under photochemical C–H insertion condition, 395 nm.

3.5.2 Assessment of thermal parameters for representative aryl ether crosslinkers

General Protocol for DSC analysis

A sample of the substance to be analyzed (typically 3–5 mg) was placed in a Tzero aluminum hermetic pan and sealed by a matching lid. The pan was pierced with a small pinhole to allow evolution of nitrogen gas. The pan was placed in the oven of a DSC25 device (TA instruments) and heated from 40 °C to 200 °C at a rate of 5 °C/min, with an identical empty pan as a reference. The oven was constantly flushed by a 50 mL/min flow of nitrogen. The device recorded the difference in heat flow between the reference and the studied sample, allowing the assignment of T_{onset} and T_{max}. DSC analysis for each substrate was conducted 8 times for compound **3.9** and 7 times for compound **3.3**. Representative DSC traces for crosslinkers **3.9** and **3.3** are provided below.

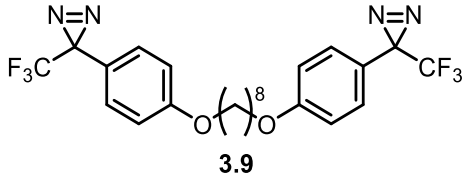

3.9

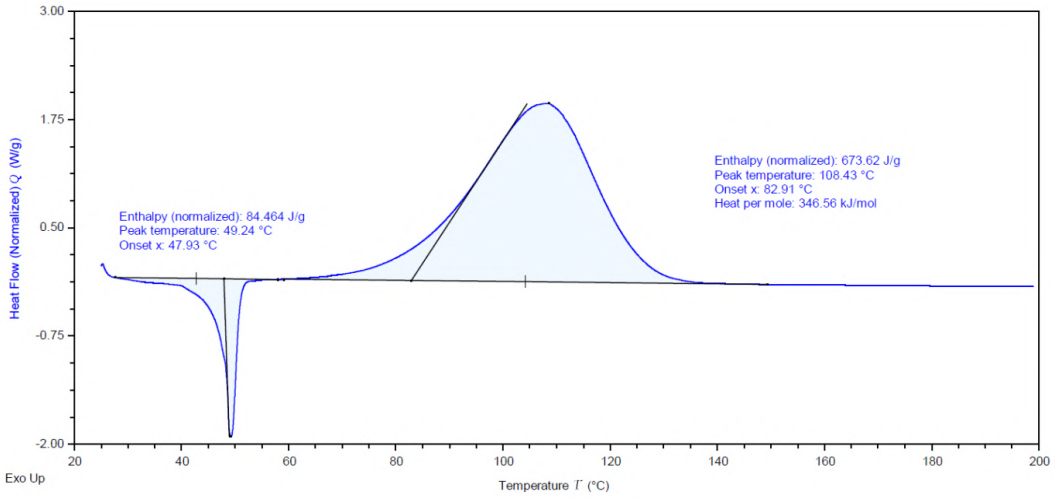

Figure S3.11 Representative DSC trace for crosslinker **3.9**.

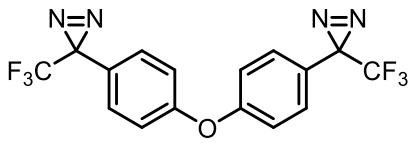

3.3

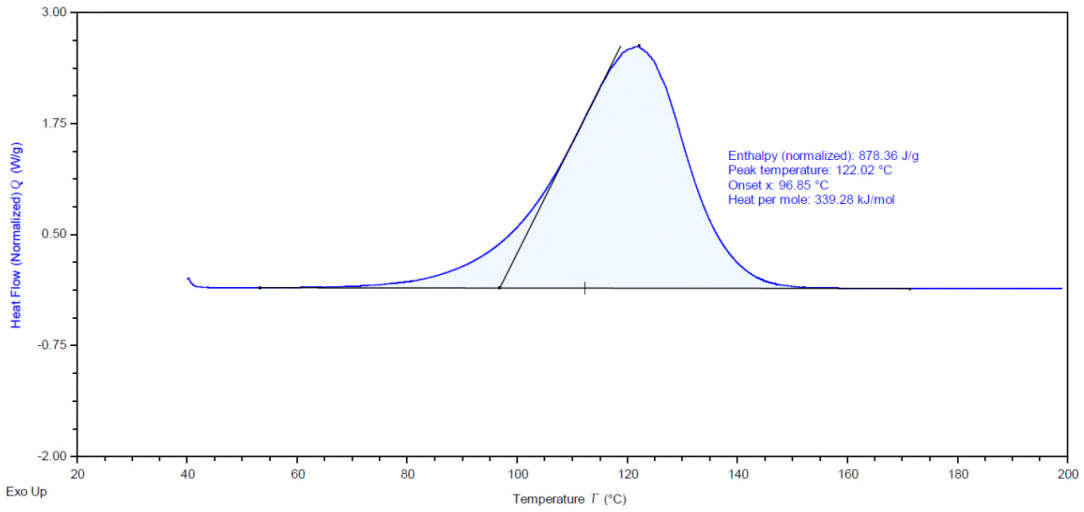

Figure S3.12 Representative DSC trace for crosslinker **3.3**.

Table S3.3 Collected thermal data for representative *bis*-diazirine crosslinkers[a]

	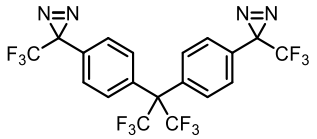 **3.1**	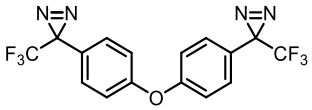 **3.3**	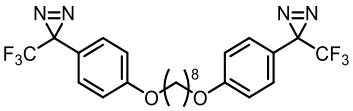 **3.9**
MP[b]	34 °C	n.d.	48.9 ± 0.2 °C
T_{onset}[c]	112.8 ± 0.2 °C	96.8 ± 0.2 °C	81.2 ± 1.3 °C
T_{peak}[d]	138.5 ± 0.2 °C	121.9 ± 0.1 °C	105.8 ± 1.5 °C
ΔH (by mass)[e]	683 ± 9 J/g	920 ± 35 J/g	680 ± 25 J/g
ΔH (by mole)[e]	355 ± 5 kJ/mol	355 ± 13 kJ/mol	350 ± 13 kJ/mol
SS[f]	–0.17 ± 0.01	+0.03 ± 0.02	–0.03 ± 0.02
EP[g]	–0.20 ± 0.01	–0.03 ± 0.02	–0.12 ± 0.02

[a] Error bars indicate standard error across multiple DSC runs. n=15 for compound **3.1**; n=7 for compound **3.3**; n=8 for compound **3.9**.

[b] The melting point (MP) for compound **3.1** was taken from reference 35. No melting point was determined for compound **3.3**, which was an oil at room temperature and did not freeze upon long term storage at –18 °C. The melting point for compound **3.9** was taken as the peak of the endothermic melting transition visible in the DSC trace.

[c] The onset temperature (T_{onset}) was determined by extrapolation of the tangent of the upward slope in the DSC experiment, to the fitted baseline of the plot.

[d] The peak temperature (T_{peak}) was determined as the temperature at which the maximum heat flow was observed in the DSC experiment.

[e] ΔH refers to the total integrated peak area (per unit mass or per mole), for the exotherm associated with diazirine activation.

[f] The shock sensitivity metric (SS) was determined according to the method of Yoshida and co-workers.[118] SS = log (Q_{DSC}) – 0.72 x log (T_{onset} – 25) – 0.98; where Q_{DSC} is the enthalpy of nitrogen release (in cal/g), and T_{onset} is measured as described above. A value of >0 indicates a risk of shock sensitivity for the compound.

[g] The explosive propagation metric (EP) was likewise determined according to Yoshida's methods. EP = log (Q_{DSC}) – 0.38 x log (T_{onset} – 25) – 1.67; where Q_{DSC} is the enthalpy of nitrogen release (in cal/g), and T_{onset} is measured as described above. A value of >0 indicates a risk of explosive propagation for the compound.

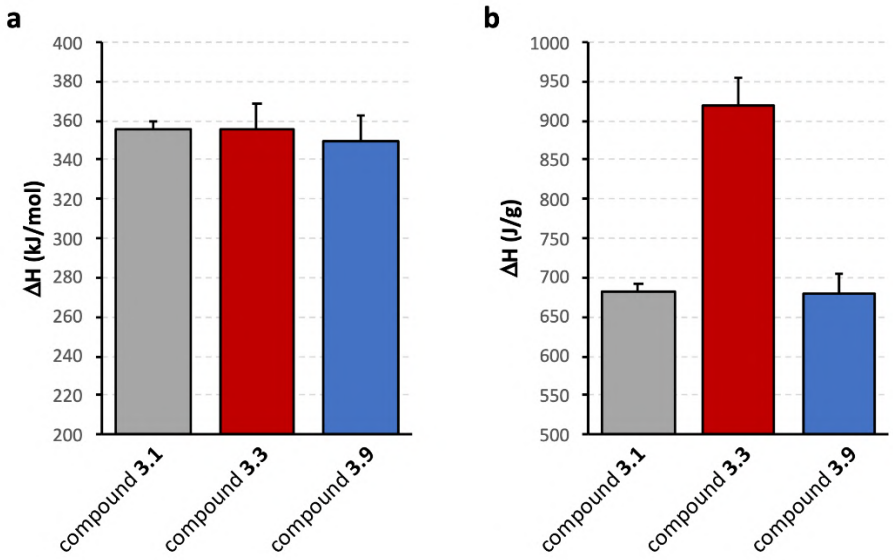

Figure S3.13 Enthalpy output associated with thermal diazirine activation for three representative *bis*-diazirines. **a.** Enthalpy per molar unit. **b.** Enthalpy per gram. The data indicate that each trifluoromethyl aryl diazirine unit produces that same amount of energy upon activation (within experimental error), regardless of the electron density associated with the aromatic ring. However, the molecular weight of the tether plays a significant role in the total energy output per unit mass. Thus, compounds **3.1** and **3.9**, which have similar molecular weights (520 and 514 g/mol, respectively), produce equivalent energy per gram, while compound **3.3**, which has a lower molecular weight (388 g/mol), produces a proportionately higher energy per gram of material. It is this larger energy output per unit mass that contributes to the potential explosion hazard associated with **3.3**.

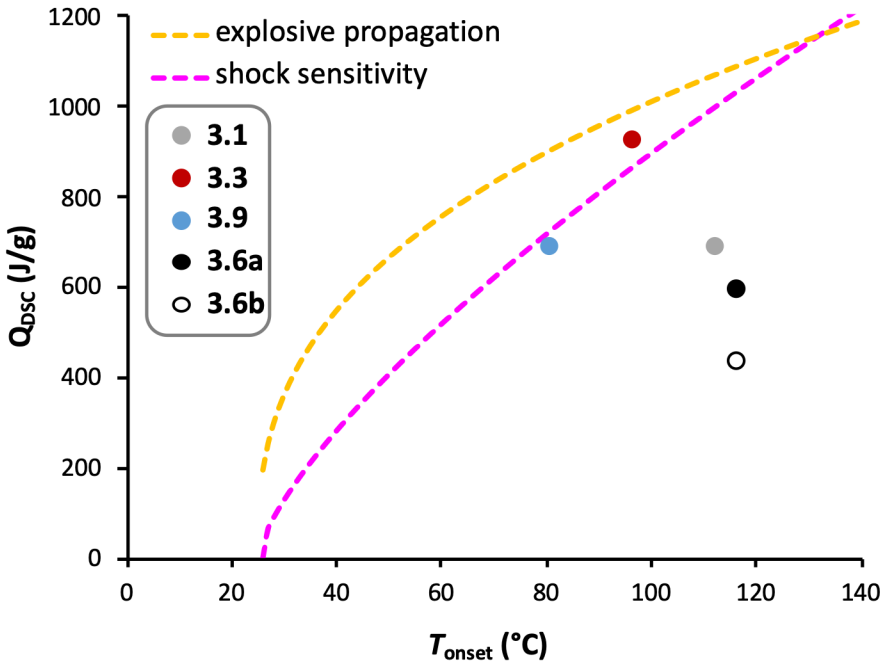

Figure S3.14 Yoshida correlation data for compounds **3.1**, **3.3**, **3.9**, **3.6a** and **3.6b**. Compounds for which Q_{DSC} vs. T_{onset} falls above either of the two curves are predicted to have an inherent risk of shock sensitivity or explosive propagation. For the compounds analyzed herein, only compound **3.3** falls into this danger zone.

3.5.3 Crosslinking of monodisperse poly(ethylene glycol) (PEG-1000 Da)

A series of samples was prepared by mixing monodisperse poly(ethylene glycol) (PEG-1000 Da) (20 mg) with various amounts of **3.1**, **3.9**, or **3.3** in glass vials (Table S3.4). Four different stock solutions with PEG-1000, **3.1**, **3.9**, or **3.3** in DCM were prepared. All vials were mixed for 15 seconds on a vortex mixer, sonicated (280 W for 30 seconds), and left to dry in the fume hood overnight. The contents of the vials were further dried by placing them under high vacuum (*ca.* 10^{-2} mbar) after mixing them for 15 seconds on a vortex mixer. The removal of solvents was monitored by measuring the weights of each vial over the whole process. The samples were placed in a heat block and heated at 110 °C for 16 hours. This induced crosslinking via thermal activation. Once cooled, each sample was homogenized (vortex mixer) and 1 mg was dissolved in 1 mL THF. The solutions were then filtered through a 0.2 µm PTFE filter directly into vials for SEC analysis. A vehicle control was prepared in the same way without the addition of any crosslinker and an untreated sample was prepared by dissolving 1 mg of PEG-1000 into 1 mL of THF and filtering the resulting solution through a 0.2 µm PTFE filter. All filtered samples were clear solutions.

Size Exclusion Chromatography (SEC)

SEC was carried out using a Malvern Viscotek TDAmax system equipped with two analytical SEC columns made from styrene-divinyl benzene (T5000 and T3000 Org SEC Col). Measurements were carried out at 1.0 mL/min with HPLC-grade tetrahydrofuran (Fisher) containing tetrabutylammonium bromide (0.1% w/w) as the eluent at 35 °C. Results were calibrated against polystyrene standards. All samples were dissolved in the eluent (1 mg/mL) and filtered with a polytetrafluoroethylene membrane of 0.2 µm pore size before analysis.

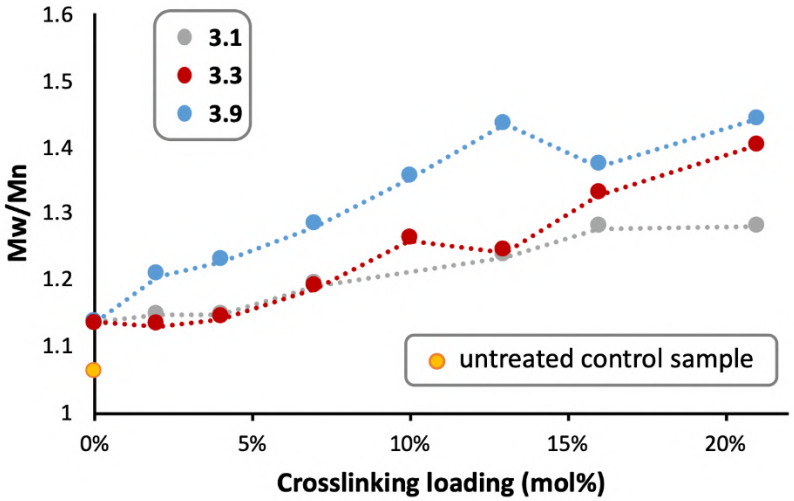

Figure S3.15 SEC data showing increasing polydispersity (Mw/Mn) as a result of crosslinking.

Table S3.4 Composition of samples prepared for crosslinking PEG-1000

vial	crosslinker	MW (g/mol)	loading (µmol/g)	PEG (mg)	crosslinker (µmol)	crosslinker (mg)	loading (wt%)	loading (mol%)
A1	**3.1**	520.28	20	20	0.4	0.21	1.0%	2.1%
A2	**3.1**	520.28	40	20	0.8	0.42	2.1%	4.1%
A3	**3.1**	520.28	70	20	1.4	0.73	3.6%	7.2%
A4	**3.1**	520.28	100	20	2	1.04	5.2%	10.3%
A5	**3.1**	520.28	130	20	2.6	1.35	6.8%	13.4%
A6	**3.1**	520.28	160	20	3.2	1.66	8.3%	16.5%
A7	**3.1**	520.28	200	20	4	2.08	10.4%	20.6%
B1	**3.9**	514.47	20	20	0.4	0.21	1.0%	2.1%
B2	**3.9**	514.47	40	20	0.8	0.41	2.1%	4.1%
B3	**3.9**	514.47	70	20	1.4	0.72	3.6%	7.2%
B4	**3.9**	514.47	100	20	2	1.03	5.1%	10.3%
B5	**3.9**	514.47	130	20	2.6	1.34	6.7%	13.4%
B6	**3.9**	514.47	160	20	3.2	1.65	8.2%	16.5%
B7	**3.9**	514.47	200	20	4	2.06	10.3%	20.6%
C1	**3.3**	386.26	20	20	0.4	0.15	0.8%	2.1%
C2	**3.3**	386.26	40	20	0.8	0.31	1.5%	4.1%
C3	**3.3**	386.26	70	20	1.4	0.54	2.7%	7.2%
C4	**3.3**	386.26	100	20	2	0.77	3.9%	10.3%
C5	**3.3**	386.26	130	20	2.6	1.00	5.0%	13.4%
C6	**3.3**	386.26	160	20	3.2	1.24	6.2%	16.5%
C7	**3.3**	386.26	200	20	4	1.55	7.7%	20.6%
D1	vehicle ctrl	N/A	0	20	0	0	0%	
D2	untreated							

3.5.4 Adhesion testing

Preparation of HDPE–HDPE samples

Pairs of 4"x1"x¼" bars of HDPE (Quadrant Engineering Plastics) were treated with 1 or 5 mg of crosslinkers **3.1**, **3.9**, or **3.3**, or 1 mg of molecular control **3.10**. After cutting the HDPE sheet into bars of the appropriate size, the edges were scraped to smoothness using a utility knife and the bars were wiped with Kimwipes and a solution of 70% isopropanol to remove grease/dust/plastic particles. Stock solution of crosslinkers and molecular control in diethyl ether were prepared and 60 µL was deposited onto the 1"x 0.5" overlap zone using a micropipette. The solvent was allowed to evaporate at room temperature, and then each pair of bars was held together with binder clamps and placed into an oven pre-heated to 110 °C. After 4 h, the samples were removed from the oven, cooled to room temperature, and challenged on a lap-shear experiment. Negative (vehicle) controls were prepared in an identical manner, except that 60 µL of pure diethyl ether was added to the bars in place of the crosslinker solution described above. Vehicle control samples were incubated at the same temperature (110 °C) as the other samples, for an identical length of time.

Lap-shear test

The lap-shear test was implemented according to ASTM D5868. The two trailing ends of the adhered HDPE samples prepared as described above were clamped in a universal testing system (Instron, Series 5969) and pulled apart at a rate of 5 mm/min until breakage of the bond.

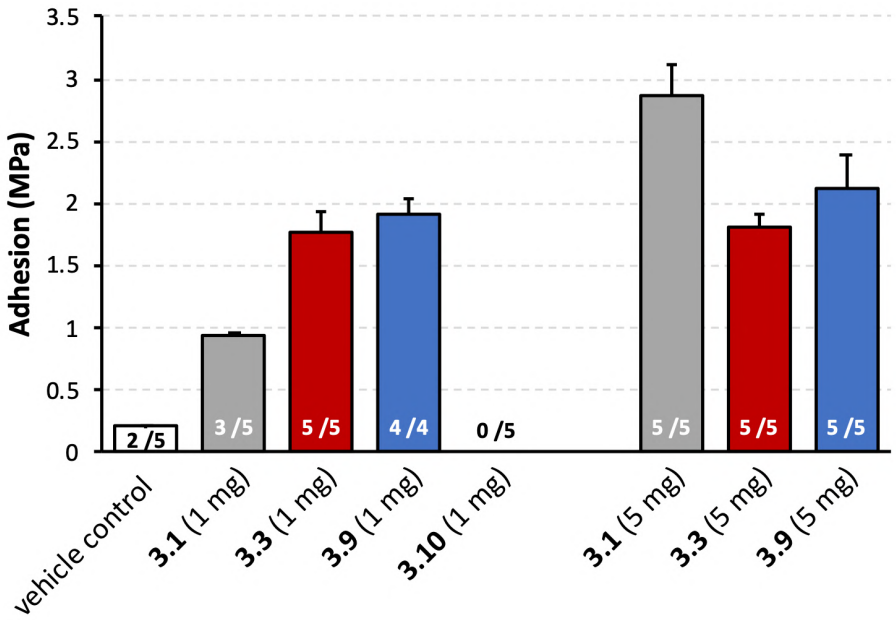

Figure S3.16 Adhesion strength of HDPE–crosslinker–HDPE lap-shear composites; numerical values indicate the number of samples that were sufficiently well adhered to be measured.

Table S3.5 Adhesion data for HDPE–crosslinker–HDPE lap-shear composites

sample	fraction bonded[a]	adhesion (MPa)
vehicle control	2 / 5	0.20 ± 0.01
3.1 (1 mg)	3 / 5	0.94 ± 0.03
3.9 (1 mg)	4 / 4	1.91 ± 0.25
3.3 (1 mg)	5 / 5	1.76 ± 0.37
3.10 (1 mg)	0 / 5	0.00 ± n/a
3.1 (5 mg)	5 / 5	2.86 ± 0.56
3.9 (5 mg)	5 / 5	2.13 ± 0.56
3.3 (5 mg)	5 / 5	1.80 ± 0.27

[a] The number of samples that were sufficiently well bonded to permit analysis.

3.5.5 Crosslinking of apparel fabric

3.5.5.1 Loading of crosslinker into UHMWPE fabric

Irreversible crosslinking of ultra-high molecular weight polyethylene (UHMWPE)

Commercial 75 g/m^2 UHMWPE fabric was impregnated with either **3.1** or **3.9**, by placing 1" x 1" pieces of fabric into close-fitting aluminum pans filled with solutions of the desired *bis*-diazirine in pentane. The concentration of the solution was calculated to correspond to 1.25 wt%, 6.25 wt%, or 12.5 wt% of crosslinker, relative to the mass of fabric being employed in the experiment. The bath was covered with aluminum foil and incubated at room temperature for 30 min. The cover was then removed to allow the pentane to evaporate in a fume hood for 20 min. After pentane evaporation, the impregnated sheets were wrapped in aluminum foil and placed into an oven at 110 °C for 4 h. Control samples were prepared following an identical procedure, but without adding crosslinker to the pentane bath.

Following thermal curing, the samples were weighed to determine the total mass of reacted crosslinker that was associated with each square of fabric. Each sample was then extracted for 5 min at room temperature using 20 mL of methanol, to remove any reaction products that were not irreversibly attached to the fabric. After drying the treated fabrics in an oven (5 min at 100 °C), each sample was weighed again to determine the mass of reaction products that were lost to the methanol extraction.

Table S3.6 Gravimetric analysis following methanol extraction of crosslinked UHMWPE fabric

crosslinker	nominal loading (wt%)	percent retention after loading and curing			percent retention after methanol extraction		
vehicle ctrl	0%	–0.27%	±	0.03%	–0.71%	±	0.08%
3.1	12.5%	8.75%	±	0.21%	0.14%	±	0.40%
3.1	6.25%	4.17%	±	0.07%	0.94%	±	0.25%
3.1	1.25%	0.93%	±	0.02%	0.13%	±	0.12%
3.9	12.5%	8.08%	±	0.49%	7.89%	±	0.53%
3.9	6.25%	4.35%	±	0.16%	3.79%	±	0.19%
3.9	1.25%	0.92%	±	0.07%	0.68%	±	0.16%

3.5.5.2 Loading of crosslinker into apparel fabric

Representative apparel fabric samples of low- and high-stretch modulus were crosslinked with *bis*-diazirines **3.1** or **3.9** at a nominal loading of 1 wt% or 5 wt%, following a similar protocol to that outlined above for UHMWPE fabric. Both types of fabrics were comprised of nylon and Lycra, but were selected on the basis of their different stretch moduli.

For each crosslinking experiment, fabric samples were cut to 5" x 6" rectangles, which were matched exactly to fit inside of a 5" x 6" aluminum tray. Each portion of fabric was weighed, and the appropriate amount of crosslinker was calculated. In order to account for losses to the pan, a mass of 1.25 wt% crosslinker was used in order to achieve a nominal loading of 1 wt% in the treated fabric. Likewise 6.25 wt% of crosslinker was used to achieve a nominal loading of 5 wt% in the treated fabric. The crosslinker of interest was dissolved in 75 mL of pentane. For vehicle control samples, 75 mL of pentane containing no crosslinker was used.

The crosslinker solution (in 75 mL of pentane, or else pure pentane for vehicle control samples) was then poured over the fabric sample in the close-fitting aluminum pan. The pan was covered with aluminum foil for 30 minutes to allow the crosslinker to penetrate into the fabric. The covering was then removed in a fume hood and the pentane solvent was allowed to evaporate. Following evaporation, the impregnated fabric sample was removed from the pan and weighed to confirm crosslinker adsorption (at *ca.* 1 wt% or 5 wt%) within the material.

Crosslinking of apparel fabrics under thermal and photochemical conditions

Thermal activation was achieved by incubating the treated samples in a 110 °C oven for 4 hours. Photochemical activation was achieved by suspending the treated samples in a Rayonet photochemical reactor (RMR-600) equipped with eight 350 nm bulbs. The light output measured at the sample location was 1640 lux (16 W/m^2). Photochemical activation was allowed to proceed for 4 hours. Following the 4-hour curing time, the fabric samples were again weighed to confirm that no significant material losses had occurred during the activation step.

Testing of crosslinked apparel fabric samples

The treated fabric samples were cut using scissors into 150 mm x 25 mm strips, and then the mechanical performance was evaluated using a James Heal Titan fabric testing machine. Each strip of fabric was pulled to 150% of its static extension, and then allowed to relax. The extension/relaxation process was repeated for 10 cycles to assess the performance of crosslinked vs. noncrosslinked material over repeated stretches.

For apparel fabric with a low starting stretch modulus (*ca.* 0.5 N peak force), addition of 1 wt% of *bis*-diazirine **3.1** (followed by thermal activation) was capable of doubling the stretch modulus (*ca.* 1 N peak force) while addition of 5 wt% **3.1** resulted in another doubling of modulus (*ca.* 2 N peak force). For apparel fabric with a higher starting stretch modulus, however (*ca.* 4 N peak force), 1wt% of **3.1** was ineffective at improving stretch modulus relative to vehicle control samples (Figure S3.17b and c). For this stronger starting fabric, 5wt% of **3.1** was required in order to achieve a significant increase in modulus (Figure S3.17c).

By contrast, 1 wt% of crosslinker **3.9** (following thermal activation) was found to affect roughly the same increase to stretch modulus as 5wt% of crosslinker **3.1** (compare Figure S3.17b to c). These data confirm the superior crosslinking performance of **3.9** relative to **3.1**. Data from photochemically crosslinked samples (also using fabric of high starting modulus) likewise showed a greater increase in stretch modulus for fabric samples treated with **3.9** than for fabric samples treated with **3.1** (Figure S3.17a). However, the maximum stretch modulus was lower for photochemically activates samples than for thermally activated samples, perhaps indicating incomplete activation under the selected UV irradiation conditions.

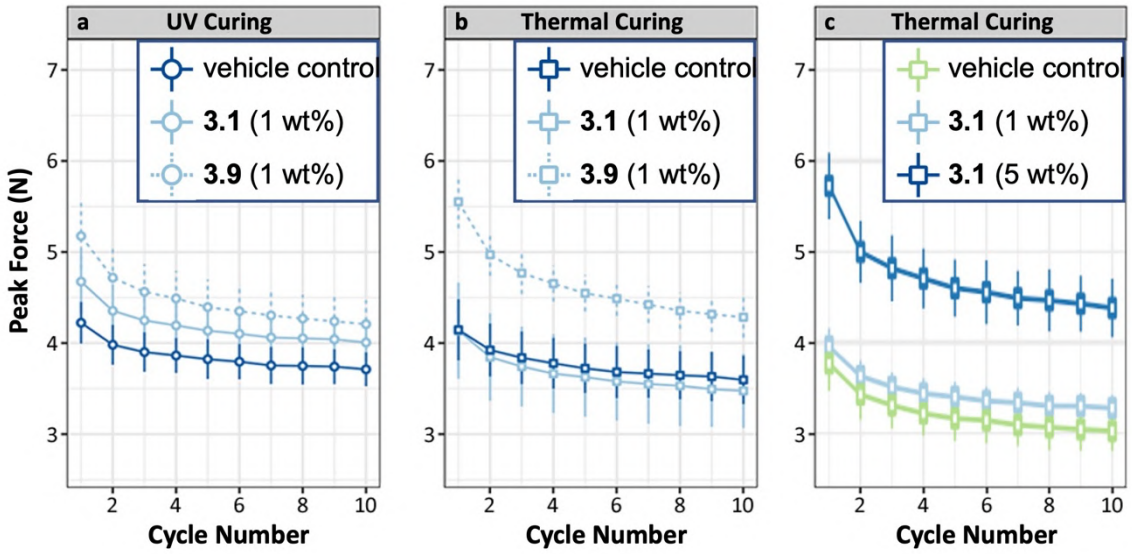

Figure S3.17 Increasing stretch modulus through crosslinking of apparel fabric with crosslinkers **3.1** and **3.9**.

3.5.6 Mechanical testing of crosslinked UHMWPE fabric

3.5.6.1 General fabric preparation procedure

A (thermo-activation): Commercial 75 g/m^2 UHMWPE fabric was impregnated with each test compound, by placing a piece of fabric of desired dimensions into close-fitting aluminum filled with a solution of the desired *bis*-diazirine or molecular control in pentane/diethyl ether at the appropriate concentration. The concentration was calculated to correspond to 1 wt% (plus an extra 0.25 wt% to compensate for crosslinker deposited on the sides and bottom of the aluminum pan), relative to the mass of fabric being employed in the experiment. The bath was covered with aluminum foil and incubated at room temperature for 30 min. The cover was then removed to allow the solvent to evaporate in a fume hood for 20 min. After solvent evaporation, the impregnated sheets were wrapped in aluminum foil and placed into an oven at 110 °C for 4 h. Vehicle control samples were prepared following the same procedure, but without adding crosslinker in the solvent bath. Molecular control samples were prepared following the same procedure but with the crosslinker replaced by the corresponding molecular control **3.10** bearing only one diazirine moiety.

B (photo-activation): Commercial 75 g/m^2 UHMWPE fabric was impregnated with each test compound, by placing a piece of fabric of desired dimensions into close-fitting aluminum filled with a solution of the desired *bis*-diazirine or molecular control in pentane/diethyl ether at the appropriate concentration. The concentration was calculated to correspond to 1 wt% and 0.2 wt% (plus an extra 0.25 wt% to compensate for crosslinker deposited on the sides and bottom of the aluminum pan), relative to the mass of fabric being employed in the experiment. The bath was covered with aluminum foil and incubated at room temperature for 30 min. The cover was then removed to allow the solvent to evaporate in a fume hood for 20 min. After solvent evaporation, the impregnated sheets were placed into a home-built photoreactor, constructed from a 15 cm diameter pyrex crystallizing dish (7.5 cm in height), wrapped laterally with 2.5 m of 395 nm LED Strip Lights, (Waveform Lighting) and irradiated for 5 min. Vehicle control samples were prepared following the same procedure, but without adding crosslinker in the solvent bath.

Tensile testing of crosslinked fabric using **procedure A (thermo-activation)**

Tensile tests were conducted on samples 75 mm × 250 mm in size, using an Instron 5969 dual column load frame. Each sample was inserted into the grips in such a way that 50 mm from each end of the fabric was clamped within each grip. Consequently, the area between the grips (i.e., the area upon which the tensile experiment was performed) had dimensions of 150 mm x 75 mm. To ensure consistent results, three samples were analyzed for each treatment condition. The loading rate was 5 mm/min. The force-displacement curves (Figure 3.3) indicated that the maximum load was considerably increased in UHMWPE that had been crosslinked with *bis*-diazirines **3.9** and **3.3**, compared to both untreated and vehicle control samples.

Table S3.7 Composition of samples prepared for tensile test

sample	loading (wt%)	wt. of fabric (g)	wt. of crosslinker (mg)	wt. of fabric after curing (g)	wt. gain /loss (mg)	wt% gain/loss	wt. after extraction with pentane (g)	wt. gain/loss (mg)	wt% gain/loss
vehicle control	0	3.4436	---	3.4442	0.0	0.0%	3.4478	0.0	0.1%
		3.4182	---	3.4197	0.0	0.0%	3.4187	0.0	0.0%
		3.4806	---	3.4791	0.0	0.0%	3.4771	0.0	-0.1%
3.1	1.25	3.4034	42.5	3.4425	39.1	1.1%	3.4397	36.3	1.1%
		3.4303	42.8	3.4509	20.6	0.6%	3.4492	18.9	0.6%
		3.4214	42.7	3.4508	29.4	0.9%	3.4503	28.9	0.8%
3.9	1.25	3.4607	43.2	3.4948	34.1	1.0%	3.4948	34.1	1.0%
		3.4224	43.7	3.4695	47.1	1.4%	3.4628	40.4	1.2%
		3.4177	42.7	3.4476	29.9	0.9%	3.4485	30.8	0.9%
3.3	1.25	3.3969	42.5	3.4392	42.3	1.2%	3.427	30.1	0.9%
		3.4284	42.8	3.4711	42.7	1.2%	3.4592	30.8	0.9%
		3.4037	42.5	3.455	51.3	1.5%	3.4405	36.8	1.1%

3.5.6.2 Tear test of crosslinked fabric using procedure A (thermo-activation)

Tear resistance of fabric was characterized according to ASTM D2261. In a sample of 100 mm × 100 mm, a centered edge cut of 50 mm in length was introduced using a hot wire cutter. The two "legs" of the sample were then clamped symmetrically, over a length of 25 mm on each, in a universal testing system (Instron, Series 5969), and pulled apart at a rate of 30 mm/min, while the force-extension curve was recorded. Five samples of each group were tested. The force–displacement results are shown in Figure S3.18.

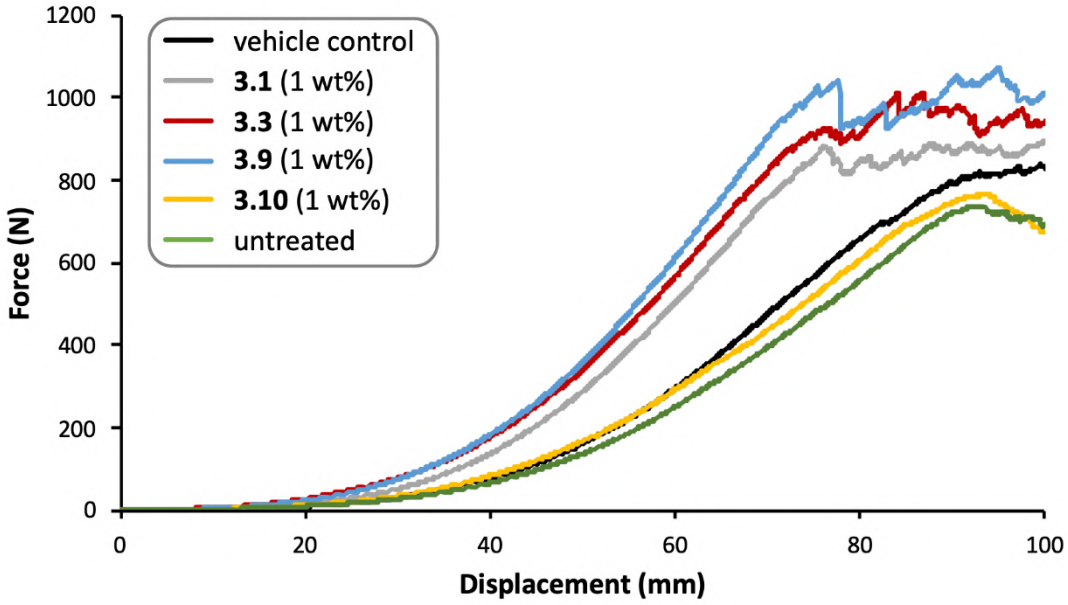

Figure S3.18 Force-displacement curves obtained during tear testing of variously treated UHMWPE samples.

Table S3.8 Composition of samples prepared for tear test

sample	loading (wt%)	wt. of fabric (mg)	wt. of crosslinker (mg)	wt. of fabric after curing (mg)	wt. gain /loss(mg)	wt% gain/loss	wt. after extraction with pentane	wt. gain/loss (mg)	wt% gain/loss
vehicle	0	796.8	---	796.2	-0.6	-0.1%	795.2	-1.6	-0.2%
control		818.6	---	805.4	-13.2	-1.6%	804.7	-13.9	-1.7%
		816.7	---	798.8	-17.9	-2.2%	799.7	-17	-2.1%
		805.2	---	809.6	4.4	0.5%	802.1	-3.1	-0.4%
		809.5	---	808.2	-1.3	-0.2%	807.5	-2	-0.2%
3.1	1.25	844.3	10.6	844	-0.3	0.0%	838.9	-5.4	-0.6%
		820.4	10.4	850.1	29.7	3.6%	811.6	-8.8	-1.1%
		915	11.4	942.2	27.2	3.0%	807.8	-107.2	-11.7%
		830.6	10.4	839.4	8.8	1.1%	790.8	-39.8	-4.8%
		825.8	10.3	805.6	-20.2	-2.4%	802.3	-23.5	-2.8%
3.9	1.25	775.1	9.7	784.9	9.8	1.3%	783.8	8.7	1.1%
		793.8	9.9	801.8	8	1.0%	801.8	8	1.0%
		797.2	10	805.6	8.4	1.1%	805.1	7.9	1.0%
		787	9.8	795.4	8.4	1.1%	795	8	1.0%
		789.8	9.9	799.3	9.5	1.2%	798.7	8.9	1.1%
3.3	1.25	779.8	9.7	786.8	7	0.9%	787.7	7.9	1.0%
		790.1	9.8	798.4	8.3	1.1%	799.2	9.1	1.2%
		807.6	10.1	816.1	8.5	1.1%	815.3	7.7	1.0%
		793.5	9.9	805.3	11.8	1.5%	801.7	8.2	1.0%
		802.2	10	813.1	10.9	1.4%	812.6	10.4	1.3%
3.10	1.25	816.3	10.4	811.1	-5.2	-0.6%	816.8	0.5	0.1%
		822.7	10.3	811.1	-11.6	-1.4%	810.2	-12.5	-1.5%
		792	9.9	795.6	3.6	0.5%	798.4	6.4	0.8%
		735.6	9.2	769.6	34	4.6%	768.4	32.8	4.5%
		790.3	9.9	790.7	0.4	0.1%	789.9	-0.4	-0.1%

3.5.6.3 Integration of tear testing curves

To better compare the results from tear testing, the force−extension curves were integrated over the first 50 mm of extension. This value was chosen because at this extension, none of the fabric samples had exhibited failure. The resulting values of tear energy, expressed in Joules (J), were then averaged for each type of crosslinked fabric.

Table S3.9 Integration of tear testing curves up to 50 mm extension

treatment	average tear energy (J)		standard deviation	number of replicates
untreated	1.70	±	0.2	5
vehicle control	1.9	±	0.5	5
3.1 (1wt%)	3.4	±	0.7	5
3.9 (1wt%)	4.5	±	0.3	5
3.3 (1wt%)	4.2	±	0.6	5
3.10 (1wt%)	2.1	±	0.3	5

3.5.6.3 Tear test of crosslinked fabric using procedure B (photo-activation)

Tear resistance of fabric was characterized according to ASTM D2261. In a sample of 100 mm × 100 mm, a centered edge cut of 50 mm in length was introduced using a hot wire cutter. The two "legs" of the sample were then clamped symmetrically, over a length of 25 mm on each, in a universal testing system (Instron, Series 5969), and pulled apart at a rate of 30 mm/min, while the force-extension curve was recorded. Five samples of each group were tested. The force–displacement results are shown in Figure S3.19.

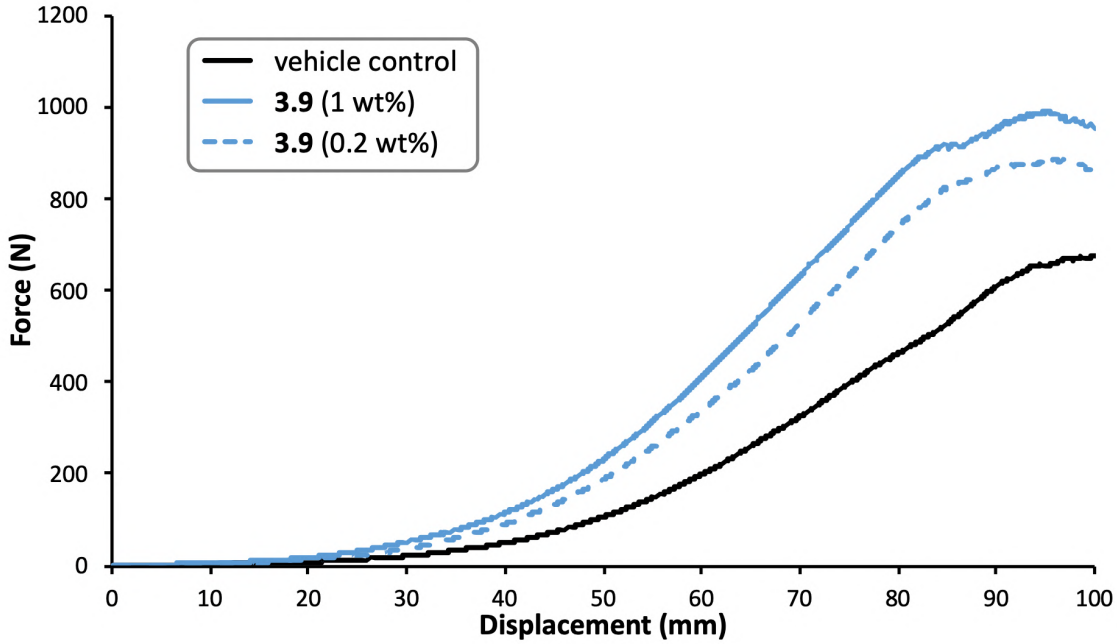

Figure S3.19 Force-displacement curves obtained during tear testing of variously treated UHMWPE samples.

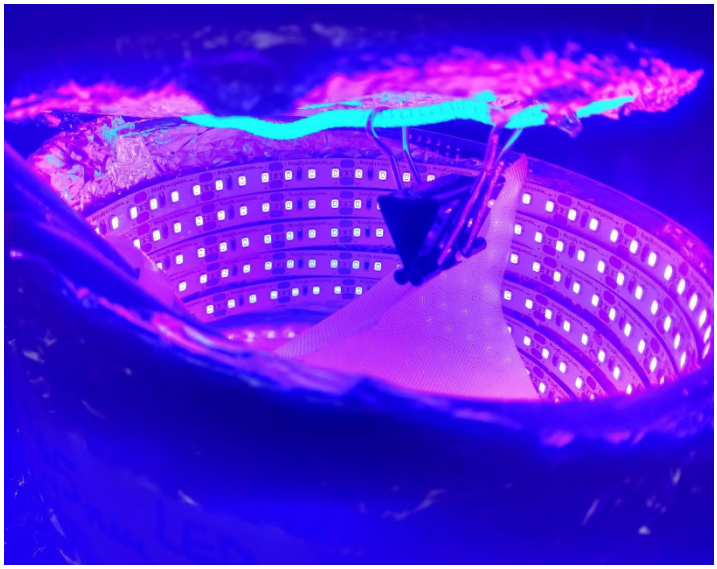

Figure S3.20 Photo-crosslinking of fabrics using a home-built photoreactor operating at 395 nm for 5 min (general procedure B).

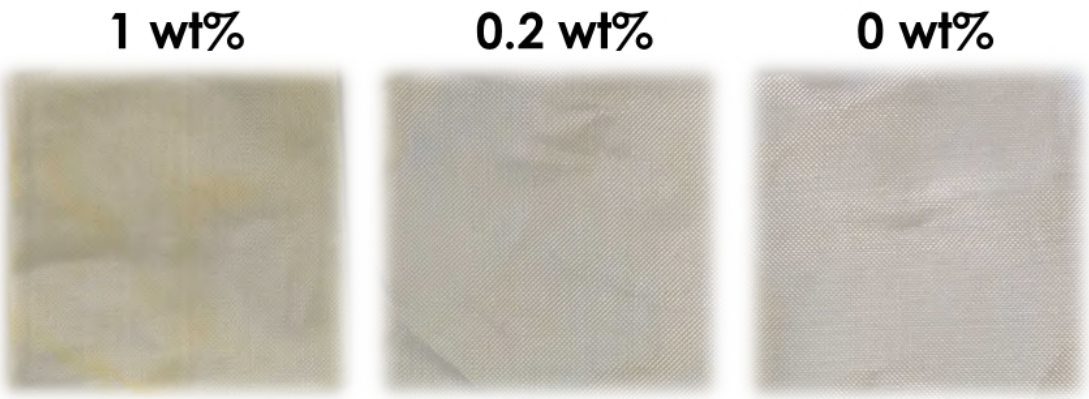

Figure S3.21 Photocured fabrics with 1, 0.2, and 0 wt% of crosslinker **3.9**.

Chapter 4: A Cleavable Crosslinking Strategy for Commodity Polymer Functionalization and Generation of Reprocessable Thermosets

This chapter has been adapted with permission from a previously accepted paper.

Liting Bi, Benjamin Godwin, Miranda J. Baran, Rashid Nazir and Jeremy E. Wulff, *Angew. Chem. Int. Ed.,* ***2023****, e202304708*.

Contributions:

Liting Bi contributed to the design and synthesis of the molecules, as well as to the crosslinking/decrosslinking experiments and the preparation of crosslinked macroscale samples and their dynamic mechanical thermal analysis. Benjamin Godwin performed the parallel plate and scanning electron microscope experiments. Miranda J. Baran contributed to the scale-up synthesis and data discussions. Rashid Nazir contributed to the initial molecule synthesis route design.

4.1. Abstract

Covalently crosslinked polymeric materials, known as thermosets, possess enhanced mechanical strength and thermal stability relative to the corresponding uncrosslinked thermoplastics. However, the presence of covalent inter-chain crosslinks that makes thermosets so attractive is precisely what makes them so difficult to reprocess and recycle. Here, we demonstrate the introduction of chemically cleavable groups into a *bis*-diazirine crosslinker. Application of this cleavable crosslinker reagent to commercial low-functionality polyolefins (or to a small-molecule model) results in the rapid, efficient introduction of molecular crosslinks that can be uncoupled by specific chemical inputs. These proof-of-concept findings provide one potential strategy for circularization of the thermoplastic/thermoset plastics economy, and may allow crosslinked polyolefins to be manufactured, used, reprocessed, and re-used without losing value. As an added benefit, the method allows the ready introduction of functionality into non-functionalized commodity polymers.

4.2. Introduction

The annual global production of thermoset polymers is over 65 million tons and comprises about 18% of polymeric materials manufactured today.[169] Addition of covalent crosslinks into polymer networks gives the resulting thermoset enhanced tensile strength, as well as thermal and chemical resistance.[170] However, this comes at the expense of reprocessability and recyclability. Transforming thermoplastics into thermosets limits the possibility of mechanical reprocessing (melt-and-remould) because the crosslinked structures preclude flow, even at elevated temperatures.[171] Consequently, most thermosets are incinerated or landfilled after their useful lifetimes.[1,172,173] Existing strategies to create reprocessable thermosets have focused on the incorporation of stimuli-triggered degradation or dynamic interactions such as the installation of silyl ether linkages within polydicylopentadiene,[174] carbamate exchange in polyurethane foams,[175] reversible enamine linkages in polydiketoenamines,[176] and boronic ester hydrolysis in vitrimers.[177] None of these methods, however, combine on-demand crosslinking with the ability to uncouple the key inter-chain bond, and most require that

bespoke polymer substrates be synthesized, rather than permitting the upgrading of existing, commodity polymer materials.

Traditional crosslinking methods include rubber vulcanization,[7] silicone hydrosilylation[178] and epoxy resin polyamine curing.[179] However, low-functionality polymers such as polyethylene and polypropylene (the most widely produced polymers in the world) lack intrinsically reactive functional groups for crosslinking. As a result, industrial polyethylene crosslinking involves either high-energy radiation (γ rays or electron beams) or peroxide-induced radical reactions. Both methods are poorly controlled, and are generally unsuitable for polypropylene (and even for certain forms of polyethylene) due to competing chain-scission events.[180,181]

Recently, trifluoromethyl aryl diazirines have shown promising efficacy in polymer crosslinking[24,36,59,61,100,163,167] and photopatterning applications.[67,68,71,72,182] Upon exposure to heat or light, the strained diazirine heterocycle loses a molecule of nitrogen gas (N_2) to generate a highly reactive carbene, which in turn can insert into neighboring C–H bonds.[40,58] Thus, the use of *bis*-, *tetrakis*-, or *poly*-diazirines provides a convenient and practical method to rationally install molecular crosslinks into commercial polyolefins without the risk of competing fragmentation reactions, and without any requirement for functional groups to be already present along the polymer chain.[36,161] Recent structure–function studies in Chapter 2 revealed that trifluoromethyl aryl diazirines bearing electron-rich aryl groups were much more efficient at undergoing C–H insertion than the corresponding electron-neutral or electron-poor systems.[50] This in turn led to the design of a prototypical, electronically optimized *bis*-diazirine crosslinker containing aryl ether linkages in Chapter 3, which showed improved performance in crosslinking both polymers and small-molecule models.[168]

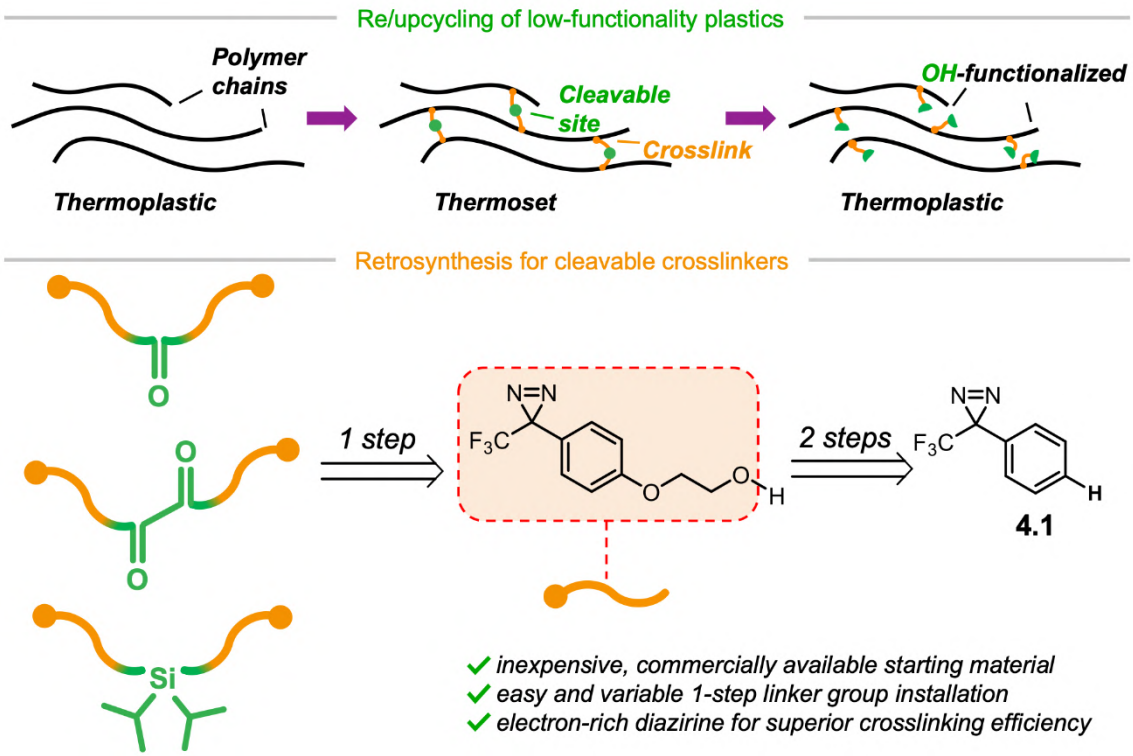

Figure 4.1 A broadly applicable, cleavable *bis*-diazirine crosslinker strategy for reprocessing thermosets. Adapted from literature.[183]

In this chapter, we describe the design, synthesis, and testing of a series of electronically optimized *bis*-diazirines that incorporate chemically cleavable functional groups (Figure 4.1). These include a carbonate, an oxalate, and a silyl ether, each of which can undergo bond cleavage/reformation under external stimuli (e.g., acid, base, fluoride etc.), thereby allowing low-functionality commodity polymers to be reversibly crosslinked through strong—yet selectively cleavable—covalent bonds. As with other *bis*-diazirines, the suite of reagents described herein can be topically applied to manufactured polymer materials without the need to melt or dissolve the polymer substrate. The addition of a cleavable group adds the potential for thermoset reprocessibility, together with facile polymer functionalization.

4.3. Results and Discussion

4.3.1 Design and synthesis of cleavable crosslinkers

Carbonate functional groups have been widely used in polymeric networks to establish reprocessable materials that can be degraded using specific chemical stimuli such as hydroxide or alkoxide anions.[184,185] Meanwhile, oxalate linkages, which benefit from higher rates of cleavage, have also been built into polymer materials.[186] These have been investigated for certain medical applications, such as drug delivery and medical sutures.[187] Silyl ether linkages have likewise been found to serve as robust and thermally stable sites in polymeric materials, which can be cleaved following the addition of acid or fluoride reagents. Such linkages can even be dynamic in nature, when amine groups are positioned nearby to facilitate fast exchange.[188–191]

We therefore set out to prepare a collection of cleavable crosslinkers with carbonate, oxalate, or silyl ether linkages installed between two electron-rich trifluoromethyl aryl diazirine warheads (**4.4**–**4.6**, Scheme 4.1b). Traditionally, *bis*-, *tetrakis*-, or *poly*-diazirine crosslinkers have either been made by functionalizing a suitable precursor with a commercially available diazirine-containing benzyl bromide,[24,62,100,163] benzyl alcohol,[67,167,71] or benzoic acid[66,162] (in which case the synthesis is straightforward, but the product does not contain electronically optimized diazirine groups) or else by first derivatizing a desirable aromatic core with trifluoromethyl ketone groups and then elaborating the resulting product through a tedious sequence of oxime formation (using hydroxylamine), activation (using either tosyl chloride or nosyl chloride), diaziridine formation (through addition of ammonia) and finally oxidation to afford the desired diazirine.[36,59,61,68,72,168,182] This latter approach allows one to exert more control over both the diazirine warhead and the linker group. However, it necessarily means that each new diazirine reagent requires a 6–8 step linear synthesis (Scheme S4.1). Seeking a faster and more efficient route to access the suite of cleavable crosslinkers proposed here, we recognized that the parent trifluoromethyl phenyl diazirine (**4.1**, Figure 4.1) was available from several different suppliers, and could be sourced for as low as US$2/gram on multi-kilogram scale. We were therefore attracted to the idea of functionalizing precursor **4.1** with a *para*-linked ethereal tether.

As discussed above, the use of an electron-rich aromatic group (which would be established through the addition of the *para*-oxygen) helps to stabilize the singlet carbene following diazirine activation,[90,112] which in turn affords up to 10-fold more efficient C–H insertion than is observed using electron-neutral or electron-poor trifluoromethyl aryl diazirines.[50] If the ether linkage were to terminate in a functional group handle, this could then be exploited for the ready introduction of the desired carbonate, oxalate, and silyl ether cleavage sites.

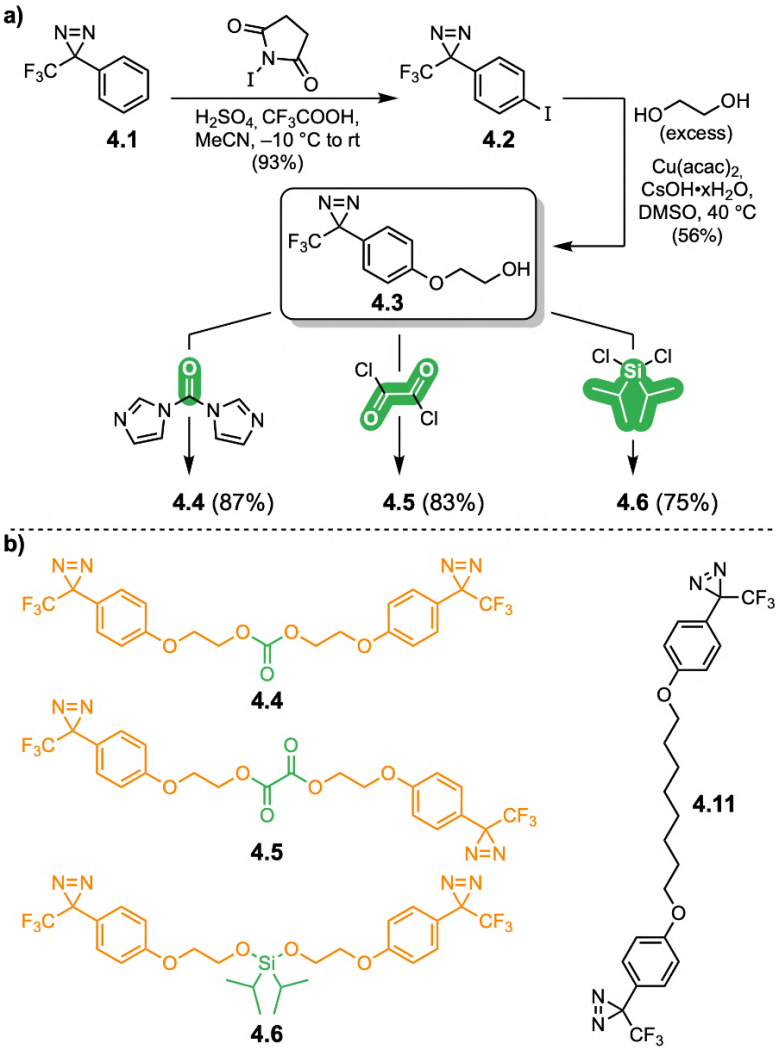

Scheme 4.1 Crosslinker design. a) Synthesis of cleavable crosslinkers from a common, readily accessible key intermediate. b) Structures of cleavable and non-cleavable *bis*-diazirine crosslinkers used in the present study. Adapted from literature.[183]

While more step-economical than previous syntheses of electron-rich *bis*-diazirines, this approach introduced an additional synthetic challenge: because

trifluoromethyl aryl diazirines containing *para*-alkoxy groups on the aromatic ring decompose above *ca.* 40 °C, we were unable to harness palladium couplings to install the key aryl–oxygen bond, without resorting to prohibitively expensive ligand sets. Fortunately, we found that a low-temperature copper coupling based upon methodology from the Chae and Sun groups[192,193] provided an efficient and cost-effective solution.

In the event, treatment of **4.1** with *N*-iodosuccinimide in a mixture of trifluoroacetic acid, acetonitrile, and sulfuric acid[194] afforded *para*-iodo functionalized aryl diazirine (**4.2**) on >100-gram scale in 93% yield (Scheme 4.1a). Subsequent reaction of **4.2** with excess ethylene glycol at 40 °C was facilitated by the use of recrystallized $Cu(acac)_2$, completing an efficient 2-step synthesis of key intermediate **4.3**, which had previously been prepared from 4-bromophenol over 7 steps, using the more traditional diazirine-construction sequence outlined above.[195] Cleavable crosslinkers **4.4**–**4.6** were then easily synthesized by subjecting glycol **4.3** to standard conditions for carbonate, oxalate, or silyl ether synthesis (refer to the section 4.5 for full details).

4.3.2 Evaluation of crosslinking-decrosslinking activity using a molecular model

To determine if our proposed method of introducing cleavable groups via *bis*-diazirine reagents would be useful for crosslinking and decrosslinking low-functionality materials, we first explored the use of a molecular model. Cyclohexane was chosen as a convenient surrogate for aliphatic polyolefins, since (like polyethylene) it contains only non-activated methylenes.

As reported previously, electronically optimized (but non-cleavable) *bis*-diazirine **4.11** (Scheme 4.1b) can crosslink this challenging substrate upon thermal or photochemical (395 nm) activation.[168] The isolated yield of the pure *bis*-cyclohexane adduct from **4.11** was 91% when the reaction was conducted at 140 °C, which is 10-fold better than a prototypical electron-poor diazirine-based crosslinker.[168] When reacted at 90 °C for two hours, **4.11** still efficiently provided 82% conversion. Repeating this experiment with **4.4**–**4.6** at 110 °C for one hour, we found that crosslinkers **4.4** and **4.6** performed similar to **4.11**, giving the carbonate-linked cyclohexane adduct **4.7** and silyl-linked **4.9** in 80% conversion (Scheme 4.2). Although crosslinker **4.5** has poor solubility in cyclohexane, it still proceeds with >70% conversion under the same reaction

conditions, to afford the desired oxalate adduct, **4.8**. Photo-activation at 395 nm provided similar percent conversions; refer to the section 4.5 for full details.

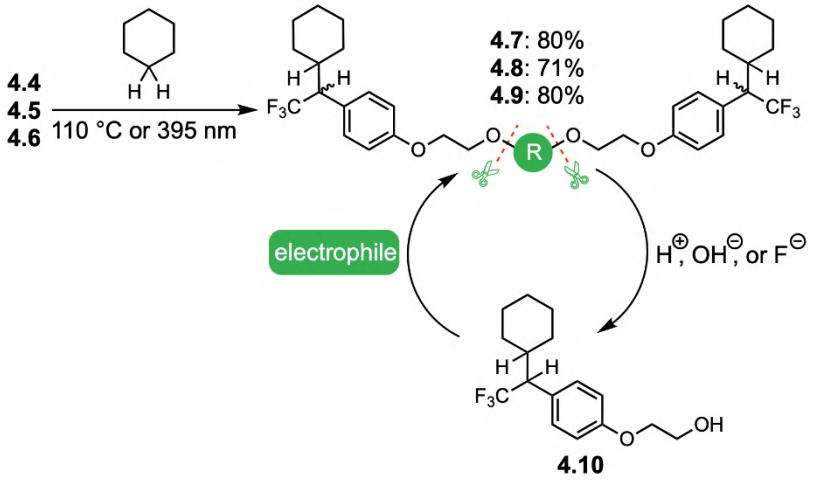

Scheme 4.2 Comparison of cyclohexane crosslinking efficacy and hydrolysis/regeneration of the resulting crosslink. Values for the cyclohexane insertion step indicate percent conversion to **4.7**–**4.9** (as diastereomeric mixtures) following thermal activation of the diazirine reagents. For isolated yields after column chromatography (which were slightly lower due to the sensitivity of the cleavable group), and for results following photochemical activation, refer to the section 4.5. Adapted from literature.[183]

To preliminarily assess the hydrolysis conditions and follow the reaction spectroscopically for each *bis*-adduct, compounds **4.7**–**4.9** were dissolved in CD_3OD, and aqueous NaOH was added directly to the NMR tube. After 4 hours, 90% of compound **4.7** hydrolyzed to afford free alcohol **4.10** (Figure 4.2). By contrast, compound **4.9** showed only 2% hydrolysis under same basic conditions. On the other hand, when the crosslinked cyclohexane adducts were exposed to aqueous HCl in CD_3OD, silyl ether **4.9** hydrolyzed within 3 hours, but carbonate **4.7** remained unreacted. In both basic and acid conditions, oxalate **4.8** hydrolyzed within 15 minutes; we hypothesize that the CD_3OD solvent was playing a role in the cleavage reaction (refer to the section 4.5 for full details). To demonstrate circularity in our molecular model, we directly added carbonyldiimidazole (CDI) into a suspension of compound **4.10** and K_2CO_3 in acetonitrile, to successfully reform the carbonate-linked *bis*-adduct **4.7** in quantitative

conversion. Adducts **4.7**–**4.10** were isolated and fully characterized following each experiment; refer to the section 4.5 for spectroscopic details.

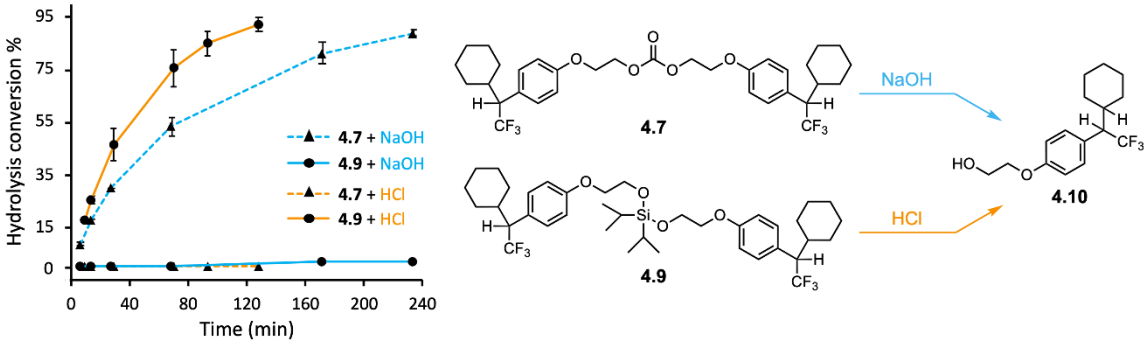

Figure 4.2 Hydrolysis of cyclohexane adducts **4.7** and **4.9** under basic (NaOH) and acidic (HCl) conditions. All experiments were performed directly in NMR tubes at room temperature, and use CD_3OD as solvent. Adapted from literature.[183]

4.3.3 Polymeric models for evaluation of crosslinking and decrosslinking activity

To evaluate the suitability of the cleavable crosslinkers for re/upcycling cycle of low-functionality plastics via *crosslink-decrosslink-recrosslink* cycles, paraffin wax (PW; m.p. 58–62 °C; estimated M_r *ca.* 440) was chosen to facilitate rapid and accurate characterization by size exclusion chromatography (SEC). We firstly compared the effectiveness of all four crosslinkers (**4.4**–**4.6**, plus compound **4.11** as a non-cleavable control) in crosslinking paraffin wax. As evidenced by the presence of a higher molecular weight shoulder at 19–20 mins in the SEC traces (Figure 4.3a), each *bis*-diazirine reagent was capable of crosslinking the polymer.

We observed that crosslinkers **4.6** and **4.11**, containing less-polar tethers, crosslinked paraffin more efficiently than did **4.4** and **4.5**, which have more-polar tethers. This was evidenced by both a decreased shift in retention time for the SEC peak associated with the crosslinked polymer, and a higher intensity for that same signal (Figure 4.3a). The incompatibility between the polar tether of crosslinkers **4.4** and **4.5** and the lipophilic polymer substrate results in phase separation (Figure S4.14) which leads to the lower crosslinking efficacy. Changing the polymer substrate to poly(ethylene glycol) (PEG; m.p. 44–48 °C; M_r *ca.* 1500), crosslinkers **4.5** and **4.11** showed similar crosslinking efficacy (Figure 4.3e) and there was no visible difference between the

crosslinked polymer samples (Figure S4.14). By increasing the crosslinker loading from 10 to 20 mol%, the crosslinking efficacy changes similarly for both crosslinkers (i.e. compare Figure 4.3e and 4.3f).

Decrosslinking procedures were then applied to each crosslinked material. The paraffin wax samples crosslinked with **4.4** and **4.5** (i.e. PW-X-**4.4** and PW-X-**4.5**) were rapidly degraded by the addition of dilute NaOH (*ca.* 140 mM) to a solution of polymer in a mixture of tetrahydrofuran and methanol. Paraffin that had been treated with silyl ether **4.6** (PW-X-**4.6**) was treated with an equivalent concentration of dilute HCl (refer to the section 4.5 for full details). SEC analysis of the crude products showed complete degradation of the crosslinked polymers to the original molecular weight with no residual high MW shoulder (Figure 4.3b and 4.3c). As expected, paraffin wax crosslinked with **4.11** (PW-X-**4.11**; employed as a negative control for the decrosslinking step) did not hydrolyze under basic or acidic conditions. The sample of PEG that was crosslinked with compound **4.5** (i.e. PEG-X-**4.5**) was also successfully degraded into its original size under basic conditions (Figure 4.3e and 4.3f); once again the negative control sample (PEG-X-**4.11**) was unaffected by the addition of NaOH.

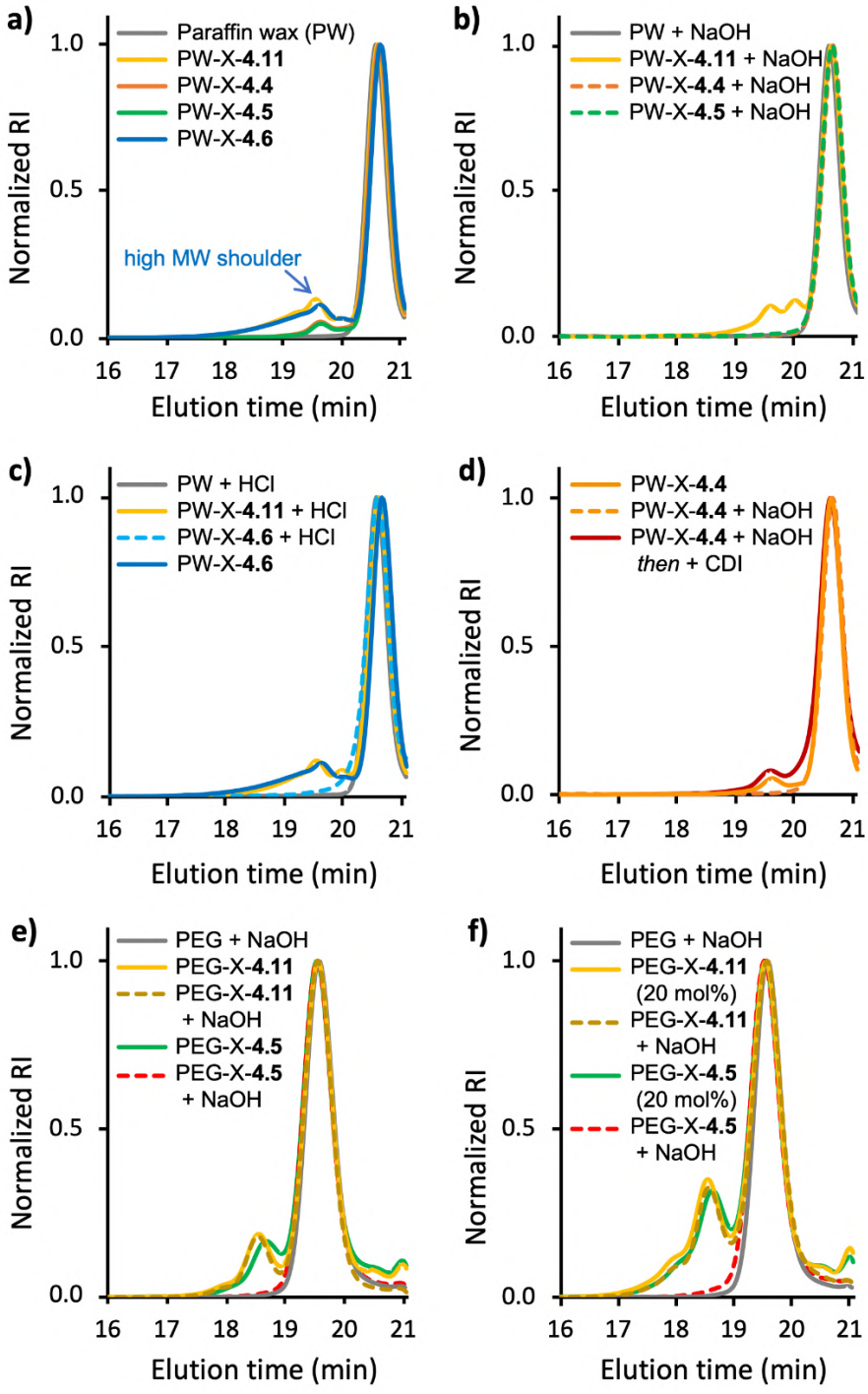

Figure 4.3 SEC traces of polymer samples after crosslinking/decrosslinking. a) Paraffin wax (PW) crosslinked (X) with 10 mol% *bis*-diazirine **4.4**, **4.5**, **4.6** or **4.11**, compared to native paraffin wax (vehicle control). b) Paraffin wax crosslinked with 10 mol% **4.4** or **4.5** treated with NaOH and compared to negative and vehicle controls. c) 10 mol% 6-

doped paraffin wax treated with HCl and compared to negative and vehicle controls. d) Decrosslinked paraffin wax (containing pendant OH groups) reacted with CDI to achieve recrosslinking. e) 10 mol% **4.5** or **4.11** (negative control)-doped PEG before and after NaOH treatment. f) 20 mol% **4.5** or **4.11**-doped PEG before and after NaOH treatment. RI, refractive index. Vehicle control samples were prepared identically to the test samples, but without the addition of crosslinker. Adapted from literature.[183]

4.3.4 Functionalization and recrosslinking

Following decrosslinking, the pendant OH groups remaining on the paraffin wax provide the opportunity for recrosslinking or other modification. To demonstrate recrosslinking, the electrophile CDI was added directly to the decrosslinked paraffin wax samples, coupling nearby hydroxyl groups to reform a carbonate linkage. SEC analysis showed the reappearance of the high MW shoulder indicative of crosslinking (Figure 4.3d).

While the *crosslink-decrosslink-recrosslink* cycle illustrated thus far affords a potentially useful means of shuttling between thermoplastic and thermoset states within a given polymer material, we were also attracted to the potential to add new functionality to the hydroxyl-containing decrosslinked thermoplastic intermediate. To explore this possibility, we chose to add diazirine groups directly to hydrolyzed PW-X-**4.4**. To this end, a sample of paraffin wax was first crosslinked with 10 mol% of crosslinker **4.4**, and the formation of the carbonate-containing crosslink was confirmed by ^{1}H NMR (Figure 4.4). The sample was then hydrolyzed through the addition of NaOH, and once again the successful transformation was confirmed spectroscopically. Finally, an excess of diazirine-containing benzyl bromide was added, and (after washing away excess electrophile), the formation of the labeled product was confirmed by both ^{1}H NMR spectroscopy and DSC (Figures S4.22 and S4.23).

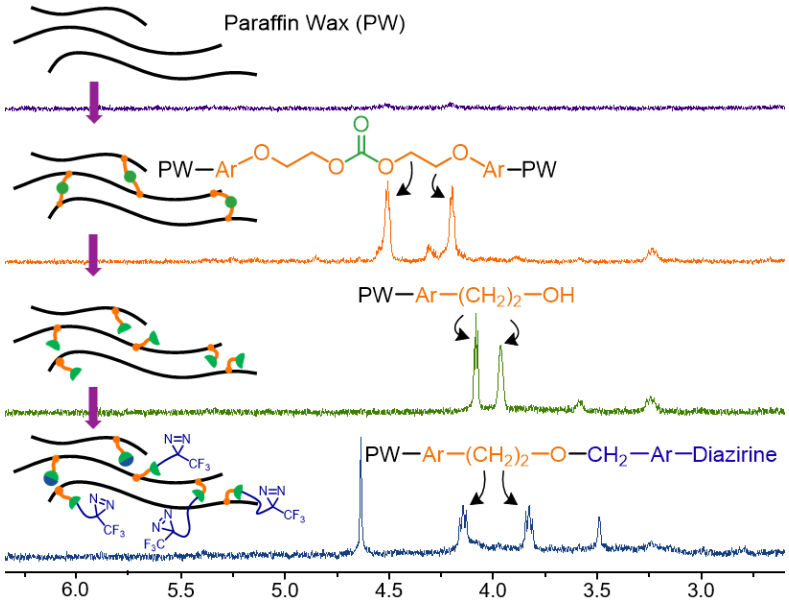

Figure 4.4 Stacked ^{1}H NMR spectra indicating the functionalization of a hydrolyzed (decrosslinked) paraffin wax sample reacted with a benzyl bromide-containing diazirine. All spectra were recorded in $CDCl_3$. See Figure S4.22 for integrations. Adapted from literature.[183]

4.3.5 Application to commercial low-funtionality polyolefins

To translate the results on cyclohexane and paraffin wax to more challenging polymeric substrates, isotactic polypropylene (iPP; M_n *ca.* 5000 g/mol) was selected as a representative low-functionality plastic. Of the three cleavable crosslinkers investigated above, oxalate-linked compound **4.5** appeared to contain the most labile linkage. We therefore added 10 wt% of crosslinker **4.5** or **4.11** (as a non-cleavable control) to commercial iPP, and thermally activated the sample (110 °C for 2 hours) to initiate crosslinking. Thermal properties for the samples (as well as those of the relevant vehicle control) were then analyzed by differential scanning calorimetry (DSC). As expected, both of the crosslinked polymer samples demonstrated decreased enthalpies in the melting transition, when compared to the vehicle control sample. These enthalpy decreases, where crosslinked regions of the polymer structure behave as thermosets and therefore no longer melt,[36,170] were consistently displayed in both the heating and cooling cycles of each DSC trace (Table 4.1). To test the reprocessability of crosslinked iPP samples, aqueous NaOH was mixed with the iPP substrates (refer to the section 4.5 for

full details). As anticipated, the iPP sample that had been crosslinked with **4.5** afforded the same enthalpy values as the vehicle control sample following the decrosslinking procedure—indicating successful restoration of thermoplastic properties. Conversely, the iPP sample crosslinked with **4.11** maintained its reduced crystallization and fusion enthalpies, indicating that no decrosslinking had taken place within the negative control.

Table 4.1 Evolution of thermal properties of crosslinked polypropylene before and after hydrolysis

Sample	$\Delta H_{crystal}$ (J/g)[a]	ΔH_{fusion} (J/g)[b]
$iPP_{(vehicle\ control)}$	94.9	99.8
iPP-X-**4.5**	81.7 (86%)	86.3 (86%)
iPP-X-**4.11**	77.6 (82%)	82.9 (83%)
$iPP_{(vehicle\ control)}$ + NaOH	96.0	100.1
iPP-X-**4.5** + NaOH	96.6 (101%)	101.8 (106%)
iPP-X-**4.11** + NaOH	82.1 (86%)	86.9 (87%)

[a] The integrated region for crystallization enthalpy was from 90 to 150 °C. [b] The fusion enthalpy was determined from the second heating cycle and integrated from 90 to 170 °C. Percentage values (shown in parentheses) are defined relative to the appropriate vehicle control.

To explore the effect of crosslinking and decrosslinking on *mixtures* of aliphatic polymers, we added crosslinkers **4.4**–**4.6**, as well as non-cleavable crosslinker **4.11**, at 10 wt% loading, to a 1:1 mixture of polyethylene (PE; m.p. 92 °C; M_n *ca.* 1700 g/mol) and iPP (m.p. 157 °C; M_n *ca.* 5000 g/mol). Once again we observed a consistent decrease in the enthalpy associated with the melting and crystallization transitions (Table 4.2), with the three cleavable crosslinkers performing more efficiently than non-cleavable *bis*-diazirine **4.11**. Reprocessability of these new thermoset materials was then demonstrated by hydrolyzing them back into their constituent thermoplastics. Basic conditions were employed for samples crosslinked with **4.4** and **4.5**, while tetrabutylammonium fluoride (TBAF) was used for samples crosslinked with **4.6**. As expected, the crystallization and fusion enthalpies for samples crosslinked with **4.4**–**4.6** returned to nearly the values associated with the corresponding vehicle control samples, while samples crosslinked with non-cleavable control **4.11** maintained lower enthalpies—indicating resistance to hydrolysis conditions.

Table 4.2 Enthalpy analysis of crosslinked and decrosslinked mixed-polyolefin plastics

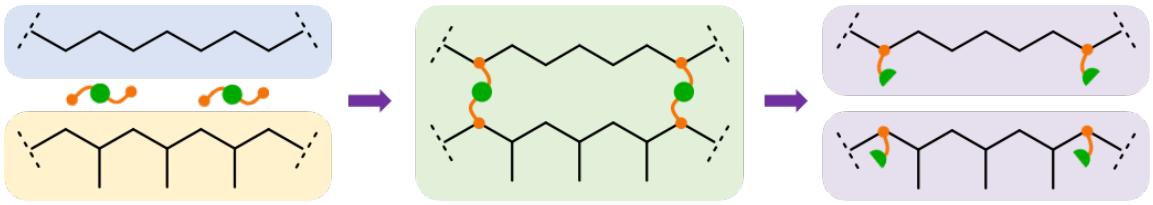

Sample	Following Crosslinking $\Delta H_{crystal}$ (J/g)[a]	ΔH_{fusion} (J/g)[b]	Sample	Following Decrosslinking $\Delta H_{crystal}$ (J/g)[a]	ΔH_{fusion} (J/g)[b]
iPP/PE$_{(vehicle\ control)}$	88.8	90.7	iPP/PE$_{(vehicle\ control)}$ + NaOH	83.3	85.3
iPP/PE-X-**4.11**[c]	79.1 (89%)	79.8 (88%)	iPP/PE-X-**4.11** + NaOH	69.6 (84%)	69.8 (82%)
iPP/PE-X-**4.4**[d]	66.1 (74%)	65.5 (72%)	iPP/PE-X-**4.4** + NaOH	78.0 (94%)	80.3 (94%)
iPP/PE-X-**4.5**[d]	70.2 (79%)	71.5 (79%)	iPP/PE-X-**4.5** + NaOH	79.1 (95%)	82.2 (96%)
iPP/PE$_{(vehicle\ control)}$	88.8	90.7	iPP/PE$_{(vehicle\ control)}$ + TBAF	105.7	110.0
iPP/PE-X-**4.11**[c]	79.1 (89%)	79.8 (88%)	iPP/PE-X-**4.11** + TBAF	87.1 (82%)	93.9 (85%)
iPP/PE-X-**4.6**[d]	68.7 (77%)	69.2 (76%)	iPP/PE-X-**4.6** + TBAF	101.8 (96%)	104.4 (95%)

[a] The integrated region for crystallization enthalpy was from 50 to 120 °C. [b] The fusion enthalpy was determined from the second heating cycle and integrated from 50 to 170 °C. Percentage values (shown in parentheses) are defined relative to the appropriate vehicle control. [c] A mixture of isotactic polypropylene (iPP) and polyethylene (PE) were reacted with non-cleavable crosslinker **4.11**, as a negative control for the decrosslinking experiment. [d] A mixture of iPP and PE were reacted with the indicated cleavable crosslinker.

4.3.6 Application to reversible PDMS crosslinking

To demonstrate curing in a representative liquid polymer matrix, we applied polydimethylsiloxane (PDMS; viscosity 18,000–22,000 cSt) containing 5 wt% of *bis*-diazirine **4.4** to a rheometer stage for direct measurement of the change in storage modulus during crosslinking. As anticipated, we observed a pronounced increase in shear modulus as the sample passed beyond the activation temperature for **4.4** (Figure S4.40). A PDMS control sample, by contrast, showed no such modulus increase upon heating. We also crosslinked bulk PDMS with **4.4**, and then decrosslinked the sample by addition of NaOH. As expected, crosslinked PDMS was a mechanically stable gel, while the decrosslinked sample regained the ability to flow with gravity (Figure S4.39).

4.3.7 Thermomechanical testing of crosslinked polymers

To assess the effective crosslink density within a representative commercial polyolefin treated with a cleavable crosslinker, 5 wt% of carbonate crosslinker **4.4** was added to injection-moulding grade low-density polyethylene (LDPE; melt flow rate 21). After thermal activation and melt-processing to generate regular-dimensioned macro-scale objects (refer to the section 4.5 for details), crosslinked samples (or vehicle controls, prepared identically but with no added crosslinker) were extracted with hot toluene to determine the gel content,[176,196] and were subjected to dynamic mechanical thermal analysis (DMTA) to measure the average apparent molecular weight difference between crosslinks ($M_{c,a}$).

Despite the low loading of *bis*-diazirine **4.4**, crosslinked LDPE samples were found to have a gel content of 95% ± 3% (compared with 0% gel content for the corresponding vehicle control samples). Perhaps most significantly, DMTA analysis of the crosslinked samples revealed a pronounced rubbery plateau above *ca.* 125 °C, confirming that these samples had been transformed into thermosets (Figure 4.5b). The corresponding vehicle control samples, by contrast, behaved as pure thermoplastics, exhibiting clean melting transitions at elevated temperature (Figure 4.5a).

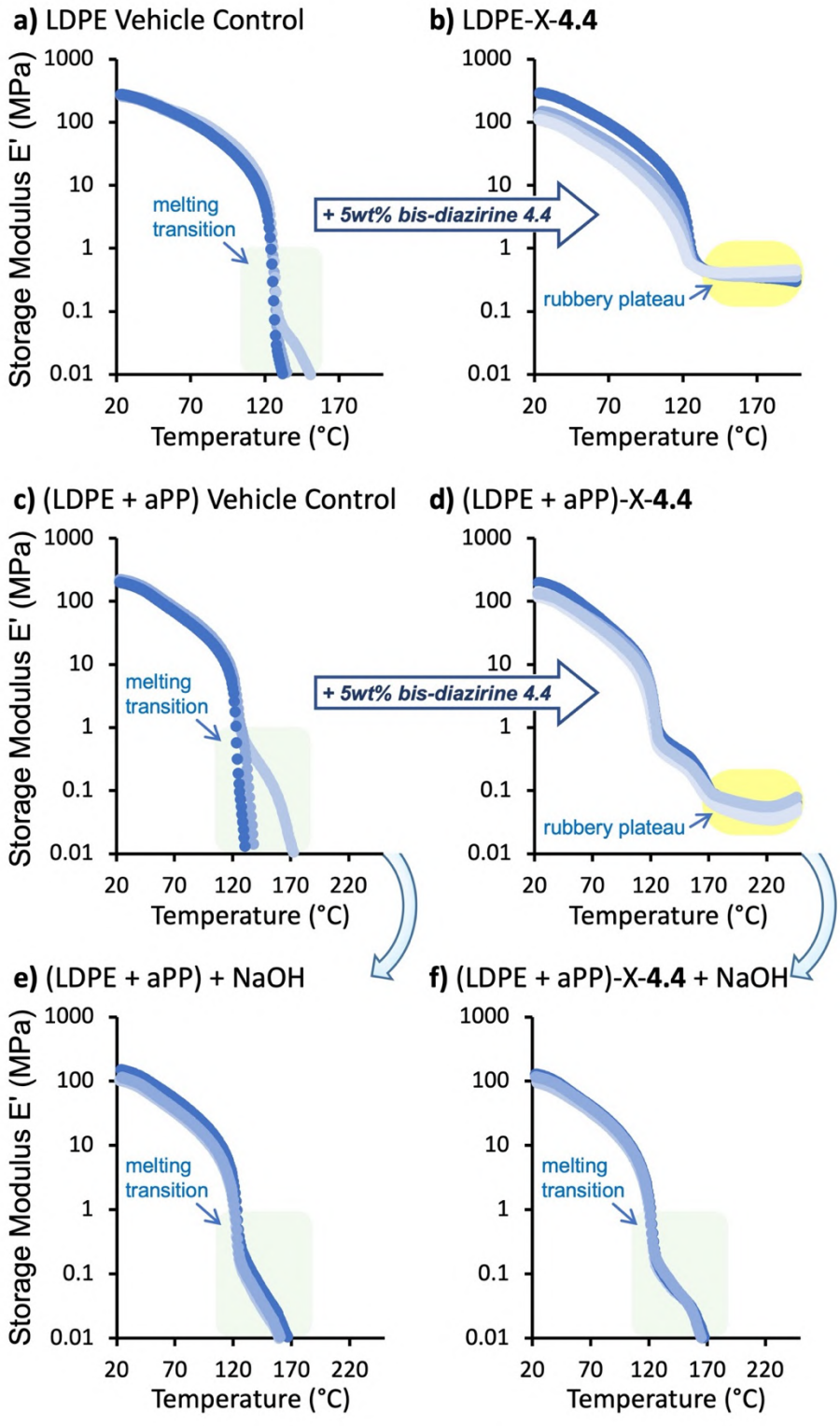

Figure 4.5 DMTA curves for polymer samples after crosslinking/decrosslinking. a) Vehicle control samples prepared from low-density polyethylene (LDPE). b) LDPE samples crosslinked with 5 wt% *bis*-diazirine **4.4**. c) Vehicle control samples prepared

from a 1:1 mixture (by weight) of amorphous polypropylene (aPP) and LDPE. d) aPP:LDPE samples crosslinked with 5 wt% *bis*-diazirine **4.4**. e) aPP:LDPE samples treated with NaOH. f) crosslinked aPP:LDPE samples (prepared identically to those tested in panel d), then treated with NaOH to trigger decrosslinking. Replicate samples are indicated in differing shades of blue; at least 3 samples were tested for each condition. Melting behavior is highlighted in light green. Rubbery plateau regions are highlighted in yellow. Refer to Tables S4.9 and S4.12 for collected DSC and WAXS data for crosslinked polymers; no significant differences in percent crystallinity were observed, even when the enthalpy of melting was substantively reduced. Adapted from literature.[183]

The rubbery plateau for LDPE samples crosslinked with 5 wt% of **4.4** corresponds to storage modulus of 0.414 ± 0.010 MPa. Calculating the $M_{c,a}$ from this value using the theory of rubbery elasticity[196–198] and the measured sample density (0.936 ± 0.007 g/cm^3) revealed a distance between mechanically productive crosslinks of approximately 23,300 g/mol (i.e. 1,660 methylene units between crosslink points). Comparison to the total number of C–H insertion events expected for **4.4** within a polyethylene matrix (based on the cyclohexane model experiments discussed above; refer to the section 4.5 for calculations) suggests a ratio of productive crosslinks (where **4.4** bridges two polyethylene chains) to unproductive loops (where **4.4** reacts twice on the same chain) of approximately 1 : 2.5. A distinct rubbery plateau was also observed for LDPE samples crosslinked with only 2 wt% of **4.4** (see Figure S4.28 in the section 4.5). While this necessarily occurs at a lower storage modulus (*ca.* 0.12 MPa) due to the very low ratio of crosslinker molecules to LDPE methylene units, it nevertheless provides compelling evidence for the ability of small-molecule *bis*-diazirines to imbue thermoplastic materials with thermoset-like performance characteristics.

We next prepared melt-processed mixtures of LDPE and amorphous polypropylene (aPP), in which the samples were either treated with 5 wt% of *bis*-diazirine **4.4** or a solvent blank. Once again, the vehicle controls showed melting transitions consistent with thermoplastic behavior (Figure 4.5c), while the samples treated with **4.4** displayed stable rubbery plateaus consistent with their conversion to thermosets. The plateau modulus was lower than that observed for the crosslinked pure LDPE samples in Figure 4.5b, indicating a lower density of mechanically productive crosslinks.

This decrease in performance is reflective of the challenge inherent in crosslinking immiscible materials, and was also reflected in a reduced gel content for the crosslinked mixture of LDPE + aPP (73% ± 6%), compared with that discussed above for crosslinked LDPE. Nevertheless, the existence of a stable and consistent rubbery plateau in these samples (together with complementary microscopy and tensile data available in Figures S4.32 and S4.36) provided good evidence that some portion of crosslinks within the material were occurring at the LDPE : aPP interface. By contrast, control samples prepared from pre-crosslinked LDPE and pre-crosslinked aPP (in which both homopolymers are individually crosslinked, but where no crosslinking is possible at the interface) performed poorly and irreproducibly in DMTA testing (Figure S4.38a).

Finally, to demonstrate the ability to convert the crosslinked LDPE : aPP thermoset composite back into a mixture of thermoplastics, we subjected (LDPE+aPP)-X-**4.4** samples to hydrolysis conditions. This served to remove the rubbery plateau (compare Figure 4.5f to Figure 4.5d), giving samples that performed identically to the corresponding vehicle controls (compare Figure 4.5f to Figure 4.5e).

4.4. Conclusions

A series of simple, yet powerful, cleavable crosslinkers has been introduced that can be used to upcycle low-functionality thermoplastic materials into reprocessable thermosets. Cleavage of the labile linker groups can be accomplished using a range of external stimuli (base, acid, or fluoride), and the decrosslinked polymer products resulting from these operations contain pendent hydroxyl groups that can either be used for recrosslinking or further functionalization.

The opportunity to crosslink mixtures of incompatible polymers (e.g. polyethylene and polypropylene) together to form novel covalent composites is particularly attractive, given the persistent problem of mixed plastic waste streams. Polyethylene is frequently contaminated with polypropylene, and polypropylene is even more frequently contaminated with polyethylene.[199–201] Simple melt-blending of these mixed materials leads to poor mechanical properties due to phase separation,[202–205] and cross-contamination challenges of this type are partially responsible for the fact that only 9% of all plastics ever produced have been recycled.[173,206] Because small-molecule *bis*-

diazirines react promiscuously with polymer substrates and cannot easily distinguish between different polymer architectures, they readily connect dissimilar polymers.[61] Together with other recently disclosed reagents for functionalization of commodity polymers through reaction at C–H bonds,[159,207–209] the cleavable crosslinkers described herein may provide a useful means of generating reprocessable thermosets from low-functionality thermoplastics and post-consumer waste.

4.5. Experimental and Supplementary Information

4.5.1 Materials and methods

4.5.1.1 General considerations

All commercial materials were used as received unless otherwise noted. Reagents used for the synthesis of target compounds were purchased from Sigma-Aldrich except for *N*-iodosuccinimide and diazirine **4.1**, which were purchased from AK Scientific and Amadis Chemicals, respectively. *bis*-Diazirine crosslinker **4.11** was a gift from XlynX Materials. Reagent grade solvents were used for extractions and purifications. Anhydrous cyclohexane was used in crosslinking experiments. All diazirine-forming reactions were performed in the dark. Removal of solvent was done below 40 °C, avoiding the use of excessive vacuum. The following polymer substrates were employed in crosslinking experiments:

- Paraffin wax (PW) from Sigma-Aldrich (ref 327212, m.p. = 58–62 °C, CAS 8002-74-2). An approximate chemical formula of $C_{31}H_{64}$ was estimated by determining the relative ratio of methyl (CH_3) and methylene (CH_2) groups observable in the ^{1}H NMR (Figure S4.8), together with the approximate molecular weight observed in the SEC experiments discussed below.
- Poly(ethylene glycol) 1500 (PEG) from Alfa Aesar (ref A16241, $H(OCH_2CH_2)_nOH$, m.p. = 44–48 °C, CAS 25322-68-3).
- Isotactic polypropylene (iPP) from Sigma-Aldrich (ref 428116, average M_w ~12000, average M_n ~5000, m.p. = 157 °C, CAS 9003-07-0).
- Amorphous polypropylene (aPP) from Sigma-Aldrich (ref 428175, CAS 9003-07-0).

- Polyethylene (PE) from Sigma-Aldrich (ref 427772, average M_w ~4000, average M_n ~1700, m.p. = 92 °C, CAS 9002-88-4).
- Low-density polyethylene (LDPE) from Goodfellow Materials (ref ET31-GL-000105, melt flow rate 21).
- Polydimethylsiloxane (PDMS) from Sigma-Aldrich (ref 432997, viscosity 18000–22000 cSt, CAS 70131-67-8).

Nuclear Magnetic Resonance (NMR) spectra were recorded at ambient temperature using either a Bruker AVANCE 300 (300 MHz for ^{1}H, 283 MHz for ^{19}F, 76 MHz for ^{13}C) or a Bruker AVANCE Neo 500 (500 MHz for ^{1}H, 471 MHz for ^{19}F, 126 MHz for ^{13}C, 99 MHz for ^{29}Si) spectrometer. Chemical shifts were reported in parts per million (ppm) and were referenced to the solvent peak ($CDCl_3$: ^{1}H NMR δ = 7.26 ppm, ^{13}C NMR δ = 77.16 ppm; CD_2Cl_2: ^{1}H NMR δ = 5.32 ppm, ^{13}C NMR δ = 53.84 ppm; CD_3OD: ^{1}H NMR δ = 3.31 ppm, ^{13}C NMR δ = 49.00 ppm). ^{13}C spectra and ^{19}F spectra were ^{1}H decoupled unless otherwise noted. Data are reported as follows: chemical shift (multiplicity (s = singlet, d = doublet, t = triplet, q = quartet, qd = quartet of doublets, m = multiplet), coupling constant in Hz, integration). Spectral assignments were made for compounds that gave well-resolved spectra in COSY, HSQC and HMBC experiments. Chemical shifts in ^{19}F spectra are reported in ppm and reported as obtained. Reaction progress was monitored by either thin-layer chromatography on pre-coated aluminum-backed silica gel 60 F254 plates followed UV visualization or by ^{1}H/^{19}F NMR spectroscopy.

Low resolution mass spectrometry (LRMS) data were acquired using electrospray ionization (EI) and conducted using a Finnigan Trace DSQ system with Direct Probe Controller (Thermo, MA).

High resolution mass spectrometry (HRMS) data were acquired using field desorption (FD) ionization on a JEOL AccuTOF GCx mass spectrometer.

Infrared (IR) spectra were recorded using a Perkin-Elmer ATR spectrometer. IR wave numbers (ν) are reported in cm^{-1}.

Differential Scanning Calorimetry (DSC) analysis: A sample of the analyzed substance (typically 3 to 10 mg) was placed in a Tzero pan (TA Instruments, 901683.901) and sealed by a Tzero hermetic lid (TA Instruments, 901684.901). The pan was placed in the oven of the DSC25 device (TA Instruments) and heated/cooled within –90 to 200 °C at a

rate of 5 or 10 °C/min with an identical empty pan as a reference. The oven was constantly flushed by a 50 mL/min flow of nitrogen gas during the analysis. Melting points (m.p.) were taken as the peak of the endothermic melting transition visible in the DSC analysis trace for diazirine-containing compounds.

Size Exclusion Chromatography (SEC) analysis: all samples were dissolved in tetrahydrofuran (*ca.* 5 mg/mL) and filtered through a polytetrafluoroethylene membrane of 0.2 μm pore size before analysis. SEC was carried out using a Malvern Viscotek TDAmax system with two analytical SEC columns made from styrene-divinyl benzene (T5000 and T3000 Org SEC Col). Measurements were carried out at 1.0 mL/min with HPLC-grade tetrahydrofuran containing tetrabutylammonium bromide (0.1% w/w) as the eluent at 35 °C. The molecular weights were calculated based on signals from a refractive index (RI) detector, and using a calibration curve prepared from monodisperse polystyrene standards.

Dynamic Mechanical Thermal Analysis (DMTA) was performed on an Anton Paar Modular Compact 302 rheometer fitted with an Anton Paar SRF12 geometry and CTD 600 oven. All samples were fabricated as rectangular specimens with ~25 mm (*L*) x 10 mm (*W*) x 4.0 mm (*T*). Samples were measured through a temperature range of 25–200/250 °C with a thermal ramp rate of 1.5 °C min^{-1}, a logarithmic strain of 0.01–0.1 % at 1 Hz, and a normal force of –0.1 N.

The molecular weight between crosslinks (M_c) was calculated from equation (1)[196–198]:

$$E' = \frac{3\rho RT}{M_c} \qquad (1)$$

where E' is the modulus of the rubbery plateau determined by DMTA, ρ is the measured density of crosslinked low-density polyethylene, R is the gas constant, and T refers to the absolute temperature (413 K).

Parallel Plate Rheometry measurements of polydimethylsiloxane (PDMS) were conducted on the same Anton Paar Modular Compact 302 rheometer, using the default MCR 203 SN82432706 plate and an Anton Paar PP25/S parallel plate geometry. PDMS with or without crosslinker sample was deposited on the lower plate, the PP25/S plate was then lowered to a gap of 1 mm and the excess was removed. Samples were measured through 25–120 °C using a constant shear strain of 0.5 % at 1 Hz (applied frequency).

Tensile Tests were performed using an ADMET eXpert 7603 single column universal tester, in conjunction with the standard procedure laid out by ISO 527-1 Plastics - Determination of Tensile Properties. The test specimens were type 5B dog bone samples. The samples were affixed in the tester by clamping the wide ends in the tester jaws. The samples were pulled in tensile until breakage at a crosshead speed of 50 mm/min. Force-displacement curves were obtained from these tests. The cross-sectional area used for the stress calculations was the middle of the gauge length, where the break was intended to happen.

Scanning Electron Microscopy (SEM) micrographs were generated using a Hitachi S-4800 cold field emission scanning electron microscope. Before imaging, samples were sputtered with gold for 2 minutes at 10 mA under 100 mTorr of argon. Images were taken using a mixed detector with an accelerating voltage of 1.0 kV, an emission current of 10.5 μA and a working distance of *ca.* 8.8–9.1 mm.

X-Ray Diffraction (XRD) analysis was carried out on an AXS D8 Discover (Bruker) diffractometer, equipped with a LynxEye strip detector and a Ge (111) focusing monochromator, providing Cu Kα1 (λ = 1.5406 Å) radiation powered at 45 kV and 40 mA.

4.5.1.2 Procedures for crosslinker synthesis

Synthesis of ethylene glycol diazirine **4.3**

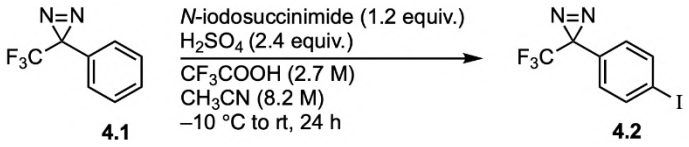

*Caution: diazirine **4.1** should be handled with extreme care when not in solution: refer to impact tests below.*

To a solution of diazirine **4.1** (80 g, 430 mmol, 1.0 equiv.) in 1:3 acetonitrile:trifluoroacetic acid (150 mL), *N*-iodosuccinimide (116 g, 516 mmol, 1.2 equiv.) was added portion-wise under ambient atmosphere. After the *N*-iodosuccinimide fully dissolved, the mixture was then cooled to 0 °C with an ice bath before adding a solution of H_2SO_4 (55 mL, 1032 mmol, 2.4 equiv.) in trifluoroacetic acid and acetonitrile (TFA: 45 mL and CH_3CN: 15 mL) dropwise over *ca.* 60 min. The reaction was slowly warmed to room temperature and stirred for 24 h before pouring over a mixture of ice, sodium bicarbonate, and water to neutralize the product mixture. The dark red aqueous solution was then extracted with ether (3 × 150 mL), and the combined organic extracts were washed with saturated aqueous sodium thiosulfate (2 × 150 mL), dried with sodium sulfate, and concentrated. The crude product was purified by passing over a silica plug with pentane to yield **2** as a pale yellow or pink liquid (124.67 g, 93%). $\mathbf{R_f}$ = 0.8 (100% pentane). **^{1}H NMR** (500 MHz, $CDCl_3$) δ 7.74 (d, *J* = 8.7 Hz, 2H), 6.93 (d, *J* = 8.7 Hz, 2H). **^{13}C NMR** (126 MHz, $CDCl_3$) δ 138.18, 128.91, 128.25, 122.05 (q, *J* = 274.7 Hz), 96.12, 29.86. **^{19}F NMR** (471 MHz, $CDCl_3$) δ –65.27. **IR** (diamond-ATR) ν: 2956, 2926, 2856, 1614, 1590, 1493, 1342, 1232, 1186, 1155, 1047, 1007, 936, 811, 744. **LRMS** (EI) m/z (% relative intensity) [ion]: 284 (100) $[M - N_2]^+$, 157 (90) $[M - N_2 - I]^+$.

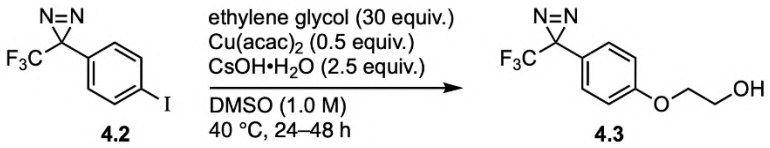

To an oven-dried 2-neck round bottom flask containing **4.2** (100 g, 320 mmol, 1.0 equiv.) in DMSO (320 mL, 1.0 M), ethylene glycol (536 mL, 9614 mmol, 30 equiv.) and $CsOH{\cdot}H_2O$ (134.6 g, 801 mmol, 2.5 equiv.) was added before warming to 40 °C. Subsequently, the reaction mixture was bubbled with argon for 15 min and $Cu(acac)_2$ (41.95 g, 160 mmol, 0.5 eq, recrystallized from ethanol) was added in three portions at 0 h (21.95 g), 20 h (10 g), and 24 h (10 g). The reaction was monitored by ^{19}F-NMR and quenched by pouring over water (500 mL) when no more conversion was observed. The dark blue-green aqueous solution was extracted with DCM (4 × 300 mL), and the combined organic extracts were washed with ammonia water (3 × 150 mL) and then water (3 × 150 mL). The crude product was purified by passing over a silica plug with pentane followed by 1:1 diethyl ether:pentane to yield **4.3** as a viscous yellow liquid (43.88 g, 56%). $\mathbf{R_f}$ = 0.3 (100% CH_2Cl_2). **^{1}H NMR** (500 MHz, $CDCl_3$) δ 7.15 (d, *J* = 8.7 Hz, 2H), 6.92 (d, *J* = 8.8 Hz, 2H), 4.08 (t, *J* = 4.3 Hz, 2H), 4.02 – 3.93 (m, 2H), 2.11 – 1.99 (m, 1H). **^{13}C NMR** (126 MHz, $CDCl_3$) δ 159.81, 128.36, 122.36 (q, *J* = 274.4 Hz), 121.58, 115.07, 69.47, 61.44, 28.35 (q, *J* = 38.8 Hz). **^{19}F NMR** (471 MHz, $CDCl_3$) δ – 65.63. **IR** (diamond-ATR) ν: 3369 (broad), 2930, 2856, 1613, 1585, 1518, 1457, 1344, 1299, 1257, 1233, 1180, 1151, 1055, 938, 825, 734. **HRMS** (FD+) m/z $[M^{\bullet}]^+$ calculated for $C_{10}H_9F_3N_2O_2$: 246.0611, found: 246.0624.

Synthesis of carbonate-linked *bis*-diazirine **4.4**

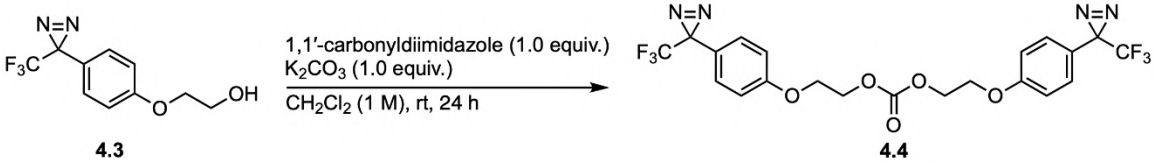

To a solution of diazirine **4.3** (3.0 g, 12 mmol, 1.0 equiv.) in dichloromethane (12 mL, 1.0 M) at room temperature, 1,1'-carbonyldiimidazole (2.0 g, 12 mmol, 1.0 equiv.) was added under ambient atmosphere. After one hour stirring at room temperature, the second equivalent of diazirine **4.3** (3.0 g, 12 mmol, 1.0 equiv.) was added into the abovementioned reaction mixture, followed by K_2CO_3 (1.7 g, 12 mmol, 1.0 equiv.). The

reaction mixture was left at room temperature and stirred for 24 hours. The reaction was then quenched with NH_4Cl saturated solution and extracted with diethyl ether (× 3). The combined organic layers were dried over sodium sulfate. After evaporation of the solvent, the residue was purified by silica gel column chromatography (0–10% ethyl acetate in pentane) to afford the desired product as a yellow oil (5.5 g; 87%). $\mathbf{R_f}$ = 0.8 (1:1 pentane:ethyl acetate). **^{1}H NMR** (500 MHz, $CDCl_3$) δ 7.14 (d, *J* = 8.8 Hz, 4H), 6.90 (d, *J* = 8.9 Hz, 4H), 4.51 (t, *J* = 4.6 Hz, 4H), 4.20 (t, *J* = 4.6 Hz, 4H). **^{13}C NMR** (126 MHz, $CDCl_3$) δ 159.47, 155.03, 128.33, 122.35 (q, *J* = 274.5 Hz), 121.76, 115.09, 66.23, 65.83, 28.32 (q, *J* = 40.4 Hz). **^{19}F NMR** (471 MHz, $CDCl_3$) δ –65.63. **IR** (diamond-ATR) ν: 3140, 2932, 1770 (sharp, strong), 1614, 1519, 1458, 1394, 1344, 1292, 1234, 1181, 1154, 1056, 938, 826. **HRMS** (FD+) m/z $[M^{\bullet}]^+$ calculated for $C_{21}H_{16}F_6N_4O_5$: 518.1019, found: 518.1011.

Synthesis of oxalate-linked *bis*-diazirine **4.5**

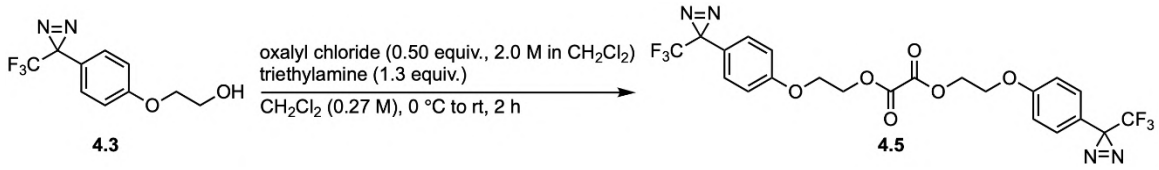

4.3 **4.5**

A flame-dried round bottom flask was charged with a solution of diazirine **4.3** (0.10 g, 0.41 mmol, 1.0 equiv.) in anhydrous dichloromethane (1.5 mL, 0.27 M), under an atmosphere of argon. The solution was cooled to 0 °C, and triethylamine (0.071 mL, 0.51 mmol, 1.3 equiv.) was added, followed by the dropwise addition of oxalyl chloride (0.10 mL, 0.20 mmol, 0.50 equiv., 2.0 M in dichloromethane). After stirring at room temperature for 2 hours, while shielding from light, the mixture was concentrated in vacuo to afford the crude mixture. Then the solid crude product was filtered and washed with cold diethyl ether to afford the desired product as a light-yellow solid (0.092 g; 83%, melting point: 86.9 ± 0.7 °C). $\mathbf{R_f}$ = 0.2 (1:1 pentane:diethyl ether). **^{1}H NMR** (500 MHz, $CDCl_3$) δ 7.15 (d, *J* = 8.8 Hz, 4H), 6.91 (d, *J* = 8.8 Hz, 4H), 4.64 (t, *J* = 4.7 Hz, 4H), 4.26 (t, *J* = 4.7 Hz, 4H). **^{13}C NMR** (126 MHz, $CDCl_3$) δ 159.34, 157.30, 128.39, 122.33 (q, *J* = 274.5 Hz), 121.95, 115.15, 65.40, 65.06, 28.30 (q, *J* = 40.7 Hz). **^{19}F NMR** (471 MHz, $CDCl_3$) δ –65.62. **IR** (diamond-ATR) ν: 2959, 2925, 1773 and 1750 (sharp, strong), 1613,

1518, 1458, 1344, 1299, 1258, 1233, 1172, 1074, 938, 825. **HRMS** (FD+) m/z $[M^{\bullet}]^+$ calculated for $C_{22}H_{16}F_6N_4O_6$: 546.0969, found: 546.0957.

Synthesis of silyl-ether-linked *bis*-diazirine **4.6**

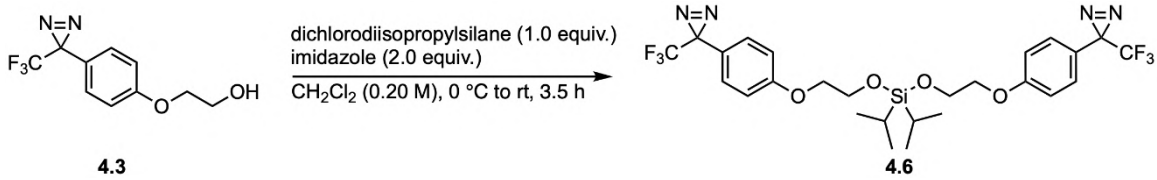

4.3 **4.6**

A flame-dried round bottom flask was charged with a solution of diazirine **4.3** (1.0 g, 4.1 mmol, 2.0 equiv.) in anhydrous dichloromethane (10 mL, 0.41 M), under an atmosphere of argon. The solution was cooled to 0 °C, and imidazole (0.28 g, 4.1 mmol, 2.0 equiv.) was added, followed by the dropwise addition of dichlorodiisopropylsilane (0.25 mL, 2.0 mmol, 1.0 equiv.). The reaction mixture was allowed to warm to room temperature over 4 hours, while shielding from light. The mixture was then filtered, and the filtrate was washed with dichloromethane. The collected dichloromethane solution containing the desired product was concentrated in vacuo, and the residue was purified by silica gel column chromatography (0–10% ethyl acetate in pentane) to afford the desired product as a yellow oil (0.92 g; 75%). $\mathbf{R_f}$ = 0.4 (100% pentane). **^{1}H NMR** (500 MHz, $CDCl_3$) δ 7.12 (d, *J* = 8.6 Hz, 4H), 6.89 (d, *J* = 8.7 Hz, 4H), 4.16 – 4.00 (m, 8H), 1.05 (s, 14H). **^{13}C NMR** (126 MHz, $CDCl_3$) δ 160.11, 128.26, 122.40 (d, *J* = 274.8 Hz), 121.20, 115.07, 69.47, 61.68, 28.36 (q, *J* = 39.6 Hz), 17.31, 12.19. **^{19}F NMR** (471 MHz, $CDCl_3$) δ –65.65. **IR** (diamond-ATR) ν: 2946, 2870, 1614, 1519, 1457, 1344, 1300, 1260, 1234, 1182, 1154, 1057, 939, 825. **HRMS** (FD+) m/z $[M^{\bullet}]^+$ calculated for $C_{26}H_{30}F_6N_4O_4Si$: 604.1935, found: 604.1963.

Linear 8-step synthesis of ethylene glycol diazirine **4.3**

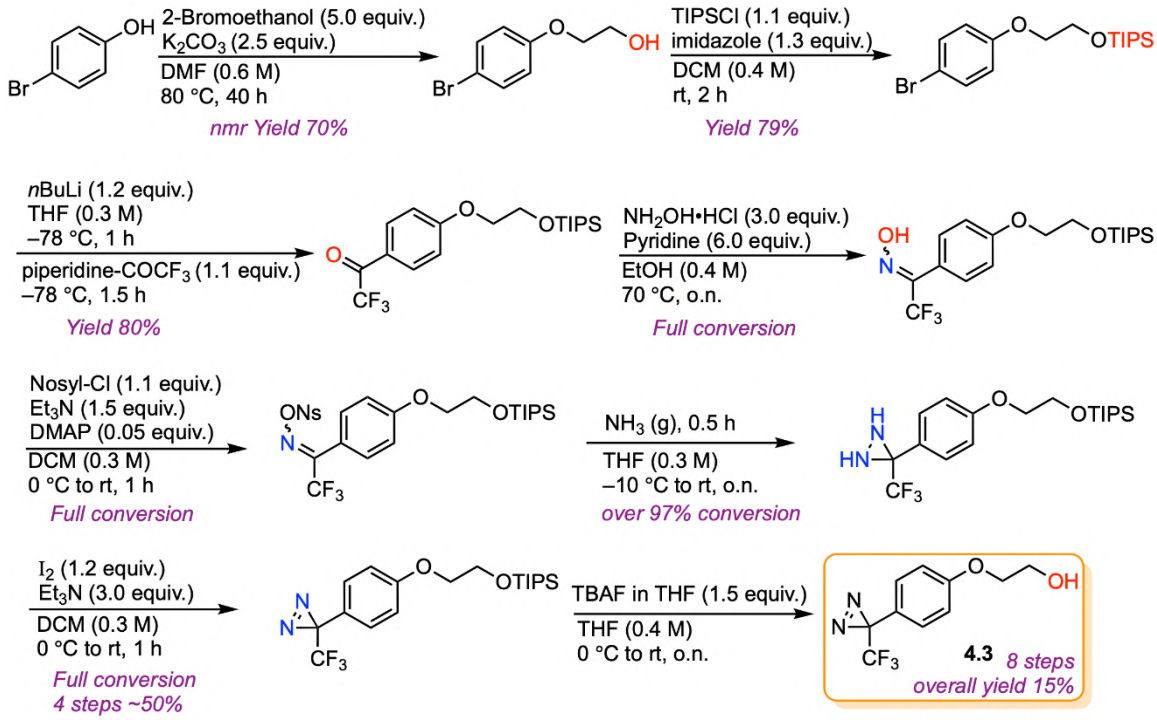

Scheme S4.1 Alternative approach to diazirine **4.3**, employing a traditional diazirine construction sequence.

4.5.1.3 Assessment of thermal parameters for diazirine-containing compounds

A sample of the analyzed substance (typically 3 to 7 mg) was placed in a Tzero pan and sealed by a Tzero hermetic lid, which was pierced with a small pinhole to allow evolution of nitrogen gas. The pan was placed in the oven of a DSC25 device and heated from 40 °C to 160 °C (180 °C upper limit for *mono*-diazirine compounds) at a rate of 5 °C/min with an identical empty pan (pierced) as a reference. The oven was constantly flushed by a 50 mL/min flow of nitrogen gas during the analysis. The device recorded the difference in heat flow between the reference and the studied sample, allowing the assignment of T_{onset} and T_{peak}. DSC analyses were conducted 12 times for compound **4.2**, 8 times for compound **4.3**, 4 times for compound **4.4**, 3 times for compound **4.5**, and 6 times for compound **4.6**. A representative DSC trace for compound **4.2** is provided below.

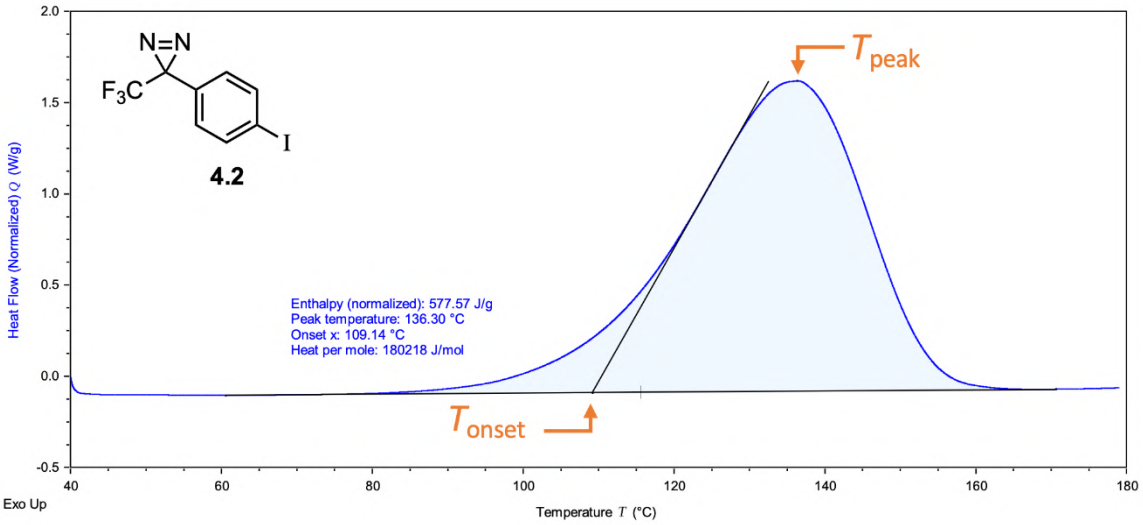

Figure S4.1 Representative DSC trace for compound **4.2**, illustrating the positions of T_{onset} and T_{peak}.

Table S4.1 Collected thermal data for *bis*-diazirine crosslinkers[a]

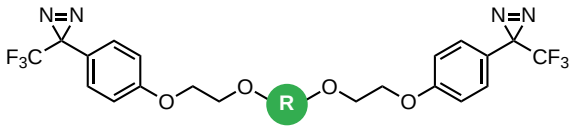

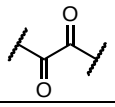

	4.4	**4.5**	**4.6**
T_{onset} (°C)	87.5 ± 0.7	88.9 ± 0.5	85.0 ± 0.1
T_{peak} (°C)	111.3 ± 0.3	110.7 ± 0.4	110.7 ± 0.1
Enthalpy[b] (J/g)	667.0 ± 11.6	583.6 ± 10.5	646.1 ± 11.6
Enthalpy[b] (kJ/mol)	345.7 ± 6.0	318.8 ± 5.7	390.6 ± 7.0
Shock Sensitivity[c]	Not likely (–0.07)	Not likely (–0.14)	Not likely (–0.07)
Explosive Propagation[d]	Not likely (–0.15)	Not likely (–0.21)	Not likely (–0.16)

[a] Error bars indicate standard error across 4 DSC runs for compound **4.4**, 3 runs for compound **4.5**, 6 runs for compound **4.6**.

[b] Enthalpy refers to the total integrated peak area (per unit mass or per mole), for the exotherm associated with diazirine activation.

[c] The shock sensitivity metric (SS) was determined according to the method of Yoshida and co-workers.[118] SS = log (Q_{DSC}) – 0.72 x log (T_{onset} – 25) – 0.98; where Q_{DSC} is the enthalpy of nitrogen release (in cal/g), and T_{onset} is determined by extrapolation of the tangent of the upward slope in the DSC experiment, to the fitted baseline of the plot (in °C). A value of ≥0 indicates that the analyzed compound may be shock-sensitive and/or explosive.[210]

[d] The explosive propagation metric (EP) was likewise determined according to Yoshida's methods. EP = log (Q_{DSC}) – 0.38 x log (T_{onset} – 25) – 1.67; where Q_{DSC} is the

enthalpy of nitrogen release (in cal/g), and T_{onset} is measured as described above. A value of ≥0 indicates a risk of explosive propagation for the compound.

Table S4.2 Collected thermal data for *mono*-diazirine compounds[a]

mono-Diazirine	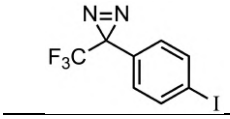	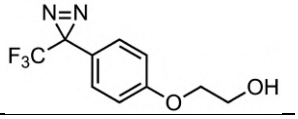
	4.2	**4.3**
T_{onset} (°C)	108.9 ± 0.1	91.5 ± 0.1
T_{peak} (°C)	136.2 ± 0.1	116.0 ± 0.1
Enthalpy[b] (J/g)	561.1 ± 17.3	1056.5 ± 11.7
Enthalpy[b] (kJ/mol)	175.1 ± 5.4	260.1 ± 2.9
Shock Sensitivity[c]	Not likely (–0.24)	Alert (0.11)[e]
Explosive Propagation[d]	Not likely (–0.27)	Alert (0.04)[e]

[a] Error bars indicate standard error across 12 DSC runs for compound **4.2**, 8 runs for compound **4.3**.

[b] Enthalpy refers to the total integrated peak area (per unit mass or per mole), for the exotherm associated with diazirine activation.

[c] The shock sensitivity metric (SS) was determined according to the method of Yoshida and co-workers.[118] SS = log (Q_{DSC}) – 0.72 x log (T_{onset} – 25) – 0.98; where Q_{DSC} is the enthalpy of nitrogen release (in cal/g), and T_{onset} is determined by extrapolation of the tangent of the upward slope in the DSC experiment, to the fitted baseline of the plot (in °C). A value of ≥0 indicates that the analyzed compound may be shock-sensitive and/or explosive.[210]

[d] The explosive propagation metric (EP) was likewise determined according to Yoshida's methods. EP = log (Q_{DSC}) – 0.38 x log (T_{onset} – 25) – 1.67; where Q_{DSC} is the enthalpy of nitrogen release (in cal/g), and T_{onset} is measured as described above. A value of ≥0 indicates a risk of explosive propagation for the compound.

[e] Yoshida correlations provide conservative estimates to ensure that all compounds which have the potential to be either shock-sensitive and/or explosive are flagged for further testing. Impact tests for *mono*-diazirine **4.3** were performed (see below for data), and no propensity for explosion was observed.

4.5.2 Evaluation of crosslinker efficiacy by crosslinking of cyclohexane

4.5.2.1 Thermal insertion reactions for *bis*-diazirine 4.4, 4.5, 4.6 and *mono*-diazirine 4.3

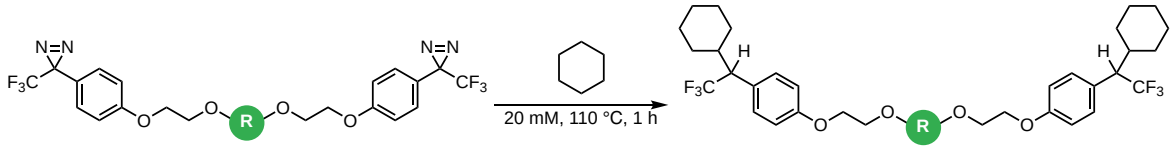

All reactions were conducted under an air atmosphere. A 20 mM solution of the desired crosslinker or *mono*-diazirine in cyclohexane was prepared in a vial. The reaction mixture was immersed in an oil bath at 110 °C for 1 hour. Upon confirming the absence of peaks at *ca.* –65 ppm (*bis*-diazirine or *mono*-diazirine) and *ca.* –57 ppm (diazo species) in the ^{19}F NMR spectra, the reaction was cooled to room temperature and concentrated *in vacuo* to provide crude product. ^{19}F NMR ($CDCl_3$) spectra of crude and isolated products were collected and compared. Conversions of *bis*-adduct products are reported in the following table.

Table S4.3 Thermal insertion reactions with cyclohexane

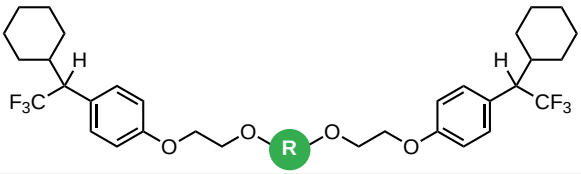	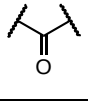 **4.7**	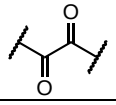 **4.8**	 **4.9**
Conversion	80%	71%	80%
Isolated yield	69%	58%	62%

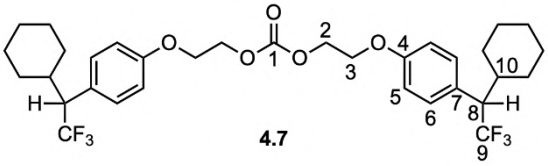

The reaction was performed as described in the above general procedure. *bis*-Diazirine **4.4** (50 mg, 0.096 mmol, 1.0 equiv.) provided 62 mg of crude product. The crude material was purified by silica gel chromatography (0–20% ethyl acetate in pentane) to afford the desired adduct **4.7** as a mixture of diastereomers (white solid, 42 mg; 69%). $\mathbf{R_f}$ = 0.2 (9:1 pentane:ethyl acetate). **^{1}H NMR** (500 MHz, $CDCl_3$) δ 7.14 (d, *J* = 8.6 Hz, 4H, H-6), 6.87 (d, *J* = 8.6 Hz, 4H, H-5), 4.51 (t, *J* = 4.7 Hz, 4H, H-2), 4.20 (t, *J* = 4.9 Hz, 4H, H-3), 2.98 (qd, *J* = 10.0, 8.2 Hz, 2H, H-8), 2.00 – 1.93 (m, 2H), 1.93 – 1.86 (m, 2H,

H-10), 1.79 – 1.72 (m, 2H), 1.67 – 1.58 (m, 4H), 1.52 – 1.45 (m, 2H), 1.34 – 1.23 (m, 2H), 1.21 – 1.02 (m, 6H), 0.85 – 0.75 (m, 2H). **^{13}C NMR** (126 MHz, $CDCl_3$) δ 157.98 (C-4), 155.16 (C-1), 130.45(C-6), 127.98 (C-7), 127.42 (q, *J* = 281.6 Hz, C-9), 114.62 (C-5), 66.42 (C-2), 65.69 (C-3), 55.45 (q, *J* = 25.1 Hz, C-8), 38.66 (C-10), 31.65, 30.80, 26.31, 26.23, 26.15. **^{19}F NMR** (471 MHz, $CDCl_3$) δ –63.71. **IR** (diamond-ATR) ν: 2926, 2855, 1749 (sharp, strong), 1614, 1514, 1452, 1229, 1183, 1151, 1134, 1099, 1081, 1041, 928, 832. **HRMS** (FD+) m/z $[M^{\bullet}]^+$ calculated for $C_{33}H_{40}F_6O_5$: 630.2774, found: 630.2791.

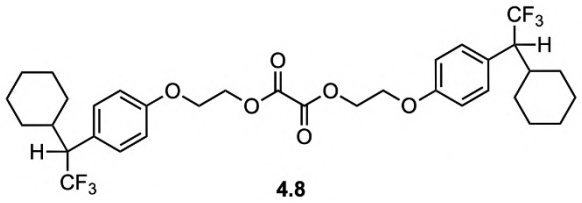

4.8

The reaction was performed as described in the above general procedure. *bis*-Diazirine **4.5** (50 mg, 0.092 mmol, 1.0 equiv.) provided 64 mg of crude product. The crude material was purified by silica gel chromatography (0–30% ethyl acetate in pentane) to afford the desired adduct **4.8** as a mixture of diastereomers (colorless oil, 35 mg; 58%). **R_f** = 0.7 (7:3 pentane:diethyl ether). **^{1}H NMR** (500 MHz, $CDCl_3$) δ 7.15 (d, *J* = 8.6 Hz, 4H), 6.88 (d, *J* = 8.7 Hz, 4H), 4.64 (t, *J* = 4.8 Hz, 4H), 4.26 (t, *J* = 4.9 Hz, 4H), 2.98 (qd, *J* = 10.1, 8.5 Hz, 2H), 2.00 – 1.94 (m, 2H), 1.94 – 1.86 (m, 2H), 1.80 – 1.72 (m, 2H), 1.69 – 1.58 (m, 4H), 1.53 – 1.45 (m, 2H), 1.32 – 1.27 (m, 2H), 1.18 – 1.05 (m, 6H), 0.85 – 0.76 (m, 2H). **^{13}C NMR** (126 MHz, $CDCl_3$) δ 157.84, 157.45, 130.49, 128.17, 127.40 (q, *J* = 281.6 Hz), 114.66, 65.29, 65.24, 55.45 (q, *J* = 24.8 Hz), 38.66, 31.65, 30.80, 26.30, 26.22, 26.14. **^{19}F NMR** (471 MHz, $CDCl_3$) δ –63.70. **IR** (diamond-ATR) ν: 2928, 2855, 1773 and 1750 (sharp, strong), 1613, 1514, 1452, 1306, 1254, 1154, 1099, 798. **HRMS** (FD+) m/z $[M^{\bullet}]^+$ calculated for $C_{34}H_{40}F_6O_6$: 658.2724, found: 658.2741.

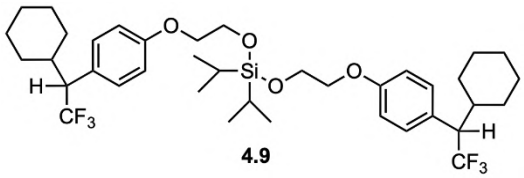

4.9

The reaction was performed as described in the above general procedure. *bis*-Diazirine **4.6** (50 mg, 0.083 mmol, 1.0 equiv.) provided 62 mg of crude product. The crude material was purified by silica gel chromatography (0–5% ethyl acetate in pentane) to afford the desired adduct **4.9** as a mixture of diastereomers (colorless oil, 37 mg; 62%). $\mathbf{R_f}$ = 0.9 (2:1 pentane:ethyl acetate). **^{1}H NMR** (500 MHz, $CDCl_3$) δ 7.12 (d, *J* = 8.7 Hz, 4H), 6.87 (d, *J* = 8.7 Hz, 4H), 4.17 – 4.01 (m, 8H), 2.97 (qd, *J* = 10.1, 7.8 Hz, 2H), 2.01 – 1.94 (m, 2H), 1.93 – 1.85 (m, 2H), 1.79 – 1.73 (m, 2H), 1.66 – 1.58 (m, 4H), 1.54 – 1.48 (m, 2H), 1.32 – 1.27 (m, 2H), 1.19 – 1.06 (m, 20H), 0.87 – 0.75 (m, 2H). **^{13}C NMR** (126 MHz, $CDCl_3$) δ 158.58, 130.35, 127.47 (q, *J* = 281.8 Hz), 127.40, 114.58, 69.23, 61.86, 55.44 (q, *J* = 25.1 Hz), 38.67, 31.66, 30.81, 26.32, 26.25, 26.17, 17.38, 12.23. **^{19}F NMR** (471 MHz, $CDCl_3$) δ –63.71. **^{29}Si NMR** (99 MHz, $CDCl_3$) δ –8.36. **IR** (diamond-ATR) ν: 2927, 2856, 1614, 1585, 1514, 1452, 1356, 1294, 1248, 1182, 1152, 1133, 1099, 969, 831, 692. **HRMS** (FD+) m/z $[M^{\bullet}]^+$ calculated for $C_{38}H_{54}F_6O_4Si$: 716.3690, found: 716.3691.

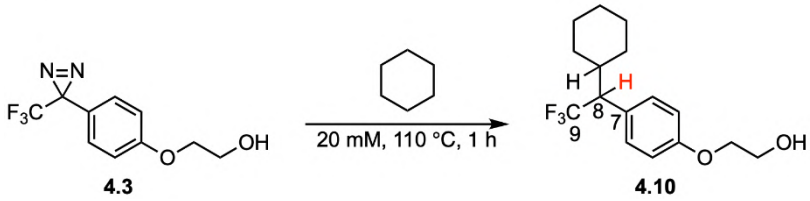

4.3 **4.10**

After cyclohexane insertion reaction, *mono*-diazirine **4.3** (36 mg, 0.15 mmol, 1.0 equiv.) provided 38 mg of crude product. The crude material was purified by silica gel chromatography (0–40% ethyl acetate in pentane) to afford the desired adduct **4.10** (pale-yellow oil, 30 mg; 66%). $\mathbf{R_f}$ = 0.6 (1:1 pentane:ethyl acetate). **^{1}H NMR** (500 MHz, CD_2Cl_2) δ 7.16 (d, *J* = 8.7 Hz, 2H), 6.90 (d, *J* = 8.8 Hz, 2H), 4.12 – 4.03 (m, 2H), 3.98 – 3.85 (m, 2H), 3.02 (qd, *J* = 10.3, 8.4 Hz, 1H), 2.09 – 2.01 (m, 1H), 2.00 – 1.88 (m, 2H), 1.80 – 1.72 (m, 1H), 1.67 – 1.59 (m, 2H), 1.51 – 1.45 (m, 1H), 1.37 – 1.25 (m, 1H), 1.22 – 1.04 (m, 3H), 0.87 – 0.77 (m, 1H). **^{13}C NMR** (126 MHz, CD_2Cl_2) δ 158.91, 130.88, 128.14 (q, *J* = 2.4 Hz, C-7), 128.05 (q, *J* = 281.4 Hz, C-9), 114.96, 69.95, 61.89, 55.71 (q, *J* = 24.8 Hz, C-8), 39.07, 32.05, 31.23, 26.73, 26.65, 26.60. **^{19}F NMR** (471 MHz, CD_2Cl_2) δ –63.98. **IR** (diamond-ATR) ν: 3368 (broad), 2927, 2855, 1614, 1514, 1452, 1294, 1245,

1182, 1152, 1134, 1098, 1081, 1048, 918, 832. **HRMS** (FD+) m/z $[M^{\bullet}]^{+}$ calculated for $C_{16}H_{21}F_3O_2$: 302.1488, found: 302.1501.

4.5.2.2 Photochemical insertion reactions at 395 nm

All reactions were conducted under an air atmosphere. A 20 mM solution of the desired crosslinker in cyclohexane was prepared in a vial. The reaction was irradiated with 395 nm LED Strip Lights (Waveform Lighting, 5129 lux, 53 W/m^2, 19 J/cm^2, when volume is 4.8 mL, *ca.* 247 J) for 1 hour. Upon confirming the absence of peaks at *ca.* –65 ppm (*bis*-diazirine) and *ca.* –57 ppm (diazo species) in the ^{19}F NMR spectra, the reaction mixture was concentrated *in vacuo* to provide the crude product. Crude ^{19}F NMR ($CDCl_3$) spectra were collected and compared. Conversions of *bis*-adduct products at 395 nm irradiation are reported in the following table. The low conversion % of compound **4.8** is due to the poor solubility of oxalate-linked *bis*-diazirine in cyclohexane at room temperature.

Table S4.4 Photochemical insertion reactions with cyclohexane

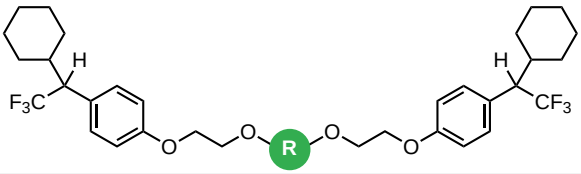		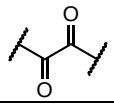	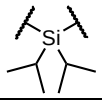
	4.7	**4.8**	**4.9**
Percent conversion to desired *bis*-adduct (measured by ^{19}F NMR)	75%	61%	75%

4.5.3 Evaluation of decrosslinking efficacy by hydrolysis of cyclohexane *bis*-adducts

4.5.3.1 Decrosslinking *bis*-adducts under basic conditions

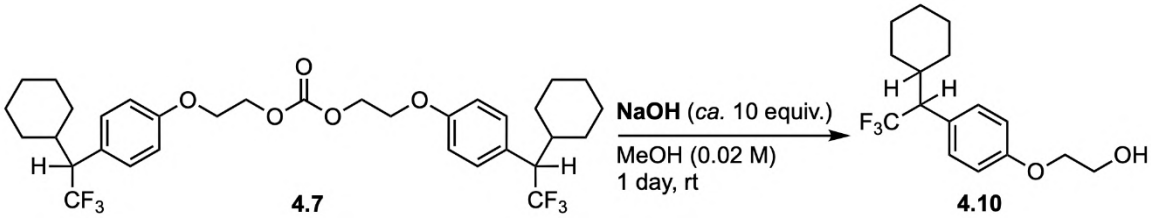

To a solution of *bis*-adduct **4.7** (0.014 g, 0.023 mmol, 1.0 equiv.) in methanol (1.4 mL, 0.023 M) at room temperature, 5 M NaOH (in water, 0.046 mL, 0.23 mmol, 10 equiv.) was added under ambient atmosphere. The reaction mixture was left at room temperature and stirred for 24 hours. After evaporation of the solvent, the residue was purified by silica gel chromatography (0–30 % ethyl acetate in pentane) to afford the desired product as a pale-yellow oil (0.017 g; 64%). Spectroscopic data are consistent with those reported above for compound **4.10**.

To follow the hydrolysis reaction spectroscopically, compound **4.7** (1–2 mg) was dissolved in CD_3OD (0.4 mL). NaOH (5 μL of 0.1 M) was added directly to the NMR tube. After *ca.* 4 hours, 90% of the starting material hydrolyzed and provided compound **4.10**. This experiment was done in triplicate and representative stacked ^1H NMR spectra are provided below (Figure S4.2).

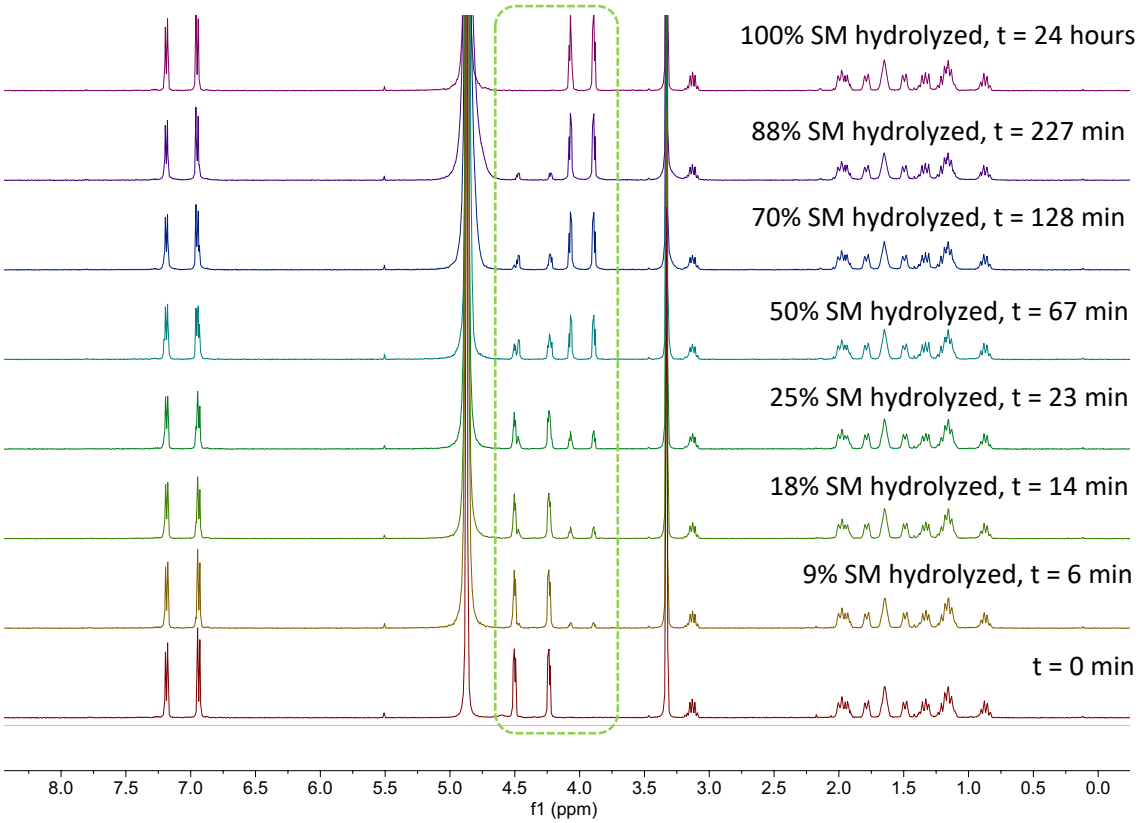

Figure S4.2 Stacked ^{1}H NMR spectra for the hydrolysis of compound **4.7** in CD_3OD under basic conditions.

4.5.3.2 Decrosslinking *bis*-adducts under acidic conditions

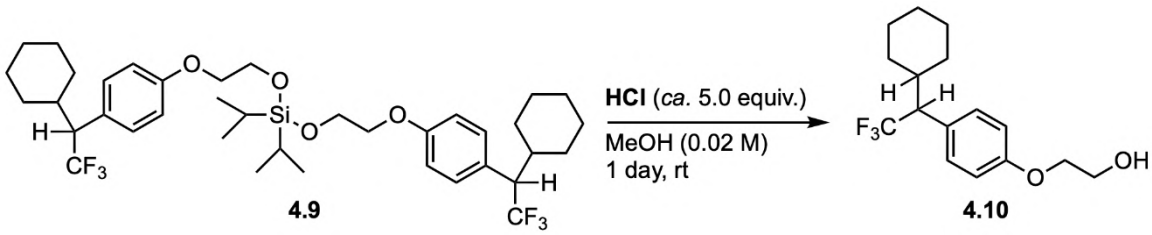

To a solution of *bis*-adduct **4.9** (0.023 g, 0.032 mmol, 1.0 equiv.) in methanol (1.4 mL, 0.023 M) at room temperature, 1 M HCl (in water, 0.16 mL, 0.16 mmol, 5.0 equiv.) was added under ambient atmosphere. The reaction mixture was left at room temperature and stirred for 24 hours. After evaporation of the solvent, the residue was purified by silica gel chromatography (0–30% ethyl acetate in pentane) to afford the desired product as a pale-yellow oil (0.017 g; 89%). Spectroscopic data are consistent with those reported above for compound **4.10**.

To follow the hydrolysis reaction spectroscopically, compound **4.9** (1–2 mg) was dissolved in CD_3OD (0.4 mL). HCl (5 µL of 0.1 M) was added directly to the NMR tube. After *ca.* 3 hours, more than 95% of the starting material hydrolyzed and provided compound **4.10**. This experiment was done in triplicate and representative stacked ^1H NMR spectra are provided below (Figure S4.3).

The oxalate-linked *bis*-adduct (compound **4.8**) was also found to hydrolyze under the acidic conditions described above, but further control experiments revealed that the MeOH solvent was playing a role in the cleavage reaction (*vide infra*).

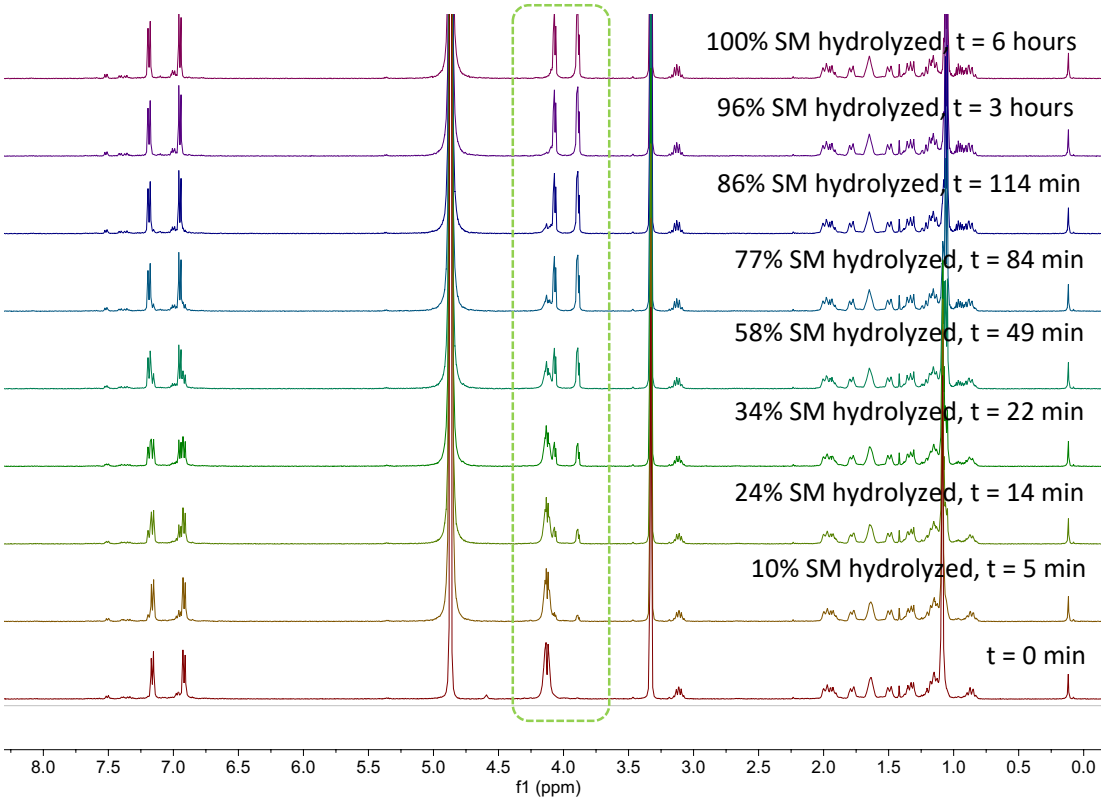

Figure S4.3 Stacked ^1H NMR spectra for the hydrolysis of compound **4.9** in CD_3OD under acidic conditions.

4.5.3.3 Decrosslinking *bis*-adduct 4.8 with MeOH and CD_3OD

In a parallel experiment, compound **4.8** (*ca.* 2 mg) was added into 0.5 mL of MeOH and CD_3OD respectively. After reacting overnight at room temperature, compound **4.8** in CD_3OD was found to be 92% hydrolyzed (including 20% hydrolyzed product present at t = 0 min) and no hydrolysis was observed in MeOH only.

We then compared the ^1H NMR of MeOH and CD_3OD (3 μL each), respectively in $CDCl_3$ with internal standard (1,3,5-trimethoxybenzene) present and found that there is more water content in MeOH ("wet MeOH") compared to CD_3OD (Figure S4.4).

Later we added 20 wt% (of 0.5 mL MeOH) 3 Å molecular sieves into the reaction in MeOH. Within 3 hours, compound **4.8** hydrolyzed completely (Figure S4.5).

In another control experiment, we mixed 0.5 mL CD_3OD and 0.15 mL distilled water and left it overnight to mimic the "wet MeOH". We then add compound **4.8** (*ca.* 2 mg) into the prepared "wet" CD_3OD and stirred for 4 hours. We then removed the CD_3OD solution and re-add $CDCl_3$ to obtain a clear ^1H NMR sample. At the same time, we examined a vehicle control sample of compound **4.8** only in $CDCl_3$ after stirring for 4 hours. From the ^1H NMR spectra (including 50% hydrolyzed product present at t = 0 min), there was less than 2% hydrolysis of compound **4.8** in "wet" CD_3OD (Figure S4.6). Therefore, we propose that hydrogen bonding within MeOH effectively renders the solvent less nucleophilic than CD_3OD.

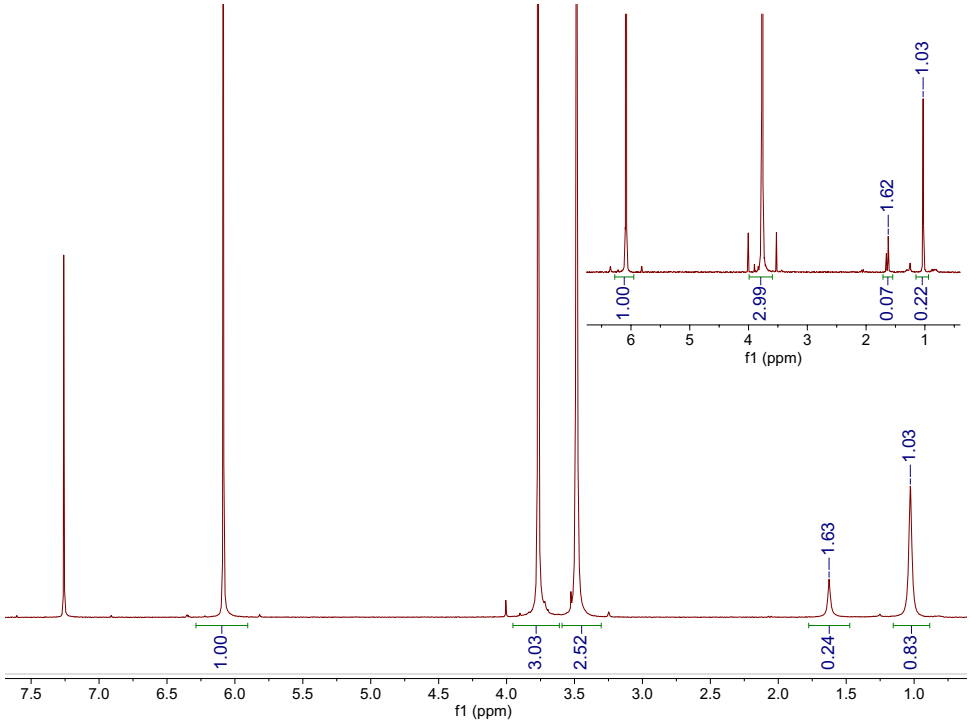

Figure S4.4 ^{1}H NMR spectra show different percentage water content in MeOH and CD_3OD (inset).

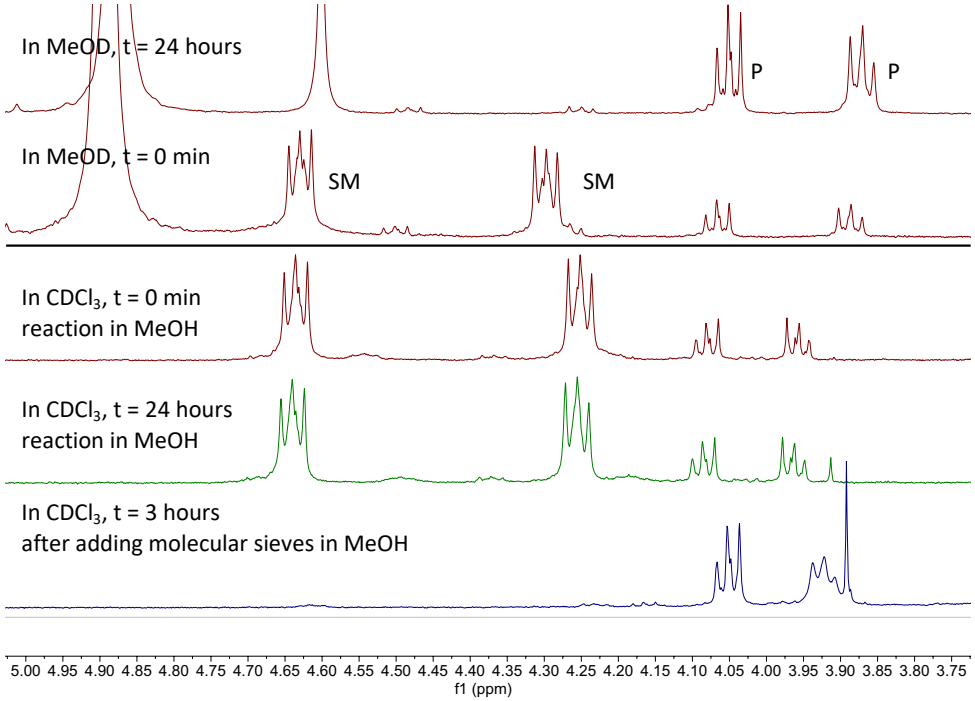

Figure S4.5 Stacked ^{1}H NMR spectra for the hydrolysis of compound **4.8** in CD_3OD and MeOH respectively.

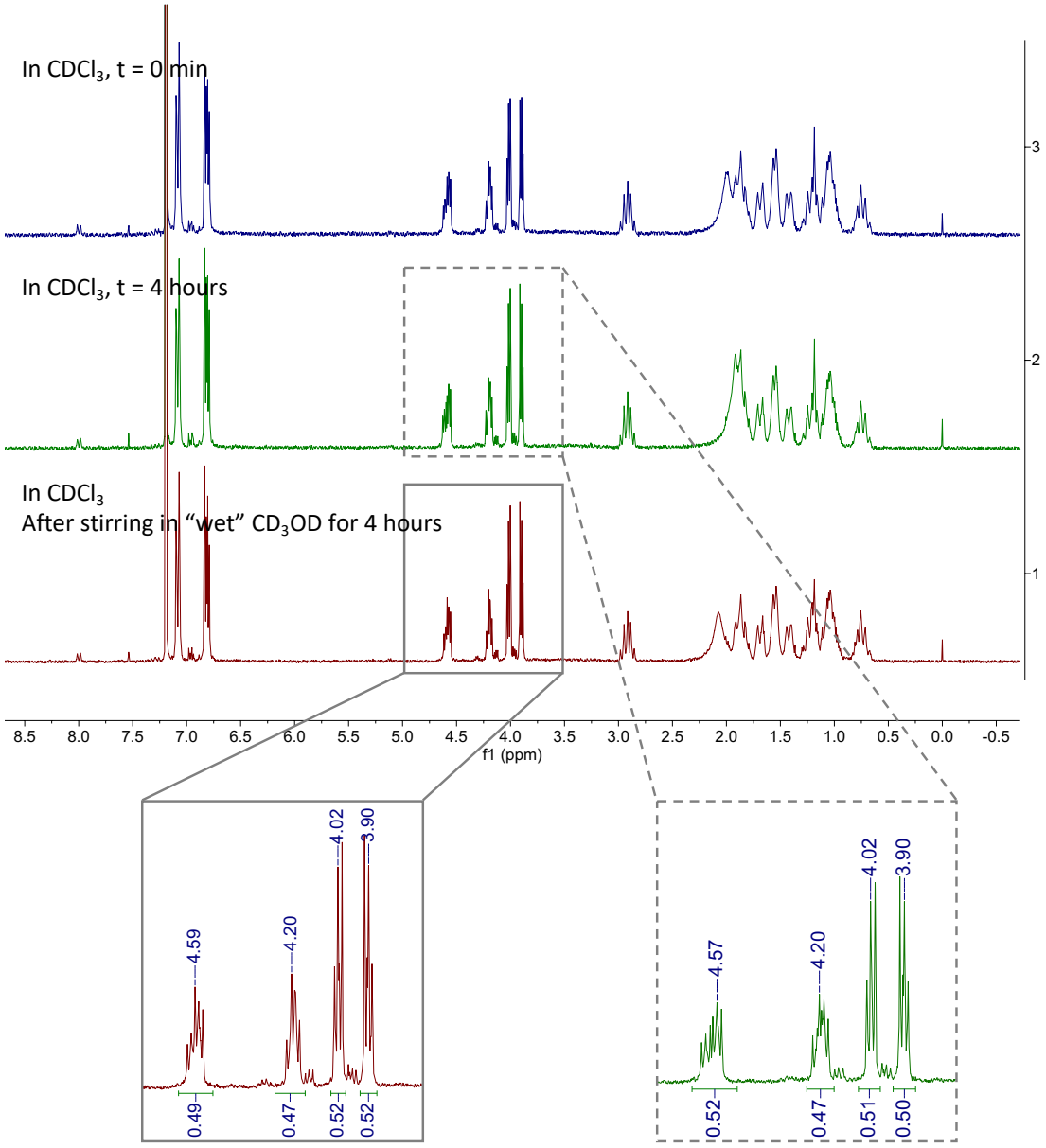

Figure S4.6 Stacked ^{1}H NMR spectra for the hydrolysis of compound **4.8** in "wet" CD_3OD and $CDCl_3$ (vehicle control) respectively.

4.5.3.4 Decrosslinking *bis*-adduct 4.9 with TBAF

To follow the hydrolysis reaction spectroscopically, compound **4.9** (2 mg) was dissolved in $CDCl_3$ (0.4 mL). TBAF (tetrabutylammonium fluoride, 5 µL of 1.0 M in THF solution) was added directly to the NMR tube. After two days, more than 90% of the starting material hydrolyzed and provided compound **4.10**. Representative stacked ^1H NMR spectra are provided below (Figure S4.7).

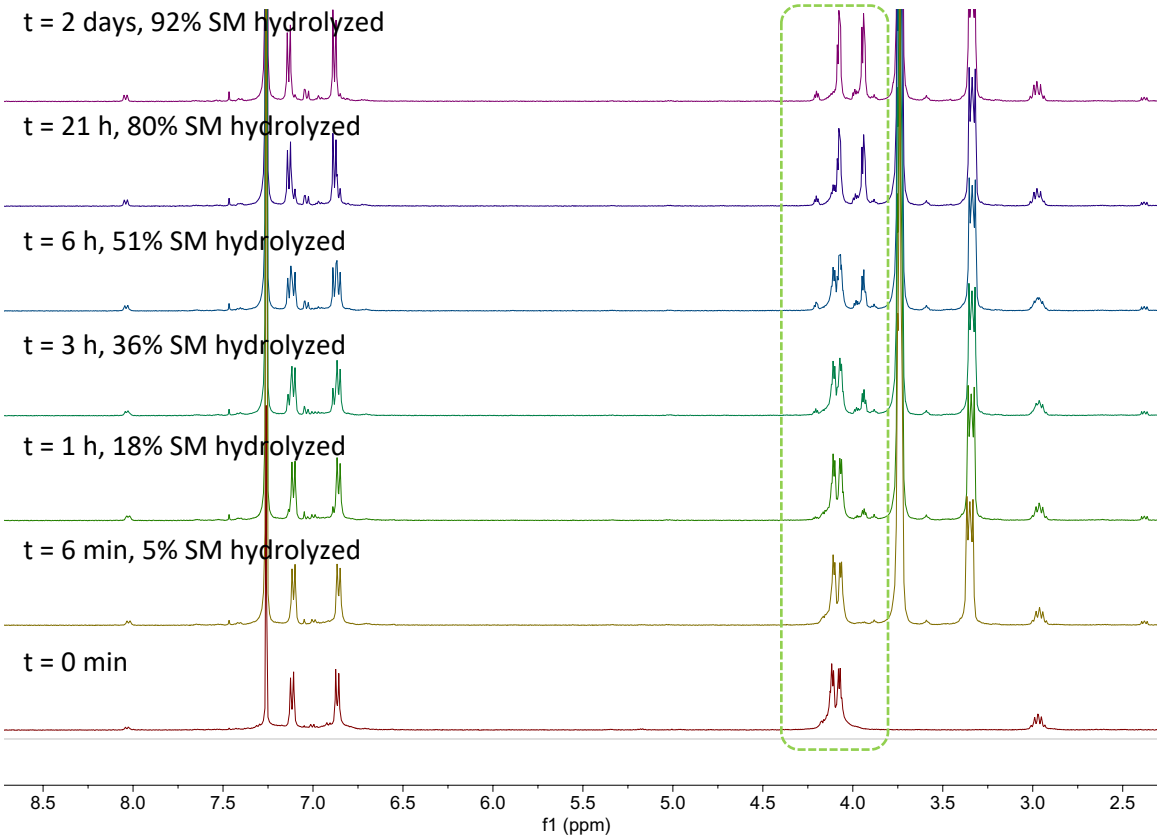

Figure S4.7 Stacked ^1H NMR spectra of compound **4.9** reacting with TBAF in $CDCl_3$.

4.5.4 Complete procedure for crosslinking/decrosslinking of paraffin wax

4.5.4.1 Crosslinking of paraffin wax

Material used: paraffin wax was purchased from Sigma-Aldrich (ref 327212, m.p. = 58–62 °C, CAS 8002-74-2). An approximate chemical formula of $C_{31}H_{64}$ was estimated by determining the relative ratio of methyl (CH_3) and methylene (CH_2) groups observable in the ^1H and DEPT-135 NMR (Figure S4.8), together with the approximate molecular weight observed in the SEC experiments discussed below.

Procedure: a series of samples was prepared by mixing paraffin wax (100 mg) with various amounts of *bis*-diazirine **4.4**, **4.5**, **4.6** or **4.11** in glass vials (Table S4.5). DCM (200 µL) was added to each vial, following which all vials were sonicated (280 W for 30 seconds) and gently heated at 40 °C for 30 min with lid, then left at 40 °C without lid 2 days for drying (Figure S4.9a). The removal of solvents was monitored by measuring the weights of each vial over the whole process. The samples were placed in a heating block (appropriately chosen to snugly fit each vial) and heated at 80 °C for 3 hours. This induced crosslinking via thermal activation. Once cooled, all samples were opaque solid at room temperature (Figure S4.9b).

SEC analysis: *ca.* 5 mg samples were each dissolved in 1 mL THF. The solutions were then filtered through a 0.2 µm PTFE filter directly into vials for SEC analysis. A vehicle control sample (VC, sample A) was prepared in the same way without the addition of any crosslinker. All filtered samples were clear solutions. The relevant portion of the chromatograms obtained from the refractive index detector are displayed in Figure S4.10.

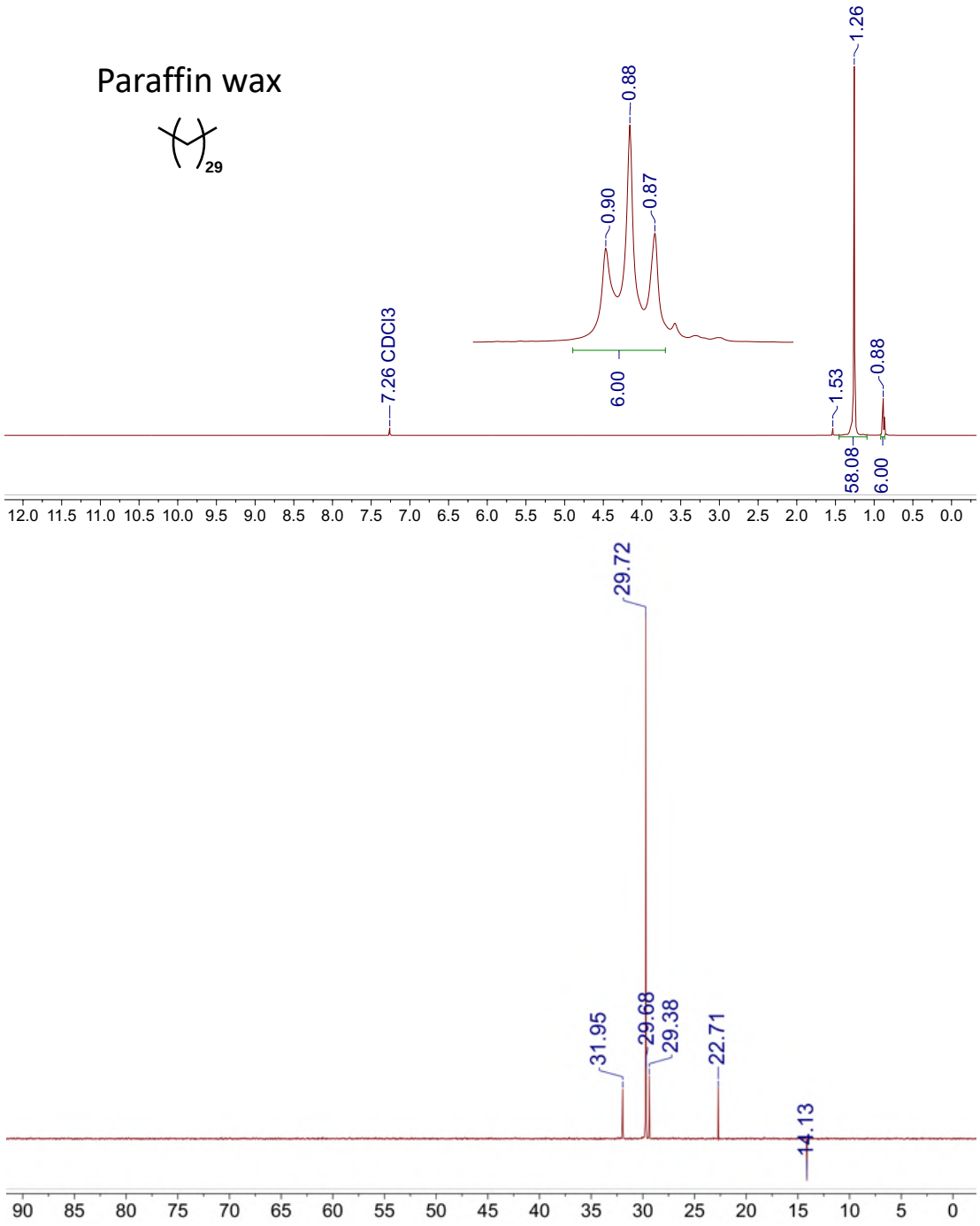

Figure S4.8 ^{1}H and DEPT-135 NMR spectra of paraffin wax in $CDCl_3$.The lack of methyne groups in the DEPT NMR spectrum indicates a low percentage of polymer branching, indicating that the sample can be represented by the approximate molecular formula CH_3-$(CH_2)_n$-CH_3. The ratio of methyl to methylene protons in the ^{1}H NMR spectrum (6:58) indicates an average of 29 methylene groups within the chain.

Table S4.5 Composition of paraffin wax samples doped with *bis*-diazirine crosslinkers

Sample	Crosslinker added	Loading (mol%)	crosslinker MW (g/mol)	Crosslinker (mg)	Loading (wt%)
A	n/a	0	n/a	0	0
B	**4.11**	10	514.5	11.8	11.8
C	**4.4**	10	518.4	11.9	11.9
D	**4.5**	10	546.4	12.5	12.5
E	**4.6**	10	604.6	13.9	13.9
F	**4.4**	20	518.4	24.0	24.0
G	**4.4**	50	518.4	59.4	59.4

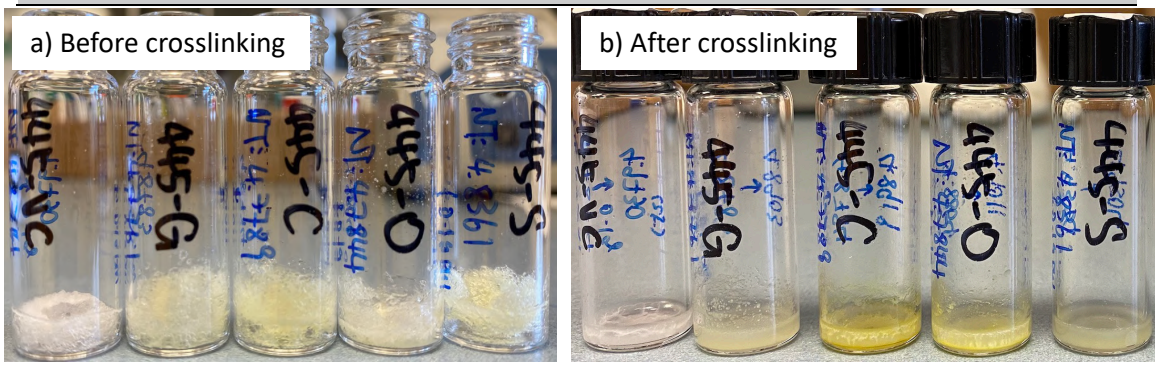

Figure S4.9 Samples of paraffin wax at various stages of the crosslinking process: a) loaded gel after drying 2 days, before crosslinking; and b) after crosslinking and cooling to room temperature.

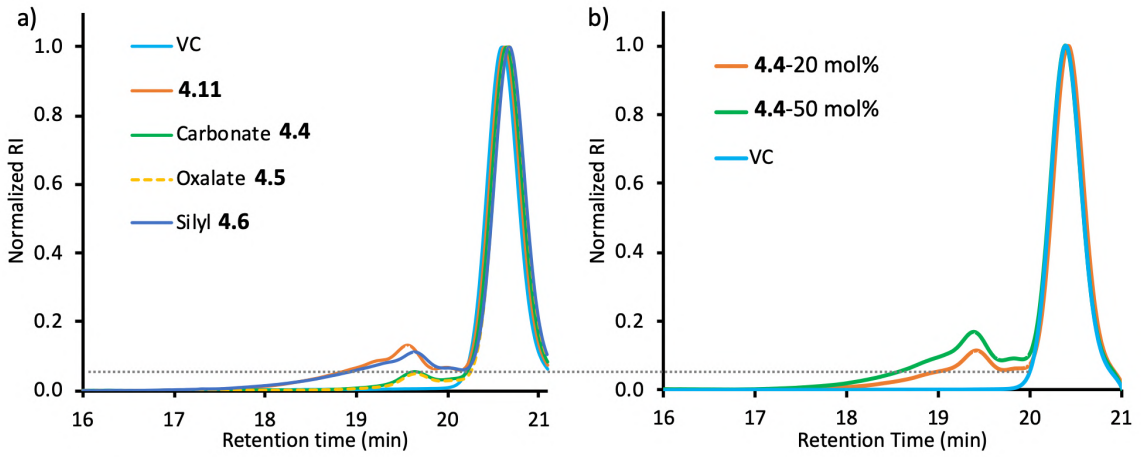

Figure S4.10 SEC traces derived from the crosslinking of: a) 10 mol% *bis*-diazirine-doped paraffin wax; and b) 20 mol% *bis*-diazirine-doped paraffin wax. Panel (a) shows

that *bis*-diazirines **4.11** and **4.6** provided similar crosslinking efficacy, whereas carbonate and oxalate linked crosslinkers afforded lower crosslinking efficacy. The incompatibility between the polar tether of the crosslinker and the polymer substrate resulted in phase separation, which leads to the lower crosslinking efficacy (Figure S4.14b). As expected, panel (b) shows that increased crosslinker **4.4** loading leads to enhanced polymer network formation, as evidenced by an increase in the size of the lower-retention time peak. RI, refractive index.

4.5.4.2 Decrosslinking of crosslinked paraffin wax

Procedure with NaOH treatment: three samples were prepared by mixing previously crosslinked materials (sample A, F and G, each 50 mg) with NaOH solution in glass vials. Ethanol (100 µL), methanol (100 µL) and 5 M NaOH (in water, 100 µL) were added to each vial, following which all vials were heated at 80 °C overnight and then sonicated (280 W for 7 hours at 60 °C). All vials were then heated at 60 °C for two more days to remove residual solvent.

The other set of samples were prepared by mixing previously crosslinked materials (sample A, B, C and D, each 50 mg) with NaOH solution in glass vials. Tetrahydrofuran (1 mL), methanol (200 µL) and 1 M NaOH (in water, 200 µL) were added to each vial, following which all vials were heated at 60 °C for *ca.* 40 hours and sonicated (280 W for 2 hours at 60 °C). All vials were then heated at 60 °C for two more days to remove residual solvent.

Procedure with HCl treatment: three samples were prepared by mixing previously crosslinked materials (sample A, B and E, each 50 mg) with HCl solution in glass vials. Tetrahydrofuran (1 mL), methanol (200 µL) and 1 M HCl (in water, 200 µL) were added to each vial, following which all vials were handled identically to the protocol described above for the NaOH procedure. The previous crosslinking vehicle control (sample A) was divided into two vials and processed with either NaOH or HCl treatment as needed.

SEC analysis: *ca.* 5 mg samples were each dissolved in 1 mL THF. The solutions were then filtered through a 0.2 µm PTFE filter directly into vials for SEC analysis. All filtered samples were clear solutions. The relevant portion of the chromatograms obtained from the refractive index detector are displayed in Figure S4.11.

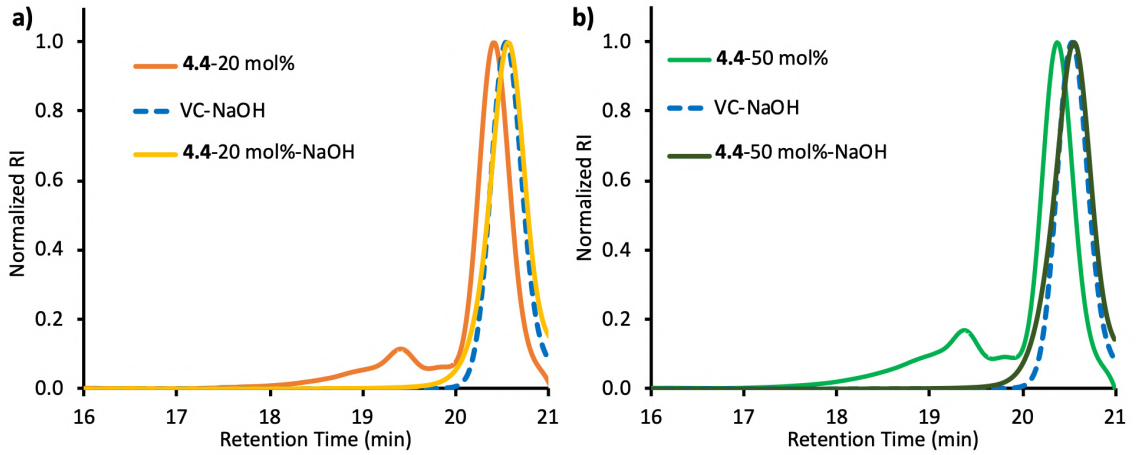

Figure S4.11 SEC traces derived from the decrosslinking of: a) 20 mol% **4.4** (carbonate)-doped paraffin wax after NaOH treatment, and b) 50 mol% **4.4** (carbonate)-doped paraffin wax after NaOH treatment.

4.5.5 Complete procedure for crosslinking/decrosslinking of poly(ethylene glycol)

4.5.5.1 Crosslinking of poly(ethylene glycol)

Material used: poly(ethylene glycol) 1500 (PEG) from Alfa Aesar (A16241, $H(OCH_2CH_2)_nOH$, m.p. = 44–48 °C, CAS 25322-68-3)

Procedure: five samples were prepared by mixing monodisperse PEG (100 mg, 1500 g/mol was used for calculation) with various amounts of *bis*-diazirine **4.5** or **4.11** in glass vials (Table S4.6). DCM (200 µL) was added to each vial, following which all vials were sonicated (280 W for 30 seconds) and gently heated at 40 °C for 6 hours without lid, then left to dry in the fume hood overnight (Figure S4.12a). The removal of solvents was monitored by measuring the weights of each vial over the whole process. The samples were placed in a heating block (appropriately chosen to snugly fit each vial) and heated at 100 °C for 2.5 hours. This induced crosslinking via thermal activation. Once cooled, all samples were opaque solid at room temperature (Figure S4.12b).

SEC analysis: *ca.* 5 mg samples were each dissolved in 1 mL THF. The solutions were then filtered through a 0.2 µm PTFE filter directly into vials for SEC analysis. A vehicle control was prepared in the same way without the addition of any crosslinker and an untreated sample was prepared by dissolving 5 mg of original PEG into 1 mL of THF and filtering the resulting solution through a 0.2 µm PTFE filter. All filtered samples were clear solutions. The relevant portion of the chromatograms obtained from the refractive index detector are displayed in Figure S4.13.

Table S4.6 Composition of PEG samples doped with *bis*-diazirine crosslinkers

Sample	PEG (mg)	Loading (mol%)	**4.5** (mg) (546.4 g/mol)	**4.11** (mg) (514.5 g/mol)	Loading (wt%)
A	100	0	0	0	0
B	100	10	0	3.4	3.4
C	100	20	0	6.9	6.9
D	100	10	3.6	0	3.6
E	100	20	7.3	0	7.3

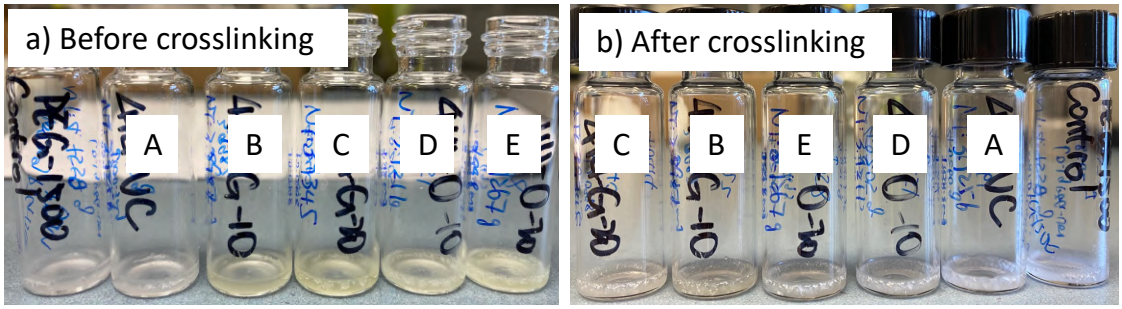

Figure S4.12 Samples of PEG at various stages of the crosslinking process: a) loaded gel after drying overnight, before crosslinking; and b) after crosslinking and cooling to room temperature.

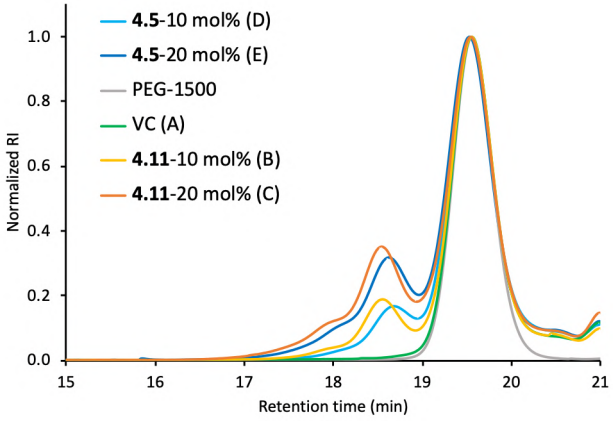

Figure S4.13 SEC traces derived from the crosslinking of compound **4.5** or **4.11**-doped PEG. As expected, increased crosslinker loading leads to larger polymer network, as evidenced by increases in retention time and concentration of larger polymer network. RI, refractive index. PEG-1500, original PEG.

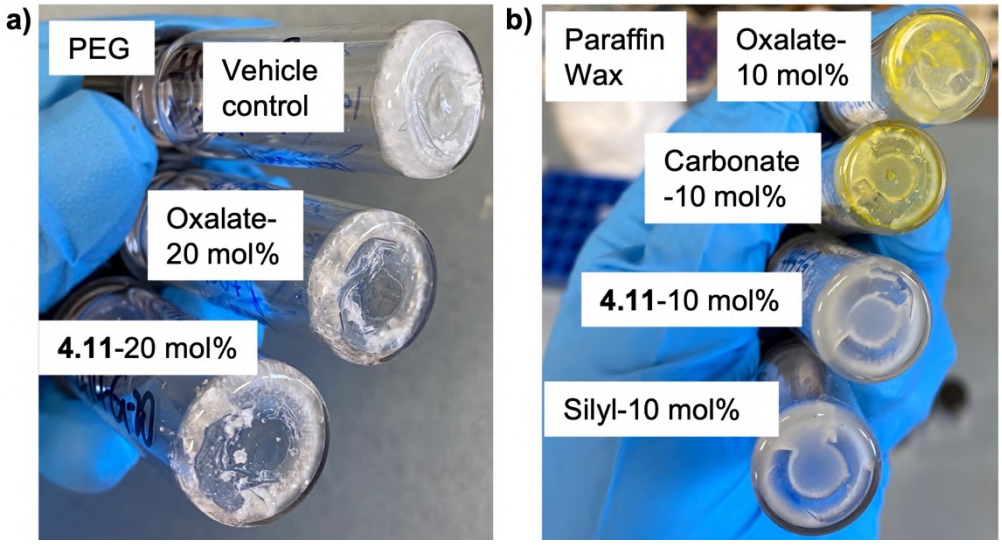

Figure S4.14 a) Within the PEG substrate, *bis*-diazirine **4.11** and **4.5** show similar crosslinking efficacy from SEC analysis and there is no visible difference between the crosslinked polymer samples. b) In non-polar polymer (paraffin wax) substrate, the relatively non-polar tether in *bis*-diazirine **4.11** and **4.6** (silyl-linked) provided more homogenous crosslinked sample that led to higher crosslinking efficacy (Figure S4.10a).

4.5.5.2 Decrosslinking of crosslinked poly(ethylene glycol)

Procedure with NaOH treatment: five samples were prepared by mixing previous materials (samples A–E, each 10 mg) with 0.5 M NaOH (in water, 5 µL) in glass vials. Methanol (*ca.* 300 µL) was added to each vial, following which all vials were mixed for 2 hours on a vortex mixer and then left at ambient temperature (*ca.* 20 °C) for drying overnight.

SEC analysis: *ca.* 5 mg samples were each dissolved in 1 mL THF. The solutions were then filtered through a 0.2 µm PTFE filter directly into vials for SEC analysis. All filtered samples were clear solutions. The relevant portion of the chromatograms obtained from the refractive index detector are displayed in Figure S4.15.

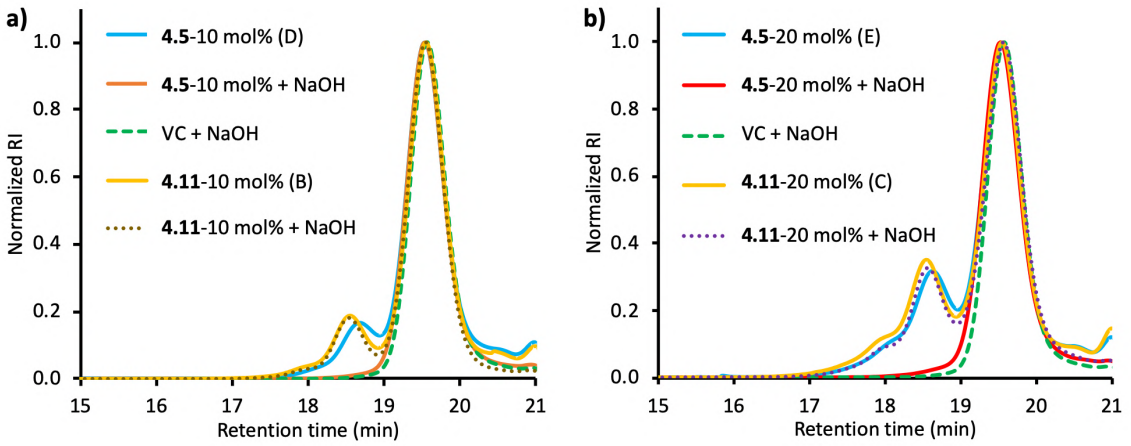

Figure S4.15 SEC traces derived from the decrosslinking of: a) 10 mol% **4.5** (oxalate) or **4.11**-doped PEG after NaOH treatment; and b) 20 mol% **4.5** (oxalate) or **4.11**-doped PEG after NaOH treatment.

4.5.6 Complete procedure for crosslinking/decrosslinking of isotactic polypropylene and analysis of thermal properties by DSC

4.5.6.1 Crosslinking of isotactic polypropylene

Material used: isotactic polypropylene (Sigma-Aldrich, ref 428116, average M_w ~12000, average M_n ~5000, m.p. = 157 °C, CAS 9003-07-0)

Procedure: Three samples were prepared by mixing isotactic polypropylene (iPP, 100 mg) with various amounts of *bis*-diazirine **4.5** or **4.11** in glass vials (Table S4.7). Toluene (300 µL) was added to each vial, following which all vials were sonicated (280 W for 30 seconds) and gently heated at 40 °C for drying overnight. The removal of solvents was monitored by measuring the weights of each vial over the whole process. Upon drying, the gels turned into white solids. Overall, this procedure allowed the homogenous dispersion of *bis*-diazirine crosslinkers into iPP matrices. The samples were placed in a heating block (appropriately chosen to snugly fit each vial) and heated at 110 °C for 2 hours. This induced crosslinking via thermal activation. Once cooled, all samples were opaque solid at room temperature and a small portion (3–10 mg) was taken from each vial for DSC analysis. A vehicle control (VC) was prepared in the same way without the addition of any crosslinker (Sample A).

DSC analysis: Samples of the analyzed substance (typically 4 to 9 mg) were placed in Tzero pans and sealed by a Tzero hermetic lid. The sample was placed in the oven of a DSC25 device (with an identical-sealed empty pan as a reference) and analyzed on the following cycle under a flow of nitrogen (50 mL/min) at 10 °C/min: –90 °C → 200 °C → –90 °C → 200 °C. The corresponding enthalpies of crystallization (exotherm, $\Delta H_{crystal}$) and melting (endotherm, ΔH_{fusion}) transitions were recorded from the cooling and second heating phase. Representative DSC traces were provided below.

Table S4.7 Composition of iPP samples doped with *bis*-diazirine crosslinkers

Sample	iPP (mg)	Loading (wt%)	**4.5** (mg) (546.4 g/mol)	**4.11** (mg) (514.5 g/mol)
A	100	0	0	0
B	100	10	10	0
C	100	10	0	10

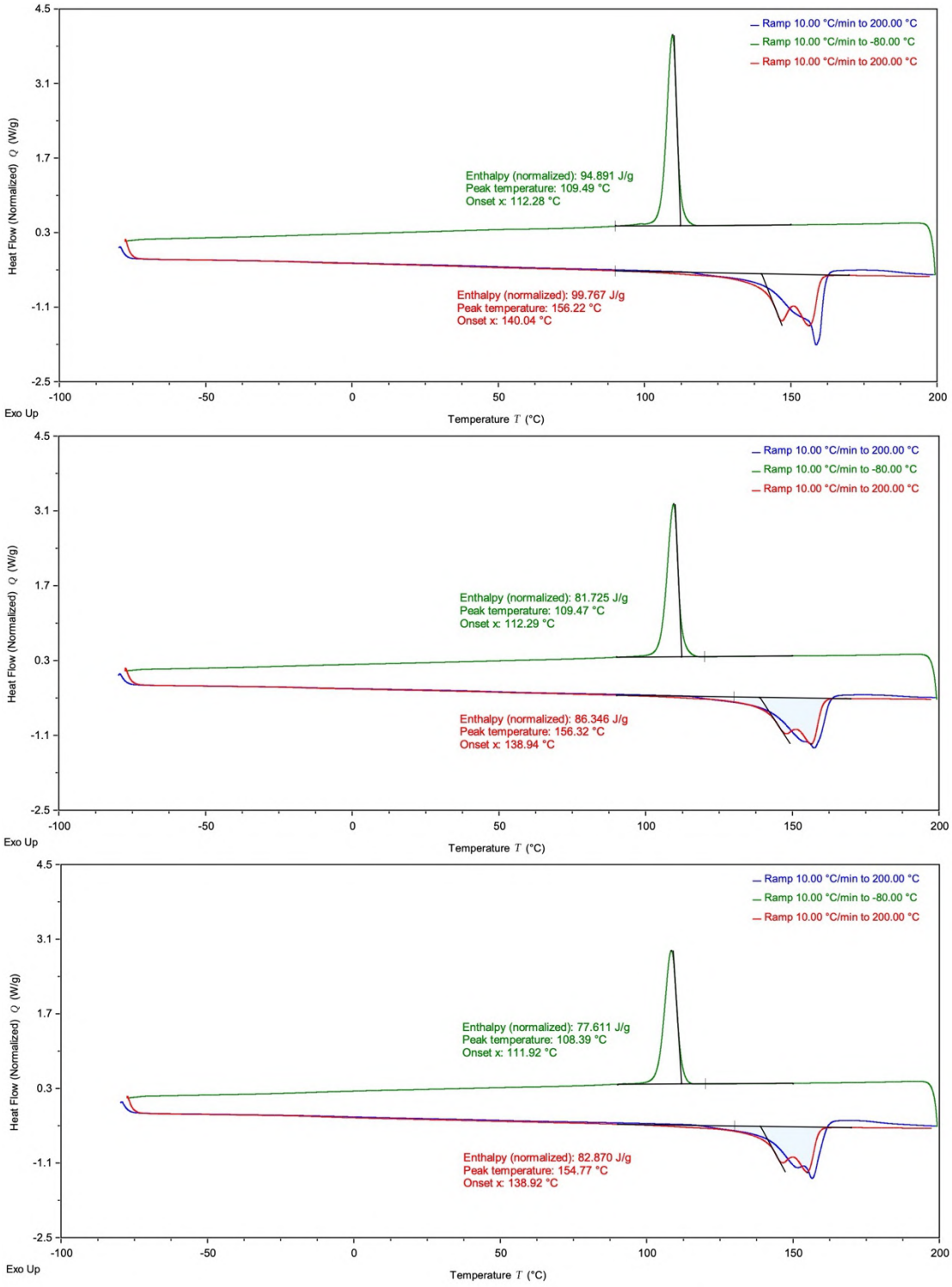

Figure S4.16 DSC traces for iPP vehicle control (top, sample A, no crosslinker added), iPP crosslinked with 10 wt% of **4.5** (middle, sample B), iPP crosslinked with 10 wt% of **4.11** (bottom, sample C).

4.5.6.2 Decrosslinking of crosslinked isotactic polypropylene

Procedure: three samples were prepared by mixing the crosslinked materials described above (sample A, B and C, 50 mg) with NaOH solution in glass vials. Toluene (200 μL), ethanol (200 μL), 1 M NaOH (in MeOH, 400 μL) and 5 M NaOH (in water, 100 μL) were added to each vial, following which all vials were sonicated (280 W for 5.5 hours) and heated at 70 °C for two more days to remove residual solvent. Then water (1–2 mL) was added to wash off (30 seconds sonication) the residual NaOH by filtration and this process was repeated two times for each sample. Once the sample was dry, a small portion (3–10 mg) was taken from each vial for DSC analysis. The previous vehicle control (VC) was brought through an identical treatment procedure.

DSC analysis: samples were analyzed by the method described above for crosslinked iPP. The corresponding enthalpies of crystallization (exotherm, $\Delta H_{crystal}$) and melting (endotherm, ΔH_{fusion}) transitions were recorded from the cooling and second heating phase. Representative DSC traces are provided below.

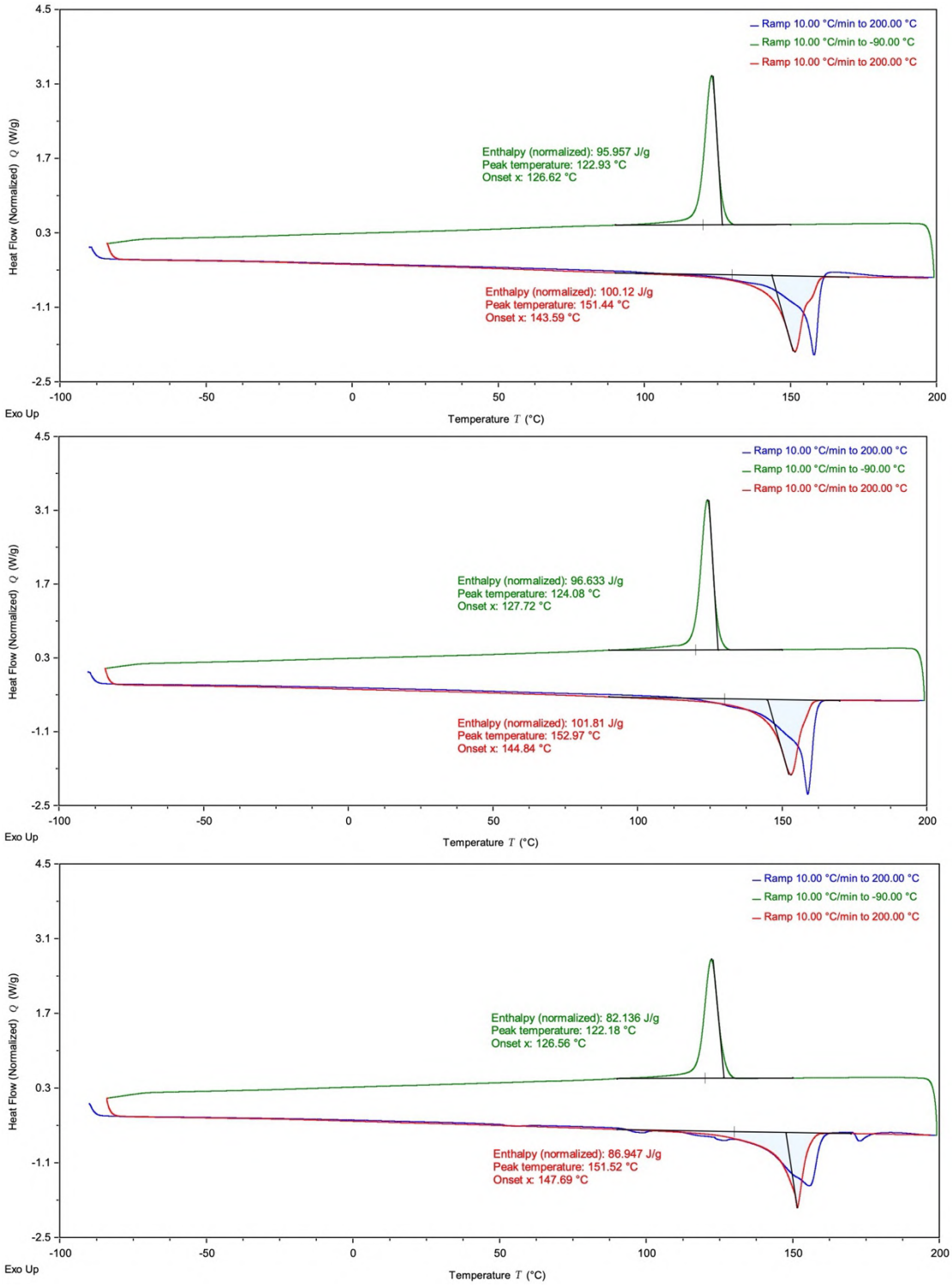

Figure S4.17 DSC traces for iPP vehicle control after NaOH treatment (top, sample A), iPP crosslinked with 10 wt% of **4.5** after NaOH treatment (middle, sample B), iPP crosslinked with 10 wt% of **4.11** after NaOH treatment (bottom, sample C).

4.5.7 Complete procedure for crosslinking/decrosslinking of iPP and PE composite materials, and analysis of thermal properties by DSC

4.5.7.1 Crosslinking of iPP and PE composites

Material used: isotactic polypropylene (Sigma-Aldrich, ref 428116, average M_w ~12000, average M_n ~5000, m.p. = 157 °C, CAS 9003-07-0) and polyethylene (Sigma-Aldrich, ref 427772, average M_w ~4000, average M_n ~1700, m.p. = 92 °C, CAS 9002-88-4).

Procedure: five samples were prepared by mixing isotactic polypropylene (iPP, 100 mg) and polyethylene (PE, 100 mg) with *bis*-diazirine **4.4**, **4.5**, **4.6** or **4.11** (10 wt% = 20 mg for each crosslinker) in glass vials. Toluene (400 µL) and dichloromethane (100 µL) were added to each vial, following which all vials were sonicated (280 W for 30 seconds) and gently heated at 40 °C for drying overnight (Figure S4.18a). The removal of solvents was monitored by measuring the weights of each vial over the whole process. Upon drying, the gels turned into white-yellow solids. Overall, this procedure allowed the homogenous dispersion of *bis*-diazirine crosslinkers into iPP and PE matrices. The samples were placed in a heating block (appropriately chosen to snugly fit each vial) and heated at 110 °C for 2 hours. This induced crosslinking via thermal activation. Once cooled, all samples were opaque solid at room temperature (Figure S4.18b) and a small portion (3–10 mg) was taken from each vial for DSC analysis.

DSC analysis: samples were placed in Tzero pans and sealed by a Tzero hermetic lid. The sample was placed in the oven of a DSC25 device (with an identical-sealed empty pan as a reference) and analyzed on the following cycle under a flow of nitrogen (50 mL/min) at 10 °C/min: –90 °C → 200 °C → –90 °C → 200 °C. The corresponding enthalpies of crystallization (exotherm, $\Delta H_{crystal}$) and melting (endotherm, ΔH_{fusion}) transitions were recorded from the cooling and second heating phase (Table S4.8). Representative DSC traces are provided in the Appendix B.

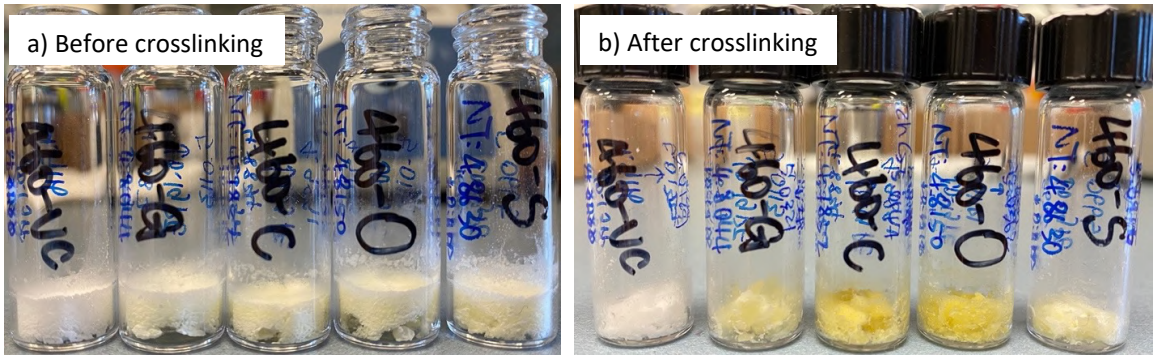

Figure S4.18 Samples of iPP and PE mixture at various stages of the crosslinking process: a) loaded gel after drying overnight; and b) after crosslinking and cooling to room temperature.

Table S4.8 Evolution of thermal properties of iPP and PE mixture with different *bis*-diazirine crosslinkers

Sample	iPP (mg)	PE (mg)	Loading (wt%)	Crosslinker (mg)	$\Delta H_{crystal}$ (J/g)[a]	ΔH_{fusion} (J/g)[b]
VC	100	100	0	0	88.8	90.7
G (**4.11**)	100	100	10	20	79.1 (89%)	79.8 (88%)
C (**4.4**)	100	100	10	20	66.1 (74%)	65.5 (72%)
O (**4.5**)	100	100	10	20	70.2 (79%)	71.5 (79%)
S (**4.6**)	100	100	10	20	68.7 (77%)	69.2 (76%)

[a] In all five samples, the integrated region for crystallization enthalpy is from 50 to 120 °C.
[b] In all five samples, the integrated region for fusion enthalpy is from 50 to 170 °C.

4.5.7.2 Decrosslinking of crosslinked iPP and PE composites

Basic hydrolysis: four samples were prepared by mixing the samples prepared above (sample VC, G, C and O, 100 mg) with NaOH solution in glass vials. Toluene (400 µL), ethanol (400 µL), 1 M NaOH (in MeOH, 400 µL) and 5 M NaOH (in water, 200 µL) were added to each vial, following which all vials were sonicated (280 W for 7 hours) and heated at 60 °C for two days to remove residual solvent. Then water (1–2 mL) was added to wash off (using 30 seconds sonication) the residual NaOH by filtration and this process was repeated three times for each sample. Once the sample was dry, a small portion (3–10 mg) was taken from each vial for DSC analysis. The previously described

samples VC and G were brought through the same abovementioned procedure as negative and positive controls.

TBAF hydrolysis: three samples were prepared by mixing previously crosslinked sample S (100 mg), VC (50 mg, negative control) and G (50 mg, positive controls) respectively with TBAF solution in glass vials. Toluene (200 μL) and TBAF (1 M in THF, 400 μL) were added to each vial, following which all vials were sonicated (280 W for 3 hours) and heated at 60 °C for overnight to remove residual solvent. Then water (1–2 mL) was added to wash off (using 30 seconds sonication) the residual salts by filtration and this process was repeated three times for each sample. After aqueous wash, DCM (1–2 mL) was added to wash off the residual organic by-products and repeated three times. Once the sample was dry, a small portion (3–10 mg) was taken from each vial for DSC analysis.

DSC analysis: samples were analyzed by the method described above for crosslinked iPP+PE. The corresponding enthalpies of crystallization (exotherm, $\Delta H_{crystal}$) and melting (endotherm, ΔH_{fusion}) transitions were recorded from the cooling and second heating phase. Representative DSC traces are provided in the Appendix B.

4.5.8 Post-cleavage functionalization

4.5.8.1 Recrosslinking a functionalized (decrosslinked) cyclohexane adduct

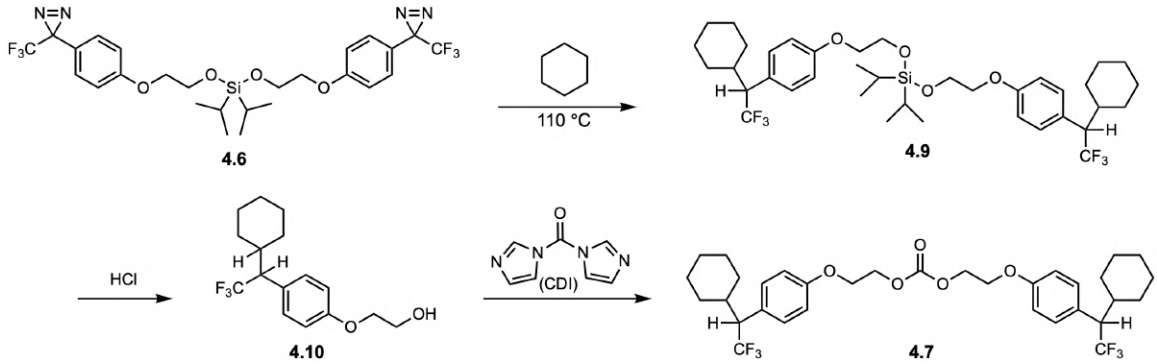

To a solution of *mono*-adduct **4.10** (from hydrolyzed compound **4.9**, 0.01 g, 0.033 mmol, 1.0 equiv.) in CH_3CN (0.2 mL, 0.2 M) at room temperature, 1,1'-carbonyldiimidazole (CDI, 0.0054 g, 0.033 mmol, 1.0 equiv.) was added under ambient atmosphere. After 30 min stirring at room temperature, the second equivalent of *mono*-adduct **4.10** (0.01 g, 0.033 mmol, 1.0 equiv.) was added into the abovementioned reaction mixture, followed by K_2CO_3 (0.0069 g, 0.05 mmol, 1.5 equiv.). The reaction mixture was left at room temperature and stirred for 24 hours. The reaction was then quenched with NH_4Cl saturated solution and extracted with diethyl ether (× 3). The combined organic layers were dried over sodium sulfate. After evaporation of the solvent, the desired product was afforded as white solid (0.019 g; 92%). Spectroscopic data are consistent with those reported above for compound **4.7**. Representative ^1H NMR spectra are provided below.

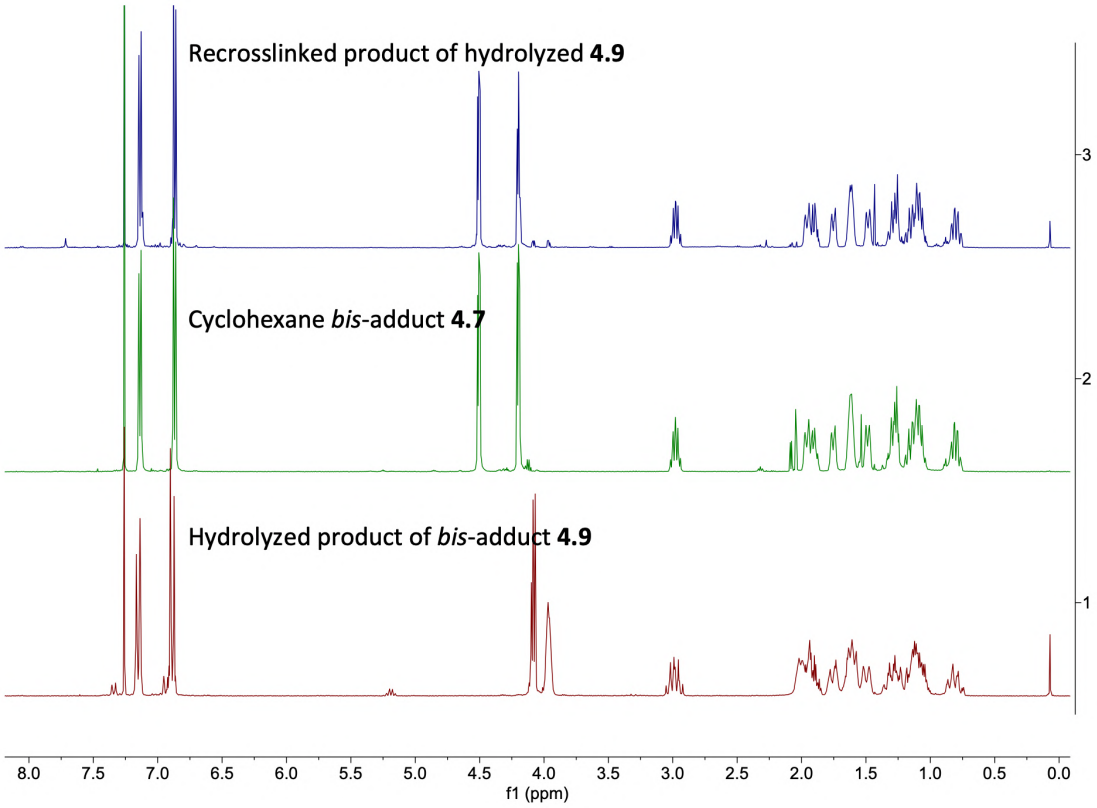

Figure S4.19 Stacked ^{1}H NMR spectra in $CDCl_3$ of recrosslinking functionalized cyclohexane *mono*-adduct (from decrosslinked compound **4.9**) reacting with CDI.

4.5.8.2 Recrosslinking functionalized (decrosslinked) paraffin wax

Procedure: to a solution of decrosslinked sample F (*ca.* 10 mg, from Table S4.5) in $CDCl_3$ (0.5 mL), carbonyl diimidazole (CDI, 2 mg, 0.011 mmol) and K_2CO_3 (4 mg, 0.029 mmol) was added. After stirring overnight, decrosslinked sample G (*ca.* 10 mg, from Table S4.5) and more K_2CO_3 (4 mg, 0.029 mmol) were added into the solution. The reaction mixture was left stirring overnight at 50 °C. After evaporation of the solvent, the residue was dissolved in 1 mL THF and then filtered through a 0.2 μm PTFE filter directly into a vial for SEC analysis. The filtered sample was a clear solution and the relevant portion of the chromatogram obtained from the refractive index detector is displayed in Figure S4.20.

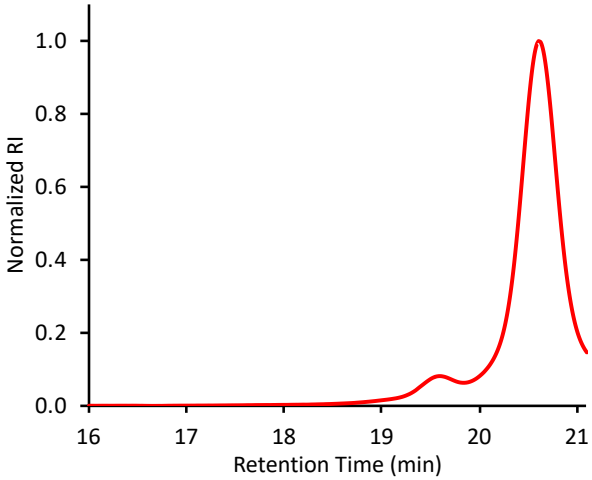

Figure S4.20 SEC trace derived from reacting CDI with decrosslinked carbonate **4.4** crosslinked paraffin wax sample. The appearance of a new peak at *ca.* 19.5 minutes indicates the successful re-crosslinking of the functionalized polymer.

4.5.8.3 Reacting functionalized (decrosslinked) paraffin wax with benzyl bromide diazirine

To a solution of hydrolyzed (i.e. decrosslinked) paraffin wax sample (from 10 mol% **4.4** crosslinked, 0.04 g) in THF (0.2 mL) at room temperature, NaH (60% dispersion in mineral oil, 0.007 g, excess) was added under ambient atmosphere. After 10 min stirring at room temperature, a solution of benzyl bromide diazirine (0.016 g, 0.057 mmol, excess) in THF (0.2 mL) was added dropwise into the abovementioned reaction mixture. The reaction mixture was left at room temperature and stirred for 24 hours. The reaction was then quenched with saturated aqueous NH_4Cl and extracted with CH_2Cl_2 (× 3). The combined organic layers were dried over sodium sulfate. After evaporation of the solvent, the obtained yellow solid was further washed with CH_3OH (× 3) to remove unreacted benzyl bromide diazirine. After filtering through a Kimwipe and drying, the desired product was afforded as white solid (0.022 g). Representative ^1H NMR spectra are provided below.

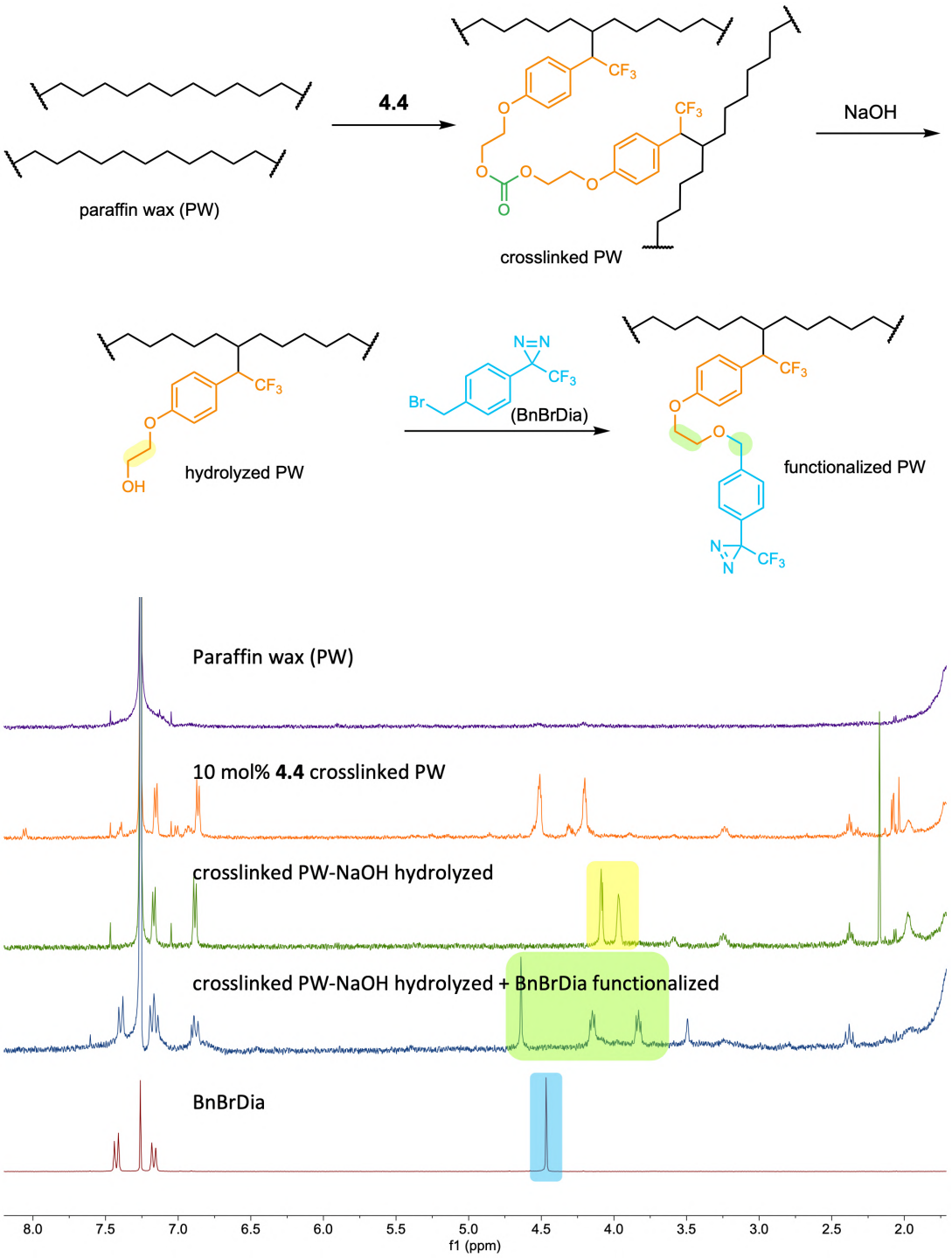

Figure S4.21 Stacked ^{1}H NMR spectra in $CDCl_3$ indicating the functionalization of a hydrolyzed (decrosslinked) paraffin wax sample reacted with a benzyl bromide-containing diazirine.

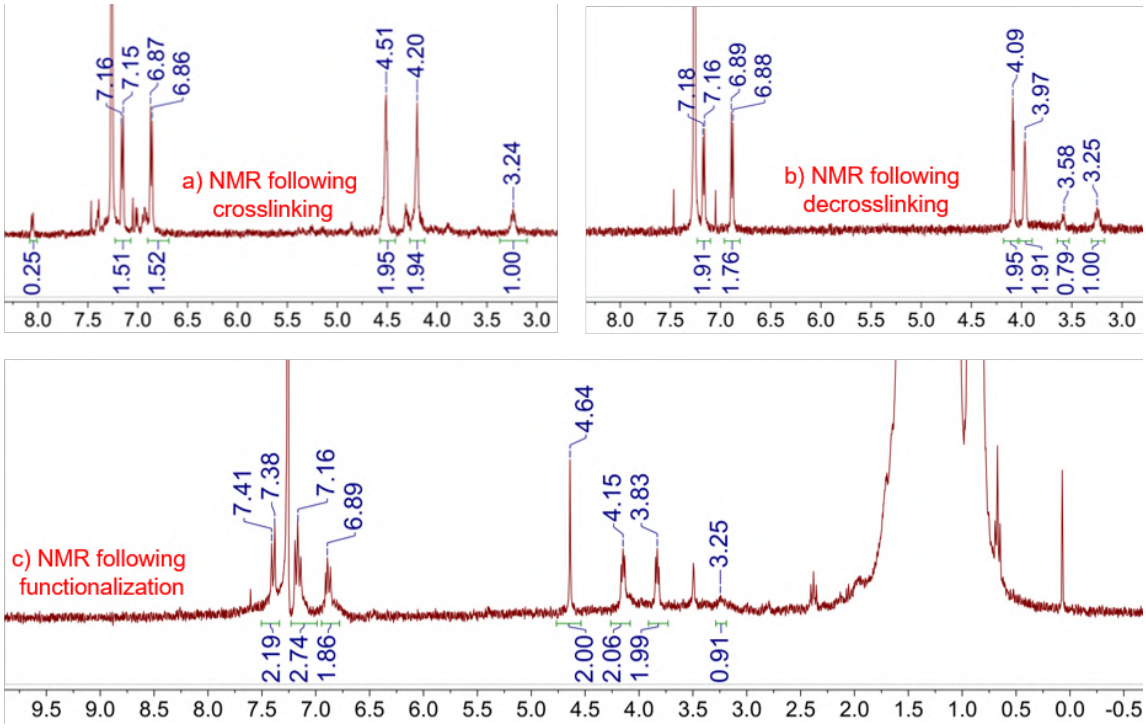

Figure S4.22 Integrated ^{1}H NMR spectra for: a) paraffin wax following crosslinking with **4.4**; b) after decrosslinking with NaOH; and c) after functionalization with BnBrDia. Integrations indicate a C–H insertion efficiency in the first step of >80% (determined from the relative ratios of the signals at 3.05 ppm and 4.20 / 4.51 ppm), with only *ca.* 15% production of ketone side-product (indicated by a signal at *ca.* 8.05 ppm,[168] lost in the subsequent washing step) due to quenching of the intermediate carbene by O_2. The yield of the 2-step hydrolysis / functionalization protocol was also >80%, as determined by the relative integrations for the benzylic protons (4.64 ppm) to the glycol group (4.15 / 3.83 ppm). Integrations of the paraffin methyl and methylene signals relative to crosslinker signals were inconsistent, due to poor solubility of the crosslinker within the PW matrix, in the initial treatment step.

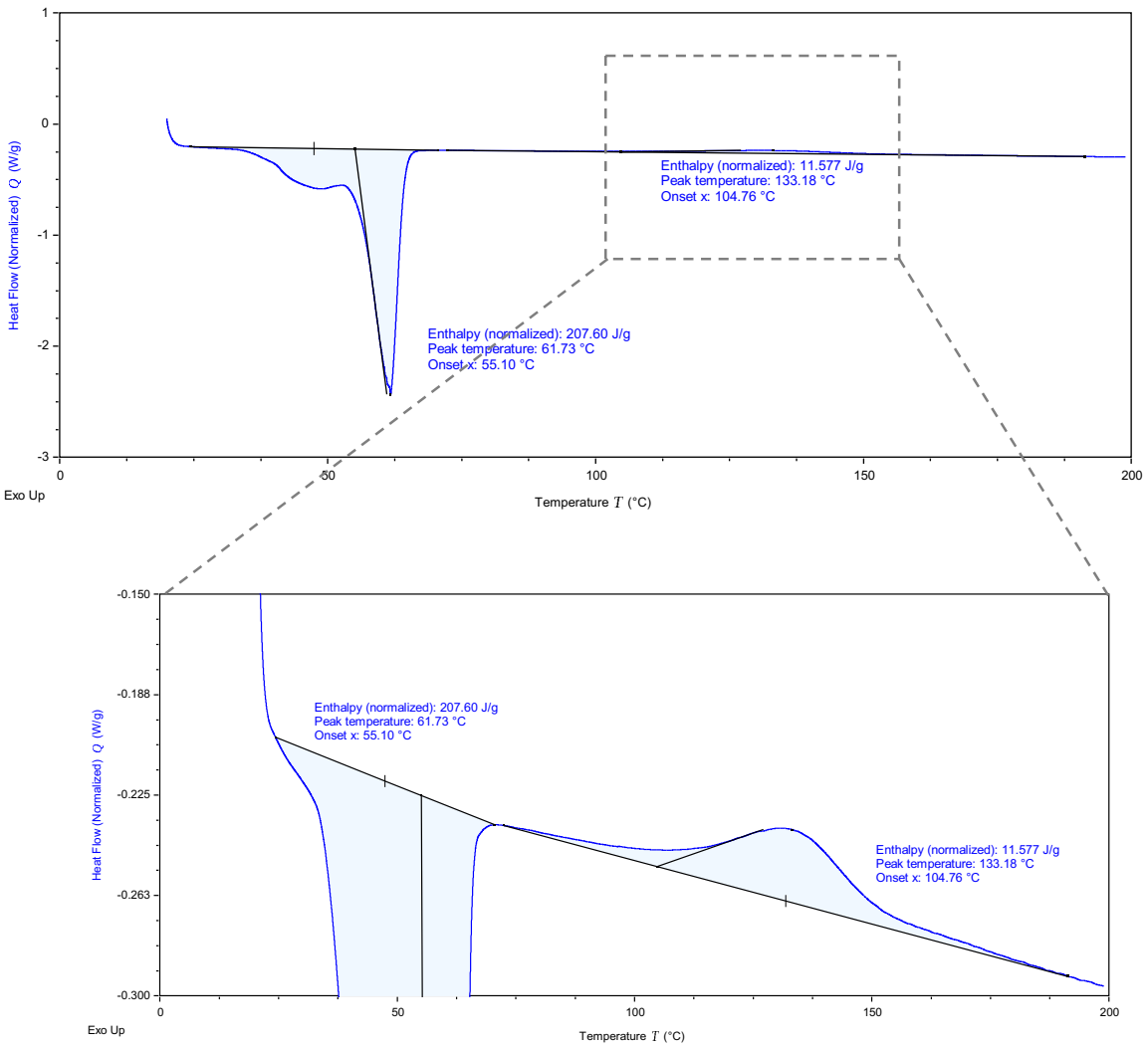

Figure S4.23 DSC trace for BnBrDia functionalized paraffin wax, illustrating a characteristic activation exotherm with a T_{max} of 133 °C. The total recorded enthalpy for the activation (in J/g) was variable, due to poor solubility of the crosslinker (**4.4**) within the PW matrix, in the initial treatment step.

4.5.9 Complete procedure for crosslinking/decrosslinking of low-density polyethylene (LDPE), and thermomechanical testing of prepared samples

4.5.9.1 Crosslinking of LDPE

Material used: low-density polyethylene (LDPE, Goodfellow, product code ET31-GL-000105, melt flow rate 21). Unless otherwise stated, crosslinked samples used 5 wt% ($m_{crosslinker}/m_{polymer}$) loading of crosslinker **4.4**.

Procedure: LDPE (40 g) was dissolved in toluene (170 mL, in a 150 × 75 mm crystalizing dish, covered with aluminum foil) at 80 °C. The solution temperature was decreased to 70 °C, and then a solution of crosslinker was added (2 g of compound **4.4** dissolved in 5 mL toluene). The mixture was quickly stirred for 20 s and then cooled in an ice bath for 10 min. Solvents were removed under ambient temperature (*ca.* 25 °C) and pressure in a well-ventilated fume hood over 24 h. The removal of solvents was monitored by measuring the weights of samples over the whole process. Upon drying, the mixture turned into white-yellow solids. Overall, this procedure allowed the homogenous dispersion of cleavable crosslinker **4.4** into the LDPE matrix. The sample was placed in an oven at 120 °C for 1 h. This induced crosslinking via thermal activation. Meanwhile, a vehicle control sample was prepared following the same procedure from beginning to end. The same amount of toluene (with no crosslinker) was added to the vehicle control.

4.5.9.2 Melt-processing of crosslinked LDPE

To process the crosslinked LDPE materials, the sample was cut into small pieces (3–10 mm) by use of scissors and a utility knife, and then placed into a two-piece rectangular-shaped aluminum mold (10 × 65 × 90 mm), glued with a silicone sealant and covered with a Teflon sheet. Melt-processing was carried out using a 3912 Hydraulic Unit Carver press. The Al mold was filled with small pieces of crosslinked sample and covered by a Teflon sheet, which was pressed under an applied load of 3000 lbs at 150 °C for 1 h, followed by fast cooling (directly removed from the Carver press and left at room temperature). Once the mold cooled, more small pieces of samples were added into the mold and it was pressed again under an applied load of *ca.* 4000 lbs at 180 °C for 1 h, followed by fast cooling. The melt-processing step (applied load of *ca.* 4000 lbs at 180 °C for 1 h) was repeated 3–5 times. Each pressure cycle, fresh pieces of crosslinked

LDPE materials were added and compressed together under pressure and heat. Following this process, a good-quality rectangular plaque was obtained (as shown in Figure S4.24a). The vehicle control plaque was prepared following the same procedure, but without adding crosslinker. Waterjet cutting was then applied to both plaques to obtain different sample dimensions for gel content and DMTA measurements (Figure S4.24b and c).

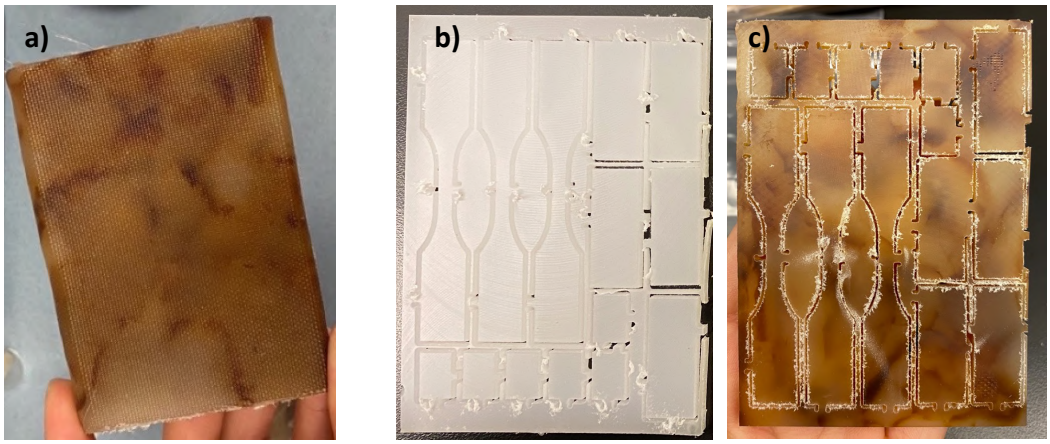

Figure S4.24 a) Crosslinked LDPE (with 5 wt% cleavable crosslinker **4.4** loading) plaque obtained from melt-processing. b) UVic machine shop polished and cut vehicle control plaque (*ca.* 4 × 62 × 87 mm). c) UVic machine shop polished and cut crosslinked LDPE plaque (*ca.* 4 × 62 × 87 mm) from panel (a).

4.5.9.3 DSC analysis of LDPE samples

Samples were placed in Tzero pans and sealed by a Tzero hermetic lid. The sample was placed in the oven of a DSC25 device (with an identical-sealed empty pan as a reference) and analyzed on the following cycle under a flow of nitrogen (50 mL/min) at 10 °C/min: 0/–10 °C → 200 °C → 0/–10 °C → 200 °C. The corresponding enthalpies of crystallization (exotherm, $\Delta H_{crystal}$) and melting (endotherm, ΔH_{fusion}) transitions were recorded from the cooling and second heating phase (Table S4.9). Representative DSC traces are provided below.

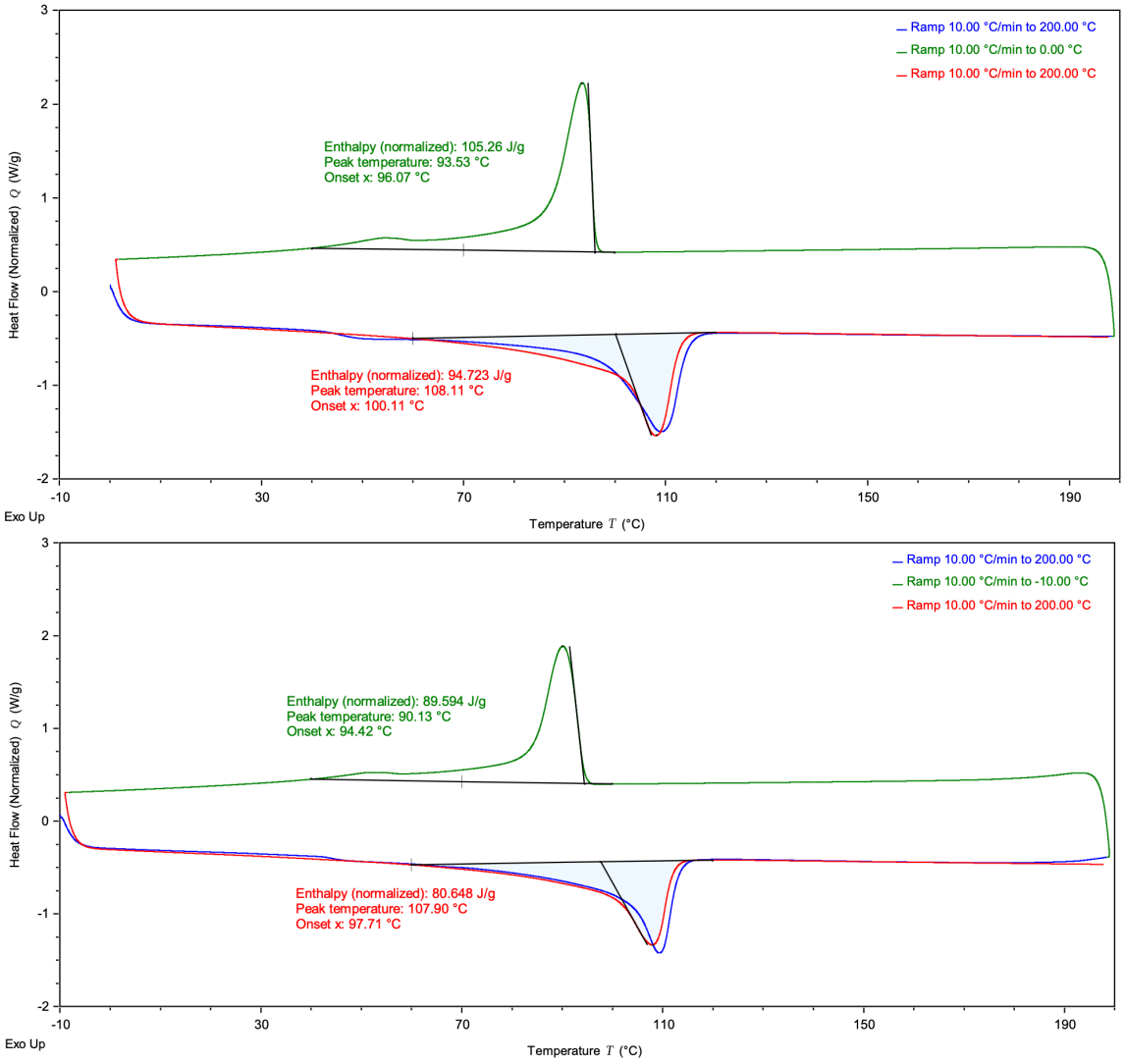

Figure S4.25 DSC traces for LDPE vehicle control sample (top) and 5 wt% compound **4.4** crosslinked LDPE (bottom, both DSC samples were taken from melt-processed plaques).

4.5.9.4 XRD (WAXS) analysis of LDPE samples

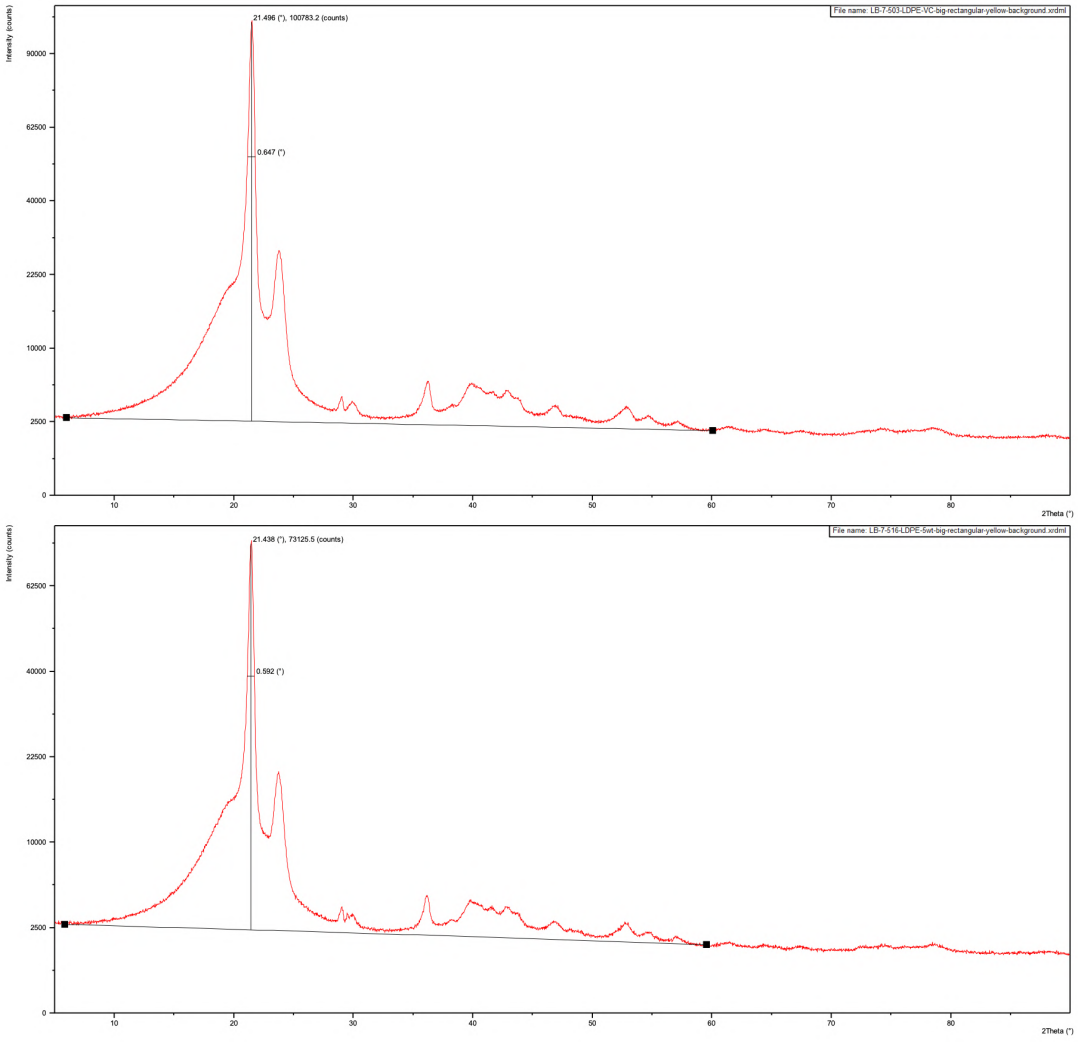

Figure S4.26 WAXS spectra for LDPE vehicle control (top) and 5 wt% compound **4.4** crosslinked LDPE (bottom, both samples were taken from melt-processed plaques).

Table S4.9 Evolution of thermal properties of LDPE and assessment of crystallinity

Sample	$\Delta H_{crystalization}$ (J/g)[a]	ΔH_{fusion} (J/g)[a]	$X_{c,XRD}$[b]
LDPE-VC	105	94.7	35.9%
LDPE-X-**4**	89.6 (85%)	80.6 (85%)	35.6%

[a] In both VC and crosslinked samples, the integrated regions for crystallization and fusion enthalpy are from 40 to 100 °C and 60 to 120 °C respectively.
[b] In both VC and crosslinked samples, obtained area values from WAXS data (*ca.* 6–60°) were used to calculate % crystallinity.

4.5.9.5 Gel content analysis of LDPE samples

Swelling tests were performed by soaking samples (crosslinked LDPE and vehicle control) in 2 mL of toluene at 100 ˚C for 24 h. After removing the solvent and washing the sample by soaking in a fresh 2 mL of toluene at 100 ˚C for 5 min, the samples were finally dried at 100 ˚C for 48 h under ambient pressure. Samples were weighed every 24 h to guarantee solvents are fully removed. The gel fraction was calculated using equation (2):

$$Gel\% = \frac{m_{dry}}{m_{initial}} \times 100\% \qquad (2)$$

where $m_{initial}$ is the original weight of the sample, and m_{dry} is the weight of sample after drying from the solvent. This experiment was done in triplicate (Table S4.10) and the representative flow chart is provided below (Figure S4.27).

Table S4.10 Gel content of LDPE samples (XL indicates the use of 5 wt% compound **4.4**; the inset photo shows three crosslinked LDPE samples after the swelling tests)

Sample	$m_{initial}$ (g)	m_{dry} (g)	$m_{supernatant}$ (g)	Gel content (%)
XL-1	0.2438	0.2333	0.0080	95.7
XL-2	0.2527	0.2457	0.0037	97.2
XL-3	0.2438	0.2228	0.0177	91.4
VC-1	0.2464	0.0002	0.2369	< 2
VC-2	0.2460	0.0025	0.2413	< 2
VC-3	0.2481	0.0028	0.2429	< 2

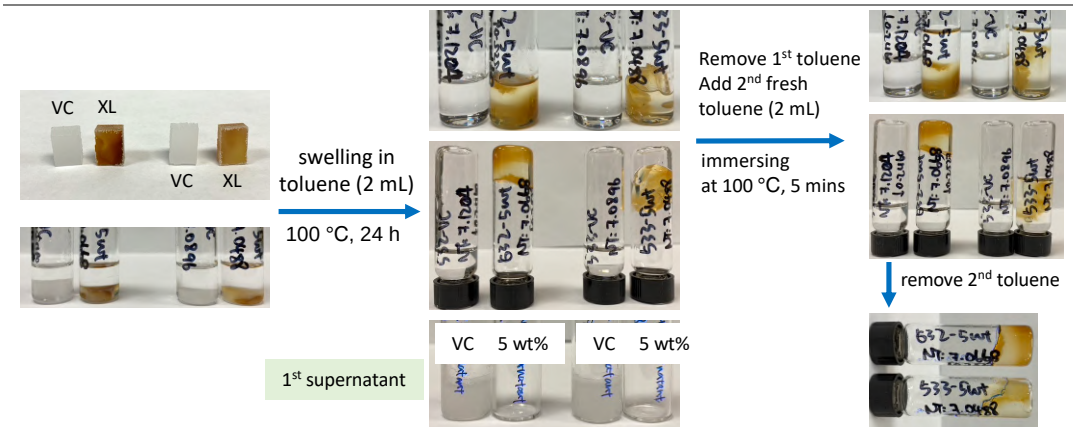

Figure S4.27 Swelling tests procedure for LDPE samples.

4.5.9.6 DMTA analysis of LDPE samples, and calculation of M_c

Dynamic mechanical thermal analysis was carried out following the general procedure specified above.

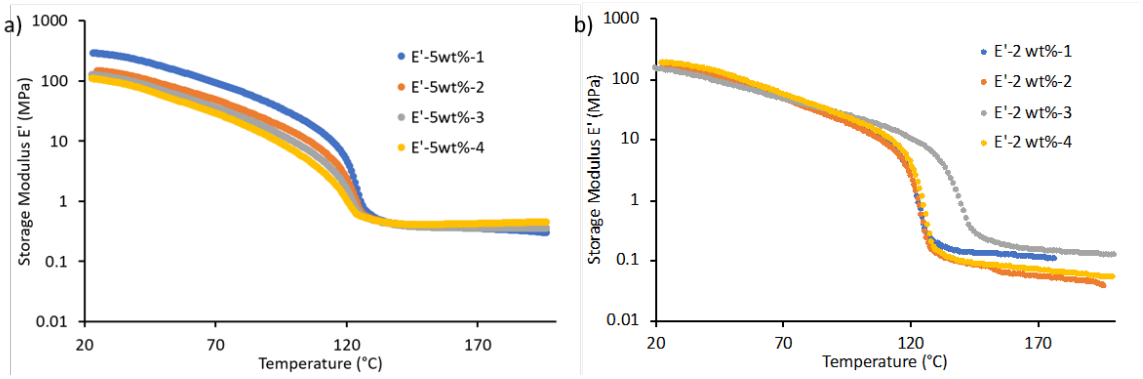

Figure S4.28 DMTA curves for LDPE polymer samples after crosslinking with *bis*-diazirine **4.4**, at loadings of: a) 5 wt%; and b) 2 wt%. Replicate samples are indicated with different colors.

Table S4.11 Storage modulus (E') of crosslinked LDPE determined at *ca.* 140 ˚C by DMTA

Sample	XL-1	XL-2	XL-3	XL-4
E'-5 wt% in the rubbery state (MPa)	0.4197	0.4194	0.3998	0.4186
E'-2 wt% in the rubbery state (MPa)	0.1365	0.0925	0.1697	0.0957

The molecular weight between crosslinks was assessed from the storage modulus of the rubbery plateau region at 140 °C (413 K) using the following formula, determined by rearranging equation 1:

$$M_{c,a} = \frac{3\rho RT}{E'_r}$$

where $M_{c,a}$ is the apparent molecular weight difference between crosslinks, ρ is the density of the sample (measured at 0.936 ± 0.007 g/cm^3), R is the gas constant, T is the temperature, and E'_r is the storage modulus at the rubbery plateau region (reported in Table S4.11). When 5 wt% of crosslinker **4.4** was used, the average storage modulus of the rubbery plateau was 0.414 ± 0.010 MPa, and the calculated $M_{c,a}$ was 23,300 ± 560 g/mol (equivalent to 1,660 ± 40 methylene units between mechanically productive crosslinks).

The total amount of methylene-to-methylene linkages, meanwhile, can be estimated from the cyclohexane crosslinking experiments, which have previously shown

to correlate closely with gravimetric measurements of polymer crosslinking efficiency in polyethylene materials.[168] Crosslinker **4.4** was 80% efficient at converting cyclohexane to **4.7** under thermal activation conditions (as described above), and this level of efficiency was consistent with the C–H insertion efficiency determined by ^{1}H NMR for compound **4.4** in paraffin wax (see Figure S4.22).

A representative 1 g sample of LDPE treated with 5 wt% (50 mg) of **4.4** (518.37 g/mol) contains 71.3 mmol of methylene groups and 0.096 mmol of compound **4.4** (i.e. 0.19 mmol of diazirine groups). From the cyclohexane insertion measurement, we can estimate that 80% of these 0.096 mmol of **4.4** (i.e. 0.077 mmol) react twice with methylene groups within the LDPE, resulting in 0.15 mmol of methylene units becoming linked together. The remaining 20% of compound **4.4** reacts unproductively, such that one or both of the generated carbenes undergoes some undesirable reaction: e.g. quenching by O_2 to form a ketone, reaction with a linear diazo species to form an azo linkage, etc.

At 5 wt% loading of **4.4**, therefore, we can estimate that 0.21% (0.15 mmol / 71.3 mmol) of methylene groups within the sample have become linked together—an estimate that is supported by NMR integrations of crosslinked and decrosslinked.

The remaining 99.79% of methylenes within the sample will either be unmodified, or will contain a "dead" modification where only one end of compound **4.4** has undergone C–H insertion. The distance between productively modified methylene groups can therefore be estimated as:

$$\frac{[(71.3 - 0.15)/\,71.3]}{(0.15\,/\,71.3)} = 474\ \text{methylenes}$$

Many of these methylene-to-methylene linkages will constitute loops, wherein crosslinker **4.4** has reacted twice along the same LDPE chain. The ratio of these loops to the mechanically productive crosslinks determined above from the modulus of the rubbery plateau (assumed to result from inter-chain crosslinks) can be estimated as follows:

$$\frac{[1{,}660\ methylenes - 474\ methylenes]}{474\ methylenes} = 2.5 : 1$$

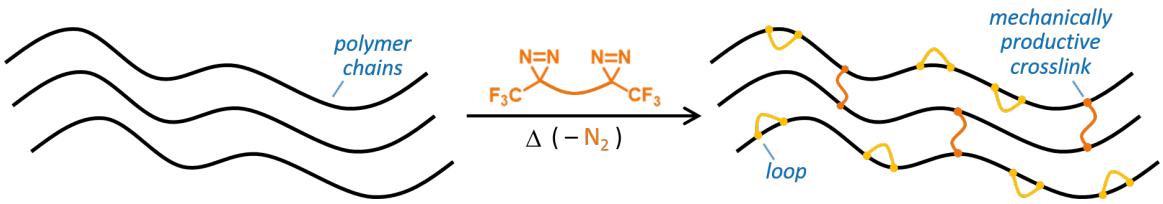

Figure S4.29 Cartoon illustration of the estimated 2.5:1 ratio of loops (i.e. intra-chain crosslinks) to mechanically productive inter-chain crosslinks in LDPE. The illustration is not to scale: when 5 wt% crosslinker is used, very long stretches of unmodified polymer chains will be present within the sample.

4.5.9.7 Decrosslinking of crosslinked LDPE

Material: used DMTA samples (crosslinked and vehicle control), cut into 2–10 mm pieces.

Basic hydrolysis: in a 100 mL round bottom flask, the crosslinked LDPE sample (5.0 g) was combined with toluene (30 mL), followed by ethanol (10 mL) and 5 M NaOH (in water, 10 mL). The mixture was then heated to reflux at 100 °C overnight. The next day, the mixture was sonicated (280 W for 5–7 hours at *ca.* 60 °C). The reflux-sonication process was repeated three to four times until no remaining particles were visible. The mixture was then poured into a crystalizing dish and left overnight for evaporation. Then the decrosslinked material was filtered and washed with 0.25 M aqueous HCl and water (pH was monitored along the washing process) to afford the neutralized product. The resulting solids were then dried under ambient conditions overnight. The dried material was then left in oven at 140 °C for 5 min and the weights were measured through the process to ensure that no residual solvents remained. The samples were then remolded (using an applied load of 1500 lbs at 140 °C for 20 min) for gel content analysis (Figure S4.30). The vehicle control (VC) sample was processed following an identical procedure. As shown in Figure S4.30, decrosslinked XL-LDPE (deXL) has less than 2% gel content which is the same as the vehicle control.

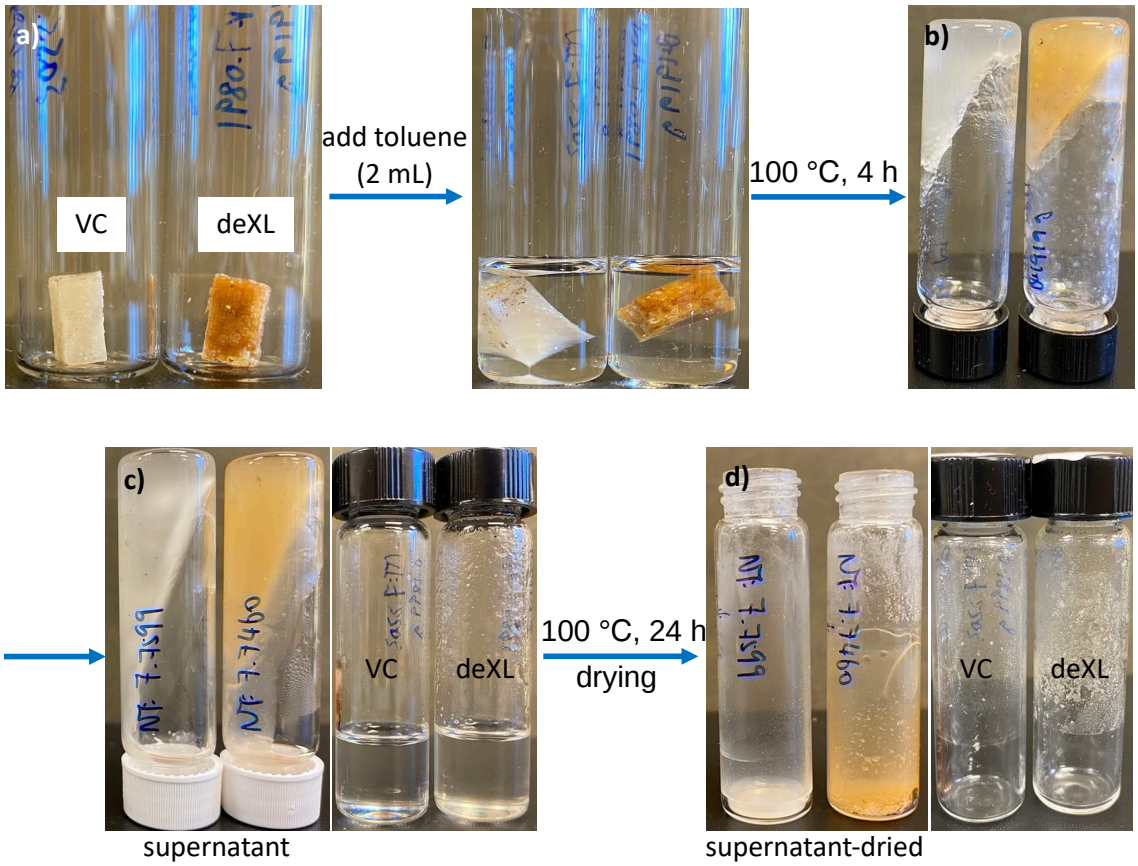

Figure S4.30 Decrosslinking process for LDPE samples, all pictures were taken at room temperature (*ca.* 23 °C). a) Remolded vehicle control and decrosslinked samples for gel content analysis. b) Both vehicle control and decrosslinked samples were dissolved in toluene after heating at 100 °C for 4 h. c) The 1st supernatants were poured into new vials (with white caps). Fresh toluene (2 mL) was then added into the sample vials (black cap), soaked for 5 min at 100 °C, then combined with the 1st supernatant. d) All four vials were dried at 100 °C under ambient pressure for 24 h. Vial masses were measured along the process to determine the gel content for both vehicle control and decrosslinked materials are less than 2%.

4.5.10 Complete procedure for crosslinking/decrosslinking of mixed amorphous PP and LDPE (aPP+LDPE) composites, and thermomechanical testing of prepared samples

4.5.10.1 Crosslinking of (aPP+LDPE) composites

Material used: amorphous polypropylene (aPP, Sigma-Aldrich, ref 428175, CAS 9003-07-0) and low-density polyethylene (LDPE, Goodfellow, product code ET31-GL-000105, melt flow rate 21). All crosslinked materials are based on 5 wt% ($m_{crosslinker}/m_{polymer}$) crosslinker **4.4** loading.

Procedure: A mixture of aPP (20 g) and LDPE (20 g) was dissolved in toluene (150 mL, in a 150 × 75 mm crystalizing dish, covered with aluminum foil) at 90 °C. The solution temperature was decreased to 75 °C, and then a solution of crosslinker was added (2 g of compound **4.4** dissolved in 5–7 mL toluene). The mixture was quickly stirred for 20 s and then cooled in an ice bath for 10 min. Solvents were removed under ambient temperature (*ca.* 25 °C) and pressure in a well-ventilated fume hood over 24 h. The removal of solvents was monitored by measuring the weights of samples over the whole process. Upon drying, the mixture turned into white-yellow solids. Overall, this procedure allowed the homogenous dispersion of cleavable crosslinker **4.4** into the mixed aPP and LDPE matrix. The sample was placed in an oven at 120 °C for 1 h. This induced crosslinking via thermal activation. Meanwhile, a vehicle control sample was prepared following the same procedure from beginning to end. The same amount of toluene (with no crosslinker) was added to the vehicle control.

4.5.10.2 Melt-processing of crosslinked (aPP+LDPE) composites

To process the crosslinked (aPP+LDPE) materials, the same procedure was followed as described above for crosslinked LDPE. The Al mold was filled with small pieces of crosslinked sample and covered by a Teflon sheet, which was pressed under an applied load of 2500 lbs at 150 °C for 1 h, followed by fast cooling. Once the mold cooled, more small pieces of samples were added into the mold and it was pressed again under an applied load of 2500 lbs at 160 °C for 1 h, followed by fast cooling. The melt-processing step (applied load of 2500 lbs at 160 °C for 1 h) was repeated 3–5 times, with fresh pieces of crosslinked materials being added between each application of pressure.

Following this process, a good-quality rectangular plaque was obtained. A **vehicle control** (VC) plaque was prepared following the same procedure, but without adding crosslinker. A **crosslinked control sample** (XLPP-XLPE) was prepared by mixing a 1:1 ratio (by mass) of pre-crosslinked LDPE (prepared as described above) and pre-crosslinked aPP (following the same procedure as for crosslinked LDPE, and using the same loading of crosslinker **4.4**: 5 wt%) then processing using the same melt-processing procedure. All three plaques were cut into different dimensions for further analysis by waterjet cutting (Figure S4.31a–c, *ca.* 4 × 62 × 87 mm).

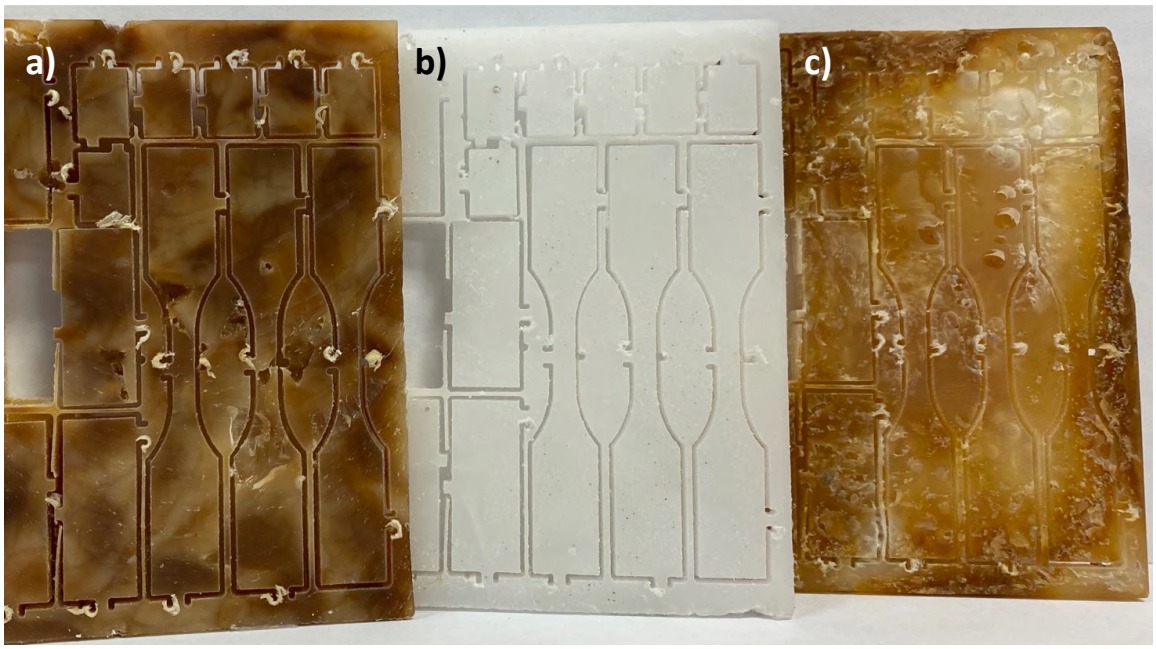

Figure S4.31 a) UVic machine shop polished and cut crosslinked (aPP+LDPE) plaque. b) Vehicle control plaque. c) XLPP-XLPE plaque. The crosslinked control sample in panel (c) shows severe voids due to grain boundaries.

4.5.10.3 SEM images of (aPP+LDPE) composites

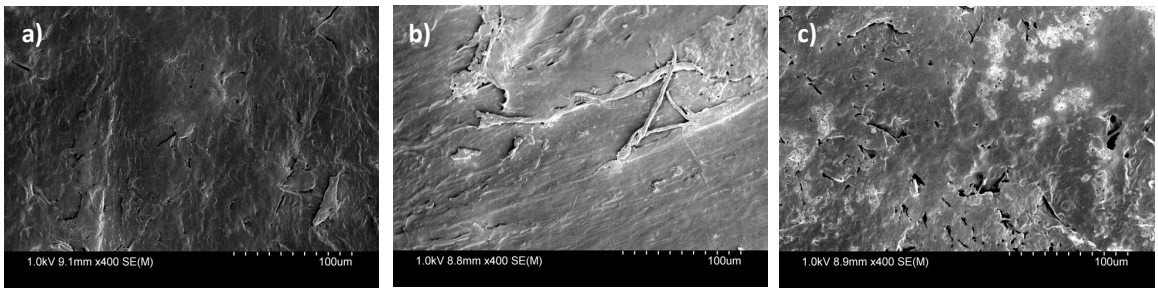

Figure S4.32 SEM images of melt-processed plaques (taken from the samples in Figure S4.31) for: a) crosslinked (aPP+LDPE); b) a representative vehicle control sample; and c) a blend of precrosslinked XLPP and XLPE. The crosslinked control sample in panel (c) shows severe voids due to grain boundaries.

4.5.10.3 DSC analysis of (aPP+LDPE) composites

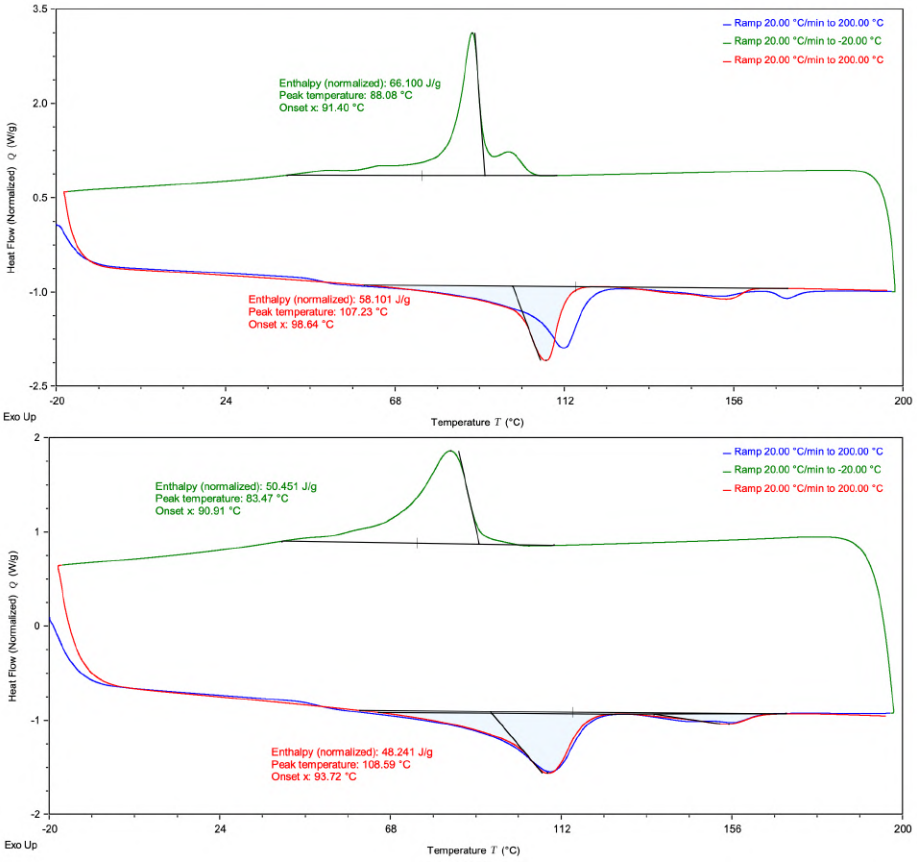

Figure S4.33 DSC traces for (aPP+LDPE) vehicle control (top) and crosslinked (bottom, both DSC samples were taken from melt-processed plaques).

4.5.10.4 XRD (WAXS) analysis of (aPP+LDPE) composites

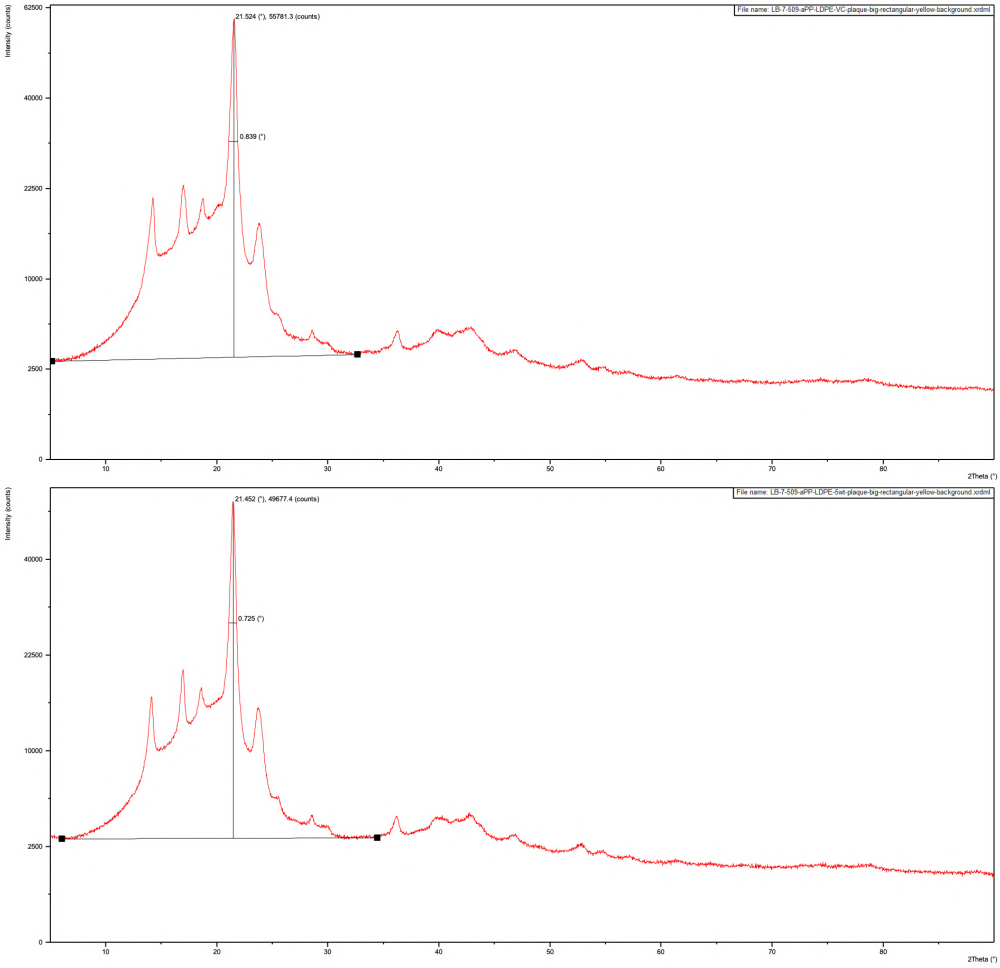

Figure S4.34 WAXS spectra for aPP+LDPE vehicle control (top) and crosslinked (bottom, both samples were taken from melt-processed plaques).

Table S4.12 Evolution of thermal properties of (aPP+LDPE) and assessment of crystallinity from XRD.

Sample	$\Delta H_{crystal}$ (J/g)[a]	ΔH_{fusion} (J/g)[a]	$X_{c,XRD}$[b]
(aPP+LDPE)-VC	66.1	58.1	30.1%
(aPP+LDPE)-X-**4**	50.5 (76%)	48.2 (83%)	28.6%

[a] In both VC and crosslinked samples, the integrated regions for crystallization and fusion enthalpy are from 40 to 110 °C and 60 to 170 °C respectively.
[b] In both VC and crosslinked samples, obtained area values from XRD data (*ca.* 6–60°) were used to calculate % crystallinity.

4.5.10.5 Gel content analysis of (aPP+LDPE) composites

Swelling tests were performed using the same procedure as outlined above for crosslinked LDPE samples. Five replicates were performed for each sample type (Table S4.13), and the representative gel picture is provided below (Figure S4.35).

Table S4.13 Gel content of aPP+LDPE samples (XL is 5 wt% compound **4.4** crosslinked (aPP+LDPE) sample)

Sample	$m_{initial}$ (g)	m_{dry} (g)	$m_{supernatant}$ (g)	Gel content (%)
XL-1	0.2244	0.1408	0.0781	62.7
XL-2	0.2270	0.1743	0.0484	76.8
XL-3	0.2296	0.1724	0.0539	75.1
XL-4	0.2268	0.1697	0.0540	74.8
XL-5	0.2281	0.1685	0.0554	73.9
VC-1	0.2271	0.0018	0.2246	< 2
VC-2	0.2326	0.0017	0.2294	< 2
VC-3	0.2239	0.0009	0.2200	< 2
VC-4	0.2310	0.0010	0.2283	< 2
VC-5	0.2332	0.0013	0.2241	< 2

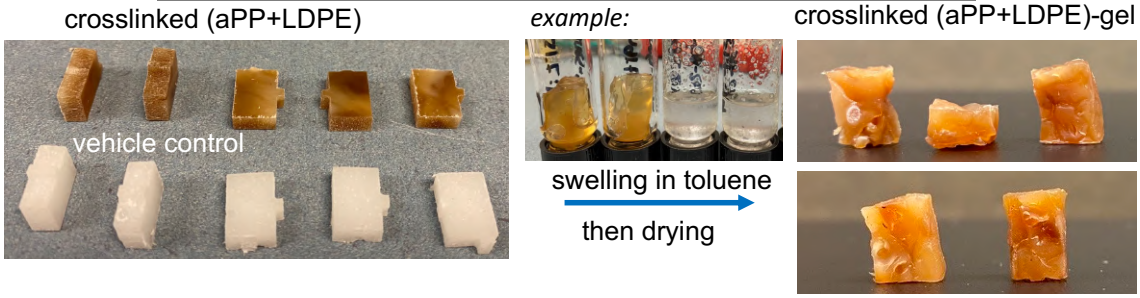

Figure S4.35 Crosslinked (aPP+LDPE) and vehicle control samples before and after swell tests.

4.5.10.6 Tensile tests of (aPP+LDPE) composites

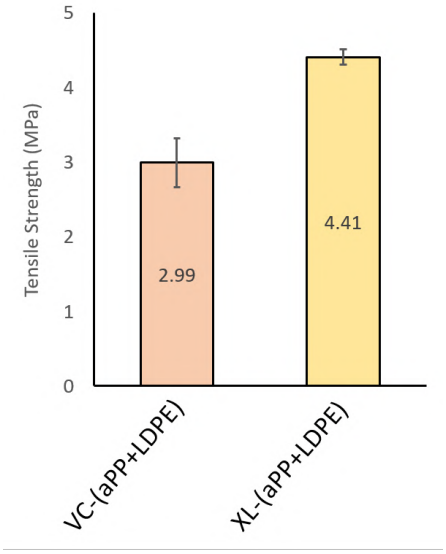

Figure S4.36 The tensile strength of vehicle control (aPP+LDPE) samples was measured at 2.99 ± 0.92 MPa. The tensile strength of the crosslinked (aPP+LDPE) samples was measured at 4.41 ± 0.18 MPa (eight replicates were used for the VC samples, while the crosslinked sample was analyzed in triplicate). The dogbone samples were prepared by remolding (applied load of 2500 lbs at 160 °C for 1 h) the crosslinked and vehicle control materials into dogbone-shaped Al-molds. Bars indicate standard error.

4.5.10.7 Decrosslinking of crosslinked (aPP+LDPE) composites

Material: used DMTA and tensile test samples (crosslinked (XL) and vehicle control), cut into 2–7 mm pieces (Figure S4.37a).

Basic hydrolysis: in a 100 mL round bottom flask, the crosslinked polymer sample (aPP+LDPE, 3.5 g) was combined with toluene (20 mL), followed by ethanol (10 mL) and 5 M NaOH (in water, 10 mL). The mixture was then heated to reflux at 100 °C overnight. The next day, the mixture was sonicated (280 W for 5–7 hours at *ca.* 60 °C). The reflux-sonication process was repeated two to three times until no remaining particles were visible (Figure S4.37b). The mixture was then poured into a crystalizing dish and left overnight for evaporation (Figure S4.37c). Then the orange solid (decrosslinked) material was filtered and washed with 0.25 M aqueous HCl and water (pH was monitored along the washing process) to afford the neutralized product as a

light-brown solid. The resulting solids were then dried under ambient conditions overnight. The resulting dried material was then left in oven at 140 °C for 5 min and the weights were measured through the process to guarantee no residual solvents left (Figure S4.37d and e). The samples were then remolded (applied load of 1500 lbs at 140 °C for 20 min) for DMTA analysis (Figure S4.37f). The vehicle control (VC) sample was processed following an identical procedure.

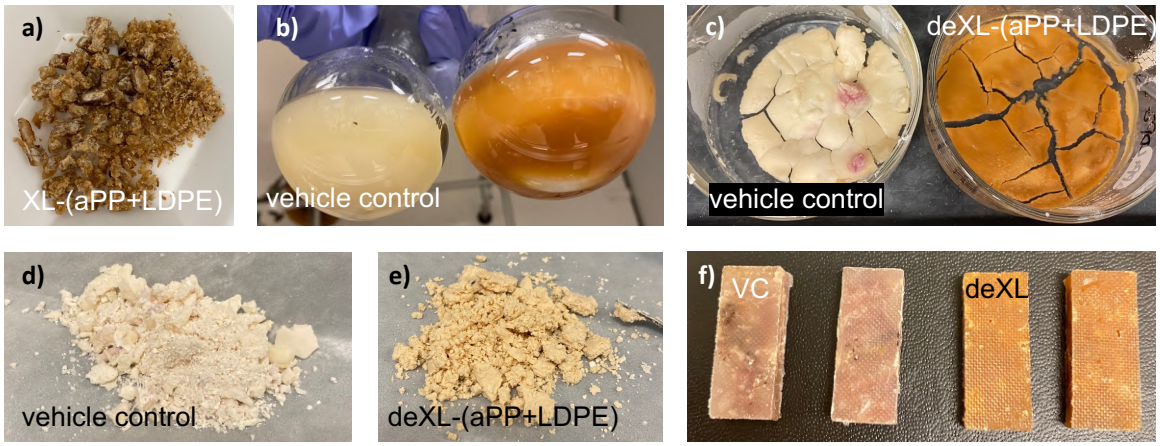

Figure S4.37 a) Used XL-(aPP+LDPE) DMTA and tensile test samples (cut into 2–7 mm pieces). b) VC and XL-(aPP+LDPE) samples after reflux-sonication treatment with no visible particles. c) VC and deXL samples after overnight solvent evaporation. d–e) Both samples after washing and drying. f) Samples remolded for DMTA analysis.

4.5.10.8 DMTA analysis of crosslinked control sample (XLPP-XLPE) and a representative aPP sample

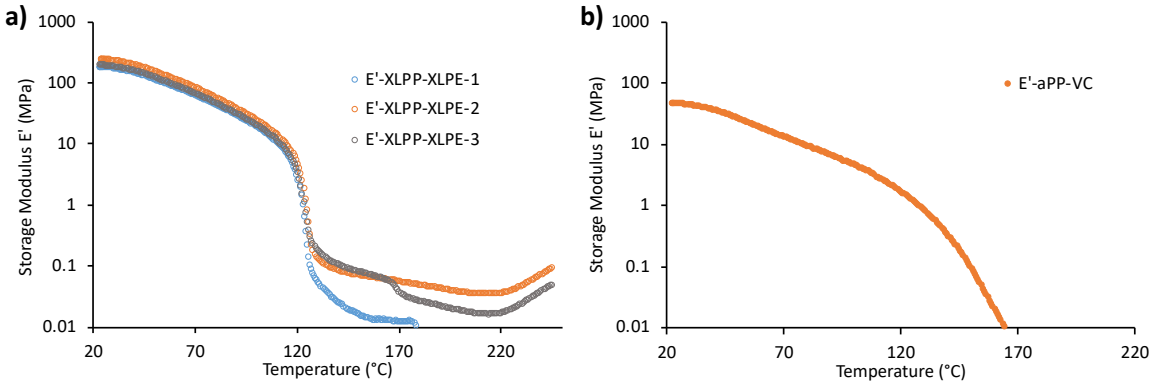

Figure S4.38 DMTA curves for: a) crosslinked control samples (XLPP-XLPE, in triplicate) after melt-processing; and b) amorphous polypropylene (aPP) processed using the same procedure as the crosslinked samples, but with no crosslinker added.

4.5.11 Complete procedure for crosslinking/decrosslinking of PDMS (inverted vial and parallel plate experiments)

4.5.11.1 Crosslinking of PDMS

Material used: polydimethylsiloxane (PDMS, Sigma-Aldrich, ref 432997, CAS 70131-67-8, with a viscosity of 18000-22000 cSt).

Procedure: To a vial containing liquid PDMS (500 mg) was added **4.4** (5 wt%, 25 mg) and diethyl ether (0.1 mL). The mixture was manually stirred with a thin needle to disperse the crosslinker. Sonication for 5 min removed bubbles created during the manual stirring. The resulting mixture became a pale-yellow cloudy liquid. A duplicate sample of 5 wt% **4.4** in PDMS was prepared identically (for use in the decrosslinking experiment described below), while a vehicle control sample was prepared using the same protocol (and the same amount of diethyl ether) but with no added crosslinker. All three vials were then gently heated at 40 °C for 2 h to remove the diethyl ether. The sample weights were measured throughout the evaporation process to ensure complete removal of solvent. The three vials were then placed in an oven at 120°C for 1 h. As shown in Figure S4.39, the crosslinked PDMS sample did not flow when the vial was inverted, confirming the crosslinked state of the substance.

4.5.11.2 Decrosslinking of crosslinked PDMS

To a vial containing crosslinked PDMS (prepared as described above; *ca.* 520 mg) was added toluene (1 mL), ethanol (0.5 mL) and NaOH (2 M in H_2O, 0.3 mL). The vial was then capped and heated at 100 °C for 1.5 h (until no visible yellow particles remained). The decrosslinked sample was then extracted with pentane (× 3). The combined organic layers were dried at 90 °C overnight. The sample weights were measured throughout the evaporation process to ensure complete removal of solvent. A non-crosslinked control sample (the vehicle control from the preparation described above) was treated identically. As shown in Figure S4.39, the decrosslinked sample regained the ability to flow when the vial was inverted.

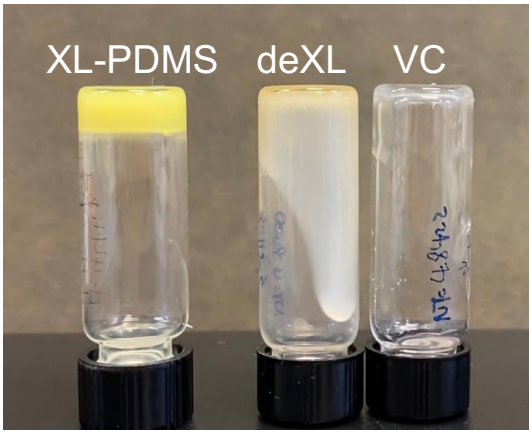

Figure S4.39 Vials containing crosslinked (left), decrosslinked (middle) and vehicle control (right) PDMS.

4.5.11.3 Crosslinking of PDMS by parallel plate experiment

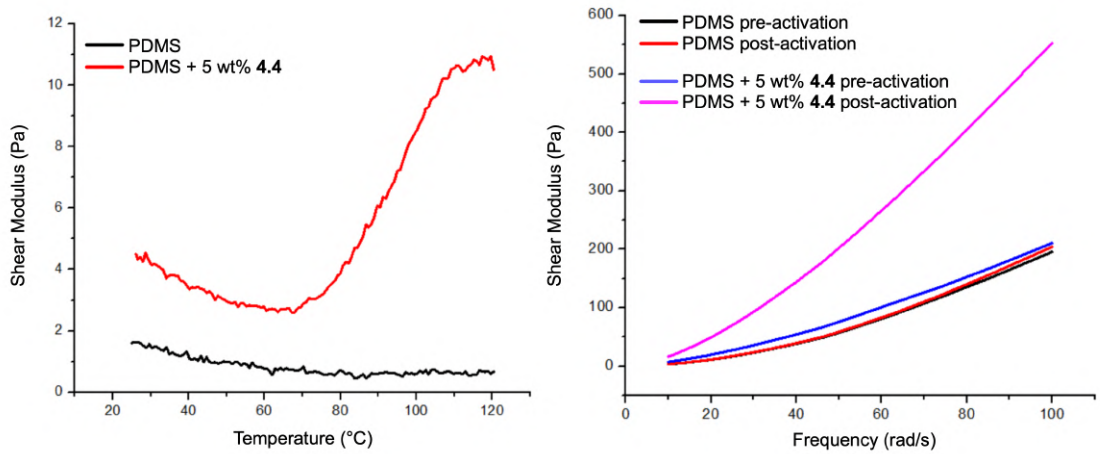

Figure S4.40 A parallel plate in a rheometer was charged with a pre-mixed sample of crosslinker **4.4** (5 wt%) in PDMS. a) The shear modulus (G'; red curve) was monitored as the temperature was increased. As the temperature of the sample exceeded the activation temperature of the diazirine groups in **4.4** (*ca.* 80 °C), the shear modulus increased sharply, indicating crosslinking of the PDMS polymer matrix. By contrast, a control sample (PDMS with no crosslinker present; blue curve) showed no increase in shear modulus with increasing temperature. b) Following crosslinking, the crosslinked sample exhibited a sharp increase in frequency-dependent shear modulus, indictating successful crosslinking. Prior to crosslinking, both the treated sample and vehicle control samples had similar characteristics.

4.5.12 Impact-testing of diazirines 4.1 and 4.3

Diazirine building blocks **4.1** and **4.3** (10 mL each) were submitted to Fauske & Associates for Drop-Weight Impact Testing analysis, conducted according to the UN Manual of Tests and Criteria for Transportation of Dangerous Goods (Test code 3 (a) (ii)). A BAM Fallhammer apparatus was used for the analysis, which consisted of dropping a series of weights (1, 2, 5, and 10 kg) on a measured sample (40 mm^3) from varying heights, in order to expose the sample to impacts of increasing energy from 2–100 J. As indicated in Table S4.14 below, diazirine **4.1** exhibited explosive decomposition at all tested impacts, while diazirine **4.3** did not explode at the highest impact energy used in the analysis.

Table S4.14 Impact results for diazirines **4.1** and **4.3**[a]

Sample	Impact Energy (J)	Trial 1	Trial 2	Trial 3	Trial 4	Trial 5	Trial 6
diazirine **4.1**	100	E	–	–	–	–	–
"	50	E	E	–	–	–	–
"	10	E	–	–	–	–	–
"	5	E	E	–	–	–	–
"	2	E	–	–	–	–	–

Sample	Impact Energy (J)	Trial 1	Trial 2	Trial 3	Trial 4	Trial 5	Trial 6
diazirine **4.3**	100	NR	NR	NR	NR	NR	NR

[a] 'E' indicates the observation of explosive decomposition. 'NR' indicates that no reaction was observed. '–' indicates that the sample was not tested further, since sufficient data had already been collected.

Chapter 5: Functionalization of Polydimethylsiloxane (PDMS) with Diazirine-Based Linkers for Covalent Protein Immobilization

This chapter has been adapted from:

Jie Li, Liting Bi, Stefania F. Musolino, Jeremy E. Wulff, Kyla N. Sask

manuscript submitted.

Contributions:

Liting Bi and Stefania F. Musolino contributed to the design and synthesis of the diazirine reagents. Furthermore, Liting Bi conducted the small molecule model experiments. Jie Li performed the surface modifications of PDMS with the diazirine reagents, conducted and analyzed the surface characterization experiments, including X-ray photoelectron spectroscopy, infrared analysis, water contact angle measurements, and atomic force microscopy. Additionally, Jie Li performed experiments for BSA and IgG immobilization, quantifying the results using iodine-125, and conducted confocal microscopy experiments.

5.1. Abstract

Biomolecule attachment to solid supports is critical for biomedical devices such as biosensors and implants. Polydimethylsiloxane (PDMS) is commonly used for these applications due to its advantageous properties. To enhance biomolecule immobilization on PDMS, a novel technique is demonstrated using newly synthesized diazirine molecules for the surface modification of PDMS. This non-destructive process involves a reaction between diazirine molecules and PDMS through C–H insertion with thermal or ultraviolet activation. The success of the PDMS modification is confirmed with various surface characterization techniques. Bovine serum albumin (BSA) and immunoglobulin G (IgG) are covalently immobilized on the modified PDMS surfaces, and the amount of protein is quantified using iodine-125 radiolabeling. The results demonstrate that PDMS is rapidly functionalized, and the stability of the immobilized proteins is significantly improved with multiple types of diazirine molecules and activation methods. Confocal microscopy provides three-dimensional images of the distribution of immobilized IgG on the surfaces and the penetration of diazirine-based linkers through the PDMS substrate during the coating process. Overall, this study presents a promising new approach for functionalizing PDMS surfaces to enhance biomolecule immobilization, and its potential applications can extend to multi-material modifications for various diagnostic and medical applications with relevant bioactive proteins.

5.2. Introduction

Surface modification of low-functionality substrates and the subsequent immobilization of biomolecules is important in the fields of biotechnology and biomedicine with a wide range of applications in biosensors, biomaterials, and microfluidics.[211] Biosensors, such as immunosensors and enzyme electrodes, heavily rely on immobilized proteins and are extensively used for medical diagnostics, food analysis, and environmental monitoring.[212] For biomaterials, immobilized biomolecules can be used to regulate cell adhesion or to enhance the biocompatibility of implants.[213] Particular microfluidic devices also require the attachment of proteins for applications in immunoassays, cell studies and protein microarrays.[214] However, challenges still remain

in ensuring consistent and stable activity of biomolecules on surfaces while also preventing their denaturation and undesirable interactions with the surface.[215,216] Additionally, in order to obtain the greatest level of sensitivity and specificity in detection and response, a large amount of desired biomolecules need to be immobilized uniformly over the material with outward presentation of the active site.[217] Various methods have been developed to improve biomolecule immobilization on solid surfaces, which can be divided into three categories: physical adsorption, electrostatic interaction, and covalent bonding.[218,219] The first two methods are relatively simple to apply, however, their effects are often temporary and reversible due to the dissociation of immobilized molecules from the surface.[220,221] Alternatively, covalent tethering with specific functional groups can be used for immobilization, and this binding process is usually irreversible due to the stable nature of the bond. However, the required reactive functional groups must be present on the surface of the material and many polymers inherently lack these groups. Furthermore, for applications that use multiple materials within a device or system, different surface modifications for each material type are typically needed.

Polydimethylsiloxane (PDMS) is a widely used polymer in biomedical applications including oxygenators,[222] implants,[223] biosensors[224] and microfluidics,[225] due to its attractive features such as chemical stability, good mechanical properties, relatively good biocompatibility and simple fabrication by replica moulding.[226] Despite these advantages, the inherent chemical inertness of PDMS surfaces and the lack of functional groups (i.e. sites for protein attachment) present a challenge in directly immobilizing biomolecules on its surfaces.[226–228] Thus, chemical treatment to induce functional groups on PDMS surfaces or synthesis of PDMS copolymers is generally required to permit protein immobilization. These usually involve complicated and harsh reaction conditions where functional groups must first be present, such as with PEG-grafted and carboxybetaine-modified PDMS surfaces.[229,230] Therefore, a broadly applicable approach to modify the PDMS surface for biomolecule immobilization is highly desirable to achieve maximum recognition capacity and ensure the long-term stability of the immobilized biomolecules.

Diazirines are effective carbene precursors which have been applied as photoaffinity labeling groups,[57] as crosslinkers for photopatterning of polymers and

semiconductors,[67,70,72] as adhesives for low-surface-energy materials and tissue surfaces,[61,164] as well as for transforming thermoplastic polyolefins into thermosets.[36,183] Carbene surface modification has also been applied on glass fiber membranes to introduce the enzyme cellulase with successful maintenance of activity.[231] Upon thermal- or photo-activation, the diazirine motif loses N_2 and generates a reactive carbene that rapidly forms covalent bonds with any nearby available substrate through C–H, N–H, and O–H insertions without forming new high-energy species which can lead to substrate damage.[161] Although a few studies using diazirine motifs for surface functionalization exist, their occasional application to biomolecule immobilization is limited to tedious diazirine synthesis procedures (5 or 7 steps) and often they are lacking optimization of the substrate.[101,232,233] For example, the Leipzig group used alkyl *mono*-diazirine **5.1** (Figure 5.1) to functionalize chitosan, and then covalently bonded maleimide groups for protein immobilization.[232] However, activation of alkyl diazirine **5.1** affords a dialkyl carbene that is prone to rapid 1,2-hydrogen shifts. This leads mostly to production of undesirable alkene reaction products, which decreases the surface functionalization efficiency and prevents **5.1** from being used with low-functionality polymer surfaces.[234] More recently, Shestopalov et al. and Marchand-Brynaert et al. designed trifluoromethyl aryl diazirine **5.2** (Figure 5.1) with an electrophilic *N*-hydroxysuccinimide (NHS) ester reactive group for functionalizing different material surfaces or grafting NHS esters on polyethylene glycol (PEG).[101,233] According to previous studies from Musolino et al., the presence of electron-withdrawing groups present in the *para*-position of aryl diazirine molecules (as present in **5.2**) resulted in only 6% thermal C–H insertion yield in a cyclohexane model experiment, which implies low efficiency in surface functionalization.[50] By contrast, electron-donating groups present in the *para*-position of aryl diazirine molecules resulted in high C–H insertion yields, up to 92% using cyclohexane as a model compound. Additionally, electron-rich diazirine molecules can be activated at low temperatures (approximately 80 °C) or through the use of visible light (395 nm), which are both milder conditions in comparison to the corresponding electroneutral or electron-poor diazirine molecules.[50]

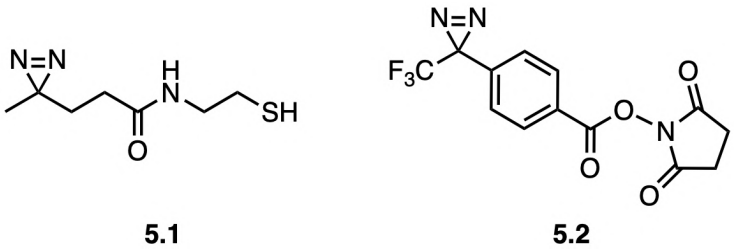

Figure 5.1 Structures of compounds **5.1** and **5.2**.

Herein we propose a simple, efficient, and scalable approach to covalently immobilize proteins of interest onto a polymeric surface using electronically optimized diazirine-based small molecule linkers. We designed two types of *mono*-diazirine compounds containing different electrophilic moieties: imidazole carbamate **5.3** and benzyl bromide **5.4**, both of which incorporate an electronically optimized aryl diazirine moiety (Figure 5.2), which encodes an electron-rich aryl group to stabilize the desired singlet carbene. In the absence of this stabilization, the singlet carbene that is initially generated following diazirine activation rapidly relaxes to the corresponding triplet state, which can suffer unwanted quenching by O_2.[90,232] The carbamate and benzyl halide in compound **5.3** and **5.4** respectively are efficient electrophilic units where the amino groups present on the proteins can interact and easily provide covalent protein immobilization onto the surface. Compared to other commonly used protein immobilization methods such as polydopamine (PDA) coatings, which can result in inhomogeneous surface coverage and non-covalent interactions with the PDMS surface,[235,236] this diazirine-based approach allows covalent conjugation of the protein to the PDMS, increasing protein immobilization after elution steps. The durability and strength of protein attachment, combined with the potential for scalability, make this method particularly suitable for applications that require permanent properties, such as biosensors, medical devices, and implants.

To investigate the efficacy of the diazirine molecules for protein immobilization, bovine serum albumin (BSA) and immunoglobulin G (IgG) were selected as model biomolecules. Albumin is a globular plasma protein and is an attractive natural biomolecule for surface modification and functionalization. BSA is commonly used as a passivating agent to prevent non-specific adhesion and as a "backfiller" to fill residual spaces on solid surfaces after a biomolecule has been immobilized.[237,238] IgG is the most

common antibody and is found in blood and extracellular fluid. It plays an important role in the immune system and in controlling infections by binding to pathogens such as viruses, bacteria and fungi.[239] Additionally, antibodies have high specificity and binding affinity toward their corresponding antigen molecules,[240] providing them with an essential role in the development of immunosensors.[241,242]

In this study, we hypothesized that newly synthesized diazirine molecules **5.3** and **5.4** can be used as a tool for functionalization of PDMS surfaces to covalently immobilize biomolecules. To validate this hypothesis, the three diazirine molecules (**5.3**, **5.4** and a control diazirine **5.5**) were applied to modify PDMS and subsequently activated through thermal and ultraviolet (UV) methods. Compared to traditional PDMS modification approaches, the diazirine modification process did not need complicated steps and harsh reaction conditions. The success of the PDMS surface modifications was confirmed by X-ray photoelectron spectroscopy (XPS) analysis, attenuated total reflectance (ATR)-Fourier transform infrared spectroscopy (FTIR), contact angle measurements and atomic force microscopy (AFM). In addition, two models were presented using cyclohexane as a small-molecule model for C–H containing polymers and isopropylamine as a model for amino groups on proteins to demonstrate the incorporation of carbene into PDMS and the reaction of diazirines with biomolecules for immobilization. The effectiveness of BSA and IgG immobilization on diazirine-modified PDMS surfaces was quantified using iodine-125 radiolabeling and the stability of the immobilized proteins was determined by sodium dodecyl sulfate (SDS) elution. Further, confocal microscopy was performed to visualize the distribution of immobilized IgG on the modified PDMS surface. This surface modification strategy with new diazirine derivatives provides a promising and novel pathway for polymeric surface functionalization to enhance protein immobilization for various biomedical applications.

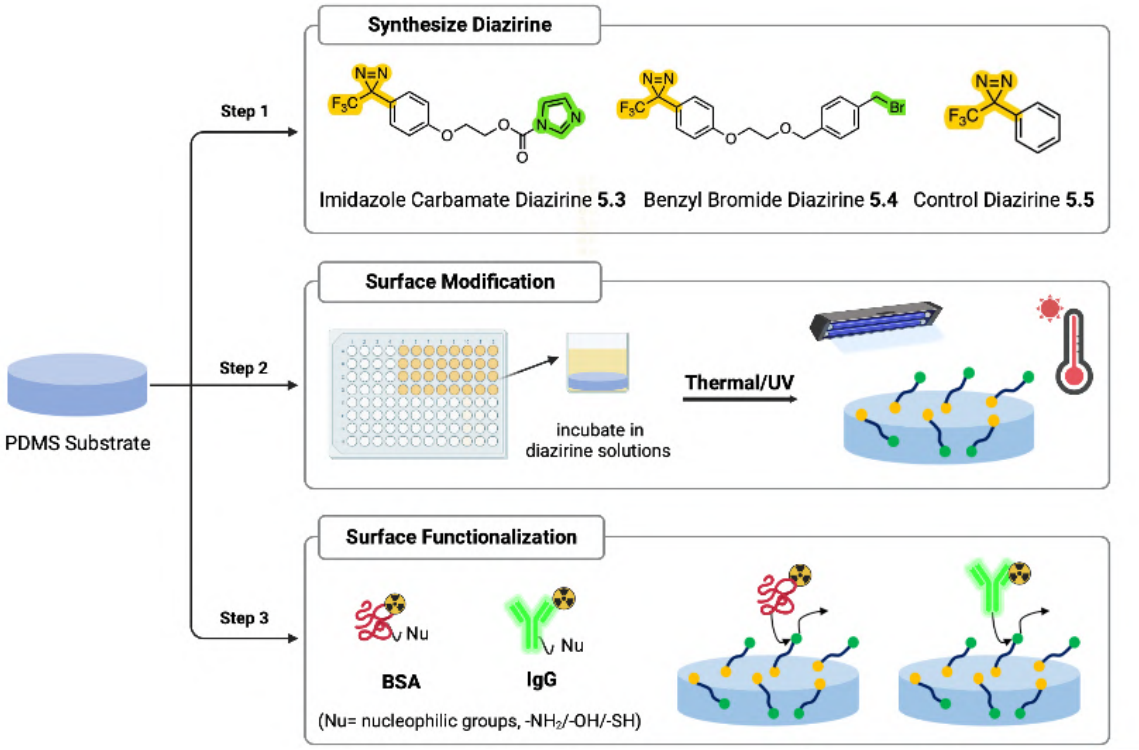

Figure 5.2 Schematics showing surface modification with diazirines on PDMS substrates through carbene C–H insertion, and the protein reaction with the electrophilic moieties of the small molecules.

5.3. Results and Discussion

5.3.1 Synthesis of electronically optimized diazirine reagents for surface functionalization

The target compounds **5.3** and **5.4** were readily synthesized from ethylene glycol diazirine **5.6** in one step, as illustrated in Scheme 5.1. To achieve a rapid and clean protein immobilization in subsequent steps, efficient electrophilic groups on linkers have been selected: imidazole carbamate[243,244] and benzyl bromide, where the latter has been widely used for polymer grafting[24,163,245] and small molecular functionalization,[246] and the former is known to react efficiently with amine-containing nucleophiles.

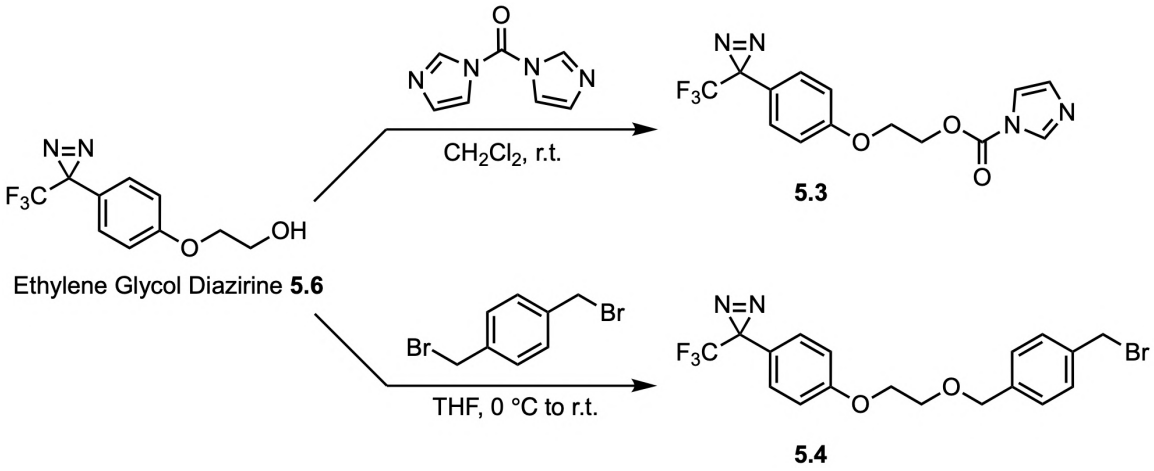

Scheme 5.1 Synthetic procedures for diazirine-based reagents **5.3** and **5.4**.

5.3.2 Benchmarking of diazirine-based linkers performance on surface functionalization and protein immobilization

In previous studies, the insertion of a diazirine molecule crosslinker into PDMS polymer was validated by studying the insertion efficiency into the small-molecule model hexamethyldisiloxane (HMDSO).[27] To evaluate C–H insertion efficiencies of the two new electronically optimized diazirine-based linkers **5.3** and **5.4**, we employed cyclohexane as a molecular model of low-functionality PDMS, since the previously reported model compound HMDSO did not dissolve compounds **5.3** and **5.4**, and since cyclohexane has previously been employed as a general model for aliphatic polymers.[36,50] As shown in Scheme 5.2, both linkers **5.3** and **5.4** successfully insert into C–H bonds of cyclohexane upon thermal activation at 100 °C with over 80% efficiency. Finally, to

probe the protein immobilization efficacy of **5.7** and **5.8**, we selected isopropylamine as a small molecular model for proteins, since amines (-NH_2) are one of the most abundant reactive groups on the protein chains. Isolated yields of the pure amine-adducts **5.9** and **5.10** were 92% and 70%, respectively. Both small-molecule model experiments successfully proved that our electronically optimized diazirine linkers can efficiently functionalize low-functionality polymer surfaces. This also occurred without the electrophilic motifs suffering undesirable reactions with the intermediate carbenes, a significant advantage compared to other methods. The covalently linked electrophilic groups can then readily react with protein substrates to functionalize the surface.

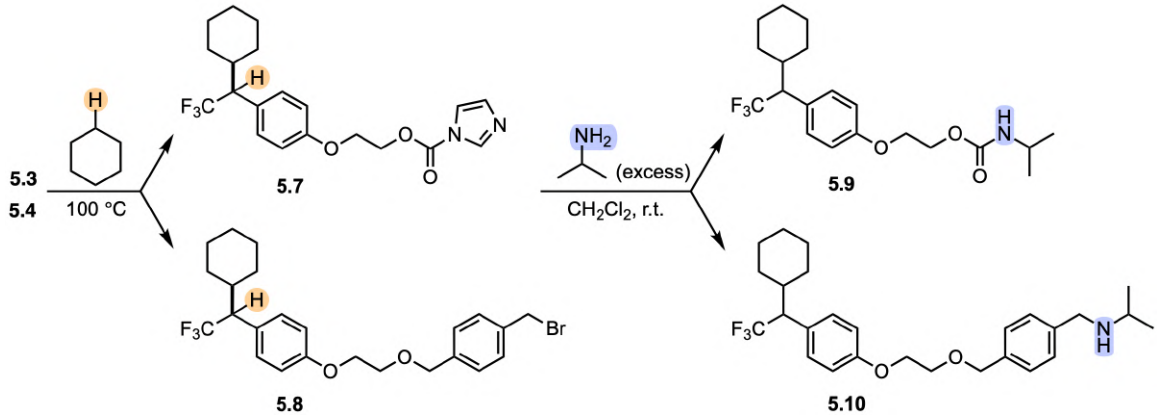

Scheme 5.2 Comparison of cyclohexane C–H insertion efficacy and amine reactivity to simulate protein immobilization.

5.3.3 Surface characterization

The wettability and roughness of the surface are both important in the interaction between biomolecules and materials. The water contact angle of various PDMS surfaces is shown in Figure 5.3. The unmodified PDMS surface exhibited a contact angle of 102.7 °, a value that is in the typical range for hydrophobic silicone materials. After applying thermal (100 °C) or UV (360 nm) treatment on the PDMS surface, no significant change in contact angle was observed demonstrating that these methods alone do not alter the surface wettability. However, the contact angle values of diazirine-modified surfaces showed a significant decrease for all types of diazirines with both activation methods ($p < 0.0001$). This reduction in water contact angle (indicating a decrease in hydrophobicity) confirms a modification to the surface properties.

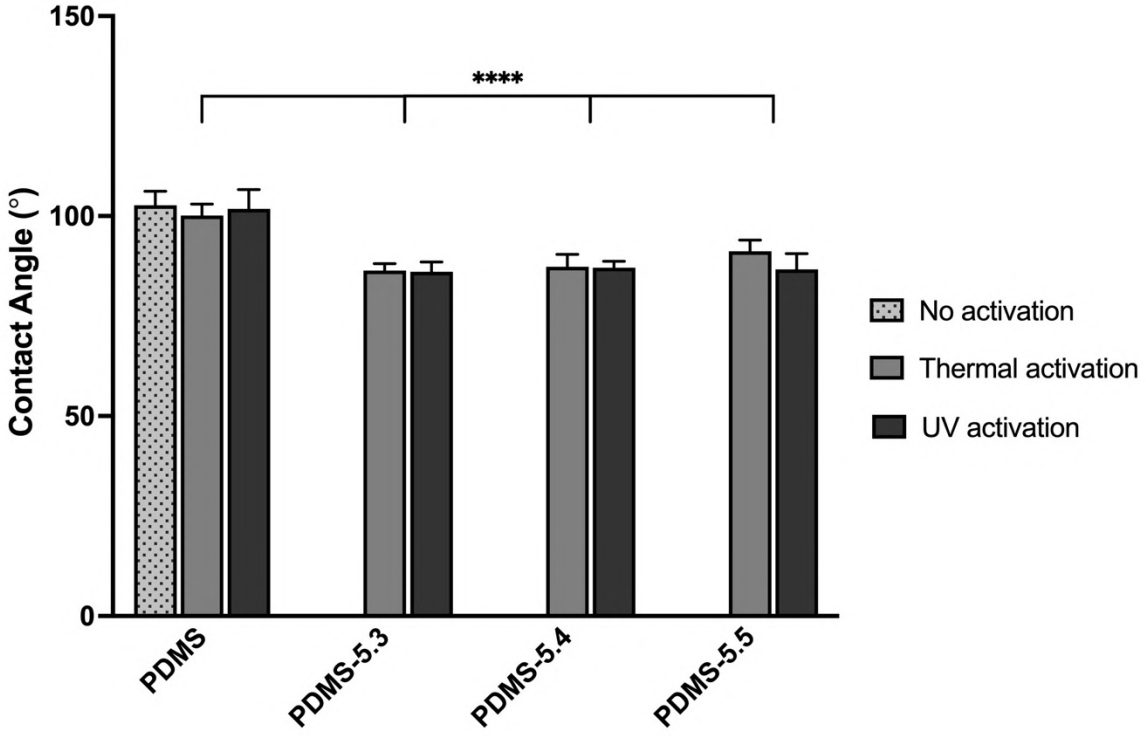

Figure 5.3 Advancing contact angle measurements of control and diazirine-modified PDMS surfaces (**5.3**: carbamate diazirine, **5.4**: benzyl bromide diazirine and **5.5**: control diazirine). Data are mean ± SD (n= 6), ****p < 0.0001.

The surface roughness and heterogeneity of PDMS and modified PDMS was analyzed using AFM to determine topographical changes that may influence subsequent interactions (Figure 5.4 and S5.1). The root-mean-square (RMS) roughness of native PDMS was measured to be 1.01 nm, with no apparent surface irregularities observed (Table 5.1). Thermal treatment of native PDMS surfaces did not result in an increase in roughness, while UV treatment increased the PDMS surface roughness by just over 1 nm. The thermally activated compound **5.3** modified surface had an increase in roughness, and particles appeared on the surface. The roughness of the UV-activated PDMS-**5.3** surfaces dramatically increased to 109.6 nm, likely due to the aggregation of diazirine molecules during the activation process demonstrating a very heterogeneous surface. Meanwhile, the PDMS surfaces modified with compounds **5.4** and **5.5** had a much smoother and uniform surface with both activation methods, with roughness values of approximately 2–6 nm.

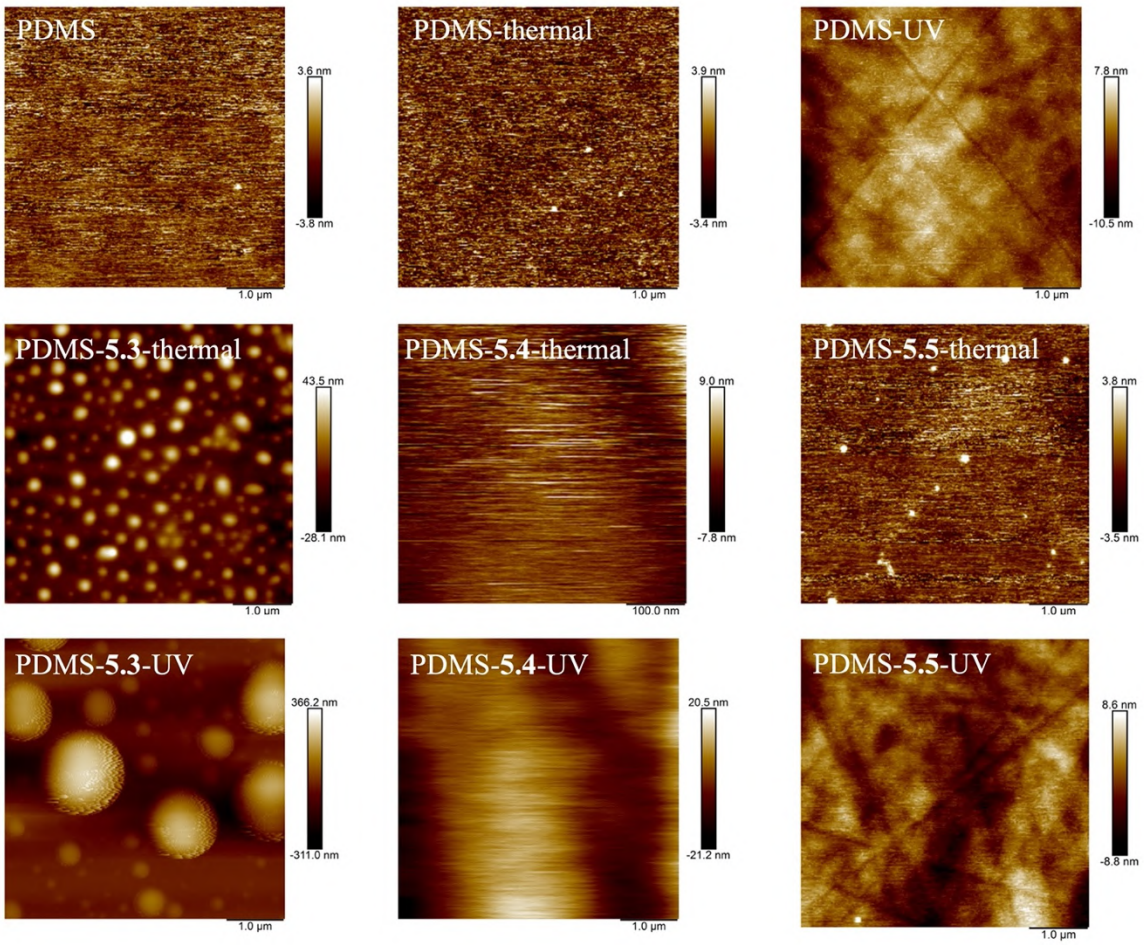

Figure 5.4 AFM characterization of control and diazirine-modified PDMS surfaces; Scans are 5 µm x 5µm.

Table 5.1 The surface roughness of control and diazirine modified PDMS surfaces determined by AFM (**5.3**: carbamate diazirine, **5.4**: benzyl bromide diazirine and **5.5**: control diazirine).

Sample	Roughness (nm)
PDMS	1.01 ± 0.07
PDMS-thermal	1.07 ± 0.06
PDMS-UV	2.19 ± 0.24
PDMS-**5.3**-thermal	8.04 ± 1.64
PDMS-**5.3**-UV	109.60 ± 17.14
PDMS-**5.4**-thermal	2.25 ± 0.3
PDMS-**5.4**-UV	5.76 ± 1.74
PDMS-**5.5**-thermal	1.09 ± 0.09
PDMS-**5.5**-UV	2.36 ± 0.08

The surface modifications on control and modified PDMS surfaces were also analyzed using ATR-FTIR (Figure 5.5). The bands observed between 1100 and 1020 cm^{-1} were characteristic of the asymmetric stretching of Si–O–Si in a PDMS polymer network.[247] The bands at 1408 and 1258 cm^{-1} were associated with the asymmetric and symmetrical deformations of the C–H bond of the $Si(CH_3)_2$ groups, respectively.[248] The rocking deformation of C–H and Si–C bond stretching were observed at 843 and 790 cm^{-1}, respectively (Figure 5.5a). The symmetric stretching of the $-CF_3$ groups in the analysed diazirines was seen in the 1140 cm^{-1} region.[249] The diazirine ring was expected to be observed near 1630 cm^{-1}, but this band was weak in control molecule **5.5** (Figure 5.5b).[250] The peak at 1631 cm^{-1} was related to N=N, while the peaks at 1610 cm^{-1} and 1344 cm^{-1} were assigned to the C–N bond.[251] The peaks around 1700 cm^{-1} were indicative of the presence of a carbonyl group, which is specific for compound **5.3** (Figure 5.5c). Overall, the data clearly demonstrate modification of the PDMS with the diazirine compounds.

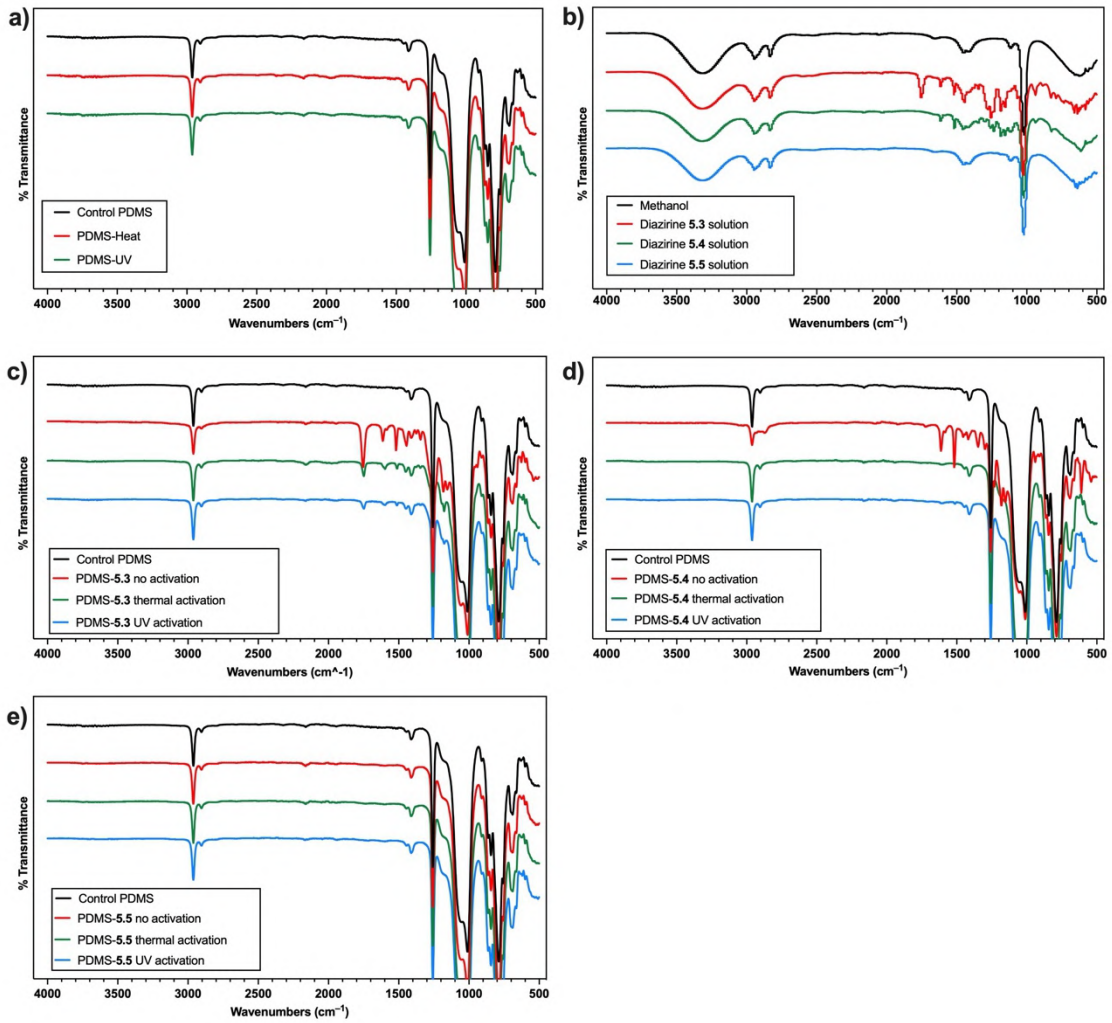

Figure 5.5 FTIR-ATR spectra of a) PDMS, b) diazirine solutions of compound **5.3**, **5.4** and **5.5**, c) PDMS modified with compound **5.3**, carbamate specific peak have been observed at 1700 cm^{-1}, d) PDMS modified with compound **5.4** and e) PDMS modified with compound **5.5** (**5.3**: carbamate diazirine, **5.4**: benzyl bromide diazirine and **5.5**: control diazirine).

Table 5.2 presents the XPS analysis of the elemental composition on PDMS surfaces displayed as a percentage. The control PDMS has high levels of carbon, silicon and oxygen as expected. Trace levels of nitrogen and fluorine are also seen that are likely due to low levels of surface contaminants evident in the highly surface sensitive and vacuum environment of the XPS. With all modifications, there is an increase in the nitrogen and fluorine, and a corresponding decrease in the silicon, indicating the successful modification of a diazirine layer on the PDMS surfaces. For surfaces modified

with compounds **5.3** and **5.5**, the amount of nitrogen and fluorine after thermal activation was lower than that of UV activation, likely due to the mobility of the molecules at high temperatures and loss of nitrogen and fluorine. The detection of elemental bromine confirms the presence of benzyl bromide diazirine (from **5.4**) on the modified PDMS surfaces. After activation, both fluorine and bromine content in PDMS-**5.4** samples decreased. Thermal activation resulted in a greater decrease in nitrogen compared to UV activation, which may be attributed to the high temperature promoting molecule mobility and evaporation.

Table 5.2 XPS elemental composition (%) of native PDMS and PDMS modified with compounds **5.3**–**5.5** (**5.3**: carbamate diazirine, **5.4**: benzyl bromide diazirine and **5.5**: control diazirine).

Sample	Si	C	N	O	F	Br
PDMS	28.18 ± 0.32	43.51 ± 0.44	0.05 ± 0.04	27.86 ± 0.30	0.44 ± 0.09	
PDMS-**5.3**	25.14 ±1.73	42.85 ± 0.58	1.11 ± 0.40	27.62 ± 0.61	3.18 ± 1.44	
PDMS-**5.3**-thermal	24.49 ± 1.19	44.21 ± 0.52	0.64 ± 0.13	27.88 ± 0.18	2.77 ± 0.70	
PDMS-**5.3**-UV	23.74 ± 0.75	44.53 ± 1.23	0.93 ± 0.12	27.49 ± 1.02	3.28 ± 0.43	
PDMS-**5.4**	19.03 ± 5.02	49.01 ± 4.17	1.64 ± 0.50	22.25 ± 1.91	6.17 ± 1.57	1.82 ± 0.68
PDMS-**5.4**-thermal	24.78 ± 0.32	45.27 ± 0.22	0.57 ± 0.09	27.45 ± 0.16	1.91± 0.10	0.5
PDMS-**5.4**-UV	21.27 ± 3.26	49.20 ± 3.22	0.71 ± 0.22	25.55 ± 1.78	3.23 ± 1.59	0.6
PDMS-**5.5**	26.85 ± 0.37	43.26 ± 0.32	0.41 ± 0.08	28.22 ± 0.34	1.26 ± 0.10	
PDMS-**5.5**-thermal	26.99 ± 0.41	42.86 ± 0.29	0.28 ± 0.16	28.90 ± 0.21	0.96 ± 0.18	
PDMS-**5.5**-UV	26.35± 0.69	43.88 ± 0.64	0.40 ± 0.17	28.22 ± 0.56	1.15 ± 0.43	

5.3.4 Protein immobilization and stability

The amount of BSA immobilized on native and modified PDMS surfaces was measured through radiolabeling experiments (Figure 5.6). The native PDMS surfaces were used as controls to compare physical adsorption of BSA to the modified surfaces. The thermal and UV treated PDMS surfaces also served as controls to ensure that no change in protein adsorption occurred with these treatments alone. The results indicate that the PDMS surfaces do not exhibit a noticeable change in BSA adsorption compared to the thermal or UV treated surfaces, confirming that these modifications themselves do not impact the BSA adsorption on PDMS. In contrast, the PDMS surfaces modified with diazirine compounds **5.3** and **5.4** and activated thermally both showed significant improvements in BSA immobilization compared with PDMS controls, with both modifications reaching similarly high levels. Specifically, the amount of BSA immobilized on PDMS-**5.4** surfaces activated thermally was approximately 3.5 times higher than that on the control PDMS surfaces. However, with UV activation, only compound **5.4**-modified surfaces showed a significant increase in the amount of BSA immobilized, with an amount much lower compared to thermal activation ($p < 0.0001$). We hypothesized that the distinct polarity difference between compound **5.3** (polar) and the PDMS substrate (containing a hydrophobic surface) results in phase separation. Consequently, this leads to the observed aggregation of **5.3** on the surfaces. During UV activation, when the reagents **5.3** aggregate, they tend to form diazo linkages (along with other undesirable species) instead of inserting into the polymer substrate. Under thermal activation conditions, there is likely to be greater mobility of the molecules (as well as of the surface), reducing the impact of these effects. The control diazirine **5.5**-modified surfaces adsorbed levels of BSA similar to the PDMS controls, regardless of whether they were activated thermally or photochemically. This was expected since the control diazirine **5.5** compounds do not have specific functional groups to bind to the proteins.

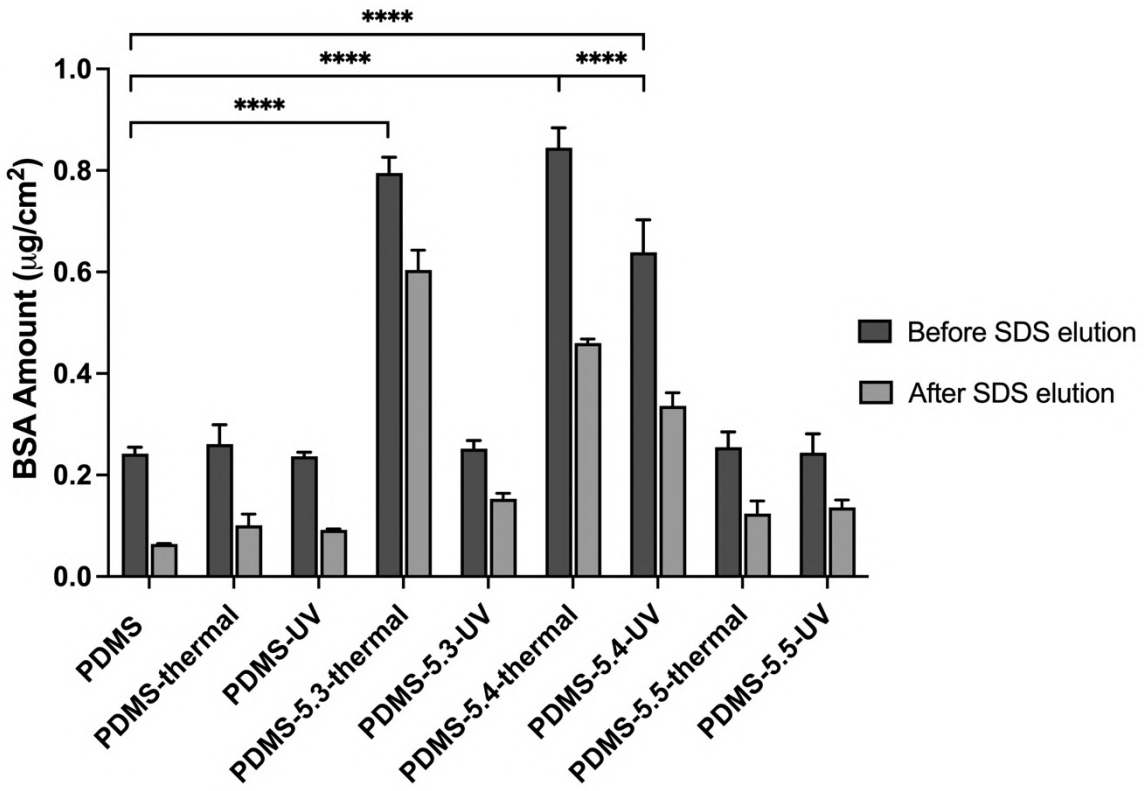

Figure 5.6 BSA adsorption from PBS buffer (2 mg/mL) to various modified PDMS surfaces and the amount of protein remaining after 2% SDS elution (**5.3**: carbamate diazirine, **5.4**: benzyl bromide diazirine and **5.5**: control diazirine). Data are mean ± SD, n=3, ****$p < 0.0001$.

The stability of the immobilized BSA on diazirine-modified PDMS surfaces was evaluated by eluting the loosely bound proteins with 2% of SDS for 24 hours with shaking. The results after SDS elution demonstrate that there is a significantly high amount of BSA remaining on **5.3**- and **5.4**-modified PDMS surfaces with thermal activation. In particular, the immobilized BSA on the compound **5.3**-modified surfaces showed significantly increased stability after elution in comparison to compound **5.4** ($p < 0.0001$, Figure 5.6). Slightly lower levels of BSA remaining after elution are detected when compound **5.4** is treated photochemically on the PDMS surface. In contrast, there is no significant increase in the amount of BSA remaining on the compound **5.3**-modified PDMS surfaces activated photochemically likely due to insufficient modification of the surface as indicated in the AFM images.

Compound **5.3**- and **5.4**-modified surfaces activated by thermal treatment exhibited the highest amount of BSA immobilization. The enhanced immobilization of BSA on diazirine **5.3** and **5.4** modified PDMS can be attributed to the formation of covalent bonds between the protein and the carbamate imidazole and benzyl bromide functional groups in diazirine **5.3** and **5.4**, respectively. During the thermal activation process, the high temperature can promote the mobility of these molecules, leading to a uniform coating on the surface. However, with UV activation, the AFM results show that compound **5.3** molecules appear to self-aggregate on the PDMS, causing heterogeneities in the surface and greatly reducing the effectiveness of protein immobilization. The compound **5.4** modified surfaces show some inhomogeneities, likely due to alteration of the benzyl bromide diazirine-coated surfaces during the UV activation process, resulting in lower immobilization levels. However, these levels are still much greater than the control samples after SDS elution demonstrating their stability and potential use for advanced material applications, including the combination of photolithography for UV activation to achieve functional patterning on surfaces. These results suggest that modifying PDMS with diazirine-based linkers is an effective approach for functionalizing the surfaces and increasing protein immobilization, with potential advantages over other common coating methods. The immobilization amounts and stability were significantly influenced by the different functional groups and activation methods. It is expected that modifications with these diazirine molecules could be applied for attaching various bioactive molecules to provide specific functionality to materials and devices, for example with anticoagulant or fibrinolytic molecules to improve the blood compatibility of devices.

5.3.5 Antibody immobilization and stability

To investigate the effect of the diazirine-modified PDMS surfaces on antibody immobilization, IgG was chosen as the model antibody to be measured on diazirine-modified PDMS. The amount of immobilized IgG on different surfaces was quantified through radiolabeling experiments, as shown in Figure 5.7. Consistent with the previous BSA immobilization results, the thermally activated **5.3**- and **5.4**-modified surfaces had the highest amount of immobilized IgG, indicating that both imidazole and bromide

groups efficiently react with IgG under these conditions. Specifically, compared to the control PDMS, the compound **5.3**-modified surface immobilized an approximately 5-fold higher level of IgG. With UV activation, only the compound **5.4**-modified surfaces demonstrated a significant increase in the amount of immobilized IgG, although this effect was not as pronounced as with thermal activation. Similar to the BSA results, during UV activation, compound **5.3** and **5.4**-coated PDMS surfaces showed molecular aggregation and surface distortion, respectively, as detected by AFM, resulting in lower IgG immobilization amounts. The control molecule **5.5**-modified surfaces did not show a significant increase in the IgG immobilization amount, which can be attributed to the absence of functional groups on the control diazirine molecule and its inability to enhance antibody immobilization.

To evaluate the stability of the immobilized IgG on different surfaces, the samples were incubated in 2% SDS for 24 hours. On control samples, the IgG amounts remaining after SDS elution were lower than for BSA. The compound **5.3**-modified surfaces activated thermally, and the **5.4**-modified surfaces activated thermally and with UV, retained a significantly higher amount of immobilized IgG compared to the control PDMS surfaces ($p < 0.0001$, Figure 5.7). The levels of IgG remaining on the thermally activated surfaces modified with **5.3** and **5.4** were similar. Despite the different functionalization routes, the thermal activation of PDMS surfaces with either of these two diazirine molecules not only demonstrated similar abilities to immobilize antibodies, but also exhibited comparable stability in retaining the immobilized antibodies. In this case of IgG, the control molecule **5.5**-modified surfaces activated by UV retained a slightly higher amount of IgG compared to the control PDMS ($p < 0.05$). However, significantly less IgG was retained on surfaces treated with compound **5.5** compared to surfaces treated with **5.3** or **5.4**.

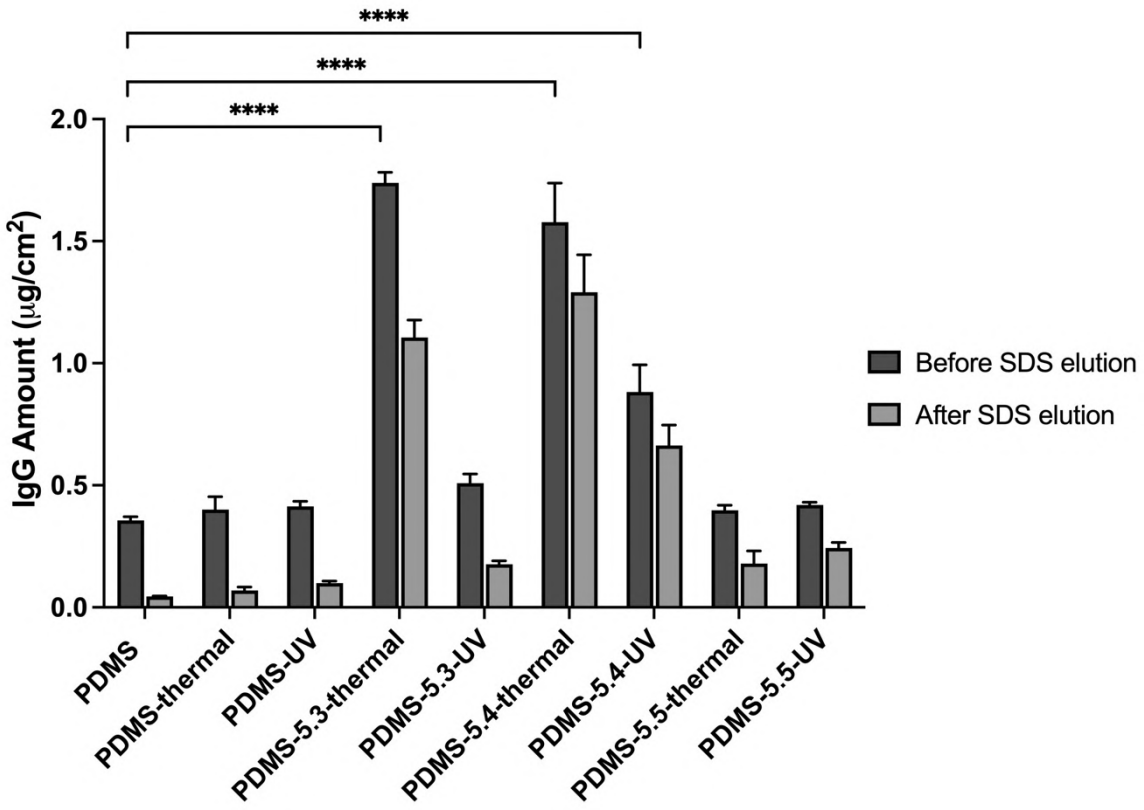

Figure 5.7 IgG adsorption from PBS buffer (1 mg/mL) to various modified PDMS surfaces and the amount of protein remaining after 2% SDS elution (**5.3**: carbamate diazirine, **5.4**: benzyl bromide diazirine and **5.5**: control diazirine). Data are mean ±SD, n=3, ****$p < 0.0001$.

Therefore, both the carbamate diazirine (**5.3**) and benzyl bromide diazirine (**5.4**) effectively functionalized the surfaces to enhance the immobilization of different biomolecules. This improvement is attributed to the specific covalent reactions between these two diazirine molecules and the biomolecules. Surfaces modified using thermal activation showed superior effectiveness compared to UV activation, likely due to the achievement of more uniform coatings. These diazirine-modified surfaces have a stable and reliable ability for functionalization evidenced by the similar trends observed in the immobilization amount of different biomolecules. The small variations in amount and stability observed for the BSA protein and IgG antibody are likely a result of the distinct structures of these two biomolecules, including their size and number of amine groups available for binding. For biosensing applications, the ability to immobilize higher amounts of IgG can lead to enhanced sensitivity. These model studies with IgG can

readily be translated to attach particular monoclonal antibodies with specificity for various protein biomarkers in biological fluids such as blood.

5.3.6 Distribution of immobilized IgG

The distribution of immobilized IgG on various PDMS surfaces was investigated using confocal microscopy. Confocal microscopy provides a significant advantage over traditional fluorescence microscopy due to its ability to perform optical sectioning, which allows for the creation of 3D reconstructions of a sample from high-resolution image stacks.[252] This offers valuable information on the distribution of IgG throughout the bulk of the PDMS substrate, along with surface distribution, and helps determine if the diazirine molecules have permeated into the inner layers of PDMS.

The IgG adsorption on the control PDMS surface was relatively uniform, with more non-covalent adsorption on the top side and less on the bottom (Figure 5.8). The control compound **5.5**-modified surfaces also displayed an even distribution of IgG, similar to the control PDMS surface. On the compound **5.3**-modified PDMS surfaces with thermal activation, the IgG seems to be distributed into the bulk of the PDMS substrate, with possible penetration into the PDMS polymer network (Figure 5.9). This is likely due to the high temperature during modification promoting the movement of compound **5.3**, enabling a greater number of molecules to penetrate into the bulk. In contrast, the IgG was primarily distributed on the surface of the compound **5.4**-modified PDMS samples, demonstrating that compound **5.4** is not able to penetrate into the PDMS. Additionally, despite the high amount of immobilized antibody on the **5.4**-modified surfaces, the distribution of IgG was more uniform on the compound **5.3**- and **5.5**-modified PDMS surfaces. With UV activation, the IgG still penetrated into the bulk of the **5.3**-modified PDMS substrate, but to a lesser extent than with thermal activation (Figure 5.10). Compared to the benzyl bromide diazirine **5.4**, the imidazole carbamate diazirine **5.3** appears to have a greater capacity to penetrate into the bulk of the PDMS, and the high temperature promotes this phenomenon. This suggests that the degree of penetration is influenced by both the type of diazirine functional groups and the activation method.

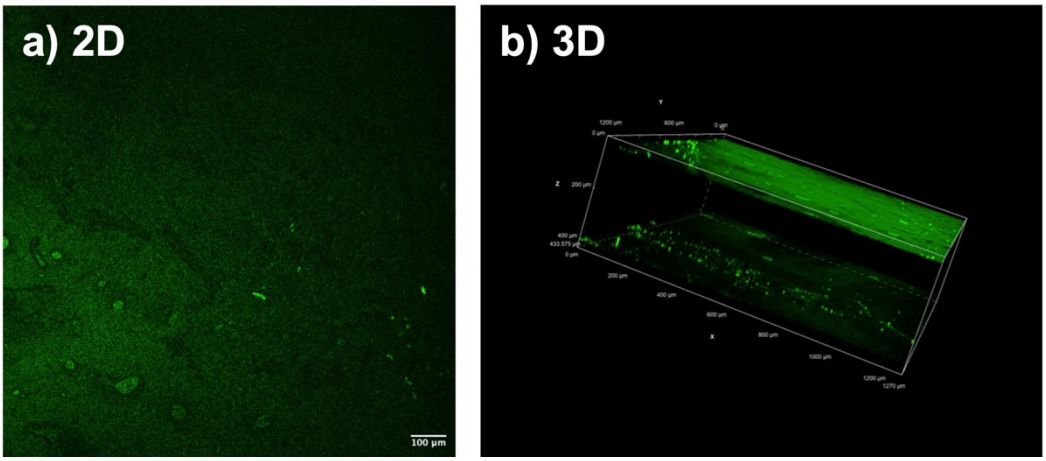

Figure 5.8 a) 2D and b) 3D confocal images of IgG-FITC (1 mg/mL) distribution on the native PDMS surface.

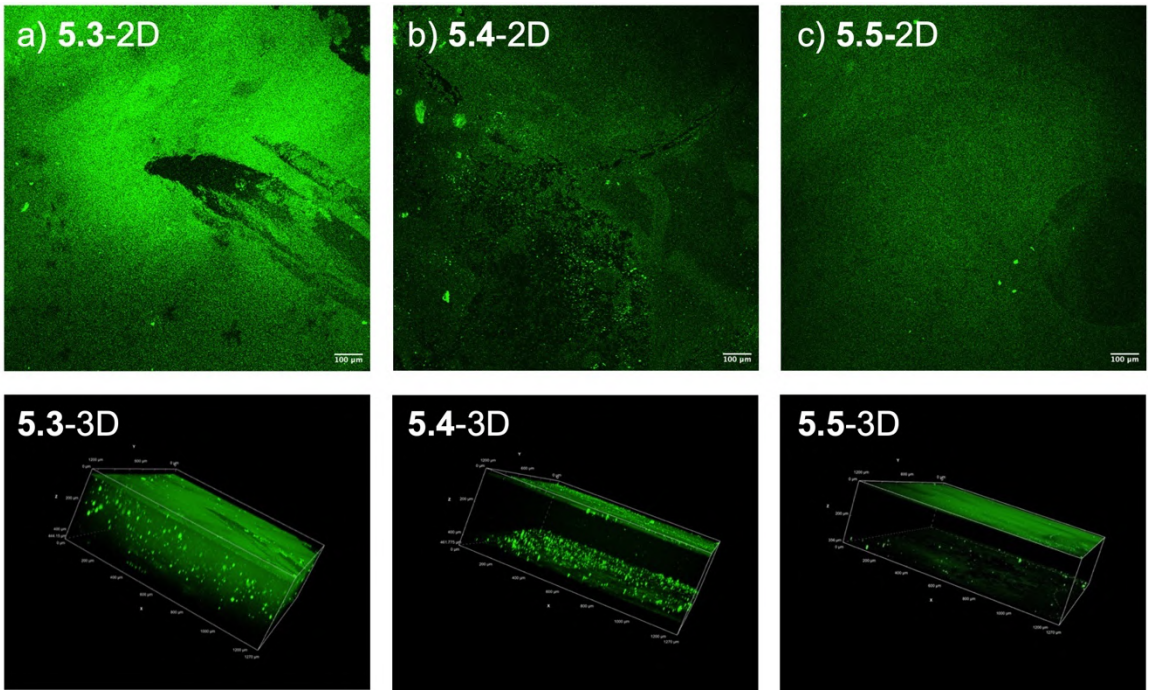

Figure 5.9 The 2D (top) and 3D (bottom) confocal images of immobilized IgG-FITC (1 mg/mL) distribution on PDMS modified with a) compound **5.3**, b) compound **5.4** and c) compound **5.5** thermally activated at 100 °C (**5.3**: carbamate diazirine, **5.4**: benzyl bromide diazirine and **5**: control diazirine).

Comparatively, the surfaces modified with compound **5.4** exhibited a more homogeneous distribution of IgG with thermal activation, while UV activation resulted in a layered distribution, as observed with AFM. Combining these observations with the radiolabeling results, it was found that the surfaces modified with compound **5.3**

activated with UV exhibited lower immobilization compared to thermal activation. This could be partly attributed to the molecules aggregating on the surfaces and partly due to a lower amount of compound **5.3** penetrating into the substrate. The surfaces modified with compound **5.4** show less effective immobilization with UV activation compared to thermal activation, possibly due to the surface distortion that limits its ability to bind more IgG. Therefore, by analyzing confocal 3D images, the influence of the functional group and activation methods on the degree of penetration of different diazirine molecules on modified PDMS surfaces can be observed, along with a better understanding of the role of the activation methods on the uniformity of the coating layer. These factors can impact the immobilization of biomolecules and the enhanced ability to penetrate polymeric materials may be beneficial in applications with substrates and devices of complex geometries including porous and other structured materials requiring thorough and sustained functionalization.

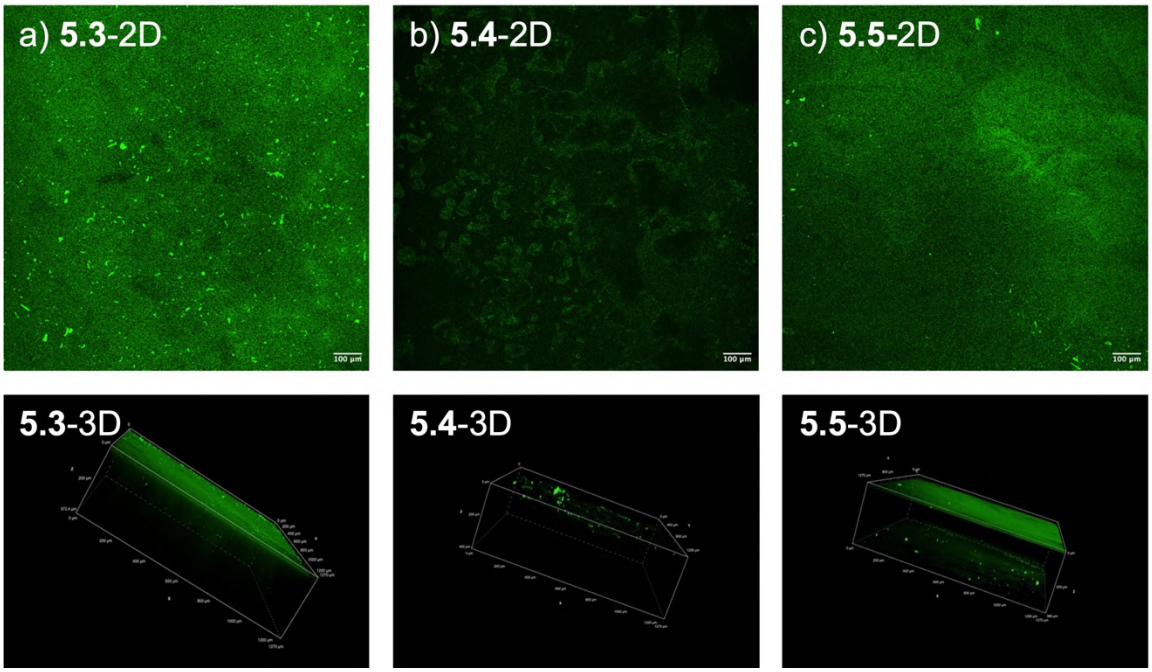

Figure 5.10 The 2D (top) and 3D (bottom) confocal images of immobilized IgG-FITC (1 mg/mL) distribution on PDMS modified with a) compound **5.3**, b) compound **5.4** and c) compound **5.5** UV activated with 360 nm (**5.3**: carbamate diazirine, **5.4**: benzyl bromide diazirine and **5.5**: control diazirine).

5.4. Conclusions

In this work, PDMS was successfully modified by newly synthesized diazirine molecules to enhance the immobilization of proteins. Small-molecule model experiments were performed with cyclohexane and isopropylamine to prove that the diazirine linkers could functionalize polymer surfaces without undesirable reactions. The modified substrates were characterized by water contact angle measurements, AFM, ATR-FTIR, and XPS to confirm changes in the surface wettability, roughness, chemical, and elemental composition, respectively. Radiolabelling the proteins BSA and IgG with ^{125}I provided a sensitive and effective method to quantify the amount of protein on the surface and determine the stability of the immobilization following SDS elution. Both carbamate **5.3** and bromide **5.4** diazirine-modified surfaces were able to increase the BSA and IgG immobilization amount, with greater effects when activated thermally compared to ultraviolet activation. Additionally, the **5.3**- and **5.4**-modified surfaces with thermal activation maintained a significantly greater amount of immobilized proteins following SDS elution, demonstrating the stability of this method based on the strong interactions between the functionalized diazirine molecules and proteins. Confocal microscopy images revealed the differences in immobilized antibody distribution between diazirine **5.3** and **5.4**-modified surfaces, highlighting the impact of the diazirine functional groups on the distribution of the molecule within the substrate, and their importance in the design of PDMS modified biomaterials.

Compared to other surface modification methods, functionalization can be achieved without complicated reaction steps or harsh conditions and can allow covalent conjugation of proteins to the surface. The successful UV activation of the benzyl bromide **5.4** diazirines provides the opportunity to apply these modifications with photolithography for functional surface patterning. Furthermore, the modifications can be translated to other substrates as long as C–H bonds are available for insertion. This versatility would be especially important in multi-material device applications, for example in a blood oxygenator system where an oxygenator may be a different material (e.g., PDMS) than the catheters used for connection (e.g., polyurethane). Applying just this one modification method to multiple materials could reduce manufacturing costs significantly. In addition, the simplicity and stability of the technique has advantages for

complex devices including porous materials, microfluidics, and structured implants, that are otherwise difficult to modify. Thus, this novel surface modification approach has the potential to contribute to the development of advanced biomaterials and devices for various biotechnological and medical applications.

5.5. Experimental and Supplementary Information

5.5.1 Synthesis of diazirine reagents and small molecule experiments

5.5.1.1 General considerations

All commercial materials were used as received unless otherwise noted. Reagents used for the synthesis of target compounds were purchased from Sigma-Aldrich except for *N*,*N*′-carbonyldiimidazole, which was purchased from AK Scientific. Reagent grade solvents were used for extractions and purifications. Anhydrous cyclohexane was used in crosslinking experiments. All diazirine-forming reactions were performed in the dark. Removal of solvent was done below 40 °C. Control diazirine **5.5** and ethylene glycol diazirine **5.6** were obtained from XlynX Materials Inc (Victoria, BC, Canada).

NMR spectra were recorded at ambient temperature using either a Bruker AVANCE 300 (300 MHz for ^{1}H, 283 MHz for ^{19}F, 76 MHz for ^{13}C) or a Bruker AVANCE Neo 500 (500 MHz for ^{1}H, 471 MHz for ^{19}F, 126 MHz for ^{13}C) spectrometer. Chemical shifts were reported in parts per million (ppm) and were referenced to the solvent peak ($CDCl_3$: ^{1}H NMR δ = 7.26 ppm, ^{13}C NMR δ = 77.16 ppm). ^{13}C spectra and ^{19}F spectra were ^{1}H decoupled unless otherwise noted. Data is reported as follows: chemical shift (multiplicity (s = singlet, d = doublet, t = triplet, q = quartet, qd = quartet of doublet, hept = heptet, m = multiplet), coupling constant in Hz, integration). Spectral assignments were made for compounds that gave well-resolved spectra in COSY, HSQC and HMBC experiments. Chemical shifts in ^{19}F spectra are reported in ppm and reported as obtained. Reaction progress was monitored by ^{1}H/^{19}F NMR spectroscopy.

High resolution mass spectrometry (HRMS) data were acquired using field desorption (FD) ionization on a JEOL AccuTOF GCx mass spectrometer. IR spectra were recorded using a Perkin-Elmer ATR spectrometer. IR wave numbers (ν) are reported in cm^{-1}.

5.5.1.2 Synthetic procedures of diazirine molecules

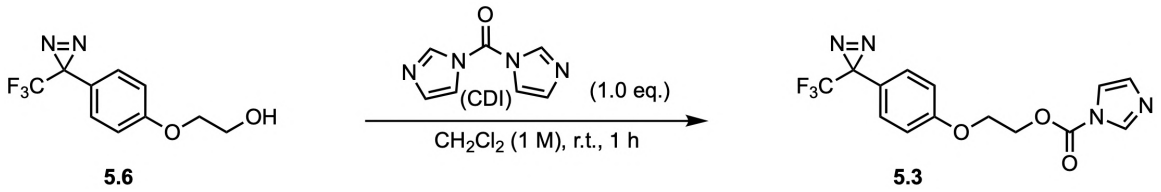

Compound **5.3**: To a solution of diazirine **5.6** (1.0 g, 4.1 mmol, 1.0 equiv.) in dichloromethane (4.0 mL, 1.0 M) at room temperature, *N*,*N*'-carbonyldiimidazole (CDI, 0.66 g, 4.1 mmol, 1.0 equiv.) was added under ambient atmosphere. After one hour of stirring at room temperature, the reaction was then quenched with NH_4Cl saturated solution and extracted with diethyl ether three times. The combined organic layer was dried over sodium sulfate. The solvent was removed to achieve the desired product **5.3** as a yellow solid without further purification (1.3 g; 94%). **^{1}H NMR** (500 MHz, $CDCl_3$) δ 8.14 (s, 1H), 7.42 (s, 1H), 7.17 (d, *J* = 8.4 Hz, 2H), 7.07 (s, 1H), 6.93 (d, *J* = 8.5 Hz, 2H), 4.80 – 4.70 (m, 2H), 4.37 – 4.24 (m, 2H). **^{13}C NMR** (126 MHz, $CDCl_3$) δ 159.15, 148.61, 137.17, 130.87, 128.35, 123.30 (q, *J* = 274.9 Hz), 121.97, 117.14, 114.97, 66.03, 65.45, 28.29. **^{19}F NMR** (471 MHz, $CDCl_3$) δ –65.62. **HRMS** (FD+) m/z $[M^{\bullet}]^+$ calculated for $C_{14}H_{11}F_3N_4O_3$: 340.0783, found: 340.0777.

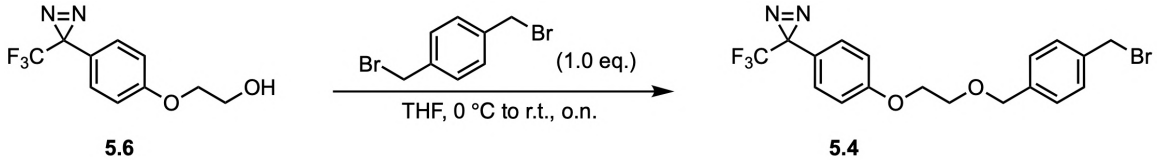

Compound **5.4**: To a suspension of sodium hydride (60% in mineral oil, 1.2 equiv.) in anhydrous THF (8 mL) at 0 °C under argon, a solution of **5.6** (4.4 g, 17.7 mmol, 1.0 equiv.) in anhydrous THF (10 mL) was added dropwise. After stirring the reaction for 10 min, a solution of α,α′-dibromo-*p*-xylene (4.67 g, 17.7 mmol, 1 equiv.) in anhydrous THF (20 mL) was added dropwise at 0 °C and then, the reaction was left stirring overnight at room temperature. The reaction was filtrated on a celite plug and washed with dichloromethane and then filtrated over silica using pentane affording the pure product **5.4** as a yellow solid (5.7 g, 75%). **^{1}H NMR** (300 MHz, $CDCl_3$) δ 7.43 – 7.29 (m, 4H), 7.13 (d, *J* = 9.0 Hz, 2H), 6.92 (d, *J* = 8.9 Hz, 2H), 4.61 (s, 2H), 4.49 (s, 2H), 4.18 – 4.10 (m, 2H), 3.87 – 3.79 (m, 2H). **^{13}C NMR** (126 MHz, $CDCl_3$) δ 159.94, 138.43, 137.45, 129.62, 129.31, 128.22, 128.03, 121.31, 115.14, 73.10, 68.58, 67.69, 33.36, 28.52.

^{19}F NMR (283 MHz, $CDCl_3$) δ –65.60. **HRMS** (FD+) m/z $[M^{\bullet}]^+$ calculated for $C_{18}H_{16}BrF_3N_2O_2$: 428.0347, found: 428.0337.

5.5.1.3 General procedure for the thermal crosslinking of cyclohexane, as a small-molecule model for C–H containing polymer substrate

Cyclohexane was degassed by sparging with argon for 10 minutes, while stirring. A 11–12 mM solution of the desired diazirine in the degassed substrate was then prepared in a flame-dried heavy-walled pressure vessel with a PTFE bushing as a pressure seal. After sealing the vessel under an argon atmosphere, the reaction was immersed in an oil bath at 100 °C and stirred at that temperature for 1 hour. After cooling the mixture to room temperature, the reaction was transferred into a round bottom flask and concentrated in vacuum to provide the crude product.

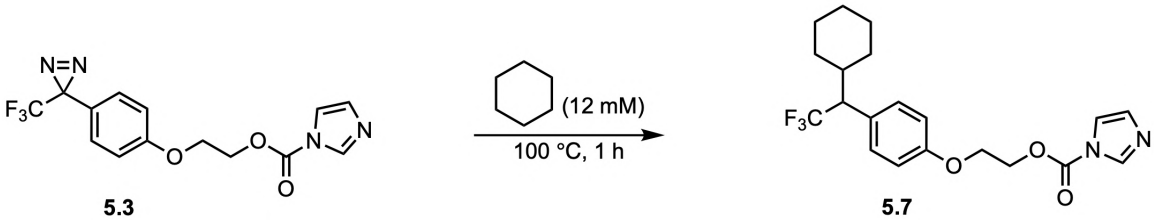

5.3 **5.7**

*C–H insertion product **5.7**:* Following the above general procedure for the C–H insertion experiment, diazirine **5.3** (30 mg, 0.088 mmol) was activated in cyclohexane (8 mL, 11 mM). After completion, the batch was concentrated under reduced pressure and the desired product **5.7** (28 mg, 0.071 mmol) was obtained as a colorless oil, which was used without further purification. **^{1}H NMR** (300 MHz, $CDCl_3$) δ 8.16 (d, *J* = 1.1 Hz, 1H), 7.42 (s, 1H), 7.17 (d, *J* = 8.7 Hz, 2H), 7.07 (s, 1H), 6.89 (d, *J* = 8.7 Hz, 2H), 4.80 – 4.69 (m, 2H), 4.36 – 4.27 (m, 2H), 2.99 (qd, *J* = 10.1, 8.1 Hz, 1H), 2.02 – 1.84 (m, 2H), 1.81 – 1.71 (m, 1H), 1.66 – 1.58 (m, 2H), 1.53 – 1.44 (m, 1H), 1.38 – 1.31 (m, 1H), 1.17 – 1.01 (m, 3H), 0.84 – 0.73 (m, 1H). **^{19}F NMR** (283 MHz, $CDCl_3$) δ –63.72.

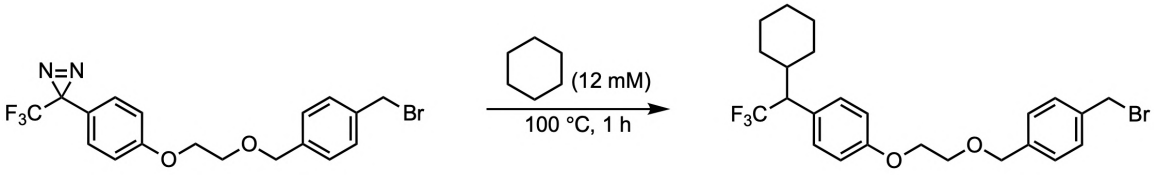

5.4 **5.8**

*C–H insertion product **5.8***: Following the above general procedure for the C–H insertion experiment, diazirine **5.4** (100 mg, 0.23 mmol) was activated in cyclohexane

(20 mL, 12 mM). After completion, the batch was concentrated under reduced pressure and the desired product **5.8** (110 mg, 0.23 mmol) was obtained as a colorless oil, which was used without further purification. **^{1}H NMR** (500 MHz, $CDCl_3$) δ 7.39 – 7.32 (m, 4H), 7.13 (d, *J* = 8.2 Hz, 2H), 6.89 (d, *J* = 8.3 Hz, 2H), 4.63 (s, 2H), 4.51 – 4.46 (m, 2H), 4.21 – 4.10 (m, 2H), 3.87 – 3.77 (m, 2H), 3.08 – 2.89 (m, 1H), 2.02 – 1.85 (m, 2H), 1.79 – 1.72 (m, 1H), 1.67 – 1.58 (m, 2H), 1.52 – 1.46 (m, 1H), 1.34 – 1.28 (m, 1H), 1.18 – 1.05 (m, 3H), 0.85 – 0.78 (m, 1H). **^{19}F NMR** (471 MHz, $CDCl_3$) δ –63.71.

5.5.1.4 Synthetic procedures to simulate the reactivity of C–H insertion products 7 and 8 during protein immobilization using isopropylamine as a small molecule model

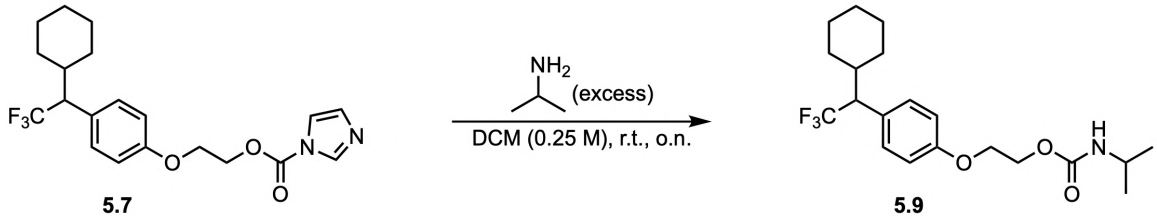

*Small-molecule model immobilization product **5.9**:* Compound **5.7** (20 mg, 0.05 mmol, 1.0 equiv.) was reacted with isopropylamine (0.043 mL, 0.51 mmol, 10 equiv.) in dichloromethane (0.2 mL, 0.25 M) under ambient atmosphere. After overnight stirring at room temperature, the reaction was concentrated under reduced pressure and then quenched with NaOH solution (0.5 M) and extracted with diethyl ether (× 3). The combined organic layer was extracted further with NH_4Cl saturated solution. The solvent was removed to afford the desired product **5.9** (18 mg; 92%) as a colorless oil without the need for further purification. **^{1}H NMR** (500 MHz, $CDCl_3$) δ 7.14 (d, *J* = 8.2 Hz, 2H), 6.88 (d, *J* = 8.2 Hz, 2H), 4.60 (s, 1H, NH), 4.47 – 4.34 (m, 2H), 4.22 – 4.11 (m, 2H), 3.81 (hept, *J* = 6.5 Hz, 1H), 2.98 (qd, *J* = 10.2, 7.9 Hz, 1H), 2.02 – 1.86 (m, 2H), 1.79 – 1.72 (m, 1H), 1.66 – 1.58 (m, 2H), 1.53 – 1.46 (m, 1H), 1.35 – 1.25 (m, 2H), 1.15 (d, *J* = 6.4 Hz, 6H), 1.12 – 1.05 (m, 2H), 0.86 – 0.78 (m, 1H). **^{13}C NMR** (126 MHz, $CDCl_3$) δ 158.21, 155.48, 130.43, 127.80, 127.43 (q, *J* = 281.1 Hz), 114.59, 66.60, 63.08, 55.44 (q, *J* = 25.2 Hz), 43.28, 38.66, 31.64, 30.80, 26.30, 26.23, 26.15, 23.12. **^{19}F NMR** (471 MHz, $CDCl_3$) δ –63.71 (d, *J* = 10.2 Hz). **HRMS** (FD+) m/z $[M^{\bullet}]^+$ calculated for $C_{20}H_{28}F_3NO_3$: 387.2021, found: 387.2026.

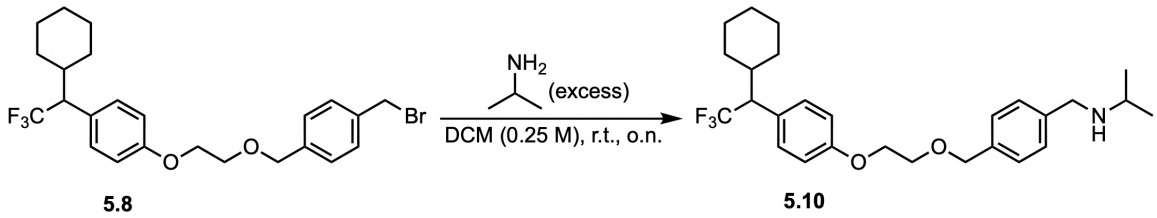

5.8 **5.10**

*Small-molecule model immobilization product **5.10**:* To a solution of C–H insertion product **5.8** (30 mg, 0.062 mmol, 1.0 equiv.) in dichloromethane (0.25 mL, 0.25 M) at room temperature, isopropylamine (0.053 mL, 0.62 mmol, 10 equiv.) was added under ambient atmosphere. After overnight stirring at room temperature, the reaction was concentrated under reduced pressure and then quenched with NaOH solution (0.5 M) and extracted with diethyl ether (× 3). The combined organic layer was dried over sodium sulfate. The solvent was removed to afford the desired product as a colorless oil. The crude materials were purified by silica gel chromatography using pentane and ethyl acetate mixture as eluent. Several 1–3 mL fractions were collected in 1-dram vials. Fractions that contained the desired product were combined and concentrated to afford desired product **5.10** (20 mg; 70%) as a colorless oil. **^{1}H NMR** (500 MHz, $CDCl_3$) δ 7.39 – 7.30 (m, 4H), 7.14 (d, *J* = 8.5 Hz, 2H), 6.90 (d, *J* = 8.6 Hz, 2H), 4.60 (s, 2H), 4.13 (t, *J* = 4.9 Hz, 2H), 3.85 – 3.77 (m, 4H), 2.98 (qd, *J* = 10.1, 7.6 Hz, 1H), 2.89 (hept, *J* = 6.4 Hz, 1H), 2.03 – 1.85 (m, 2H), 1.81 – 1.71 (m, 1H), 1.68 – 1.57 (m, 2H), 1.54 – 1.46 (m, 1H), 1.33 – 1.26 (m, 1H), 1.14 (d, *J* = 6.2 Hz, 6H), 1.12 – 1.03 (m, 2H), 0.86 – 0.76 (m, 1H). **^{13}C NMR** (126 MHz, $CDCl_3$) δ 158.42, 137.21, 130.35, 128.73, 128.11, 127.55, 127.53, 127.42 (q, *J* = 281.3 Hz), 114.62, 73.23, 68.59, 67.52, 55.43 (q, *J* = 25.2 Hz), 50.75, 48.18, 38.66, 31.65, 30.79, 26.32, 26.23, 26.16, 22.37. **^{19}F NMR** (471 MHz, $CDCl_3$) δ –63.70 (d, *J* = 10.2 Hz). **HRMS** (FD+) m/z $[M^{\bullet}]^+$ calculated for $C_{27}H_{36}F_3NO_2$: 463.2698, found: 463.2741.

5.5.2 Materials and methods for immobilization tests

Materials: All commercial materials were used as received unless otherwise noted. Polydimethylsiloxane SYLGARD 184 silicone elastomer kit was obtained from Ellsworth Adhesives Inc., (Stoney Creek, ON, Canada). Methanol, bovine serum albumin (BSA), human immunoglobulin G (Ig G) and IgG-FITC were ordered from Sigma-

Aldrich, USA. The $Na^{125}I$ was obtained from the McMaster University Nuclear Reactor (Hamilton, ON, Canada).

Preparation of PDMS Substrates: To prepare the native PDMS substrates, the prepolymer base and curing reagents were combined at a 10:1 mass ratio, stirred for 10 minutes to ensure even distribution, and poured into a petri dish. To eliminate bubbles, the mixture was placed in a desiccator for 30 minutes before being cured at room temperature for 48 hours. Following the curing process, circular disks with a diameter of 6 mm were punched out from the PDMS substrates and utilized either as controls or for subsequent surface modification.

Surface Modification with Diazirine Molecules: Three diazirine molecules **5.3**, **5.4** and **5.5** were dissolved in methanol to prepare 10 mg/mL solutions respectively. The PDMS disks were rinsed three times with Milli-Q water and immersed in a 96-well plate containing diazirine solution (250 µL/well). The plate was then placed in a fume hood and left to evaporate the solvent overnight. After evaporation, the PDMS disks were activated by heating in an oven at 100 °C or exposure to 360 nm UV light for 1 hour. The PDMS surface was then washed twice with methanol to remove any side reaction products.

Water contact angle measurements: Surface wettability was evaluated using a goniometer (Ramé-hart, Model No. 100-00 115)). In brief, 5 µL droplets of Milli-Q water were deposited onto the sample surfaces utilizing a micro syringe. The contact angles of the water droplets on the PDMS surfaces were then observed and recorded via the sessile drop method. To ensure accurate measurements, six different disks were chosen for each sample type to measure the water contact angle on the surface.

Atomic force microscopy (AFM): The surface roughness of both control and modified PDMS surfaces was assessed by utilizing AFM (Bruker Dimension iCon). The AFM images were obtained in tapping mode under ambient conditions in air. A carbon cantilever with a spring constant of k= 2.8 N/m was automatically adjusted to a scan rate of 1 Hz, and the scan area was 5 µm × 5 µm. The obtained AFM data were analyzed using Gwyddion software, and the average root-mean-square (RMS) roughness taken over the entire image was reported as the surface roughness.

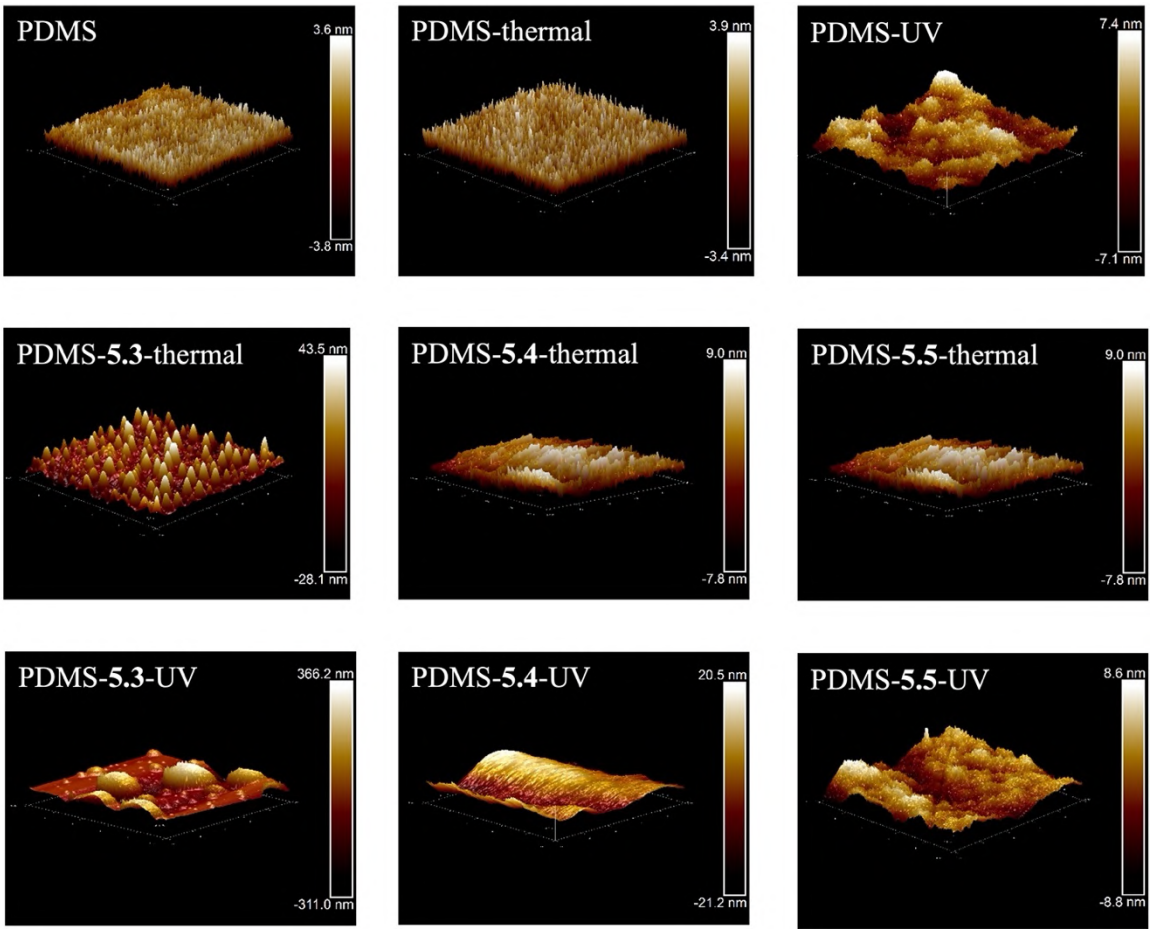

Figure S5.1 Three-dimensional images of AFM characterization of control and diazirine-modified PDMS surfaces; Scans are 5 µm x 5µm.

ATR-Fourier transform infrared (FTIR) spectroscopy : Fourier transform infrared spectroscopy (FTIR) with attenuated total reflectance (ATR) mode was used to analyze the diazirine-modified PDMS surface. Spectra of native PDMS, PDMS-diazirine, and diazirine solution were acquired to investigate the chemical composition. Prior to FTIR analysis, all samples were freshly prepared and air-dried at room temperature. An ATR-FTIR spectrometer (Nicolet 6700, Thermo) was utilized to record the spectra in the 500-4000 cm^{-1} range.

X-ray photoelectron spectroscopy (XPS): X-ray photoelectron spectroscopy analysis was performed using a K-Alpha XPS system (ThermoFisher Scientific, East Grinstead, UK) with an Al K-Alpha monochromatized X-ray source with a 400 µm spot size. Charge neutralization was achieved using a low-energy electron/ion (Ar) flood

source. Survey spectra were acquired with a pass energy of 200 eV and a point density on the energy axis of 1 eV/step to identify all detectable surface species. Regional scans were performed with lower pass energy (50 eV) and a correspondingly higher point density (0.1 eV between points) for quantification. Spectra were collected at a 20° angle relative to the surface plane with minimized analysis time and X-ray exposure. ThermoFisher's Avantage software was used to process the data, with surface elemental compositions calculated from background-subtracted peak areas derived from transmission function-corrected regional spectra. Relative atomic percentages were calculated using sensitivity factors provided by the instrument manufacturer. One measurement per sample type was carried out on three independent sample surfaces to ensure data reproducibility.

Radiolabelling and Immobilization of BSA and IgG: BSA and IgG were labelled with $Na^{125}I$ using the iodine monochloride (ICl) method. The labelled protein was filtered with an AG 1-X4 anion exchange resin to eliminate free ^{125}I. Labeled protein was precipitated in 20% trichloroacetic acid (TCA) and centrifuged for 5 min. The supernatant, containing free iodide ion (*i.e.* not bound to protein) was counted on a Wizard Automatic Gamma Counter. Tests were conducted to determine residual free iodide and levels were maintained below 3%. For studies of protein adsorption from buffer, solutions were prepared with labelled and unlabelled protein in a 1:9 mass ratio. BSA and IgG solutions were prepared, at concentrations of 2 mg/mL and 1 mg/mL, respectively. The PDMS substrates were equilibrated in phosphate buffered saline (PBS, pH 7.4) overnight and then samples were incubated with BSA and IgG for 24 hours at room temperature. Following adsorption, the samples were rinsed three times with PBS, for 10 min each. The samples were lightly wiped to remove the residual adherent buffer and the radioactivity was counted with a gamma counter (Wizard Automatic, PerkinElmer). Radioactivity was converted to protein adsorption amounts based on corresponding solution counts. For each type of sample, 3 disks were repeated.

Sodium Dodecyl Sulfate (SDS) Elution of the Immobilized Proteins: Following radioactivity counting, 1 mL of 2% SDS was added to each sample to elute loosely adsorbed protein. The samples were then incubated in SDS for 24 hours at room temperature with shaking. The SDS solution was subsequently removed, and the sample

surfaces were rinsed three times with PBS buffer for 10 min each. Finally, the samples were dried, and the gamma counter was used to measure the radioactivity.

Confocal Laser Scanning Microscopy (CLSM): The diazirine modified PDMS surfaces were incubated with 1 mg/mL of FITC-labelled IgG for 24 hours in the dark. After incubation, the samples were rinsed three times with PBS. The distribution of FITC-labeled IgG on the modified PDMS surfaces was visualized by confocal laser scanning microscopy (Nikon A1R Upright) with a 10X objective and a 488 nm excitation laser. Image analysis was performed using Image J software.

Statistical Analysis: For each test method, data for at least three independent samples was collected. Data are presented as means ± standard deviation. To assess statistical significance, a one-way ANOVA was performed with Tukey's post hoc analysis using GraphPad Prism software. Results were considered statistically significant for $*p < 0.05$, $**p < 0.01$, $***p < 0.001$, and $****p < 0.0001$.

Chapter 6: Summary and Future Work

6.1. Contributions to the Field of Aryl Diazirine Chemistry and Applications in Materials Science

The research work described in this thesis has focused on the design, synthesis, optimization, and applications of trifluoromethyl aryl diazirine molecules in materials science. The central core of this work is based on a fundamental investigation of aryl diazirine reactivity towards C–H insertion reactions, which provided valuable insights into the design and synthesis of optimal crosslinkers for low-functionality commodity polymers. In addition, to build upon this success, the modification of the tether which connects the two diazirine moieties was explored, and in particular, cleavable linkages were incorporated into the rationally designed small molecule crosslinkers, enabling the exploration of new applications in polymer upcycling and polymer functionalization. Finally, alternative methods for polymer functionalization were explored by directly linking a reactive functional group to the diazirine motif, retaining its functionality through surface functionalization steps. Through this work, the potential uses of trifluoromethyl aryl diazirine chemistry are expanded beyond materials science, with significant contributions to fundamental understanding and innovative solutions for polymer science.

Chapter 2 described a detailed assessment of structure–function relationships within several families of *mono*-aryl-diazirines via a combination of synthetic and computational investigations, calorimetry experiments (DSC), and model C–H and O–H insertion reactions. Ultimately, we identified the optimal electronics for favoring C–H insertion reactions with low-functionality polyolefins. The yield of C–H insertion to cyclohexane (a convenient small-molecular model for polyethylene) was significantly improved by up to ~15-fold under thermal activation conditions, and up to ~4-fold using photochemical activation. We also showed that these reactions work under ambient conditions, exposing reagents and substrates to air and moisture. These highly significant findings will be of use to many other research groups who are currently using diazirines

in a broad range of applications from photoaffinity probes to tissue adhesion, photopatterning, and polymer crosslinking.

Building upon this study, we then explored a new generation of ether-linked *bis*-diazirine crosslinker in Chapter 3. Our electronically optimized crosslinking reagent was more than 10 times as effective as previous generations[36,61] and, for the first time, enabled the use of visible light and low temperatures for diazirine activation. The effectiveness of the electron-rich tether has been shown at the molecular and polymer level through the ability of the new linkers to covalently adhere low functionality substrates and to strengthen ultra-high molecular weight polyethylene fabrics.

We furthered the field of low-functionality polymer upcycling by developing new generation crosslinkers where cleavable linkages were installed into electronically optimized *bis*-diazirine reagents. The result is a useful new series of chemical tools that can be exploited to turn commodity, low-functionality thermoplastics into reversible thermosets: crosslinked materials in which the linkage between polymer chains can be cleaved with the application of specific chemical inputs (acid, base, or fluoride anions). In Chapter 4, for the first time, we used dynamic mechanical thermal analysis to both qualitatively and quantitatively characterize the crosslinked thermosets. Additionally, we see substantial possibilities for these cleavable *bis*-diazirine crosslinkers to upcycle mixed polyethylene/polypropylene wastes into covalent composites.

Chapter 5 explores the broader application of trifluoromethyl aryl diazirine reagents for protein immobilization on low-functionality surfaces. To enhance protein immobilization, newly synthesized diazirine molecules conjugated with electrophiles were used to modify PDMS substrates. Importantly, the study demonstrates that reactive electrophiles can be directly attached to the surface without undergoing unwanted reactions with reactive singlet or triplet carbenes. The resulting substrates were characterized, and the amount of protein on the surface was quantified. This result highlights the potential for this broadly applicable surface modification technique to be translated to other materials and contribute to the development of biotechnological and medical devices.

6.2. Future Work

Following on from the results presented in this thesis a number of future research directions could be pursued and are outlined below.

Expanding the structural diversity of the aryl diazirine scaffold is a major direction of interest for future development of this technology. Research on diazirines has focused predominately on trifluoromethyl-substituted aryl diazirine since Brunner's discovery in 1980, as discussed in Chapter 2. However, fluorinated molecules in materials are becoming increasingly unfavorable due to their environmental persistence and potential risks to human health.[253,254] As a result, it is prudent to consider alternatives for the α-trifluoromethyl group. In Chapter 2, we studied the activation temperature and activation free energy for aryl diazirines containing different α-substituents using calorimetry and computational analysis. However, we did not investigate the relationship between these substituents and their ability to efficiently insert X–H (X = C, N, O) bonds experimentally.

To address this gap, I propose conducting a future study on X–H insertion reactions using thermally and photochemically activated aryl diazirines containing a variety of α-substituents (Figure 6.1a). Due to the ability of electron-withdrawing groups to stabilize diazirines,[112] I suggest exploring a series of aryl diazirines with alpha electron-withdrawing groups such as nitrile, ester and trichloromethyl groups. Trifluoromethyl aryl diazirines are traditionally synthetized starting from the corresponding trifluoromethyl ketone and several steps are required to produce the desired product. Conversely, the synthetic route to α-Cl aryl diazirine is known since 1965, when Graham *et al* reported a one-step oxidation reaction that converts amidine to diazirine using sodium hypochlorite (bleach) as reagent.[255] The chloride substituent in the diazirine formed from the Graham reaction can also be displaced with various nucleophiles such as fluoride (using TBAF) or as cyanide (using tetrabutylammonium cyanide).[256] The nitrile is a great isosteric replacement of the trifluoromethyl group and eliminates the issue of having fluorine content in the molecule. Previous literature reports suggest that cyanophenyl diazirine is thermally unstable,[257–259] however, this problem could be potentially addressed by tuning the electronics around the aromatic ring. Alternatively, the inclusion of an ester group can be considered. Ethyl diazoacetate (EDA,

Figure 6.1b) is a commonly used diazo compound, in which the ester group is utilized for safe manipulation and increasing the degree of electrophilicity of the carbenoid.[260,261] The results from these future investigations will not only help us to design new molecules without the presence of fluorinated carbons but also allow us to compare the X–H insertion efficiency of different diazirine scaffolds.

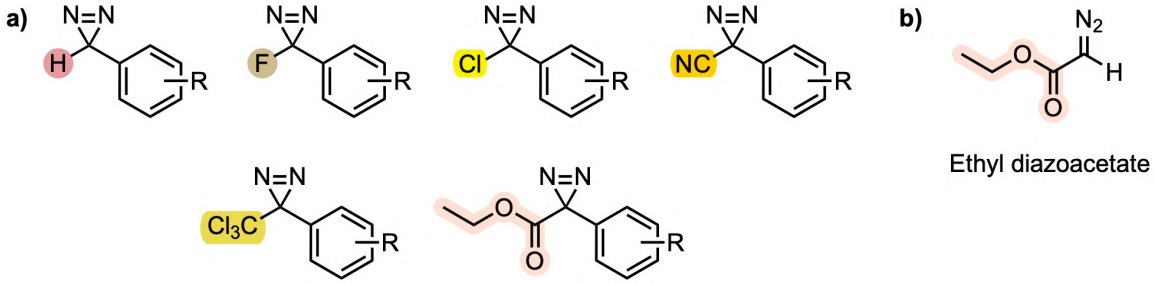

Figure 6.1 a) Proposed α-substituent electronics to examine X–H insertion efficiency. b) The structure of ethyl diazoacetate.

In Chapter 4, we successfully developed a more efficient route to electronically optimized diazirine reagents. This same approach can also be applied to streamline the synthesis of non-cleavable electronically optimized *bis*-diazirine **4.11**. To achieve this, we can react suitable linkers with the key building block, ethylene glycol diazirine as illustrated in Figure 6.2. Furthermore, our research in Chapter 4 revealed that crosslinkers containing less-polar tethers (compound **4.6** and **4.11**) crosslinked paraffin wax more efficiently than crosslinkers **4.4** and **4.5**, which have more-polar tethers. To enhance polymer crosslinking performance, a range of different linkers (Figure 6.2) can be incorporated into bivalent or multivalent diazirine reagents to facilitate effective recycling purposes on different substrates.

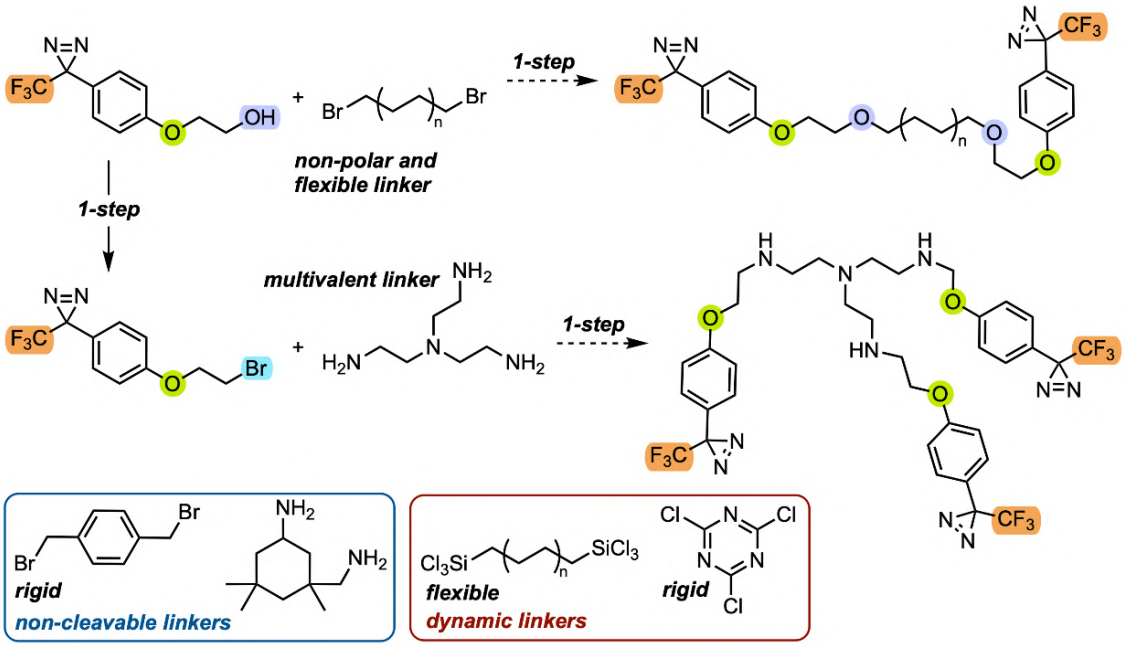

Figure 6.2 Schematic representation of potential linkers for one-pot synthesis of electronically optimized diazirine crosslinkers.

With the proof-of-concept of recycling low-functionality polymers having been developed in Chapter 4, the next step is to focus on the real-life application of post-consumer mixed plastic wastes. One approach is to integrate a melt-extrusion step using a twin-screw extruder, which can mix plastic waste streams and crosslinkers more efficiently, as illustrated recently in the work from the Chen group.[209] We can also incorporate dynamic linkages such as boronic esters with internal B–N coordination bonds (Figure 6.3) into diazirine reagents. Dynamic B–O bonds have been widely used for constructing multifunctional recyclable polymers due to their dynamic properties.[177,262] The dissociation of B–N coordination bonds upon loading provides an efficient energy dissipation pathway for the crosslinked network.[263,264] Therefore, introducing dynamic B–O bonds with internal B–N coordination into covalent networks would be an ideal platform for designing high performance thermoset materials.

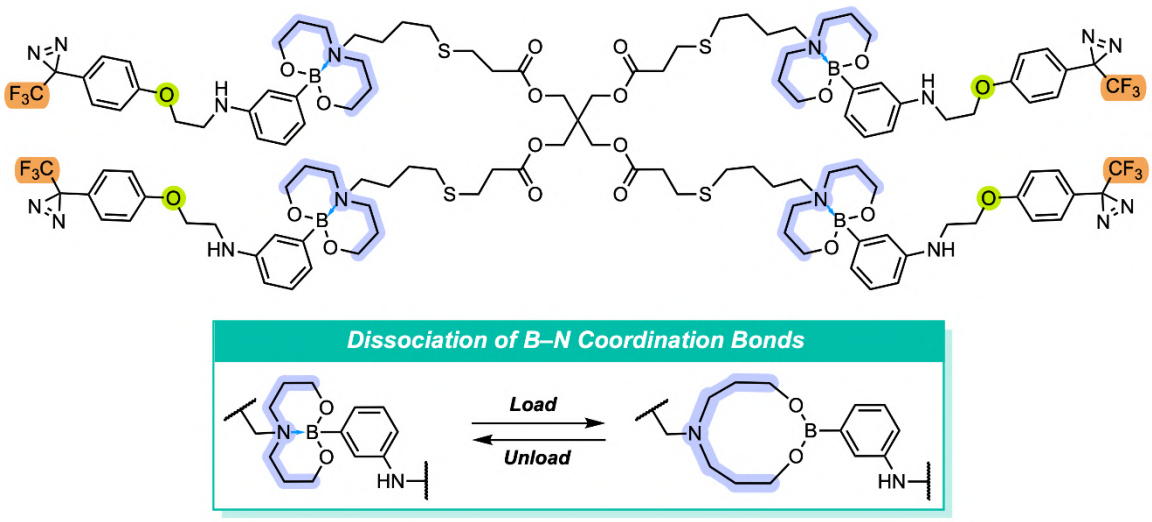

Figure 6.3 The proposed structure of the *tetra*-diazirine crosslinker with internal B–N coordination bonds in cyclic boronic esters.

In conclusion, the trifluoromethyl aryl diazirine reagents studied in this work demonstrate exceptional efficiency in C–H insertion reactions, and in the crosslinking of low-functionality polymers. The unique features of these diazirine reagents make them an excellent choice for addressing the recyclability issues of existing low-functionality commodity polymers. With a better understanding of diazirine chemistry, researchers can develop novel and innovative methods for converting used plastic waste into recyclable and degradable materials. This research provides a strong foundation for the development of new strategies for the sustainable management of plastic waste, opening up new possibilities for sustainable materials and reducing the environmental impact of plastic waste.

Bibliography

(1) Fortman, D. J.; Brutman, J. P.; De Hoe, G. X.; Snyder, R. L.; Dichtel, W. R.; Hillmyer, M. A. Approaches to Sustainable and Continually Recyclable Cross-Linked Polymers. *ACS Sustain. Chem. Eng.* **2018**, 6 (9), 11145–11159.

(2) Ma, S.; Webster, D. C. Degradable Thermosets Based on Labile Bonds or Linkages: A Review. *Prog. Polym. Sci.* **2018**, 76, 65–110.

(3) Farag, R. K.; Hani, S. Crosslinked Polymer Hydrogels. In *Reactive and Functional Polymers Volume Two: Modification Reactions, Compatibility and Blends*; Gutiérrez, T. J., Ed.; Springer International Publishing: Cham, 2020; pp 91–116.

(4) Lin, W.; Shao, Z.; Dong, J.; Chung, T. C. M. Cross-Linked Polypropylene Prepared by PP Copolymers Containing Flexible Styrene Groups. *Macromolecules* **2009**, 42 (11), 3750–3754.

(5) Dong, Y.; Zhao, Y.; Wang, H.; Liu, P.; He, Y.; Lin, G. Integration of Life Cycle Assessment and Life Cycle Costing for the Eco-Design of Rubber Products. *Sci. Rep.* **2022**, 12 (1), 595.

(6) Tiseo, Ian. *Consumption of natural and synthetic rubber worldwide from 1990 to 2020*. https://www.statista.com/statistics/275399/world-consumption-of-natural-and-synthetic-caoutchouc/.

(7) Kruželák, J.; Sýkora, R.; Hudec, I. Sulphur and Peroxide Vulcanisation of Rubber Compounds – Overview. *Chem. Pap.* **2016**, 70 (12), 1533–1555.

(8) Hamed, G. R. Materials and Compounds. In *Engineering with Rubber (Third Edition)*; Gent, A. N., Ed.; Hanser, 2012; pp 11–36.

(9) Marković, G.; Marinović-Cincović, M.; Samaržija-Jovanović, S.; Jovanović, V.; Budinski-Simendić, J. Crosslinking of Polymers: Rubber Vulcanization. In *Reactive and Functional Polymers Volume Two: Modification Reactions, Compatibility and Blends*; Gutiérrez, T. J., Ed.; Springer International Publishing: Cham, 2020; pp 117–134.

(10) Fazli, A.; Rodrigue, D. Waste Rubber Recycling: A Review on the Evolution and Properties of Thermoplastic Elastomers. *Materials* **2020**, 13 (3).

(11) Karger-Kocsis, J.; Mészáros, L.; Bárány, T. Ground Tyre Rubber (GTR) in Thermoplastics, Thermosets, and Rubbers. *J. Mater. Sci.* **2013**, 48 (1), 1–38.

(12) Liang, L.; Bhagia, S.; Li, M.; Huang, C.; Ragauskas, A. J. Cross-Linked Nanocellulosic Materials and Their Applications. *ChemSusChem* **2020**, 13 (1), 78–87.

(13) Schubert, M.; Panzarasa, G.; Burgert, I. Sustainability in Wood Products: A New Perspective for Handling Natural Diversity. *Chem. Rev.* **2023**, 123 (5), 1889–1924.

(14) Lam, Y. L.; Kan, C. W.; Yuen, C. W. M. Wrinkle-Resistant Finishing of Cotton Fabric with BTCA - the Effect of Co-Catalyst. *Text. Res. J.* **2010**, 81 (5), 482–493.

(15) Harifi, T.; Montazer, M. Past, Present and Future Prospects of Cotton Cross-Linking: New Insight into Nano Particles. *Carbohydr. Polym.* **2012**, 88 (4), 1125–1140.

(16) Dhiman, G.; Chakraborty, J. N. Assessment of Durable Press Performance of Cotton Finished with Modified DMDHEU and Citric Acid. *Fash. Text*. **2017**, 4 (1), 18.

(17) İlleez, A. A.; Dalbaşıi, E. S.; Kayseri, G. Ö. Seam Properties and Sewability of Crease Resistant Shirt Fabrics. *AATCC J. Res.* **2017**, 4 (1), 28–34.

(18) Lepage, M. L.; Takaffoli, M.; Simhadri, C.; Mandau, R.; Gashti, M. P.; Nazir, R.; Mohseni, M.; Li, W.; Liu, C.; Bi, L.; Falck, G.; Berrang, P.; Golovin, K.; Milani, A. S.; DiLabio, G. A.; Wulff, J. E. Influence of Topical Cross-Linking on Mechanical and Ballistic Performance of a Woven Ultra-High-Molecular-Weight Polyethylene Fabric Used in Soft Body Armor. *ACS Appl. Polym. Mater.* **2021**, 3 (11), 6008–6018.

(19) Sonnenschein, M. F. *Polyurethanes: Science, Technology, Markets, and Trends*; Wiley, 2021.

(20) Szycher, M. *Szycher's Handbook of Polyurethanes*, 2nd ed.; Taylor & Francis, 2013.

(21) Akindoyo, J. O.; Beg, M. D. H.; Ghazali, S.; Islam, M. R.; Jeyaratnam, N.; Yuvaraj, A. R. Polyurethane Types, Synthesis and Applications – a Review. *RSC Adv* **2016**, 6 (115), 114453–114482.

(22) Delebecq, E.; Pascault, J.-P.; Boutevin, B.; Ganachaud, F. On the Versatility of Urethane/Urea Bonds: Reversibility, Blocked Isocyanate, and Non-Isocyanate Polyurethane. *Chem. Rev.* **2013**, 113 (1), 80–118.

(23) Odian, G. Step Polymerization. In *Principles of Polymerization*; 2004; pp 39–197.

(24) Nazir, R.; Bi, L.; Musolino, S. F.; Margoto, O. H.; Çelebi, K.; Mobuchon, C.; Takaffoli, M.; Milani, A. S.; Falck, G.; Wulff, J. E. Polyamine–Diazirine Conjugates for

Use as Primers in UHMWPE–Epoxy Composite Materials. *ACS Appl. Polym. Mater.* **2022**, 4 (3), 1728–1742.

(25) Brook, M. A. *Silicon in Organic, Organometallic, and Polymer Chemistry*; Wiley, 1999.

(26) Pouget, E.; Tonnar, J.; Lucas, P.; Lacroix-Desmazes, P.; Ganachaud, F.; Boutevin, B. Well-Architectured Poly(Dimethylsiloxane)-Containing Copolymers Obtained by Radical Chemistry. *Chem. Rev.* **2010**, 110 (3), 1233–1277.

(27) Zhao, X.; Bi, L.; Khatir, B.; Serles, P.; Filleter, T.; Wulff, J. E.; Golovin, K. Crosslinking Inert Liquidlike Polydimethylsiloxane Brushes Using Bis-Diazirine Chemical Insertion for Enhanced Mechanical Durability. *Chem. Eng. J.* **2022**, 442, 136017.

(28) Shit, S. C.; Shah, P. A Review on Silicone Rubber. *Natl. Acad. Sci. Lett*. **2013**, 36 (4), 355–365.

(29) Marciniec, B. Functionalisation and Cross-Linking of Organosilicon Polymers. In *Hydrosilylation: A Comprehensive Review on Recent Advances*; Marciniec, B., Ed.; Springer Netherlands: Dordrecht, 2009; pp 159–189.

(30) Cervantes, J.; Zárraga, R.; Salazar-Hernández, C. Organotin Catalysts in Organosilicon Chemistry. *Appl. Organomet. Chem*. **2012**, 26 (4), 157–163.

(31) Azevedo, M.; Monks, A.-M.; Kerschbaumer, R. C.; Schlögl, S.; Holzer, C. Peroxide-Based Crosslinking of Solid Silicone Rubber, Part I: Insights into the Influence of Dicumylperoxide Concentration on the Curing Kinetics and Thermodynamics Determined by a Rheological Approach. *Polymers* **2022**, 14 (20).

(32) Thomas, J.; Joseph, B.; Jose, Josmin. P.; Maria, H. J.; Main, P.; Rahman, A. A.; Francis, B.; Ahmad, Z.; Thomas, S. Recent Advances in Cross-Linked Polyethylene-Based Nanocomposites for High Voltage Engineering Applications: A Critical Review. *Ind. Eng. Chem. Res*. **2019**, 58 (46), 20863–20879.

(33) de Zwart, F. J.; Bootsma, J.; de Bruin, B. Cross-Linking Polyethylene through Carbenes. *Science* **2019**, 366 (6467), 800–800.

(34) Chodák, I. Crosslinking of Polypropylene. In Polypropylene: An A-Z reference; Karger-Kocsis, J., Ed.; Springer Netherlands: Dordrecht, 1999; pp 128–134.

(35) Jaydev, S. D.; Usteri, M.-E.; Martín, A. J.; Pérez-Ramírez, J. Identifying Selective Catalysts in Polypropylene Hydrogenolysis by Decoupling Scission Pathways. *Chem Catal*. **2023**, 3 (5), 100564.

(36) Lepage, M. L.; Simhadri, C.; Liu, C.; Takaffoli, M.; Bi, L.; Crawford, B.; Milani, A. S.; Wulff, J. E. A Broadly Applicable Cross-Linker for Aliphatic Polymers Containing C–H Bonds. *Science* **2019**, 366 (6467), 875–878.

(37) Saed, M. O.; Lin, X.; Terentjev, E. M. Dynamic Semicrystalline Networks of Polypropylene with Thiol-Anhydride Exchangeable Crosslinks. *ACS Appl. Mater. Interfaces* **2021**, 13 (35), 42044–42051.

(38) Wong, B.; Baker, W. E. Melt Rheology of Graft Modified Polypropylene. *Polymer* **1997**, 38 (11), 2781–2789.

(39) Lu, H.; Zhou, Q.; He, J.; Jiang, Z.; Peng, C.; Tong, R.; Shi, J. Recent Advances in the Development of Protein–Protein Interactions Modulators: Mechanisms and Clinical Trials. *Signal Transduct. Target. Ther.* **2020**, 5 (1), 213.

(40) Seath, C. P.; Trowbridge, A. D.; Muir, T. W.; MacMillan, D. W. C. Reactive Intermediates for Interactome Mapping. *Chem. Soc. Rev*. **2021**, 50 (5), 2911–2926.

(41) Kotzyba-Hibert, F.; Kapfer, I.; Goeldner, M. Recent Trends in Photoaffinity Labeling. *Angew. Chem. Int. Ed. Engl*. **1995**, 34 (12), 1296–1312.

(42) Petrotchenko, E. V.; Borchers, C. H. Protein Chemistry Combined with Mass Spectrometry for Protein Structure Determination. *Chem. Rev*. **2022**, 122 (8), 7488–7499.

(43) Singh, A.; Thornton, E. R.; Westheimer, F. H. The Photolysis of Diazoacetylchymotrypsin. *J. Biol. Chem*. **1962**, 237 (9), 3006–3008.

(44) Murale, D. P.; Hong, S. C.; Haque, Md. M.; Lee, J.-S. Photo-Affinity Labeling (PAL) in Chemical Proteomics: A Handy Tool to Investigate Protein-Protein Interactions (PPIs). *Proteome Sci*. **2017**, 15 (1), 14.

(45) Dorman, G.; Prestwich, G. D. Benzophenone Photophores in Biochemistry. *Biochemistry* **1994**, 33 (19), 5661–5673.

(46) Dormán, G.; Nakamura, H.; Pulsipher, A.; Prestwich, G. D. The Life of Pi Star: Exploring the Exciting and Forbidden Worlds of the Benzophenone Photophore. *Chem. Rev*. **2016**, 116 (24), 15284–15398.

(47) Sumranjit, J.; Chung, S. J. Recent Advances in Target Characterization and Identification by Photoaffinity Probes. *Molecules* **2013**, 18 (9), 10425–10451.

(48) Preston, G. W.; Wilson, A. J. Photo-Induced Covalent Cross-Linking for the Analysis of Biomolecular Interactions. *Chem. Soc. Rev*. **2013**, 42 (8), 3289–3301.

(49) Xia, Y.; Peng, L. Photoactivatable Lipid Probes for Studying Biomembranes by Photoaffinity Labeling. *Chem. Rev.* **2013**, 113 (10), 7880–7929.

(50) Musolino, S. F.; Pei, Z.; Bi, L.; DiLabio, G. A.; Wulff, J. E. Structure–Function Relationships in Aryl Diazirines Reveal Optimal Design Features to Maximize C–H Insertion. *Chem. Sci.* **2021**, 12 (36), 12138–12148.

(51) Dubinsky, L.; Krom, B. P.; Meijler, M. M. Diazirine Based Photoaffinity Labeling. *Bioorg. Med. Chem.* **2012**, 20 (2), 554–570.

(52) Halloran, M. W.; Lumb, J.-P. Recent Applications of Diazirines in Chemical Proteomics. *Chem. – Eur. J.* **2019**, 25 (19), 4885–4898.

(53) Paulsen, S. R. 3.3-Dialkyl-Diazacyclopropen-(1). *Angew. Chem.* **1960**, 72 (21), 781–782.

(54) Schmitz, E.; Ohme, R. Neue Diaziridin-Synthese. *Angew. Chem*. **1961**, 73 (6), 220–221.

(55) Modarelli, D. A.; Morgan, S.; Platz, M. S. Carbene Formation, Hydrogen Migration, and Fluorescence in the Excited States of Dialkyldiazirines. *J. Am. Chem. Soc.* **1992**, 114 (18), 7034–7041.

(56) Smith, R. A. G.; Knowles, J. R. Aryldiazirines. Potential Reagents for Photolabeling of Biological Receptor Sites. *J. Am. Chem. Soc.* **1973**, 95 (15), 5072–5073.

(57) Blencowe, A.; Hayes, W. Development and Application of Diazirines in Biological and Synthetic Macromolecular Systems. *Soft Matter* **2005**, 1 (3), 178–205.

(58) Brunner, J.; Senn, H.; Richards, F. M. 3-Trifluoromethyl-3-Phenyldiazirine. A New Carbene Generating Group for Photolabeling Reagents. *J. Biol. Chem*. **1980**, 255 (8), 3313–3318.

(59) Blencowe, A.; Blencowe, C.; Cosstick, K.; Hayes, W. A Carbene Insertion Approach to Functionalised Poly(Ethylene Oxide)-Based Gels. *React. Funct. Polym*. **2008**, 68 (4), 868–875.

(60) Mehenni, H.; Pourcelle, V.; Gohy, J.-F.; Marchand-Brynaert, J. Synthesis and Application of New Photocrosslinkers for Poly(Ethylene Glycol). *Aust. J. Chem*. **2012**, 65 (2), 193–201.

(61) Simhadri, C.; Bi, L.; Lepage, M. L.; Takaffoli, M.; Pei, Z.; Musolino, S. F.; Milani, A. S.; DiLabio, G. A.; Wulff, J. E. Flexible Polyfluorinated Bis-Diazirines as Molecular Adhesives. *Chem. Sci*. **2021**, 12 (11), 4147–4153.

(62) Ping, J.; Gao, F.; Chen, J. L.; Webster, R. D.; Steele, T. W. J. Adhesive Curing through Low-Voltage Activation. *Nat. Commun.* **2015**, 6 (1), 8050.

(63) Gao, F.; Djordjevic, I.; Pokholenko, O.; Zhang, H.; Zhang, J.; Steele, T. W. J. On-Demand Bioadhesive Dendrimers with Reduced Cytotoxicity. *Molecules* **2018**, 23 (4).

(64) Djordjevic, I.; Pokholenko, O.; Shah, A. H.; Wicaksono, G.; Blancafort, L.; Hanna, J. V.; Page, S. J.; Nanda, H. S.; Ong, C. B.; Chung, S. R.; Chin, A. Y. H.; McGrouther, D.; Choudhury, M. M.; Li, F.; Teo, J. S.; Lee, L. S.; Steele, T. W. J. CaproGlu: Multifunctional Tissue Adhesive Platform. *Biomaterials* **2020**, 260, 120215.

(65) Ellis, E.; Djordjevic, I.; Bin Mohd Ali, M. N.; Steele, T. W. J. Carbene-Based Bioadhesive Blended with Amine, Thiol, and Acrylate Liquid Additives. *ACS Appl. Polym. Mater*. **2023**, 5 (2), 1440–1452.

(66) Djordjevic, I.; Wicaksono, G.; Solic, I.; Steele, T. W. J. In Vitro Biocompatibility of Diazirine-Grafted Biomaterials. *Macromol. Rapid Commun*. **2020**, 41 (21), 2000235.

(67) Burgoon, H.; Cyrus, C.; Skilskyj, D.; Thoresen, J.; Ebner, C.; Meyer, G. A.; Filson, P.; Rhodes, L. F.; Backlund, T.; Meneau, A.; Cull, T.; Afonina, I. Photopatterning of Low Dielectric Constant Cycloolefin Polymers Using Azides and Diazirines. *ACS Appl. Polym. Mater*. **2020**, 2 (5), 1819–1826.

(68) Dey, K.; Chowdhury, S. R.; Dykstra, E.; Koronatov, A.; Lu, H. P.; Shinar, R.; Shinar, J.; Anzenbacher, P. Diazirine-Based Photo-Crosslinkers for Defect Free Fabrication of Solution Processed Organic Light-Emitting Diodes. *J. Mater. Chem. C* **2020**, 8 (34), 11988–11996.

(69) Duan, L.; Hou, L.; Lee, T.-W.; Qiao, J.; Zhang, D.; Dong, G.; Wang, L.; Qiu, Y. Solution Processable Small Molecules for Organic Light-Emitting Diodes. *J Mater Chem* **2010**, 20 (31), 6392–6407.

(70) Dey, K.; Roy Chowdhury, S.; Dykstra, E.; Lu, H. P.; Shinar, R.; Shinar, J.; Anzenbacher, P. Jr. Effect of Bis-Diazirine-Mediated Photo-Crosslinking on Polyvinylcarbazole and Solution-Processed Polymer LEDs. *ACS Appl. Electron. Mater*. **2021**, 3 (8), 3365–3371.

(71) Zheng, Y.-Q.; Liu, Y.; Zhong, D.; Nikzad, S.; Liu, S.; Yu, Z.; Liu, D.; Wu, H.-C.; Zhu, C.; Li, J.; Tran, H.; Tok, J. B.-H.; Bao, Z. Monolithic Optical Microlithography of High-Density Elastic Circuits. *Science* **2021**, 373 (6550), 88–94.

(72) Wu, C.; Li, C.; Yu, X.; Chen, L.; Gao, C.; Zhang, X.; Zhang, G.; Zhang, D. An Efficient Diazirine-Based Four-Armed Cross-Linker for Photo-Patterning of Polymeric Semiconductors. *Angew. Chem. Int. Ed*. **2021**, 60 (39), 21521–21528.

(73) Doyle, M. P.; Duffy, R.; Ratnikov, M.; Zhou, L. Catalytic Carbene Insertion into C−H Bonds. *Chem. Rev*. **2010**, 110 (2), 704–724.

(74) Wentrup, C. Carbenes and Nitrenes: Recent Developments in Fundamental Chemistry. *Angew. Chem. Int. Ed.* **2018**, 57 (36), 11508–11521.

(75) Bayly, A. A.; McDonald, B. R.; Mrksich, M.; Scheidt, K. A. High-Throughput Photocapture Approach for Reaction Discovery. *Proc. Natl. Acad. Sci.* **2020**, 117 (24), 13261–13266.

(76) Schmitz, E.; Ohme, R. 3,3-Pentamethylenediazirine. *Org. Synth*. **1965**, 45 (83).

(77) Wang, L.; Murai, Y.; Yoshida, T.; Ishida, A.; Masuda, K.; Sakihama, Y.; Hashidoko, Y.; Hatanaka, Y.; Hashimoto, M. Alternative One-Pot Synthesis of (Trifluoromethyl)Phenyldiazirines from Tosyloxime Derivatives: Application for New Synthesis of Optically Pure Diazirinylphenylalanines for Photoaffinity Labeling. *Org. Lett*. **2015**, 17 (3), 616–619.

(78) Kumar, A. B.; Manetsch, R. Ammonia-Free Synthesis of 3-Trifluoromethyl-3-Phenyldiaziridine. *Synth. Commun*. **2018**, 48 (6), 626–631.

(79) Ichiishi, N.; Moore, K. P.; Wassermann, A. M.; Wolkenberg, S. E.; Krska, S. W. Reducing Limitation in Probe Design: The Development of a Diazirine-Compatible Suzuki–Miyaura Cross Coupling Reaction. *ACS Med. Chem. Lett*. **2019**, 10 (1), 56–61.

(80) Hatanaka, Y.; Hashimoto, M.; Kurihara, H.; Nakayama, H.; Kanaoka, Y. A Novel Family of Aromatic Diazirines for Photoaffinity Labeling. *J. Org. Chem*. **1994**, 59 (2), 383–387.

(81) Nakashima, H.; Hashimoto, M.; Sadakane, Y.; Tomohiro, T.; Hatanaka, Y. Simple and Versatile Method for Tagging Phenyldiazirine Photophores. *J. Am. Chem. Soc.* **2006**, 128 (47), 15092–15093.

(82) Geri, J. B.; Oakley, J. V.; Reyes-Robles, T.; Wang, T.; McCarver, S. J.; White, C. H.; Rodriguez-Rivera, F. P.; Parker, D. L.; Hett, E. C.; Fadeyi, O. O.; Oslund, R. C.; MacMillan, D. W. C. Microenvironment Mapping via Dexter Energy Transfer on Immune Cells. *Science* **2020**, 367 (6482), 1091–1097.

(83) Singh, M.; Webster, R. D.; J. Steele, T. W. Voltaglue Electroceutical Adhesive Patches for Localized Voltage Stimulation. *ACS Appl. Bio Mater.* **2019**, 2 (6), 2633–2642.

(84) Singh, M.; Yin, C. S.; Page, S. J.; Liu, Y.; Wicaksono, G.; Pujar, R.; Choudhary, S. K.; Kulkarni, G. U.; Chen, J.; Hanna, J. V.; Webster, R. D.; Steele, T. W. J. Synergistic Voltaglue Adhesive Mechanisms with Alternating Electric Fields. *Chem. Mater.* **2020**, 32 (6), 2440–2449.

(85) Moss, R. A.; Doyle, M. P. Contemporary Carbene Chemistry; Wiley: Hoboken, New Jersey, 2014.

(86) Gordon, M. S.; Gano, D. R. Ab Initio Study of the Insertions of Methylene and Silylene into Methane, Silane, and Hydrogen. *J. Am. Chem. Soc.* **1984**, 106 (19), 5421–5425.

(87) Wang, J.; Kubicki, J.; Peng, H.; Platz, M. S. Influence of Solvent on Carbene Intersystem Crossing Rates. *J. Am. Chem. Soc.* **2008**, 130 (20), 6604–6609.

(88) Moss, R. A.; Jones Jr., M. Singlet Carbenes. In Reactive Intermediate Chemistry; Wiley-Interscience: Hoboken, N.J., 2004; pp 273–328.

(89) Lee, H.; Miyamoto, Y.; Tateyama, Y. Excited State Carbene Formation from UV Irradiated Diazomethane. *J. Org. Chem.* **2009**, 74 (2), 562–567.

(90) Song, M.-G.; Sheridan, R. S. Regiochemical Substituent Switching of Spin States in Aryl(Trifluoromethyl)Carbenes. *J. Am. Chem. Soc.* **2011**, 133 (49), 19688–19690.

(91) Manzi, L.; Barrow, A. S.; Scott, D.; Layfield, R.; Wright, T. G.; Moses, J. E.; Oldham, N. J. Carbene Footprinting Accurately Maps Binding Sites in Protein–Ligand and Protein–Protein Interactions. *Nat. Commun.* **2016**, 7 (1), 13288.

(92) MacKinnon, A. L.; Garrison, J. L.; Hegde, R. S.; Taunton, J. Photo-Leucine Incorporation Reveals the Target of a Cyclodepsipeptide Inhibitor of Cotranslational Translocation. *J. Am. Chem. Soc.* **2007**, 129 (47), 14560–14561.

(93) Tulloch, L. B.; Menzies, S. K.; Fraser, A. L.; Gould, E. R.; King, E. F.; Zacharova, M. K.; Florence, G. J.; Smith, T. K. Photo-Affinity Labelling and Biochemical Analyses Identify the Target of Trypanocidal Simplified Natural Product Analogues. *PLoS Negl. Trop. Dis.* **2017**, 11 (9), e0005886.

(94) Gao, J.; Mfuh, A.; Amako, Y.; Woo, C. M. Small Molecule Interactome Mapping by Photoaffinity Labeling Reveals Binding Site Hotspots for the NSAIDs. *J. Am. Chem. Soc.* **2018**, 140 (12), 4259–4268.

(95) Frederike M. Müskens; Richard J. Ward; Dominik Herkt; Helmus van de Langemheen; Andrew B. Tobin; Rob M. J. Liskamp; Graeme Milligan. Design, Synthesis, and Evaluation of a Diazirine Photoaffinity Probe for Ligand-Based Receptor Capture Targeting G Protein–Coupled Receptors. *Mol. Pharmacol.* **2019**, 95 (2), 196.

(96) Sakurai, K.; Ozawa, S.; Yamada, R.; Yasui, T.; Mizuno, S. Comparison of the Reactivity of Carbohydrate Photoaffinity Probes with Different Photoreactive Groups. *ChemBioChem* **2014**, 15 (10), 1399–1403.

(97) Preston, G. W.; Radford, S. E.; Ashcroft, Alison. E.; Wilson, A. J. Analysis of Amyloid Nanostructures Using Photo-Cross-Linking: In Situ Comparison of Three Widely Used Photo-Cross-Linkers. *ACS Chem. Biol.* **2014**, 9 (3), 761–768.

(98) Tippmann, E. M.; Liu, W.; Summerer, D.; Mack, A. V.; Schultz, P. G. A Genetically Encoded Diazirine Photocrosslinker in Escherichia Coli. *ChemBioChem* **2007**, 8 (18), 2210–2214.

(99) Blencowe, A.; Cosstick, K.; Hayes, W. Surface Modification of Nylon 6,6 Using a Carbene Insertion Approach. *New J Chem* **2006**, 30 (1), 53–58.

(100) Cuthbert, T. J.; Ennis, S.; Musolino, S. F.; Buckley, H. L.; Niikura, M.; Wulff, J. E.; Menon, C. Covalent Functionalization of Polypropylene Filters with Diazirine–Photosensitizer Conjugates Producing Visible Light Driven Virus Inactivating Materials. *Sci. Rep.* **2021**, 11 (1), 19029.

(101) Li, X.; Ma, W.; Shestopalov, A. A. Vapor-Phase Carbenylation of Hard and Soft Material Interfaces. *Langmuir* **2016**, 32 (44), 11386–11394.

(102) Suzuki, T.; Okamura, T.; Tomohiro, T.; Iwabuchi, Y.; Kanoh, N. Third Generation Photo-Cross-Linked Small-Molecule Affinity Matrix: A Photoactivatable and Photocleavable System Enabling Quantitative Analysis of the Photo-Cross-Linked Small Molecules and Their Target Purification. *Bioconjug. Chem.* **2015**, 26 (3), 389–395.

(103) Liu, M. T. H.; Toriyama, K. Pyrolysis of 3-Chloro-3-Aryldiazirines, Kinetics and Mechanism. *Can. J. Chem.* **1972**, 50 (18), 3009–3016.

(104) Soundararajan, N.; Platz, M. S.; Jackson, J. E.; Doyle, M. P.; Oon, S. Min.; Liu, M. T. H.; Anand, S. M. Addition of Arylchlorocarbenes to .Alpha.,.Beta.-Unsaturated Esters. Absolute Rates, Substituent Effects, and Variable Reactivities. *J. Am. Chem. Soc.* **1988**, 110 (21), 7143–7152.

(105) Liu, M. T. H.; Suresh, R. V. Studies on Benzylchlorocarbene. *J. Org. Chem.* **1989**, 54 (2), 486–488.

(106) Bonneau, R.; Liu, M. T. H. A Laser Flash Photolysis Study of Carbonyl Ylides of Arylchlorocarbenes: Kinetics and Reversibility of the Formation, Cyclization, and Cycloaddition. *J. Am. Chem. Soc.* **1990**, 112 (2), 744–747.

(107) Moss, R. A.; Ma, Y.; Sauers, R. R. A Duality of Mechanisms for the Fragmentation of Substituted Benzyloxychlorocarbenes. *J. Am. Chem. Soc.* **2002**, 124 (47), 13968–13969.

(108) Martinu, T.; Dailey, W. P. Reactivity of 1-Chloro-3-Phenyldiazirines. *J. Org. Chem.* **2006**, 71 (13), 5012–5015.

(109) Moya-Barrios, R.; Cozens, F. L. Generation and Reactivity of Simple Chloro(Aryl)Carbenes within the Cavities of Nonacidic Zeolites. *J. Am. Chem. Soc.* **2006**, 128 (46), 14836–14844.

(110) Zhang, Y.; Wang, L.; Moss, R. A.; Platz, M. S. Ultrafast Spectroscopy of Arylchlorodiazirines: Hammett Correlations of Excited State Lifetimes. *J. Am. Chem. Soc.* **2009**, 131 (46), 16652–16653.

(111) Peng, X.-L.; Migani, A.; Li, Q.-S.; Li, Z.-S.; Blancafort, L. Theoretical Study of Non-Hammett vs. Hammett Behaviour in the Thermolysis and Photolysis of Arylchlorodiazirines. *Phys Chem Chem Phys* **2018**, 20 (2), 1181–1188.

(112) Raimer, B.; Lindel, T. Photoactivation of (p-Methoxyphenyl)(Trifluoromethyl)Diazirine in the Presence of Phenolic Reaction Partners. *Chem. – Eur. J.* **2013**, 19 (21), 6551–6555.

(113) Kumar, A. B.; Tipton, J. D.; Manetsch, R. 3-Trifluoromethyl-3-Aryldiazirine Photolabels with Enhanced Ambient Light Stability. *Chem Commun* **2016**, 52 (13), 2729–2732.

(114) Hatanaka, Y.; Yoshida, E.; Nakayama, H.; Kanaoka, Y. Chromogenic Diazirine: A New Spectrophotometric Approach for Photoaffinity Labeling. *Bioorganic Chem.* **1989**, 17 (4), 482–485.

(115) Hatanaka, Y.; Yoshida, E.; Nakayama, H.; Abe, T.; Satake, M.; Kanaoka, Y. Photolabile μ-Conotoxins with a Chromogenic Phenyldiazirine. *FEBS Lett*. **1990**, 260 (1), 27–30.

(116) Shimotahira, H.; Fusazaki, S.; Ikeda, I.; Ozoe, Y. A Photoreactive Probe That Differentiates the Binding Sites of Noncompetitive GABA Receptor Antagonists. *Bioorg. Med. Chem. Lett.* **2011**, 21 (6), 1598–1600.

(117) Liu, M. T. H.; Choe, Y.-K.; Kimura, M.; Kobayashi, K.; Nagase, S.; Wakahara, T.; Niino, Y.; Ishitsuka, M. O.; Maeda, Y.; Akasaka, T. Effect of Substituents on the Thermal Decomposition of Diazirines: Experimental and Computational Studies. *J. Org. Chem.* **2003**, 68 (19), 7471–7478.

(118) Yoshida, T.; Wada, Y.; Foster, N. Experimental Evaluation of Fire and Explosion Hazards of Reactive Substances. In Safety of Reactive Chemicals and Pyrotechnics; Industrial safety series; Elsevier, 1995; Vol. 5, pp 75–253.

(119) Green, S. P.; Wheelhouse, K. M.; Payne, A. D.; Hallett, J. P.; Miller, P. W.; Bull, J. A. On the Use of Differential Scanning Calorimetry for Thermal Hazard Assessment of New Chemistry: Avoiding Explosive Mistakes. *Angew. Chem. Int. Ed.* **2020**, 59 (37), 15798–15802.

(120) Hansch, C.; Leo, A.; Taft, R. W. A Survey of Hammett Substituent Constants and Resonance and Field Parameters. *Chem. Rev.* **1991**, 91 (2), 165–195.

(121) Brown, H. C.; Okamoto, Y. Electrophilic Substituent Constants. *J. Am. Chem. Soc.* **1958**, 80 (18), 4979–4987.

(122) Dust, J. M.; Arnold, D. R. Substituent Effects on Benzyl Radical ESR Hyperfine Coupling Constants. The .Sigma..Alpha..Cntdot. Scale Based upon Spin Delocalization. *J. Am. Chem. Soc.* **1983**, 105 (5), 1221–1227.

(123) Creary, X.; Mehrsheikh-Mohammadi, M. E.; McDonald, S. Methylenecyclopropane Rearrangement as a Probe for Free Radical Substituent Effects. .Sigma..Bul. Values for Commonly Encountered Conjugating and Organometallic Groups. *J. Org. Chem.* **1987**, 52 (15), 3254–3263.

(124) Creary, X. Super Radical Stabilizers. *Acc. Chem. Res.* **2006**, 39 (10), 761–771.

(125) Jiang, X.; Ji, G. A Self-Consistent and Cross-Checked Scale of Spin-Delocalization Substituent Constants, the .Sigma.JJ.Bul. Scale. *J. Org. Chem.* **1992**, 57 (22), 6051–6056.

(126) Jiang, X.-K. Establishment and Successful Application of the ΣJJ• Scale of Spin-Delocalization Substituent Constants. *Acc. Chem. Res.* **1997**, 30 (7), 283–289.

(127) O'Rourke, N. F.; Wulff, J. E. Investigation of Quantitative Structure–Reactivity Relationships in the Aliphatic Claisen Rearrangement of Bis-Vinyl Ethers Reveals a Dipolar, Dissociative Mechanism. *Org Biomol Chem* **2014**, 12 (8), 1292–1308.

(128) Moss, R. A.; Shen, S.; Hadel, L. M.; Kmiecik-Lawrynowicz, G.; Wlostowska, J.; Krogh-Jespersen, K. Absolute Rate and Philicity Studies of Methoxyphenylcarbene. An Extended Range for Carbenic Ambiphilicity. *J. Am. Chem. Soc.* **1987**, 109 (14), 4341–4349.

(129) Schwickert, K.; Andrzejewski, M.; Grabowsky, S.; Schirmeister, T. Synthesis, X-Ray Structure Determination, and Comprehensive Photochemical Characterization of (Trifluoromethyl)Diazirine-Containing TRPML1 Ligands. *J. Org. Chem.* **2021**, 86 (9), 6169–6183.

(130) Briner, K.; Vasella, A. Glycosylidene Carbenes. Part 2. Synthesis of O-Aryl Glycosides. *Helv. Chim. Acta* **1990**, 73 (6), 1764–1778.

(131) Blüchel, C.; Ramana, C. V.; Vasella, A. Synthesis of Monosaccharide-Derived Spirocyclic Cyclopropylamines and Their Evaluation as Glycosidase Inhibitors. *Helv. Chim. Acta* **2003**, 86 (9), 2998–3036.

(132) Moss, R. A.; Wlostowska, J. The Extraordinary Selectivity of Methoxyphenylcarbene; The Case of the Curious “Olefin.” *Tetrahedron Lett.* **1988**, 29 (21), 2559–2561.

(133) Włostowska, J.; Moss, R. A.; Guo, W.; Chang, M. J. Methoxyphenyldiazirine as Precursor to Methoxyphenylcarbene. *J Chem Soc Chem Commun* **1982**, No. 8, 432–433.

(134) Ghafarian Shirazi, R.; Neese, F.; Pantazis, D. A. Accurate Spin-State Energetics for Aryl Carbenes. *J. Chem. Theory Comput.* **2018**, 14 (9), 4733–4746.

(135) Sakurai, M.; Masuda, K.; Wang, L.; Murai, Y.; Sakihama, Y.; Hashidoko, Y.; Hatanaka, Y.; Hashimoto, M. Synthesis of Methoxy-Substituted Diazirinyl Phenylalanine – A Novel Photoreactive Aspartame Derivative for Functional Analysis of Sweet Receptors. *Heterocycles* **2014**, 88 (1), 629–637.

(136) Tian, Z.; Fattahi, A.; Lis, L.; Kass, S. R. Cycloalkane and Cycloalkene C−H Bond Dissociation Energies. *J. Am. Chem. Soc.* **2006**, 128 (51), 17087–17092.

(137) Iacobucci, C.; Götze, M.; Piotrowski, C.; Arlt, C.; Rehkamp, A.; Ihling, C.; Hage, C.; Sinz, A. Carboxyl-Photo-Reactive MS-Cleavable Cross-Linkers: Unveiling a Hidden Aspect of Diazirine-Based Reagents. *Anal. Chem.* **2018**, 90 (4), 2805–2809.

(138) Jiang, H.; Guo, G.; Chen, W.; Cui, Z. Reactive Dyeing of Synthetic Fibers Employing Dyes Containing a Diazirine Moiety. *Dyes Pigments* **2021**, 194, 109555.

(139) Johansen, M. B.; Gedde, O. R.; Mayer, T. S.; Skrydstrup, T. Access to Aryl and Heteroaryl Trifluoromethyl Ketones from Aryl Bromides and Fluorosulfates with Stoichiometric CO. *Org. Lett.* **2020**, 22 (11), 4068–4072.

(140) Gao, X.; Cheng, R.; Xiao, Y.-L.; Wan, X.-L.; Zhang, X. Copper-Catalyzed Highly Enantioselective Difluoroalkylation of Secondary Propargyl Sulfonates with Difluoroenoxysilanes. *Chem* **2019**, 5 (11), 2987–2999.

(141) Kelly, C. B.; Mercadante, M. A.; Carnaghan, E. R.; Doherty, M. J.; Fager, D. C.; Hauck, J. J.; MacInnis, A. E.; Tilley, L. J.; Leadbeater, N. E. Synthesis of Perfluoroalkyl-Substituted Vinylcyclopropanes by Way of Enhanced Neighboring Group Participation. *Eur. J. Org. Chem.* **2015**, 2015 (19), 4071–4076.

(142) Bender, T.; Huss, M.; Wieczorek, H.; Grond, S.; von Zezschwitz, P. Convenient Synthesis of a [1-14C]Diazirinylbenzoic Acid as a Photoaffinity Label for Binding Studies of V-ATPase Inhibitors. *Eur. J. Org. Chem.* **2007**, 2007 (23), 3870–3878.

(143) Shi, F.; Shen, J. K.; Chen, D.; Fog, K.; Thirstrup, K.; Hentzer, M.; Karlsson, J.-J.; Menon, V.; Jones, K. A.; Smith, K. E.; Smith, G. Discovery and SAR of a Series of Agonists at Orphan G Protein-Coupled Receptor 139. *ACS Med. Chem. Lett.* **2011**, 2 (4), 303–306.

(144) Tomohiro, T.; Yamamoto, A.; Tatsumi, Y.; Hatanaka, Y. [3-(Trifluoromethyl)-3H-Diazirin-3-Yl]Coumarin as a Carbene-Generating Photocross-Linker with Masked Fluorogenic Beacon. *Chem Commun* **2013**, 49 (98), 11551–11553.

(145) Zou, L.-H.; Priebbenow, D. L.; Wang, L.; Mottweiler, J.; Bolm, C. Copper-Catalyzed Synthesis of α-Thioaryl Carbonyl Compounds Through S–S and C–C Bond Cleavage. *Adv. Synth. Catal.* **2013**, 355 (13), 2558–2563.

(146) Wu, W.; Tian, Q.; Chen, T.; Weng, Z. Copper-Mediated Trifluoroacetylation of Arenediazonium Salts with Ethyl Trifluoropyruvate. *Chem. – Eur. J.* **2016**, 22 (46), 16455–16458.

(147) Kwiatkowski, S.; Crocker, P. J.; Chavan, A. J.; Nobuyuki, I.; Haley, B. E.; Watt, D. S.; Ren-jye, H. Thiazolidine and Thiazoline Derivatives of 3-Aryl-3-Trifluoromethyldiazirines for the Preparation of Fluorescent or 35S-Radiolabeled Photoaffinity Probes. *Tetrahedron Lett.* **1990**, 31 (15), 2093–2096.

(148) Naumann, D.; Finke, M.; Lange, H.; Dukat, W.; Tyrra, W. Die Reaktionen von Bis(Perfluoralkyl)Cadmium-Komplexen Mit Arylcarbonsäurechloriden: Synthese von Aryl-(Perfluoralkyl)Ketonen, (Perfluoralkyl-Dihydropyridin)-Arylcarbonsäureamiden, α,α-Bis(Trifluormethyl)Benzyl-Alkoholen Und Benzoesäure-α,α-Bis(Trifluormethyl)-Benzylestern. *J. Fluor. Chem.* **1992**, 56 (2), 215–237.

(149) Hatanaka, Y.; Hashimoto, M.; Kanaoka, Y. A Rapid and Efficient Method for Identifying Photoaffinity Biotinylated Sites within Proteins. *J. Am. Chem. Soc.* **1998**, 120 (2), 453–454.

(150) Terpinski, J.; Denney, D. Z.; Beveridge, R.; Cox, D. P.; Moss, R. A. A Substituent Chemical Shift (SCS) Effect Study by 13C and 19F NMR of Para-Substituted Phenylhalodiazirines. *Magn. Reson. Chem.* **1987**, 25 (10), 923–927.

(151) Moss, R. A.; Terpinski, J.; Cox, D. P.; Denny, D. Z.; Krogh-Jespersen, K. Azide and Fluoride Exchange Reactions of Halodiazirines. *J. Am. Chem. Soc.* **1985**, 107 (9), 2743–2748.

(152) Liu, Z.; Cao, S.; Yu, W.; Wu, J.; Yi, F.; Anderson, E. A.; Bi, X. Site-Selective C–H Benzylation of Alkanes with N-Triftosylhydrazones Leading to Alkyl Aromatics. *Chem* **2020**, 6 (8), 2110–2124.

(153) Brazel, C. S.; Rosen, S. L. Fundamental Principles of Polymeric Materials; Wiley, 2012.

(154) Taddei, P.; Affatato, S.; Fagnano, C.; Toni, A. Oxidation in Ultrahigh Molecular Weight Polyethylene and Cross-Linked Polyethylene Acetabular Cups Tested against Roughened Femoral Heads in a Hip Joint Simulator. *Biomacromolecules* **2006**, 7 (6), 1912–1920.

(155) Lukin, R. Yu.; Kuchkaev, A. M.; Sukhov, A. V.; Bekmukhamedov, G. E.; Yakhvarov, D. G. Platinum-Catalyzed Hydrosilylation in Polymer Chemistry. *Polymers* **2020**, 12 (10).

(156) Hashimoto, M.; Hatanaka, Y. Recent Progress in Diazirine-Based Photoaffinity Labeling. *Eur. J. Org. Chem.* **2008**, 2008 (15), 2513–2523.

(157) Smith, E.; Collins, I. Photoaffinity Labeling in Target- and Binding-Site Identification. *Future Med. Chem.* **2015**, 7 (2), 159–183.

(158) Hill, J. R.; Robertson, A. A. B. Fishing for Drug Targets: A Focus on Diazirine Photoaffinity Probe Synthesis. *J. Med. Chem.* **2018**, 61 (16), 6945–6963.

(159) Plummer, C. M.; Li, L.; Chen, Y. The Post-Modification of Polyolefins with Emerging Synthetic Methods. *Polym Chem* **2020**, 11 (43), 6862–6872.

(160) Liu, M. T. H. The Thermolysis and Photolysis of Diazirines. *Chem Soc Rev* **1982**, 11 (2), 127–140.

(161) Ollevier, T.; Carreras, V. Emerging Applications of Aryl Trifluoromethyl Diazoalkanes and Diazirines in Synthetic Transformations. *ACS Org. Inorg. Au* **2022**, 2 (2), 83–98.

(162) Welle, A.; Billard, F.; Marchand-Brynaert, J. Tri- and Tetravalent Photoactivable Cross-Linking Agents. *Synthesis* **2012**, 44 (14), 2249–2254.

(163) Singh, M.; Varela, C. E.; Whyte, W.; Horvath, M. A.; Tan, N. C. S.; Ong, C. B.; Liang, P.; Schermerhorn, M. L.; Roche, E. T.; Steele, T. W. J. Minimally Invasive Electroceutical Catheter for Endoluminal Defect Sealing. *Sci. Adv.* **2021**, 7 (14), eabf6855.

(164) Singh, M.; Solic, I.; Steele, T. W. J. Hydrophobic Bioadhesive Composites for Human Motion Detection. *ACS Macro Lett.* **2021**, 10 (11), 1353–1358.

(165) Tomohiro, T.; Tachi, N.; Azuma, Y.; Hatanaka, Y. Hydrophilic Diazirine Polymer for One-Step Photo-Fabrication of Proteins on Polypropylene Surface. *Heterocycles* **2009**, 79 (1), 897–908.

(166) Ghiassian, S.; Ismaili, H.; Lubbock, B. D. W.; Dube, J. W.; Ragogna, P. J.; Workentin, M. S. Photoinduced Carbene Generation from Diazirine Modified Task Specific Phosphonium Salts To Prepare Robust Hydrophobic Coatings. *Langmuir* **2012**, 28 (33), 12326–12333.

(167) Bexis, P.; Arno, M. C.; Bell, C. A.; Thomas, A. W.; Dove, A. P. Thermally-Induced Hyperbranching of Bromine-Containing Polyesters by Insertion of in Situ Generated Chain-End Carbenes. *Chem. Commun.* **2021**, 57 (35), 4275–4278.

(168) Musolino, S. F.; Mahbod, M.; Nazir, R.; Bi, L.; Graham, H. A.; Milani, A. S.; Wulff, J. E. Electronically Optimized Diazirine-Based Polymer Crosslinkers. *Polym. Chem.* **2022**, 13 (25), 3833–3839.

(169) Ma, S.; Webster, D. C. Degradable Thermosets Based on Labile Bonds or Linkages: A Review. *Prog. Polym. Sci.* **2018**, 76, 65–110.

(170) Khonakdar, H. A.; Morshedian, J.; Wagenknecht, U.; Jafari, S. H. An Investigation of Chemical Crosslinking Effect on Properties of High-Density Polyethylene. *Polymer* **2003**, 44 (15), 4301–4309.

(171) Rahimi, A.; García, J. M. Chemical Recycling of Waste Plastics for New Materials Production. *Nat. Rev. Chem.* **2017**, 1 (6), 1–11.

(172) Post, W.; Susa, A.; Blaauw, R.; Molenveld, K.; Knoop, R. J. I. A Review on the Potential and Limitations of Recyclable Thermosets for Structural Applications. *Polym. Rev.* **2020**, 60 (2), 359–388.

(173) Chemical Sciences and Society Summit. Science to Enable Sustainable Plastics; 2020.

(174) Shieh, P.; Zhang, W.; Husted, K. E. L.; Kristufek, S. L.; Xiong, B.; Lundberg, D. J.; Lem, J.; Veysset, D.; Sun, Y.; Nelson, K. A.; Plata, D. L.; Johnson, J. A. Cleavable Comonomers Enable Degradable, Recyclable Thermoset Plastics. *Nature* **2020**, 583 (7817), 542–547.

(175) T. Sheppard, D.; Jin, K.; S. Hamachi, L.; Dean, W.; J. Fortman, D.; J. Ellison, C.; R. Dichtel, W. Reprocessing Postconsumer Polyurethane Foam Using Carbamate Exchange Catalysis and Twin-Screw Extrusion. *ACS Cent. Sci.* **2020**, 6 (6), 921–927.

(176) Christensen, P. R.; Scheuermann, A. M.; Loeffler, K. E.; Helms, B. A. Closed-Loop Recycling of Plastics Enabled by Dynamic Covalent Diketoenamine Bonds. *Nat. Chem.* **2019**, 11 (5), 442–448.

(177) Röttger, M.; Domenech, T.; van der Weegen, R.; Breuillac, A.; Nicolaÿ, R.; Leibler, L. High-Performance Vitrimers from Commodity Thermoplastics through Dioxaborolane Metathesis. *Science* **2017**, 356 (6333), 62–65.

(178) Radchenko, A. V; Ganachaud, F. Photocatalyzed Hydrosilylation in Silicone Chemistry. *Ind. Eng. Chem. Res.* **2022**, 61 (23), 7679–7698.

(179) J. Marks, M.; Vernon Snelgrove, R. Effect of Conversion on the Structure−Property Relationships of Amine-Cured Epoxy Thermosets. *ACS Appl. Mater. Interfaces* **2009**, 1 (4), 921–926.

(180) Chodák, I. Crosslinking of Polypropylene. In Polymer Science and Technology Series; Karger-Kocsis, J., Ed.; Springer Netherlands: Dordrecht, 1999; pp 128–134.

(181) Thomas, J.; Joseph, B.; Jose, Josmin. P.; Maria, H. J.; Main, P.; Ali Rahman, A.; Francis, B.; Ahmad, Z.; Thomas, S. Recent Advances in Cross-Linked Polyethylene-Based Nanocomposites for High Voltage Engineering Applications: A Critical Review. *Ind. Eng. Chem. Res.* **2019**, 58 (46), 20863–20879.

(182) Lu, S.; Fu, Z.; Li, F.; Weng, K.; Zhou, L.; Zhang, L.; Yang, Y.; Qiu, H.; Liu, D.; Qing, W.; Ding, H.; Sheng, X.; Chen, M.; Tang, X.; Duan, L.; Liu, W.; Wu, L.; Yang, Y.; Zhang, H.; Li, J. Beyond a Linker: The Role of Photochemistry of Crosslinkers in the Direct Optical Patterning of Colloidal Nanocrystals. *Angew. Chem. Int. Ed.* **2022**, 61 (23), e202202633.

(183) Bi, L.; Godwin, B.; Baran, M. J.; Nazir, R.; Wulff, J. E. A Cleavable Crosslinking Strategy for Commodity Polymer Functionalization and Generation of Reprocessable Thermosets. *Angew. Chem. Int. Ed.* e202304708.

(184) Häußler, M.; Eck, M.; Rothauer, D.; Mecking, S. Closed-Loop Recycling of Polyethylene-like Materials. *Nature* **2021**, 590 (7846), 423–427.

(185) Maschmeyer, P. G.; Liang, X.; Hung, A.; Ahmadzai, O.; Kenny, A. L.; Luong, Y. C.; Forder, T. N.; Zeng, H.; Gillies, E. R.; Roberts, D. A. Post-Polymerization "click" End-Capping of Polyglyoxylate Self-Immolative Polymers. *Polym. Chem.* **2021**, 12 (47), 6824–6831.

(186) Garcia, J. J.; Miller, S. A. Polyoxalates from Biorenewable Diols via Oxalate Metathesis Polymerization. *Polym. Chem.* **2014**, 5 (3), 955–961.

(187) Song, C.-C.; Du, F.-S.; Li, Z.-C. Oxidation-Responsive Polymers for Biomedical Applications. *J. Mater. Chem. B* **2014**, 2 (22), 3413–3426.

(188) Barth, M.; Fischer, R.; Brock, R.; Rademann, J. Reversible Cross-Linking of Hyperbranched Polymers: A Strategy for the Combinatorial Decoration of Multivalent Scaffolds. *Angew. Chem. Int. Ed.* **2005**, 44 (10), 1560–1563.

(189) Parrott, M. C.; Luft, J. C.; Byrne, J. D.; Fain, J. H.; Napier, M. E.; DeSimone, J. M. Tunable Bifunctional Silyl Ether Cross-Linkers for the Design of Acid-Sensitive Biomaterials. *J. Am. Chem. Soc.* **2010**, 132 (50), 17928–17932.

(190) Nishimura, Y.; Chung, J.; Muradyan, H.; Guan, Z. Silyl Ether as a Robust and Thermally Stable Dynamic Covalent Motif for Malleable Polymer Design. *J. Am. Chem. Soc.* **2017**, 139 (42), 14881–14884.

(191) Shieh, P.; Nguyen, H. V.-T.; Johnson, J. A. Tailored Silyl Ether Monomers Enable Backbone-Degradable Polynorbornene-Based Linear, Bottlebrush and Star Copolymers through ROMP. *Nat. Chem.* **2019**, 11 (12), 1124–1132.

(192) Liu, Y.; Park, S. K.; Xiao, Y.; Chae, J. Copper(Ii)-Catalyzed C–O Coupling of Aryl Bromides with Aliphatic Diols: Synthesis of Ethers, Phenols, and Benzo-Fused Cyclic Ethers. *Org. Biomol. Chem.* **2014**, 12 (26), 4747–4753.

(193) Zheng, Y.; Zou, W.; Luo, L.; Chen, J.; Lin, S.; Sun, Q. Ligand-Free Cu-Catalyzed O-Arylation of Aliphatic Diols. *RSC Adv.* **2015**, 5 (81), 66104–66108.

(194) Bergström, M.; Suresh, G.; Naidu, V. R.; Unelius, C. R. N-Iodosuccinimide (NIS) in Direct Aromatic Iodination. *Eur. J. Org. Chem.* **2017**, 2017 (22), 3234–3239.

(195) Morita, C.; Hashimoto, K.; Okuno, T.; Shirahama, H. Synthesis of 3-Trifluoromethyl-3-Aryldiazirines for Photoaffinity-Labeling Probes and Their Labeling Ability. *Heterocycles* **2000**, 52, 1163–1169.

(196) He, C.; Christensen, P. R.; Seguin, T. J.; Dailing, E. A.; Wood, B. M.; Walde, R. K.; Persson, K. A.; Russell, T. P.; Helms, B. A. Conformational Entropy as a Means to Control the Behavior of Poly(Diketoenamine) Vitrimers In and Out of Equilibrium. *Angew. Chem. Int. Ed.* **2020**, 59 (2), 735–739.

(197) Long, T. R.; Elder, R. M.; Bain, E. D.; Masser, K. A.; Sirk, T. W.; Yu, J. H.; Knorr, D. B.; Lenhart, J. L. Influence of Molecular Weight between Crosslinks on the Mechanical Properties of Polymers Formed via Ring-Opening Metathesis. *Soft Matter* **2018**, 14 (17), 3344–3360.

(198) Barszczewska-Rybarek, I. M.; Korytkowska-Wałach, A.; Kurcok, M.; Chladek, G.; Kasperski, J. DMA Analysis of the Structure of Crosslinked Poly(Methyl Methacrylate)s. *Acta Bioeng. Biomech.* **2017**, 19 (1), 47–53.

(199) Juan, R.; Paredes, B.; García-Muñoz, R. A.; Domínguez, C. Quantification of PP Contamination in Recycled PE by TREF Analysis for Improved the Quality and Circularity of Plastics. *Polym. Test.* **2021**, 100, 107273.

(200) Karaagac, E.; Jones, M. P.; Koch, T.; Archodoulaki, V.-M. Polypropylene Contamination in Post-Consumer Polyolefin Waste: Characterisation, Consequences and Compatibilisation. *Polymers* **2021**, 13 (16), 2618.

(201) Karaagac, E.; Koch, T.; Archodoulaki, V.-M. The Effect of PP Contamination in Recycled High-Density Polyethylene (RPE-HD) from Post-Consumer Bottle Waste and Their Compatibilization with Olefin Block Copolymer (OBC). *Waste Manag.* **2021**, 119, 285–294.

(202) Yin, S.; Tuladhar, R.; Shi, F.; Shanks, R. A.; Combe, M.; Collister, T. Mechanical Reprocessing of Polyolefin Waste: A Review. *Polym. Eng. Sci.* **2015**, 55 (12), 2899–2909.

(203) Nwabunma, D.; Kyu, T. Overview of Polyolefin Blends. In Polyolefin blends; Wiley-Interscience: Hoboken, N.J., 2008; pp 1–26.

(204) Jehanno, C.; Alty, J. W.; Roosen, M.; Meester, S. D.; Dove, A. P.; Chen, E. Y.-X.; Leibfarth, F. A.; Sardon, H. Critical Advances and Future Opportunities in Upcycling Commodity Polymers. *Nature* **2022**, 603 (7903), 803–814.

(205) Eagan, J. M.; Xu, J.; Girolamo, R. D.; Thurber, C. M.; Macosko, C. W.; LaPointe, A. M.; Bates, F. S.; Coates, G. W. Combining Polyethylene and Polypropylene:

Enhanced Performance with PE/IPP Multiblock Polymers. *Science* **2017**, 355 (6327), 814–816.

(206) Geyer, R.; Jambeck, J. R.; Law, K. L. Production, Use, and Fate of All Plastics Ever Made. *Sci. Adv.* **2017**, 3 (7), e1700782.

(207) Plummer, C. M.; Zhou, H.; Li, S.; Zhong, H.; Sun, Z.; Bariashir, C.; Sun, W.-H.; Huang, H.; Liu, L.; Chen, Y. A Direct Functionalization of Polyolefins for Blend Compatibilization by an Insertion of 1,1-Bis(Phenylsulfonyl)Ethylene (BPSE). *Polym Chem* **2019**, 10 (24), 3325–3333.

(208) Fazekas, T. J.; Alty, J. W.; Neidhart, E. K.; Miller, A. S.; Leibfarth, F. A.; Alexanian, E. J. Diversification of Aliphatic C–H Bonds in Small Molecules and Polyolefins through Radical Chain Transfer. *Science* **2022**, 375 (6580), 545–550.

(209) Clarke, R. W.; Sandmeier, T.; Franklin, K. A.; Reich, D.; Zhang, X.; Vengallur, N.; Patra, T. K.; Tannenbaum, R. J.; Adhikari, S.; Kumar, S. K.; Rovis, T.; Chen, E. Y.-X. Dynamic Crosslinking Compatibilizes Immiscible Mixed Plastics. *Nature* **2023**, 616 (7958), 731–739.

(210) Sperry, J. B.; Minteer, C. J.; Tao, J.; Johnson, R.; Duzguner, R.; Hawksworth, M.; Oke, S.; Richardson, P. F.; Barnhart, R.; Bill, D. R.; Giusto, R. A.; Weaver, J. D. Thermal Stability Assessment of Peptide Coupling Reagents Commonly Used in Pharmaceutical Manufacturing. *Org. Process Res. Dev.* **2018**, 22 (9), 1262–1275.

(211) Wronska, M. A.; O'Connor, I. B.; Tilbury, M. A.; Srivastava, A.; Wall, J. G. Adding Functions to Biomaterial Surfaces through Protein Incorporation. *Adv. Mater.* **2016**, 28 (27), 5485–5508.

(212) Mohamad, N. R.; Marzuki, N. H. C.; Buang, N. A.; Huyop, F.; Wahab, R. A. An Overview of Technologies for Immobilization of Enzymes and Surface Analysis Techniques for Immobilized Enzymes. *Biotechnol. Biotechnol. Equip.* **2015**, 29 (2), 205–220.

(213) Ainsworth, M. J.; Lotz, O.; Gilmour, A.; Zhang, A.; Chen, M. J.; McKenzie, D. R.; Bilek, M. M. M.; Malda, J.; Akhavan, B.; Castilho, M. Covalent Protein Immobilization on 3D-Printed Microfiber Meshes for Guided Cartilage Regeneration. *Adv. Funct. Mater.* **2023**, 33 (2), 2206583.

(214) Khnouf, R.; Karasneh, D.; Albiss, B. A. Protein Immobilization on the Surface of Polydimethylsiloxane and Polymethyl Methacrylate Microfluidic Devices. *ELECTROPHORESIS* **2016**, 37 (3), 529–535.

(215) Hartmann, M.; Jung, D. Biocatalysis with Enzymes Immobilized on Mesoporous Hosts: The Status Quo and Future Trends. *J Mater Chem* **2010**, 20 (5), 844–857.

(216) Fopase, R.; Paramasivam, S.; Kale, P.; Paramasivan, B. Strategies, Challenges and Opportunities of Enzyme Immobilization on Porous Silicon for Biosensing Applications. *J. Environ. Chem. Eng.* **2020**, 8 (5), 104266.

(217) Williams, D. M.; Kaufman, G.; Izadi, H.; Gahm, A. E.; Prophet, S. M.; Vanderlick, K. T.; Osuji, C. O.; Regan, L. Facile Protein Immobilization Using Engineered Surface-Active Biofilm Proteins. *ACS Appl. Nano Mater.* **2018**, 1 (6), 2483–2488.

(218) Enemchukwu, N. O.; García, A. J. 4.13 Peptide- and Protein-Modified Surfaces☆. In Comprehensive Biomaterials II; Ducheyne, P., Ed.; Elsevier: Oxford, 2017; pp 200–220.

(219) Hoffman, A. S.; Hubbell, J. A. Chapter I.2.17 - Surface-Immobilized Biomolecules. In Biomaterials Science (Third Edition); Ratner, B. D., Hoffman, A. S., Schoen, F. J., Lemons, J. E., Eds.; Academic Press, 2013; pp 339–349.

(220) Robinson, G. K. Methods in Biotechnology—Immobilization of Enzymes and Cells; Edited by G F Bickerstaff. Pp 367. Humana Press, New Jersey. 1996 ISBN 0-89603-386-4. *Biochem. Educ.* **1997**, 25 (4), 232–232.

(221) Enzyme Immobilization in Biodegradable Polymers for Biomedical Applications. In Biodegradable Systems in Tissue Engineering and Regenerative Medicine; Reis, R. L., Román, J. S., Eds.; CRC Press, 2004; pp 301–323.

(222) Leung, J. M.; Berry, L. R.; Atkinson, H. M.; Cornelius, R. M.; Sandejas, D.; Rochow, N.; Selvaganapathy, P. R.; Fusch, C.; Chan, A. K. C.; Brash, J. L. Surface Modification of Poly(Dimethylsiloxane) with a Covalent Antithrombin–Heparin Complex for the Prevention of Thrombosis: Use of Polydopamine as Bonding Agent. *J Mater Chem B* **2015**, 3 (29), 6032–6036.

(223) Yoo, B. Y.; Kim, B. H.; Lee, J. S.; Shin, B. H.; Kwon, H.; Koh, W.-G.; Heo, C. Y. Dual Surface Modification of PDMS-Based Silicone Implants to Suppress Capsular Contracture. *Acta Biomater.* **2018**, 76, 56–70.

(224) Wang, B.; Koo, B.; Huang, L.; Monbouquette, H. G. Microbiosensor Fabrication by Polydimethylsiloxane Stamping for Combined Sensing of Glucose and Choline. *Analyst* **2018**, 143 (20), 5008–5013.

(225) Fujii, T. PDMS-Based Microfluidic Devices for Biomedical Applications. *Micro-Nano-Eng. 2001* **2002**, 61–62, 907–914.

(226) Mata, A.; Fleischman, A. J.; Roy, S. Characterization of Polydimethylsiloxane (PDMS) Properties for Biomedical Micro/Nanosystems. *Biomed. Microdevices* **2005**, 7 (4), 281–293.

(227) Bai, Y.; Koh, C. G.; Boreman, M.; Juang, Y.-J.; Tang, I.-C.; Lee, L. J.; Yang, S.-T. Surface Modification for Enhancing Antibody Binding on Polymer-Based Microfluidic Device for Enzyme-Linked Immunosorbent Assay. *Langmuir* **2006**, 22 (22), 9458–9467.

(228) Yuan, Y.; He, H.; Lee, L. J. Protein A-Based Antibody Immobilization onto Polymeric Microdevices for Enhanced Sensitivity of Enzyme-Linked Immunosorbent Assay. *Biotechnol. Bioeng*. **2009**, 102 (3), 891–901.

(229) Kovach, K. M.; Capadona, J. R.; Gupta, A. S.; Potkay, J. A. The Effects of PEG-Based Surface Modification of PDMS Microchannels on Long-Term Hemocompatibility. *J. Biomed. Mater. Res. A* **2014**, 102 (12), 4195–4205.

(230) Zhang, A.; Cheng, L.; Hong, S.; Yang, C.; Lin, Y. Preparation of Anti-Fouling Silicone Elastomers by Covalent Immobilization of Carboxybetaine. *RSC Adv* **2015**, 5 (107), 88456–88463.

(231) Wang, D.; Hartz, W. F.; Moloney, M. G. Surface Modified Materials for Active Capture of Enzymes. *J Mater Chem B* **2023**, 11 (11), 2377–2388.

(232) McCormick, A. M.; Wijekoon, A.; Leipzig, N. D. Specific Immobilization of Biotinylated Fusion Proteins NGF and Sema3A Utilizing a Photo-Cross-Linkable Diazirine Compound for Controlling Neurite Extension. *Bioconjug. Chem.* **2013**, 24 (9), 1515–1526.

(233) Pourcelle, V.; Duff, C. S. L.; Freichels, H.; Jérôme, C.; Marchand-Brynaert, J. Clickable PEG Conjugate Obtained by “Clip” Photochemistry: Synthesis and Characterization by Quantitative 19F NMR. *J. Fluor. Chem.* **2012**, 140, 62–69.

(234) West, A. V.; Amako, Y.; Woo, C. M. Design and Evaluation of a Cyclobutane Diazirine Alkyne Tag for Photoaffinity Labeling in Cells. *J. Am. Chem. Soc.* **2022**, 144 (46), 21174–21183.

(235) Dreyer, D. R.; Miller, D. J.; Freeman, B. D.; Paul, D. R.; Bielawski, C. W. Perspectives on Poly(Dopamine). *Chem Sci* **2013**, 4 (10), 3796–3802.

(236) Chuah, Y. J.; Koh, Y. T.; Lim, K.; Menon, N. V.; Wu, Y.; Kang, Y. Simple Surface Engineering of Polydimethylsiloxane with Polydopamine for Stabilized Mesenchymal Stem Cell Adhesion and Multipotency. *Sci. Rep.* **2015**, 5 (1), 18162.

(237) Goh, S. C.; Luan, Y.; Wang, X.; Du, H.; Chau, C.; Schellhorn, H. E.; Brash, J. L.; Chen, H.; Fang, Q. Polydopamine–Polyethylene Glycol–Albumin Antifouling Coatings on Multiple Substrates. *J Mater Chem B* **2018**, 6 (6), 940–949.

(238) Carter, D. C.; He, X.-M.; Munson, S. H.; Twigg, P. D.; Gernert, K. M.; Broom, M. B.; Miller, T. Y. Three-Dimensional Structure of Human Serum Albumin. *Science* **1989**, 244 (4909), 1195–1198.

(239) Vidarsson, G.; Dekkers, G.; Rispens, T. IgG Subclasses and Allotypes: From Structure to Effector Functions. *Front. Immunol.* **2014**, 5.

(240) Shen, M.; Rusling, J. F.; Dixit, C. K. Site-Selective Orientated Immobilization of Antibodies and Conjugates for Immunodiagnostics Development. *Antibodies –Analytical Masterpieces Prod. Appl.* **2017**, 116, 95–111.

(241) Khanmohammadi, A.; Jalili Ghazizadeh, A.; Hashemi, P.; Afkhami, A.; Arduini, F.; Bagheri, H. An Overview to Electrochemical Biosensors and Sensors for the Detection of Environmental Contaminants. *J. Iran. Chem. Soc.* **2020**, 17 (10), 2429–2447.

(242) Deng, F.; Li, Y.; Hossain, M. J.; Kendig, M. D.; Arnold, R.; Goldys, E. M.; Morris, M. J.; Liu, G. Polymer Brush Based Fluorescent Immunosensor for Direct Monitoring of Interleukin-1β in Rat Blood. *Analyst* **2019**, 144 (19), 5682–5690.

(243) Bansagi, J.; Wilson-Konderka, C.; Debrauwer, V.; Narayanan, P.; Batey, R. A. N-Alkyl Carbamoylimidazoles as Isocyanate Equivalents: Exploration of the Reaction

Scope for the Synthesis of Ureas, Hydantoins, Carbamates, Thiocarbamates, and Oxazolidinones. *J. Org. Chem.* **2022**, 87 (17), 11329–11349.

(244) Ghosh, A. K.; Brindisi, M. Organic Carbamates in Drug Design and Medicinal Chemistry. *J. Med. Chem.* **2015**, 58 (7), 2895–2940.

(245) Zhang, H.; Wang, W.; Wei, L.; Wu, D.; Cheng, J.; Gao, F. Fabrication of PAMAM Antimicrobial Monolayer via UV Induced Grafting on the Surface of Polyethylene Terephthalate. *Colloids Surf. B Biointerfaces* **2021**, 201, 111601.

(246) Musolino, S. F.; Shatila, F.; Tieman, G. M. O.; Masarsky, A. C.; Thibodeau, M. C.; Wulff, J. E.; Buckley, H. L. Light-Induced Anti-Bacterial Effect Against Staphylococcus Aureus of Porphyrin Covalently Bonded to a Polyethylene Terephthalate Surface. *ACS Omega* **2022**, 7 (33), 29517–29525.

(247) Pissetti, F. L.; Magosso, H. A.; Yoshida, I. V. P.; Gushikem, Y.; Myernyi, S. O.; Kholin, Y. V. N-Propylpyridinium Chloride-Modified Poly(Dimethylsiloxane) Elastomeric Networks: Preparation, Characterization, and Study of Metal Chloride Adsorption from Ethanol Solutions. *J. Colloid Interface Sci.* **2007**, 314 (1), 38–45.

(248) Pissetti, F. L.; Araújo, P. L. D.; Silva, F. A. B.; Poirier, G. Y. Synthesis of Poly(Dimethylsiloxane) Networks Functionalized with Imidazole or Benzimidazole for Copper(II) Removal from Water. *J. Braz. Chem. Soc.* **2015**, 26 (2), 266–272.

(249) Balachandran, V.; Karpagam, V.; Santhi, G.; Revathi, B.; Ilango, G.; Kavimani, M. Conformational Stability, Vibrational (FT-IR and FT-Raman) Spectra and Computational Analysis of m-Trifluoromethyl Benzoic Acid. *Spectrochim. Acta. A. Mol. Biomol. Spectrosc.* **2015**, 137, 165–175.

(250) Djordjevic, I.; Wicaksono, G.; Solic, I.; Steele, T. W. J. Diazoalkane Decay Kinetics from UVA-Active Protein Labelling Molecules: Trifluoromethyl Phenyl Diazirines. *Results Chem.* **2020**, 2, 100066.

(251) Gambi, A.; Winnewisser, M.; Christiansen, J. Johs. The Infrared Spectrum of Diazirine: . Rovibrational Analysis of the N3 Fundamental. *J. Mol. Spectrosc.* **1983**, 98 (2), 413–424.

(252) Elliott, A. D. Confocal Microscopy: Principles and Modern Practices. *Curr. Protoc. Cytom.* **2020**, 92 (1), e68.

(253) Pan, Y. The Dark Side of Fluorine. *ACS Med. Chem. Lett.* **2019**, 10 (7), 1016–1019.

(254) 3M to Stop Making PFAS by 2025. *CEN Glob. Enterp.* **2023**, 101 (1), 4–4.

(255) Graham, W. H. The Halogenation of Amidines. I. Synthesis of 3-Halo- and Other Negatively Substituted Diazirines1. *J. Am. Chem. Soc.* **1965**, 87 (19), 4396–4397.

(256) Moss, R. A. Diazirines: Carbene Precursors Par Excellence. *Acc. Chem. Res.* **2006**, 39 (4), 267–272.

(257) Cox, D. P.; Moss, R. A.; Terpinski, J. Exchange Reactions of Halodiazirines. Synthesis of Fluorodiazirines. *J. Am. Chem. Soc.* **1983**, 105 (21), 6513–6514.

(258) Moss, R. A.; Kmiecik-ławrynowicz, G.; Cox, D. P. Novel Preparation of Cyanophenylcyclopropanes Via Cyanophenylcarbene. *Synth. Commun.* **1984**, 14 (1), 21–25.

(259) Moss, R. A.; Zdrojewski, T.; Krogh-Jespersen, K.; Włostowski, M.; Matro, A. Push-Pull Carbenes: Alkoxycyanocarbenes. *Tetrahedron Lett.* **1991**, 32 (17), 1925–1928.

(260) Green, S. P.; Wheelhouse, K. M.; Payne, A. D.; Hallett, J. P.; Miller, P. W.; Bull, J. A. Thermal Stability and Explosive Hazard Assessment of Diazo Compounds and Diazo Transfer Reagents. *Org. Process Res. Dev.* **2020**, 24 (1), 67–84.

(261) Davies, H. M. L.; Beckwith, R. E. J. Catalytic Enantioselective C−H Activation by Means of Metal−Carbenoid-Induced C−H Insertion. *Chem. Rev.* **2003**, 103 (8), 2861–2904.

(262) Bapat, A. P.; Sumerlin, B. S.; Sutti, A. Bulk Network Polymers with Dynamic B–O Bonds: Healable and Reprocessable Materials. *Mater Horiz* **2020**, 7 (3), 694–714.

(263) Ono, T.; Taema, A.; Goto, A.; Hisaeda, Y. Switching of Monomer Fluorescence, Charge-Transfer Fluorescence, and Room-Temperature Phosphorescence Induced by Aromatic Guest Inclusion in a Supramolecular Host. *Chem. – Eur. J.* **2018**, 24 (66), 17487–17496.

(264) Zhao, Z.-H.; Zhao, P.-C.; Chen, S.-Y.; Zheng, Y.-X.; Zuo, J.-L.; Li, C.-H. Tough, Reprocessable, and Recyclable Dynamic Covalent Polymers with Ultrastable Long-Lived Room-Temperature Phosphorescence. *Angew. Chem. Int. Ed.* e202301993.

Appendix

Appendix A: NMR Spectra

^{1}H and ^{13}C NMR spectra of **S3.1** in $CDCl_3$:

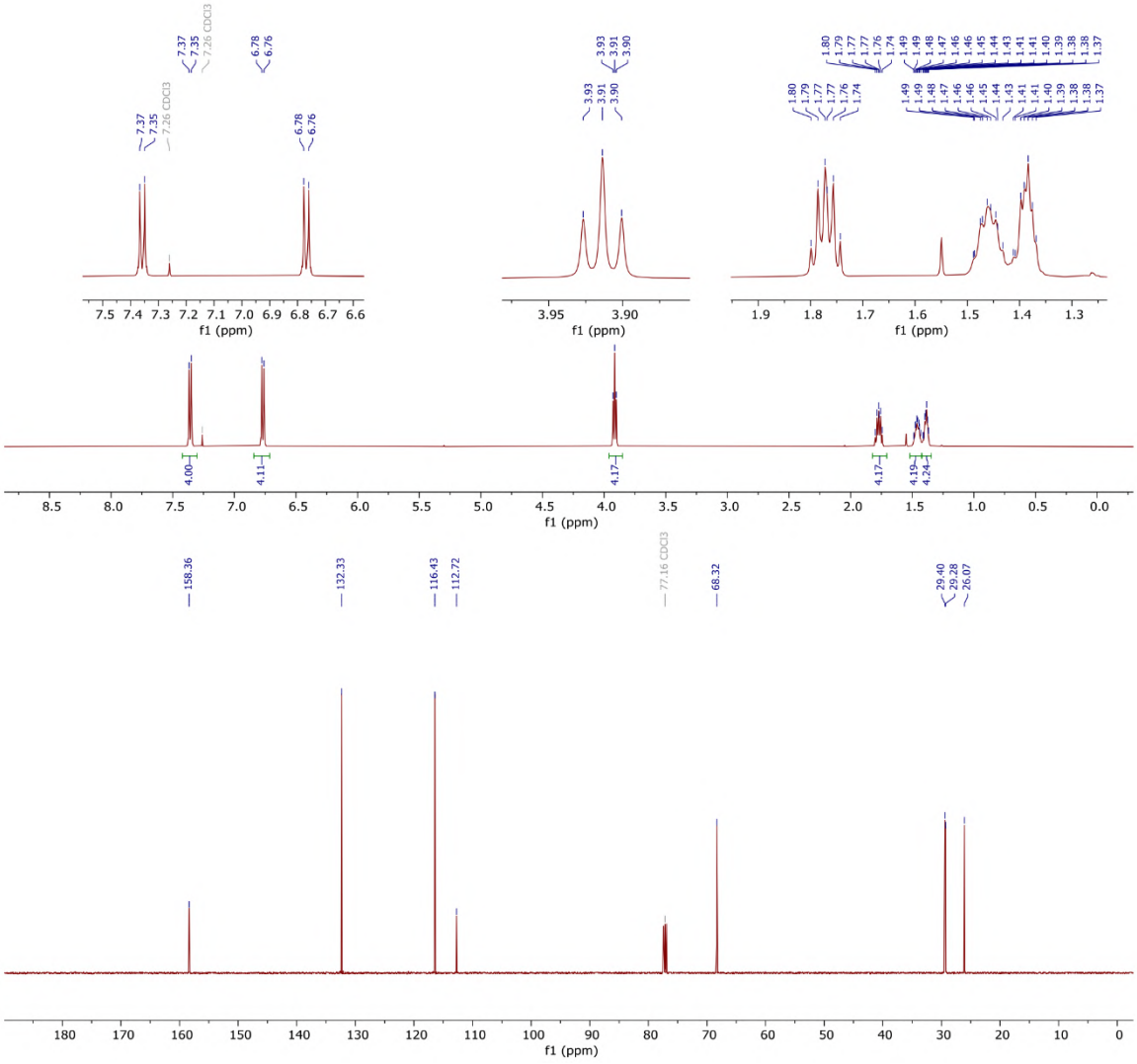

^{1}H, ^{13}C, and ^{19}F NMR spectra of **S3.2** in $CDCl_3$:

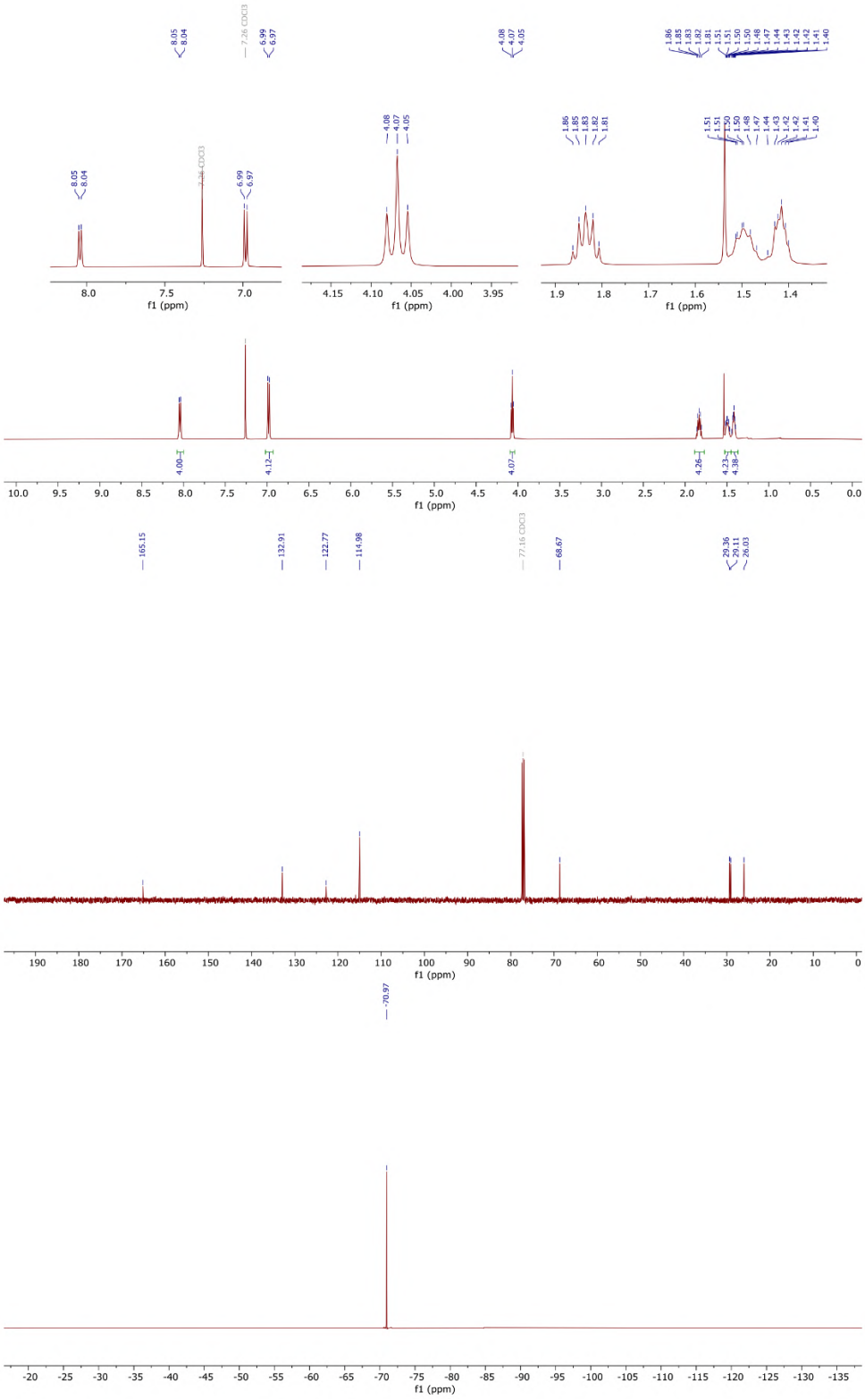

^{1}H and ^{19}F NMR spectra of **S3.3** in $(CD_3)_2CO$:

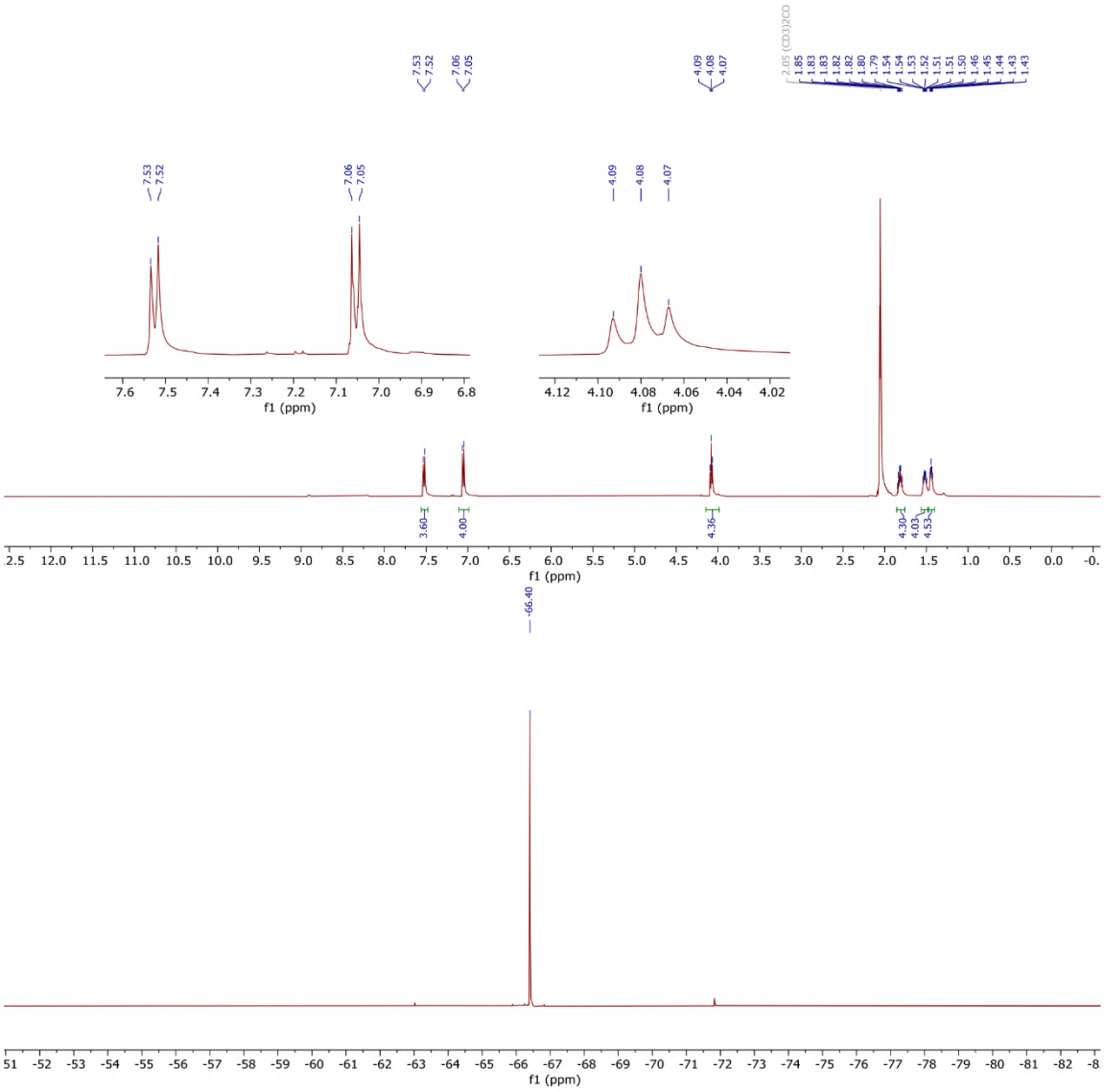

^{1}H and ^{19}F NMR spectra of **S3.4** in $CDCl_3$:

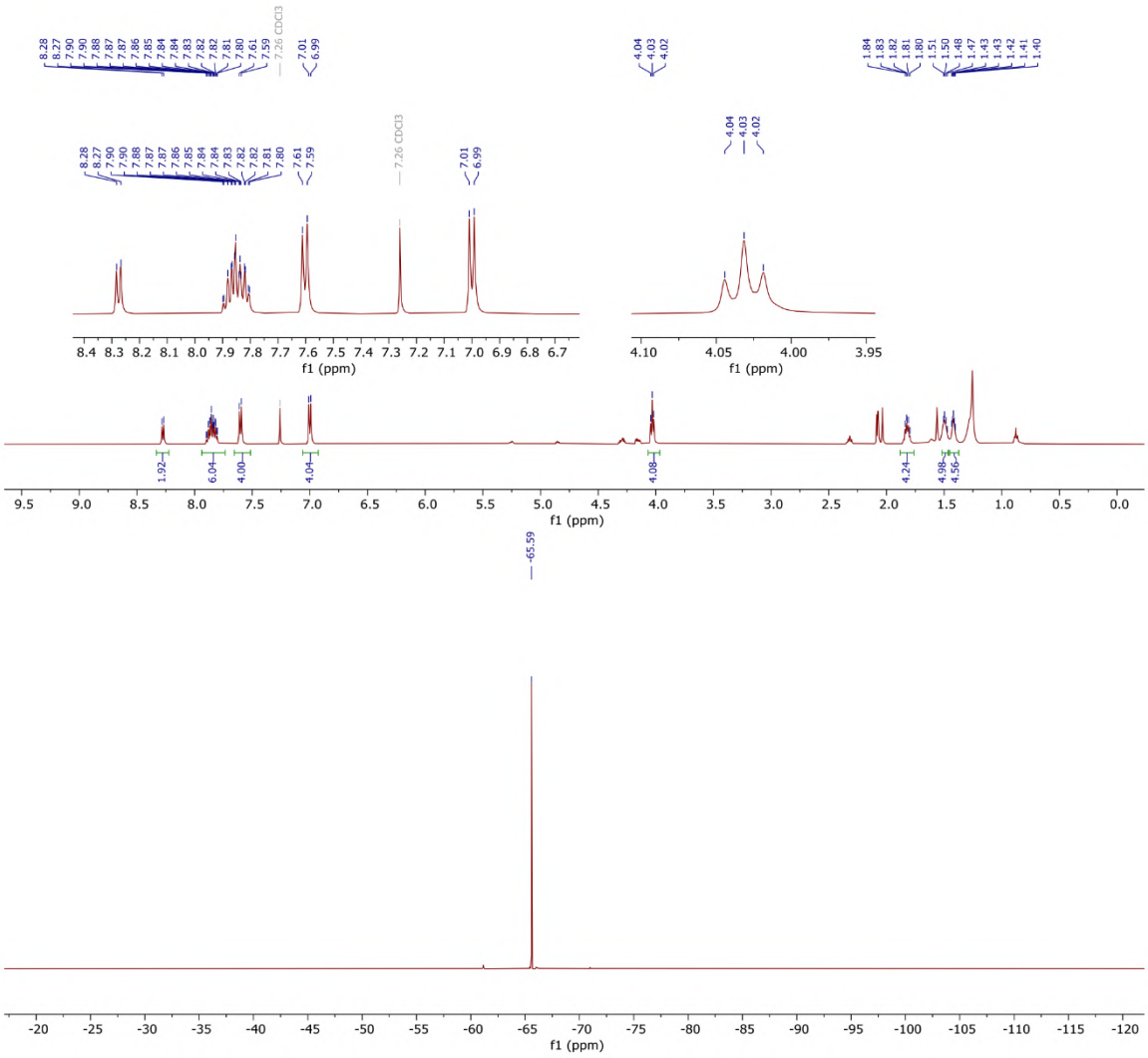

^{1}H, ^{13}C, and ^{19}F NMR spectra of **S3.5** in $CDCl_3$:

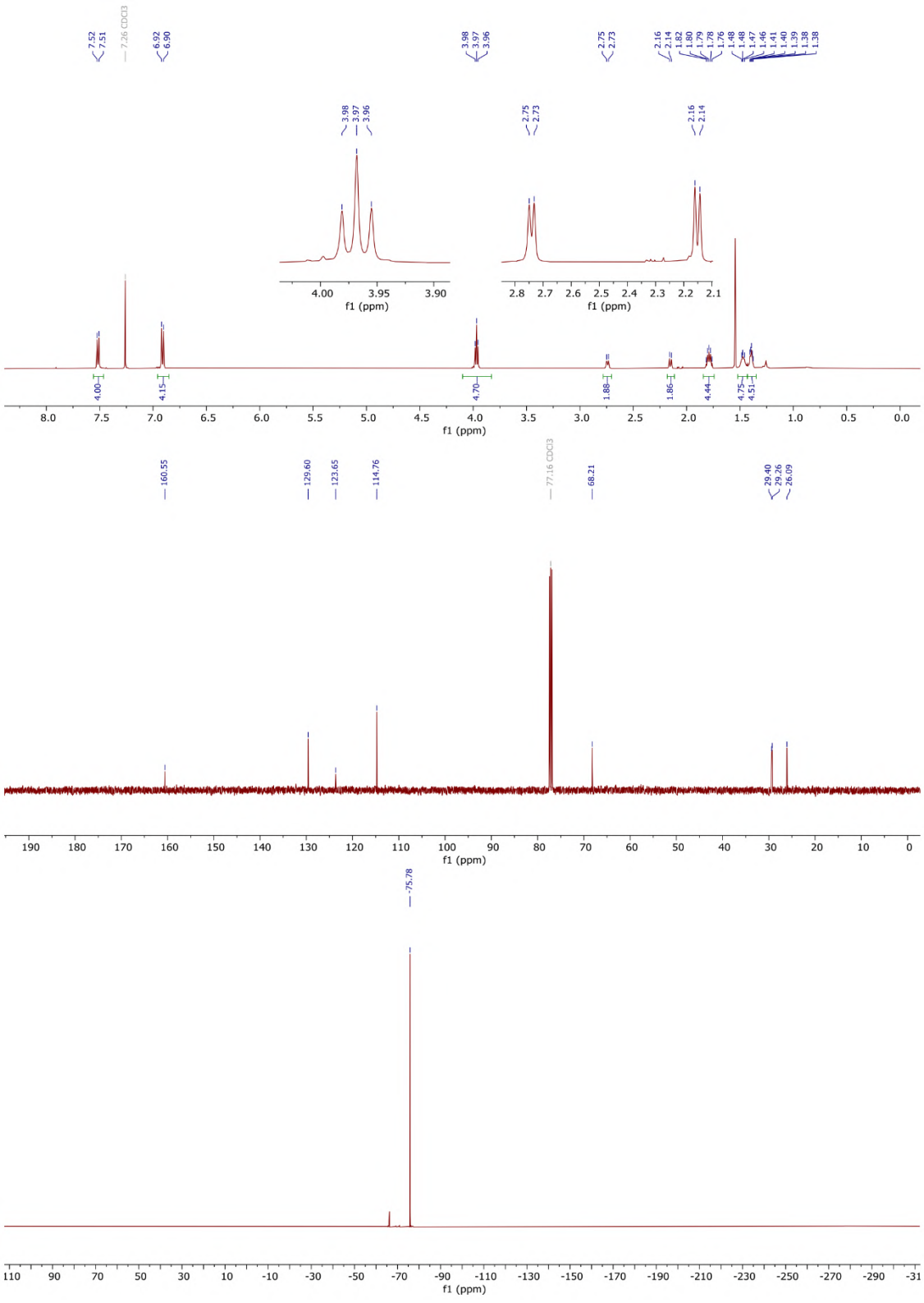

^{1}H and ^{19}F NMR spectra of **S3.6** in $CDCl_3$:

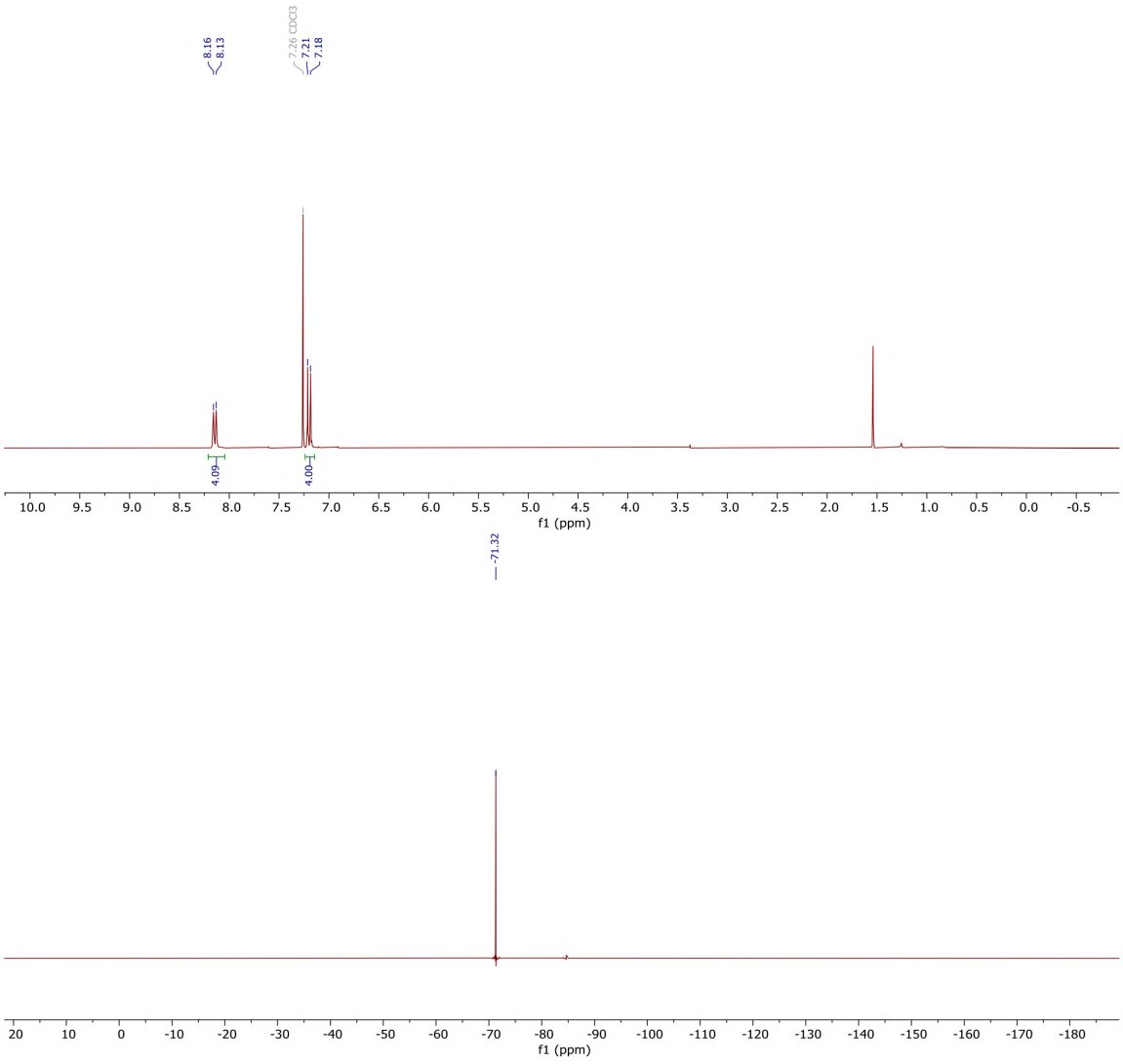

^{1}H and ^{19}F NMR spectra of **S3.7** in CD_3OD:

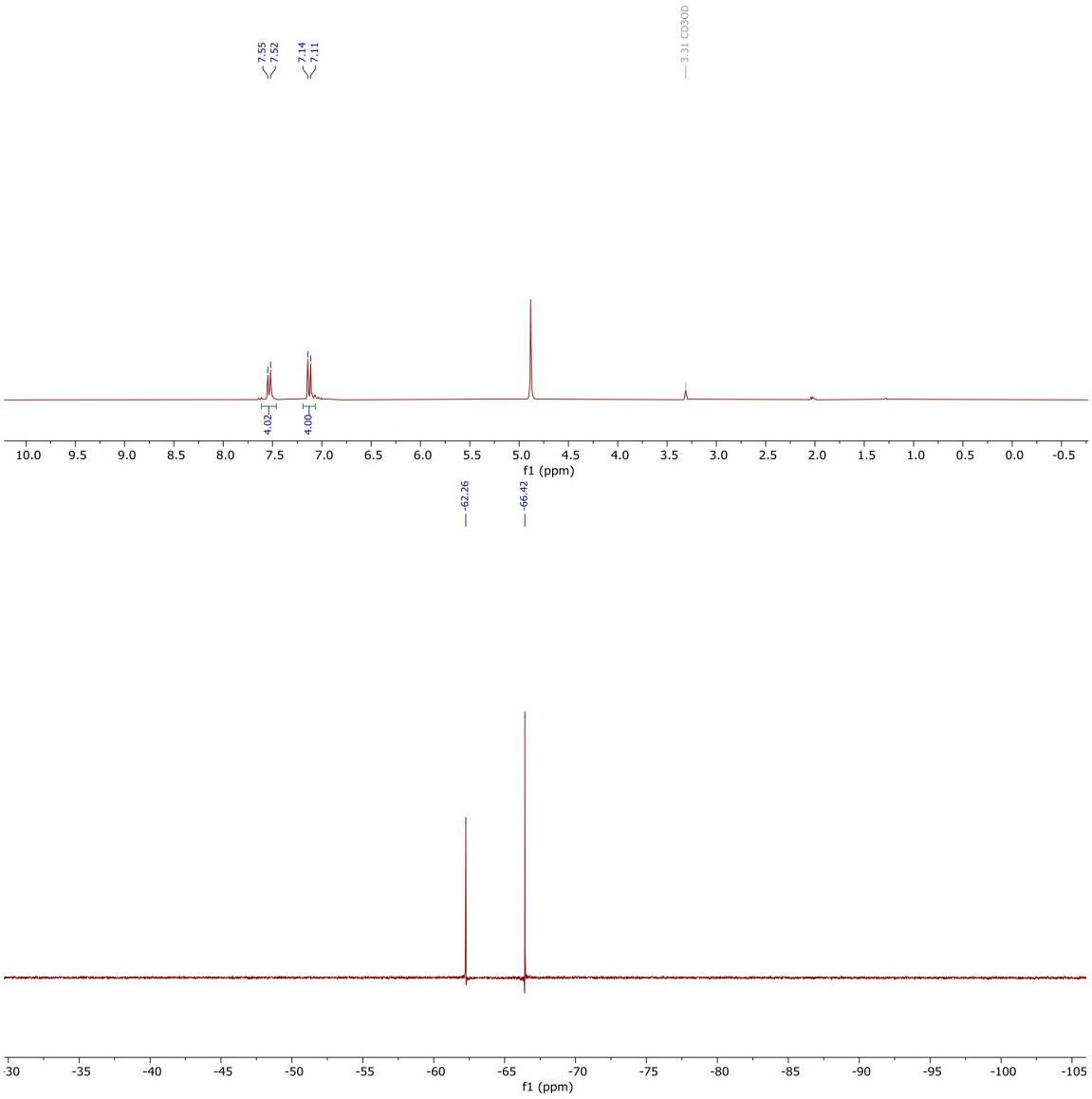

^{1}H, ^{13}C, and ^{19}F NMR spectra of **S3.8** in $CDCl_3$:

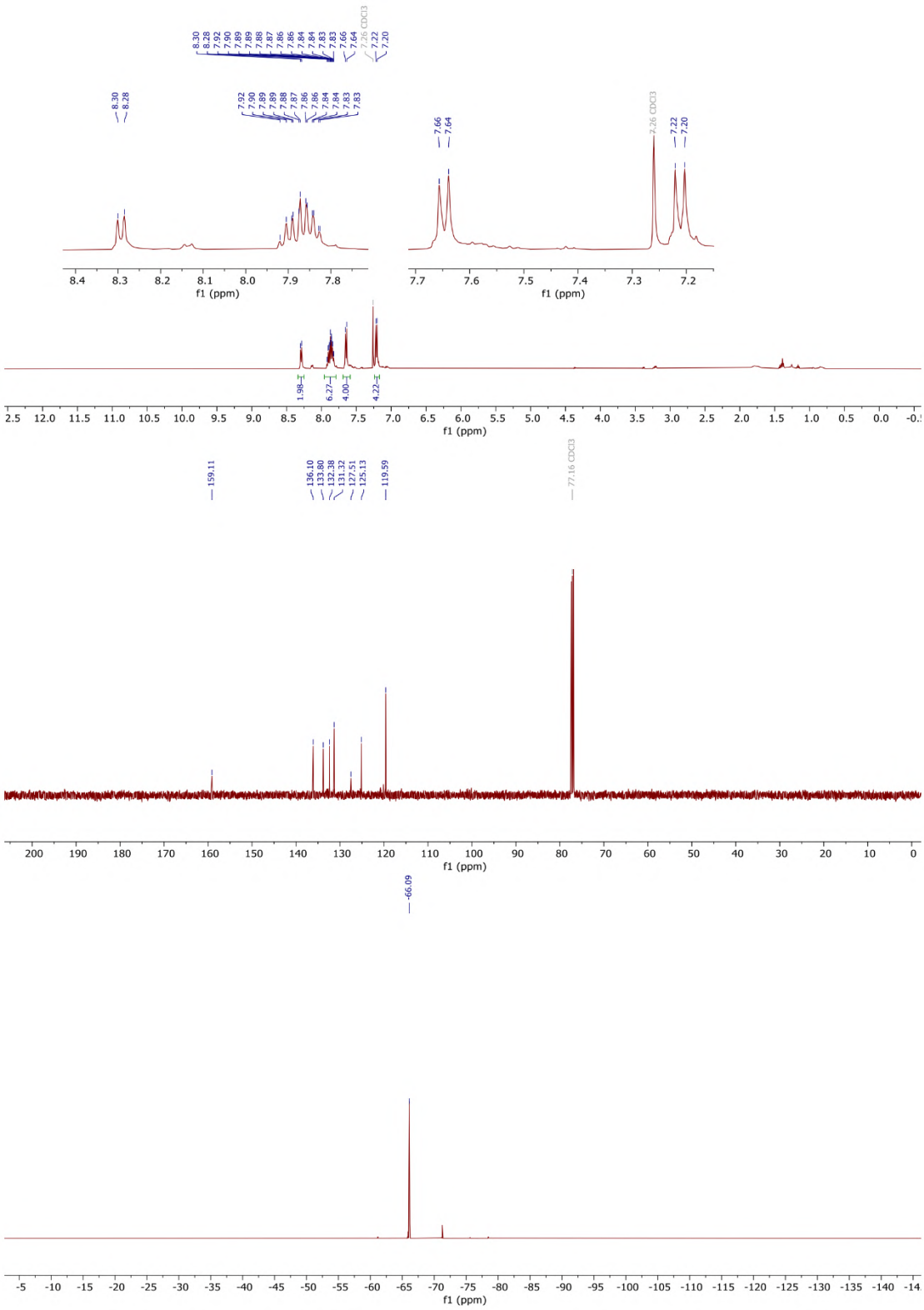

^{1}H and ^{19}F NMR spectra of **S3.9** in $CDCl_3$:

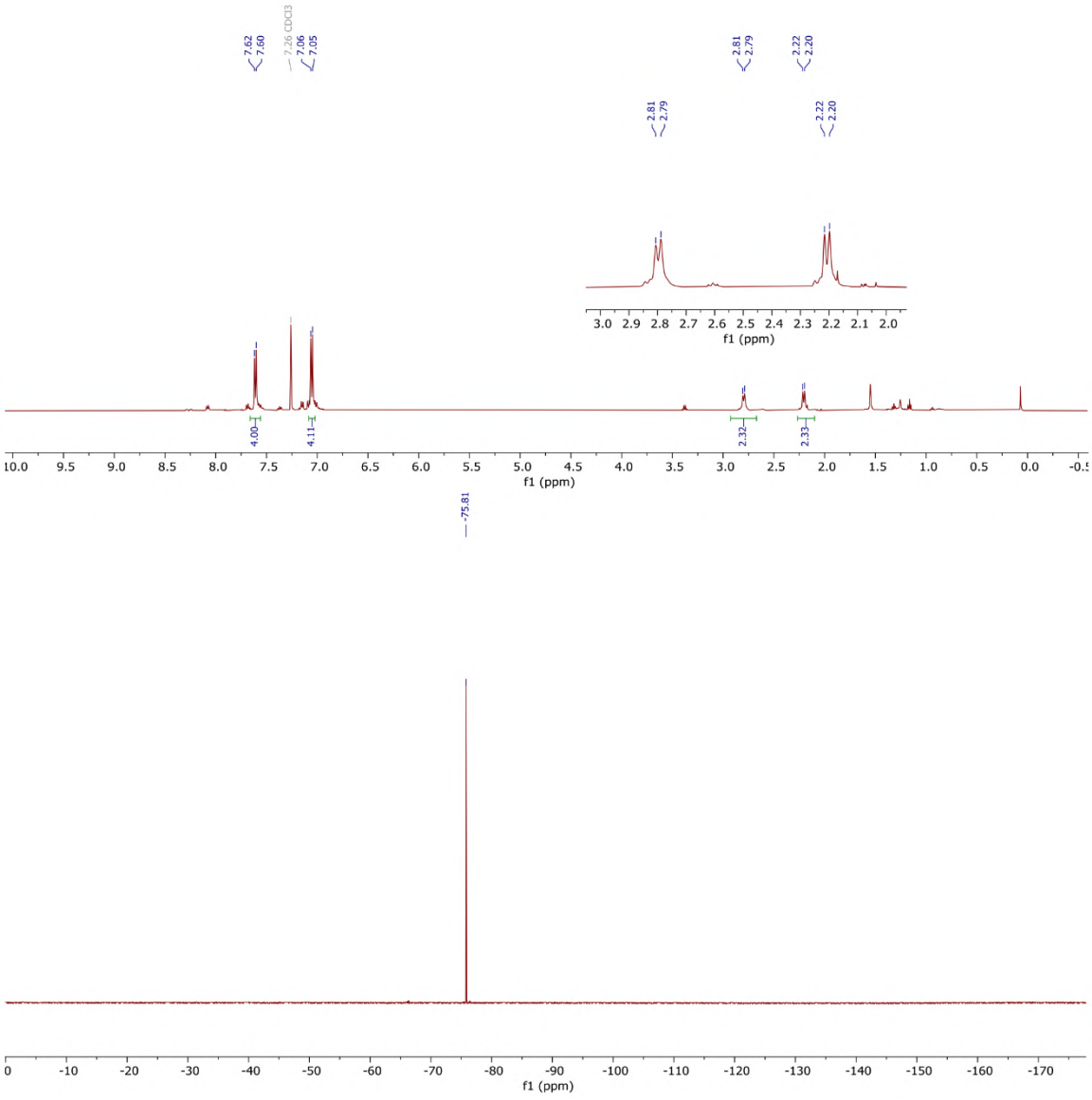

^{1}H, ^{13}C, and ^{19}F NMR spectra of **S3.10** in CD_2Cl_2:

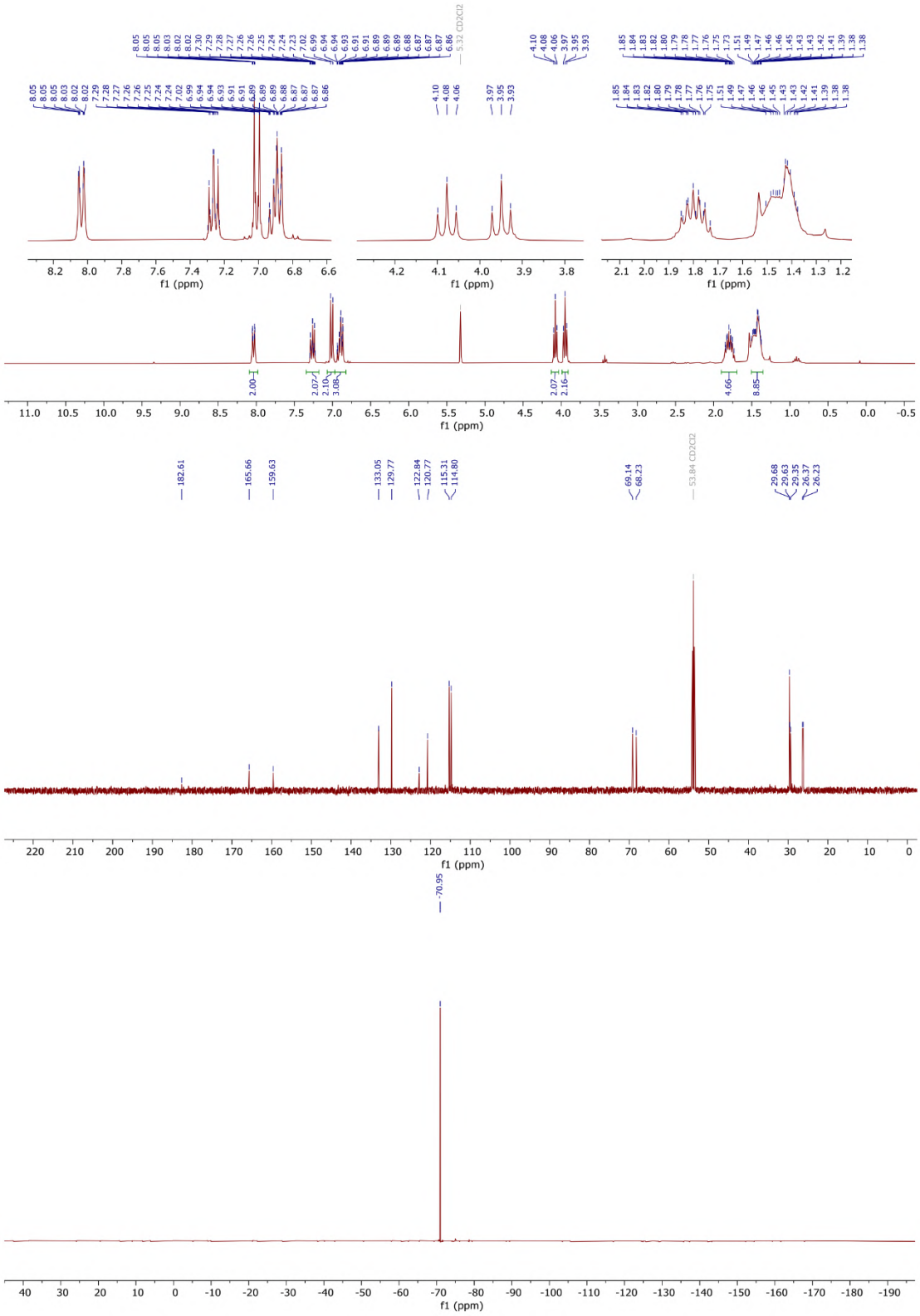

^{1}H and ^{19}F NMR spectra of **S3.11** in $(CD_3)_2CO$:

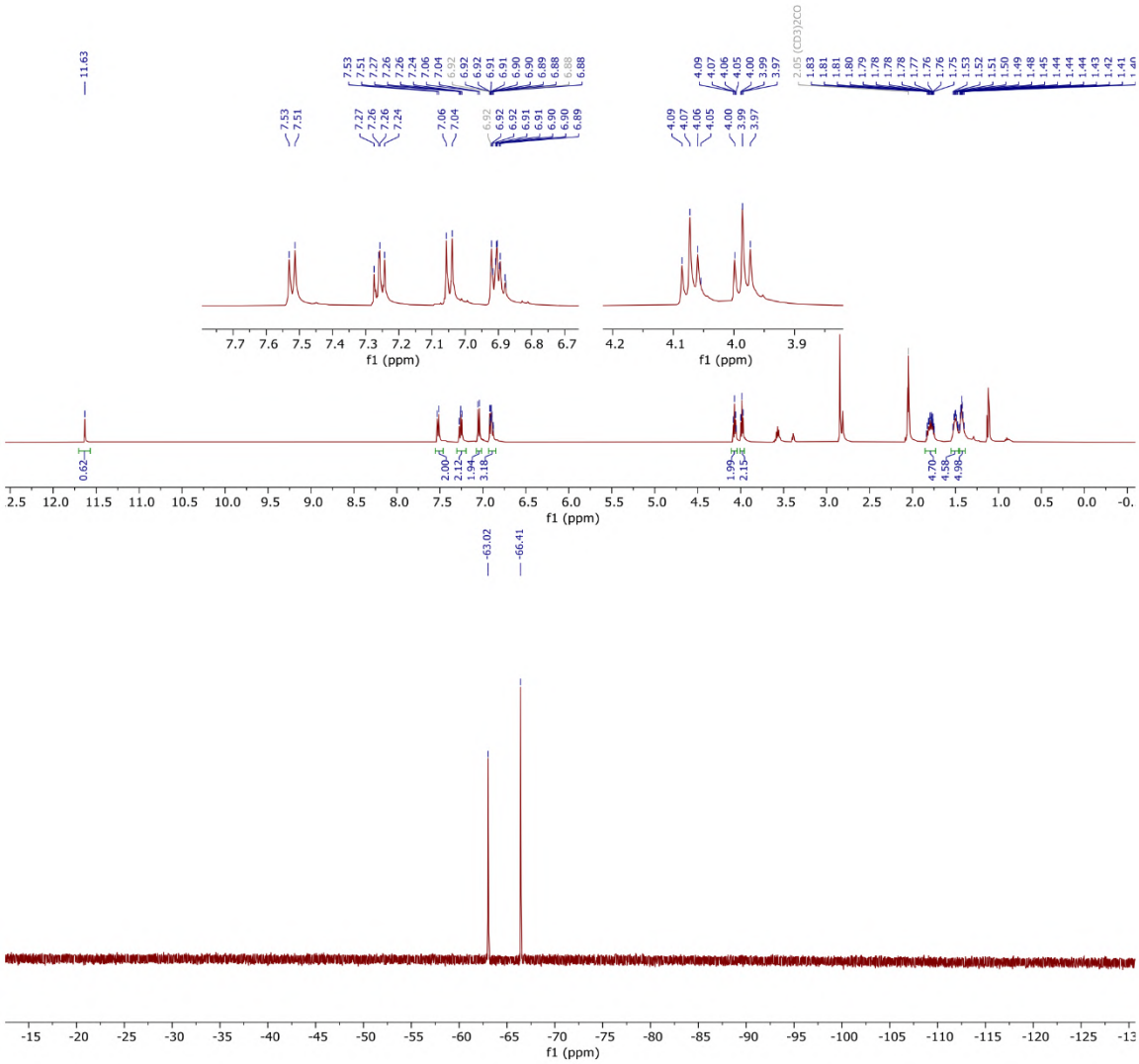

^{1}H and ^{19}F NMR spectra of **S3.12** in $CDCl_3$:

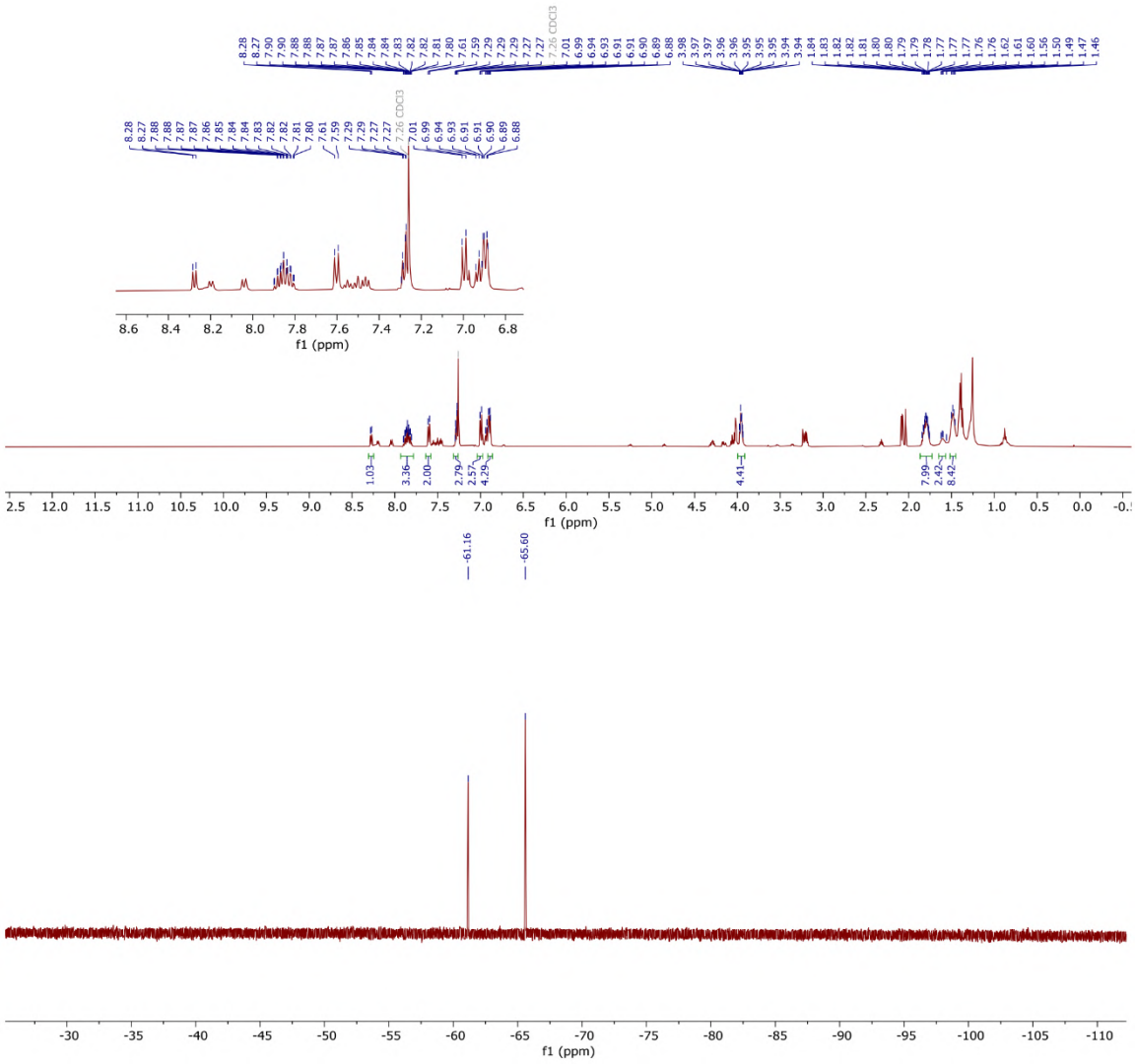

^{1}H, ^{13}C, and ^{19}F NMR spectra of **S3.13** in $CDCl_3$:

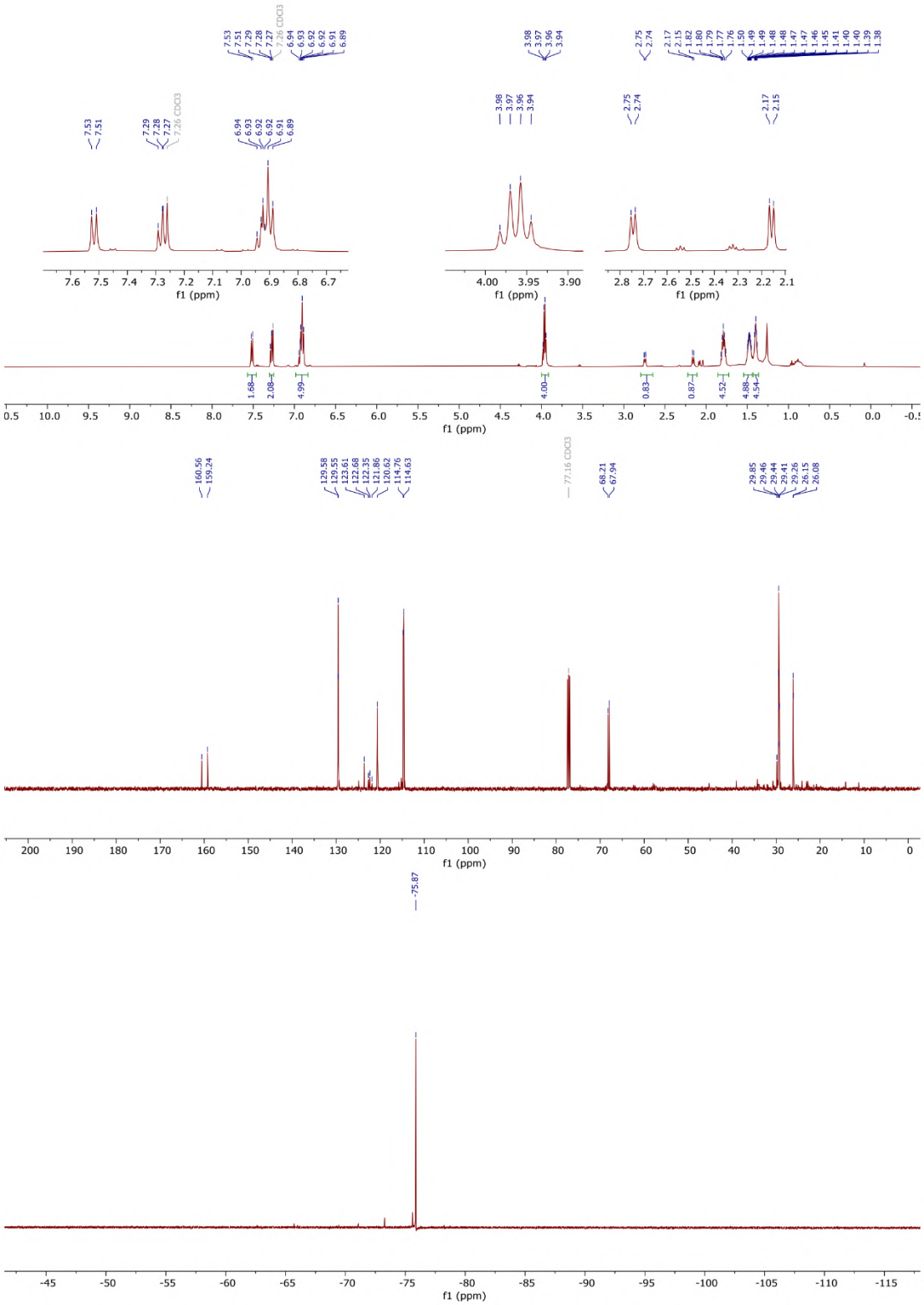

^{1}H, ^{13}C, and ^{19}F NMR spectra of *mono*-diazirine **4.2** in $CDCl_3$:

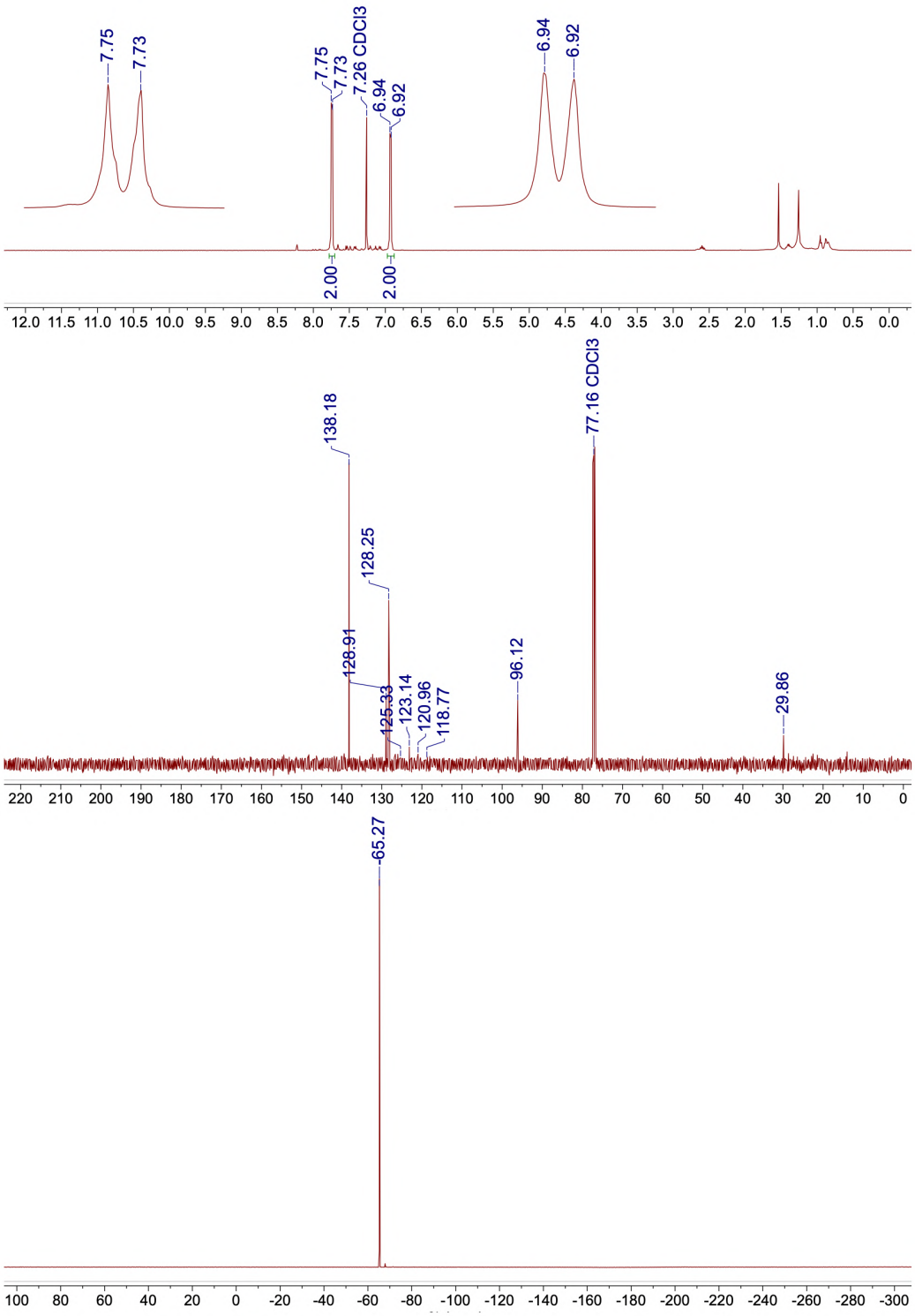

^{1}H, ^{13}C, and ^{19}F NMR spectra of *mono*-diazirine **4.3** in $CDCl_3$:

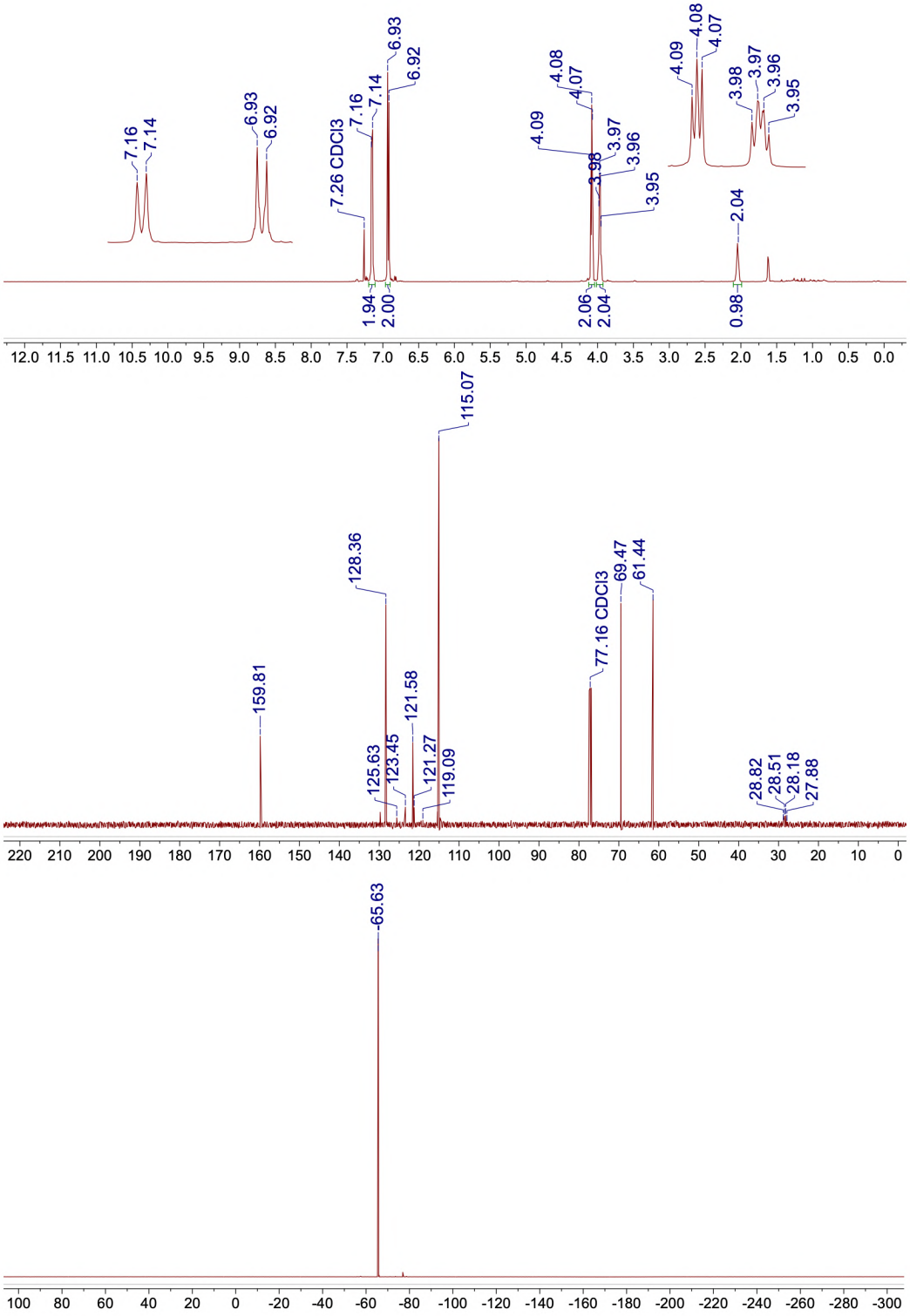

^{1}H, ^{13}C, and ^{19}F NMR spectra of *bis*-diazirine **4.4** in $CDCl_3$:

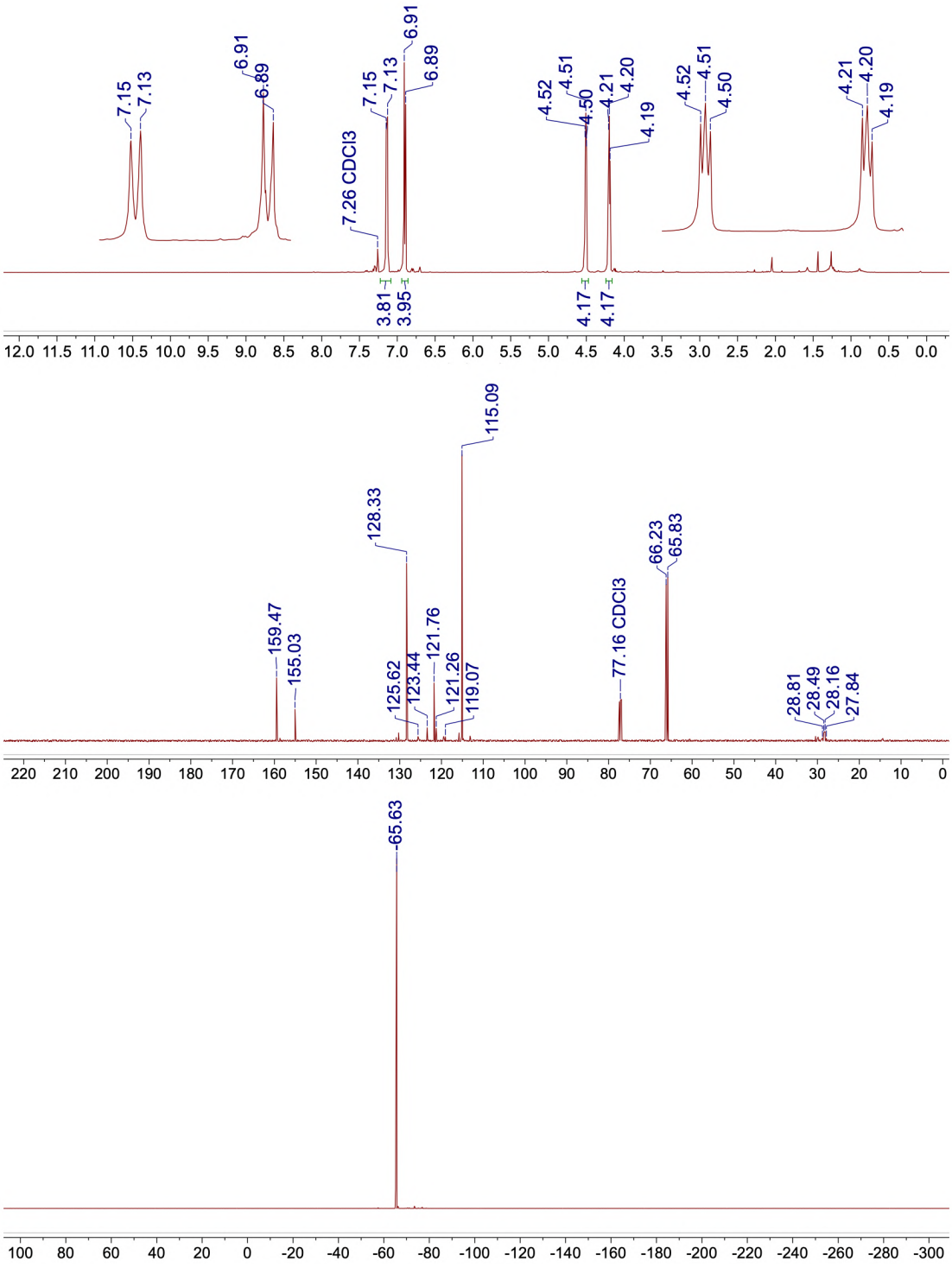

^{1}H, ^{13}C, and ^{19}F NMR spectra of *bis*-diazirine **4.5** in $CDCl_3$:

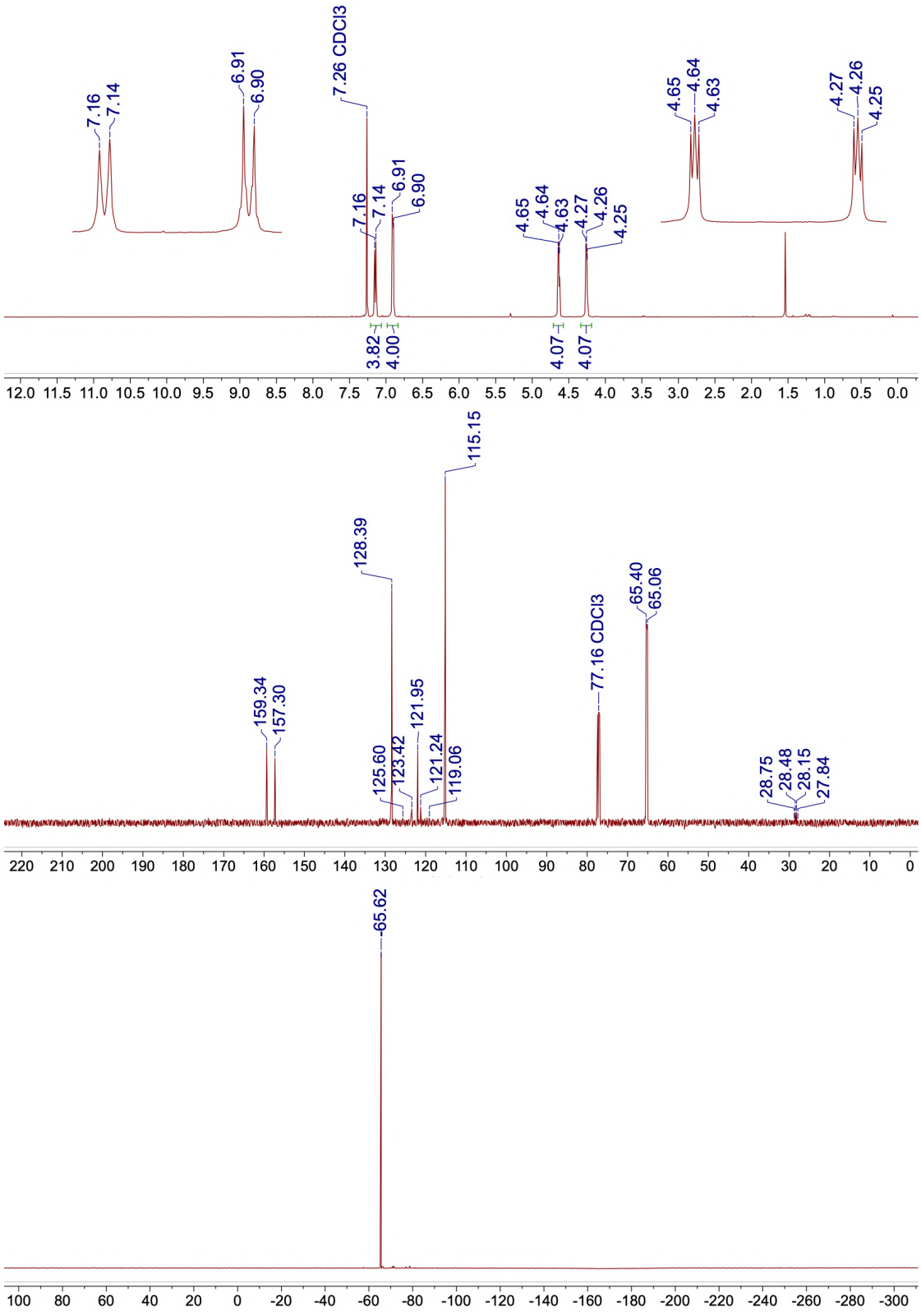

^{1}H, ^{13}C, and ^{19}F NMR spectra of *bis*-diazirine **4.6** in $CDCl_3$:

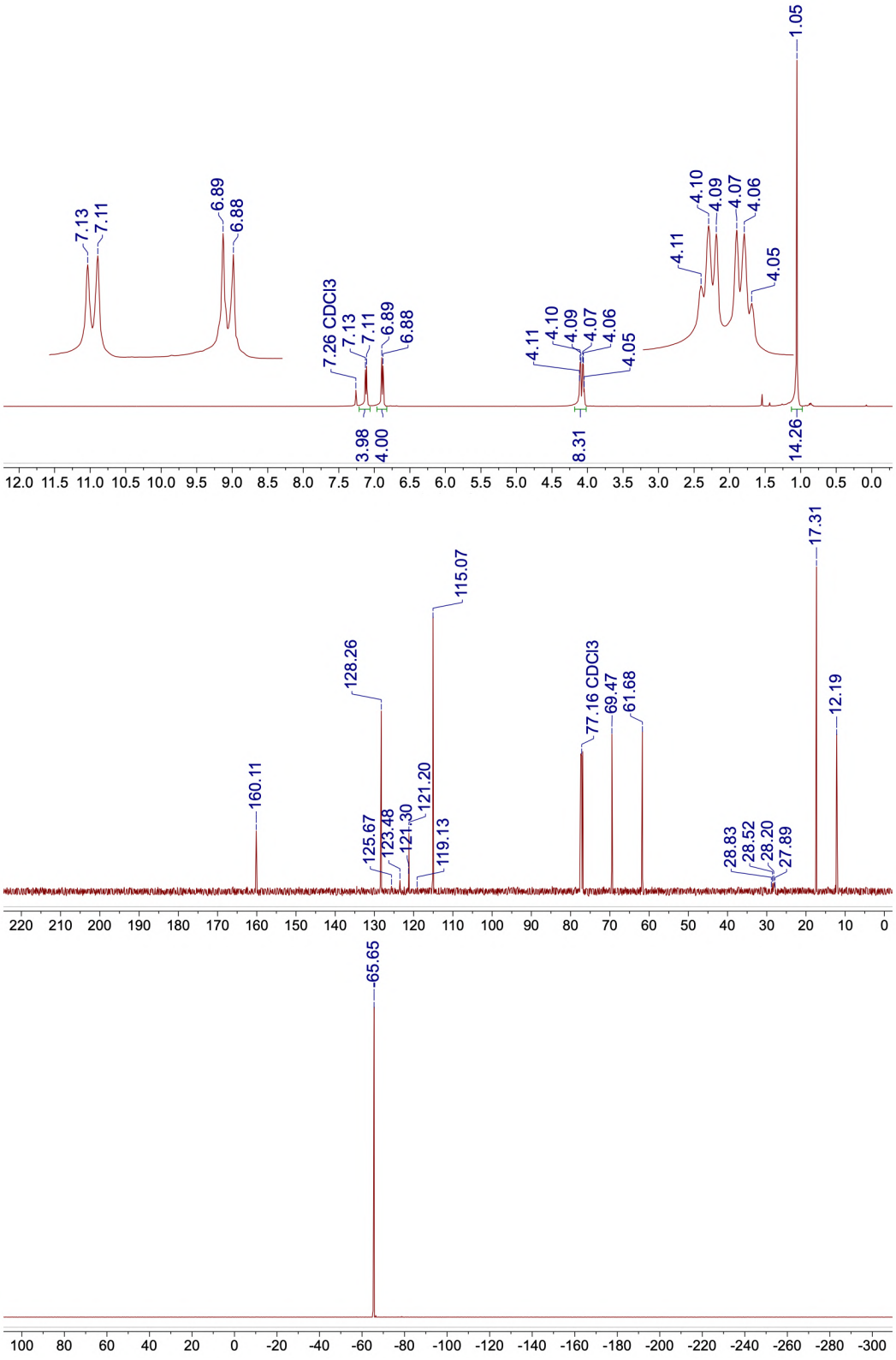

^{1}H, ^{13}C, and ^{19}F (inset shows proton coupled ^{19}F) NMR spectra of compound **4.7** in $CDCl_3$:

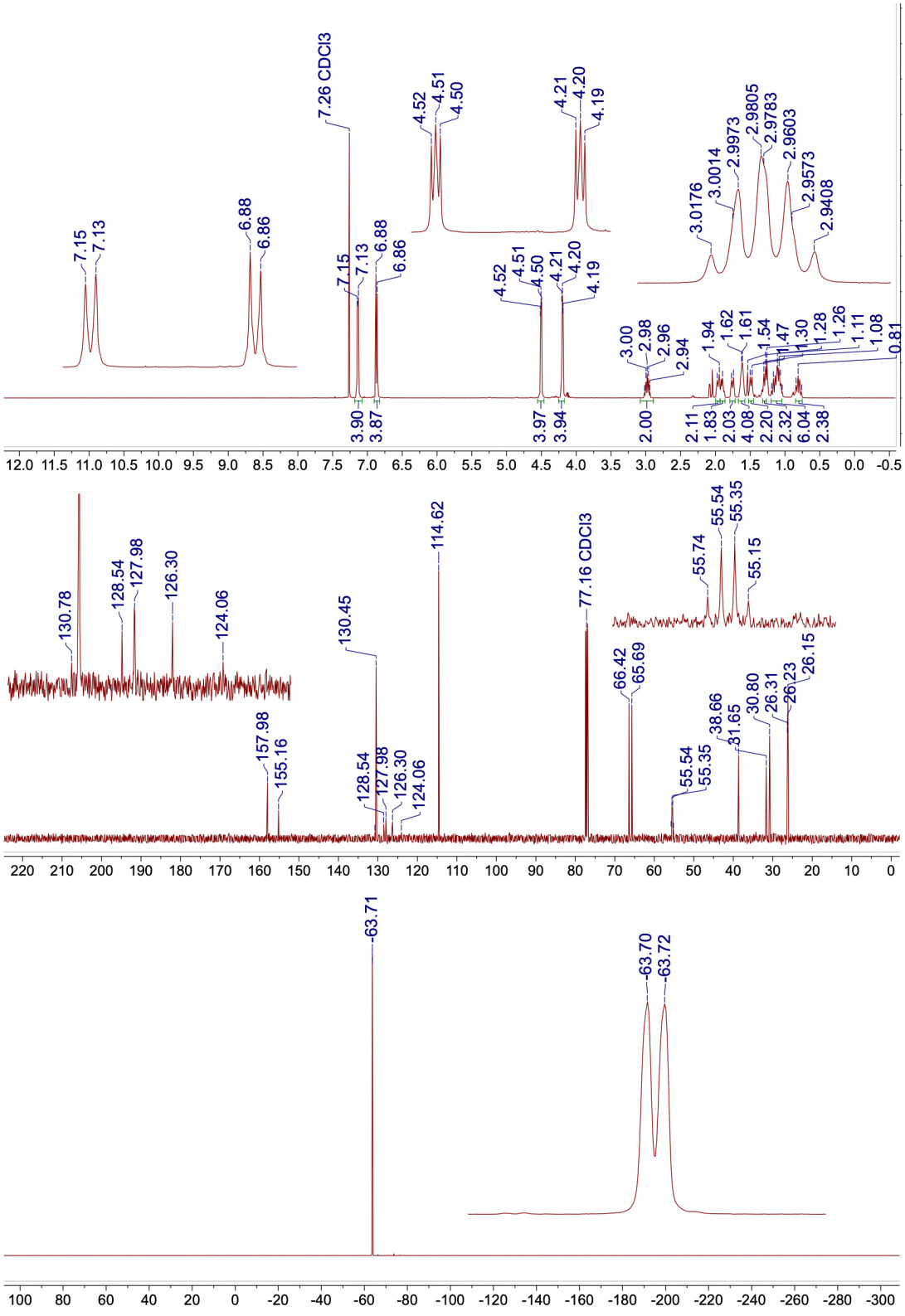

^{1}H, ^{13}C, and ^{19}F (inset shows proton coupled ^{19}F) NMR spectra of compound **4.8** in $CDCl_3$:

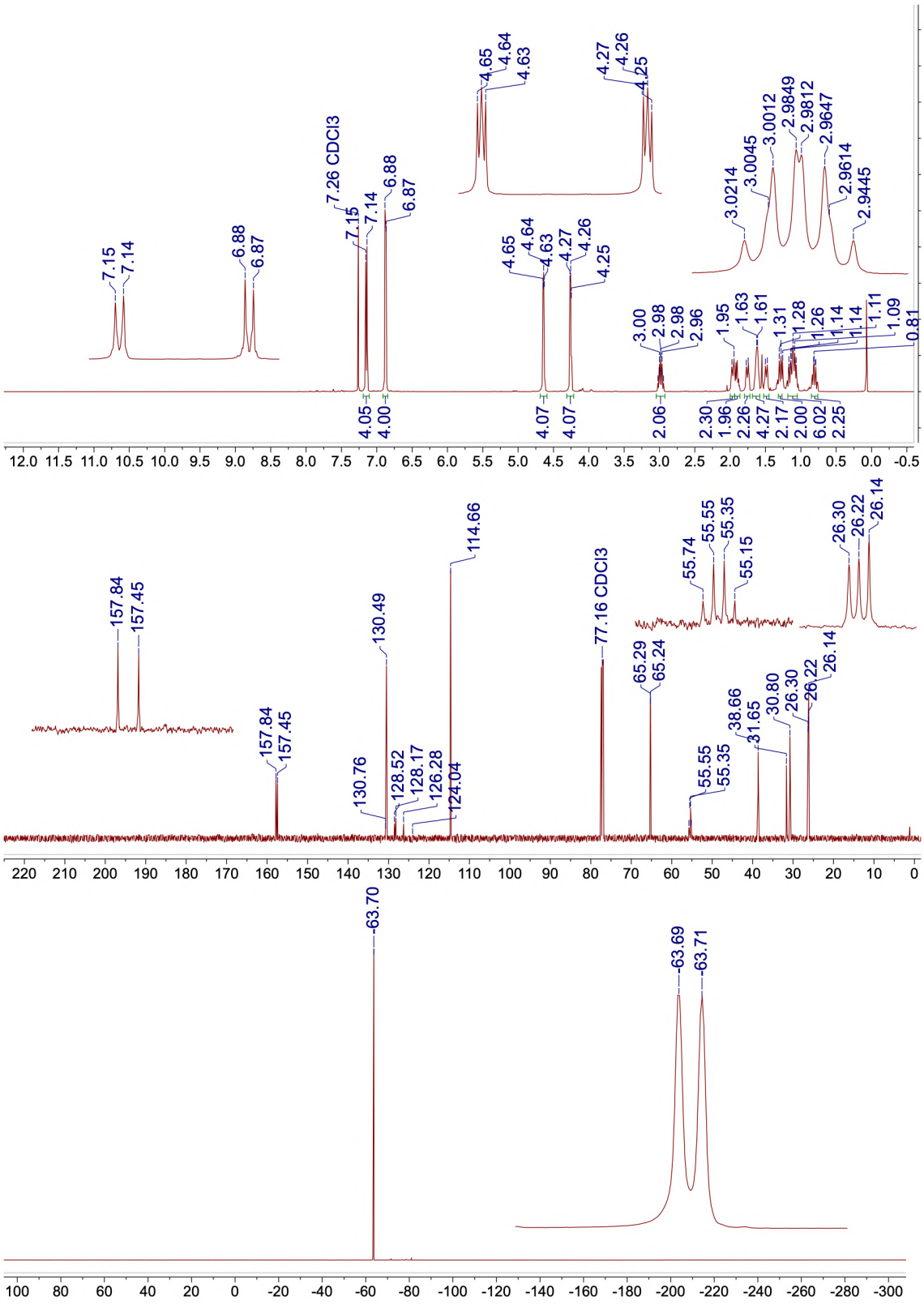

^{1}H, ^{13}C, and ^{19}F (inset shows proton coupled ^{19}F) NMR spectra of compound **4.9** in $CDCl_3$:

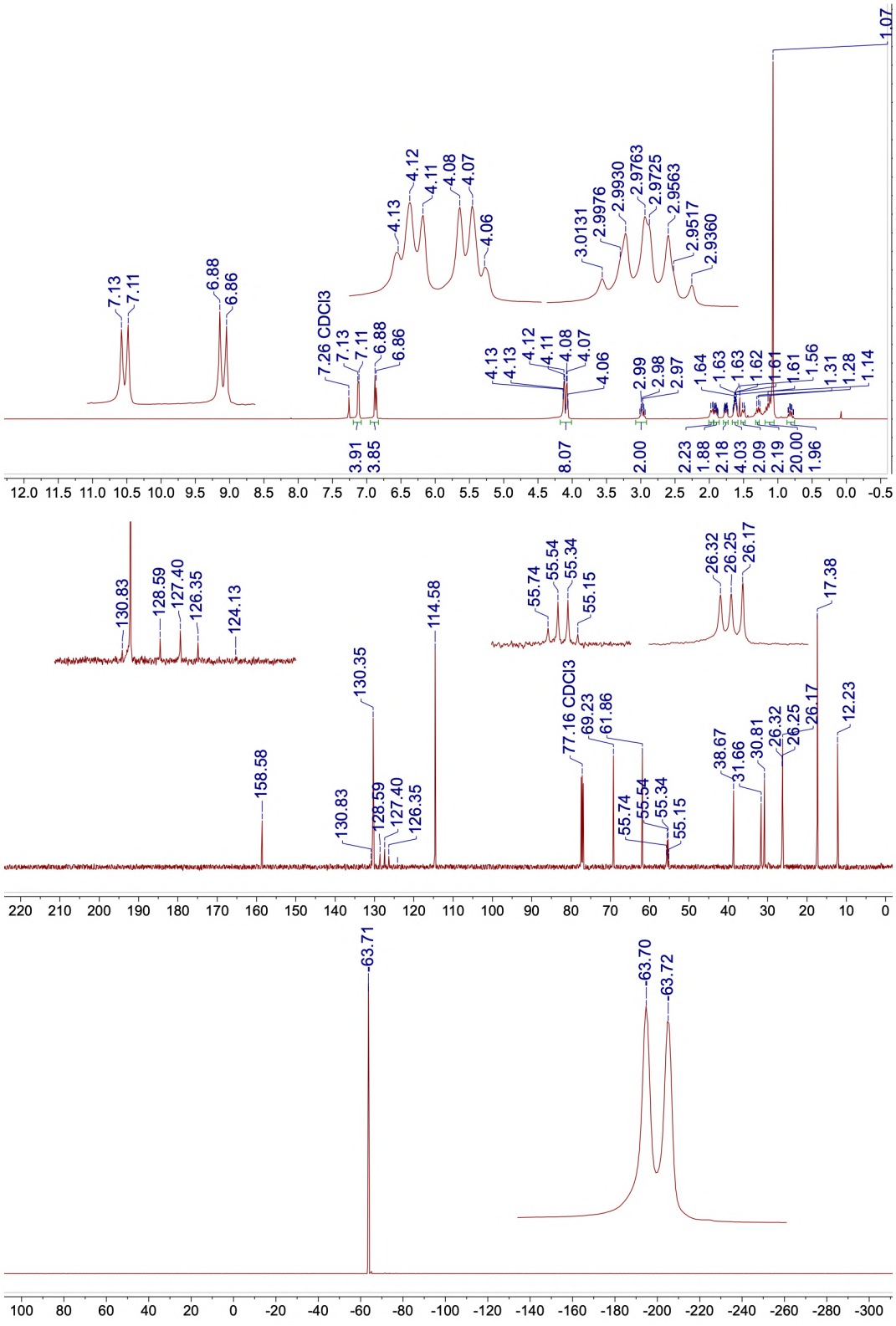

^{29}Si NMR spectrum of compound **4.9** in $CDCl_3$:

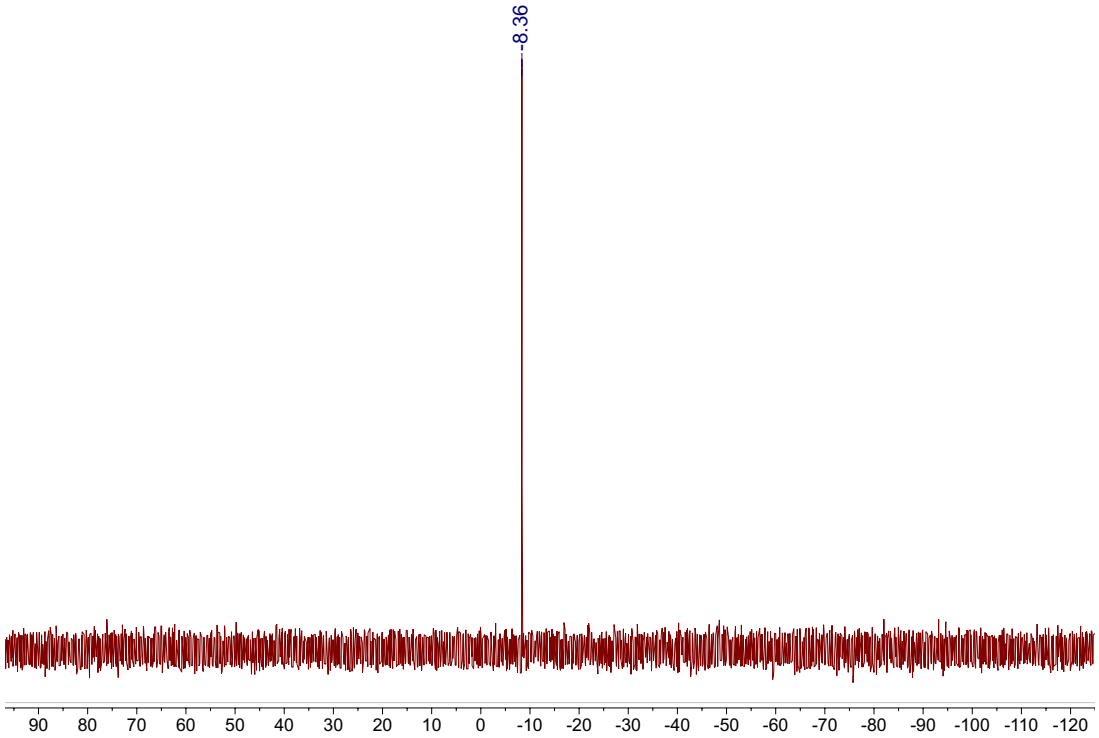

^{1}H, ^{13}C, and ^{19}F (inset shows proton coupled ^{19}F) NMR spectra of compound **4.10** in CD_2Cl_2:

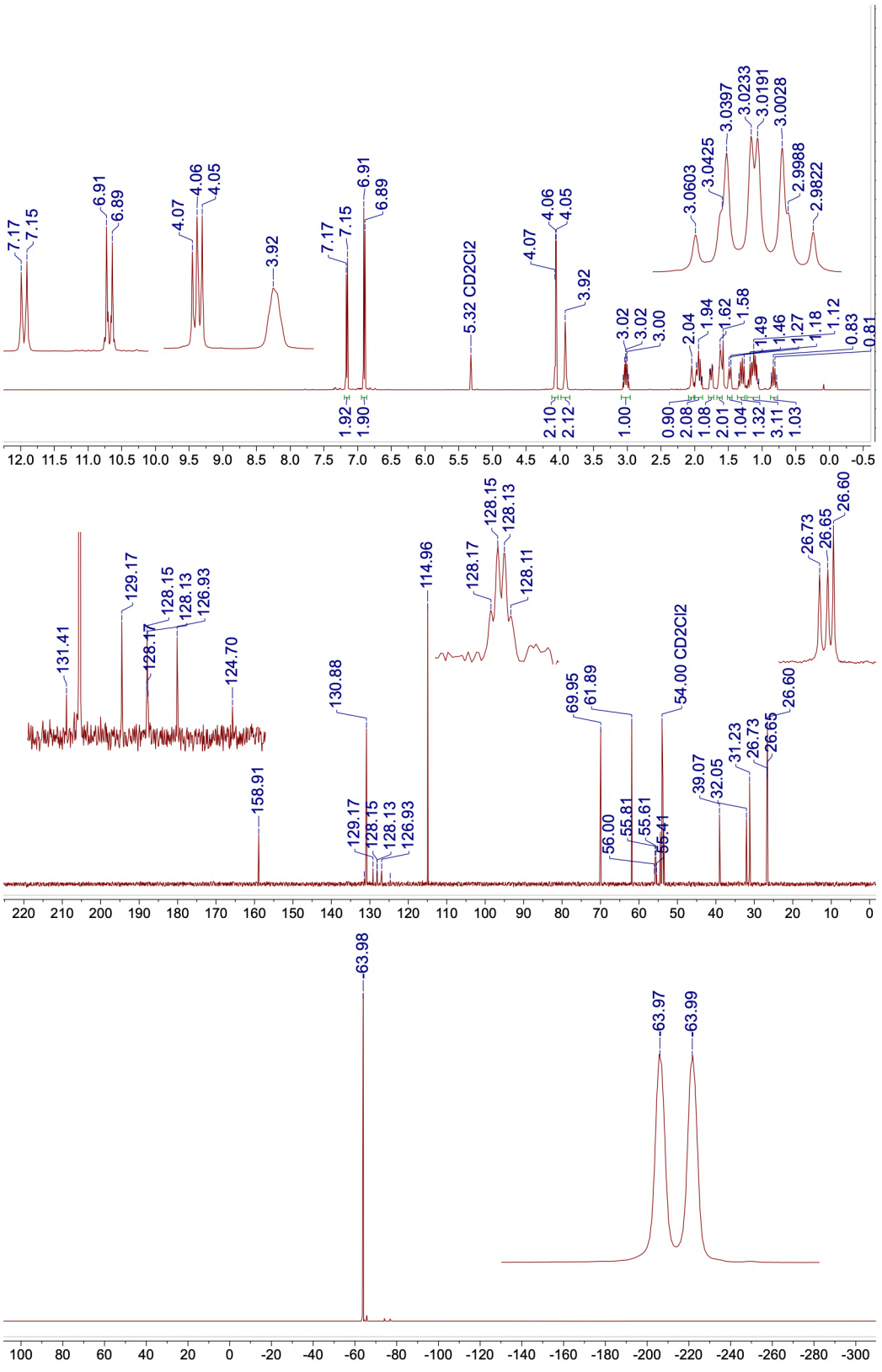

^{1}H, ^{13}C, and ^{19}F NMR spectra of imidazole carbamate diazirine **5.3** in $CDCl_3$:

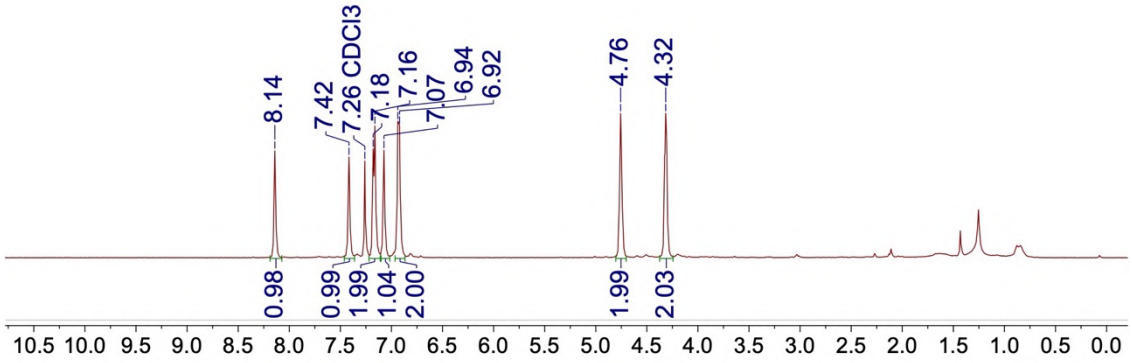

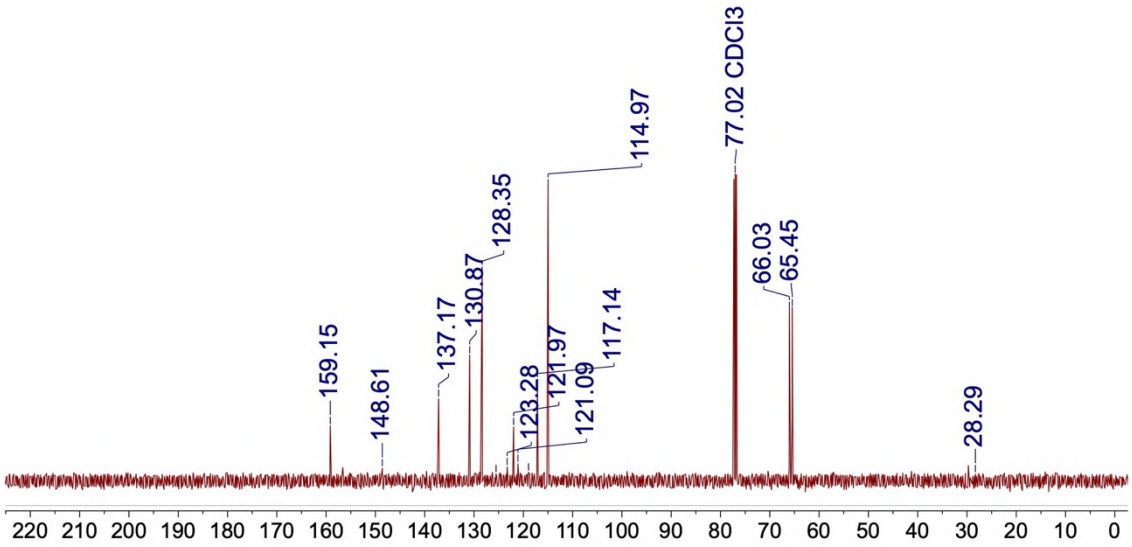

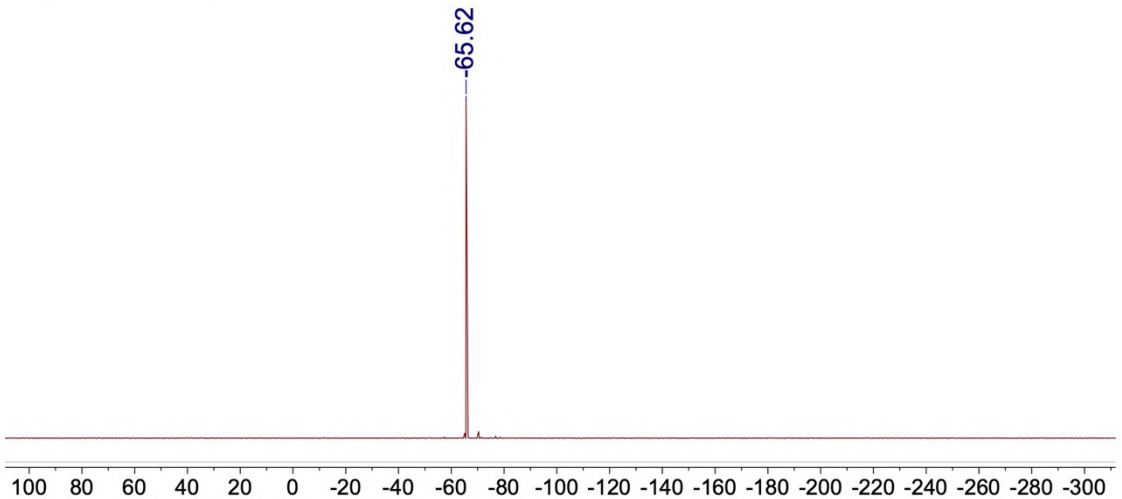

^{1}H, ^{13}C, and ^{19}F NMR spectra of benzyl bromide glycol diazirine **5.4** in $CDCl_3$:

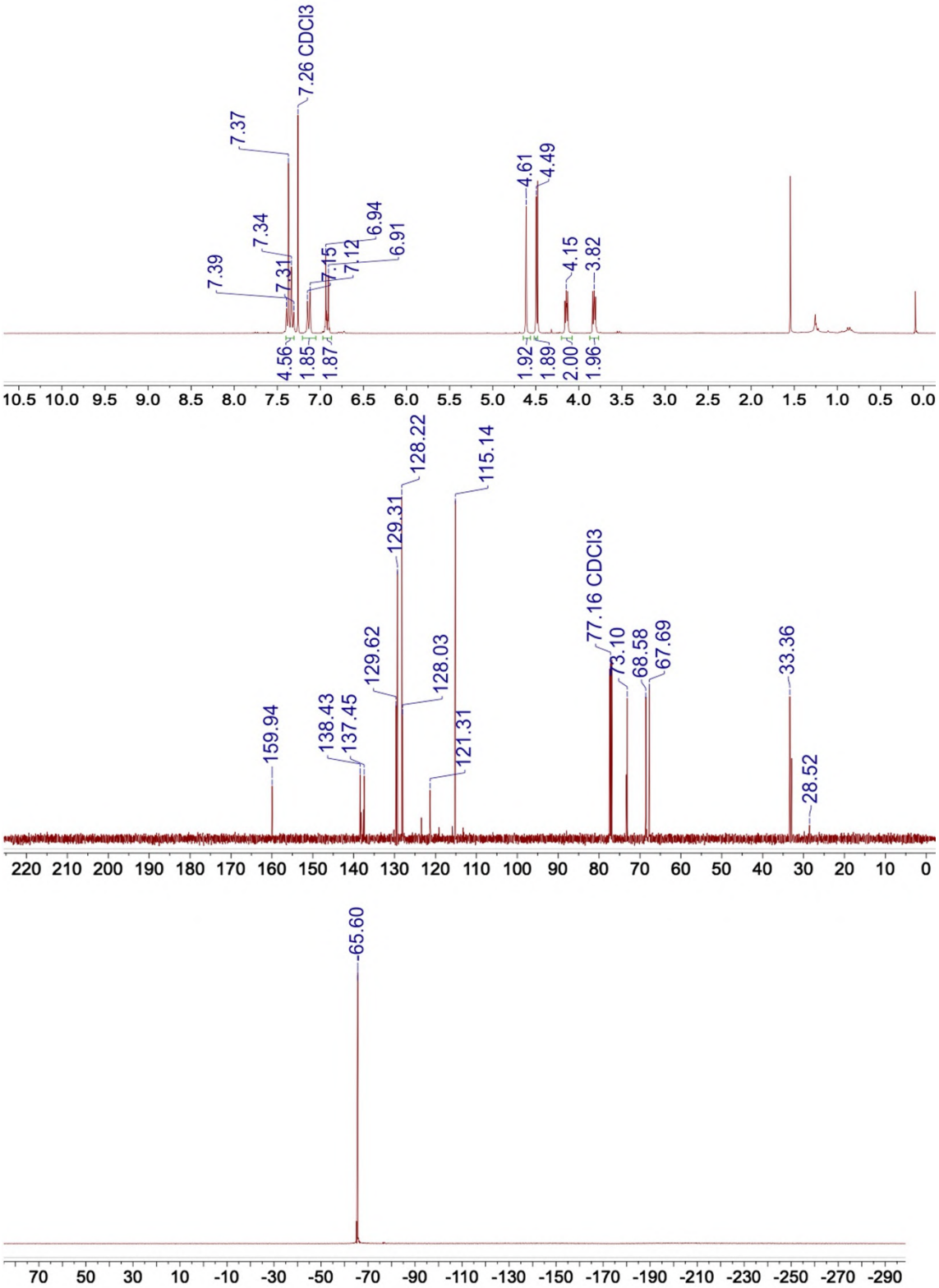

^{1}H and ^{19}F NMR spectra of C–H insertion product **5.7** in $CDCl_3$:

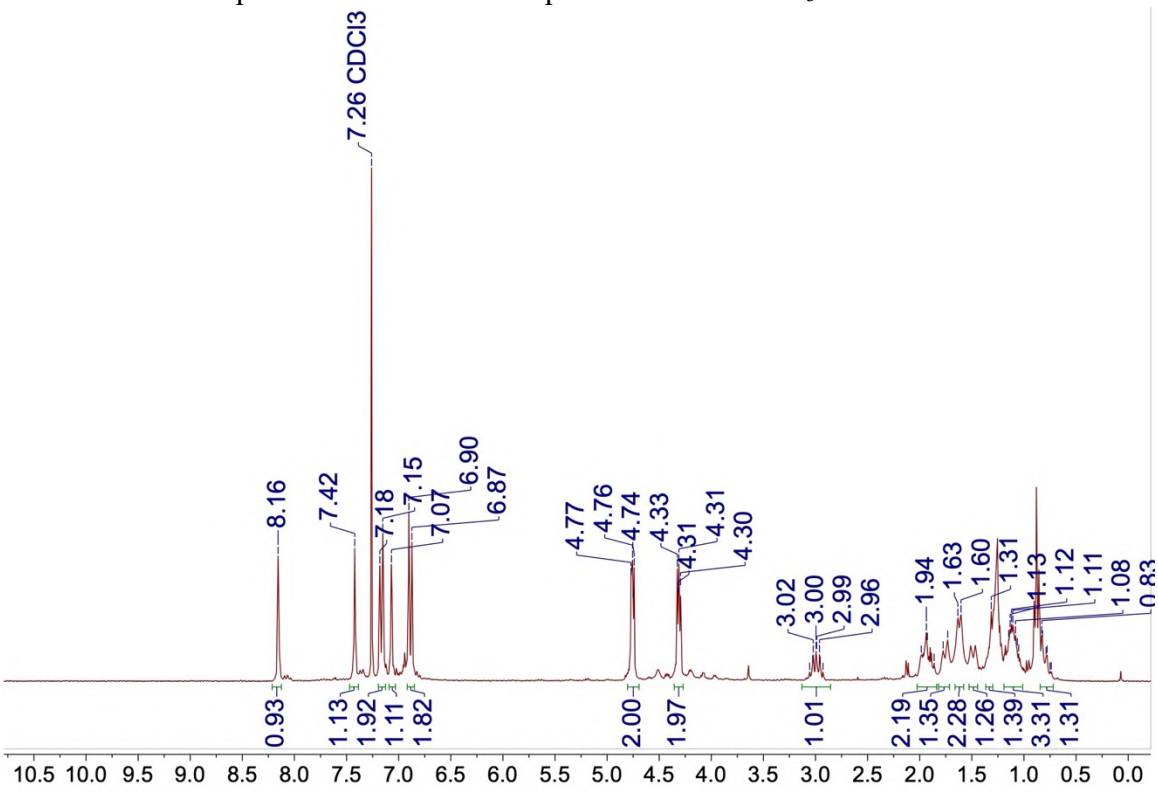

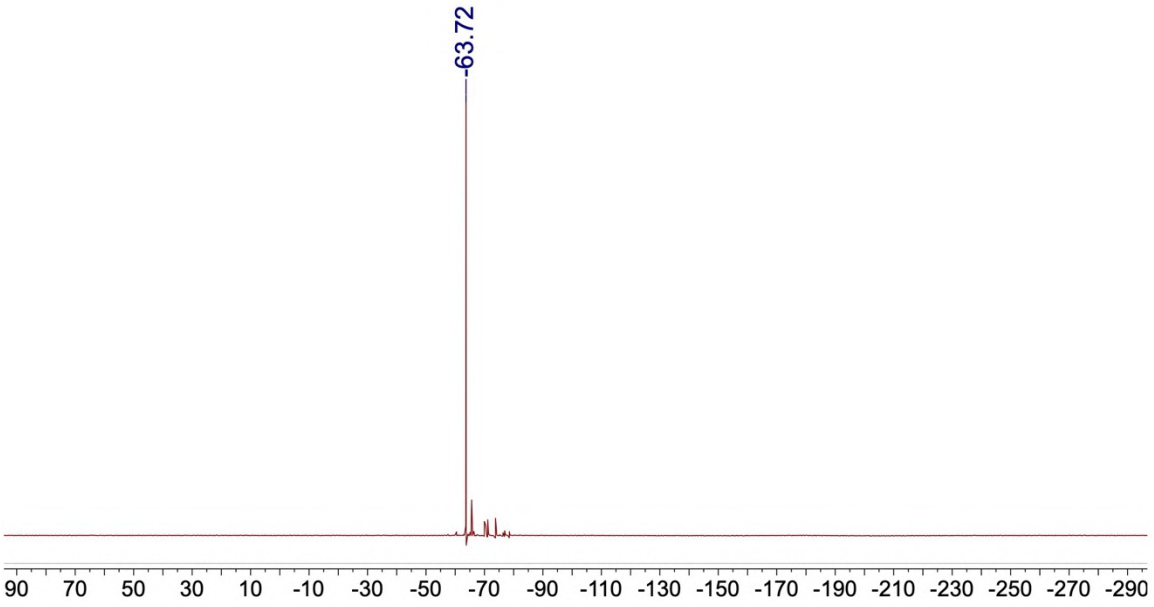

^{1}H and ^{19}F NMR spectra of C–H insertion product **5.8** in $CDCl_3$:

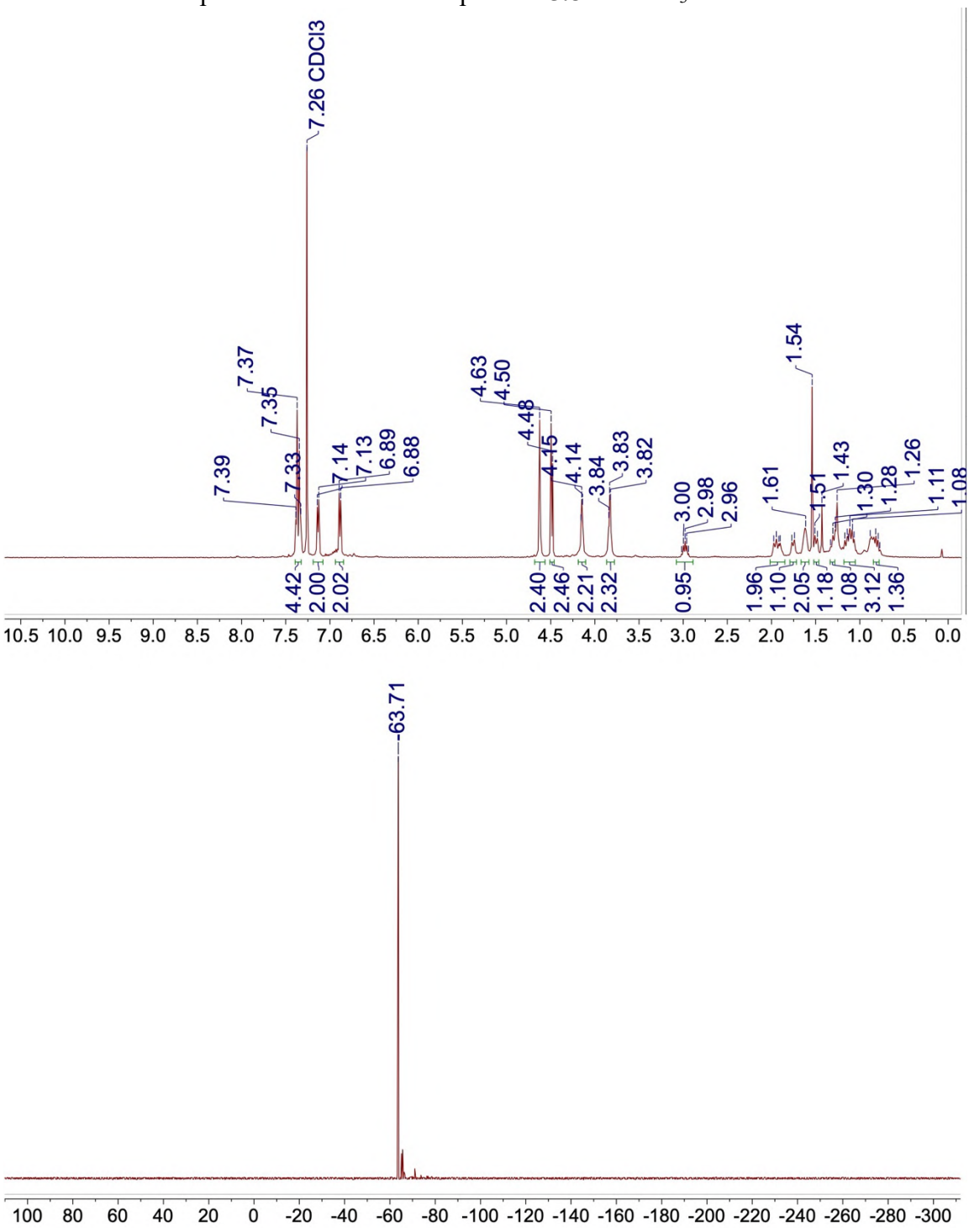

^{1}H, ^{13}C, and ^{19}F (inset shows proton coupled ^{19}F) NMR spectra of amine-functionalized compound **5.9** in $CDCl_3$:

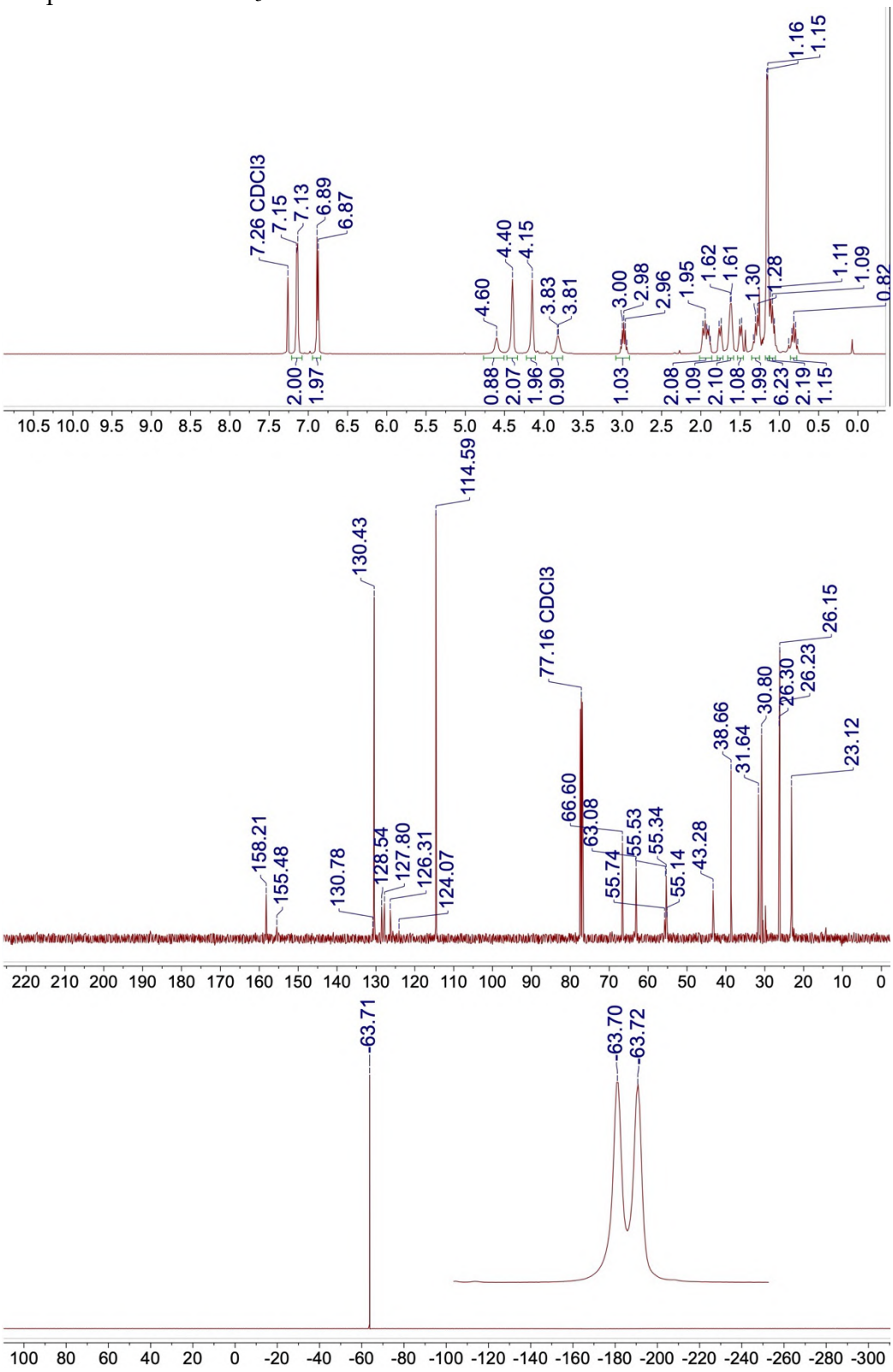

^{1}H, ^{13}C, and ^{19}F (inset shows proton coupled ^{19}F) NMR spectra of amine-functionalized compound **5.10** in $CDCl_3$:

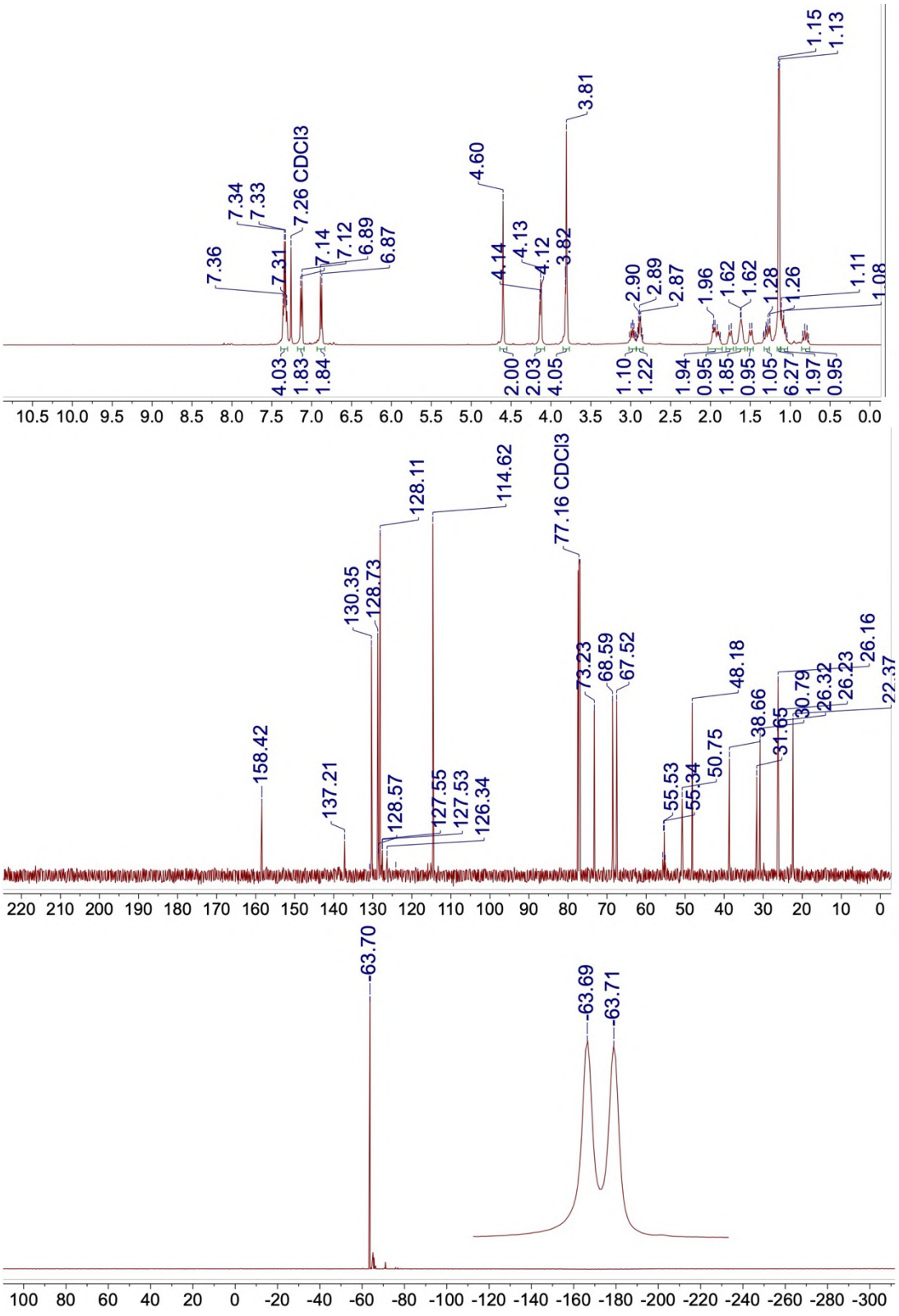

Appendix B: DSC Data

Representative DSC data for **D2.2** (top) and **D2.3** (bottom):

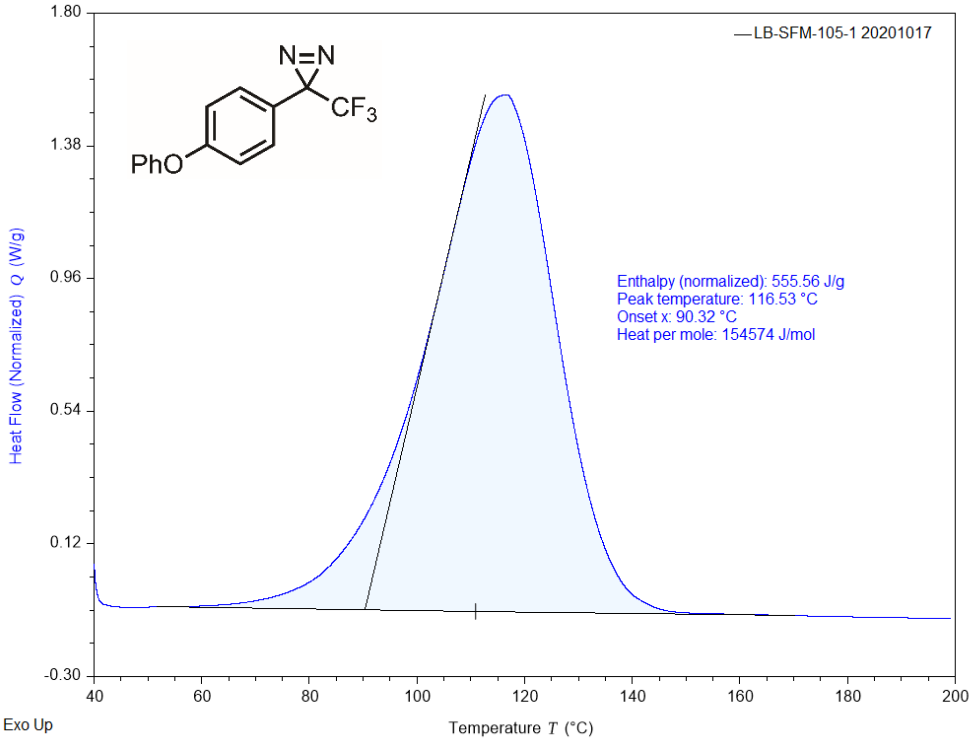

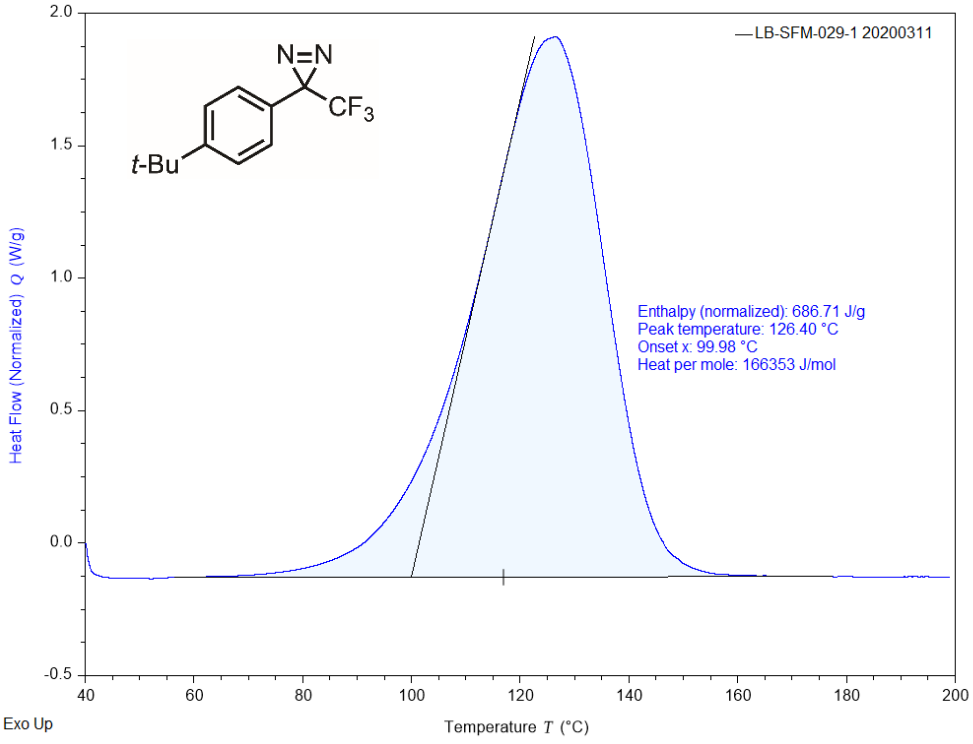

Representative DSC data for **D2.4** (top) and **D2.5** (bottom):

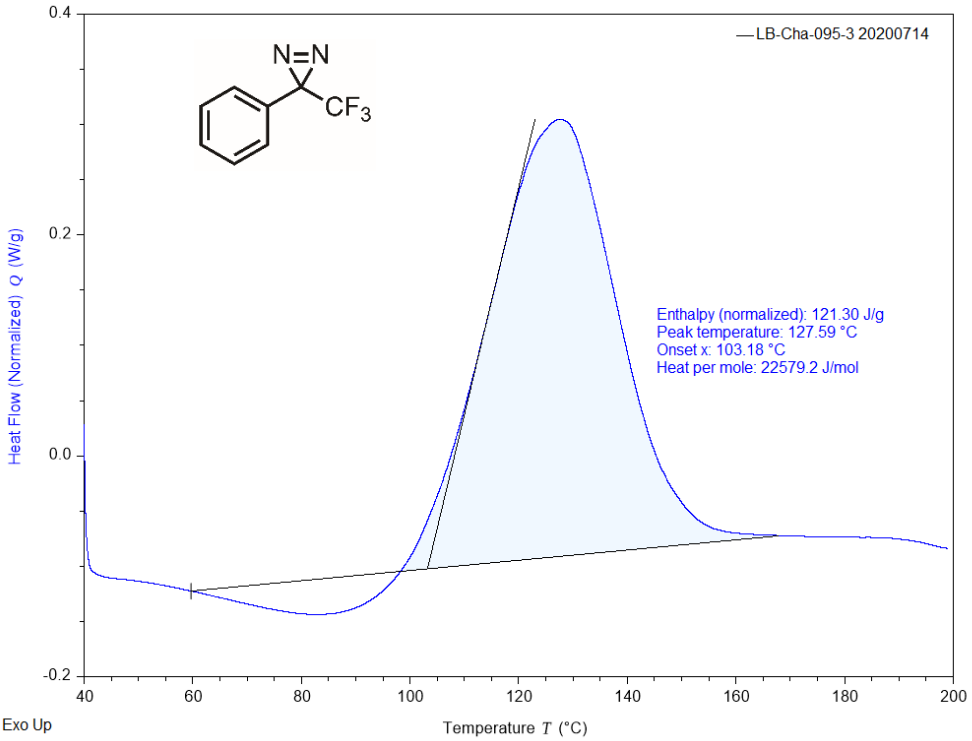

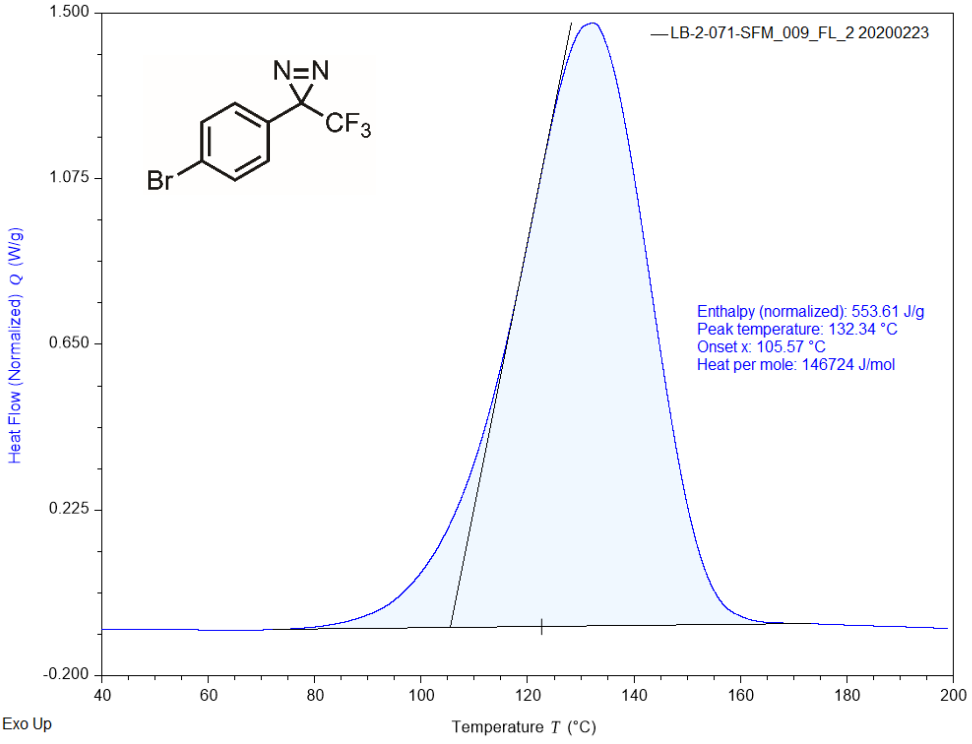

Representative DSC data for **D2.6** (top) and **D2.7** (bottom):

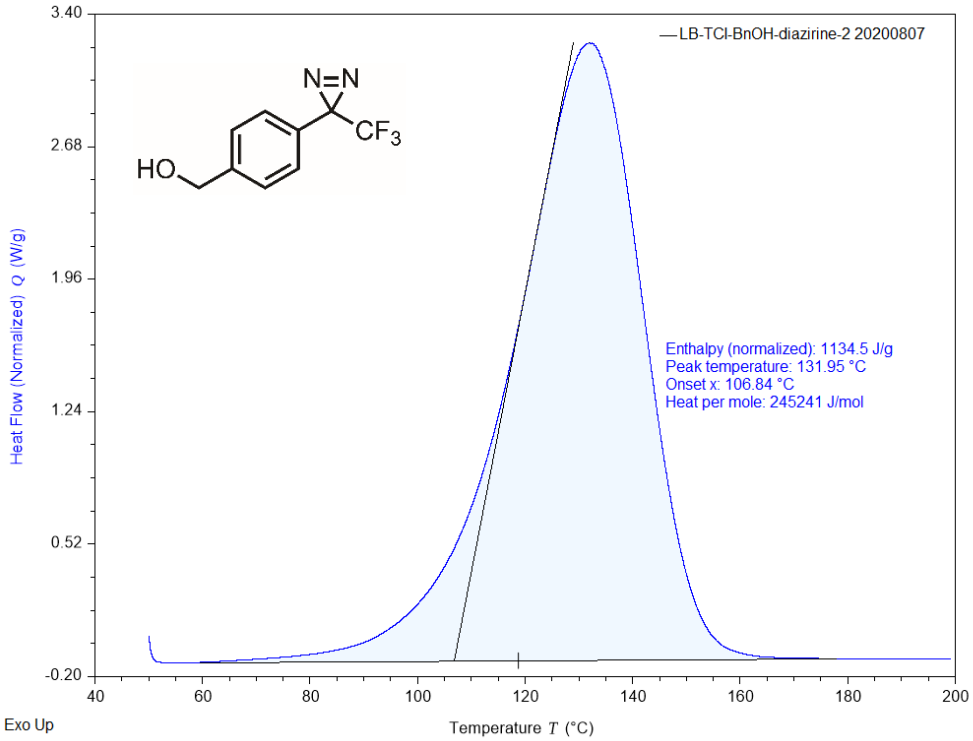

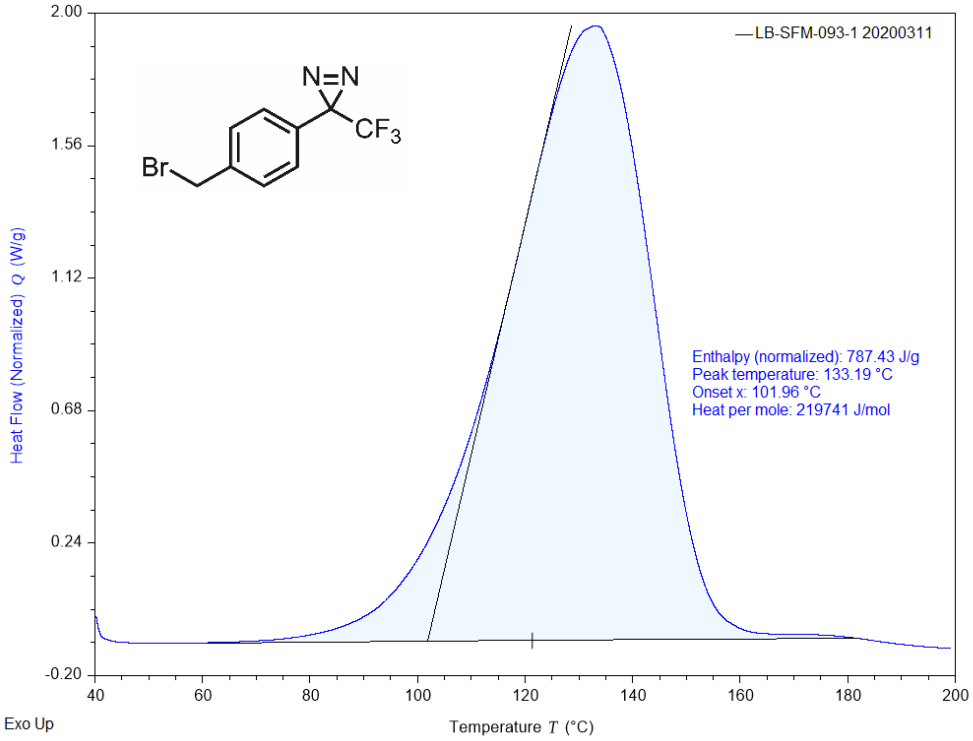

Representative DSC data for **D2.8** (top) and **D2.9** (bottom):

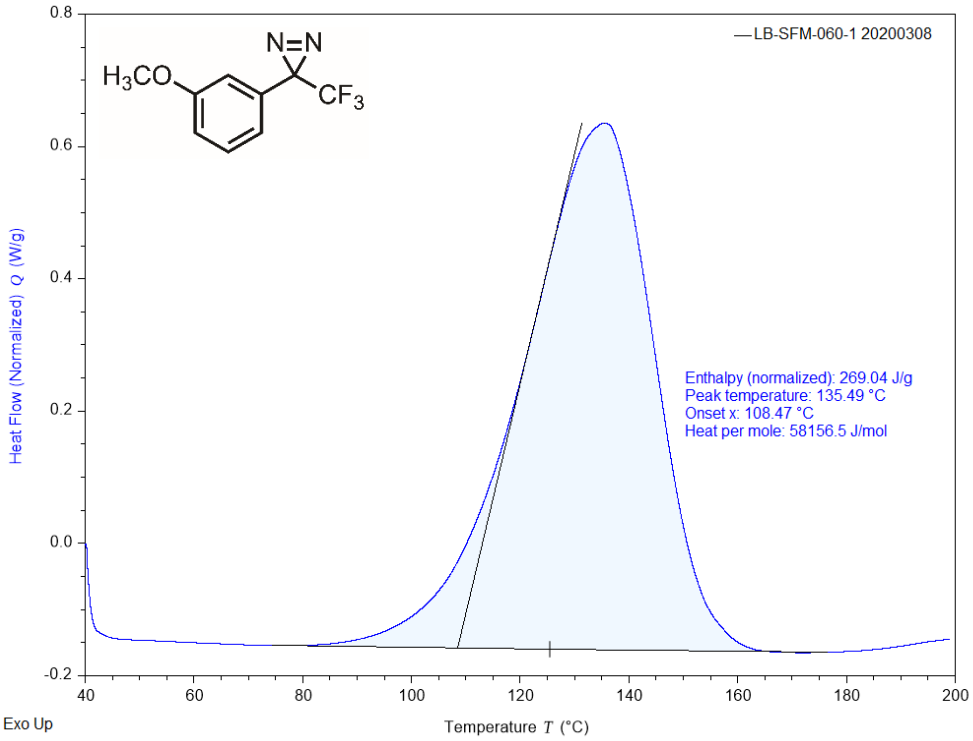

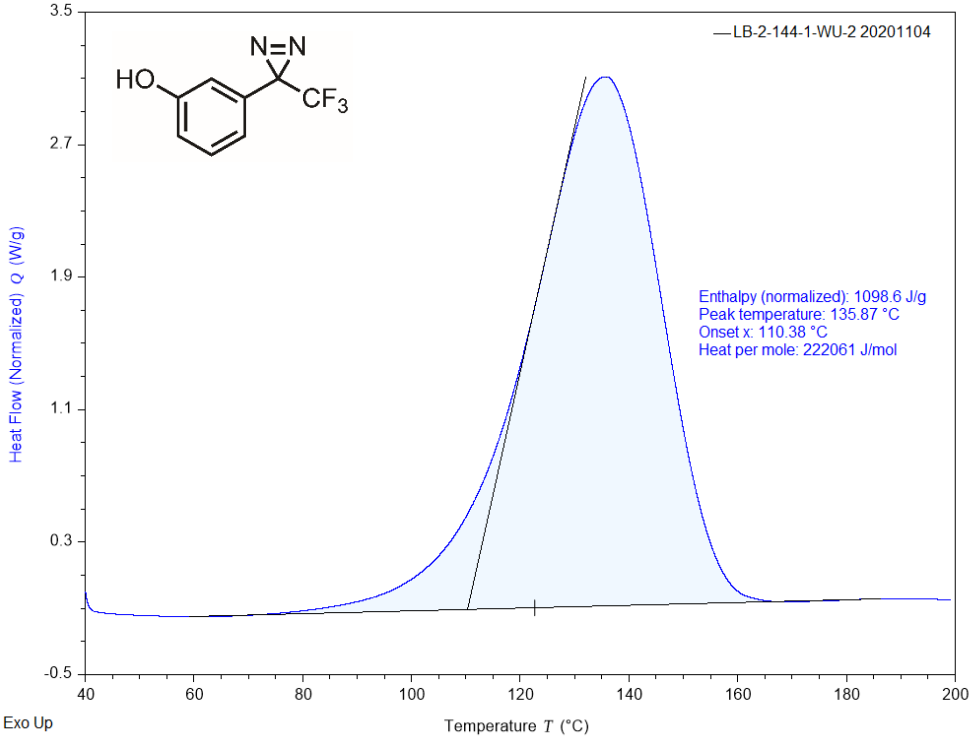

Representative DSC data for **D2.10** (top) and **D2.11** (bottom):

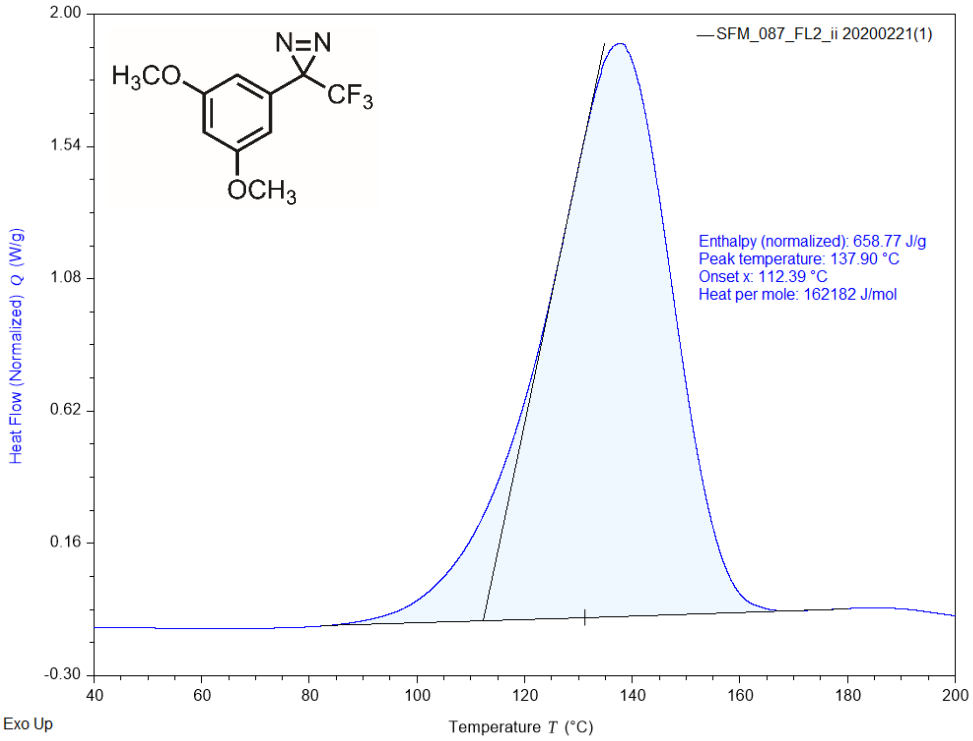

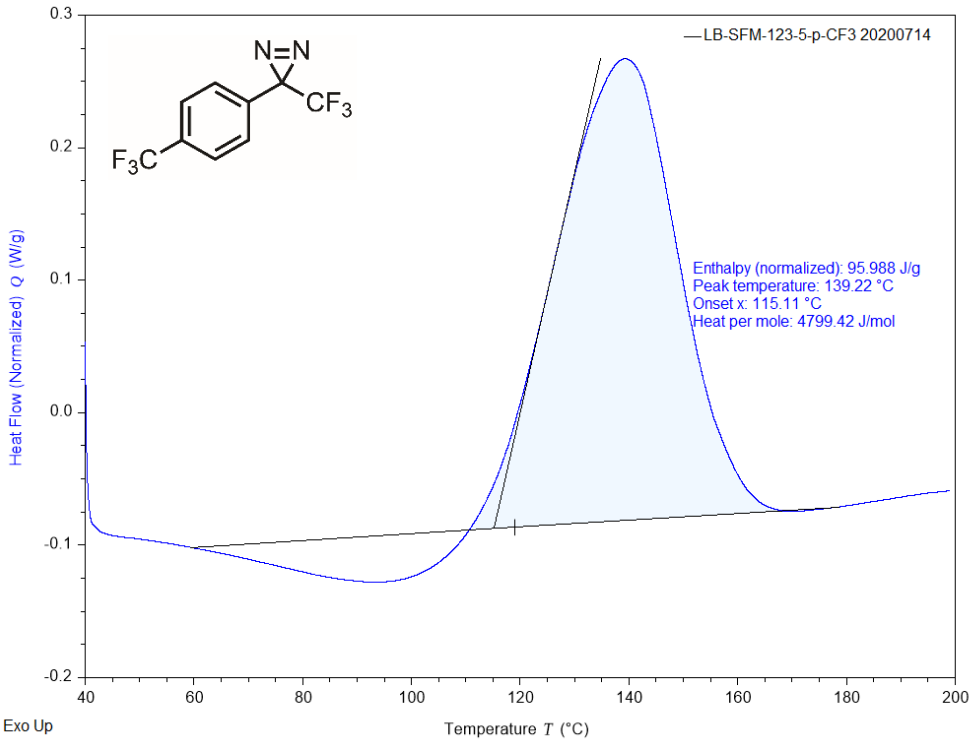

Representative DSC data for **D2.12** (top) and **D2.13** (bottom):

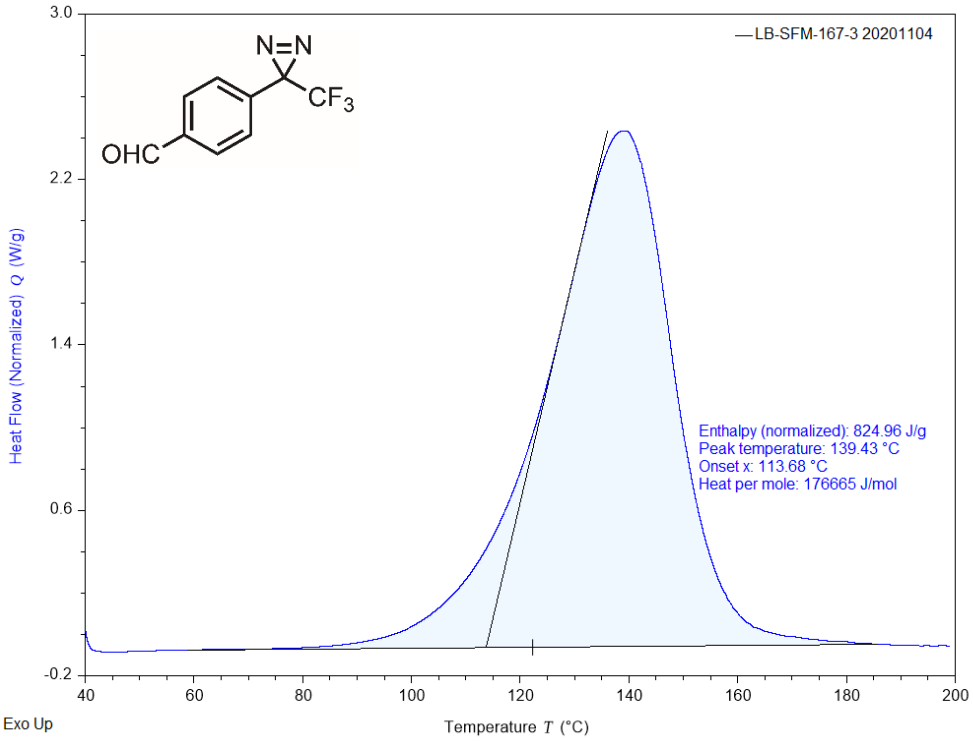

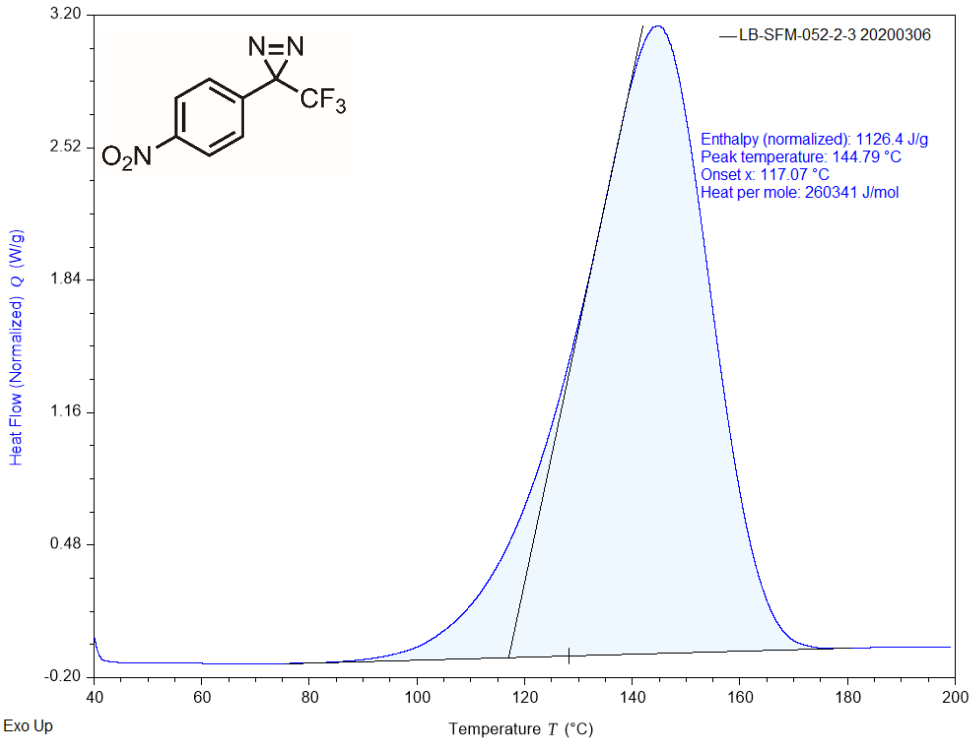

Representative DSC data for **D2.14** (top) and **D2.15** (bottom):

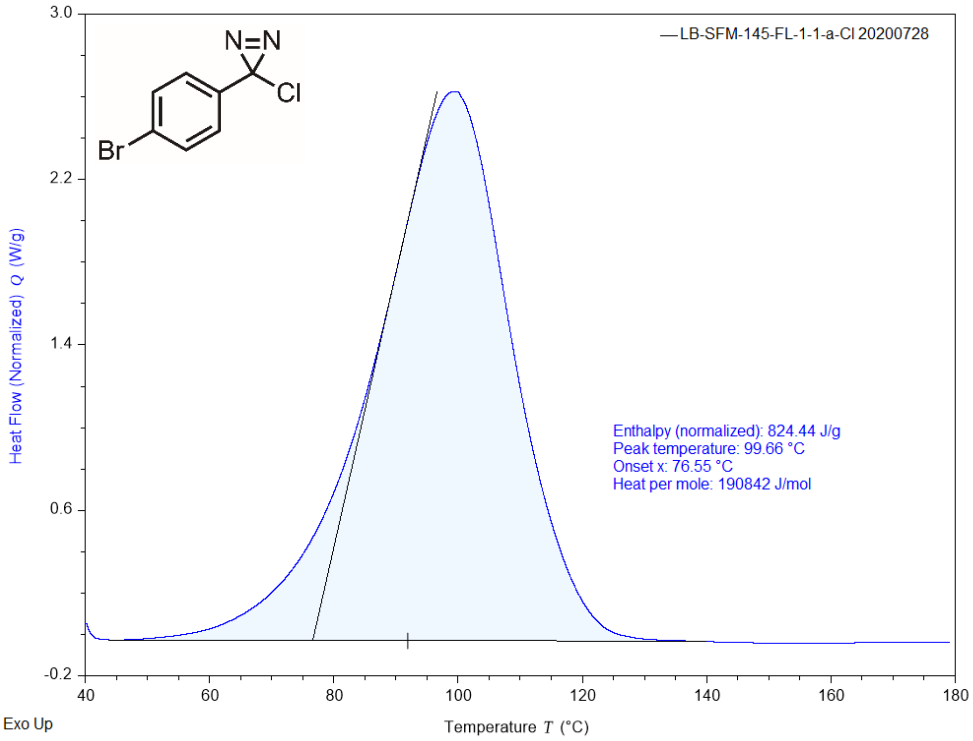

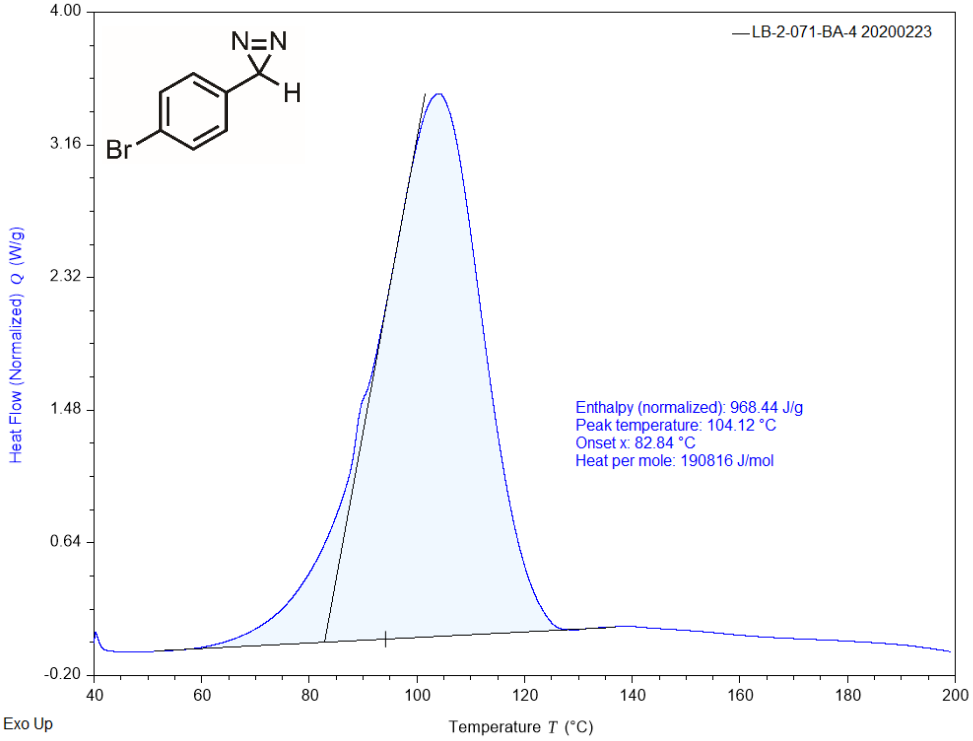

Representative DSC data for **D2.16** (top) and **D2.17** (bottom):

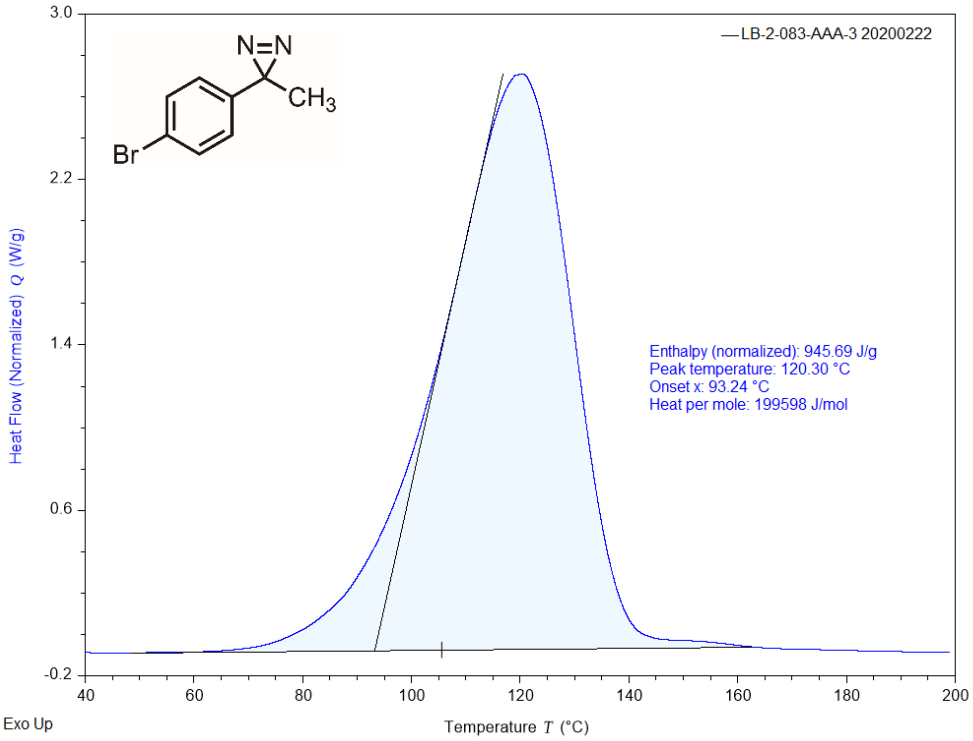

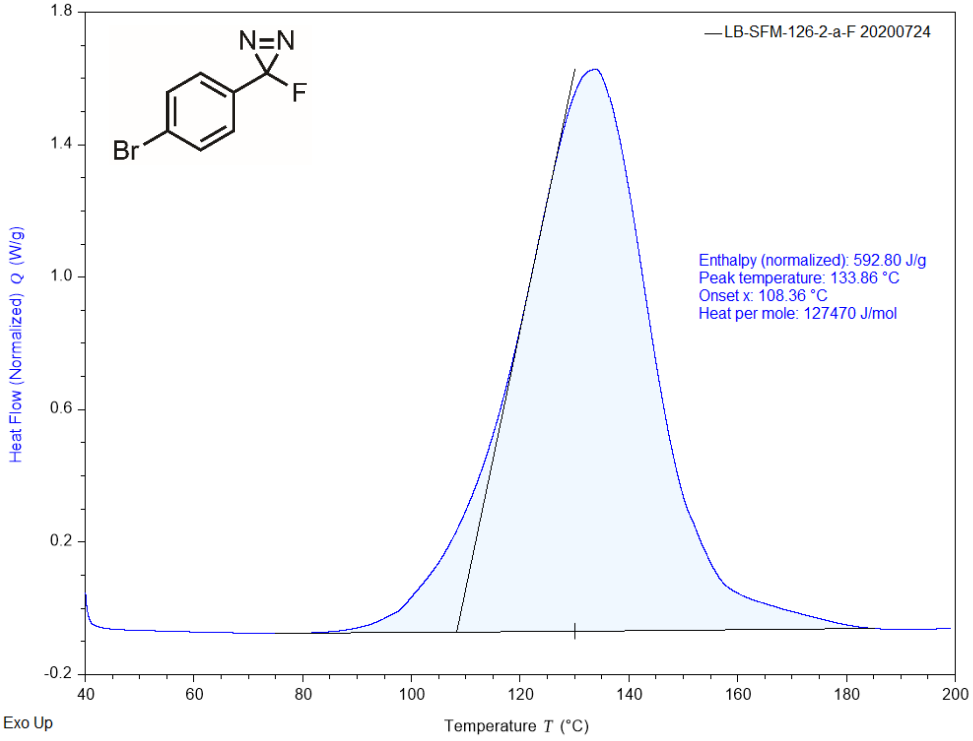

Representative DSC data for **4.3** (top) and **4.4** (bottom):

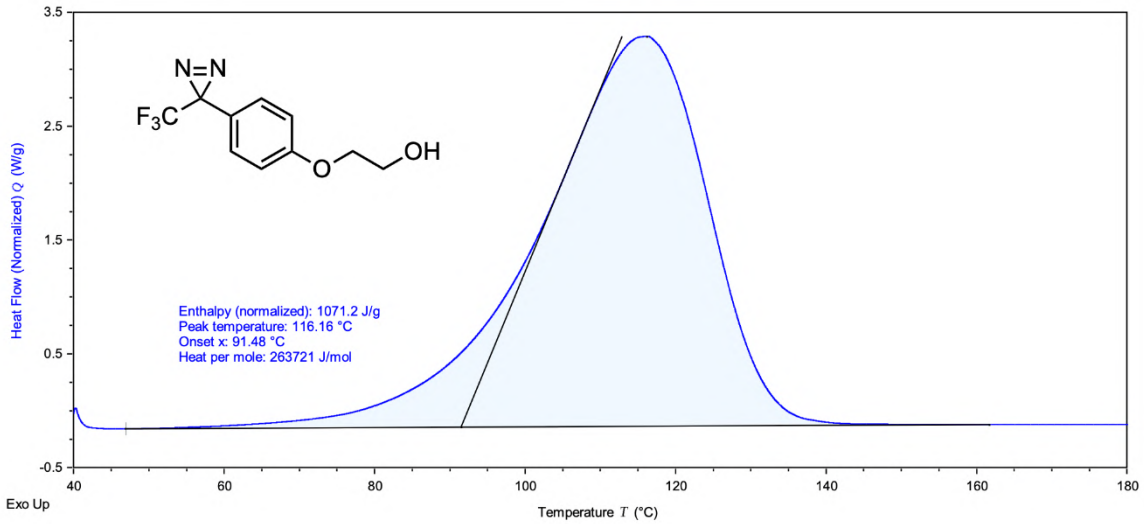

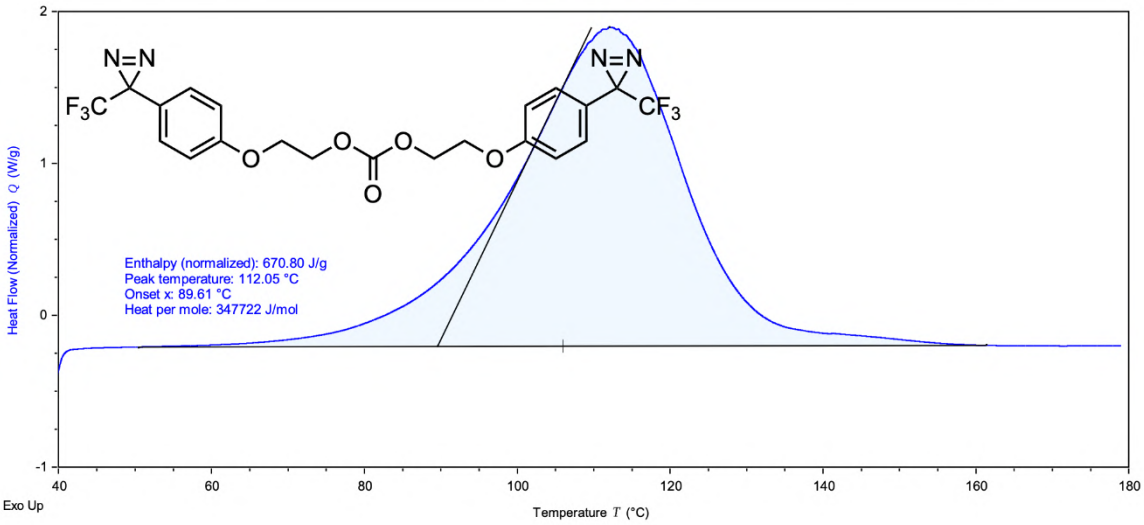

Representative DSC data for **4.5** (top) and **4.6** (bottom):

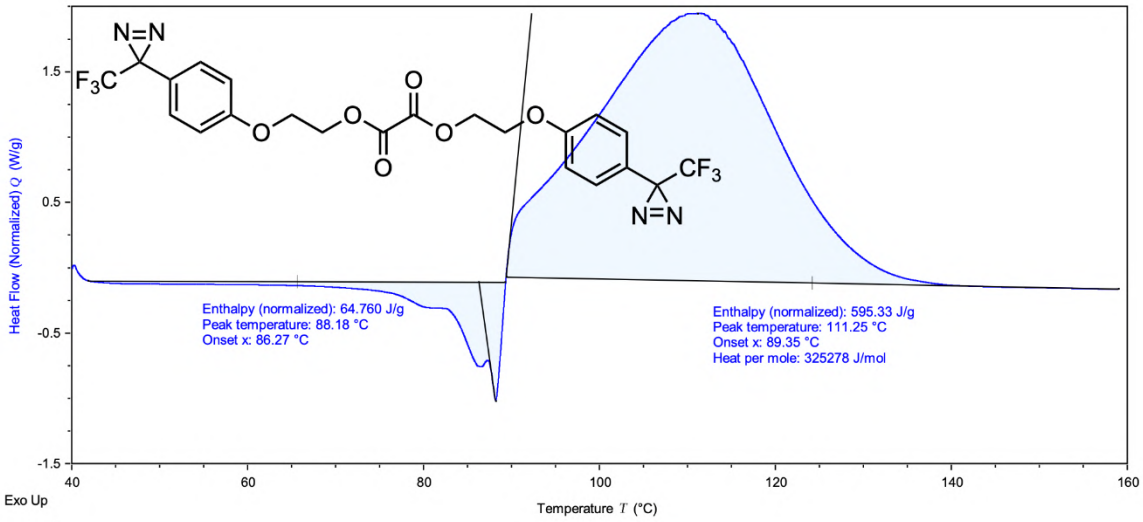

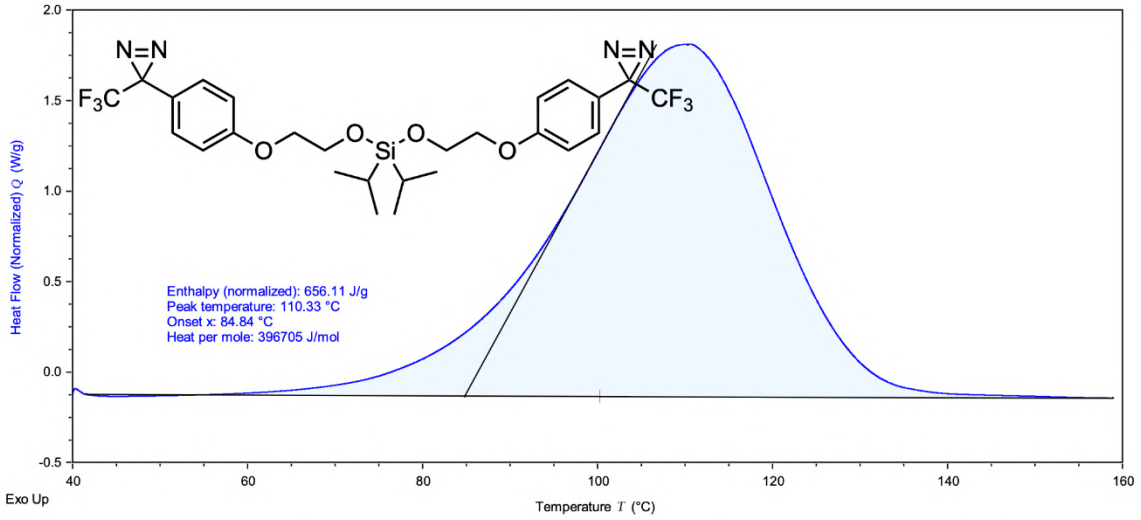

DSC traces for iPP and PE mixture vehicle control (top, sample VC) and crosslinked with 10 wt% of **4.11** (bottom, sample G):

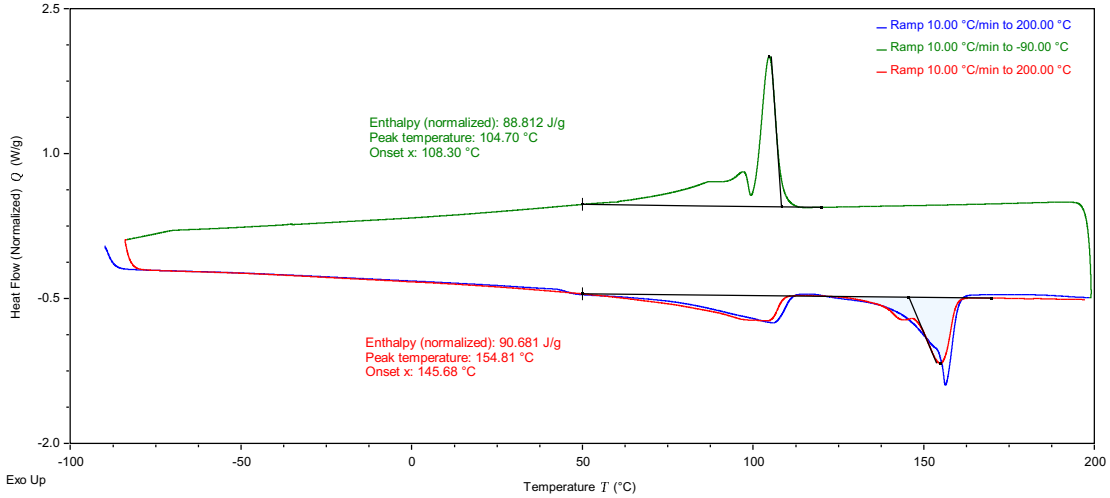

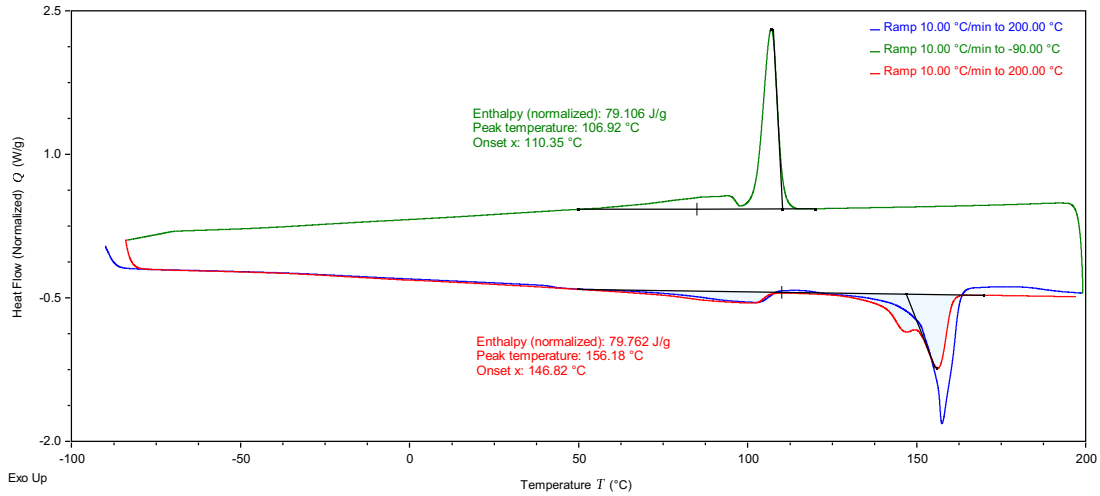

DSC traces for iPP and PE mixture crosslinked with 10 wt% of **4.4** (top, sample C), **4.5** (middle, sample O), and **4.6** (bottom, sample S):

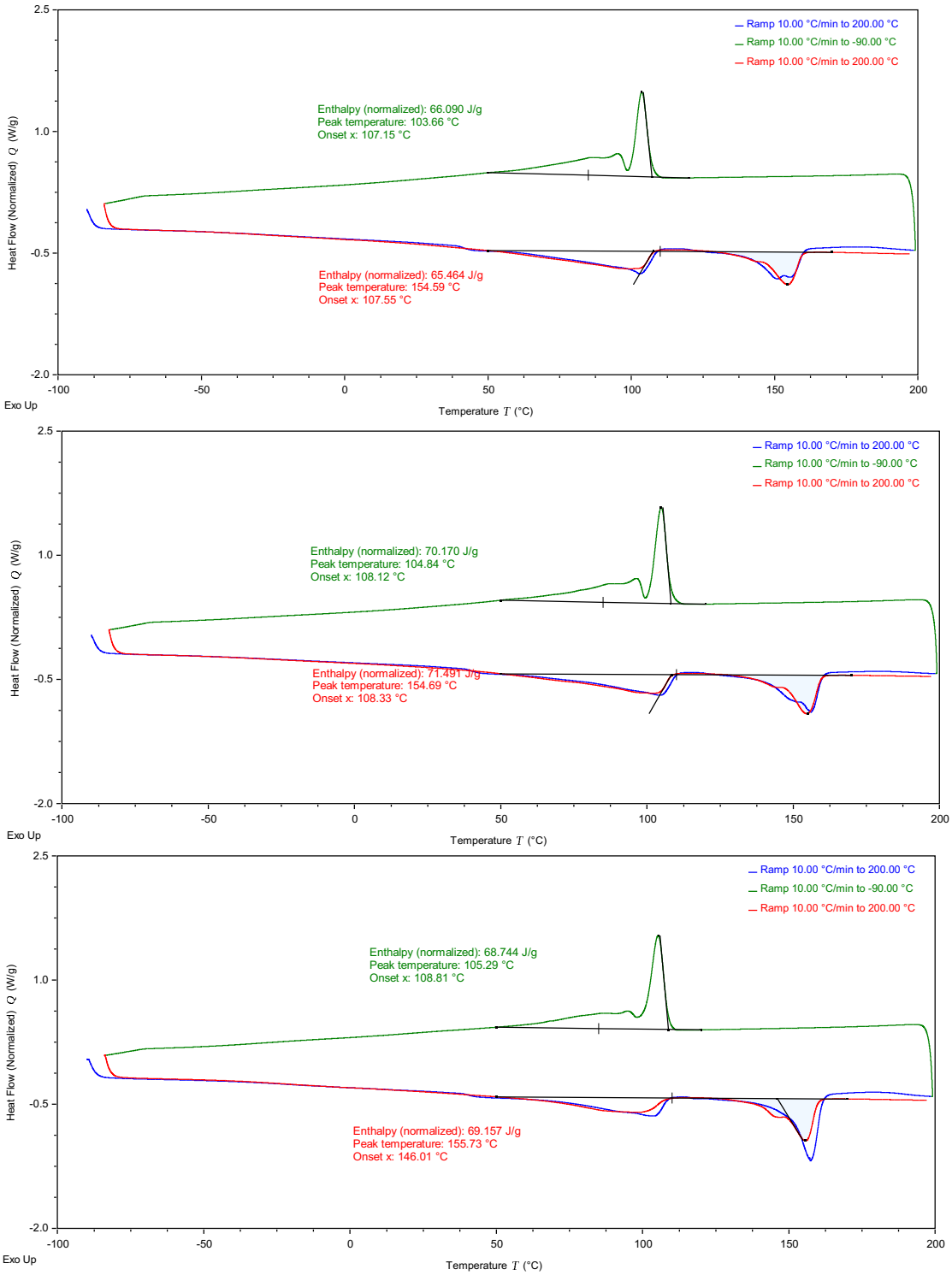

DSC traces for iPP and PE mixture vehicle control after NaOH treatment (top, sample VC) and crosslinked with 10 wt% of **4.11** after NaOH treatment (bottom, sample G):

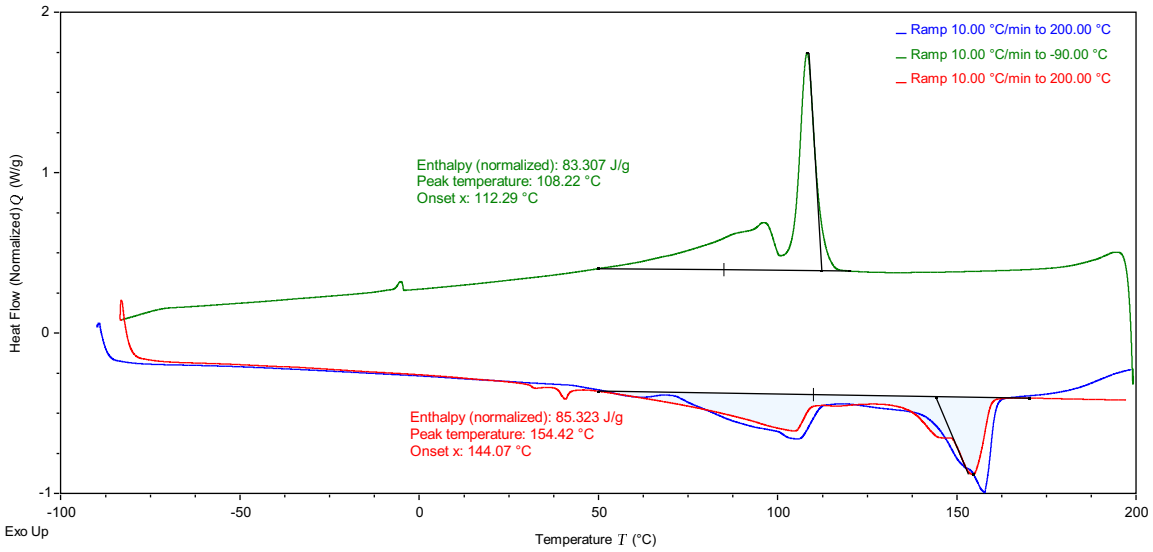

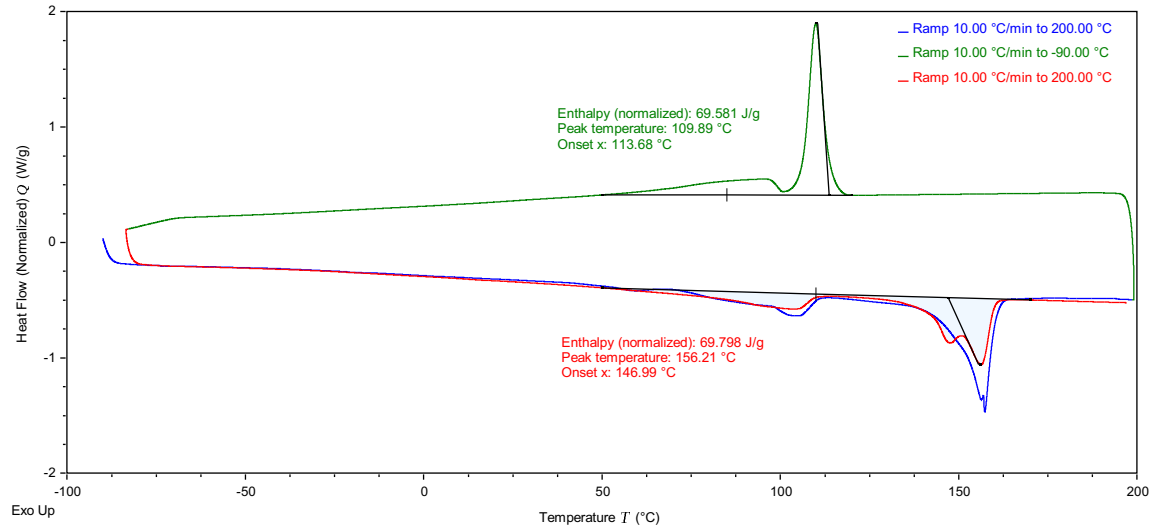

DSC traces for iPP and PE mixture crosslinked with 10 wt% of **4.4** (top, sample C) after NaOH treatment and **4.5** (bottom, sample O) after NaOH treatment:

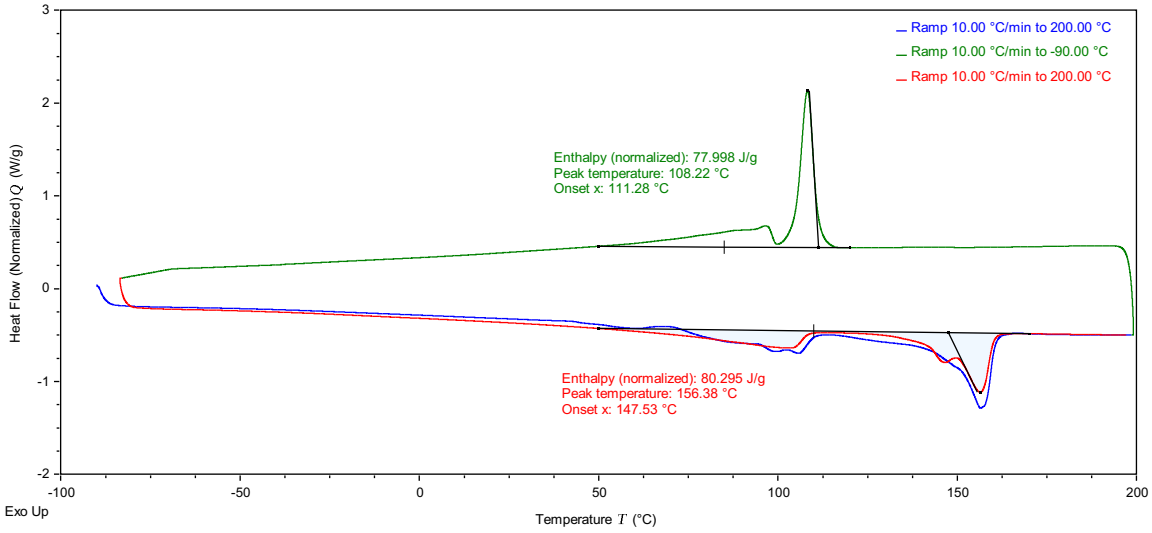

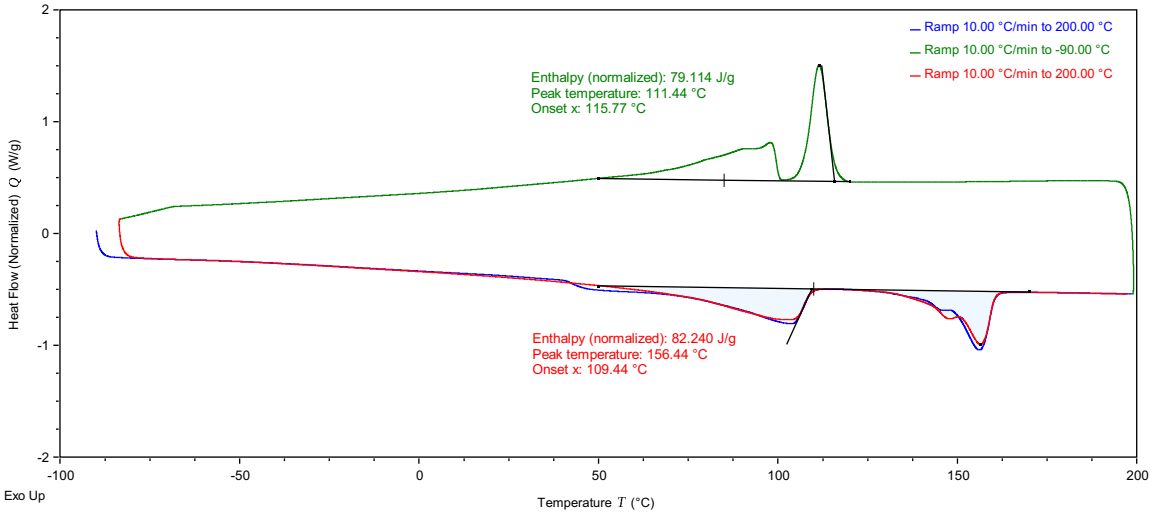

DSC traces for iPP and PE mixture vehicle control after TBAF treatment (top, sample VC), crosslinked with 10 wt% of **4.11** after TBAF treatment (middle, sample G), and 10 wt% of **4.6** after TBAF treatment (bottom, sample S):